Investigating the effect of age-related mitochondrial dysfunction on intestinal tumour formation and progression

Anna Louise Murray Smith
BSc (Hons) MSc

This thesis is submitted for the degree of Doctor of Philosophy at Newcastle University

Wellcome Centre for Mitochondrial Research
Institute of Biosciences
Newcastle University
2020

Author's Declaration

This thesis is submitted for the degree of Doctor of Philosophy at Newcastle University. The research was conducted at the Wellcome Centre for Mitochondrial Research, Biosciences Institute, under the supervision of Dr Laura Greaves and Professor Sir Doug Turnbull. All research is my own unless stated otherwise.

I certify that none of the material offered in this thesis has been previously submitted by me for a degree of any other qualification at this or any other university.

Abstract

The clonal expansion of mitochondrial DNA (mtDNA) point mutations and associated defects of oxidative phosphorylation (OXPHOS) are observed within the ageing colorectal epithelium. Clonally expanded mtDNA point mutations are also observed within colorectal tumours, however whether these mutations are passive bystanders or if they functionally contribute to tumour progression is unknown. In order to address this, a mouse model was developed in which *PolγA* mediated mtDNA mutation accumulation preceded the intestinal *Lgr5+* stem cell specific deletion of *Apc.* In comparison with controls, mice harbouring OXPHOS defects demonstrated an accelerated clinical deterioration characterised by anaemia, impaired thermoregulation and weight loss. The reduced survival of these animals was attributed to a significantly greater intestinal adenoma burden in which a prominent complex I defect was revealed following immunofluorescent quantification of OXPHOS protein levels. A double thymidine analogue labelling technique demonstrated accelerated proliferation within complex I deficient intestinal adenomas while apoptotic cells were significantly fewer.

Total RNA sequencing of OXPHOS deficient intestinal crypts prior to *Apc* deletion identified the upregulation of transcripts specific to the *de novo* serine synthesis pathway and mitochondrial one-carbon cycle (Whitehall, 2019). These pathways provide essential nucleotides, antioxidants and anabolic precursors vital to maximal tumour growth. RNA sequencing results were validated at the protein level within OXPHOS deficient intestinal crypts and adenomas and were further demonstrated to be upregulated in response to an age-related accumulation of OXPHOS defects in the murine small intestine and colon. Finally, these data are directly translatable to the normal human colonic epithelium in which the upregulation of serine synthesis and mitochondrial one-carbon cycle enzymes was identified within OXPHOS deficient crypts. These data show that age-related OXPHOS deficiency creates a permissive metabolic environment which in the event of malignant transformation, can actively contribute to accelerated intestinal cancer growth.

Acknowledgements

Firstly, I would like to thank my supervisors; Dr Laura Greaves and Professor Sir Doug Turnbull for allowing me the opportunity to undertake this PhD. During my years of study, the support I have received from Dr Greaves has been unfaltering. Extended to my colleagues, Dr Julia Whitehall, Carla Bradshaw and Dr Angela Pyle; I would like to thank you all for your endless encouragement and friendship. Thank you to Dr David Bulmer, Dr Glyn Nelson, Dr Rolando Berlinguer-Palmini, and Dr Alex Laude in the Bioimaging Unit, Newcastle University. I sincerely appreciate all of the time, advice and coffee you have shared with me. I would also like to thank my assessors Professor Robert Taylor, Professor Rakesh Heer and Professor Neil Perkins for their guidance throughout, and Dr Alasdair Blain for his statistical support. While I would like to thank Matthew Hunt specifically for his contribution in assisting with OXPHOS and thymidine analogue small intestinal data collection, my thanks are extended to all of my colleagues at the Centre past and present. You have all supported me in different ways and I am grateful to every member of the group.

To my parents, thank you for encouraging and inspiring me to aim to be the best version of myself. To my mum especially, thank you for always being there and always saying what I have needed to hear. My final thank you is to my son, Stanley. Although my work has been challenging for both of us, at times you have shown patience and understanding beyond your years. I hope that one day you might read 'mum's book' and if anything, I hope it will inspire you to work hard, challenge yourself and persevere as you strive to achieve your own goals.

Publications

Anna L. M. Smith, Julia C. Whitehall, Carla Bradshaw, David Gay, Fiona Robertson, Alasdair P. Blain, Gavin Hudson, Angela Pyle, David Houghton, Matthew Hunt, James N. Sampson, Craig Stamp, Grace Mallett , Shoba Amarnath, Jack Leslie, Fiona Oakley, Laura Wilson, Angela Baker, Oliver M. Russell, Riem Johnson, Claire A. Richardson, Bhavana Gupta, Iain McCallum, Stuart A. C. McDonald, Seamus Kelly, John C. Mathers, Rakesh Heer, Robert W. Taylor, Neil D. Perkins, Doug M. Turnbull, Owen J. Sansom and Laura C. Greaves. Age-associated mitochondrial DNA mutations cause metabolic remodelling contributing to accelerated intestinal tumorigenesis. *Nature Cancer* (2020). https://doi.org/10.1038/s43018-020-00112-5

Abbreviations used

1C	one carbon
3PG	3-phosphoglycerate
3PHP	3-phosphohydroxypyruvate
3PSer	3-phosphoserine
AARE	amino acid response element
ACP	acyl carrier protein
ADOA	autosomal dominant optic atrophy
ADP	adenosine diphosphate
AJCC/UICC	American Joint Committee on Cancer/Union Internationale Contre le Cancer
α-KG	α–ketoglutarate
Akt	AKT serine/threonine kinase
Aldh1l2	aldehyde dehydrogenase 1 family member L2
AMPK	AMP activated protein kinase
ANOVA	analysis of variance
Apaf-1	apoptotic protease activating factor-1
APC	adenomatous polyposis coli
APOBEC1	apolipoprotein B (apoB) mRNA editing catalytic polypeptide 1
Ascl2	achaete-scute family basic helix loop helix transcription factor 2
ASNS	asparagine synthetase
ATAD3	ATPase AAA domain-containing protein 3
ATF	activating transcription factor
Atoh1	atonal basic helix loop helix transcription factor 1
ATP	adenosine triphosphate

ATPB	ATP synthase subunit beta
AU	airy unit
AU	arbitrary unit
Bad	Bcl2-associated agonist of cell death
Bak	Bcl-2 homologous antagonist/killer
BAT	brown adipose tissue
Bax	Bcl-2-associated X protein
Bcl-2	B-cell lymphoma 2
Bcl-xL	Bcl-2-like protein 1 isoform x
BER	base excision repair
BH3	Bcl-2 homology domains (3)
BMC	bone mineral composition
BMD	bone mineral density
Bmi1	proto-oncogene, polycomb ring finger
BMP	bone morphogenetic protein
Bp	base pairs
BRAF	V-Raf murine sarcoma viral oncogene homologue B serine/threonine kinase
Ca^{2+}	calcium
CAF	cancer associated fibroblast
Cas9	CRISPR associated protein 9
CaMK	calcium/calmodulin-dependent protein kinase
cAMP	cyclic adenosine monophosphate
CBC	crypt base columnar
CC3	cleaved caspase 3

CCK	cholecystokinin
CD	cluster of differentiation
CIMP	CpG island methylator phenotype
CIN	chromosomal instability
cKIT	KIT proto-oncogene receptor tyrosine kinase
CldU	5-chloro-2’-deoxyuridine
CMS	consensus molecular subtype
CO	cytochrome *c* oxidase
CO_2	carbon dioxide
coA	coenzyme A
COX	cytochrome *c* oxidase
CPEO	chronic progressive external ophthalmoplegia
CpG	5'-cytosine-phosphate-guanine-3'
CRC	colorectal cancer
CRISPR	clustered regularly interspaced short palindromic repeats
CSC	cancer stem cell
CTH	cystathionine gamma-lyase
CuA/B	copper centre A/B
CYP1A	cytochrome P450 family 1 subfamily A
CYTB	cytochrome *b*
DAB	3,3’-diaminobenzidine
DDIT	DNA damage-inducible transcript 3 protein
DHFR	dihydrofolate reductase
Dll1/4	delta like canonical Notch ligand 1/4

D-loop	displacement loop
DNA	deoxyribonucleic acid
dNTP	deoxynucleoside triphosphate
DPX	dibutylphthalate polystyrene xylene
DRP1	dynamin related protein 1
DSB	double stranded break
Dsh	dishevelled
ECM	extracellular matrix
EDTA	ethylenediaminetetraacetic acid
EGF	epidermal growth factor
EGFR	epidermal growth factor receptor
EGFP	enhanced green fluorescent protein
eIF2α	eukaryotic initiation factor 2, α subunit
EMT	epithelial-to-mesenchymal-transition
ENU	ethylnitrosourea
EpCAM	epithelial cell adhesion molecule
ER	endoplasmic reticulum
ERK	extracellular signal-regulated kinase
ES cell	embryonic stem cell
EtOH	ethanol
FACS	fluorescence-activated cell sorting
$FADH_2$	dihydroflavin adenine dinucleotide
FAP	familial adenomatous polyposis coli
Fas	Fas cell surface death receptor

FASTK	Fas-activated serine/threonine kinase
Fe-S	iron sulphur
FFPE	formalin fixed paraffin embedded
FGF21	fibroblast growth factor 21
FH	fumarate hydratase
FPKM	fragments per kilobase of transcript per million mapped reads
FMN	flavin mononucleotide
FOXO	forkhead box O transcription factor
FXN	frataxin
Fz	frizzled
GAPDH	glyceraldehyde-3- phosphate dehydrogenase
GCN2	general control nonderepressible 2, eIF2α kinase
GDF15	growth differentiation factor 15
GEMM	genetically engineered mouse model
GFP	green fluorescent protein
GI	Galon Immunoscore
GLUT1/3/4	glucose transporter 1/3/4
GMS	Glasgow microenvironment score
Gpx1	glutathione peroxidase 1
GREM1	gremlin 1 BMP antagonist
GSH	glutathione
GSK-3β	glycogen synthase kinase 3 beta
GSSG	oxidised glutathione
GTP	guanosine-5'-triphosphate

H_2O_2	hydrogen peroxide
HDAC1	histone deacetylase 1
HDR	homology-directed repair
H&E	haematoxylin and eosin
HER2	human epidermal growth factor receptor 2
Hes1	hairy and enhancer of split family basic helix loop helix transcription factor 1
HIF	hypoxia-inducible factor
HNPCC	hereditary non-polyposis colon cancer
H+L	heavy and light chains
Hopx	homeobox only
HPLC-MS	high performance liquid chromatography-mass spectrometry
HR	heptad repeat
HR	homologous recombination
HRP	horseradish peroxidase
HSC	haematopoietic stem cell
HSC20	HscB mitochondrial iron sulphur cluster cochaperone
HSP	heavy strand promoter
HSP	heat shock protein
iAP	conditional null alleles of *Apc* and *Tp53* (GEMM)
IAP	inhibition of apoptosis
IDH1/2	isocitrate dehydrogenase 1/2
IDO1	indoleamine-2,3-dioxygenase-1
IdU	5-iodo-2'-deoxyuridine
IF	immunofluorescence

Ig	immunoglobulin
IHC	immunohistochemistry
IMC	imaging mass cytometry
IVC	individually ventilated cage
IF2MT	mitochondrial initiation factor 2
IF3MT	mitochondrial initiation factor 3
iKAP	inducible oncogenic *Kras* allele, conditional null alleles of *Apc* and *Tp53* (GEMM)
IL	interleukin
IOSCA	infantile onset spinocerebellar ataxia
IMM	inner mitochondrial membrane
IP	intraperitoneal
IRES	internal ribosome entry site
ISC	intestinal stem cell
ISCU	iron-sulfur cluster assembly scaffold protein
ISD11	Cysteine desulphurase (NFS1) activator
ISR^{mt}	mitochondrial integrated stress response
JNK	c-Jun N-terminal kinase
KM	Klintrup-Makinen
KRAS	Kirsten rat sarcoma viral oncogene homologue, GTPase
KSS	Kearns-Sayre syndrome
LBD	ligand binding domain
LED	light-emitting diode
Lgr5	leucine-rich-repeat-containing G protein-coupled receptor 5
LoxP	locus of X over P1

Lrp	LDL receptor related Protein
LSP	light strand promoter
MAPK	mitogen-activated protein kinase
MEK	mitogen-activated protein kinase kinase
Mcl1	myeloid cell leukaemia 1
MCU	mitochondrial Ca^{2+} uniporter
MDH1	malate dehydrogenase 1
MELAS	mitochondrial encephalopathy, lactic acidosis and stroke-like episodes
MERFF	myoclonic epilepsy with ragged red fibres
Mff	mitochondrial fission factor
MFN1	mitofusin 1
MFN2	mitofusin 2
MFRTA	mitochondrial free radical theory of ageing
MiD49	mitochondrial dynamics protein 49
MiD51	mitochondrial dynamics protein 51
Min	multiple intestinal neoplasia
MKK6	mitogen-activated protein kinase kinase 6
MLH1	mutL homolog 1
ML-IAP	melanoma inhibitor of apoptosis
MLL1	mixed lineage leukaemia 1
MMR	mismatch repair
MnSOD	mitochondria-specific manganese superoxide dismutase
MOMP	mitochondrial outer membrane permeability
MPC	mitochondrial pyruvate carrier

Mrfn1	mitoferrin 1/2
MSH2/6	mutS homolog 2/6
mtDNA	mitochondrial DNA
mtEFG1	mitochondrial elongation factor G1
mtEFG2	mitochondrial elongation factor G2
mtEFTs	mitochondrial elongation factor Ts
mtEFTu	mitochondrial elongation factor Tu
mTERF1	mitochondrial termination factor 1
MTHFD	methylenetetrahydrofolate dehydrogenase
MTHFR	methylene tetrahydrofolate reductase
MTORC1	mammalian target of rapamycin complex 1
mtPAP	polyadenylic acid RNA polymerase
MTR	methionine synthase
mtRF1a	mitochondrial release factor 1a
mtRRF1	mitochondrial ribosomal recycling factors 1
MSI	microsatellite instability
mtSSB	mitochondrial single-strand binding protein
mtTF1	human mitochondrial transcription factor 1
mtTFB2	mitochondrial transcription factor B2
MT-TK	mitochondrially encoded tRNA-Lys (AAA/G)
MT-TL1	mitochondrially encoded tRNA-Leu (UUA/G) 1
mtZFN	mitochondrially targeted zinc-finger nuclease
Muc2	mucin 2, oligomeric mucus/gel-forming
MUL1	mitochondrial E3 ubiquitin protein ligase 1

MYC	avian myelocytomatosis viral oncogene homologue, basic helix loop helix transcription factor
NAD+	nicotinamide adenine dinucleotide
NADH	reduced nicotinamide adenine dinucleotide
NADPH	reduced nicotinamide adenine dinucleotide phosphate
ND1/4L/6	NADH: ubiquinone oxidoreductase core subunit 1/4L/6
NDUFA4	cytochrome *c* oxidase subunit NDUFA4
NDUFB8	NADH: ubiquinone oxidoreductase subunit B8
NDUFS3	NADH: ubiquinone oxidoreductase subunit S3
NER	nucleotide excision repair
NF-kB	nuclear factor kappa B subunit 1
NFS1	mitochondrial cysteine desulphurase
NFY	nuclear transcription factor Y
NGS	normal goat serum
NHEJ	non-homologous end joining
NICD	Notch intracellular domain
NMN	nicotinamide mononucleotide
NMNAT	nicotinamide mononucleotide adenylyl transferase
NNT	nicotinamide nucleotide transhydrogenase
NPC	no primary control
NR	nicotinamide riboside
NRF1	nuclear respiratory factor 1
NRF2	nuclear respiratory factor 2
NSCLC	non-small cell lung cancer
NUMT	nuclear-encoded mitochondrial segment

O_2-	superoxide radical
•OH	hydroxyl radical
O_H	origin of heavy strand replication
O_L	origin of light strand replication
OMM	outer mitochondrial membrane
OPA1	optic atrophy 1 mitochondrial dynamin-like GTPase
OTC	ornithine transcarbamylase
OXPHOS	oxidative phosphorylation
PABA	para-aminobenzoic acid
PAM	protospacer adjacent motif
PBS	phosphate buffered saline
PC/GPC	phosphocoline/glycerophosphocoline ratio
PCR	polymerase chain reaction
PDE	patient derived explant
PDE12	phosphodiesterase 12
PDH	pyruvate dehydrogenase
PDHK	pyruvate dehydrogenase kinase
PEO	progressive external ophthalmoplegia
PERK	protein kinase R (PKR)-like endoplasmic reticulum kinase
PET	positron emission tomography
PFK	phosphofructokinase
PGC-1α	peroxisome proliferator activated receptor γ coactivator 1 α
PHB1/2	prohibitin 1/2
PHGDH	phosphoglycerate dehydrogenase

Pi3k	phosphatidylinositol-4,5-bisphosphate 3-kinase
PKC	protein kinase C
PKM1/2	pyruvate kinase M1/2 isoform
PMS2	post meiotic segregation increased 2
Polγ	mitochondrial DNA polymerase gamma
PolγA	catalytic subunit of polymerase gamma
PolγB	accessory subunit of polymerase gamma
POLMRT	mitochondrial RNA polymerase
PPARα	peroxisome proliferator activated receptor alpha transcription factor
PSAT1	phosphoserine aminotransferase 1
PSPH	phosphoserine phosphatase
PTEN	phosphatase and tensin homologue
Q	ubiquinone
QH_2	ubiquinol
R-2HG	(*R*)-2-hydroxyglutarate
Raf	rapidly accelerated fibrosarcoma serine/threonine kinase
Ras	rat sarcoma GTPase
Rbpj	recombination signal binding protein for immunoglobulin kappa J region
Reg4	regenerating family member 4
RET	reverse electron transport
RFID	radio frequency identification chip
RIN	RNA integrity
RITOLS	RNA incorporation throughout the lagging strand
RM	rat and mouse

RNA	ribonucleic acid
RNaseP	ribonuclease P
RNase H1	encoding ribonuclease H1
RNaseZ	ribonuclease Z
RNF43	ring finger protein 43 ubiquitin ligase
ROI	region of interest
ROS	reactive oxygen species
SA	succinate
SAH	S-adenosylhomocysteine
SAM	S-adenosylmethionine
SAM	sorting and assembly machinery
SD	standard deviation
SDH	succinate dehydrogenase
SDS	sodium dodecyl sulphate
SEM	standard error of the mean
sgRNA	single guide RNA
SHMT	serine hydroxymethyltransferase
SI	small intestine
SIRT	sirtuin (silent mating type information regulation 2 homologue)
SIV	Simian immunodeficiency virus
Slc1a4	solute carrier family 1 member 4
SMAC	second mitochondria-derived activator of caspase
Smad	mothers against decapentaplegic homologue
Sod2	superoxide dismutase 2

Sox9	SRY (sex determining region Y) - box transcription factor 9
SP1	specificity protein 1
SSBR	single strand break repair
SSP	serine synthesis pathway
Stat1	signal transducer and activator of transcription 1
T_3	triiodothyronine
T_4	thyroxine
TA	transit amplifying progenitor cell
TALE	transcription activator-like effector array
TBST	tris buffered saline plus tween
TCA	tricarboxylic acid
Tcf4	transcription factor 4
TCF/LEF	transcription factor/lymphoid enhancer binding factor
TEFM	mitochondrial transcription elongation factor
TFAM	mitochondrial transcription factor A
TfR	transferrin receptor
TGF	transforming growth factor
THF	tetrahydrofolate
TIM	translocase of the inner membrane
TME	tumour microenvironment
TNF	tumour necrosis factor
TNM	tumour node metastases
TOM	translocase of the outer membrane
Top3α	type IA topoisomerase 3α

TP53	tumour protein 53
TPO	thyroid peroxidase
tracrRNA	transactivating crRNA region
TRAIL	TNF-related apoptosis inducing ligand
Treg	regulatory T cell
Trib3	tribbles pseudokinase 3
tRNA	transfer ribonucleic acid
TRNT1	tRNA nucleotidyltransferase
Tsc1	tuberous sclerosis 1
TSP	tumour stroma percentage
TWINKLE	mitochondrial helicase
UCP-1/2	mitochondrial uncoupling protein 1/2
UPR^{mt}	mitochondrial unfolded protein response
UQCRFS1	ubiquinol-cytochrome *c* reductase, Rieske iron-sulphur polypeptide 1
VDAC	voltage-dependant ion channel
Wnt	wingless integration
XIAP	X-linked inhibitor of apoptosis
YME1L1	YME1-like ATP-dependent zinc metalloprotease 1
ZNRF3	zinc and ring finger 3 ubiquitin ligase

Table of Contents

List of figures

List of tables

Chapter 1. Introduction

Worldwide, colorectal cancer (CRC) is the third most commonly diagnosed cancer in men and the second most commonly diagnosed malignancy in women. In 2018, colorectal cancer accounted for 9.2% of global cancer deaths with 5-year survival rates in the UK reported as relatively poor at approximately 50% (Arnold et al., 2019). The incidence of CRC rises steeply from around 50-55 years of age and as such, CRC and indeed many malignancies are strongly associated with advancing age. Described by López-Otín and colleagues in 2013, the pathology of ageing is characterised by nine molecular hallmarks which together lead to the manifestation of an ageing phenotype (López-Otín et al., 2013). A similar set of hallmarks has been described with regard to cancer (Hanahan & Weinberg, 2011). While some hallmarks such as proteostasis and cellular senescence are divergent between the two pathologies of ageing and cancer, several are shared. Perturbed mitochondrial function is one such common hallmark.

Previous work carried out within the group has demonstrated an exponential increase in the frequency of colonic crypts harbouring clonally expanded somatic mitochondrial DNA point mutations and associated defects of oxidative phosphorylation (OXPHOS) within the ageing colorectal epithelium (Taylor et al., 2003). A similar mtDNA mutational spectrum has also been observed within human colorectal cancers (Ericson et al., 2012; He et al., 2010; Larman et al., 2012; Polyak et al., 1998). The enrichment of somatic mtDNA mutations and their co-segregation with oxidative phosphorylation defects as colorectal adenomas progress to carcinoma suggests a contribution to tumorigenesis (Smith et al., 2020), however whether this is active, or passive remains to be elucidated. In the absence of experimental evidence supporting or refuting the role of age-associated mtDNA mutations in the development of colorectal cancer, this thesis aims to address this with the use of a biologically relevant mouse model of mtDNA mutation accumulation, ageing and colorectal cancer.

1.1. Mitochondria

Mitochondria are organelles present in the cytoplasm of almost every eukaryotic cell. They were first described by Altmann in the 1890s as ‘‘bioblasts’’; “elementary organisms” that live inside cells and carry out vital functions (Altmann, 1894). Mitochondria very closely resemble bacteria, and as such, are thought to have evolved from them via a process known as endosymbiosis. Endosymbiosis describes the engulfment of free living, respiring Eubacteria by anaerobic, hydrogen dependant Archaebacteria creating primitive eukaryotic cells (Martin & Müller, 1998; Sagan, 1967).

Mitochondria play an essential role in metabolism, converting carbohydrates and fatty acids into ATP, the energy currency of the cell via a process known as oxidative phosphorylation (Belitzer & Tsybakova, 1939). Alongside this critical function, mitochondria are also involved in cytosolic calcium regulation (McCormack et al., 1990), apoptosis (Liu et al., 1996), and the biosynthesis of haem and iron sulphur (Fe-S) clusters (Sano et al., 1959).

Unlike other organelles, mitochondria contain their own genome, mitochondrial DNA (mtDNA). This circular, self-replicating, double stranded molecule was fully sequenced in 1981 and comprises 16,569 base pairs in humans. The mitochondrial genome encodes a proportion of the proteins essential for ATP production, the additional proteins required are encoded by the nuclear genome (Anderson et al., 1981).

1.1.1. Mitochondrial structure

The first high resolution electron micrograph images of mitochondria were produced in 1952 (Palade, 1952). Individual mitochondria are typically shown as rod shaped, double plasma membrane encased organelles which these early works placed as measuring around 2.5µm in length and 0.5 µm in width. A schematic is shown in Figure 1-1.

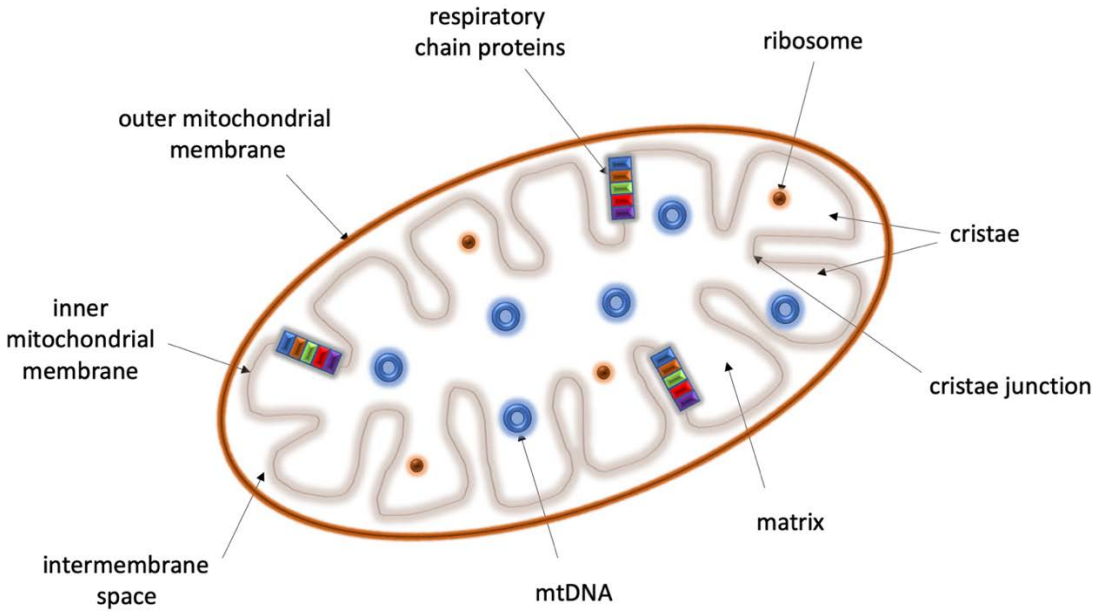

Figure 1-1. Schematic detailing the basic structure of a mitochondrion. The outer mitochondrial membrane houses an inner mitochondrial membrane which is folded into connected projections known as cristae. Respiratory chain proteins comprising the mitochondrial oxidative phosphorylation system are located on the inner mitochondrial membrane with the inner matrix containing multiple copies of the mitochondrial genome.

The outer mitochondrial membrane (OMM) is a porous structure which presents no barrier to the passage of ions and small uncharged molecules. These molecules traverse the membrane through the abundant voltage-dependant ion channels (VDAC). Larger molecules such as mitochondrial precursor proteins are transported across the OMM by dedicated translocases of the outer membrane (TOMs), with sorting and assembly of these precursors being facilitated by the sorting and assembly machinery (SAM) complex of proteins, also present in the OMM (Wiedemann et al., 2003).

The OMM surrounds the inner mitochondrial membrane (IMM), and the space between the two is termed the intermembrane space. The inner mitochondrial membrane is extensively folded into cristae which protrude into the mitochondrial matrix within. In contrast to the porous OMM, transport across the IMM is tightly regulated. This results in an electrochemical membrane potential across the membrane fundamental to oxidative phosphorylation. Molecules and ions may only pass across the IMM via specific transport proteins of which there are several types. Like the TOM proteins of the outer membrane, translocase of the inner membrane (TIM) proteins allow the movement of proteins across the IMM. The ATP/ADP carrier complex exports ATP from the mitochondrial matrix into the

cytoplasm while importing ADP back into the matrix for resynthesis of ATP (Pebay-Peyroula et al., 2003).

The innermost compartment of mitochondria is the matrix. It houses multiple copies of the mitochondrial genome in addition to the mitochondrial transcription and translation machinery. Replication of mitochondrial DNA occurs in the matrix as does fatty acid oxidation and the tricarboxylic acid (TCA) cycle, both reactions being important precursors to oxidative phosphorylation.

1.1.2. Mitochondrial functions

1.1.2.1. ATP synthesis

A major function of mitochondria is the production of cellular energy in the form of adenosine triphosphate (ATP). This occurs via oxidative phosphorylation on the IMM with the carriage of electrons from one respiratory protein complex to the next (Hatefi, 1985). ATP can be generated with the breakdown of lipids proteins and nucleotides; however, the primary source of cellular energy is derived from the breakdown of carbohydrates which, via a series of biochemical reactions, provide the substrates for oxidative phosphorylation (Berg et al., 2012). In the cytoplasm, glycolysis essentially describes the conversion of one molecule of glucose into two molecules of pyruvate. A net gain of two molecules of ATP, two molecules of water and one molecule of NADH are also generated during glycolysis, which can occur in both presence and absence of oxygen. In the absence of oxygen, pyruvate is converted to lactate which can be resynthesised to glucose via the Cori cycle in the liver, however under aerobic conditions pyruvate is transported into the mitochondrial matrix by the mitochondrial pyruvate carrier (MPC) (Papa et al., 1971) . The subsequent decarboxylation of pyruvate by pyruvate dehydrogenase (PDH) generates acetyl-coA; the primary substrate of the ensuing series of reactions encompassing the TCA cycle within the mitochondrial matrix. The completion of all eight stages of the TCA cycle generates one molecule of GTP, two of carbon dioxide, three molecules of NADH and one of $FADH_2$. NADH and $FADH_2$ are important electron carriers or reducing equivalents which are fundamental to the next stage of aerobic respiration; oxidative phosphorylation (Berg et al., 2012). The donation of electrons from NADH and $FADH_2$ to complexes I and II of the mitochondrial

electron transport chain permits the coupled translocation of protons from the mitochondrial matrix to the cristae lumen. This maintains an electrochemical gradient which is used by complex V at the end of the chain of respiratory protein complexes. The movement of protons from an area of high concentration in the cristae lumen to that of a lower concentration in the matrix provides a proton motive force sufficient to drive the phosphorylation of adenosine diphosphate (ADP) to ATP by complex V (Mitchell, 1961). The depiction of glycolysis and the TCA cycle are presented in Figure 1-2.

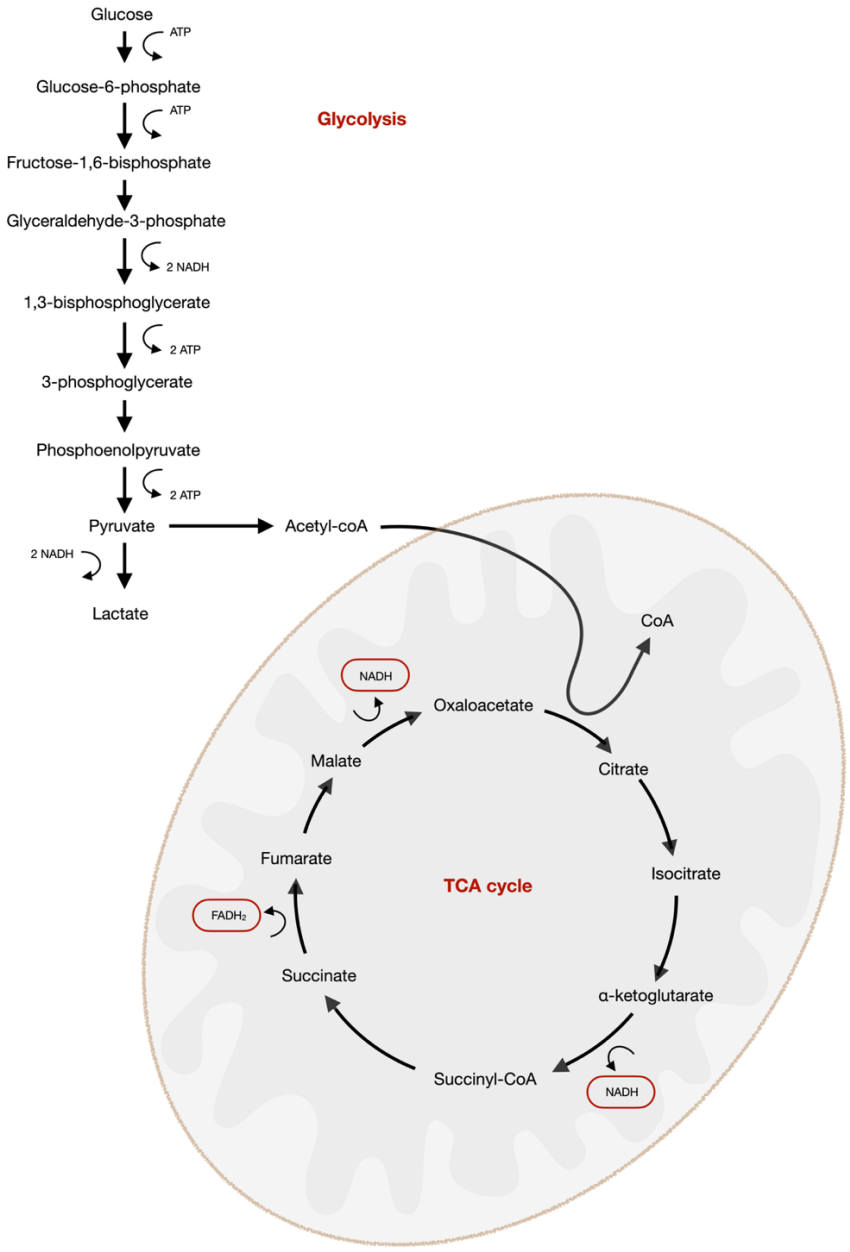

Figure 1-2. Glycolysis and the tricarboxylic acid cycle. A net gain of two ATP molecules and two molecules of pyruvate are generated from one molecule of glucose. The TCA cycle; a series of enzyme catalysed reactions occurring within the mitochondrial matrix. GTP and CO_2 are produced, as are the electron carriers NADH and $FADH_2$. NADH and $FADH_2$ donate electrons to Complexes I and II of the mitochondrial respiratory chain respectively.

1.1.2.1.1. Complex I

Complex I, also known as NADH-ubiquinone oxidoreductase, is a large, multi-subunit enzyme representing the first respiratory complex of the mitochondrial oxidative phosphorylation system. Mammalian complex I consists of a total of 45 subunits, 7 of which are encoded by mtDNA (ND1-ND6 and ND4L) (Carroll et al., 2006; Chomyn et al., 1986; Chomyn et al., 1985). The remaining 38 subunits are encoded by the nuclear genome and together all subunits comprise three distinct functional modules (Ragan & Hatefi, 1986). The hydrophilic peripheral arm which protrudes into the mitochondrial matrix constitutes the electron input module (N module) and an electron output module (Q module), while the hydrophobic membrane embedded arm (P module) facilitates proton translocation (Hunte et al., 2010; Wikström, 1984). Complex I catalyses the oxidation of NADH to NAD+ with the resultant two electrons being transferred to the flavin mononucleotide (FMN) group of the peripheral arm. This group then passes the electrons to ubiquinone in the inner mitochondrial membrane via a chain of iron-sulphur clusters (Hinchliffe & Sazanov, 2005). On accepting electrons, ubiquinone is reduced to ubiquinol, which transfers these electrons to complex III. Four protons are released into the mitochondrial intermembrane space which contributes to the creation of the proton gradient which drives ATP synthesis by ATP synthase at the end of the respiratory chain (Mitchell, 1961).

1.1.2.1.2. Complex II

Mitochondrial complex II, also known as succinate dehydrogenase or succinate-ubiquinone oxidoreductase, is composed of four subunits (SDHA-D) which are all encoded by the nuclear genome. The hydrophobic subunits C and D are embedded within the inner mitochondrial membrane, with the catalytic subunits, A and B projecting into the matrix. Complex II has dual functionality; it has a role in the TCA cycle in addition to its role in the electron transport chain. In the TCA cycle, subunit SDHA catalyses the oxidation of succinate to fumarate generating $FADH_2$. $FADH_2$ is oxidised to FAD+ releasing two electrons which are transferred to ubiquinone via Fe-S and haem prosthetic groups thus permitting the subsequent reduction of ubiquinone to ubiquinol. Ubiquinol is then released from SDH-C and subsequently transfers electrons to complex III (Hagerhall, 1997).

1.1.2.1.3. Complex III

Complex III, also known as ubiquinol: cytochrome c oxidoreductase, is composed of 11 subunits, one of which; *cyt b*, is encoded by the mitochondrial genome. Complex III catalyses electron transfer from ubiquinol to cytochrome *c*. This is coupled with the transfer of two protons across the inner mitochondrial membrane (Mitchell, 1976). Complex III possesses two quinone binding sites; one quinone oxidation site (Q_O or QP) and one quinone reduction site (Q_i or QN). When ubiquinol (QH_2) binds Q_O, one electron is transferred to the Rieske iron sulphur cluster, on to cytochrome *c1*, then to cytochrome *c*. The other electron takes a different route via cytochrome *b* and the haem groups to the Q_i site where it reduces ubiquinone (Q) to the unstable semi-ubiquinone Q-. A second molecule of QH_2 binds Q_O with the same electron bifurcation occurring again. An additional cytochrome *c* is reduced and simultaneously at Q_i, Q- receives a second electron and is further reduced to Q**.** This is known as the Q cycle and facilitates the transfer of electrons between respiratory chain complexes in addition to the translocation of two protons across the inner mitochondrial membrane for each molecule of QH_2 entering the cycle (Mitchell, 1975a, 1975b).

1.1.2.1.4. Complex IV

Complex IV, also known as cytochrome *c* oxidase (COX), is composed of 14 subunits and represents the final enzyme of the mitochondrial respiratory chain. Complex IV was initially considered to be composed of 13 subunits, however in 2012 the NDUFA4 subunit of complex I was reassigned to complex IV and placed at the location of dimerisation of the enzyme (Balsa et al., 2012; Zong et al., 2018). Initially resolved as a monomer (Fuller et al., 1979), it is currently suggested that dimerisation of complex IV is reversible with transition between the two forms occurring continuously (Ramzan et al., 2019).

Three of the 14 subunits of complex IV; COX I, II and III are encoded by the mtDNA and comprise the catalytic core of the complex (reviewed in Capaldi, 1990). The remaining 11 subunits are encoded by the nuclear DNA and are thought to be involved in enzyme assembly and regulation of enzyme activity (Galati et al., 2009; Li et al., 2006). The basic function of complex IV is the acceptance of electrons from cytochrome *c* in order to facilitate

the reduction of oxygen (O_2) into H_2O (Hatefi, 1985). Simultaneously, four protons are translocated across the inner mitochondrial membrane (Wikström, 1977). Complex IV contains four redox-active metal groups that facilitate this function. Electrons from cytochrome c are received by CuA within subunit COXII. They are transferred to the haem a3-CuB group of subunit COXI via haem a, also of COXI. Four electrons are transferred one at a time to an O_2 molecule bound at haem a3, with the formation of water and translocation of four protons (Faxén et al., 2005).

1.1.2.1.5. Complex V

Complex V, also known as F_OF_1 ATP synthase, is comprised of 16 subunits, two of which are encoded by the mitochondrial genome. Its main function is to synthesise ATP using the H+ electrochemical gradient set up by the transport of H+ ions across the IMM from the matrix to the intermembrane space by complexes I, III and IV. Complex V is comprised of two domains, the F_O domain, which is fixed within the membrane, and the F1 domain, which projects into the matrix (Yoshida et al., 2001). The F_O domain comprises eight hydrophobic c subunits, which form a c ring. The c ring allows protons to pass from the intermembrane space back into the matrix. The F_1 domain constitutes five subunits in total (α, β, γ, δ and ε), with 3α and 3β subunits making up the stationary ring, and the γ, δ and ε subunits forming the rotary stalk (Wittig et al., 2008). The flow of H+ ions through the F_O domain drives the rotation of the c ring around the central stalk. Protonation and deprotonation of glutamate residues within c ring subunits result in conformational changes which then drive the rotation of α and β subunits of the F_1 domain, allowing the formation of ATP from ADP and Pi (Noji et al., 1997).

1.1.2.1.6. Supercomplexes

Although traditionally depicted as discrete units adjacent to one another within the inner mitochondrial membrane, the respiratory chain complexes can reportedly assemble into multi-complex structural units known as supercomplexes (Schägger & Pfeiffer, 2000). Known as the ‘respirasome’, the association of complex I with complexes III and IV, is described as the predominant supercomplex formation (Gu et al., 2016). An increased stability of

individual complexes is reportedly enhanced by supercomplex formation (Acín-Pérez et al., 2004; Diaz et al., 2006; Schägger et al., 2004). Additional advantages include a reduced reactive oxygen species generation by complex I (Maranzana et al., 2013), and an augmented electron flux efficiency through the respiratory chain (Lapuente-Brun et al., 2013); both as a result of supercomplex formation.

1.1.2.2. Calcium homeostasis

Mitochondria play an important role in the buffering of intracellular calcium (Ca^{2+}). In doing so, they regulate metabolism, cell signalling and cell survival; functions of the cell which are sensitive to variations in cytosolic Ca^{2+}. With regards to metabolism, enzymes critical to the TCA cycle rely on Ca^{2+}mediated activation. The stimulatory effect of Ca^{2+} on the TCA cycle subsequently increases the rate of ATP production by OXPHOS via the increased availability of metabolic substrates (Jouaville et al., 1999; McCormack et al., 1990).

The OMM is permeable to small ions and uncharged molecules, and therefore presents little barrier to the passage of Ca^{2+}. The tightly regulated IMM possesses a dedicated, selective channel; the mitochondrial Ca^{2+} uniporter (MCU), which facilitates the transport of Ca^{2+} across the IMM (Kirichok et al., 2004). A massive influx of Ca^{2+} into the mitochondrial matrix is generally associated with cell death via necrosis or apoptosis, particularly when in conjunction with oxidative stress (reviewed in Duchen, 2000).

1.1.2.3. Apoptosis

Apoptosis, also known as programmed cell death, is a process by which cellular populations are maintained during the normal development and ageing of an organism. This homeostatic mechanism is characterised by a distinct set of morphological features including chromatin condensation, cell shrinkage and plasma membrane blebbing which precedes the death of the cell (reviewed in Saraste & Pulkki, 2000). There are two apoptotic signalling pathways that are well conserved between different animal species and represent the predominant routes by which cell death is programmed. One responds to extrinsic stress-mediated signals, and the apoptotic machinery is activated following ligand binding to cell surface

receptors. The other is initiated in response to intrinsic signals and is orchestrated by the mitochondrion (reviewed in Elmore, 2007).

Mitochondria act in response to death signals such as DNA damage, oncogene activation or withdrawal of growth factors which ultimately leads to apoptosis. Upon receipt of these signals, pro-apoptotic effector members of the Bcl-2 family (for example Bax and Bak) promote mitochondrial outer membrane permeability (MOMP) which allows the release of cytochrome *c*. While Bax and Bak promote apoptosis, other members of the Bcl-2 family, for example Bcl-2 itself and Bcl-xL, are anti-apoptotic regulators (Kharbanda et al., 1997; Yang et al., 1997). In conjunction with support from the Bcl-2 subgroup; the BH3-only pro-apoptotic proteins (Zha et al., 1996), the balance between pro- and anti-apoptotic regulators determines the fate of the cell.

As cytochrome *c* is released from the mitochondria into the cytoplasm, it binds and activates the apoptotic protease activating factor-1 (Apaf-1) which in an ATP-dependant manner forms the apoptosome. The apoptosome facilitates the cleavage of procaspase-9 forming the active caspase-9. Caspase-9 then activates further caspase proteases, namely 3, 6, and 7, mediating the death of the cell via the breakdown of its constituents (Li et al., 1997).

1.1.2.4. Iron sulphur cluster biogenesis

Iron-sulphur clusters (Fe-S) and haem are cofactors which are synthesised within the mitochondrial matrix. They function within numerous processes of the cell such as electron transport, the TCA cycle and DNA and RNA metabolism (reviewed in Rouault, 2019). The transport of iron into the mitochondrial matrix is facilitated by mitoferrins 1 and 2 (Mrfn1 and Mrfn2) in mammalian cells (Paradkar et al., 2009). In the matrix, the Fe-S synthesis machinery consists of a scaffold protein known as ISCU and sulphur generating cysteine desulphurase (NFS1) in addition to its functionally required partner; ISD11 (Pandey et al., 2012; Shi et al., 2010; Shi et al., 2009). ISD11 has been shown to stabilise NFS1 and also interact with the acyl carrier protein (ACP) (Van Vranken et al., 2016). Together these components form the core Fe-S cluster synthesis complex. Following initial cluster assembly on ISCU, the transfer of sulphur from NFS1 to ISCU is promoted by frataxin (FXN) completing cluster synthesis (Bridwell-Rabb et al., 2014; Fox et al., 2019). The delivery of newly

synthesised Fe-S clusters to recipient proteins is achieved via chaperone mediated transfer. In mammalian cells HSPA9 and HSC20 coordinate the direct transfer of Fe-S clusters to respiratory chain complexes (Maio et al., 2017; Uhrigshardt et al., 2010). In complexes I to III, the ability of Fe-S clusters to accept and donate electrons renders them fundamental to the transport of electrons in oxidative phosphorylation. Nuclear DNA polymerases also contain Fe-S clusters which assist in the stabilisation and formation of active enzymatic complexes (Netz et al., 2011), and their involvement in the maintenance of genome stability has also been described (Stehling et al., 2012). Fe-S clusters also function as regulators of cellular iron concentrations; yeast that are deficient in enzymes that release sulphur from cysteine for Fe-S formation demonstrate accumulation of iron within the mitochondrial matrix (Li et al., 1999).

1.1.2.5. ROS production

Mitochondria and the electron transport chain specifically, have long been regarded as major producers of cellular reactive oxygen species (Jensen, 1966). The demonstration that isolated mitochondria generate peroxide (H_2O_2) (Loschen et al., 1971) was closely followed by the identification of the superoxide radical (O_2-), as the precursor of H_2O_2, catalysed by the mitochondria-specific superoxide dismutase (MnSOD) (Loschen et al., 1974; Weisiger & Fridovich, 1973). Reactive oxygen species are primarily produced by complexes I (Hinkle et al., 1967) and III of the electron transport chain (Cadenas et al., 1977; Turrens et al., 1985). At complex I, a high NADH/NAD+ ratio can lead to a fully reduced FMN site and subsequent reduction of oxygen generating O_2-. Additionally, an abundant electron supply leading to a reduced coenzyme Q /ubiquinone pool can lead to reverse electron transport (RET) back through complex I when coupled with a high protonmotive force (reviewed in Murphy, 2009). At complex III, superoxide generation has been shown to originate from the Q_O site as inhibition of the Q_i site with antimycin promotes O_2- production (Cadenas et al., 1977; Turrens et al., 1985). An increase in membrane potential can enhance ROS production at complex III (Rottenberg et al., 2009), while the location of the site of origin; the Q_O site, has important implications for the effects of complex III generated ROS. In contrast to the matrix protruding FMN site of complex I, the Q_O site of complex III is parallel to the inner mitochondrial membrane and as such, ROS can be released into the intermembrane space in

addition to the matrix (Muller et al., 2004; St-Pierre et al., 2002). While ROS have been generally considered as harmful by virtue of the damage they can exert upon cellular components such as DNA and proteins, they are also involved in the regulation of cellular signalling pathways such as the response to hypoxia (Chandel et al., 1998), NF-κB, and TNFα-mediated cell death (Kamata et al., 2005). The close proximity to the cytoplasm of complex III generated intermembrane space resident ROS may therefore deem these species of particular importance in signal transduction pathways (Bell et al., 2007).

1.2. Mitochondrial biogenesis

The biogenesis of mitochondria requires the convergence of multiple events. Nuclear and mtDNA encoded mitochondrial proteins must be synthesised, mitochondrial proteins must be imported, cofactors such as haem and Fe-S clusters must be formed, and the mitochondrial genome replicated. The PGC-1 family of coactivators are major players in mitochondrial biogenesis, with peroxisome proliferator activated receptor γ coactivator 1 α (PGC-1α) being key. PGC-1α activates nuclear respiratory factors 1 and 2 (NRF1 and NRF2); transcription factors which are responsible for the activation of mitochondrial gene promoters (Scarpulla, 2008; Virbasius et al., 1993a; Virbasius et al., 1993b).

Following external stimuli such as increased exercise, a decrease in temperature or decreased nutrient availability, mitochondrial mass increases to meet new metabolic demands. Such stimuli increase intracellular Ca^{2+}levels and thus activate kinases such as calcium/calmodulin-dependent protein kinase (CaMK) or protein kinase C (PKC). Subsequent activation of p38 mitogen-activated protein kinase (p38 MAPK) by CaMK increases PGC-1α expression and mitochondrial biogenesis as a result (Wright et al., 2007).

1.3. Mitochondrial dynamics

1.3.1. Mitochondrial fusion

Mitochondria do not always exist as single entities; the double membranes of adjoining mitochondria can fuse together, creating a syncytium of interlinked organelles. The size,

shape and subcellular locations of mitochondrial networks is maintained by balancing mitochondrial fusion with the opposing state of fission and has a marked effect on the viability of the organelles and cellular processes in which they participate. The dynamin related protein family (DRP) members mitofusin 1 and 2 (MFN1 and MFN2) facilitate outer mitochondrial membrane fusion, with mutations in the gene encoding the latter causing Charcot-Marie-Tooth neuropathy type 2A, a progressive axonal condition characterised by distal muscle weakness, atrophy and sensory loss (Zuchner et al., 2004). Similarly, mutation of the gene encoding OPA1; the dynamin related GTPase responsible for inner mitochondrial membrane fusion, causes autosomal dominant optic atrophy (ADOA); the most common inherited optic neuropathy (Alexander et al., 2000). The process of fusion is initiated by the interaction between two outer membrane anchored MFN1 molecules on adjacent organelles. Earlier studies have proposed that contacts between MFN1 molecules are established via the HR2 domains of each protein (Koshiba et al., 2004), however more recent works have described the association of GTPase domains as the fusion-promoting interaction (Cao et al., 2017; Qi et al., 2016). Regardless of the specific MFN1 region involved in mitochondrial tethering, it is generally understood that the subsequent stages in fusion are facilitated by MFN conformational change, GTPase hydrolysis and outer membrane fusion (Ishihara et al., 2004; Legros et al., 2002). Following outer membrane fusion, OPA1 and MFN1 mediate fusion of the inner membrane (Cipolat et al., 2004), however for this to occur, OPA1 must be appropriately processed. The enzyme is proteolytically cleaved in order to generate short OPA1 fragments (S-OPA1), primarily catalysed by the ATP-dependent zinc metalloprotease; YME1L1 (Griparic et al., 2007). Although the specific mechanism by which OPA1 mediates fusion has not been fully elucidated, it has been proposed that S-OPA1 enhances the interaction of long, unprocessed OPA1 with the inner mitochondrial membrane lipid cardiolipin. In contrast to this heterotypic interaction, the homotypic interaction of OPA1 reportedly supports cristae structure (Ban et al., 2017). Similarly, while the second mitofusin MFN2 is required for fusion, its precise mechanistic action is unclear and the protein has also been shown to play a supportive role with regards mitochondrial-endoplasmic reticulum contact (de Brito & Scorrano, 2008).

1.3.2. Mitochondrial fission

Mitochondrial fission describes the division of single mitochondria into two distinct organelles and like fusion, is required to maintain mitochondrial function. Fission also allows damaged mitochondria to be isolated and removed via autophagy (Twig et al., 2008). The major orchestrator of mitochondrial fission is an evolutionarily conserved dynamin related GTPase known as DRP1 which was first described in yeast and *Caenorhabditis elegans* (Bleazard et al., 1999; Labrousse et al., 1999). DRP1 is a soluble cytosolic protein which requires post-translational modification to allow its translocation to the outer mitochondrial membrane (Chang & Blackstone, 2007; Cribbs & Strack, 2007). DRP1 recruitment to the outer membrane also relies on colocalisation with the outer membrane bound proteins; mitochondrial fission factor (Mff) (Gandre-Babbe & van der Bliek, 2008) and mitochondrial dynamic proteins 49 and 51 (MiD49 and MiD51) (Losón et al., 2013; Palmer et al., 2011). The subsequent binding of GTP to DRP1 promotes linear polymerisation of DRP1 supported by MiD49 and MiD51. GTP hydrolysis facilitates the dissociation of MiD49 and MiD51 while DRP1 polymers shorten into closed, constrictive rings (Kalia et al., 2018). These events commonly occur at sites of mitochondrial contact with the endoplasmic reticulum (ER). The ER is described as an important participant in the process of mitochondrial fission by marking the site of division and providing an initial mechanical force (Friedman et al., 2011). It has recently been demonstrated that that DRP1 also provides the final constrictive force required for the separation of mitochondria (Fonseca et al., 2019; Kamerkar et al., 2018).

The importance of mitochondrial fission with regard to the distribution and integrity of mtDNA has been demonstrated via the knockdown of key mediators. In comparison to control cardiomyocytes in which small nucleoids were dispersed throughout the mitochondrial network, the examination of fluorescent micrographs of cardiomyocytes from muscle-specific *DRP1*-KO mice revealed an enlargement and aggregation of mtDNA nucleoids. Also demonstrated was a respiratory defect and a mosaic pattern of COX1 fluorescent labelling, with larger nucleoids displaying an increased intensity in comparison to those that were smaller (Ishihara et al., 2015).

Appropriate mitochondrial dynamics are additionally required to facilitate apoptosis (Frank et al., 2001; Scorrano et al., 2002), mitosis (Taguchi et al., 2007) and with reference to the

intestinal tract; the maintenance of stemness (Katajisto et al., 2015). Accordingly, mitochondrial dynamics are critical to the life and death of the cell.

1.4. The mitochondrial genome

Unlike other organelles, mitochondria contain their own genome; mtDNA. This circular, self-replicating, double stranded mtDNA was fully sequenced in 1981 and comprises 16,569 base pairs in humans (Anderson et al., 1981). The circular genome consists of the heavy (H) G rich strand and the light (L) C rich strand. Together they encode 37 genes of which 22 are transfer RNAs, 2 are ribosomal RNAs (12S and 16S ribosomal subunits) and the remaining 13 encode polypeptides involved in oxidative phosphorylation. The mitochondrial genome is very compact, and unlike that of the nucleus, does not contain any introns. There is only one major non-coding region, known as the D-loop. It contains O_H; the origin of heavy strand replication and also HSP, the heavy strand transcription promoter.

Small numbers of non-coding bases separate coding sequences, and in some instances, there is an overlap of protein encoding regions (Anderson et al., 1981; Fearnley & Walker, 1986). Furthermore, complete termination codons are not associated with all genes. Instead, endonucleocytic cleavage and polyadenylation at sites typically before and after tRNA sequences processes polycistronic RNA molecules prior to their maturation (Ojala et al., 1981).

In contrast to the nuclear genome which is packaged into nucleosomal structural units by association with histones, mtDNA lacks histone support and is instead organised into discrete units known as nucleoids which the earliest reports describe as containing one or two mtDNA molecules (Satoh & Kuroiwa, 1991). Nucleoid organisation ensures the appropriate distribution of mtDNA throughout the mitochondrial network and core components have been proposed to comprise factors which are involved in mitochondrial replication and transcription. Further to its role as the mtDNA transcription factor, mitochondrial transcription factor A (TFAM) provides a key packaging function central to the nucleoid structure (Kaufman et al., 2007). Additional core components include the dedicated mitochondrial DNA polymerase gamma (Polγ), mitochondrial RNA polymerase (POLRMT), mitochondrial single-strand binding protein (mtSSB) and the mitochondrial helicase TWINKLE

to varying degrees depending on functional demand (Rajala et al., 2014). Peripherally, proteins such as ATPase AAA domain-containing protein 3 (ATAD3) and the prohibitins 1 and 2 (PHB1 and PHB2) facilitate inner mitochondrial membrane tethering while also mediating ribosomal contact and thus supporting protein synthesis (He et al., 2012). This central DNA and protein core surrounded by peripheral proteins forms the multi-layered model of mitochondrial nucleoid organisation (Bogenhagen et al., 2008; Wang & Bogenhagen, 2006) however more recently, alternative models have been proposed. Using electron microscopy, cryo-ET microscopy and super-resolution microscopy it was demonstrated that the mitochondrial nucleoid consists of a single mtDNA molecule compacted by cross-strand binding of approximately 1000 molecules of TFAM per mtDNA molecule in the absence of additional proteins (Kukat et al., 2015; Kukat et al., 2011). Furthermore, the abundance of TFAM and thus the level of DNA compaction has been shown to impact the proportion of mtDNA molecules available for transcription or replication (Farge et al., 2014). Nucleoid organisation therefore supports mitochondrial form and function. A schematic of the mitochondrial genome is depicted in Figure 1-3.

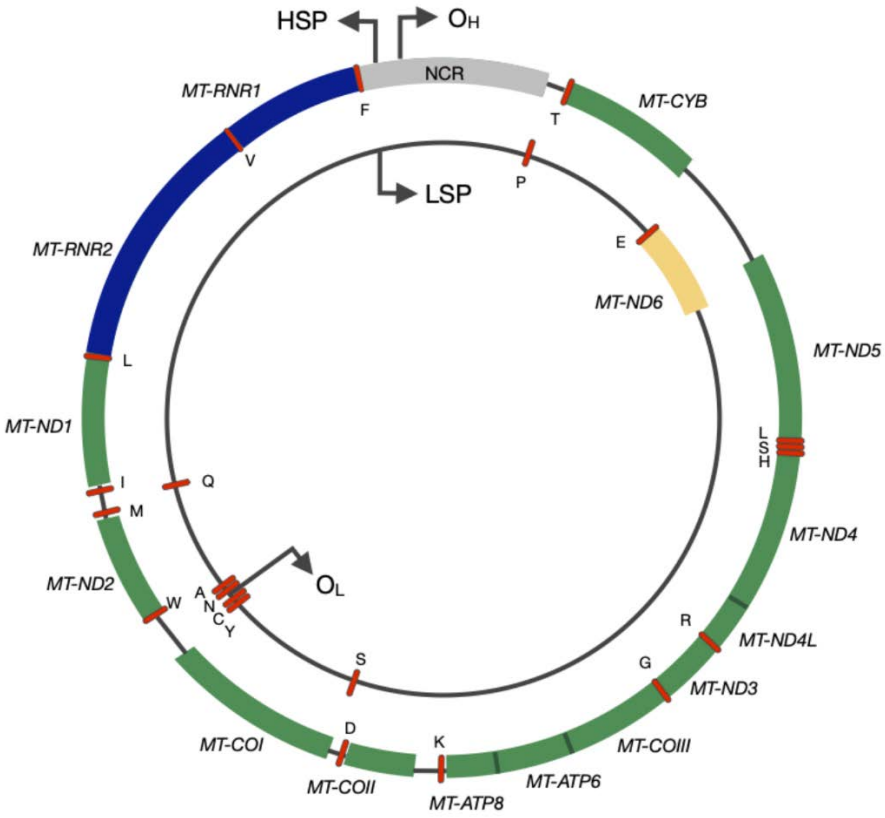

Figure 1-3. The human mitochondrial genome. The outer circle depicts the heavy strand with the inner circle representing the light strand. Genes encoding proteins of the mitochondrial respiratory chain are shown as coloured blocks labelled accordingly (MT-ND1–6, MT-COI–III, MT-ATP6 and 8 and MT-CYB). The blue blocks denote the two ribosomal RNAs and red dashes represent each of the 22 tRNAs.

1.4.1. Mitochondrial DNA replication

In addition to containing their own DNA, mitochondria also have their own machinery for its replication. The mitochondrial replisome consists of several key proteins. The mitochondrial DNA polymerase gamma, Polγ, is encoded by the nuclear genome. The RNA dependant DNA polymerase activity of Polγ was first described in 1970 (Baltimore, 1970; Temin & Mizutani, 1970) , however it wasn't until 1975 that Polγ was named as such (Weissbach et al., 1975) and in 1977 it was found to be localised to the mitochondria (Bolden et al., 1977). Human Polγ was first characterised as two distinct polypeptides of 140 kDa and 54 kDa in size (Gray & Wong, 1992). The larger 140 kDa subunit, PolγA, is now known to represent the catalytic domain of the enzyme with 3'-5' exonuclease proofreading activity (Longley et al., 1998). The smaller accessory subunit, PolγB, has been characterised as a 55 kDa polypeptide and constitutes the processivity component of the complex. Both subunits bind double stranded DNA with moderate strength, however when in their functional configuration as a $Pol\gamma AB_2$ heterotrimer (Yakubovskaya et al., 2006), PolγB substantially enhances the affinity of Polγ for DNA, preventing dissociation and thus increasing the catalytic capacity and processivity of the polymerase (Lim et al., 1999).

Also encoded by the nuclear genome and fundamental to the mitochondrial replisome is the mitochondrial helicase, TWINKLE. As Polγ is unable to utilise double stranded DNA as a template, the ATP dependant helicase TWINKLE unwinds the double stranded DNA in a 5'-3' direction to form single strands of DNA prior to polymerase replication (Korhonen et al., 2004). The mitochondrial single-stranded binding protein (mtSSB) stabilises the single stranded DNA generated by TWINKLE, and also has a stimulatory effect on the helicase (Korhonen et al., 2003). The mitochondrial replisome also contains a DNA dependant mitochondrial RNA polymerase (POLRMT), which is responsible for the synthesis of RNA primers required for DNA replication (Kühl et al., 2016) with the removal of these primers by encoding ribonuclease H1 (RNase H1) (Holmes et al., 2015). It is unclear exactly how mtDNA replicates, and as such there are two main schools of thought in which both asynchronous and synchronous replication mechanisms have been described. Furthermore, the mechanism of replication has recently been described as tissue specific and associated with the OXPHOS activity level of the tissue in question (Herbers et al., 2019).

1.4.1.1. Asynchronous mtDNA replication

The strand displacement model of mitochondrial DNA replication, also known as asynchronous or asymmetric strand displacement, was first described in 1972 (Robberson et al., 1972). Replication begins at the heavy strand origin of replication (O_H) with TWINKLE unwinding the double stranded DNA and mtSSB binding to the parental H strand as it is exposed (Miralles Fuste et al., 2014). POLRMT synthesises an RNA primer to enable Polγ to proceed and the new H strand is produced independently until the replisome reaches the second origin of replication on the light strand (O_L). The exposure of single stranded DNA at O_L causes the exposed parental H strand to fold into a stem-loop conformation (Martens & Clayton, 1979) which prevents mtSSB from binding but does allow POLMRT to initiate synthesis of RNA (Fuste et al., 2010). The short RNA primer provides a template from which Polγ can begin light strand synthesis. Each strand is now synthesised simultaneously until completion and ligated into a closed circular form (Berk & Clayton, 1974).

The RNA incorporation throughout the lagging strand (RITOLS) model is similar to the strand displacement model in that replication begins at or very close to O_H and proceeds until O_L is exposed, allowing replication of the light strand. In the strand displacement model, the displaced parental strand is stabilised by the mtSSB, however in the RITOLS model, RNA intermediates bind the parental strand and are later replaced by DNA via maturation (Yasukawa et al., 2006).

1.4.1.2. Synchronous mtDNA replication

Detection of replication intermediates also led to the proposition of a third mechanism of mtDNA replication; the coupled leading - lagging strand model, also known as the synchronous model (Holt et al., 2000).The use of two-dimensional agarose gel electrophoresis identified partially single-stranded replication intermediates in cultured cells in which maintenance synthesis of the mitochondrial genome was occurring in growing cells. This was in contrast to the double stranded intermediates observed in cells in which proliferative replication was taking place. The presence of double stranded intermediates is suggestive of a bidirectional, coupled replication, with leading and lagging strand replication

occurring simultaneously. This is hypothesised to be the preferred mode of replication in cells undergoing rapid proliferation as opposed to those that are maintaining the mitochondrial genome (Holt et al., 2000).

Following replication, the parent and newly synthesised mtDNA molecules remain connected to one another and must be separated. The presence of structures known as catenanes, describing the linked branches of reportedly newly replicated molecules of mtDNA, was documented in 1967 following electron microscopic investigation of human mitochondria (Hudson & Vinograd, 1967). Until recently, the enzymatic mediators of the separation of mitochondrial catenanes had remained elusive, however recent work has identified the mitochondrial isoform of Top3α; a type IA topoisomerase as indispensable for the separation of newly replicated mtDNA molecules (Nicholls et al., 2018).

1.4.2. Mitochondrial DNA transcription

Transcription of mtDNA is carried out by a group of dedicated proteins. They are all encoded by the nuclear genome, and the group comprises mtRNA polymerase (POLRMT), mitochondrial transcription factor A (TFAM) and the mitochondrial transcription factor B2; mtTFB2 (Falkenberg et al., 2002). Within the D-loop; the major non-coding region of the mitochondrial genome, transcription can initiate from one heavy strand promoter, HSP and one light strand promoter region, LSP.

As a result of experiments in which nascent RNA transcripts were labelled and mapped to the mitochondrial genome, it was initially believed that transcription of the genes encoding both rRNA genes and two tRNA genes ($tRNA^{Phe}$ and $tRNA^{Val}$), and transcription of the majority of the genes remaining on the H strand initiated from two different promoters: HSP1 and HSP2 respectively (Cantatore & Attardi, 1980; Chang & Clayton, 1984; Montoya et al., 1982; Montoya et al., 1983). However, it was subsequently demonstrated that HSP2 is not recognised by POLRMT and cannot be transcribed *in vitro* using purified components of the transcription system (Litonin et al., 2010). Accordingly, it is currently understood that heavy strand transcription initiates from only one promoter.

Formation of the transcription initiation complex begins with the TFAM mediated introduction of a sharp U-bend in the promoter DNA This structural conformation facilitates the recruitment of POLRMT and is required for transcription initiation (Ngo et al., 2011). The subsequent binding of mtTFB2 induces promoter melting and a conformational change in POLRMT; both of which facilitate promoter opening and transcription initiation (Hillen et al., 2017; Posse & Gustafsson, 2017). The interaction of the mitochondrial transcription elongation factor (TEFM) with the catalytic region of POLRMT and the release of mtTFB2 allows transcription to enter the elongation phase (Minczuk et al., 2011). TEFM forms a 'sliding clamp' downstream of POLMRT and thus ensures high processivity (Hillen et al., 2017).

Despite the discovery of mitochondrial termination factor 1 (mTERF1) (Kruse et al., 1989) and its demonstration as an efficient transcription termination factor *in vitro* (Asin-Cayuela et al., 2005), the exact mechanism of the process *in vivo* remains somewhat unclear. Initially reported as the mediator of termination of HSP-driven transcription via an unwinding and base flipping mechanism at the $tRNA^{Leu}$ (UUR) termination site (Martin et al., 2005a; Shang & Clayton, 1994; Yakubovskaya et al., 2010) the protein has since been shown to be dispensable for transcription from HSP promoter regions and is suggested only to be required for light strand transcription termination (Terzioglu et al., 2013). Accordingly, further investigation may be required to elucidate additional factors that may be involved in mitochondrial transcription termination.

1.4.3. Post-transcriptional mtRNA processing and modification

In order to generate each of the proteins encoded by the mitochondrial genome, the maturation of nascent precursor polycistronic transcripts is required prior to translation. This involves endonucleocytic processing followed by various post-transcriptional modifications which vary depending on the nature of the transcript. Primary processing events take place in structures known as RNA granules which are typically located in close proximity to mtDNA nucleoids (Antonicka et al., 2013; Iborra et al., 2004; Jourdain et al., 2013). As described by Ojala and colleagues in 1981, the endonucleocytic cleavage of the precursor mRNA occurs at sites before and after tRNA coding regions releasing the mt-mRNA and mt-rRNA transcripts situated between them (Ojala et al., 1981). The enzymatic machinery responsible for this

cleavage comprises RNaseP facilitating 5' mt-tRNA processing, with processing at the 3' end of mt-tRNAs carried out by RNaseZ (Brzezniak et al., 2011; Holzmann et al., 2008). In the instance of mt-mRNAs which are not delimited by mt-tRNAs, members of the Fas-activated serine/threonine kinase (FASTK) family of proteins have been implicated in their processing and thus mitochondrial gene expression (Jourdain et al., 2015).

Following mt-tRNA release, mt-tRNA maturation involves the addition of a 3' CCA trinucleotide by tRNA nucleotidyltransferase TRNT1 (Nagaike et al., 2001). In certain species of mt-tRNA, the removal of aberrant poly(A) tails by the exoribonuclease PDE12 is also required, the ablation of the *PDE12* gene leading to perturbed mt-tRNA aminoacylation, reduced OXPHOS subunit expression and impaired respiration in human embryonic kidney cell lines as a result (Pearce et al., 2017). Given the limited number of mitochondrial tRNAs in comparison to that of the nucleus, the required gene expression relies on a vast array of post-transcriptional RNA processing events which regarding those of mitochondrial tRNAs, are particularly complex. Modifications at position 34 of the anticodon loop of mt-tRNAs and position 37 immediately adjacent are especially common and facilitate the recognition of multiple codons by single mt-tRNAs (reviewed in Rebelo-Guiomar et al., 2019).
The maturation of mitochondrial mRNA transcripts firstly involves the 3' polyadenylation of all species with the exception of the MT-ND6 mRNA, carried out by the polyadenylic acid RNA polymerase (mtPAP) (Tomecki et al., 2004). In seven of the thirteen mRNA transcripts this adds a stop codon to the reading frame. Polyadenylation is also required to stabilise specific mRNAs such as CO1 and CO2, however in the case of ND1 and ND2 transcripts, the opposite is observed as deadenylation increases the steady state levels of these species (Nagaike et al., 2005; Rorbach et al., 2011).

A total of ten post-transcriptional modification sites have been described with regard to mitochondrial rRNAs, which in contrast to those of bacterial and eukaryotic cytoplasmic ribosomes at over 30 and 200 respectively, is comparatively low. At each of these ten sites, the chemical modification is either methylation, 2'-O-ribose methylation or pseudouridylation with the final two enzymes responsible for these modifications; N4-methylcytidine (m^{4C}) methyltransferase (METTL15) and tRNA (uracil(54)-C(5))-methyltransferase homologue (TRMT2B) having recently been identified (Powell & Minczuk, 2020; Van Haute et al., 2019). Owing to their key roles in the regulation of mitochondrial

gene expression, mutations causing defects in the enzymes responsible for the post-transcriptional modification of mitochondrial RNA manifest as a wide variety of clinical conditions (Bohnsack & Sloan, 2018). Accordingly, this represents an important area of mitochondrial biology, the understanding of which may assist in the development of therapeutic interventions to alleviate such pathologies.

1.4.4. Mitochondrial DNA translation

The mitochondrial translation machinery, also known as the mitoribosome, consists of a small 28S subunit and a large 39S subunit and is responsible for the synthesis of each of the mitochondrially encoded subunits of the electron transport chain. In addition to 82 nuclear genome encoded proteins, the 12S rRNA located in the small 28S subunit and the 16S rRNA located in the large 39S subunit form the mature mitoribosome (Greber et al., 2015). Mitochondrial ribosomes have a much lower rRNA content when compared to their cytosolic counterparts (Pietromonaco et al., 1991) however they contain their own tRNAs; a set of 22 which translate all codons of the polycistronic molecules produced at transcription.

Mitochondrial translation utilises either AUG or AUA start codons and follows an initiation, elongation and termination sequence. Initiation begins with mitochondrial initiation factor 3 (IF3MT) mediated dissociation of the two subunits of the mitoribosome. IF3MT is also thought to aid mRNA binding to the small subunit of the ribosome and positioning of the start codon at the P site of the mitoribosome (Bhargava & Spremulli, 2005; Haque & Spremulli, 2008). At the P site, fMet-tRNA binds the start codon, assisted by mitochondrial initiation factor 2 (IF2MT) (Liao & Spremulli, 1990; Ma & Spremulli, 1996). Elongation proceeds when the large subunit of the mitoribosome re-joins the complex and initiation factors are subsequently released**.** The first step of elongation involves the formation of a complex comprising a GTP bound mitochondrial elongation factor Tu (mtEFTu) and an aminoacyl tRNA (aa-tRNA). This complex carries the tRNA to the A site of the mitoribosome where codon: anticodon recognition causes GTP to be hydrolysed and mtEFTu is released and its GTP restored by mitochondrial elongation factor Ts (mtEFTs) (Cai et al., 2000). The aminoacyl tRNA moves to the peptidyl transferase centre of the large subunit where the peptide bond formation takes place. Mitochondrial elongation factor mtEFG1-GTP catalyses the movement of tRNAs in the A and P sites to the P and exit sites of the ribosome. The exit

of the tRNA allows another elongation cycle to occur at the next codon of the mRNA. Termination of translation occurs when the presence of a stop codon (UAA or UAG in humans) at the A site is recognised by mitochondrial release factor 1a (mtRF1a) which possesses a peptidyl-tRNA hydrolase activity owing to a GGQ motif (Frolova et al., 1999). Upon stop codon recognition, the movement of the GGQ domain of mtRF1a into the peptidyl transferase centre causes hydrolysis of the bond between the P site tRNA and the completed polypeptide facilitating its subsequent release (Soleimanpour-Lichaei et al., 2007). In the case of MT-CO1 and MT-ND6 mRNAs which lack the putative UAA or UAG stop codons, a mitoribosome frameshift is believed to facilitate mtRF1a recognition and thus termination (Temperley et al., 2010). Following the release of the polypeptide, dissociation of the ribosomal subunits, mRNAs and deacetylated tRNAs is promoted by the ribosomal recycling factors, mtRRF1 and mtEFG2 (Rorbach et al., 2008; Tsuboi et al., 2009). After their own ensuing release, the transcription cycle may subsequently resume.

1.4.5. Mitochondrial DNA mutagenesis and repair

The mutational rate of mtDNA is reportedly much higher than that of the nucleus with this historically being attributed to an absence of protective histones, an incompetent DNA repair system and the proximity of the mitochondrial genome to the reactive oxygen species generated by the electron transport chain. While the mutagenic potential of ROS has been well studied; the generation of the hydroxyl radical (•OH) following the reaction of H_2O_2 with ferric iron being particularly damaging to DNA (Henle et al., 1996), the nucleoid packaging of mtDNA has been reported to offer protection against mutagenic agents (Guliaeva et al., 2006). Furthermore, the presence of the majority of DNA repair pathways have been described within mitochondria with the most prevalent oxidative DNA base lesion, 8-oxodG being repaired via base excision repair (BER) with greater efficiency in mitochondria in comparison to the nucleus (Thorslund et al., 2002). Although the repair of double strand breaks via homologous recombination (HR) or non-homologous end joining (NHEJ) has been described in the mitochondria of plants (Manchekar et al., 2006), yeast (Foury & Lahaye, 1987) and *Drosophila melanogaster* (Morel et al., 2008), recombination events following induced double strand breaks in mammalian mitochondria are at a reportedly low frequency and also promote the formation of mtDNA deletions (D'Aurelio et al., 2004; Srivastava & Moraes, 2005). Single strand break repair (SSBR) (Sykora et al., 2011),

mismatch repair (MMR) (Mason et al., 2003), and direct reversal repair of alkylated purines (Myers et al., 1988) have all been localised to mitochondria with the main notable exception being nucleotide excision repair (NER). In the event of irreparable mtDNA damage, genome degradation by components of the mtDNA replication machinery (Nissanka et al., 2018; Peeva et al., 2018) facilitates mtDNA turnover, homeostasis and thus evasion of the accumulation of damaged mtDNA molecules (Gross & Rabinowitz, 1969).

Despite such competent mtDNA repair mechanisms in place, the mtDNA mutation rate remains much higher in comparison to that of the nucleus (Wallace, 1989). Accumulating evidence suggests that contrary to earlier considerations, ROS may not be the primary source of mtDNA mutagenesis. Although ROS induced 8-oxodG formation can lead to mitochondrial DNA polymerase (Polγ) mediated misincorporation of an A base in place of C and subsequent incorporation of T in place of 8-oxodG, the resultant G:C to T:A transversion is superseded by the G:C to A:T transition in terms of frequency of reporting (Greaves et al., 2014; Kennedy et al., 2013). Furthermore, in mice with deficient mitochondrial base-excision repair and increased exposure to ROS and oxidative damage via superoxide dismutase 2 (*Sod2*) knockout, no mtDNA mutational load changes were observed (Kauppila et al., 2018). As transition mutations are associated with errors in Polγ mediated replication, base misincorporation and miscopying events are considered a major contributor to a significant number of mutations of human mitochondrial DNA (Zheng et al., 2006).

In terms of inherited pathological mtDNA mutations, the first were reported in 1988 (Holt et al., 1988; Wallace et al., 1988) and since then a great many more have been elucidated. The Mitomap.org database lists all mutations and polymorphisms of mtDNA currently known. The most common types of mutations are point mutations with a pathogenic population prevalence being estimated at 1 in 200 (Chinnery et al., 2012; Elliott et al., 2008). Point mutations; the transition of a single nucleotide to another, can occur in any of the mitochondrial tRNA, rRNA and protein encoding genes and are often maternally inherited. The most common mtDNA disease causing point mutation of the mitochondrial genome is a single nucleotide transition from A to G at position 3243 (m.3243A>G) within the $tRNA^{Leu\ (UUR)}$ (*MT-TL1*) gene. Mutations in tRNA encoding genes such as *MT-TL1* are thought to hinder overall mitochondrial protein synthesis (Mariotti et al., 1994). Clinically, this mutation frequently gives rise to maternally inherited diabetes and deafness (MIDD) (van den

Ouweland et al., 1992), and is also associated with mitochondrial encephalomyopathy, lactic acidosis and stroke-like episodes (MELAS) (Goto et al., 1990). The m.8344A>G substitution in the *MT-TK* gene encoding $tRNA^{Lys}$ also causes a debilitating neurological disorder; myoclonic epilepsy with ragged-red fibres (MERRF) (Wallace et al., 1988).

In contrast to mtDNA point mutations, single large-scale mtDNA deletions are not typically inherited; they are acquired sporadically within the developing embryo (Chinnery et al., 2004; Holt et al., 1988). Three major clinical phenotypes are associated with single, large-scale mtDNA deletions. Chronic progressive external ophthalmoplegia (CPEO) is the most common but least severe of the three. Kearns-Sayre syndrome (KSS) is a disorder characterised by ptosis and retinopathy presenting before the age of 20. Multiple systems may be affected in cases of KSS with pathologies such as hearing loss, ataxia, cardiomyopathy and cardiac conduction defects being observed (Mancuso et al., 2015). The most severe and least common syndrome associated with single, large-scale mtDNA deletions is Pearson syndrome. Pearson syndrome is a fatal disorder presenting in infancy with sideroblastic anaemia and pancreatic insufficiency/failure (Rotig et al., 1990). The formation of mtDNA deletions was initially proposed to be due to a slipped replication error in which strand displacement allows the mis-annealing of a repeat region on the heavy strand with a complementary sequence on the light strand. The single stranded loop which forms is degraded and both a wild type and deleted mtDNA molecule are generated upon the completion of replication (Shoffner et al., 1989). This mechanism results in the flanking of the deleted region by repeat sequences which thus does not account for deleted regions flanked by partial or no repeat regions at all. As such a similar model has recently been proposed in which the chance dissociation of the replication machinery during the replication of a repeat region of the parental heavy strand may permit incorrect reassociation with a downstream repeat sequence. This results in the loss of the sequence between the repeats as replication is completed. While this 'copy-choice recombination' mechanism is promoted by repeat sequences it can also account for deletion formation in the absence of repeat sequences (Persson et al., 2019). As previously mentioned, double strand breaks within mtDNA can promote deletion formation (Srivastava & Moraes, 2005). When this occurs, the partial degradation of the linear DNA by the replication machinery with subsequent recombination of free ends describes the final known mechanism of mtDNA deletion formation (Fukui & Moraes, 2009; Nissanka et al., 2018).

1.5. Mitochondrial genetics

1.5.1. Maternal inheritance

MtDNA is inherited strictly through the maternal lineage in mammals. This is known as uniparental or more specifically, maternal inheritance and is a widely accepted process (Giles et al., 1980). Despite this, paternal mtDNA transmission has been reported in inter-species bred mice (Gyllensten et al., 1991), following *in vitro* embryo manipulation in cattle (St John & Schatten, 2004) and in an isolated case of paternally transmitted human mitochondrial disease (Schwartz & Vissing, 2002). These rare findings have questioned the dogma of maternal mtDNA inheritance and additionally the mechanisms by which it is maintained remains unclear. Fertilisation of most mammalian oocytes by sperm results in a zygote in which paternally derived mtDNA is excessively diluted by the maternal mtDNA. At a much lower copy number than that of the oocyte, the paternal mtDNA is thought to be diluted to such an extent that it is undetectable in the next generation. This has shaped the so-called simple dilution model of uniparental mode of mtDNA inheritance (Gyllensten et al., 1991), however this hypothesis has been refuted by a recent study utilising ultra-deep sequencing in a human cohort. The failure to identity common mtDNA population haplotypes in any of the individuals studied, as would be expected if there were frequent paternal leakage in the human population suggests an active mechanism of paternal mtDNA elimination (Pyle et al., 2015). The ubiquitin labelling of parental mitochondria within the oocyte and their subsequent elimination via lysosomes and/or proteasomes has been described in mammals (Sutovsky et al., 1999, 2000) as has the involvement of the E3 ubiquitin ligases, PARKIN and MUL1, in mediating mitophagy of paternal mitochondria (Rojansky et al., 2016). The direct elimination of sperm mtDNA however has not been demonstrated and further reports of parental mtDNA which has escaped the constraints of such active removal mechanisms have been documented (Luo et al., 2018). Given the rarity of such reports and the recent observation that paternally inherited large nuclear-encoded mitochondrial segments (NUMTs) can mimic paternally inherited mtDNA heteroplasmy (Wei et al., 2020), the inheritance of mtDNA as strictly maternal remains the established mode of transmission.

In asexual populations, the genome can be at an increased risk of extinction due to the accumulation of unfavourable mutations which may otherwise have been purged as a result of genetic recombination. This is known as Muller's ratchet (Muller, 1964) and as an effectively asexual population, the mitochondrial genome is vulnerable to this process. The highly variable transmission of mtDNA mutation load from mother to child (Larsson et al., 1992a; Larsson et al., 1992b), in addition to the observed rapid expansion of variant mtDNA molecules from mother to offspring in animal studies led to the development of the mtDNA genetic bottleneck hypothesis (Hauswirth & Laipis, 1982) in which a segregation or selection of mtDNA molecules at the primordial germ cell level protects against the effects of Muller's ratchet. The segregation of mtDNA molecules occurs as cell division events generate primordial germ cells in the developing embryo, each daughter cell containing a fraction of the mtDNA molecules present in the parent cell. Subsequent rapid replication of the selected mtDNA molecules ensues as these cells then mature into oocytes (Cao et al., 2007). In the case of mutated mtDNA molecules, the level of heteroplasmy within the primordial germ cell therefore dictates the transmission to the next generation in the event of fertilisation.

1.5.2. Heteroplasmy and the threshold effect

Hundreds to thousands of copies of the mitochondrial genome are present within each cell. Homoplasmy describes the state in which all copies of mtDNA are identical whereas heteroplasmy refers to the state in which there is more than one mtDNA variant in a cell. (Lightowlers et al., 1997; Wallace, 2010)**.** The heteroplasmic mutant mtDNA population, or mutation load, is expressed as the percentage of mutant versus wild type mtDNA clones. At low levels, cells and tissues are largely unaffected by mutant copies of the mitochondrial genome as wild type mtDNA molecules are able to compensate for mutant clones. A threshold level must be reached before mitochondrial function is compromised and a biochemical defect is observed. This threshold level, however, differs between specific mutations and their affected tissues. For example, the common point mutations m.3243A>G and m.8344A>G must typically reach a mutation load of 80-90% before their respective conditions of MELAS and MERRF are manifested (Chinnery et al., 1997). In contrast, a rare m.14723T>C point mutation within the mt-tRNA^{Glu} (*MTTE*) gene segregates with a biochemical defect as evidenced by COX deficient muscle fibres at a heteroplasmy as low as

7% (Alston et al., 2010). Large scale mtDNA deletions, frequently observed in cases of chronic progressive external ophthalmoplegia (CPEO), are typically associated with a threshold level of approximately 60% (Hayashi et al., 1991).

1.5.3. Clonal expansion

Clonal expansion describes the process by which a mutated molecule of mtDNA accumulates within a cell over time to become the dominant species. At present, it is unclear exactly how this occurs, however there are several mechanistic theories. The first is based upon the theory that copies of mtDNA in which there are mutations in the form of large-scale deletions, have an advantage over wild type molecules due to their smaller genome taking less time to replicate (Wallace, 1989). This is known as the 'survival of the smallest' theory however, with regard to point mutations in which genome size is unaffected, this mechanism is unable to account for expansion of these clones as is observed in mitotic tissues (Fellous et al., 2009; McDonald et al., 2008; Taylor et al., 2003). Support for the survival of the smallest hypothesis with regard to mtDNA deletions has been provided with the use of the PstI mouse model in which the largest induced mtDNA deletions in CNS neurons accumulated faster than smaller deletions (Fukui & Moraes, 2009). Arguing against this mechanism on observational and experimentally simulated grounds; Kowald and colleagues reported that while a reduction in genome size can theoretically provide a selective advantage, as genome size further reduces in relation to mtDNA molecule half-life, this advantage is lost. Additionally, this mechanism while plausible in longer lived species, cannot account for mutant mtDNA clonal expansion in shorter lived species (Kowald et al., 2014).

Two further theories also centre on mutated mitochondria possessing a replicative advantage over their wild type counterparts; however, the size of the genome is not a factor and thus they can also be applied to the clonal expansion of point mutations. Mitochondria with mutated genomes affecting their respiratory capacity were hypothesised to evade lysosomal degradation and therefore persist and replicate, whereas fully functional mitochondria suffered increased damage and death due to an increased production of ROS (de Grey, 1997). A postulated slower metabolic rate of mitochondria harbouring mtDNA

mutations and resultant reduction in ROS production led to the hypothesis being dubbed the 'survival of the slowest' theory. This theory has also been disputed with the observation that damaged or dysfunctional mitochondria undergo degradation in preference of those that are fully functional (Kim & Lemasters, 2011; Twig et al., 2008).

The third and least challenged clonal expansion theory is known as random genetic drift. MtDNA replicates independently of the nuclear genome and the cell cycle. Replication is continuous but random with different molecules of mtDNA replicating at different times, producing a small number of replicates with each cycle. It is entirely plausible that a mutated copy of mtDNA may, by chance, replicate more frequently than a wild type copy and accumulate within a cell, influencing the cell's heteroplasmy. It is also plausible that it will not, having little or no effect on heteroplasmy and subsequent biochemical function. This may be true at a particular point in time but via this alternative mechanism of clonal expansion, known as random genetic drift or relaxed replication, mutated copies of mtDNA while present, have the potential to accumulate and manifest pathologically with time (Chinnery & Samuels, 1999) . Computational modelling of random genetic drift also supported the theory that mutations occurring in childhood or early adulthood, having had an extended period of time to propagate, may have the potential to expand to greater levels than mutations occurring later in life (Elson et al., 2001). Importantly, this hypothesis is able to account for both the expansion of mtDNA point mutations in dividing tissues and those that occur in short lived species in addition to humans (Baines et al., 2014; Greaves et al., 2014; Stamp et al., 2018).

With regard to the clonal expansion of mtDNA deletions, two additional mechanistic theories have been recently proposed. The negative feedback loop theory posits that a deletion that removes the protein product of that gene also removes the negative feedback inhibition of transcription of the genome. Theoretically this bestows a replicative advantage on the mutant genome and is supported by both experimental and computer simulated data (Kowald & Kirkwood, 2014; Kowald & Kirkwood, 2018). Finally, the perinuclear niche theory proposes that should mtDNA deletions arise in the perinuclear region of skeletal muscle fibres, via retrograde stress signalling to the nucleus, replication of these mutant molecules is triggered, and clonal expansion ensues (Vincent et al., 2018).

1.5.4. Mitotic segregation

Replication of the mitochondrial genome occurs independently of the cell cycle, however mitochondrial dynamics and morphology coordinate with particular cell cycle stages in order to facilitate the partitioning of mitochondria to daughter cells at cell division. Prior to division, the mitochondrial genome must replicate to ensure sufficient copies are transmitted to daughter cells. Between G1 and S phase the fusion of mitochondria is promoted, and the network can be visualised as an extensive, hyperfused system (Mitra et al., 2009). In the early stages of mitosis, the phosphorylation of the fission promoting DRP1 results in fragmentation of the mitochondrial network prior to their segregation as the cell divides (Taguchi et al., 2007). As the segregation of mitochondria at mitosis is a stochastic process, should there be a heteroplasmic variant present within the parent cell, daughter cells have equal chances of acquiring more, less or the same level of mutant mtDNA molecules as the cell from which they are descended. Accordingly, mitotic segregation may inadvertently contribute to, and potentially accelerate, the clonal expansion of mutant clones as has been demonstrated using simulated modelling within normal buccal epithelial cells and tumour cells (Coller et al., 2001b) and more recently within colonic crypts (Stamp et al., 2018).

1.6. Ageing

The ageing process has been described as the accumulation of molecular and cellular damage that results in reduced function in adulthood, diminished fecundity and an increased probability of death (Kirkwood, 2008). As the average human life expectancy has risen steadily over the past two centuries, an increasing proportion of the population today and those of the future will be represented by individuals over the age of 65. This trend brings with it an increased need to understand the complex mechanisms by which the process of ageing occurs and accordingly obtain a position from which associated disease and frailty may be challenged.

1.6.1. Evolutionary theories of ageing

The variation in life expectancy observed among different species formed the basis from which initial evolutionary theories of ageing developed. The genomic differences between species were hypothesised as the underpinning determinant of longevity according to a pre-determined genetic programme. In 1891 August Weismann proposed that such programming existed in order to facilitate the demise of older generations, removing the burden they place upon younger members of the population and thus allowing the younger, more valuable individuals to flourish (Weismann et al., 1891). An alternative theory was proposed by Peter Medawar in 1952 and is known as the mutation accumulation theory. Medawar's theory postulates that ageing is the result of an accumulation of mutations within the genome of an individual that collectively contribute to a physiological deterioration or an ageing phenotype. Genes which are beneficial to the organism, acting early in life facilitating optimal health and reproduction were proposed to be subject to natural selection and transmitted to offspring. Conversely, late acting genes which may be detrimental to health later in life but posed negligible risk in an organism's youth were suggested to be effectively resistant to natural selection pressures and thus permitted to accumulate in subsequent generations (Medawar, 1952). Following on from the work of Medawar, the antagonistic pleiotropy theory was developed by George Williams. This theory proposed that genes that increase reproductive advantage and propagation of the species are naturally selected and favoured, despite any adverse effects that those same genes may have later in life (Williams, 1957). With limited evidence documenting specific genes supportive of antagonistic pleiotropic and mutation accumulation theories, evolutionary theories of ageing have deviated somewhat towards a more physiological rather than genetic basis. The disposable soma theory of ageing as described by Thomas Kirkwood in 1977 describes the process of ageing as the allocation of finite organismal energy into the maintenance of the germline regardless of the consequential detriment to the 'disposable soma' or somatic cells (Kirkwood, 1977).

1.6.2. Molecular theories of ageing

The advances in science, technology and medicine that have developed since Weismann's evolutionary observations have allowed gerontologists to gain intricate knowledge and expand theoretical hypotheses to a cellular and molecular level. Accordingly, experimentally derived modern theories of ageing have been described, and centralise around a time-dependant accumulation of cellular damage (reviewed in López-Otín et al., 2013).

Throughout the lifetime of an organism, physical and chemical mediated damage is incurred both as result of exogenous insult and during the normal metabolic and homeostatic processes a cell undergoes. Despite the numerous repair mechanisms which organisms have evolved in order to rectify DNA damage, the continuous exposure to endogenous and exogenous mutagens over time can lead to an accumulation of DNA damage and thus increasing genomic instability with advancing age (reviewed in Moskalev et al., 2013). Increasing age has also been associated with a reduction in the efficacy of the majority of DNA damage repair mechanisms (Hart & Setlow, 1974) and age-associated changes in the patterns of usage of different repair mechanisms has also been described (Engels et al., 2007). An imbalance between the rate of genomic damage and that by which it can be repaired inevitably results in cellular dysfunction and a decline in tissue functionality and homeostasis.

Damage to DNA is exhibited in numerous forms and can extend from single nucleotide point mutations to the loss or gain of entire chromosomes. The frequency of chromosomal aberrations has been documented to increase in both mice and humans with advancing age (Ramsey et al., 1995; Tucker et al., 1999). At the extremities of chromosomes, telomeres form protective, repetitive clusters which are also susceptible to a degeneration that is associated with increasing age. As DNA polymerase is incapable of fully replicating the telomeric ends of linear DNA, in the absence of telomerase enzymes which carry out this function, each replication of the cell results in a progressive telomere attrition until a critical or threshold level is reached and the cell enters replicative senescence (Greider & Blackburn, 1985; Harley et al., 1990; Hayflick & Moorhead, 1961; Olovnikov, 1973; Watson, 1972) thus describing the telomere hypothesis of ageing (Harley et al., 1992).Telomerase enzymes expressed in embryonic and some adult stem cells extend the 3' ends of telomeres and

effectively counteract the countdown to senescence observed in somatic cells that lack this enzyme. The importance of telomerase in the pathophysiology of ageing has been demonstrated *in vitro* by the significant extension of the lifespan of normal human telomerase-lacking cells by the introduction of telomerase (Bodnar et al., 1998), and also *in vivo* with telomerase gene therapy delaying ageing and extending the lifespan of mice (Bernardes de Jesus et al., 2012). Current understanding is that regulation of telomere length is much more complex than a simple 'biological clock'. Inflammation and oxidative stress, both of which can increase with advancing age, have been demonstrated to also accelerate the damage to and loss of telomere integrity (Jurk et al., 2014; von Zglinicki, 2002).

1.6.3. Mitochondrial free radical theory of ageing

Initially described in 1956, the free radical theory of ageing proposed that cellular oxidative stress is central to the ageing process (Harman, 1956). Mitochondria, as major producers of reactive oxygen species, have since been implicated in this theory and thus led to its revision as the mitochondrial free radical theory of ageing (MFRTA) (Harman, 1972). As a by-product of oxidative phosphorylation, mitochondria generate around 90% of cellular reactive oxygen species (Balaban et al., 2005). Due to the close proximity of mtDNA to the source of ROS; the electron transport chain, the mitochondrial genome is postulated to be subject to ROS mediated damage and mutation. This mutation may impair OXPHOS function, leading to increased production of ROS which in turn precipitates further mtDNA mutation and cellular damage. This process has been described as the vicious cycle, contributing to molecular theories of ageing and decline (Harman, 1972). Experimental support for the MFRTA can be taken from numerous animal models, for example a decrease in oxidative stress and increased longevity has been achieved in mice via the overexpression of mitochondrially targeted catalase (Schriner et al., 2005), while production of the superoxide anion radical in the liver and muscle is reportedly lower in longer-lived species (Sohal et al., 1989). Furthermore, in humans, the total levels of oxidised protein in several tissue types has been shown to increase with advancing age (Moskovitz et al., 2002). Despite evidence such as this, the MFRTA has been challenged in more recent times. The naked mole rat is an extremely long-lived rodent with a lifespan up to 15 times longer than that of the mouse in spite of evidence of high levels of oxidative damage (reviewed in Lewis et al., 2013). Additionally, the

overexpression of superoxide dismutase 2 (*Sod2*), an O_2^- scavenging antioxidant enzyme, while attenuating lipid peroxidation, oxidative stress and an age-associated reduction in mitochondrial ATP production, did not alter age-associated pathology nor longevity in mice (Jang et al., 2009). The converse also applies, in that mice deficient in *Sod2* and glutathione peroxidase 1 (*Gpx1*), also an antioxidant enzyme, have elevated oxidative damage and age-related pathologies such as tumour incidence, however no reduction in longevity is observed (Zhang et al., 2009). These seemingly contradictory findings may be reconciled by the gradual elucidation of additional roles of reactive oxygen species. No longer are they exclusively considered as damaging agents, rather the fine tuning of their generation in response to cellular stressors and subsequent involvement in cell signalling pathways now deems them essential to the promotion of cellular survival (reviewed in Sena & Chandel, 2012).

1.6.4. Mitochondrial dysfunction and ageing

Over the past three decades, the accumulation of mtDNA mutations in a variety of aged, post-mitotic tissues has been well documented. In 1989, Muller-Hocker described an association between increasing age and the frequency of COX deficient cardiomyocytes (Muller-Hocker, 1989). A similar phenomenon has also been observed in the brain, with a significantly higher frequency of the common 4977 nucleotide pair deletion, $mtDNA^{4977}$, detected in aged brain tissues when compared to younger controls (Corral-Debrinski et al., 1992). Several different brain regions were investigated, the putamen and cortical regions being more profoundly affected than occipital and parietal regions, with this particular deletion being barely detected in the cerebellum. The differences observed between different regions suggest a cell type specific variation in mtDNA mutations amongst cells of the same tissue type. In 1998, Brierley et al. described the clonal expansion of different mtDNA deletions within individual skeletal muscle fibres in aged subjects (Brierley et al., 1998). Additionally, Bender et al., reported a significant accumulation of mtDNA deletions in aged substantia nigra neurons (Bender et al., 2006). These observations provide an important indication of an association between mtDNA mutations and the role they may play in the ageing process.

Age-related mtDNA defects have also been observed in mitotic tissues maintained by adult stem cells. The detection of mtDNA point mutations in the human aged colon by Taylor et al., represented the first such finding (Taylor et al., 2003). Readily identifiable as COX deficient crypts using COX/SDH enzyme histochemistry, the subsequent single-cell laser microdissection and whole genome mtDNA sequencing revealed pathogenic mtDNA point mutations in COX deficient crypts, the majority of which were transitions involving G residues (Taylor et al., 2003). The presence of single mutations in entirely COX deficient crypts implied the expansion of stem cell derived mtDNA mutations from parent stem cells to all progeny. Similarly, the demonstration of continuous COX deficient ribbons in partially deficient crypts also supported this mechanism (Taylor et al., 2003). Identical point mutations have since been shown to be present in the two arms of a bifurcating crypt and also in adjacent crypts. This suggests that mtDNA mutations first clonally expand within a crypt which then divides by fission, allowing the mutation to propagate through the tissue (Greaves et al., 2006). Additional studies have shown that this is not exclusive to the colonic epithelium; OXPHOS defects and mtDNA point mutations have been detected in a variety of mitotic tissues such as the liver (Fellous et al., 2009) and the stomach (McDonald et al., 2008). The consequences of mtDNA mutation accumulation with age extend beyond the impairment of oxidative phosphorylation and the functional decline that this elicits. For example, mitochondrial dysfunction and ROS production facilitate telomere shortening and promote cellular senescence; both additional hallmarks of ageing (Passos et al., 2007). Understanding the mechanisms by which mitochondrial dysfunction can promote the ageing phenotype may therefore have important implications in the treatment or even the prevention of age-related diseases.

1.6.5. Stem cells, ageing and mitochondria

Almost all mammalian tissues are maintained by small numbers of specialised cells known as adult stem cells. Residing within specific compartments known as niches, the relationship between stem cells and their niche serves to support tissue homeostasis by maintaining tight control over self-renewal, differentiation and regeneration following injury. As adult stem cells possess the capacity to self-renew, they are the longest living cell type and as such are placed at an increased risk of sustaining molecular damage over time (reviewed in Liu & Rando, 2011). Accordingly, with advancing age, stem cell populations exhibit a decline in

function and regenerative capacity, however the accumulation of molecular damage represents just one mechanism by which stem cell ageing arises. Extrinsic to the stem cells themselves, circulatory systemic factors such as cytokines, hormones and immune system related components have been shown to change with age and impact stem cell function (Elabd et al., 2014; Sinha et al., 2014) . As demonstrated by heterochronic parabiosis experiments in which the surgical pairing of young and old animals allows the circulatory system to be shared, the exposure of young neural stem cells to an ageing systemic circulation facilitated a decline in the activity of these cells (Villeda et al., 2011). The converse is also true and aged skeletal muscle stem cells (satellite cells) are rejuvenated by exposure to a young milieu (Conboy et al., 2005).

Age-related changes in epigenetic modifications such as DNA methylation have also been described. In aged haematopoietic stem cells (HSCs), the reduction of methylation marks at transcription factor binding sites of self-renewal promoting genes is coupled with increased methylation of those associated with differentiation (Sun et al., 2014). Perturbations in epigenetic modifications are also linked with metabolic functions which are additionally dysregulated in an age-associated manner. Stem cells in a quiescent state are often associated with a glycolytic metabolic phenotype (Simsek et al., 2010; Takubo et al., 2013; Zheng et al., 2016) which upon differentiation switches to a metabolism relying on oxidative phosphorylation (O'Brien et al., 2015; Wüst et al., 2018; Zheng et al., 2016). The homeostasis of stem cells relies heavily on the balance between glycolysis and OXPHOS and the availability of specific cofactors and epigenetic modifiers generated by each process. For example, in response to low levels of oxygen within the HSC niche, quiescence is maintained via activation of hypoxia-inducible factor 1, (HIF-1) which restricts the entry of pyruvate into the TCA cycle and subsequent oxidative phosphorylation in the mitochondria by its activation of pyruvate dehydrogenase kinase (PDHK) (Takubo et al., 2013). The predominance of a glycolytic metabolism favours the generation of the cofactor acetyl-CoA and histone acetylation in HSCs maintaining pluripotency (Moussaieff et al., 2015), whereas oxidative phosphorylation supports the maintenance of α–ketoglutarate (α-KG) levels favouring demethylation of DNA and HSC differentiation (Ho et al., 2017). Evidently, perturbations in this balance can have major implications on stem cell fate and have been linked with the age-associated impairment of autophagy in murine HSCs (Ho et al., 2017) and impaired glucose uptake resulting from reduced expression of the glucose transporter 3

(GLUT3) in aged pluripotent stem cells (Zhang et al., 2017); both of which may promote aberrant differentiation at the expense of maintaining stemness.

Mitochondria have been implicated in the pathophysiology of stem cell ageing by several additional mechanisms. A reduction in intracellular levels of the critical cofactor NAD+ has been described in association with advancing age (Braidy et al., 2011; Massudi et al., 2012). This has consequences for countless processes within the cell, however with regard to ageing, the involvement of a family of NAD+ dependant enzymes known as sirtuins is becoming apparent. The NAD+-dependent deacetylase and mono-ADP-ribosyl transferase activity of sirtuins facilitates their regulation of proteins involved senescence, apoptosis, differentiation, and metabolism. Of seven known mammalian sirtuins, three are located within the mitochondria; SIRT3, 4 and 5, however the activities of the remaining sirtuins are intricately involved with mitochondrial function (reviewed in Michan & Sinclair, 2007). SIRT3 is downregulated with increasing age and as such, its promotion of antioxidant activity and ROS scavenging is impaired. In haematopoietic stem cells, SIRT3 deficiency results in a reduction in pool size and in self-renewal capacity (Brown et al., 2013). Mechanistically, the deacetylation of FOXO3a of the forkhead family of transcription factors by SIRT3 promotes the expression of the mitochondrial antioxidant SOD2, however an additional role of SIRT3 in the induction of mitophagy as part of the UPR^{mt} (mitochondrial unfolded protein response) in cells exposed to proteotoxic stress has been described (Papa & Germain, 2014). An additional sirtuin, SIRT7 is also linked to another axis of the UPR^{mt} and has been shown to decrease in expression in ageing HSCs rendering them less capable of dealing with an age-related increased level of mitochondrial protein folding stress (Mohrin et al., 2015). A premature HSC ageing phenotype with increased apoptosis, a myeloid differentiation bias and reduced regenerative potential in SIRT7 deficient mice was subsequently rescued by SIRT7 overexpression and linked to the repression of nuclear respiratory factor 1 (NRF1). This reduces mitochondrial biogenesis and respiration alleviating protein folding stress (Mohrin et al., 2015). Similarly, SIRT1, although its primary localisation is nuclear, its activation is linked to the regulation of mitochondrial function and stem cell ageing via several mechanisms such as the promotion of mitochondrial biogenesis (Cantó et al., 2009), autophagy (Huang et al., 2015), and the upregulation of antioxidant gene expression via FOXO3 activation thus preventing the induction of senescence (Hori et al., 2013).

Stem cell fate has been shown to be sensitive to levels of reactive oxygen species which are primarily produced by the mitochondrial oxidative phosphorylation system. Increasing levels of ROS with advancing age are associated with a loss of stemness whereas low levels of ROS reportedly bestow HSCs with a greater capacity for self-renewal (Jang & Sharkis, 2007). Furthermore, increased levels of ROS lead to the activation of p38 MAPK, a member of the mitogen-activated protein kinase family which subsequently upregulates $p16^{Ink4a}$ and $p19^{Arf}$ in the HSC population inducing senescence and thus limiting stem cell lifespan (Ito et al., 2006). The activation of p38 MAPK has been further implicated in the age-related exhaustion of intestinal stem cells. In comparison to young animals, aged murine intestinal *Lgr5+* stem cells demonstrated an increased activation of the nutrient and growth factor sensing mammalian target of rapamycin complex 1 (MTORC1). The *Lgr5+* specific deletion of an MTORC1 suppressor, tuberous sclerosis 1(*Tsc1*), induced a premature intestinal ageing phenotype in young mice which was ameliorated with administration of the MTORC1 inhibitor rapamycin. In the absence of rapamycin, *Tsc1* ablation led to mTORC1 activation, increased mitogen-activated protein kinase kinase 6 (MKK6) expression, p38 MAPK activation, and the enhancement of p53 expression. Subsequently this resulted in the exhaustion of intestinal stem cells in addition to reductions in villus size and density, which again could be rescued by p38 MAPK or p53 inhibition (He et al., 2020). Given that mitochondrial ROS can activate p38 and drive intestinal crypt differentiation (Rodríguez-Colman et al., 2017), the involvement of mitochondria in stem cell homeostasis and ageing is further supported.

Collectively, the mechanisms involved in stem cell ageing have grave implications with regard the development of pathologies associated with advancing age such as degenerative disorders and cancer. The understanding of age-related changes at the stem cell level, particularly those that are targetable such as epigenetic and metabolic aberrations may therefore assist in the development of therapeutics with the aim of rejuvenating stem cell function and thus ameliorating the disorders their functional decline may promote (reviewed in Liu & Rando, 2011; Neves et al., 2017).

1.6.6. Mouse models of mitochondrial dysfunction and ageing

Mouse models of disease are extensively used to recapitulate a wide array of pathologies seen in humans. Mice breed prolifically, are short-lived, and most importantly share a similar anatomy, physiology and genome with humans. These features make them an excellent comparator in the study of human disease and over decades of use, they have significantly contributed to a greater understanding of many human conditions.

Genetically engineered mouse models of disease are conventionally created by targeting modified genetic constructs into mouse embryonic stem (ES) cells. These vectors either carry a mutation in the gene of interest, or the gene of interest is flanked by recombination sites such as *LoxP* sites. A selection cassette such as one which confers neomycin resistance is also included in the construct and is similarly flanked by recombination sites to enable subsequent *in vivo* excision. Once transfected into the ES cells, clones which have successfully integrated the 'foreign' DNA via homologous recombination are selected using Southern blotting, injected into mouse blastocysts and implanted into a pseudo-pregnant female mouse. The resultant chimeric mice are crossed with wild-type animals to produce founder animals in which the genetic manipulation will be transmitted through the germline. The first report of a mitochondrial mouse model of disease was published in 1995 and described the effect of inactivation of the intra-mitochondrial free radical scavenging enzyme, manganese superoxide dismutase (MnSOD) via homologous recombination of a mutated vector into the mouse MnSOD gene (*Sod2*) (Li et al., 1995). Since then, further models involving the inactivation of antioxidant genes have been developed, in addition to many more in which genes involved in mtDNA replication, transcription, translation, mitochondrial dynamics, protein quality control and OXPHOS components themselves have been manipulated in order to model mitochondrial disease or dysfunction.

Human mitochondrial transcription factor 1 (mtTF1) was first isolated from human mitochondria in 1985 (Fisher & Clayton, 1985), then later sequenced and characterised as a nuclear genome encoded DNA binding protein (Parisi & Clayton, 1991). Now known as TFAM, the disruption of the gene encoding this transcription factor has been utilised to model disorders of mitochondrial DNA mutation in place of unsuccessful attempts at direct manipulation of the mitochondrial genome itself. Initial studies demonstrated the essential

requirement for TFAM for mtDNA maintenance and mitochondrial biogenesis, as homozygous knock-out mice (*Tfam*$^{-/-}$) were severely depleted of mtDNA and embryonically lethal. Their heterozygous knock-out counterparts (*Tfam*$^{+/-}$) also demonstrated a profound reduction in mtDNA copy number with an associated respiratory chain deficiency in the heart (Larsson et al., 1998). Interestingly, despite the global reduction in mtDNA copy number, not all tissues were uniformly affected in terms of mtDNA transcripts and OXPHOS dysfunction, suggesting the existence of translational compensatory mechanisms such as an increased stability of mtDNA transcripts in some tissues to a greater degree than in others.

The discovery of the Cre-Lox system in the P1 bacteriophage (Sternberg, 1979; Sternberg & Hamilton, 1981) has allowed the development of cell-type specific animal models of disease, thus facilitating the dissection of multiple pathologies into tissue specific entities. The technique was used to disrupt TFAM in a tissue specific manner. Cre-recombinase enzymes catalyse the recombination between two *LoxP* sites, excising the genetic material between them. If *Cre* is situated under a tissue specific promoter, the gene of interest around which the *LoxP* sites are inserted will only be lost in those specific cell types. Heart and muscle specific *Tfam* disruption was investigated by crossing *Tfam*$^{loxP/loxP}$ mice with mice expressing the Cre-recombinase gene under muscle creatinine kinase promoter control (Wang et al., 1999). This model faithfully reproduced the physiological and biochemical elements of the dilated cardiomyopathy observed in Kearns-Sayre syndrome. Similarly, with Cre-recombinase under the control of the insulin-2 promoter expressed in pancreatic β cells, *Tfam* disruption led to the development of mitochondrial diabetes and β cell loss in older animals (Silva et al., 2000). An adult-onset neurodegeneration with progressive symptoms of tremor and rigidity was also modelled in mice with a dopamine transporter *Cre* transgene (Ekstrand et al., 2007). Reduced levels of mtDNA expression and respiratory chain enzyme activity in midbrain dopaminergic neurons of these animals resulted in a Parkinsonism characterised by a progressive loss of these cell types. Although these models provide an excellent means by which mitochondrial disorders initiated by an mtDNA transcription defect can be studied, not all of the models reflect an mtDNA-associated ageing phenotype as such.

As discussed in 1.6.4, mitochondrial dysfunction has been associated with ageing in a multitude of both mitotic and post-mitotic tissue types with increased levels of mutated mtDNA in these aged tissues contributing to their functional decline. Tissue-specificity is observed with regard to the type of mutation found in different tissue types. Large scale mtDNA deletions are most frequent in post-mitotic tissues such as the brain (Bender et al., 2006), and mtDNA point mutations are more commonly reported within mitotic tissues such as the intestine (Greaves et al., 2012). In order to investigate the link between mtDNA mutation accumulation and ageing, the *PolγA* mutator mouse was developed in 2004 (Trifunovic et al., 2004). Knock-in mice harbour an altered catalytic *PolγA* subunit containing an alanine instead of the highly conserved aspartate residue at the second proofreading domain (D257A). This confers a reduction of exonuclease activity on the catalytic *PolγA* subunit, making mtDNA three to five times more susceptible to mutation events during replication. Mice with the homozygous $PolγA^{mut/mut}$ genotype demonstrated an increased load of somatic mtDNA point mutations in the brain, heart and liver. Furthermore, mice demonstrated an advanced ageing phenotype characterised by weight loss, curvature of the spine (kyphosis), hair loss (alopecia), reduced subcutaneous fat, anaemia and osteoporosis. A very similar mouse was developed in 2005, again with an aspartate to alanine substitution at residue 257 of the conserved proofreading domain of *PolgA* impairing the exonuclease activity of the enzyme (Kujoth et al., 2005). The models differ in the constructs and recombination enzyme systems used in their generation and as a result the Trifunovic mouse retains two *LoxP* sites flanking the *PolγA* gene whereas the Kujoth mouse contains one residual *LoxP* site; an important consideration to be made if animals are to be crossed with other models utilising *Cre-Lox* technology. Observations made by Trifunovic *et al.* were corroborated by Kujoth *et al*., however somewhat surprisingly, neither model could attribute these findings to an increase in oxidative stress as would be predicted by the mitochondrial free radical theory of ageing (Trifunovic et al., 2005). The aspersions that were cast upon the involvement of oxidative stress and free radicals in the propagation of ageing were later refuted by studies that reported increased levels of hydrogen peroxide in aged mtDNA mutator mice *in vivo* (Logan et al., 2014), increased markers of oxidative damage within the skeletal muscle of mutator mice (Kolesar et al., 2014), and the extension of lifespan and delayed onset of progeroid features in mutator mice treated with a mitochondrially targeted antioxidant (Shabalina et al., 2017). Despite these findings potentially reinstating the role of reactive oxygen species in the ageing process, their additional involvement in critical

physiological processes as signalling molecules suggests there is a much greater complexity than the historical 'vicious cycle' would suggest.

The ability of the mutator mouse to accurately model human ageing has also been challenged. Firstly, the level of mtDNA mutation is much higher in the mouse than in aged human tissues (Khrapko et al., 2006) , and despite a significant increase in mtDNA mutation load, the heterozygous *PolγA* mouse did not present with a premature ageing phenotype (Vermulst et al., 2007). Nonetheless, the mutator mouse remains a widely accepted model of premature ageing associated with mtDNA mutation.

1.7. The intestinal tract

1.7.1. Intestinal structure and function

The overarching function of the small intestine is to absorb essential nutrients from ingested food in order to provide the body with energy. Distal to the stomach in which the mechanical process of digestion begins, carbohydrates, proteins, fats, minerals and vitamins are absorbed by the small intestine which comprises the duodenum, jejunum and ileum and measures approximately 24 feet long in humans The chemical digestion which precedes absorption is facilitated by secretions from the liver, gall bladder and exocrine pancreas which are discharged into the duodenum (McCance & Huether, 2015). In order to maximise nutrient absorption, the luminal surface of the small intestine is organised into Kerckring's folds upon which villi and microvilli project into the lumen increasing surface area by a factor of 600 beyond that of a simple cylindrical tube. Depending on the substrate, nutrients traverse the epithelial membrane via passive diffusion, carrier-mediated diffusion, active transport or pinocytosis (Caspary, 1992).

Distal to the ileum is the large intestine or colon; the main function of which is to absorb water and electrolytes from dietary waste before it is expelled from the anus. The colon consists of four sections: the ascending, transverse, descending and sigmoid colon. Additionally, each section has four distinct layers: the mucosa, the muscularis mucosae, the submucosa, and the muscularis externa comprising circular and longitudinal muscle layers.

The colorectal mucosa forms millions of epithelial invaginations known as crypts. The base of a colorectal crypt rests on the muscularis mucosae and extends upwards to the mucosal surface of the large intestine where it opens into the gut lumen.

Although the majority of consumed food is digested in the stomach and small intestine, a proportion of ingested fat, protein and carbohydrate passes into the colon where it is metabolised into hydrogen, carbon dioxide, methane and short chain fatty acids (Cummings, 1975). Non-digestible food components such as resistant starch and dietary fibre are subject to microbial fermentation in the colon generating hydrogen, carbon dioxide and methane gas. The short chain fatty acids butyrate, acetate and propionate are also produced from starch and fibre fermentation. Butyrate is the colonocyte's preferred energy source and is subject to oxidation by the colonic epithelium (Roediger, 1982) whereas propionate and acetate are absorbed and used by the liver for gluconeogenesis and as fuel, respectively (Priebe et al., 2002). The production of short chain fatty acids thus has a beneficial role for the organism, however by-products which pose a more detrimental effect are also yielded. Fermentation products of protein breakdown also include short and branched chain fatty acids with the additional generation of potentially toxic metabolites such as phenols, sulphides, amines and ammonia. Ammonia can be reabsorbed, and the nitrogen utilised by colonic bacteria to facilitate their growth and metabolism, however amines and nitrates can also be used by colonic bacteria to produce *N*-nitrosamines. These have been shown experimentally to be carcinogenic compounds (Mirvish, 1995) and are associated with a significantly increased colorectal cancer risk in individuals with a high dietary intake of *N*-nitrosamine or *N*-nitrosodiumethylamine (Knekt et al., 1999). Furthermore, the generation of hydrogen sulphide via the action of sulphate reducing bacteria has been implicated in the modification of expression of DNA repair, inflammatory and cell-cycle progression genes in human intestinal epithelial cells (Attene-Ramos et al., 2010) with the perturbation of intestinal epithelial cell viability and permeability being mediated by phenol exposure (McCall et al., 2009; Pedersen et al., 2002). The colonic metabolism of protein and the resultant metabolites have thus been associated with an increased risk of inflammatory intestinal pathologies such as ulcerative colitis and Crohn's disease (Hou et al., 2011). Although a 'Western diet' high in fat and animal protein has long been associated with colorectal cancer (Drasar & Irving, 1973), it is considered that the potentially toxic and

carcinogenic effects of a high protein diet are compensated for by a balanced diet high in resistant starch or fibre.

The base of an intestinal crypt is known as the proliferative compartment and is populated by a pool of intestinal stem cells (ISCs). These multipotent cells generate transit amplifying progenitor cells (TAs) which divide a limited number of times, migrating upwards along the crypt axis before they differentiate into the functional cell lineages of the crypt. In the colon, these include goblet cells (secretory), enterocytes (absorptive), and gastrointestinal hormone secreting enteroendocrine cells (Umar, 2010). Small intestinal crypts contain a fourth cell type; the Paneth cell. Paneth cells secrete granules containing lysozyme, secretory phospholipase A2, and alpha defensins; proteins that are involved in host defence and immunity (Ouellette, 1997). Figure 1-4 depicts crypt and crypt-villous structure in the colon and small intestine respectively.

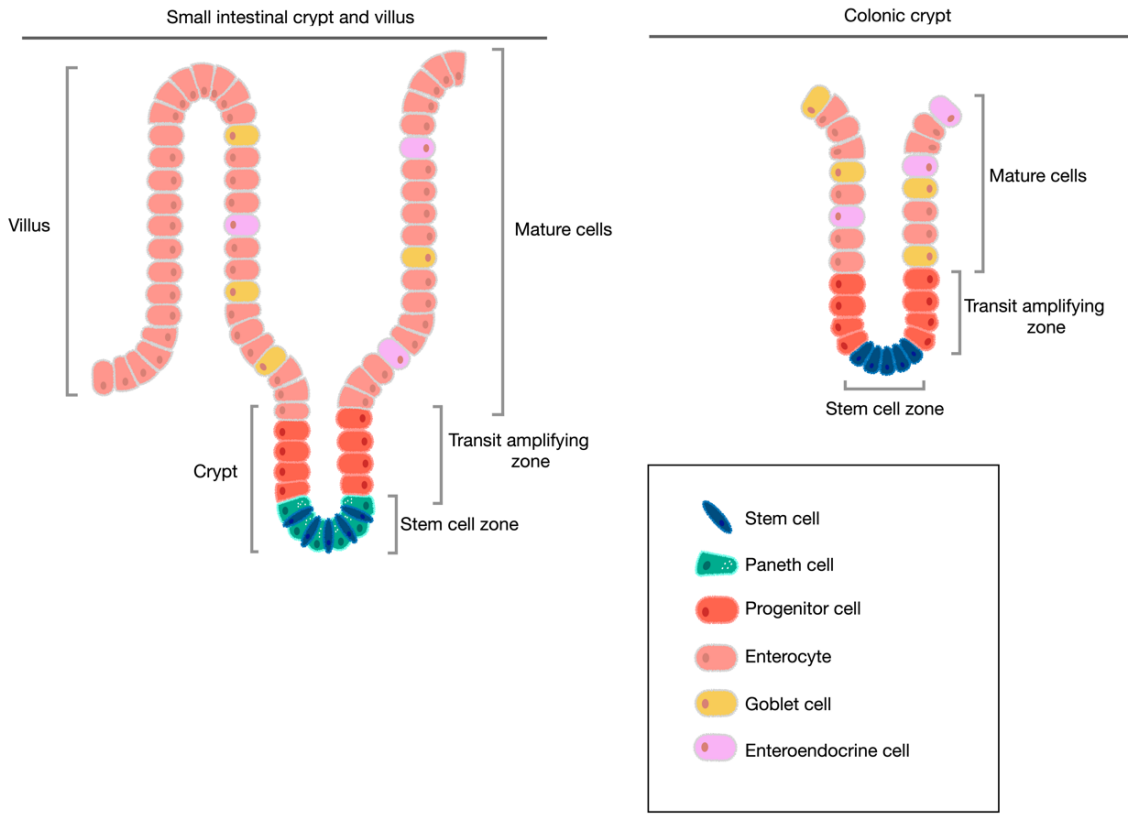

Figure 1-4. Crypt and crypt-villus structures in the colon and small intestine. In the small intestine (left), the stem cell zone or stem cell niche at the base of the crypt comprises Paneth cells intercalated between the stem cells which are responsible for generation of each of the differentiated intestinal epithelial lineages. Immediate progeny of crypt base stem cells form the transit amplifying cellular compartment; cells of which differentiate into the mature epithelial cells which populate the remainder of the crypt and villus projections. In the colon (right) there are no villus projections or Paneth cells.

1.7.2. Intestinal crypt stem cells

Initially described by Cheng and Leblond as crypt base columnar cells, stem cells are termed as such owing to their abilities to proliferate, self-maintain, produce of a variety of differentiated, functional progeny, regenerate the tissue after injury, and possess a flexibility in the use of these options (Cheng & Leblond, 1974; Potten & Loeffler, 1990). The mammalian intestinal epithelium has an extremely high turnover rate, with complete renewal occurring every 4-5 days (van der Flier & Clevers, 2009). It is understood that this process is maintained by a non-uniform population of stem cells capable of generating all intestinal lineages. Early studies aimed at characterising these stem cells utilised mutation-induced markers which facilitated the identification of stem cell descendants within the mouse intestine (Winton et al., 1988) however technological advances have greatly expanded current knowledge. Due to its establishment as a notable target of Wnt signalling in intestinal crypts, the *Lgr5* (leucine-rich-repeat-containing G protein-coupled receptor 5) was selected for investigation as a potential intestinal stem cell marker. The *Lgr5-EGFP-Ires-CreERT2* mouse model was engineered and crossed with mice bearing a Cre inducible *Rosa26-lacZ* reporter gene which upon the administration of tamoxifen, facilitated lineage tracing as *lacZ* was continuously expressed in *Lgr5+* cells and their progeny (Barker et al., 2007). Indeed, these experiments demonstrated that *Lgr5* expressing cells were able to generate each of the differentiated cell types observed in the mouse small intestine and colon. It is now understood that *Lgr5+* cells are the crypt base columnar cells; actively cycling stem cells largely responsible for homeostatic maintenance of the colonic and small intestinal epithelium. In the small intestinal crypt base, between six and eight cells situated between the Paneth cells were identified as *Lgr5* expressing stem cells, with smaller numbers being identified in the colonic crypt base (Barker et al., 2007).

By virtue of their label-retaining capacity, an additional population of slowly cycling cells located at the +4 position above the intestinal crypt base have also been purported to be intestinal stem cells (Potten et al., 1974). *Bmi1* is a member of the Polycomb group gene family and plays an essential role in the self-renewal of hematopoietic and neural stem cells. Investigations into the potential involvement of *Bmi1* in the maintenance of intestinal stem cell populations demonstrated that *Bmi1* was indeed expressed in the +4 intestinal cells. Again with the use of continuous labelling methodologies in mouse models, it was also

shown that these cells possessed the capacity to proliferate, expand, self-renew and give rise to all the differentiated cell lineages of the small intestine epithelium (Sangiorgi & Capecchi, 2008).

Lgr5+ stem cells have been described as an actively cycling, Wnt sensitive, proliferative population responsible for homeostatic maintenance of the intestinal epithelium. In contrast, *Bmi1+* cells are reported to act as a reserve pool of quiescent, Wnt insensitive stem cells with minimal involvement in tissue homeostasis, able to repopulate the *Lgr5+* pool following injury (Tian et al., 2011; Yan et al., 2012). Despite these distinct functionalities, it has since been demonstrated that *Lgr5+* cells can also express +4 markers such as *Bmi1* (Munoz et al., 2012) Furthermore, it has been shown that +4 cells express the atypical homeobox gene *Hopx*, and while they can give rise to *Lgr5* expressing stem cells, the converse is also true; *Lgr5+* cells can give rise to +4 cells expressing *Hopx* (Takeda et al., 2011). Investigations such as this highlight a plasticity within the intestinal stem cell compartments which has been further evidenced by studies observing the tissue response to injury. Not only is there an interconversion between stem cell populations but following exposure to radiation mediated damage and ablation of *Lgr5+* cells, committed secretory precursors can be recalled back to the stem cell pool fuelling regeneration and epithelial restoration (Buczacki et al., 2013). A recent paper, however, has challenged the validity of the +4-reserve stem cell concept with the demonstration that following *Lgr5+* stem cell depletion, the pool is regenerated almost entirely via the dedifferentiation of immediate *Lgr5+* progeny. Via *Lgr5+* continuous labelling and the ablation of the master transcriptional regulators of the secretory and enterocyte lineages; *Atoh1* and *Rbpj* respectively, regeneration of the stem cell pool was shown to be driven by the dedifferentiation of both precursor populations and not +4 'reserve' stem cells (Murata et al., 2020). Furthermore, the group demonstrate the post-injury regenerative requirement of the Wnt target gene *Ascl2,* the loss of which has been previously implicated in impaired intestinal stem cell survival (van der Flier et al., 2009). RNA sequencing of regenerating *Ascl2+* cells and immunoprecipitation identification of *Ascl2* target promoter regions further highlighted the upregulation of the IL-11 receptor gene *Il11ra1* in facilitating stem cell regeneration with IL-11 supplementation enhancing the organoid formation of *Ascl2+* cells (Murata et al., 2020).

1.7.3. The stem cell niche

Not only are the crypt stem cells themselves critical for the maintenance of epithelial homeostasis, their position within the crypt and their corresponding interaction with multiple signalling systems and extracellular cues are required to coordinate cellular activity. This complex interplay is known as the stem cell niche (Medema & Vermeulen, 2011). The major orchestrator of stem cell self-renewal and proliferation is the Wnt signalling pathway. The Wnt signalling system is a critical pathway that regulates self-renewal in stem cells of the colon, epidermis and haematopoietic system (reviewed in Reya & Clevers, 2005). The adenomatous polyposis coli (APC) protein is a key player in this pathway, as are several other cytosolic components namely, GSK- 3β, axin, the axin binding molecule Dishevelled (Dsh), and the central figure β-catenin. Together, these components form what is known as the destruction complex.

In the absence of Wnt ligand signals, the accumulation of β-catenin is prevented by the actions of the destruction complex. The destruction complex mediates the phosphorylation of β-catenin and targets it for proteasomal degradation (Aberle et al., 1997). When renewal signals are received via extracellular Wnt ligand binding to the cell surface receptors Frizzled and Lrp5/6, β-catenin is destabilised, released from the destruction complex and accumulates in the cytoplasm. It is now free to translocate to the nucleus where it binds transcription factors of the TCF/LEF family, primarily Tcf-4 (Behrens et al., 1996; Korinek et al., 1997), facilitating the activation of target genes such as the oncogene c-myc and cyclin D1 (He et al., 1998; Shtutman et al., 1999; Tetsu & McCormick, 1999). Fundamentally this results in proliferation; however, the pathway also provides differentiation and positional cues (reviewed in Nusse & Clevers, 2017). In addition to the Wnt ligands themselves, R-spondin proteins are also required to facilitate Wnt activation. In the absence of R-spondin, the ubiquitin ligases RNF43 and ZNRF3 constitutively degrade Frizzled Wnt receptors (Hao et al., 2012; Koo et al., 2012). However, when R-spondin proteins are present, these secreted factors bind to Lgr4 and Lgr5 receptors and facilitate the sequestration of RNF43 and ZNRF3. This enhances the stability of Frizzled Wnt receptors and thus potentiates Wnt signalling (Carmon et al., 2011; de Lau et al., 2011). The pathway is depicted schematically in Figure 1-5.

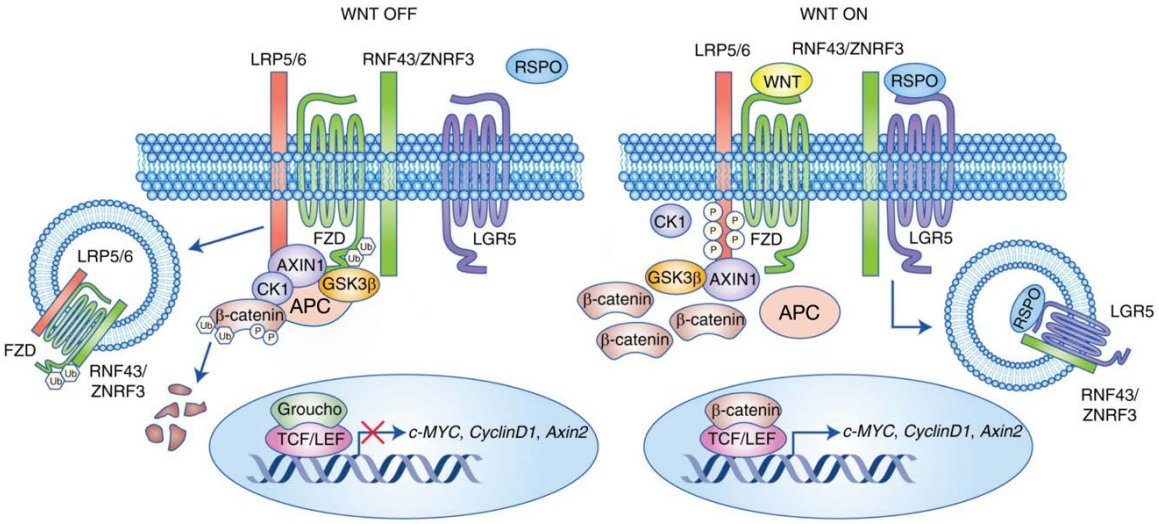

Figure 1-5. The Wnt signalling system. In the absence of Wnt ligand and R-spondin activation, the ubiquitin ligases RNF43 and ZNRF3 constitutively degrade Frizzled Wnt receptors. This facilitates the phosphorylation of β-catenin by the destruction complex, targeting it for proteasomal degradation. Wnt target genes are thus repressed. In the presence of Wnt ligand and R-spondin activation, RNF43 and ZNRF3 are sequestered allowing the destabilisation of the destruction complex. β-catenin is able to translocate to the nucleus and target gene transcription activated. Image adapted from (Morgan et al., 2018).

Bone morphogenetic protein (BMP) signalling represents the second major system crucial to the control of self-renewal and proliferation of stem cells in the intestinal crypt. In contrast to Wnt signalling however, BMP activation inhibits the proliferative response and promotes cellular differentiation (Haramis et al., 2004; He et al., 2004).BMP ligands are members of the TGFβ family and exert their actions by binding to type II receptors and recruiting type I receptors which together facilitate the translocation of Smad transcription family members to the nucleus (Heldin et al., 1997). BMP family members BMP2 and BMP4 are the predominant isoforms within the intestine and are secreted by mesenchymal cells (Haramis et al., 2004; Hardwick et al., 2004). In addition to the Smad mediated regulation of gene expression, these proteins reportedly inhibit Wnt signalling in a more direct manner. The inactivation of the tumour suppressor PTEN has been shown to activate Akt and promote the nuclear localisation of β-catenin (Persad et al., 2001). Similarly, the inactivation of BMP signalling in *Bmpr1a* receptor knockout mice was shown to associate with increased levels of inactive PTEN, activated Akt and nuclear β-catenin in intestinal stem cells indicating an additional means by which BMP can regulate stem cell self-renewal (He et al., 2004). Additionally, BMP signalling and Smad activation has also been shown to restrict *Lgr5+* stem cell self-renewal via the recruitment of histone deacetylase 1 (HDAC1) which epigenetically represses the transcription of stem cell signature genes such as *Lgr5* and *Sox9* thus inhibiting

their stemness (Qi et al., 2017). Interestingly, this study failed to identify an increase in nuclear localisation of β-catenin in *Bmpr1a* deficient mice and as such the mechanism by which BMP directly inhibits Wnt signalling remains somewhat unclear. Regulation of BMP signalling is achieved with important input from the mesenchymal tissue surrounding the intestinal crypt. In addition to the secretion of R-spondin1, myofibroblasts also secrete Noggin, an antagonist of BMP signalling (Lei et al., 2014).

The Notch signalling pathway represents the key means by which intestinal early progenitor cell fate is controlled and differentiation decisions are made. Enterocyte differentiation is driven by the activation of Notch signalling. Following the binding of Notch ligands such as Dll1 and Dll4, the Notch intracellular domain (NICD) of the Notch receptor is proteolytically cleaved and translocates to the nucleus where it facilitates the expression of target genes such as that encoding the Hes1 Notch effector transcription factor (Heitzler et al., 1996; Oellers et al., 1994). Accordingly, the expansion of secretory epithelial cell and decreased absorptive cell populations are observed in mice lacking Hes1 (Jensen et al., 2000). Conversely, mice with increased expression of NICD demonstrate an increase in stem cell proliferation with an associated decrease in secretory epithelial cell numbers (Fre et al., 2005). The activation of the Hes1 transcription factor results in the repression of another transcription factor; Atoh1. Atoh1 is considered the master regulator of the intestinal secretory cell lineage and thus directs Notch inactivated cells to become goblet, enteroendocrine, and Paneth cells (Yang et al., 2001). Notch signalling acts over very short distances as cells respond to ligands expressed by their neighbours. The cell in which Notch signalling is activated and thus Atoh1 is repressed expresses a reduced frequency of cell surface Notch ligands. Accordingly, Notch is not activated in neighbouring cells, Atoh1 repression is released and these cells are committed to the secretory lineage. This process is known as lateral inhibition and ensures a proportional distribution of different cell types within the intestinal crypt (reviewed in Sancho et al., 2015). Additional players in the Notch mediated control of cell fate decision making have recently been identified; namely the transcriptional co-repressors Mtg8 and Mtg16. These proteins were found to be expressed at high levels in early progenitor cells leaving the intestinal niche as a result of Notch signal loss at the +4/5 cell position. While the loss of Notch classically results in the activation of Atoh1 secretory lineage commitment, Mtg8 and Mtg16 expression begins to dominate as a result of the loss of Notch repression. This inhibits Atoh1 expression in addition to stem cell

gene expression and the expression of cell surface Notch ligands. Thus Mtg8/Mtg16 expression promotes intestinal niche exit, enterocyte differentiation in the cells in which they are highly expressed, and the lateral inhibition of adjacent cells driving the neighbour secretory differentiation (Baulies et al., 2020).

It is becoming apparent that the positioning of a stem cell within the niche and its resultant exposure to the differing gradients of signalling molecules is of as equal importance as the inherent clonogenicity and functional capacity of the stem cell itself. Indeed, Wnt isoforms and their downstream effectors are differentially expressed throughout the crypt-villus axis with those involved in proliferation and differentiation being expressed at the highest level at the crypt base (Gregorieff et al., 2005). Conversely, BMP activity increases along the crypt axis in the opposite direction with the crypt base being shielded from BMP activation by the secretion of BMP antagonists such as Gremlin1 and Noggin by Paneth and mesenchymal cells (Kosinski et al., 2007; Stzepourginski et al., 2017). The secretion of essential components of stem cell maintenance by Paneth cells dictates that stem cell homeostasis is shaped by the proximity of the two cell types. Paneth cells secrete Wnt3, an agonist of Wnt/βcatenin, epidermal growth factor (EGF), transforming growth factor α (TGF α) and Delta-like ligand1/4 (Dll1/4, ligands of Notch receptors) (Sato et al., 2011b). Accordingly, the immediacy and abundance of Paneth cell contact influences the potential for individual stem cells to become the dominant clone of the crypt. Those *Lgr5+* stem cells which are centrally placed and in contact with the greatest number of Paneth cells possess a survival advantage over those in contact with fewer Paneth cells at the niche border (Ritsma et al., 2014).

In contrast to small the small intestine, the colonic crypt stem cell population is less well characterised. Colonic crypts do not contain +4 cells, *Bmi1+* or Paneth cells however in place of the small intestinal Paneth cell, supportive cKIT+ (CD117) and Reg4+ cells secrete growth factors and Notch ligands which support *Lgr5+* cell homeostasis within the colonic crypt niche (Rothenberg et al., 2012; Sasaki et al., 2016).

1.7.4. Intestinal ageing

With increasing age numerous physiological changes occur within the gastrointestinal tract, collectively contributing to a functional decline. Colonic transit time is often increased in the ageing intestine and is linked with a reduction in the contractility of smooth muscle (reviewed in O'Mahony et al., 2002) and also myenteric neuron loss and changes in the gut microbiota (reviewed in Saffrey, 2013). The digestive function of the intestine is impaired with age and contributing to this are associated changes in the levels of hormones such as cholecystokinin (CCK) which stimulates the release of digestive enzymes from the pancreas (reviewed in Moss et al., 2012). Although found to be largely increased post-prandially in the elderly, a decreased sensitivity of the gall bladder to CCK has been reported with advancing age (Masclee et al., 1988). The reduction in absorptive capacity of the intestine in ageing individuals has previously been attributed to villus degeneration, with decreases in intestinal villus height (Höhn et al., 1978) and intestinal surface area (Keelan et al., 1985) described in ageing animal models. Further histological changes such as fewer, larger intestinal villi and reduced numbers of small intestinal crypts have been described in aged compared to young mice (Martin et al., 1998), however these findings have not been corroborated in humans nor have such changes been strongly linked with defective absorption.

In addition to the absorptive and digestive functions of the intestine, the epithelial surface of the intestine acts as a barrier against digestive enzymes and acid, microbes and ingested material all of which may be harmful to the underlying tissue. Epithelial enterocytes apically linked by tight junctions of claudin, zonulin and occludin proteins maintain a physical barrier in conjunction with the secretion of Muc2 containing mucus and antimicrobial peptides from goblet and Paneth cells respectively. Additionally, the immunoglobulin IgA is secreted by plasma cells into the luminal space in response to the presence of commensal bacteria (Macpherson et al., 2000). The diminishing integrity of the mucosal barrier and subsequent increase in intestinal permeability has been associated with increasing age for some time (Hollander & Tarnawski, 1985) however, the complex interplay between mucosal immunity, chronic inflammation and the host microbiota in driving this phenotype is more recent in its investigation. Although a recent study comparing numerous parameters such as mucus layer thickness, goblet and Paneth cell abundance and the transcriptomic analysis of genes related to innate and adaptive immunity of the young versus old murine intestine reports an

extensive impairment of barrier function with increasing age (Sovran et al., 2019), an equally comprehensive study in humans refutes the 'leaky gut hypothesis' and details the maintenance of intestinal barrier function in aged individuals (Wilms et al., 2020). The concept of 'inflammageing' in which a global pro-inflammatory phenotype evolves as the ability to deal with continuous antigenic exposure and stress decreases with advancing age (Franceschi et al., 2000) is supported by the work of Sovran et al. It is also supported by a study of the age-associated changes in innate immunity in the human small intestine (Man et al., 2015). Man et al. describe the increased expression of the pro-inflammatory cytokine interleukin-6 (IL-6) within the ageing ileum and an associated increased permeability to solutes mediated by the IL-6 induced expression of the tight junction protein claudin-2. In contrast, the work of Wilms et al. detected no differences in the expression of tight junction proteins in human colonic biopsies. These discrepancies may reflect differences in ileal versus colonic physiology, however the putative association of impaired barrier function and resultant increasing intestinal permeability with advancing age in human populations still requires further investigation.

In contrast, work characterising the intestinal microbiota of ageing populations is more abundant. Alterations in the function and physiology of the intestinal tract in concert with the dampened immunity, lifestyle changes and comorbidities of older age have implications on the gut microbiota profile which in turn impacts intestinal health and beyond. Disturbances in intestinal microbiota composition have been implicated in the pathogenesis of conditions such as diabetes (reviewed in Bleau et al., 2015) and Parkinson's disease (Forsyth et al., 2011), in addition to intestinal specific pathologies and as such represent a wide-ranging challenge to human health. Although a specific elderly microbiome profile has not been characterised, likely due to many confounding factors which may influence this signature more so than age, a general trend towards a decreased abundance of bifidobacteria coupled with increased levels of streptococci and Enterobacteriaceae has been observed (reviewed in An et al., 2018). Interestingly, the first extensive characterisation of elderly versus young faecal microbiota report an increased abundance of lactobacilli in the elderly profile (Mitsuoka, 1990), a genus which has also been documented as significantly increased in *PolγA*$^{mut/mut}$ versus *PolγA*$^{+/+}$ stool (Houghton et al., 2018). Probiotic supplementation with lactobacilli is generally considered to be advantageous in terms of host health. Lactate and urolithin A are the major metabolites of lactobacilli and in

addition to short chain fatty acids produced by numerous bacterial strains represent the key compounds by which intestinal health is promoted (Franco-Obregón & Gilbert, 2017). Microbiome diversity is promoted by urolithin A and also by short chain fatty acids such as butyrate. Furthermore, these compounds enhance their own production by augmenting the growth of bacterial strains that produce them. Butyrate is the primary colonocyte energy source, and its production is further facilitated by lactobacilli and bifidobacteria, as the lactate they generate can subsequently be converted to butyrate by alternate colonic bacterial strains. The connection between microbiome metabolites and mitochondria is an area which has received recent attention, and butyrate has been shown to rescue fatty acid β oxidation, oxidative phosphorylation and TCA cycling in mice in which these processes have been diminished by a germ-free intestinal environment (Donohoe et al., 2011). With reference to *Lactobacillus* supplementation, this has been shown to drive intestinal barrier repair via peroxisome proliferator activated receptor alpha (PPARα) activation and restoration of mitochondrial structure and fatty acid β-oxidation in the Simian immunodeficiency virus (SIV)-inflamed intestinal lumen of rhesus macaques (Crakes et al., 2019). With this in mind it may be presumed that an abundance of lactobacilli in the *PolyA*$^{mut/mut}$ colon could alleviate mitochondrial dysfunction to some extent. Also described in the *PolyA*$^{mut/mut}$ colon is a decreasing bacterial diversity from 4 months of age in comparison to *PolyA*$^{+/+}$ animals (Houghton et al., 2018) and as such, the benefit of profuse lactobacilli may therefore be negated by an apparent dysbiosis associated with this advanced ageing phenotype.

1.8. Colorectal cancer

After breast cancer in women and lung and prostate cancer in men, colorectal cancer (CRC) is respectively the second and third most commonly diagnosed cancer worldwide, and age is the biggest risk factor for CRC development. In 2018, colorectal cancer accounted for 9.2% of global cancer deaths (Bray et al., 2018). In addition to age, additional risk factors include environmental components such as smoking, a diet high in processed foods and alcohol and a sedentary lifestyle (Botteri et al., 2008; Cai et al., 2014; Wolin et al., 2009). While approximately 60-65% of colorectal cancers are sporadic, the remaining 35-40% are associated with genetic components that are heritable and confer an increased propensity towards CRC development (Graff et al., 2017; Lichtenstein et al., 2000). Although the

hereditary intestinal cancer syndromes such as Lynch syndrome and familial adenomatous polyposis (FAP) contribute to a relatively small (~5%) proportion of CRC cases (Jasperson et al., 2010), the genetic events that underlie these conditions are frequently observed in sporadic CRC and thus represent important molecular changes highly relevant to CRC pathogenesis (Muzny et al., 2012).

FAP is an autosomal dominant inherited condition characterised by the development of multiple polyps throughout the intestine. These polyps have the propensity to become malignant and as such, the condition places sufferers at an increased risk of colorectal cancer (Vogelstein & Kinzler, 2002). The *APC* gene resides in band q21-q22 of chromosome 5 and encodes a 312 kDa tumour suppressor protein (Groden et al., 1991; Kinzler et al., 1991). In cases of FAP, one copy of the gene is mutated, and its tumour suppressor function is perturbed. This truncating mutation is inherited with a somatically acquired mutational event impairing tumour suppression function at the second *APC* locus permitting the development of multiple benign polyps. This occurs as a result of the negative regulation the APC protein has on the Wnt signalling system; a critical pathway that controls self-renewal in stem cells of the colon, epidermis and haematopoietic system (reviewed in Reya & Clevers, 2005). The increased risk of colorectal cancer in FAP patients occurs as additional genetic and epigenetic changes facilitate disease progression. As *APC* is mutated in a large proportion of colorectal cancers it is considered a major event in tumorigenesis and forms the initiating event in the adenoma-carcinoma sequence; a pathway that leads to approximately 80% of CRCs (Fearon & Vogelstein, 1990).

Historically, colorectal cancers have been classified using the Dukes system in which the stages A, B, C and D indicate the extent of tumour growth from the lowest stage (A) where the tumour remains epithelial in its location to more advanced stages in which the tumour has grown through the bowel musculature (B), to regional lymph nodes (C) and to the most advanced stage of metastatic dissemination (D) (Dukes, 1932). Using similar principles, the tumour, node, metastases (TNM) staging system has been developed by the American Joint Committee on Cancer/Union Internationale Contre le Cancer (AJCC/UICC) and is widely used in the evaluation of CRC patient prognosis today, however the disparity in prognosis between patients of the same stage has deemed this system unsatisfactory (Dienstmann et al., 2017). Colorectal cancers are extremely heterogeneous in nature with tumour location

(left-sided versus right-sided), molecular features (microsatellite instability, MSI; chromosome instability, CIN; and CpG island methylator phenotype, CIMP discussed further in subsequent sections) and the tumour microenvironment all contributing to patient survival but not assessed by TNM staging. Accordingly, additional systems have been developed in order to better stratify the disease and thus patient outcome. As a result of several large genomic investigations, the consensus molecular subtypes (CMS) of colorectal cancer were described in 2015 (Guinney et al., 2015). Each subtype (MSI immune, CMS1; canonical, CMS2; metabolic, CMS3; and mesenchymal, CMS4) possesses a distinct set of molecular features which can assist in the prediction of patient outcome and response to particular therapies. While this specific subtyping is beneficial with regards patient management, the transcriptomic, genomic and proteomic analyses required to delineate CRCs in this manner are not readily applicable to routine pathology (reviewed in Roseweir et al., 2017). As such, several histological subtyping protocols have been developed in order to provide additional prognostic value with the use of routine histological tissue sections. The tumour microenvironment, in particular the stromal and immune infiltrate is an important determinant of CRC progression and is easily evaluated with the analysis of H&E and immunohistochemically labelled tissue sections. The Galon Immunoscore (GI) (Galon et al., 2006; Galon et al., 2014; Pagès et al., 2010), Klintrup- Mäkinen (KM) grade (Klintrup et al., 2005) and combined KM/tumour stroma percentage (TSP), the Glasgow Microenvironment Score (GMS) (Park et al., 2015) have been shown to associate with CMS subtyping, patient prognosis and with adjuvant chemotherapy response (Alexander et al., 2020; Becht et al., 2016; Marliot et al., 2020; Roseweir et al., 2020).

While surgical resection is the most common primary treatment for colorectal cancer, this is not always curative and treatment regimens are guided by TNM stage, tumour location, histological, molecular and phenotypic characteristics, and patient specific factors such as age or existing comorbidities. For example, patients in which tumour invasion of the colonic musculature has not occurred, adjuvant therapies are not always administered. In patients in which lymph node involvement or metastases are detected, a combination of chemotherapy, targeted therapies and immunotherapies are often required to target residual malignant cells, prevent recurrence and to restrict the growth of inoperable lesions. Fluoropyrimidine-based therapeutics have been the mainstay of CRC adjuvant chemotherapies for over 50 years (Heidelberger et al., 1957) with the addition of oxaliplatin

(forming the FOLFOX regime) further improving survival (André et al., 2009; Kuebler et al., 2007). Left-sided colorectal cancer patients with microsatellite stable lesions benefit more from fluoropyrimidine based regimes in comparison to patients with right-sided MSI high or CMS4 lesions in which these conventional therapies are less effective (De Sousa E Melo et al., 2013; Ribic et al., 2003). Additionally, the specific fluoropyrimidine administered has been shown to have differential effects within CMS immune subtype stage III or GMS low tumours with these lesions responding better to FOLFOX rather than the fluoropyrimidine precursor capecitabine based CAPOX regime (Alexander et al., 2020; Roseweir et al., 2020). Targeted therapeutics such as anti-VEGF monoclonal antibodies which target angiogenesis (bevacizumab, regorafenib) and anti-EGFR therapies (cetuximab and panitumumab) are also selected based upon tumour classifications. While patients with left-sided lesions can benefit from anti-VEGF and anti-EGFR therapeutics, right-sided lesions are largely refractory to anti-EGFR agents (Venook et al., 2016). Similarly, *RAS* and *RAF* mutational status are important determinants of targeted therapies with *RAS* and *RAF* wild type lesions responding well to targeted agents in addition to conventional chemotherapies while no benefit is seen in *RAF* mutant lesions (Heinemann et al., 2014; Pietrantonio et al., 2015; Venook et al., 2017). Finally, immunotherapeutic agents constitute an additional arm of CRC treatments in which much like chemo and targeted therapeutics, response to treatment is influenced by specific tumour characteristics. For example, the anti-PD-1 inhibitor pembrolizumab has shown promise in the treatment of right-sided/MSI-high/CMS1 tumours in comparison to MSI stable lesions (Le et al., 2015). To summarise, the appropriate staging and subtyping of colorectal cancers is vital in guiding the selection of efficacious treatment plans in order to provide patients with the most favourable outcomes.

1.8.1. The adenoma-carcinoma sequence and chromosome instability

The seminal work by Fearon and Vogelstein, describes the development of CRC as an accumulation of mutations, each facilitating progression through individual stages in what is referred to as the adenoma–carcinoma sequence (Fearon & Vogelstein, 1990). In this model, the primary mutational event activates the Wnt pathway and initiates the epithelial transition from normal to polypoid tissue. Subsequent mutations over a number of years drive progression to adenoma and carcinoma. Typical mutational events within this pathway include the oncogenic activation of *RAS* genes. The Ras proteins encoded by *RAS* genes are

small GTPases that relay signals from the cell surface to the nucleus via effector pathways such as the PI3K-Akt survival pathway (Rodríguez-Viciana et al., 1994; Sjölander et al., 1991) and the RAS-RAF-MEK-ERK-MAPK mitogenic pathway (Moodie et al., 1993; Warne et al., 1993). Their tumorigenic effects are mediated when mutant oncogenic Ras proteins are locked in an active GTP bound state, constitutively activating their target pathways (Trahey & McCormick, 1987). Chromosomal instability (CIN) is a characteristic feature of colorectal malignancies that evolve via this pathway with deletion of the long arm of chromosome 18 being a common event associated with poor prognosis (Popat & Houlston, 2005). Residing at this location are genes encoding members of the SMAD family of proteins that function as mediators of the TGFβ and BMP signalling pathways (reviewed in Attisano & Tuen Lee-Hoeflich, 2001). *SMAD4* loss in particular is associated with colorectal cancer, concomitant inactivation of TGFβ facilitating tumour progression following *Apc* loss (Takaku et al., 1998) and resistance to fluorouracil-based therapeutics (Boulay et al., 2002).

A critical event in the adenoma-carcinoma sequence that promotes invasive transition of CIN phenotype CRCs is inactivation of the tumour suppressor *p53* (Baker et al., 1989; Baker et al., 1990a; Baker et al., 1990b). First discovered in 1979 as a protein bound to the simian (SV40) oncogenic DNA virus, and initially thought to be a proto-oncogene (Lane & Crawford, 1979; Linzer & Levine, 1979; Rotter et al., 1980), the p53 tumour suppressor protein encoded by the *TP53* gene is mutated in around 50% of human colorectal cancers (Bouaoun et al., 2016). Wild type p53 is activated in response to cellular stress, and via its function as a transcription factor can induce metabolic homeostasis, DNA repair and antioxidant defence, and under severe stress, cellular senescence, cell-cycle arrest, and apoptosis (Levine & Oren, 2009). Due to such functions, the loss of wild type p53 as is the case in roughly half of all human cancers has a fundamental role in tumour development. In addition to loss of the wild-type function of p53, point mutations in the *Tp53* gene can confer gain of function properties on the mutant protein which in the cancer setting can promote tumour progression via an increased level of genome instability or enhanced metastatic potential (Lang et al., 2004; Olive et al., 2004).

1.8.2. The serrated pathway and molecular phenotypes

Despite the high prevalence of *APC* loss in human colorectal cancer, this event is not essential for tumorigenesis and around 20% of cases are wild type for *APC.* Lesions within this group differ histopathologically from those of the 'classical' *APC* loss Wnt-dependant pathway and they present with a more "saw-toothed" or serrated morphology than 'traditional' adenocarcinomas (Hawkins et al., 2002). Accordingly, they are termed serrated lesions and precursor foci are categorised into sessile serrated and the less frequently diagnosed traditional serrated adenoma. While *APC* and Wnt driven CRCs originate in the stem cell compartment of the intestinal crypt (Barker et al., 2009), serrated CRCs originate from progenitor cells outside the stem cell niche. In the case of traditional serrated adenomas, the disruption of BMP signalling as a result of increased expression of the BMP antagonist *GREM1* drives progenitor cell expansion and ectopic crypt formation (Davis et al., 2015). This precedes a major genetic event which is common to the majority of serrated adenomas; the acquisition of an activating mutation within the *BRAF* proto-oncogene (Kambara et al., 2004). RAF proteins exist in three forms within humans: ARAF, BRAF and CRAF. These serine/threonine kinases function downstream of RAS proteins as part of the RAS-RAF-MEK-ERK-MAP kinase pathway (Carragher et al., 2010; Davies et al., 2002; Marais & Marshall, 1996). An activating mutation in the *BRAF* gene brings about constitutive signalling through this pathway, and although primarily associated with malignant melanoma, *BRAF* mutations are associated with an incidence of up to 22% in colorectal cancer (Davies et al., 2002; Garnett & Marais, 2004). Also common within lesions developing via this pathway, more so with those of the traditional serrated phenotype, is an activating mutation in the *KRAS* gene (Jass et al., 2006; O'Brien et al., 2006). *BRAF* and *KRAS* mutations, however, are considered to be mutually exclusive from one another (Rajagopalan et al., 2002). In contrast to the chromosomal instability observed in *APC*-Wnt mediated colorectal neoplasms, colorectal tumours of the serrated phenotype are typically characterised by a CpG island methylator phenotype (CIMP) which leads to high levels of epigenetic modulation of gene expression via DNA hypermethylation at CG repeats within gene promoter regions (Toyota et al., 1999). Methylation of tumour suppressor promoters such as that of the p16 cell cycle regulation protein allows benign serrated lesions to evade the oncogene induced senescence associated with initiating *BRAF* mutations (Michaloglou et al., 2005; Serrano et al., 1997).

Also secondary to CIMP, aberrant methylation of DNA mismatch repair genes leads to an additional CRC molecular phenotype known as microsatellite instability (MSI) (Weisenberger et al., 2006). Microsatellite instability describes the frequent insertion and/or deletion of nucleotides at microsatellite sequences throughout the genome and while often observed in association with *BRAF*-mediated CIMP, this phenotype also occurs independently of CIMP as is demonstrated by hereditary non-polyposis colon cancer (HNPCC), also known as Lynch Syndrome. HNPCC is characterised by a susceptibility to colorectal cancer that is inherited in an autosomal dominant manner. First studied by Warthin in 1913 (Warthin, 1913) and later described by Lynch (Lynch et al., 1966), Lynch syndrome is caused by a defective DNA mismatch repair system attributable to a germline mutation in at least one of the mismatch repair genes; mutL homolog 1 (*MLH1*), mutS homolog 2 (*MSH2*), mutS homolog 6 (*MSH6*) and post meiotic segregation increased 2 (*PMS2*). Microsatellite instable colorectal cancers also occur via somatic acquisition of mutations in DNA mismatch repair genes and are estimated to account for 10-15% of sporadic CRCs (Ionov et al., 1993). Progression of microsatellite instable CRCs is associated with the inactivation of tumour suppressor function via microsatellite mutation of the TGFβ receptor gene *TGFβR2* (Markowitz et al., 1995) and the apoptosis promoting *BAX* (Rampino et al., 1997).

While the serrated pathways of colorectal carcinogenesis have traditionally been considered as occurring independently of the Wnt activation epitomised by *APC* loss mediated colorectal carcinogenesis, recent studies identifying the presence of Wnt activating mutations in both sessile and traditional serrated colorectal cancers (Giannakis et al., 2014; Sekine et al., 2016; Seshagiri et al., 2012) suggests that despite their fundamental differences there is much overlap between CRC phenotypes. Figure 1-6 depicts the molecular pathways of colorectal carcinogenesis.

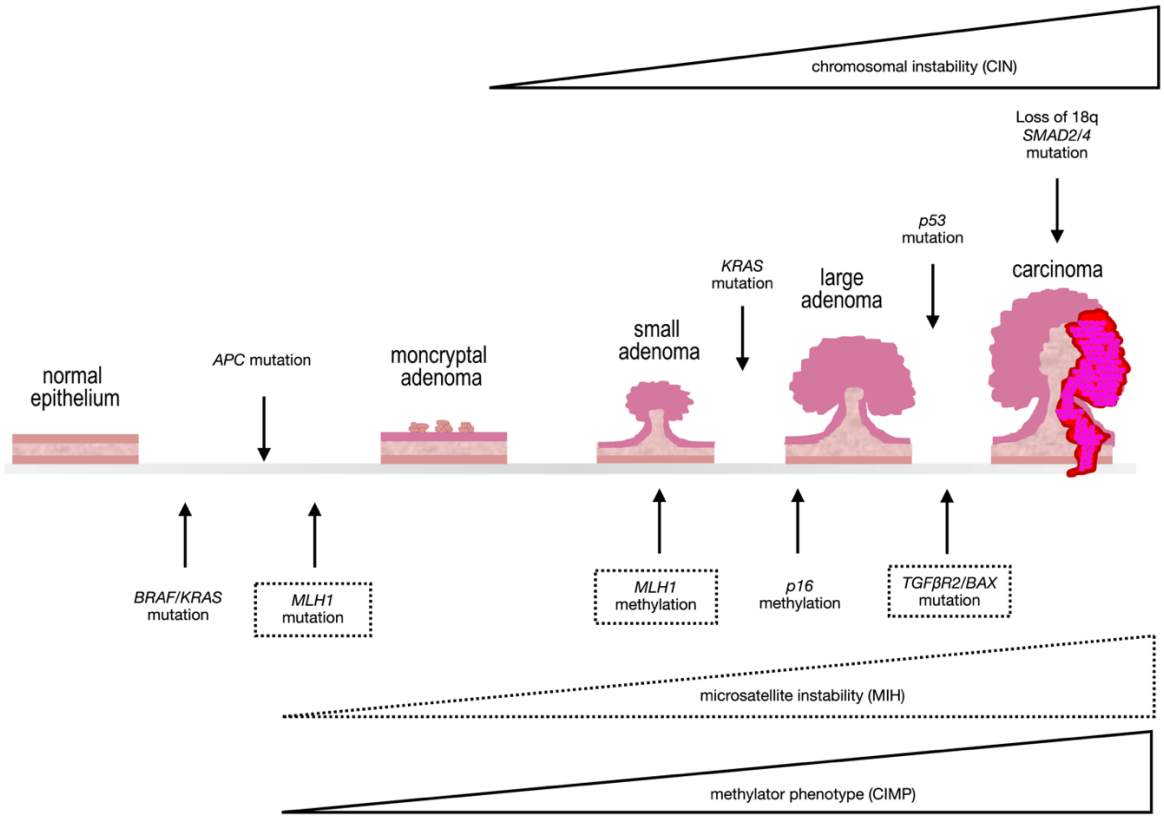

Figure 1-6. Molecular pathways of colorectal carcinogenesis. Major genetic events contributing to tumorigenesis are indicated with black arrows. The conventional *APC*-Wnt mediated adenoma-carcinoma sequence is presented above the schematic with the serrated pathway being presented below. Dashed lines indicated events associated with a microsatellite unstable phenotype. Image adapted from (Kaiser et al., 2014).

1.8.3. Colorectal cancer stem cells

Colorectal cancer is an extremely heterogeneous disease, demonstrating a great variety of genotypic and phenotypic traits. The cell of origin likely contributes to this inter-tumoral heterogeneity and plays an important role in defining tumour features. Specific activation of Wnt signalling in *Lgr5+* and *Bmi1+* stem cells results in adenoma generation, leading to the supposition that intestinal stem cells are the cells of origin of colorectal cancer (Barker et al., 2009; Sangiorgi & Capecchi, 2008). Capable of generating an extensive adenoma burden at a rapid rate, these models provide insights into a cell-autonomous mode of tumour initiation, however multiple epigenetic and micro-environmental factors create a more complex interplay in the human situation.

It is suggested that a hierarchical organisation exists within human colorectal cancers with a small population of cancer stem cells (CSCs) driving tumour growth and self-renewal, in addition to a larger population of tumour cells at advanced stages of differentiation

(Vermeulen et al., 2008). CSCs are defined as such by their ability to generate a phenotypic copy of the original tumour and its differentiated progeny upon xenotransplantation (Clarke et al., 2006). Furthermore, CSCs are considered important drivers in disease relapse. While non-stem tumour cells may be eradicated by conventional chemotherapies, cancer stem cells may persist and facilitate subsequent tumour recurrence (reviewed in Batlle & Clevers, 2017). Much as normal stem cells respond to niche signals; it is becoming apparent that CSCs are also influenced by their micro-environment to the extent that differentiated tumour cells can acquire CSC characteristics in response to myofibroblast-derived signals (Vermeulen et al., 2010). Additionally, an increase in signalling mediated by NF-kB, a transcription factor involved in regulation of inflammation, has been shown to enhance Wnt activation and bring about the de-differentiation of non-stem cells bestowing them with tumour-initiating capabilities (Schwitalla et al., 2013). Together, such observations suggest that stemness is in fact a fluid state with the convergence of genetic, epigenetic and micro-environmental factors shaping the stem cell pool, the malignancies they drive and indeed a plasticity that provides them with chemotherapeutic resistance.

Numerous molecular markers have been identified and posited as colorectal cancer stem cell specific. For example, epithelial cell adhesion molecule (EpCAM) and CD166 (Dalerba et al., 2007), aldehyde dehydrogenase 1 (ALDH1) (Huang et al., 2009) and Lgr5 (Barker et al., 2009; Barker et al., 2007) have been well characterised. Originally identified as a marker of haematopoietic stem and progenitor cells; CD133 (Yin et al., 1997), as also known as prominin-1 glycoprotein has also been described as a colorectal cancer stem cell marker with CD133+ colon cancer cells capable of reproducing the original tumour in immunodeficient mice (O'Brien et al., 2007; Ricci-Vitiani et al., 2007). Furthermore, the expression of CD133 has been associated with an enhanced apoptotic evasion via the production of IL-4 by CD133+ species (Todaro et al., 2007). A contradictory report, however, describes the same property in CD133- cells, thus questioning the stem cell specificity of the marker. The same study however identifies the metastatic CD133- population as more aggressive and positive in the expression of another CRC stem cell marker; CD44 (Shmelkov et al., 2008). CD44 is a transmembrane glycoprotein involved in the regulation of cell-cell interactions, migration and adhesion (Spring et al., 1988). The malignant potential of CD44+ cells were first described in rat pancreatic carcinoma and mammary adenocarcinoma cell lines (Günthert et al., 1991) however CD44+ colon cancer cells have since been characterised as tumorigenic in

nude mice with CD44 knockdown inhibiting xenograft growth (Du et al., 2008). The interaction of CD44 with components of the extracellular matrix, namely hyaluronan has additionally been described as a key connection that promotes colon carcinoma cell invasion (Kim et al., 2004). Given the involvement of colorectal cancer stem cells in critical aspects of tumour biology, an in depth understanding of these species aided by their specific markers may elucidate their vulnerabilities. In addition to traditional therapeutics that eliminate the non-stem tumour bulk, this may represent an important means by which the persistent cancer stem cells are also targeted and the efficacy of cancer therapies augmented.

1.8.4. Mouse models of intestinal cancer

One of the first mouse models of intestinal cancer was developed in 1990 during a mouse germline mutagenesis project (Moser et al., 1990). Male mice were treated with the mutagen ethylnitrosourea (ENU) and subsequently mated with females. A progressive anaemia was reported in the offspring of this cross, as was the incidence of multiple adenomas throughout the length of the murine intestine. Described as *Min*/+ (multiple intestinal neoplasia) mice, their phenotype was later shown to be caused by a nonsense mutation in codon 850 of the murine homolog of the *APC* tumour suppressor gene (Su et al., 1992). The administration of ENU caused a loss of function mutation at codon 850 of the murine *Apc* gene with spontaneous loss of heterozygosity occurring as the second *APC* allele is lost during adulthood. This model mimics the inherited autosomal dominant human disorder of familial adenomatous polyposis coli (FAP) in which a germline *APC* mutation is inherited, allowing the development of multiple colorectal polyps with loss of heterozygosity (Groden et al., 1991). Malignant transformation of these polyps occurs following additional genetic and epigenetic changes and as such, FAP patients are at great risk of the development of colorectal carcinoma. Although the *APC* gene is mutated in the majority of human colorectal cancers (Goss & Groden, 2000), malignant transformation of adenomas in mice carrying an *APC* mutation alone are very rare. This is likely due to the large tumour burden and resultant bowel obstruction coupled with the short life span of the animal. In order to model another hereditary colorectal cancer syndrome, homozygous *Msh2−/−* germline knock out mice were developed in 1995 (Reitmair et al., 1995). Despite its similarity to human HNPCC, and its promise for use in such modelling, the *MSH2* mutation was not

restricted to the intestine. Its global effect on the *MSH2* genes of other tissues and organ systems resulted in the prolific development of lymphoma and hence a reduced lifespan.

Villin is an actin binding protein associated with the microfilament core of mammalian intestinal epithelial cell microvilli (Bretscher & Weber, 1979). The Cre-Lox system has been utilised to excise *MSH2* specifically in intestinal cells by crossing $Msh2^{LoxP}$ mice with animals carrying a *Villin-Cre* transgene (Kucherlapati et al., 2010). Cre-Lox technology has also been used to excise *APC* in a tissue-specific manner with additional experimental control in the form of inducible Cre expression (Sansom et al., 2004). *CYP1A* is a member of the cytochrome P450 family extensively expressed in the intestine. It becomes transcriptionally active upon the addition of lipophilic xenobiotics such as β-napthoflavone. If *Cre* is inserted under the *CYP1A* promoter, administration of β-napthoflavone initiates expression of *Cre* and the subsequent recombination of *LoxP* sites. This *AhCre* mouse has been crossed with strains of mice expressing defective forms of other genes implicated in the development of CRC. The consequences of the loss of the p53 tumour suppressor was shown when the *AhCre* $Apc^{fl/+}$ mouse was crossed with animals containing an inducible knock-in allele of mutated *p53* ($Tp53172^{H/+)}$. Invasive adenocarcinoma had not been observed in the aforementioned mouse models, however all mice in the *AhCre* $Apc^{fl/+}$, $Tp53172^{H/+}$cohort demonstrated invasive adenocarcinoma, providing an excellent model for the later stages of CRC and the role that mutant p53 plays in its development (Muller et al., 2009).

In 2007, the Wnt target gene *Lgr5* (leucine-rich-repeat-containing G-protein-coupled receptor 5) was discovered as a marker of stem cells of the small intestine and colon. (Barker et al., 2007). The later identification of *Lgr5* positive stem cells as the cells-of-origin of intestinal cancer, marked an extremely important discovery in the study of colorectal cancer and hence the mouse models used to characterise it (Barker et al., 2009). A gene knock in model was created via homologous recombination of *EGFP-IRES-creERT2* into the first exon of *Lgr5*. This cassette expressing enhanced green fluorescent protein (EGFP) allowed for microscopic visualisation of *Lgr5* positive crypt base stem cells, with the *creERT2* component of the cassette allowing for *Cre-Lox* mediated gene excision. With the previously described *AhCre* $Apc^{fl/+}$ mouse, deletion of *Apc* occurred in all cell types throughout the intestine. The discovery of the *Lgr5* gene enabled stem-cell specific deletion of *Apc* to be induced by crossing the *Lgr5-EGFP-IRES-creERT2* mice with $Apc^{flox/flox}$ mice (Barker et al., 2009). An

intraperitoneal (IP) injection of tamoxifen allowed translocation of creERT2 to the nucleus, recombination of *LoxP* sites and excision of *Apc*. With the induced loss of *Apc*, microadenomas formed throughout the small intestine and colon. Upon histological analysis, these lesions were found to be expressing high levels of β-catenin, indicative of Wnt signalling activation mediated through deletion of *Apc*.

Although the *APC* gene is lost in the majority of human colorectal cancers, *APC* loss alone is not sufficient to drive the progression of adenoma to carcinoma, to invasive disease and metastases. According to the classical pathway described by Fearon and Vogelstein, the progression from an adenomatous lesion to full-blown metastatic disease is a multistep sequence initiated by the loss of *APC* but propagated to more advanced disease stages by additional genetic and epigenetic changes (Fearon & Vogelstein, 1990). As around 40% of human colorectal cancers carry a mutation in the *KRAS* proto-oncogene (The Cancer Genome Atlas et al., 2012), mouse models combining oncogenic *Kras* mutations with *Apc* loss have been developed in order to better recapitulate human pathology. Mice with both *Apc* loss and the expression of an oncogenic $Kras^{V12}$ allele display accelerated adenoma growth and stromal invasion in comparison to mice bearing mutated *Apc* alone (Janssen et al., 2006; Sansom et al., 2006). Similarly, the introduction of a loss of function mutation in the *p53* tumour suppressor gene in mice with an $Apc^{Min/+}$ background increased tumour burden and invasiveness (Halberg et al., 2000).

Mouse models of intestinal cancer with *Apc* loss as the initiating mutation are often characterised by a rapid accumulation of adenoma burden predominantly within the small intestine. Animals in which both copies of *Apc* are lost simultaneously quickly become ill with euthanasia becoming necessary as soon as 5 days post *Apc* deletion (Sansom et al., 2004). In order to extend the latency of disease potentially allowing pathology to progress, a *Cre*-expressing adenovirus was surgically administered to only the colons of mice homozygous for floxed *Apc.* In line with human colorectal cancer, this method restricted the development of adenomas to the distal colon, with a lower level of *Cre*-recombination reducing tumour multiplicity. A small proportion of these lesions demonstrated invasion of the muscularis with stromal reactions and were thus classified as carcinomas. The progression of adenoma to carcinoma was further enhanced by the addition of an activated *Kras* allele with around 20% of animals demonstrating liver metastases, thus describing the first report of a

metastatic *Apc* mouse model of colorectal cancer (Hung et al., 2010). Further evidence supporting the role of *Kras* mutations in driving and maintaining colorectal cancer invasion and metastases comes from a similar model described in 2017 in which mice were administered with a syringe-delivered colonic tamoxifen enema in order to restrict *Cre*-recombination to the colon (Boutin et al., 2017). *CreERT2* expression was controlled by the intestine specific *Villin* promoter, and the excision of floxed *Apc* and *p53* genes achieved upon induction with tamoxifen. These iKAP mice also harbour an inducible *tet-O-LSL-Kras*^{G12D} allele, which upon the administration of doxycycline facilitates the activation of the most common glycine (G) to aspartic acid (D) substitution at codon 12 of the *Kras* gene. When compared to mice with only *Apc* and *p53* deactivation (iAP), iKAP mice demonstrated an increased incidence of invasion and metastases. No metastases were observed in iAP mice whereas 25% of iKAP mice progressed through a complete adenoma-adenocarcinoma-metastases sequence. Further support for the role of activating *Kras* mutations in colorectal cancer invasion and metastasis was evidenced upon the histological analysis of tumours. GFP tagged *Kras*^{mut} were identified via anti-GFP antibody labelling with activation status verified with the use of an anti-pERK antibody; pERK signalling being a downstream consequence of *Kras* activation. As is the case in human CRC, a heterogeneous population of *Kras* clones were observed within the same tumour. Interestingly, within these heterogeneous lesions, GFP/pERK positive (*Kras*^{mut}) clones were localised to the invasive front of the tumour with GFP/pERK negative clones comprising the tumour bulk. The overwhelming presence of GFP/pERK positive cells within tumour metastases strongly suggests the selection of *Kras*^{mut} clones, highlighting the role of oncogenic *Kras* in CRC progression.

Modelling the serrated pathway of colorectal carcinogenesis, Carragher *et al*. describe a an intestine specific *Braf* ^{V600E} mutation in driving the development of hyperplastic intestinal crypts with a serrated epithelium via activation of the MEK/ERK cascade (Carragher et al., 2010). However, this mutation alone was not sufficient to maintain the hyperproliferative phenotype and oncogene induced crypt senescence was observed at later time points. High levels of expression of the senescence marker p16^{Ink4A} corroborated this observation, with subsequent inactivation of p16^{Ink4A} allowing tumour progression. This senescence inactivation and tumour progression was found to be associated with the *de novo* methylation of multiple CpG islands within p16^{Ink4A} exon 1, a finding that was corroborated at a later date by another *Braf* ^{V600E} induced mouse model of intestinal tumorigenesis (Rad et

al., 2013). The inactivation of p16 or expression of a gain of function mutant p53 in these mice permitted the development of metastases in 25% of animals.

Commonly found in CRCs with high rates of microsatellite instability are mutations in the *TGFBR2* gene which encodes a receptor for the cytokine, transforming growth factor β (TGF-β). TGF-β has an inhibitory effect on epithelial cell growth and thus loss of this inhibition is associated with tumour development (Wu et al., 1992). Loss of TGF-β signalling via intestine specific deletion of the *Tgfbr2* gene in mice is not sufficient for tumorigenesis. However, the loss of *Pten,* a negative regulator of the PI3K/Akt pro-survival pathway which is hyperactive in 40% of CRCs, results in the development of adenomas progressing to carcinomas with an 8% incidence of metastases (Parsons et al., 2005; Yu et al., 2014). Similarly, lung and regional lymph node metastases are observed in mice with an activating *Kras* mutation in addition to *Tgfbr2* loss. This cooperation facilitates the development of metastases in 15% of these animals, notably without the involvement of *Apc* (Trobridge et al., 2009).

1.8.5. Organoid models of intestinal cancer

Genetically engineered mouse models (GEMMs) have undoubtedly been fundamental in the understanding of the pathophysiology of many types of cancer. The discovery of novel cancer genes and the elucidation of signalling pathways involved in tumorigenesis are to name but two areas in which substantial knowledge has been gleaned from the use of animal models. Despite their obvious merit, it has been argued that animal models of cancer do not faithfully recapitulate human disease with species-specific differences influencing *de novo* tumour development and responses to therapeutics. The generation and establishment of GEMM colonies is also time consuming and can be costly due to animal housing expenses over lengthy study periods. In order to maintain the pathophysiological features of human malignancies, models utilising human tissue have been developed. Patient-derived primary tumour samples provide the material from which 2D cancer cell lines are expanded. Although they are relatively quick to set up and easier to maintain than animal models, not all clones expand efficiently and those that do may have acquired multiple genetic changes rendering them significantly distinct from the original tumour from which they were derived. Despite the first long-term culture of normal human cells and their formation into 3D tissue structures being described in 1975 (Rheinwald & Green, 1975), it

has not been until the last decade that the use of "organoids" in cancer biology research has become well-established. Defined as 3D tissue structures that mimic the cellular lineage and spatial organisation of the organ system from which they are derived, organoids are initiated from either pluripotent embryonic stem cells, induced pluripotent stem cells or organ specific adult stem cells (Clevers, 2016). With regard to intestinal culture and generation of intestinal organoids, Evans *et al.* succeeded in isolating crypt and villus units from rat small intestine, maintaining their structural integrity and propagating the cultures for up to 1 month (Evans et al., 1992). They describe the proliferation of intestinal epithelial cells *in vitro* as being critically dependent upon this structural integrity and the provision of factors by stromal cells which are otherwise absent in 2D culture systems; a significant limitation of such systems. With the later identification of *Lgr5+* stem cells as the crypt base columnar (CBC) stem cells from which all intestinal epithelial cell types originate (Barker et al., 2007) and the elucidation of the growth factors which tightly control their self-renewing capacity, more robust organoid culture techniques have been developed. Embedded within a laminin-rich, crypt base mimicking 3D gel matrix, single *Lgr5+* stem cells were provided with essential components of the stem cell niche. Polarised small intestinal crypt-villus units developed, self-renewed and under the correct conditions could be maintained indefinitely, notably without the requirement for a supportive stromal cell network (Sato et al., 2009).

The major orchestrator of stem cell self-renewal and proliferation is the Wnt signalling pathway. Briefly, extracellular Wnt binds to the cell surface receptors, Frizzled (Fz) and Lrp5/6 which results in an accumulation of cytoplasmic β- catenin. Translocation of β-catenin to the nucleus and its subsequent interaction with TCF/LEF transcription factors facilitates the activation of target genes such as c-myc and cyclin D1, initiating proliferation. Indeed, mice lacking the Tcf4 transcription factor do not maintain proliferative crypt-villus units; their epithelium consists of differentiated, non-dividing cells (Korinek et al., 1998). R-spondin1 is a Wnt agonist which acts via the Lgr5 receptor (Kim et al., 2005) and is thus an essential component of the crypt culture media. The addition of Wnt3a, another Wnt agonist, indefinitely extends the growth period of normal colon crypt cultures, overcoming the inherent low level of Wnt produced in the colon in comparison to the small intestine (Sato et al., 2011a). Further essential components of the culture media include the mitogenic epidermal growth factor (EGF) and Noggin, an inhibitor of the BMP pathway. BMP signalling represents the second major system crucial to the control of self-renewal and proliferation

of stem cells in the intestinal crypt, acting as an inhibitor of these processes by supressing Wnt signalling (He et al., 2004). Fine tuning of the media is required under certain circumstances such as in the case of single cell starting material as opposed to whole intestinal crypts. Anchorage-dependant single cells which have been dissociated from the extracellular matrix (ECM) undergo anoikis, a form of cell death initiated by the removal of the supportive signals their ECM anchorage provides. When added to the media, the Rho kinase inhibitor Y-27632 inhibits this process enabling cellular survival (Watanabe et al., 2007).

As *APC* loss is concomitant with constitutive Wnt activation, culture of *APC* deficient adenomas or adenocarcinomas does not require R-spondin1. Similarly, Sato and colleagues found the addition of Noggin and EGF to the media to be non-essential to the long-term propagation of mouse *Apc* deficient adenoma organoids nor human adenocarcinoma organoids. Recent advances in genetic engineering techniques such as clustered regularly interspaced short palindromic repeat (CRISPR)-Cas9 technologies are easily applied to organoid cultures, and as such increase the capacity for genome manipulation, further validating cancer organoids as invaluable research tools (Cho et al., 2013; Cong et al., 2013; Jinek et al., 2012; Jinek et al., 2013; Mali et al., 2013). The system has been used to introduce key colorectal cancer mutations into normal human intestinal organoids, thus modelling the sequential occurrence of these genetic events *in vitro* (Drost et al., 2015; Matano et al., 2015). Applying knowledge gained in the laboratory back to patients within the clinic is the unanimous end goal of biomedical research. With an expanding range of treatment options for cancer patients alongside the extremely heterogeneous nature of the disease, it is often difficult to predict which patients will respond to which therapies, if at all, with many undergoing arduous rounds of chemotherapy and only experiencing side effects. The use of patient derived colorectal cancer organoids successfully predicted patient response to irinotecan-based therapies in over 80% of patients included in a recent study (Ooft et al., 2019). Cancer organoids can be maintained long-term, retaining the genotypic and phenotypic features of the tumour from which they are derived, with this recent work supporting their role in a translational as well as basic research setting. While the advantages of organoid models in terms of reproducibility, ease of genetic manipulation, relative cost and experimental duration are evident, there are disadvantages associated with their use. Although organoids provide a superior representation of tissue structure and

physiology in comparison to 2D cell lines, the complexity of an organoid system is inferior to alternative models. In the cancer setting, the interaction of malignant cells with the tumour microenvironment (TME) is critical to tumour survival, however this interaction cannot be recapitulated with an organoid model. Patient-derived explant (PDE) cultures provide a model by which the removal and subsequent culture of a fresh tumour resection retains the original stromal architecture in addition to that of the tumour. Given the preservation of intra-tumour heterogeneity in addition to the microenvironment, patient derived explant models offer a valuable platform from which patient-specific therapeutic responses can be evaluated (Brijwani et al., 2017; Majumder et al., 2015). Alternatively, patient derived organoids may be co-cultured with patient derived TME cells such as immune cells or cancer associated fibroblasts in order to better model cellular interactions and thus improve biological relevance (reviewed in Fiorini et al., 2020).

1.8.6. Mitochondria and malignancy

Almost 100 years ago, Otto Warburg postulated that tumour cells preferentially utilise aerobic glycolysis as their primary means of energy production. In comparison to non-malignant tissues, the uptake and utilisation of glucose by tumours was described as considerably elevated (Warburg, 1956). This characteristic, which is observed despite the availability of sufficient oxygen, is still utilised today in aiding tumour diagnosis and treatment monitoring as the uptake of radioactively labelled glucose can subsequently be imaged with positron emission tomography (PET) (reviewed in Almuhaideb et al., 2011). In terms of ATP production, glycolysis represents a much less efficient system yielding two molecules of ATP per molecule of glucose in comparison to the 36 generated via mitochondrial oxidative phosphorylation. Although in part compensated for by the increased expression of glucose transporters and concomitant increase in uptake of glucose, a predominantly glycolytic metabolism bestows tumour cells with a greater abundance of glycolytic intermediates available for diversion into biosynthetic pathways such as the branching of glucose-6-phosphate into the pentose phosphate pathway, key enzymes of which are commonly overexpressed in cancer (Wang et al., 2011; Xu et al., 2009). This pathway generates ribose sugars required for nucleic acid synthesis and also NADPH which supports fatty acid synthesis and antioxidant defence (reviewed in Patra & Hay, 2014). Similarly, the diversion of fructose-6-phosphate into the hexosamine pathway has been

shown to provide substrates required for glycosylation of proteins contributing to increased proliferation and progression of colorectal cancer (Vasconcelos-dos-Santos et al., 2017). The primary growth and proliferation concerns of the tumour are thus facilitated by a glycolytic shift, however it is becoming apparent that this shift is not an event that occurs passively but as a result of active reprogramming driven by the tumour itself (reviewed in Hanahan & Weinberg, 2011). Growing evidence suggests that the main function of oncogenes and tumour suppressors is to regulate metabolism, having evolved primarily for this purpose. Members of the MYC family of transcription factors are commonly deregulated, overexpressed and oncogenic in many human cancers. MYC has been shown to promote tumour anabolism via an upregulation of the glucose transporter GLUT1 and increasing the expression of glycolytic enzymes such as glyceraldehyde-3- phosphate dehydrogenase (GAPDH) and phosphofructokinase (PFK) (Osthus et al., 2000). Conversely, the tumour suppressor p53 can inhibit glycolysis via the downregulation of GLUT1/4 (Schwartzenberg-Bar-Yoseph et al., 2004) and can regulate the balance between oxidative and glycolytic metabolism (Matoba et al., 2006). Additionally, the abundance of mutant copies of activating *Kras* has been shown to correlate with enhanced glycolysis, increased glucose-derived TCA metabolites and glutathione production facilitating detoxification in mouse non-small cell lung cancer (NSCLC) (Kerr et al., 2016). While glycolysis remains one of the most frequently altered metabolic pathways amongst multiple forms of cancer (Gaude & Frezza, 2016; Hu et al., 2013), this represents just one of the numerous means by which metabolism is altered in cancer.

Contrary to Warburg's hypothesis that the aerobic glycolysis observed in tumour metabolism occurs on account of defective mitochondria, many tumours retain oxidative phosphorylative capacity and in fact tumorigenicity is inhibited in tumour cells depleted of mtDNA (Cavalli et al., 1997; Tan et al., 2015). Resident within the mitochondrial matrix, the enzymes of the TCA cycle generate ATP and reducing equivalents which provide electrons to the electron transport chain. This classical mechanism is observed in non-proliferating tissues, however in proliferating cells, precursors derived from TCA intermediates are frequently utilised as precursors from which lipids, nucleic acids and proteins are synthesised. Furthermore, metabolites themselves have additional downstream functions that further modulate tumour behaviour, specifically due to their function in epigenetic modification (reviewed in Reid et al., 2017). The initial finding that gain of function

mutations in genes encoding both the cytoplasmic and mitochondrial isoforms of isocitrate dehydrogenase (*IDH1* and *IDH2* respectively) result in a neomorphic enzyme activity led to an increased understanding of this phenomenon (Dang et al., 2009; Ward et al., 2010). The usual catalytic interconversion of isocitrate and α –ketoglutarate (α-KG) by IDH1 and IDH2 is replaced by the reduction of α-KG generating the (*R*)-2-hydroxyglutarate (R-2HG) oncometabolite, which subsequently causes histone and DNA hypermethylation via its inhibition of α-KG-dependant demethylase enzymes (Figueroa et al., 2010; Lu et al., 2012). Similarly, loss of function mutations in additional TCA cycle enzymes fumarate hydratase (FH) and succinate dehydrogenase (SDH) can have pro-tumorigenic consequences for the cell due to an accumulation of their substrates fumarate and succinate. Also described as oncometabolites, the accumulation of fumarate and succinate, like *R*-2HG, can give rise to widespread histone and DNA hypermethylation due to the inhibition of α-KG-dependant demethylases (Jiang et al., 2015; Xiao et al., 2012). Resulting from a loss of function mutation in FH, the accumulation of fumarate has also been shown to promote epithelial-to-mesenchymal-transition (EMT) by inhibiting the demethylation of an anti-metastatic miRNA cluster (Sciacovelli et al., 2016), while the loss of either FH or SDH and accompanying accumulation of substrates can further promote tumour survival via hypoxia-inducible factor 1 (HIF-1) stabilisation mediated angiogenesis and glycolytic adaptation (Isaacs et al., 2005; Selak et al., 2005).

Since the early observation that tumour cells generate greater quantities of hydrogen peroxide than normal cells, mitochondrial reactive oxygen species have shared a relationship with malignancy (Szatrowski & Nathan, 1991). Early works demonstrated that overexpression of the mitochondrial superoxide dismutase supressed neoplastic transformation (St. Clair et al., 1992) while more recently the knockdown of genes involved in the regulation of autophagy predisposes cells to increased ROS, secondary mutations and transformation (Park et al., 2016). Further to their mutagenic potential, ROS are important mediators of both pro- and anti-tumorigenic signalling. Hydrogen peroxide in particular has been shown to oxidise and inactivate the PTEN tumour suppressor thus removing negative regulation of the PI3K/Akt/mTOR survival pathway (Lee et al., 2002), while KRAS induced mitochondrial ROS generation activates EGFR signalling via NF-κB transcription factor mediated expression of epidermal growth factor receptor and its ligands in pancreatic acinar cells (Liou et al., 2016). The progression of malignancy to metastatic disease has also been

demonstrated to involve regulatory input from reactive oxygen species. Tyrosine kinases central to the cell adhesion response are reportedly activated by ROS thus promoting anchorage independent growth of transformed cells (Giannoni et al., 2005). Furthermore, an increased ROS production elicited by mutations in the mitochondrial oxidative phosphorylation complex I gene *ND6* was shown to promote the metastatic potential of murine tumour cells with ROS scavenger pre-treatment reducing the effect (Ishikawa et al., 2008). Concomitant with matrix detachment however is a further increase in ROS production which can subsequently inhibit distant metastases (Piskounova et al., 2015; Schafer et al., 2009). Excessive oxidative stress can promote apoptotic cell death via activation of the JNK and p38 signalling pathways (Ichijo et al., 1997), therefore in order to migrate and survive, tumour cells must employ antioxidant machinery to counteract such stresses. The balance between pro- and anti-tumorigenic ROS signalling is evidently key to tumour survival and as such highlights the central role of mitochondria in the tumorigenic process. As mitochondria and compensatory metabolic reprogramming have been implicated in the development of tumour resistance to chemotherapeutic agents, successful treatment regimens are likely to consist of a combination first-line agents and metabolic modulators aimed at disabling metabolic plasticity and thus tumour survival (reviewed in Desbats et al., 2020).

1.8.7. MtDNA mutations and malignancy

Mutations of the mitochondrial genome have been reported in human cancers for decades. Initial reports documenting the presence of mtDNA deletions within human renal oncocytomas (Welter et al., 1989) were followed by studies documenting D-loop deletions within gastric adenocarcinomas (Burgart et al., 1995), *ND1* deletions within renal cell carcinoma (RCC) (Horton et al., 1996) and extensive 4977 bp mtDNA deletions within breast cancer (Bianchi et al., 1995). With regard to point mutations, a number of studies subsequently reported the presence of clonally expanded somatic mtDNA point mutations in different tumour types. D-loop mutations were identified in colorectal and gastric tumours (Alonso et al., 1997) and mutations within the D-loop and protein coding genes (primarily *ND4*) were reported within bladder, head and neck, and lung malignancies (Fliss et al., 2000). Within ovarian carcinomas, mutations within the 16S and 12S rRNA genes, the D-loop and the cytochrome *b* gene were most frequent (Liu et al., 2001). In 1998, the seminal work by Polyak et al. was the first to report the presence of somatic mtDNA mutations at

homoplasmic levels in solid human tumours (Polyak et al., 1998). The comparison of the mtDNA sequence of ten human colorectal cancer cell lines with that of the patient-matched normal colon identified homoplasmic mtDNA point mutations within seven of the lines analysed. The majority of mutations were purine (G>A) transitions; however, pyrimidine transitions (T>C) were also identified with affected genes including those encoding the 16S and 12S rRNAs and protein coding genes (*ND1, ND4L, ND5, cyt b, COXI, COXII, COXIII*). These findings were corroborated by the documentation of similar mutational spectra within subsequent studies of colorectal cancers (Ericson et al., 2012; He et al., 2010; Larman et al., 2012). Consistent with the mutational spectrum of oxidative damage (Beckman & Ames, 1997; Cadet et al., 1997), the mtDNA mutational profile observed in colorectal cancers is also very similar to that observed within normal ageing colonic crypts (Greaves et al., 2010; Greaves et al., 2012; Taylor et al., 2003). Furthermore, the detection of pathogenic truncating mtDNA mutations at high levels of heteroplasmy and homoplasmy within colorectal cancers (Yuan et al., 2020) strongly implies that age-related somatic mtDNA mutations are enriched as normal crypts transform into malignant lesions.

Whether these mutations are passive bystanders or if they functionally contribute to the progression of malignancy remains unascertained. Accordingly, the aim of this thesis is to investigate the effect of age-related mtDNA mutations on intestinal tumour formation and progression.

1.9. Aims of study

With the knowledge that the accumulation of mtDNA mutations in replicating tissues contributes to a decline in the functionality of ageing tissue, it has been hypothesised that mitochondrial function may be involved in neoplastic progression; a pathology also strongly associated with increasing age. Given that the spectrum of mtDNA mutations within colorectal carcinoma are similar to those observed in human ageing (Smith et al., 2020), it remains to be established whether these defects occur passively or if they actively contribute to tumour development. The overriding aim of this thesis is to investigate the effect age-related mtDNA mutations on intestinal tumour formation and progression with the use of a genetically engineered mouse model of disease. This is to be achieved by meeting the following objectives.

1. To investigate the effect of age-related mtDNA mutations on intestinal tumour development through the generation and characterisation of a novel mouse model of intestinal cancer.
2. To describe mitochondrial OXPHOS function in the adenomas detected in the mouse model generated in objective 1.
3. To investigate the effect of mtDNA mutations and mitochondrial OXPHOS deficiency on the rates of cell proliferation and apoptosis in intestinal adenomas in the mouse.
4. To determine the metabolic pathways upregulated in response to age-related mitochondrial OXPHOS defects in both the mouse model and normal aged human crypts.

Chapter 2. Materials and methods

2.1. Materials

2.1.1. Equipment and software

2100 Antigen Retriever (Aptum Biologics Ltd)

Aperio CS2 digital slide scanner (Leica Biosystems)

Aperio ImageScope digital pathology slide viewing software (Leica Biosystems)

AxioCam MRm monochrome digital camera (Zeiss)

Electrothermal MH8517 paraffin section flotation bath (Cole-Parmer)

GraphPad Prism 8.4.3 statistical software (GraphPad)

Identichip radio frequency identification chips (Biotherm)

ImageJ (National Institutes of Health)

Leica MZ75 stereomicroscope (Leica Microsystems)

MBF Biosciences CX9000 colour digital camera

Microm HM 325 rotary microtome (Thermo Fisher Scientific)

Nikon A1R point scanning confocal microscope (Nikon)

NIS-Elements imaging software (Nikon)

Olympus BX-51 Stereology microscope

Zeiss AxioImager M1 Epifluorescent and brightfield microscope (Zeiss)

Zeiss Celldiscoverer 7 fluorescent microscope (Zeiss)

Zeiss LSM 800 confocal laser scanning microscope (Zeiss)

Zen 2.5 Blue microscope software (Zeiss)

Zeiss Zen Lite microscope software (Zeiss)

2.1.2. Consumables

2.1.2.1. Chemicals

10% Neutral buffered formalin (HT501128, Sigma Aldrich)

Alcoholic eosin Y (RBC-0201-00A, CellPath)

CldU (5-chloro-2'-deoxyuridine, C6891, Sigma Aldrich)

DPX (SEA-1300-00A, CellPath)

Ethylenediamine tetra-acetic acid, (EDTA) Tetrasodium Salt, Dihydrate SDS (15700, Affymetrix)

Goat serum (G9023, Sigma Aldrich)

Histoclear clearing agent (HS-200, National Diagnostics)

IsoFlo (Isofluorane, 50019100, Zoetis)

IdU (5-iodo-2'-deoxyuridine, I7125-5G, Sigma Aldrich)

Mayer's haematoxylin (HS315, TCS Biosciences)

Oxoid PBS Tablets (BR0014G, Thermo Scientific)

Prolong Gold antifade mountant (P36930, Invitrogen)

Sunflower seed oil from *Helianthus annuus* (S5007, Sigma Aldrich)

Tamoxifen (T5648, Sigma Aldrich)

Tri-sodium citrate dihydrate (VWR)

2.1.2.2. Antibodies

Affinity isolated anti-PHGDH antibody produced in rabbit (HPA021241, Sigma Aldrich)

Biotinylated goat polyclonal anti-GFP (ab6658, Abcam)

Donkey anti-mouse IgG highly cross-adsorbed secondary antibody, Alexa Fluor 488 conjugated (A21202, Invitrogen)

Donkey anti-rabbit preadsorbed secondary antibody, Alexa Fluor 750 conjugated (ab175728, Abcam)

Donkey anti-rat AffiniPure Cy™5 conjugated secondary antibody (712-175-153, Jackson ImmunoResearch)

EnVision+ System- HRP labelled polymer anti-rabbit detection kit (Dako, K4003)

Goat anti-mouse IgG1 cross-adsorbed secondary antibody, Alexa Fluor 647 conjugated (A21240, Invitrogen)

Goat anti-mouse IgG2a cross-adsorbed secondary antibody, Alexa Fluor 546 conjugated (A21133, Invitrogen)

Goat anti-mouse IgG2b cross-adsorbed secondary antibody, Alexa Fluor 546 conjugated (A21143, Invitrogen)

Goat anti-mouse IgG1 cross-adsorbed secondary antibody, biotin-XX (A10519, Invitrogen)

Goat anti-rabbit IgG (H+L) cross-adsorbed secondary antibody, Alexa Fluor 488 conjugated (A11008, Invitrogen)

Hoechst 33342, trihydrochloride, trihydrate (H3570, Invitrogen)

Mouse monoclonal anti-ATPB IgG1 (ab14730, Abcam)

Mouse monoclonal anti-IdU (Abcam, ab181664)

Mouse monoclonal anti-MTCO1 IgG2a (ab14705, Abcam)

Mouse monoclonal anti-NDUFB8 IgG1 (ab110242, Abcam)

Mouse monoclonal anti-UQCRFS1 IgG2b (ab14746, Abcam)

Rabbit polyclonal anti-β-catenin primary antibody (ab6302, Abcam)

Rabbit polyclonal anti-MTHFD2 primary antibody (ab151447, Abcam)

Rabbit polyclonal anti-active caspase 3 antibody (AB3623, Merck Millipore)

Rat monoclonal anti-BrdU (NB500-169, Novus Biologicals)

Recombinant rabbit anti-PSAT1 polyclonal primary antibody (NBP1-32920, Novus Biologicals)

Recombinant rabbit anti-TOMM20 monoclonal primary antibody (ab186734, Abcam)

Streptavidin Alexa Fluor 546 conjugate (S11225, Invitrogen)

Streptavidin Alexa Fluor 647 conjugate (S32357, Invitrogen)

2.2. Methods

2.2.1. Human colorectal carcinoma and mucosal samples

Samples used were obtained from 12 patients undergone either surgical colorectal tumour resection or polyp removal. Informed written consent was obtained prior to surgery and samples were coded to maintain patient confidentiality. This project was approved by the Joint Ethics Committee of Newcastle and North Tyneside Health Authority (2001/188) and the National Research Ethics Committee London-Stanmore (11/LO/1613). Clinical details pertaining to human samples are presented in Table 2-1.

Sample Number	Age	Sex	Specimen Region	Tumour Pathology	Grade	Staging
31	73	M	Left colon	Moderately differentiated adenocarcinoma	-	T4N1M1 (liver) Dukes' C
37	73	M	Colon	-	-	-
48	72	M	Rectum	Well differentiated adenocarcinoma		T3N0M0 Duke's B
49	58	F	Caecum	Moderately differentiated adenocarcinoma	2	T3N0Mx Dukes' B
57	64	M	Right colon	Tubular adenoma with mild dysplasia	-	-
60	65	M	Rectosigmoid colon	Moderately differentiated adenocarcinoma	2	T4N0Mx Dukes' C
61	85	M	Rectosigmoid colon	Moderately differentiated adenocarcinoma	2	T4N0Mx Duke's B
63	63	F	Rectum	Moderately differentiated adenocarcinoma	2	T2N0Mx Dukes' A
65	64	M	Rectum	-	-	-
67	60	F	Rectum	Adenocarcinoma	-	- Dukes' B
68	65	F	Left colon	Moderately differentiated adenocarcinoma	2	- Dukes' B
69	75	M	Left colon	Moderately differentiated adenocarcinoma	2	- Dukes' B

Table 2-1. Clinical details of human samples included in this study. The age of patients at the time of surgery ranged from 58 to 85 years. Eight patients were male, and four were female. Original tumour locations ranged from the caecum and right colon to the rectum. Tumour pathology was moderately differentiated in 7 cases, well differentiated in one case and undisclosed in three. The sample from patient 57 was categorised as a tubular adenoma with mild dysplasia. Pathology and grading information for patients 37, 65, and 67 was limited. Staging ranged from Dukes' A – C where data was available. Dukes' A = invasion of the basement membrane without breaching of the colon wall; B = tumour has breached the colon wall without evidence of lymph node metastasis; C = evidence of lymph node metastasis.

2.2.2. *PolyA$^{mut/mut}$ /Lgr5-EGFP-Ires-CreERT2/ Apc$^{flox/flox}$ experimental mice*

Heterozygous mitochondrial mutator mice (*PolyA$^{+/mut}$*) were kindly donated by Tomas Prolla, Department of Genetics and Medical Genetics, University of Wisconsin, Madison, USA. *Lgr5-EGFP-Ires-CreERT2* and *Apc$^{flox/flox}$* mice were kindly donated by Karen Vousden, Beatson Institute for Cancer Research, Glasgow, UK. Detailed breeding schedules are presented in 3.3.1. with the final cross only presented here in Figure 2-1. A maximum of six mice were housed per individually ventilated cage (IVC) at the Comparative Biology Centre at Newcastle University. Mice were fed an RM3 expanded chow provided by Special Diet Services (SDS) and their room maintained at a constant temperature of 25˚C with a 12-hour light/dark cycle.

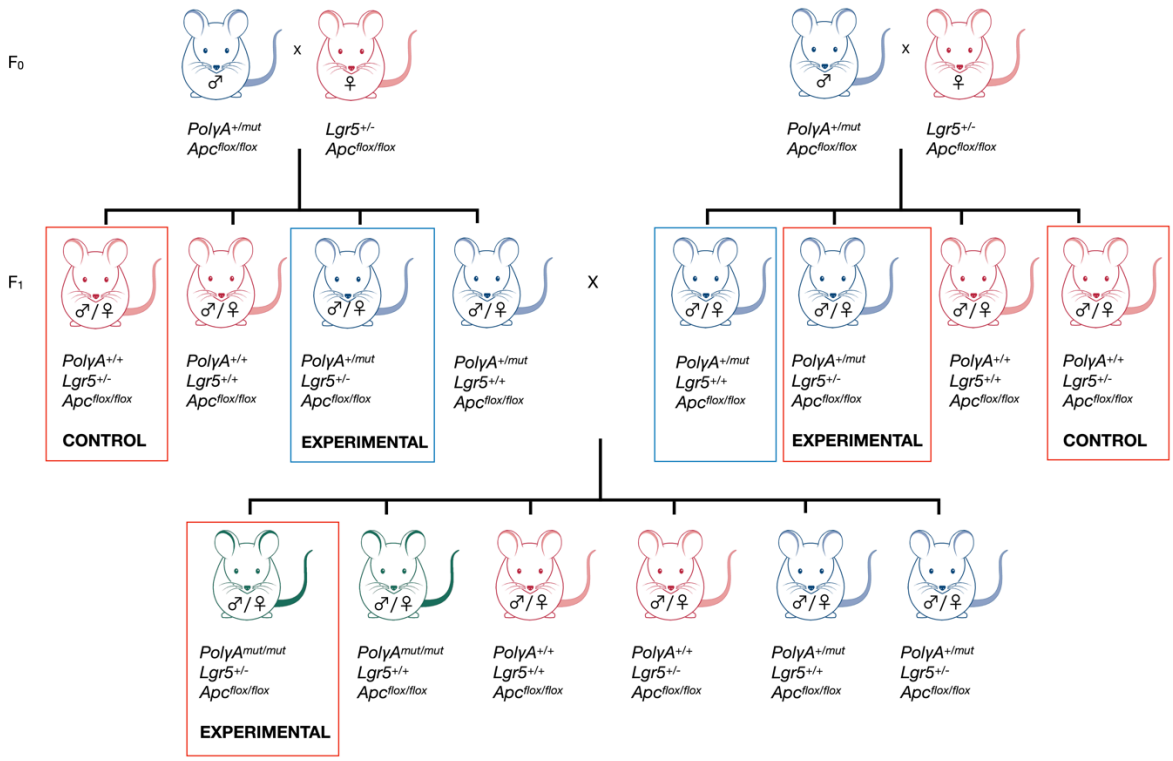

Figure 2-1. Breeding schedule depicting the mating of *PolyA$^{+/mut}$/Apc$^{flox/flox}$* males with *Lgr5$^{+/-}$/Apc$^{flox/flox}$* females. F_1 generation *PolyA$^{+/+}$ /Lgr5$^{+/-}$/Apc$^{flox/flox}$* animals highlighted accordingly were used as experimental control animals. Crossing of F_1 generation animals highlighted in blue boxes permitted the generation of *PolyA$^{mut/mut}$/ Lgr5$^{+/-}$/Apc$^{flox/flox}$* experimental animals. *PolyA$^{+/mut}$ /Lgr5$^{+/-}$/Apc$^{flox/flox}$* experimental animals were obtained at the F_1 generation.

2.2.3. Genotyping

2.2.3.1. DNA isolation from mouse ear notches

At three weeks of age mice were weaned and ear notches were samples. 47.5µL of lysis buffer (1M Tris-HCl, 0.5 M EDTA, 10% SDS in dH2O) was added to each ear notch followed by 2.5µL of proteinase K (20mg/mL) and vortexed. Ear notches were incubated on the orbital shaker overnight at 56°C at 1200 rpm. Notches were diluted 1:10 in distilled water.

2.2.3.2. Polymerase chain reaction (PCR)

The 1:10 diluted ear notch DNA lysates were amplified in 25µL PCR reaction volumes comprising 23µL master mix 5U/µL TakaRa ExTaq™, 10X Ex Taq buffer (20mM Mg2+), 2.5 mM dNTPs, 10µM forward primer, 10µM reverse primer in distilled water plus 2µL tissue lysate. Primer sequences and PCR reaction parameters used are outlined in Table 2-2.

Primer	Primer sequence	Cycling parameters
31PolG58Forward PolG59Reverse	Forward: GCCTCGCTTTCTCCGTGACT Reverse: GGATGTGGCCCAGGCTGTAACTCA	Initial denaturation at 94°C for 1 min followed by 35 cycles of • denaturation at 94 °C for 20s, • primer annealing at 64°C for 20s, • extension at 68°C for 45s. Final extension at 72°C for 5 mins.
Cre1Forward Cre2Reverse	Forward: TCCCCGCAGAACCTGAAGATGTTCG Reverse: GCCAGATTACGTATATCCTGGCAGC	Initial denaturation at 94°C for 1 min followed by 35 cycles of • denaturation at 94°C for 20s, • primer annealing at 62°C for 20s, • extension at 68°C for 45s. Final extension at 72°C for 5 mins.
APC P3 Forward APC P4 Reverse	Forward: GTTCTGTATCATGGAAAGATAGGTGGTC Reverse: CACTCAAAACGCTTTTGAGGGTTG	Initial denaturation at 94°C for 1 min followed by 35 cycles of • denaturation at 94°C for 20s, • primer annealing at 60°C for 20s, • extension at 68°C for 45s. Final extension at 72°C for 5 mins.

Table 2-2. Primer sequences and cycling parameters for PCR.

2.2.3.3. Agarose gel electrophoresis

For each PCR product, 1µL was mixed and loaded with 5µL loading dye comprising 0.25% (w/v) bromophenol blue, 30% (w/v) glycerol in distilled water onto a 1.5% agarose gel. PCR Ranger 100bp DNA ladder (Norgen) was also loaded into the gel which contained SYBR® Safe DNA Gel stain (Invitrogen) for visualisation of DNA. Gel electrophoresis was run at 120V for 45 minutes in 1X Tris acetate-EDTA buffer (Sigma). PCR products were visualised on a BIO-RAD ChemiDoc MP Imaging System. Animal genotypes were determined by the size of PCR products as presented in Table 2-3. For *Lgr5* genotyping, primer sequences target the *Cre* component where present. Accordingly, a 298bp PCR product indicates *Cre* presence and an *Lgr5-CreERT2* genotype, whereas no band indicates *Cre* absence and a wild-type *Lgr5* genotype. Ear notch sampling, PCR and agarose gel electrophoresis was performed by Carla Bradshaw, Senior Animal Technician.

Genotype	PCR product size (bp)
PolyA$^{+/+}$	296
PolyA$^{+/mut}$	468 296
PolyA$^{mut/mut}$	468
Lgr5	No band
Lgr5-CreERT2	298
Apc$^{+/+}$	226
Apc$^{flox/flox}$	314

Table 2-3. PCR product sizes for mouse genotype determination following PCR amplification and gel electrophoresis.

2.2.4. RFID chip insertion

All experimental animals were fitted with radio frequency identification chips (RFID) (Identichip, Biotherm) for the purposes of identification and the measurement of body temperature. Chip implants were inserted under the skin on the flank of each mouse between the front and back legs. Mice were under isoflurane anaesthesia (IsoFlo, Zoetis)

throughout the procedure which was performed by Carla Bradshaw at the Comparative Biology Centre, Newcastle University. Chips were implanted one month prior to *Apc* deletion through tamoxifen administration.

2.2.5. Induction regime

The fusion of a mutated oestrogen receptor ligand binding domain (LBD) with a Cre recombinase enzyme results in temporal control of this enzyme upon the addition of synthetic but not endogenous oestrogens (Feil et al., 1996; Feil et al., 1997; Zhang et al., 1996). In mice, the sensitivity of the CreERT2 fusion protein to the synthetic oestrogen 4-hydroxy-tamoxifen is ten-fold higher than that of its predecessor CreERT and is thus widely used (Indra et al., 1999). When expressed, CreERT2 is sequestered in the cytosol by heat shock proteins until the administration of 4-hydroxy-tamoxifen, or tamoxifen, which is converted to 4-hydroxy-tamoxifen in the liver. The synthetic oestrogen receptor antagonist permits translocation of CreERT2 to the nucleus where the recombination of the *LoxP* flanked gene of interest is catalysed by the recombinase.

Tamoxifen (T5648, Sigma Aldrich) was administered via intraperitoneal injection to experimental animals over the course of four days at a concentration of 10mg/ml in sunflower oil. 300µl (3mg) was administered on day one, and 200µl (2mg) administered each subsequent day. Carla Bradshaw, Senior Animal Technician performed the procedures within the Comparative Biology Centre, Newcastle University.

2.2.6. Clinical scoring of experimental mice

All mice were monitored daily until the experimental endpoint or clinical signs dictated that they be humanely killed. Number of days post tamoxifen induction was recorded for each mouse for the purposes of survival curve generation. Table 2-4 describes the clinical signs that were monitored during the experimental period. Animals were culled when they had three moderate or one severe symptom.

	Score			
	0	**1**	**2**	**3**
Weight	No weight loss/gain	5-15% weight loss	15-20% weight loss	Over 20% weight loss
Coat	Normal	Slight lack of grooming	Starey (piloerection)	
Skin tone	Normal	Tents, returns to normal in 1-2 seconds	Tents, persists	
Behaviour	Normal	Subdued but responsive. Animal shows normal behaviour patterns. Interacts with peers	Subdued- animal shows subdued behaviour. Little peer interaction. May show aggression	Animal unresponsive to extraneous activity and provocation even when provoked
Posture and mobility	Normal	Transient hunched posture, especially after dosing. Normal mobility	Hunched intermittently, reduced mobility	Hunched persistently 'frozen'. No spontaneous mobility
Abdominal distension	None	None	Abdominal distension up to the size expected in late pregnancy	Severe abdominal distension beyond that of late pregnancy affecting locomotor and/or breathing patterns
Foot colour	None	Whitening of feet due to mild anaemia	Whitening of feet due to moderate anaemia	Feet are completely white due to severe anaemia
Faeces	None	No diarrhoea or transient diarrhoea	Intermittent or continuous diarrhoea (>72h). No dehydration	Continuous diarrhoea (>72 h) with faecal soiling of perineum and/or dehydration

Table 2-4. Clinical signs monitored during experimental periods and deviations away from normal. A score of zero represents a normal presentation of the clinical sign in question. A score of 1 represents a mild presentation with scores of 2 and 3 denoting moderate and severe presentations respectively.

2.2.7. Necropsy

Mice underwent a standard necropsy in which samples of skin, heart, lungs, spleen, liver, pancreas, stomach, and kidneys were taken and fixed in 10% neutral buffered formalin (HT501128, Sigma Aldrich). The length of the intestine was flushed with formalin, opened along its length and pinned out flat for fixation. The small intestine was divided into three segments of equal length, SI1 being the most proximal and SI3 the most distal. The colon and caecum were also flushed, opened and pinned flat for fixation. After 24 hours fixation, the formalin was disposed of and any visible adenomas counted using a dissecting microscope. Only adenomas greater than 1mm x 1mm were included in the count. Following macroscopic analysis, all segments of intestine were rolled up distal end first, processed and paraffin wax embedded. This process is shown in Figure 2-2.

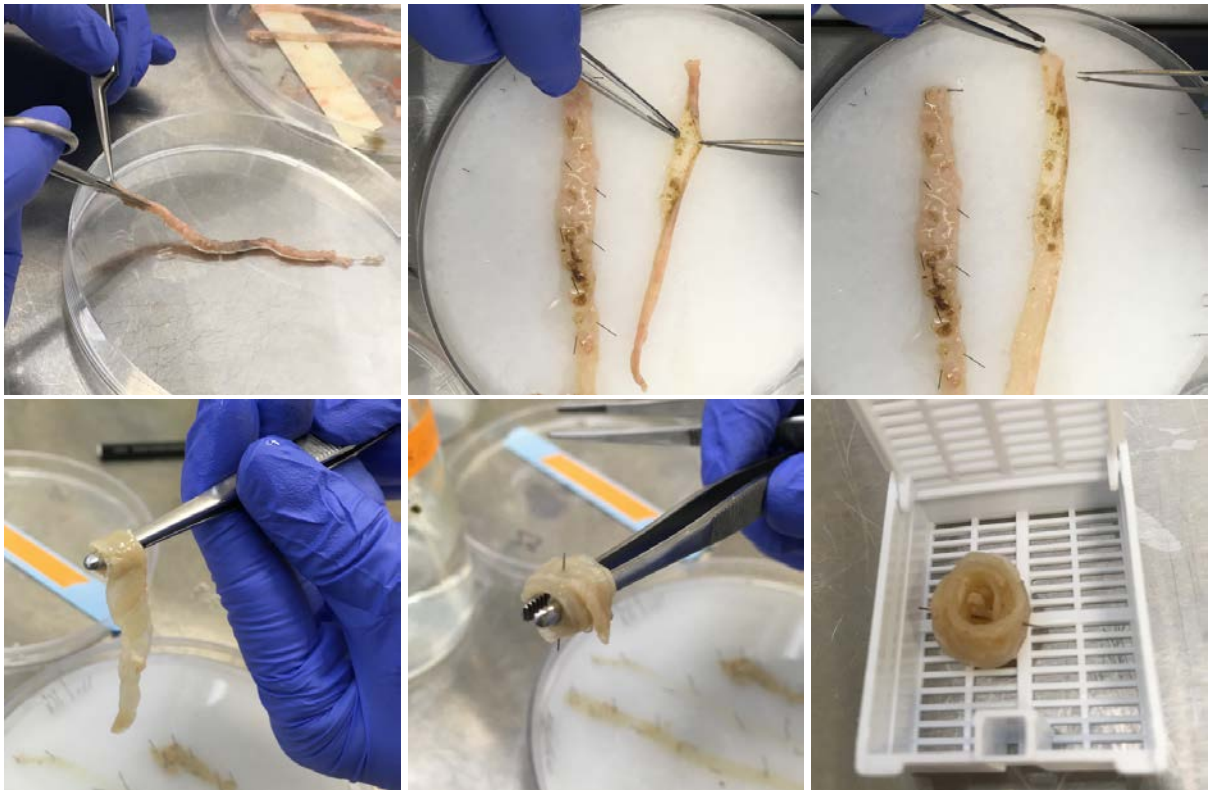

Figure 2-2. Mouse intestine dissection at necropsy. Intestinal segments are flushed with 10% neutral buffered formalin before being opened out longitudinally and pinned flat on a paraffin wax filled Petri dish. Intestines are fixed in 10% NBF for 24 hours before rolling up distal to proximal and processing for paraffin wax embedding.

2.2.8. Haematoxylin and eosin staining

After trimming blocks to full face, 4µm sections were cut using a Microm HM325 rotary microtome (Thermo Scientific Microm). Immediately prior to staining, sections were incubated for 1 hour at 60°C. They were deparaffinised in two changes of Histoclear (HS-200, National Diagnostics) and rehydrated through graded ethanol (100% EtOH, 95% EtOH, and 70% EtOH) to distilled water. Slides were washed well in water and stained with Mayer's haematoxylin (TCS Biosciences) for 10 minutes. Following a wash in water, nuclei were blued using Scott's tap water for 30 seconds. Following a wash in water sections were stained in alcoholic eosin (CellPath). Slides were washed in water, dehydrated in a graded ethanol series, cleared in two changes of Histoclear and mounted in DPX (CellPath).

2.2.9. Immunohistochemical methods

2.2.9.1. Section preparation

After trimming blocks to full face, 4µm sections were cut using a Microm HM325 rotary microtome (Thermo Scientific Microm). Immediately prior to staining, sections were incubated for 1 hour at 60°C. They were deparaffinised in two changes of Histoclear (HS-200, National Diagnostics) and rehydrated through graded ethanol (100% EtOH, 95% EtOH, and 70% EtOH) to distilled water. Antigenic sites were exposed in a heated, pressurised antigen retrieval unit (2100 Antigen Retriever, Aptum Biologics Ltd.) with either 1mM EDTA pH8.0 (beta catenin IHC) or 1mM citrate buffer pH6.0 (cleaved caspase 3 and serine synthesis pathway enzyme IHC) used as retrieval solution. Following the 20-minute warm up, 20-minute cool down cycle, slides were rinsed in distilled water. The activity of any endogenous peroxidase enzymes was blocked using the peroxidase block solution included in the EnVision+ System- HRP labelled polymer anti-rabbit detection kit (Dako, K4003). Non-specific binding sites were blocked in 10% normal goat serum (NGS) for 1 hour at room temperature.

2.2.9.2. Beta catenin immunohistochemistry

Subsequent to the preparation steps outlined in 2.2.9.1., sections were incubated overnight in a 1:1000 dilution of rabbit anti-β-catenin (ab6302, Abcam) in 10% NGS at 4°C. Slides were washed for 3x5 minutes on a rocking platform in TBST prior to incubation in secondary antibody (polymer HRP-labelled anti-rabbit, Dako Envision) for 30 minutes at room temperature. Sections were again washed for 3x5 minutes in TBST. β-catenin bound peroxidase was then visualised with DAB following a 10-minute incubation in DAB chromogen-substrate solution at room temperature. Slides were washed well in water, counterstained with Mayer's haematoxylin (TCS Biosciences) dehydrated in a graded ethanol series, cleared in two changes of Histoclear and mounted in DPX (CellPath).

2.2.9.3 Cleaved caspase 3 immunohistochemistry

Sections were prepared as outlined in 2.2.9.1. A concentration of 1:10 of rabbit polyclonal anti-active (cleaved) caspase 3 was recommended by the manufacturer for immunohistochemical detection of the target protein. Optimisation of the antibody involved evaluating the staining intensities obtained with 1:10, 1:15, 1:20, 1:25, 1:30, 1:35 and 1:40 dilutions of primary antibody in 10% NGS. An increased level of background staining was observed at the stronger concentrations which had reduced sufficiently at 1:35 therefore 1:35 was selected as the most appropriate concentration. Blocked sections were thus incubated in rabbit polyclonal anti-active caspase 3 antibody (AB3623, Merck Millipore) at a 1:35 dilution in 10% NGS overnight at 4°C.

Slides were washed for 3x5 minutes on a rocking platform in TBST prior to incubation in secondary antibody (polymer HRP-labelled anti-rabbit, Dako Envision) for 30 minutes at room temperature. Sections were again washed for 3x5 minutes in TBST. Active caspase 3 bound peroxidase was then visualised with DAB following a 10-minute incubation in DAB chromogen-substrate solution at room temperature. Slides were washed well in water, counterstained with Mayer's haematoxylin (TCS Biosciences) dehydrated in a graded ethanol series, cleared in two changes of Histoclear and mounted in DPX (CellPath).

2.2.9.4. Serine synthesis pathway enzyme immunohistochemistry

Subsequent to the preliminary steps outlined in 2.2.9.1., sections were incubated overnight in either a 1:4000 dilution of anti-PHGDH (HPA021241, Sigma Aldrich), a 1:600 dilution of anti-PSAT1 (NBP1-32920, Novus Biologicals) or a 1:600 dilution of anti-MTHFD2 (ab151447, Abcam). All antibodies were diluted in 10% NGS and sections incubated overnight at 4°C. The EnVision+ System- HRP labelled polymer anti-rabbit detection kit (Dako) was used and bound antibody visualised with DAB. Sections were counterstained with Mayer's haematoxylin (HS315, TCS Biosciences). Adenomas and regions of non-transformed mucosa were imaged using an Olympus BX-51 microscope and MBF Biosciences CX9000 colour digital camera.

2.2.10. Double thymidine analogue labelling

The administration of thymidine analogues results in their incorporation into the DNA of replicating cells during S phase of the cell cycle. Subsequent labelling using immunohistochemical or immunofluorescent assays allows identification and quantification of the number of cells which have replicated from the time of administration to the time of death. The thymidine analogue cohort was established in which five *PolγA*$^{mut/mut}$ and five *PolγA*$^{+/+}$ mice were aged to six months prior to administration of tamoxifen to induce *Apc* deletion as per the regime outlined in 2.2.5. At 15 days post *Apc* deletion, these animals underwent a series of intraperitoneal injections of the thymidine analogues CldU and IdU and were humanely killed at 16 days post *Apc* deletion. This time point was chosen from an animal welfare perspective. Mice had demonstrated signs of deteriorating health as early as 20 days post *Apc* deletion and it was deemed inappropriate to subject the animals to further procedures beyond this point. IP injections of thymidine analogues were therefore scheduled to take place prior to the deterioration of health. CldU (5-chloro-2'-deoxyuridine, C6891, Sigma Aldrich) was made up at a concentration of 5mg/ml in PBS (Oxoid PBS Tablets, BR0014G, Thermo Scientific) pH 7.4 and filter sterilised. IdU (5-iodo-2'-deoxyuridine, I7125-5G, Sigma Aldrich) was also prepared at a concentration of 5mg/ml in PBS, however it was necessary to heat the solution in a water bath at 55°C overnight to allow the IdU to fully dissolve. The pH was adjusted to pH7.4 at this point and the solution maintained at 55°C until filter sterilisation immediately prior to use. The necessary *in vivo* concentration of each analogue was 50mg/kg therefore 10µl of 5mg/ml solution was required per gram of mouse weight. Analogues were injected intraperitoneally by Carla Bradshaw according to the schedule shown in Table 2-5.

	Day 15 post *Apc* deletion	Day 16 post *Apc* deletion
10am	IP CldU 50mg/kg	IP IdU 50mg/kg
6pm	IP CldU 50mg/kg	-

Table 2-5. Thymidine analogue injection schedule for experimental animals. Animals were humanely sacrificed four hours after the final IP administration of IdU, 16 days post *Apc* deletion.

All animals were humanely culled 4 hours after IP IdU and necropsy harvesting performed as outlined in 2.2.7. Injections were performed within the Comparative Biology Centre, Newcastle University by Carla Bradshaw, Senior Animal Technician.

2.2.11. Immunofluorescent methods

2.2.11.1. Section preparation

Following tissue processing, paraffin wax embedding and trimming blocks to full face, 4µm sections were cut using a Microm HM325 rotary microtome (Thermo Scientific Microm). Immediately prior to staining, sections were incubated for 1 hour at 60°C. They were deparaffinised in two changes of Histoclear (HS-200, National Diagnostics) and rehydrated through graded ethanol (100% EtOH, 95% EtOH, and 70% EtOH) to distilled water. Antigenic sites were exposed in a heated, pressurised antigen retrieval unit (2100 Antigen Retriever, Aptum Biologics Ltd.) with either 1mM citrate buffer pH6.0 (for thymidine analogue and serine synthesis pathway enzyme IF) or 1mM EDTA pH8.0 (for mitochondrial OXPHOS IF) used as retrieval solution. Following the 20-minute warm up, 20-minute cool down cycle, slides were rinsed in distilled water. Non-specific binding sites were blocked in 10% normal goat serum (NGS) for 1 hour at room temperature.

2.2.11.2. Thymidine analogue immunofluorescence

Subsequent to the preparation steps outlined in 2.2.11.1., sections were incubated overnight in a primary antibody cocktail. The primary antibody cocktail was optimised to include mouse monoclonal anti-IdU (Abcam, ab181664) at a 1:100 dilution, rat monoclonal anti-BrdU (NB500-169, Novus Biologicals) at a 1:100 dilution and biotinylated goat polyclonal anti-GFP (Abcam, ab6658) at a 1:100 dilution. All antibodies were diluted in 10% normal goat serum and sections incubated in primary cocktails overnight at 4°C.

Slides were washed for 3x5 minutes on a rocking platform in TBST prior to incubation in fluorophore conjugated antibody cocktails. The secondary antibody cocktail was optimised to include donkey anti-mouse IgG highly cross-adsorbed secondary antibody, Alexa Fluor 488

conjugated (A21202, Invitrogen) at a dilution of 1:150, donkey anti-rat AffiniPure Cy™5 conjugated secondary antibody (712-175-153, Jackson ImmunoResearch) at a dilution of 1:150, streptavidin Alexa Fluor 546 conjugate (S11225, Invitrogen) at a 1:200 dilution and donkey anti-rabbit preadsorbed secondary antibody, Alexa Fluor 750 conjugated (ab175728, Abcam) at a dilution of 1:50. All fluorophore conjugated antibodies were diluted in 10% NGS and sections incubated in fluorophore cocktail for 2 hours at room temperature in the dark. Following 3x5 minutes on a rocking platform in TBST, sections were incubated in a 1:1200 solution of Hoescht nucleic acid stain (H3570, Invitrogen) for 15 minutes at room temperature in the dark. Following a final 3x5 minute wash in TBST, slides were mounted in Prolong Gold antifade mountant (P36930, Invitrogen).

2.2.11.3. Mitochondrial OXPHOS protein subunit immunofluorescence

Following the preparation steps outlined in 2.2.11.1., sections were incubated overnight in primary antibody cocktail. Primary antibody cocktail for section 1 included mouse anti-NDUFB8 IgG1 monoclonal primary antibody (ab110242, Abcam) at a 1:50 dilution, mouse anti-UQCRFS1 IgG2b monoclonal primary antibody (ab14746, Abcam) at a 1:100 dilution and recombinant rabbit anti-TOMM20 monoclonal primary antibody (ab186734, Abcam) at a 1:100 dilution. Primary antibody cocktail for section 2 included mouse anti-MTCO1 IgG2a monoclonal primary antibody (ab14705, Abcam) at 1:50 dilution, mouse anti-ATPB IgG1 monoclonal primary antibody (ab14730, Abcam) at a 1:100 dilution, dilution and recombinant rabbit anti-TOMM20 monoclonal primary antibody (ab186734, Abcam) at a 1:100 dilution. All antibodies were diluted in 10% normal goat serum and sections incubated in primary cocktails overnight at 4°C.

Slides were washed for 3x5 minutes on a rocking platform in TBST prior to incubation in fluorophore conjugated antibody cocktails. Sections labelled with anti-NDUFB8 required a biotin amplification step therefore a biotinylated anti-IgG1 secondary antibody step was included for these sections only. These sections were incubated in goat anti-mouse IgG1 cross-adsorbed secondary antibody, biotin-XX (A10519, Invitrogen) at a 1:200 dilution in 10% NGS for 2 hours at room temperature followed by 3x5 minute washes on a rocking platform in TBST. The fluorophore conjugated antibody cocktail for section 1 (NDUFB8 and UQCRFS1) included goat anti-rabbit IgG (H+L) cross-adsorbed secondary antibody, Alexa Fluor 488

conjugated (A11008, Invitrogen) at a 1:200 dilution, streptavidin Alexa Fluor 647 conjugate (S32357, Invitrogen) at a 1:200 dilution and goat anti-mouse IgG2b cross-adsorbed secondary antibody, Alexa Fluor 546 conjugated (A21143, Invitrogen) also at a 1:200 dilution. The fluorophore conjugated antibody cocktail for section 2 (MTCO1 and ATPB) included goat anti-rabbit IgG (H+L) cross-adsorbed secondary antibody, Alexa Fluor 488 conjugated (A11008, Invitrogen) at a 1:200 dilution, goat anti-mouse IgG2a cross-adsorbed secondary antibody, Alexa Fluor 546 conjugated (A21133, Invitrogen) and goat anti-mouse IgG1 cross-adsorbed secondary antibody, Alexa Fluor 647 (A21240, Invitrogen) also at a 1:200 dilution.

All fluorophore conjugated antibodies were diluted in 10% NGS and sections incubated in cocktails for 2 hours at room temperature in the dark. Following 3x5 minutes on a rocking platform in TBST, sections were incubated in a 1:1200 solution of Hoescht nucleic acid stain (H3570, Invitrogen) for 15 minutes at room temperature in the dark. Following a final 3x5 minute wash in TBST, slides were mounted in Prolong Gold antifade mountant (P36930, Invitrogen).

2.2.11.4. Serine synthesis pathway enzyme immunofluorescence

2.2.11.4.1. Mouse samples

In order to investigate the expression of the serine synthesis pathway enzymes PHGDH and PSAT1 and mitochondrial one carbon pathway enzyme MTHFD2 within normal non-transformed murine intestine, (3x) 4µm serial sections were taken from colon and small intestine formalin fixed paraffin embedded (FFPE) blocks from three *PolγA*$^{mut/mut}$ and three *PolγA*$^{+/+}$ mice per age group. Age groups of 1, 3, 6, 9 and 12 months were included in the analysis and sections prepared as outlined in 2.2.11.1. Sections were incubated overnight in either a 1:2000 dilution of anti-PHGDH (HPA021241, Sigma Aldrich), a 1:300 dilution of anti-PSAT1 (NBP1-32920, Novus Biologicals) or a 1:300 dilution of anti-MTHFD2 (ab151447, Abcam). All antibodies were diluted in 10% NGS and sections incubated overnight at 4°C. Slides were washed for 3x5 minutes on a rocking platform in TBST prior to incubation in fluorophore conjugated secondary antibody. For all sections, goat anti-rabbit IgG (H+L)

cross-adsorbed secondary antibody, Alexa Fluor 488 conjugated (A11008, Invitrogen) was used at 1:200 in 10% NGS dilution and sections incubated for 2 hours at room temperature in the dark. Following 3x5 minutes on a rocking platform in TBST, sections were incubated in a 1:1200 solution of Hoescht nucleic acid stain (H3570, Invitrogen) for 15 minutes at room temperature in the dark. Following a final 3x5 minute wash in TBST, slides were mounted in Prolong Gold antifade mountant (P36930, Invitrogen).

2.2.11.4.2. Human samples

In order to categorise normal human colonic crypts as either OXPHOS normal or OXPHOS deficient and subsequently correlate OXPHOS status with the level of expression of the enzymes PHGDH, PSAT1 and MTHFD2, 4 x 4μm serial sections were taken from normal colonic mucosal biopsies from 12 patients who had undergone either surgical colorectal tumour resection or polyp removal. Serial sections were labelled according to the schematic shown in Figure 2-3.

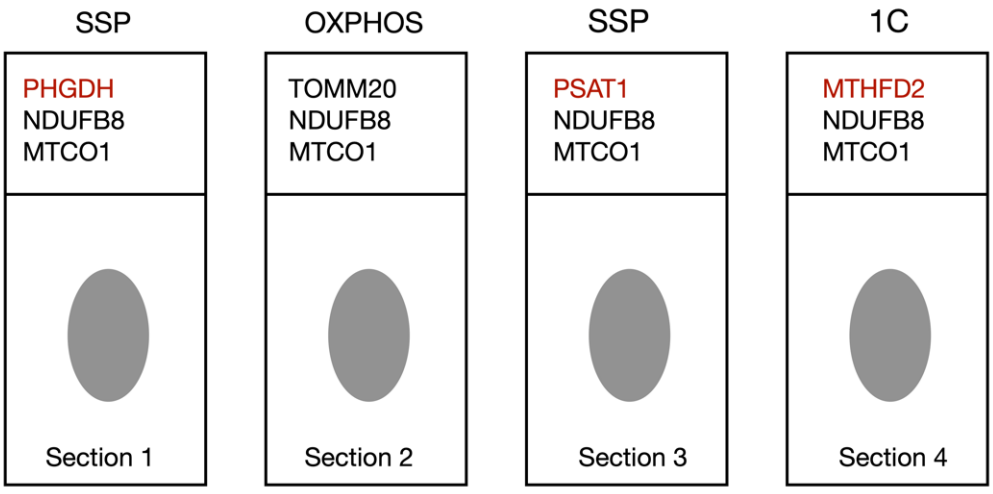

Figure 2-3. Schematic outlining labelling protocol of SSP enzymes and OXPHOS subunit proteins present in normal human colon biopsies. A ribbon of sections was cut at a thickness of 4μm with one sequential section on each slide. Antibodies targeting respective proteins were applied as noted.

2.2.11.4.2.1. OXPHOS subunit protein immunofluorescence

In order to categorise normal human colonic crypts as OXPHOS normal or deficient, the quadruple immunofluorescence protocol described by Rocha et al was applied to tissue sections (Rocha et al., 2015). This method was validated in skeletal muscle with the use of anti-VDAC1 as a mitochondrial mass marker, however the use of this antibody on intestinal tissue sections did not facilitate punctate labelling and was therefore replaced with a recombinant rabbit anti-TOMM20 monoclonal primary antibody (ab186734, Abcam). Following the preparation steps outlined in 2.2.11.1., sections were incubated overnight in primary antibody cocktail. Primary antibody cocktail included mouse anti-NDUFB8 IgG1 monoclonal primary antibody (ab110242, Abcam) at a 1:50 dilution, mouse anti-MTCO1 IgG2a monoclonal primary antibody (ab14705, Abcam) at 1:50 dilution, and recombinant rabbit anti-TOMM20 monoclonal primary antibody (ab186734, Abcam) at a 1:100 dilution. All antibodies were diluted in 10% normal goat serum and sections incubated in primary cocktails overnight at 4°C.

Slides were washed for 3x5 minutes on a rocking platform in TBST prior to incubation in fluorophore conjugated antibody cocktails. A biotin amplification step was required for adequate detection of anti-NDUFB8 required therefore a biotinylated anti-IgG1 secondary antibody step was included. Sections were incubated in goat anti-mouse IgG1 cross-adsorbed secondary antibody, biotin-XX (A10519, Invitrogen) at a 1:200 dilution in 10% NGS for 2 hours at room temperature followed by 3x5 minute washes on a rocking platform in TBST.

The fluorophore conjugated antibody cocktail consisted of goat anti-rabbit IgG (H+L) cross-adsorbed secondary antibody, Alexa Fluor 488 conjugated (A11008, Invitrogen) at a 1:200 dilution, streptavidin Alexa Fluor 647 conjugate (S32357, Invitrogen) at a 1:200 dilution and goat anti-mouse IgG2a cross-adsorbed secondary antibody, Alexa Fluor 546 conjugated (A21133, Invitrogen) also at a 1:200 dilution. All fluorophore conjugated antibodies were diluted in 10% NGS and sections incubated in cocktails for 2 hours at room temperature in the dark. Following 3x5 minutes on a rocking platform in TBST, sections were incubated in a 1:1200 solution of Hoescht nucleic acid stain (H3570, Invitrogen) for 15 minutes at room

temperature in the dark. Following a final 3x5 minute wash in TBST, slides were mounted in Prolong Gold antifade mountant (P36930, Invitrogen).

2.2.11.4.2.2. Combined serine synthesis pathway enzyme and OXPHOS subunit immunofluorescence

Following the preparation steps outlined in 2.2.11.1., sections were incubated overnight in primary antibody cocktail. Primary antibody cocktails consisted of mouse anti-NDUFB8 IgG1 monoclonal primary antibody (ab110242, Abcam) at a 1:50 dilution, mouse anti-MTCO1 IgG2a monoclonal primary antibody (ab14705, Abcam) at 1:50 dilution with one of either anti-PHGDH (HPA021241, Sigma Aldrich) at a 1:300 dilution, anti-PSAT1 (NBP1-32920, Novus Biologicals) at a 1:90 dilution or anti-MTHFD2 (ab151447, Abcam) at a 1:90 dilution. All antibodies were diluted in 10% normal goat serum and sections incubated in primary cocktails overnight at 4°C.

Following the overnight incubation, slides were washed for 3x5 minutes on a rocking platform in TBST prior to incubation in fluorophore conjugated antibody cocktails. A biotin amplification step was required for adequate detection of anti-NDUFB8 required therefore a biotinylated anti-IgG1 secondary antibody step was included. Sections were incubated in goat anti-mouse IgG1 cross-adsorbed secondary antibody, biotin-XX (A10519, Invitrogen) at a 1:200 dilution in 10% NGS for 2 hours at room temperature followed by 3x5 minute washes on a rocking platform in TBST.

The fluorophore conjugated antibody cocktail consisted of goat anti-rabbit IgG (H+L) cross-adsorbed secondary antibody, Alexa Fluor 488 conjugated (A11008, Invitrogen) at a 1:200 dilution, streptavidin Alexa Fluor 647 conjugate (S32357, Invitrogen) at a 1:200 dilution and goat anti-mouse IgG2a cross-adsorbed secondary antibody, Alexa Fluor 546 conjugated (A21133, Invitrogen) also at a 1:200 dilution. All fluorophore conjugated antibodies were diluted in 10% NGS and sections incubated in cocktails for 2 hours at room temperature in the dark. Following 3x5 minutes on a rocking platform in TBST, sections were incubated in a 1:1200 solution of Hoescht nucleic acid stain (H3570, Invitrogen) for 15 minutes at room temperature in the dark. Following a final 3x5 minute wash in TBST, slides were mounted in Prolong Gold antifade mountant (P36930, Invitrogen).

2.2.12. Microscopy and image analysis

2.2.12.1. Beta catenin immunohistochemistry imaging and analysis

Beta catenin labelled mouse sections were scanned into a Leica Aperio Slidescanner situated at the Northern Institute for Cancer Research (NICR), Newcastle University. Using the associated ImageScope software (Leica), the frequency of all visible adenomas per section was recorded, and their individual and total area measured by manually selecting each adenomatous region. Adenomas were classed as such based on their pattern of β-catenin expression. Beta catenin intense foci (adenomas) were identified as clusters of cells that showed both increased nuclear and cytoplasmic β-catenin when compared to normal, non-transformed, surrounding mucosa. The area of the clusters of β-catenin intense cells was measured, with cells being categorised as belonging to the same cluster or foci if there were no normal cells in between them.

Within ImageScope, individual adenomata were manually selected and each recorded as a layer region in which the area was listed in μm^2. The total area these layer regions circumscribed per section was then calculated and in order to determine the proportion of each tissue section comprised of adenoma, the Positive Pixel Count algorithm was used. Applying this algorithm to each section generated multiple parameters including the total area of positive pixels (or stained tissue) present in mm^2. The proportion of each tissue section comprised of adenoma was thus represented as a percentage of the total area of each section.

2.2.12.2. Cleaved caspase 3 immunohistochemistry imaging and analysis

Following labelling with anti-cleaved caspase 3 antibody as described in 2.2.9.3., a minimum of 10 adenomas were selected at random from each colonic section of *PolγA*$^{mut/mut}$ (n=7) and *PolγA*$^{+/+}$ (n=9) animals culled at 23 days post *Apc* deletion. Adenomas were imaged with a x10 objective using bright field microscopy on a Zeiss AxioImager M1 microscope. A minimum of 10 adenomas were similarly selected at random from small intestinal sections of *PolγA*$^{mut/mut}$ (n=9) and *PolγA*$^{+/+}$ (n=9) animals culled at 23 days post *Apc* deletion imaged in

the same way. Using the events tool to record frequencies, the total number of nuclei per foci and the number of cleaved caspase 3 positive cells per foci were manually counted using Zen Lite software (Zeiss).

2.2.12.3. Thymidine analogue immunofluorescence imaging and analysis

All labelled sections were imaged using a Zeiss AxioImager M1 fluorescent microscope and Zen 2.5 Blue microscope software (Zeiss). Filter cubes for Alexa Fluor fluorophores at 405 nm, 488 nm, 546 nm and 647 nm wavelengths were used and images acquired with an AxioCam MRm monochrome digital camera. Exposure times were optimised for each channel, verified against no primary antibody control sections and settings maintained throughout image acquisition. For each section from each mouse, eighteen tumour foci were selected at random and labelled cells counted manually using the events tool within Zen Lite software (Zeiss) For each adenoma, the frequencies of nuclei, *Lgr5+* cells and cells incorporating one or both thymidine analogues were quantified. For the *Lgr5+* stem cell population, cells incorporating one or both thymidine analogues were also quantified in the same manner.

2.2.12.4. Mitochondrial dysfunction immunofluorescence imaging, analysis and Z score generation

Following quadruple immunofluorescence labelling as described in 2.2.11.3., adenomas were manually identified within the colonic and small intestinal tissue of *PolγA*$^{mut/mut}$, *PolγA*$^{+/mut}$ and *PolγA*$^{+/+}$ mice culled at 23 days post *Apc* deletion and images acquired using a Nikon A1R inverted point scanning confocal microscope with a x20 Plan-Apochromat objective. In order to avoid pixel over or undersaturation, laser power was optimised for each channel using labelled and unlabelled *PolγA*$^{+/+}$ tissues. Excitatory emission was detected at wavelengths of 405, 488, 546 and 647nm within an intensity range of 0 to 4095.

Confocal images were subsequently converted into TIF format using NIS Elements software (Nikon) and analysed using Image J software (NIH). Adenomas were selected as regions of interest (ROI) and fluorophore mean intensity values recorded for each channel. Following

the collection of fluorophore mean intensity data, values in the 488nm channel (TOMM20) and 546nm channel (MTCO1 or UQCRFS1) were background corrected by subtracting the mean intensity of a no primary control (NPC) from the ROI mean. Due to the use of an additional biotin amplification step in the detection of NDUFB8 protein and thus the increased possibility of non-specific secondary antibody binding due to this, NDUFB8 mean intensity values (647nm) were corrected according to mitochondrial mass. This involved the grouping of ROIs according to mean TOMM20 expression percentiles and their correction by using the mean 647nm intensity value of the matching no primary control from that percentile. Corrected values were then normalised by log transformation. Z-scores were calculated based on the control population and adenomas (and non-transformed crypts) categorised as normal ($z > -3$), intermediate positive ($-4.5 \leq z < -3.0$), intermediate negative ($-6 \leq z < -4.5$) and negative ($z < -6$) for each protein.

2.2.12.5. Serine synthesis enzyme immunofluorescence imaging and analysis

2.2.12.5.1. Mouse samples

All labelled sections were imaged using a Zeiss Celldiscoverer 7 fluorescent microscope (Zeiss). Using the tiling function, the entire section was scanned at a x10 magnification using a x20 Plan-Apochromat objective with 0.5x Tubelens Optavar. For PHGDH imaging, 470nm and 365nm laser LED modules were set at exposure times of 80ms and 30ms respectively with both light source intensities set at 50%. For PSAT1 and MTHFD2 imaging, 470nm LED exposure time was set to 120ms. All settings remained fixed within groups and images were acquired with a Hamamatsu Fusion imaging device. Individual tile images were acquired with a 10% overlap and stitching, and fusion of tiles was carried out by the software using the 365nm channel as a reference. Quantification of PHGDH, PSAT1 and MTHFD2 expression levels was achieved by using the spline contour tool within Zen Lite software and selecting 20 crypts at random from each section.

Following whole slide scanning and SSP/1C enzyme quantification, representative regions were selected at random from one mouse per age group for each protein with specific regions being mapped across each labelled section. This process was carried out for both

colonic and small intestinal samples and high-resolution images were acquired using an LSM800 confocal laser scanning microscope with Airyscan detector (Zeiss). The Airyscan detector is a formation of 32 individual detector elements in a compound eye arrangement. Each element functions as an individual confocal pinhole, the diameter of which is relative to the maximum diameter of the detector itself; 6 elements. If a 1.25 AU pinhole is selected, the pinhole diameter of each individual element is one sixth of this value; 0.2 AU. The light collection efficiency of a large pinhole (e.g. 1.25 AU) is combined with the increased resolution of imaging with a small pinhole (0.2 AU) with the use of an Airyscan detector (Huff, 2015). A x10 Plan-Apochromat objective was used for image acquisition in conjunction with a bidirectional, linear frame scan mode. Settings applied to each group are outlined in Table 2-6.

	Laser wavelength	Laser wavelength intensity	Pinhole	Pixel dwell time	Detector gain	Detector offset
Colon PHGDH	405nm	0.99%	5.00 AU	2.06µs	750 V	0
	488nm	0.99%	5.00 AU	2.06µs	750 V	0
Colon PSAT1	405nm	0.99%	5.00 AU	2.06µs	750 V	0
	488nm	0.98%	5.00 AU	2.06µs	750 V	0
Colon MTHFD2	405nm	0.99%	5.00 AU	2.06µs	750 V	0
	488nm	0.98%	5.00 AU	2.06µs	750 V	0
Small intestine PHGDH	405nm	1.05%	5.94 AU	2.06µs	750 V	0
	488nm	1.80%	5.74 AU	2.06µs	750 V	0
Small intestine PSAT1	405nm	1.05%	5.94 AU	2.06µs	750 V	0
	488nm	2.00%	5.74 AU	2.06µs	750 V	0
Small intestine MTHFD2	405nm	1.05%	5.94 AU	2.06µs	750 V	0
	488nm	2.00%	5.74 AU	2.06µs	750 V	0

Table 2-6. LSM800 confocal microscope settings used in serine synthesis enzyme immunofluorescence image acquisition.

Acquired images measured 4096x4096 pixels in size and were subjected to Airyscan processing prior to visualising using Zen 2.5 Blue microscopy software (Zeiss). Airyscan processing utilises a deconvolution and pixel reassignment algorithm which is applied to each of the 32 detector channels individually. Identical histogram settings were applied to the resultant images to permit appropriate visual comparisons.

2.2.12.5.2. Human samples

All labelled sections were imaged using a Zeiss Celldiscoverer 7 fluorescent microscope (Zeiss). Using the tiling function, the entire section was scanned at a x10 magnification using a x20 Plan-Apochromat objective with 0.5x Tubelens Optavar. For OXPHOS section imaging, 625nm, 567nm, 470nm and 365nm LED modules were set at exposure times of 105ms, 200ms, 78ms and 16ms respectively. For PHGDH/NDUFB8/MTCO1 section imaging, 625nm, 567nm, 470nm and 365nm LED modules were set at exposure times of 300ms, 200ms, 100ms and 16ms respectively. For PSAT1/NDUFB8/MTCO1 section imaging, 625nm, 567nm, 470nm and 365nm LED modules were set at exposure times of 300ms, 400ms, 120ms and 20ms respectively. For MTHFD2/NDUFB8/MTCO1 section imaging, 625nm, 567nm, 470nm and 365nm LED modules were set at exposure times of 165ms, 200ms, 120ms and 16ms respectively. All light source intensities were set at 100%. All settings remained fixed within groups and images were acquired with an Axiocam 506 imaging device.

Analysis of OXPHOS labelled sections was undertaken using Zen Lite software (Zeiss). Using the spline contour tool, any crypt which appeared to be visually deficient in either NDUFB8 or MTCO1 was manually selected. This population formed the OXPHOS deficient crypt category which differed in quantity between subjects within a range of n=8 to n=110. At least an equal number of crypts demonstrating no visual deficiency of either of these proteins was selected at random in the same manner thus forming the normal crypt category. On a patient-by-patient basis, individual crypt Z scores were calculated using the method outlined in 2.2.11.4. Any outliers which deviated from the original classification as a result of this analysis were recategorised accordingly.

The same OXPHOS deficient and OXPHOS normal crypts were identified in adjacent serial sections labelled with PHGDH/NDUFB8/MTCO1**,** PSAT1/NDUFB8/MTCO1 and MTHFD2/NDUFB8/MTCO1. The spline contour tool was used to manually select these crypts however fluorophore intensity data were extracted from the 488nm channel only. These data represent the expression of each of the SSP/1C enzymes within the OXPHOS normal and deficient crypt compartments and were binned as such prior to enzyme expression level comparison.

2.2.13. Antibody validation and controls

The specificity of antibodies against mitochondrial OXPHOS protein complex subunits were previously validated in patients with known mutations in mtDNA or nuclear encoded complex I and complex IV subunits (Rocha et al., 2015). Similarly, antibodies targeting the UQCRFS1 subunit of complex III and ATPB subunit of complex V have been validated within the group in fibroblasts and skeletal muscle of patients harbouring pathogenic variants in genes known to impair complex III and complex V assembly (Oláhová et al., 2019; Thompson et al., 2018; Tuppen et al., 2010). All OXPHOS antibodies used in the current study are regularly used within the department and bind to proteins of the expected band size upon western blot analysis. As 6-month-old *PolγA*$^{+/+}$ colonic and small intestinal normal non-transformed crypts do not harbour age-related mtDNA mutations and thus do not exhibit OXPHOS protein defects (Greaves et al., 2011), they were used as internal positive controls in OXPHOS assays.

Antibodies targeting serine synthesis and mitochondrial one carbon cycle enzymes were previously validated and recommended for use by Prof. Owen Sansom, Beatson Institute for Cancer Research, Glasgow. Although specific positive controls were not used in individual SSP enzyme IHC/IF assays, the increased levels of these enzymes within *Apc* deficient adenomas in comparison to normal crypts in our model and the corroboration of this observation with those of the Sansom group using the same antibodies (Maddocks et al., 2017) confirmed the validity of the assay. The specificity of antibodies against thymidine analogues was previously validated in mice exposed to single thymidine analogues (Stamp, 2015). No primary controls (NPCs) were included in all assays.

2.2.14. Statistical analysis

With the exception of linear mixed effect model analyses which were carried out by Dr Alasdair Blain using the R programming language, all statistical analyses were performed using GraphPad Prism (version 8.4.3). Where pre-existing data supported a prediction in the direction of a difference between samples, a one-tailed test was used. In all other instances, two-tailed tests were used.

Chapter 3. Development and characterisation of a mouse model to investigate the effect of mitochondrial dysfunction in the pathogenesis of intestinal cancer

3.1. Introduction

Given the association of mitochondrial dysfunction and the accumulation of mtDNA mutations with increasing age, the development of two similar mouse models in 2004 and 2005 allowed the potential causative effect of mtDNA mutation accumulation on the ageing process to be investigated (Kujoth et al., 2005; Trifunovic et al., 2004). Although developed against different C57Bl/6 backgrounds using slightly different methodologies, both models share the same amino acid substitution at the same conserved residue within the mitochondrial polymerase gamma (*PolγA*) gene. This aspartate to alanine substitution at residue 257 of the conserved proofreading domain of *PolγA* impairs the exonuclease activity of the enzyme resulting in an up to eightfold increase in the likelihood of point mutations occurring during replication of the mitochondrial genome (Kujoth et al., 2005). In homozygous *PolγA* mice, multiple tissue types were shown by Southern blot to harbour shorter species of mtDNA representing deletions of the mitochondrial genome, however unlike the point mutational burden, the level of mtDNA deletions did not increase with age. Without evidence of specific mutational hotspots, the random generation of cumulative levels of mtDNA point mutations was the prevailing molecular phenotype in mutator mice (Trifunovic et al., 2004). Tissues analysed in both models including the brain, heart, liver, sperm and duodenum showed that transition mutations represented the largest class of mutation in mutator mice. This was reportedly attributed to nucleotide misincorporation by the polymerase (Kujoth et al., 2005).

In both models, the lifespan of mutator mice is significantly reduced compared with wild-type controls with mutator mice surviving a median of 11-13 months in comparison to a 28-month maximum survival of wild type animals. Clinically, *PolγA* mutator mice appear phenotypically comparable to their wild-type counterparts until around six months of age. At this time point, numerous progeroid features become apparent. First noted was the appearance of alopecia and a slight kyphosis (curvature of the spine) (Trifunovic et al., 2004). Weight loss was also noted in mutator mice from 6 months of age. X-ray densitometry of 4 and 9 month old mutator mice revealed a significant reduction in percentage body fat in mutator versus wild type animals at both time points (Trifunovic et al., 2004) and at 9

months of age, a significant loss of muscle mass (sarcopenia) was demonstrated by a reduced weight of gastrocnemius and quadriceps muscles in mutator versus wild type animals (Kujoth et al., 2005). Sarcopenia and a reduction in body fat both contribute to an overall decrease in body weight and are both also common features of ageing in humans (Rosenberg, 1997; Roubenoff, 1999). Also demonstrated using X-ray densitometry was a reduction in bone mineral composition (BMC) and bone mineral density (BMD) in 9-month-old mutator mice, consistent with the development of osteoporosis in ageing humans (Trifunovic et al., 2004). Recent *in vivo* analyses of *PolγA*$^{mut/mut}$ and wild-type lumbar spines, femurs and tibiae further demonstrate a significantly accelerated rate of bone loss associated with age-related mitochondrial respiratory chain deficiency in osteoblasts and osteoclasts in *PolγA*$^{mut/mut}$ animals. *In vitro* investigations revealed a severely impaired mineralised matrix formation and increased osteoclast resorption by *PolγA*$^{mut/mut}$ femur cells (Dobson et al., 2020).

In comparison to their wild-type counterparts, 6-month-old *PolγA* mutator mice present with significantly reduced peripheral blood haemoglobin levels with an anaemia characterised by enlarged (macrocytic), pale coloured (hypochromic) erythrocytes (Trifunovic et al., 2004). The maturation of erythrocytes involves their migration from the bone marrow into the peripheral blood when intracellular haemoglobin levels are sufficient. They enucleate and mature further within the circulation with removal of their mitochondria and clearing of transferrin receptors. The mechanism by which anaemia develops in the *PolγA* mouse has been elucidated and is reported to be due to a perturbation in these maturation steps, initiated by mutated mtDNA and resultant alterations in ROS within immature erythrocytes (Ahlqvist et al., 2015). In comparison to wild-type animals, 11-month-old *PolγA*$^{mut/mut}$ mice showed an increased frequency of reticulocytes: immature erythrocytes, with significantly elevated mitochondrial retention. The mitophagy marker NIX, indicated that the active removal of mitochondria was also significantly reduced in *PolγA*$^{mut/mut}$ reticulocytes. The transferrin receptor (TfR) was also found to be abnormally retained within *PolγA*$^{mut/mut}$ reticulocytes, causing increased loading of free iron within these cells. As free iron is highly reactive with oxygen, reactive oxygen species are generated in reticulocytes in which both TfR and mitochondria are retained. Cell surface proteins which are normally appropriated to the inner cell membrane as erythrocytes mature remain on the surface due to oxidative damage to the enzymes that facilitate their segregation. These cell surface proteins label the

erythrocytes for premature destruction by splenic macrophages, as indicated by significantly increased levels of iron loaded activated macrophages within the spleen of *PolγA*$^{mut/mut}$ mice (Ahlqvist et al., 2015).

Additional observations taken from the Trifunovic mouse included an enlargement of the hearts of 9-month-old mutator mice and the presence of a mosaic pattern of cardiomyocytes demonstrating reduced cytochrome c oxidase (COX) activity as evidenced by enzyme histochemical COX/SDH labelling. This phenotype is also demonstrated in humans with the frequency of COX deficient cardiomyocytes increasing with advancing age (Muller-Hocker, 1989). Histological analysis of the testes of 9-month-old mutator mice also revealed an absence of sperm and severe testicular tubular degeneration in concordance with the age-related decline in fertility observed in humans (Trifunovic et al., 2004). In the absence of evidence of increased markers of oxidative damage or defective cellular proliferation in mutator versus wild-type animals, Kujoth et al. suggest that the earlier induction of a caspase 3–mediated apoptotic pathway present in the normal ageing of wild type animals may be the underlying cause. Increased levels of cleaved caspase 3 were shown to be present within the heart, liver, skeletal muscle and testes of 30-month-old versus 5-month-old wild type mice which may contribute to the functional decline of tissues observed in normal ageing. Cleaved-caspase 3 levels are significantly increased at a much earlier stage in mutator mice compared to age matched wild-type controls; 3 months of age in duodenum, liver, testis, and thymus and 9 months of age in post-mitotic tissues such as the brain and skeletal muscle (Kujoth et al., 2005).

With regard to the intestinal phenotype of the Kujoth model, it has been shown that the pattern of somatic mtDNA mutations within the colon of aged *PolγA*$^{+/mut}$ mice is similar to that which is seen in aged humans. The spectrum of mutations is shown to be similarly random in both species, and subjection to selection pressures is not evident (Baines et al., 2014). Additionally, computer simulation models suggest that predominantly asymmetric stem cell division coupled with random genetic drift is sufficient to drive the clonal expansion of somatic mtDNA mutations in mitotic tissues resulting in respiratory chain deficiency in both *PolγA*$^{+/mut}$ mice and humans (Baines et al., 2014; Stamp et al., 2018). A similar situation is described within the small intestine of *PolγA*$^{+/mut}$ mice in which mtDNA point mutations with high levels of heteroplasmy were identified within COX negative villi of

15-month-old mice (Vermulst et al., 2008). The demonstration of an age-related intestinal pathology in *PolγA*$^{+/mut}$ mice and an absence of COX negative villi in aged matched wild type control mice further supports the appropriate application of this model for use in this study. Additionally, the Kujoth mouse is utilised due to its retention of only one *LoxP* site at the *PolγA* locus following homologous recombination and neomycin cassette excision. The Trifunovic mouse retains two *LoxP* sites thus rendering it incompatible with other mouse models in which Cre mediated excision is to be used.

Having identified a suitable model of age-related mitochondrial dysfunction in the intestine, an appropriate model of intestinal tumorigenesis was subsequently required in order to investigate this *in vivo*. Requirements of the model included biological relevance to human colorectal cancer and a temporospatial inducibility of tumorigenesis following an appropriate time period of intestinal mtDNA mutation accumulation. Lineage tracing experiments in which *Lgr5-EGFP-IRES-creERT2* mice were crossed with mice bearing a Cre inducible *Rosa26-lacZ* reporter gene identified *Lgr5* positive cells as being pluripotent and capable of maintaining the self-renewal of the murine colonic and small intestinal epithelium (Barker et al., 2007). The subsequent crossing of *Lgr5-EGFP-IRES-creERT2* mice with *Apc*$^{flox/flox}$ mice enabled stem cell specific deletion of *Apc* to be induced upon creERT2 activation with tamoxifen. The loss of *Apc* from *Lgr5+* cells initiated the development of and allowed the rapid expansion of numerous adenomas throughout the intestines of experimental animals with this pathology leading to their necessary culling at 36 days post *Apc* deletion (Barker et al., 2009). Immunohistochemical analysis demonstrated increased levels of β-catenin expression in isolated crypt base cells from as early as 3 days and 8 days post tamoxifen induction in the small intestine and colon respectively. This is indicative of Wnt signalling activation concurrent with *Apc* loss, also confirmed immunohistochemically by high levels of expression of the Wnt target gene *c-myc* within small intestinal lesions from 8 days post *Apc* deletion. In contrast, the deletion of *Apc* from non-stem transit amplifying and villous compartment cells using the β-naphthoflavone activated *Ah-Cre/Apc*$^{flox/flox}$*/Rosa26R* mouse facilitated the development of β-catenin^{high} clusters of cells, however these foci, despite their persistence, did not expand, nor did they progress to adenomas. As such, *Lgr5*+ve cells were identified as the cells of origin of intestinal cancer and the *Lgr5-EGFP-IREScreERT2/Apc*$^{flox/flox}$ mouse selected as an established inducible model of intestinal cancer appropriate for use in this study.

In 2012, Woo and colleagues describe a mouse model of intestinal neoplasia (*Apc*$^{Min/+}$) in which intestinal adenoma growth is promoted by mtDNA instability elicited by a *Tfam*$^{+/-}$ genotype also present within the model. TFAM is required for the expression and maintenance of mtDNA and the loss of one *Tfam* allele drives a mild phenotype in which mtDNA is slightly depleted and more susceptible to oxidative damage than wild type cells. In comparison with *Apc*$^{Min/+}$ *Tfam*$^{+/+}$ mice, *Apc*$^{Min/+}$ *Tfam*$^{+/-}$ mice demonstrated a significantly greater frequency and size of small intestinal adenomas suggesting that *Tfam*$^{+/-}$ mediated mitochondrial genome instability enhances intestinal tumour growth (Woo et al., 2012). Although highly relevant, the work of Woo and colleagues does not specifically address the accumulation of somatic mtDNA mutations that have been extensively linked with both ageing and numerous cancer types. Nor does it address the temporospatial occurrence of events that may cause mtDNA instability and/or tumorigenesis. Accordingly, the *Lgr5-EGFP-IREScreERT2/Apc*$^{flox/flox}$ mouse was selected for this study due to its intestinal stem cell specific inducible deletion of *Apc* (Barker et al., 2009). In order to investigate the potential effect of an age-related accumulation of somatic mtDNA mutations on the growth of intestinal adenomas that develop within this model, it was crossed with the *PolγA* mutator mouse and aged sufficiently prior to an intestinal stem-cell derived tumour initiation providing the final model for this study. Specifically, the Kujoth variant of the *PolγA* mutator mouse was selected due to its retention of only one *LoxP* site at the *PolγA* locus (Kujoth et al., 2005). Use of the Trifunovic *PolγA* mutator mouse in which two *LoxP* sites flanking the *PolγA* locus are retained would not be compatible with the Cre/*LoxP* mediated *Apc* deletion utilised within the *Lgr5-EGFP-IREScreERT2/Apc*$^{flox/flox}$ mouse as excision of *PolγA* would also occur with tamoxifen administration. Furthermore, it has been demonstrated that the pattern of somatic mtDNA mutations within the colon of aged Kujoth *PolγA*$^{+/mut}$ mice is similar to that which is seen in aged humans with *PolγA* derived mtDNA mutations also reaching high levels of heteroplasmy within the COX negative small intestinal crypts of 15-month-old Kujoth *PolγA*$^{+/mut}$ mice (Baines et al., 2014; Vermulst et al., 2008). The intestinal phenotype and retention of only one *LoxP* site within the Kujoth model therefore provided the rationale for its selection for this study.

3.2. Aims of study

Having identified suitable mouse models of both inducible intestinal cancer and a premature ageing phenotype caused by the accumulation of mtDNA mutations, the aims of this study were to:

1. Generate a transgenic mouse model to be used to investigate the role of mtDNA mutations in intestinal cancer development.
2. Evaluate the clinical phenotype of this mouse model with regards clinical symptoms, their severity and their effect on lifespan.
3. Macroscopically and microscopically examine adenoma burden comparing frequency, size and total burden across experimental groups all culled at the same time point post *Apc* deletion.
4. Assess the toxicity and potential effect on lifespan of the tamoxifen regime used to induce tumorigenesis in experimental animals.

3.3. Results

3.3.1. Generation of a transgenic mouse model

Each of the three mouse lines required to generate the appropriate transgenic model were obtained separately. In order to cross these lines successfully, specific features pertaining to the phenotypes of each line were taken into consideration. All animal breeding was undertaken by Dr Laura Greaves and Carla Bradshaw. Features characteristic to each model were also used to develop a clinical scoring protocol in which appropriate symptoms would be gauged. As *PolyA* mutator mice present with weight loss and anaemia, animals were weighed daily, and the colour of extremities assessed. The condition of the coat of a mouse can often be an indicator pain or distress; a lack of grooming is noted when health is deteriorating. Similarly, the presence of piloerection can indicate dehydration (Burkholder et al., 2012). As greying of the fur and alopecia are reported in *PolγA* mutators, particular attention was paid to coat condition in experimental animals.

As adenomas extensively develop within the intestine of Apc^{Min} mice, premature death occurs due to chronic anaemia and intestinal obstruction; effects which are secondary to the adenoma burden itself (Shoemaker et al., 1997). Accordingly, experimental animals were monitored for signs of intestinal blockage such as abdominal distension, diarrhoea and reduced mobility. In addition to observing the colour of extremities, stools were checked for the presence a blood, also an indicator of intestinal pathology and associated anaemia. Details of clinical symptoms monitored, and scores given for aberrations can be found in Table 2-4.

3.3.1.1. PolγA$^{mut/mut}$ mitochondrial mutator mice breeding

Homozygous *PolγA$^{mut/mut}$* mice of both genders present with reduced fertility. The testes of male mutator mice are smaller than those of wild type males at 3 months of age and by 9 months of age, a complete absence of sperm is noted in male mutator mice. Female homozygous mutator mice only give birth to one litter and do not become pregnant a second time after 4 months of age despite continuous exposure to male mice (Trifunovic et al., 2004). In order to propagate our colony of *PolγA$^{+/+}$*, *PolγA$^{+/mut}$* and *PolγA$^{mut/mut}$* animals, four *PolγA$^{+/mut}$* male mice were donated from a well-established colony and mated with female C57Bl/6J wild type mice as shown in Figure 3-1. In Figure 3-1 and subsequent breeding schedules, green mice denote a *PolγA$^{mut/mut}$* genotype while blue and red mice denote *PolγA$^{+/mut}$* and *PolγA$^{+/+}$* genotypes respectively.

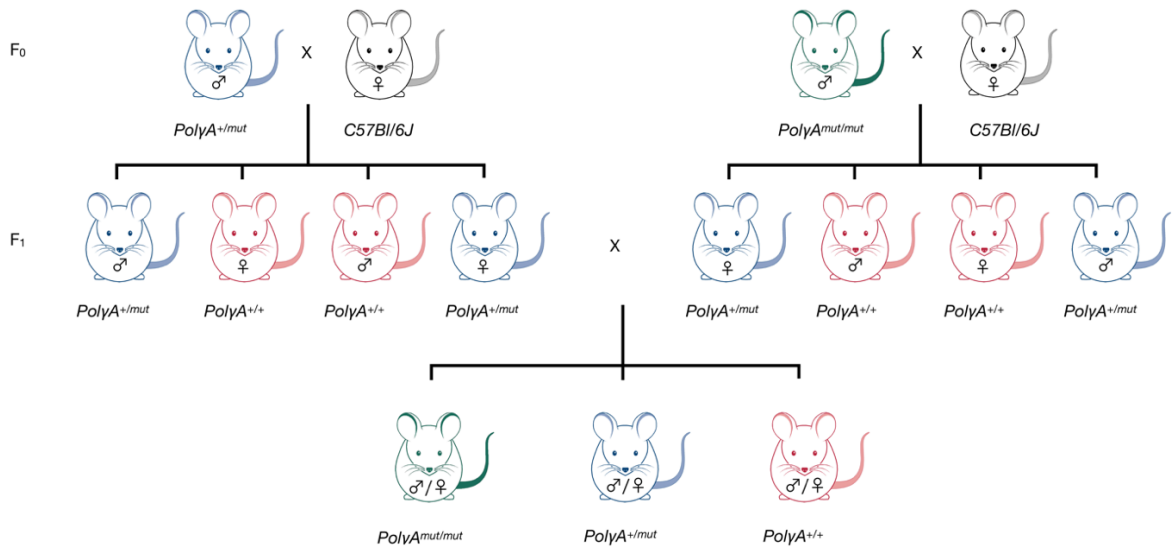

Figure 3-1. Mitochondrial mutator mouse breeding schedule. *PolγA$^{+/mut}$* male mice were mated with C57Bl/6J wild type female mice in order to generate *PolγA$^{+/mut}$* and *PolγA$^{+/+}$* males and females. Subsequent mating of heterozygous animals propagated the colony permitting the generation of *PolγA$^{mut/mut}$* animals. Green mice denote *PolγA$^{mut/mut}$* genotype while blue and red mice denote *PolγA$^{+/mut}$* and *PolγA$^{+/+}$* genotypes respectively.

3.3.1.2. Lgr5-EGFP-Ires-CreERT2 and Apc$^{flox/flox}$ mice breeding

Homozygous *Lgr5*$^{-/-}$ mice present with a craniofacial defect in which the tongue is fused to the floor of the oral cavity. This causes a suckling defect in which air is swallowed and mutant neonates die within 24 hours of birth (Morita et al., 2004). As such, breeding schemes were designed to avoid the generation of this lethal phenotype. There were no breeding issues with *Apc*$^{flox/flox}$ mice. *Lgr5*$^{+/-}$ males were donated and mated with *Apc*$^{flox/flox}$ females and only offspring with *Lgr5*$^{+/-}$ and *Lgr5*$^{+/+}$ genotypes subsequently crossed to generate *Lgr5*$^{+/-}$/*Apc*$^{flox/flox}$ females for use in experimental animal generation. This cross is depicted as shown in Figure 3-2.

Simultaneously, *Apc*$^{flox/flox}$ females were also crossed with *PolyA*$^{+/mut}$ males. This is shown in Figure 3-3. Subsequent mating of males and females from the F_1 generation provided *PolyA*$^{+/mut}$/*Apc*$^{flox/flox}$ males for use in generating experimental animals.

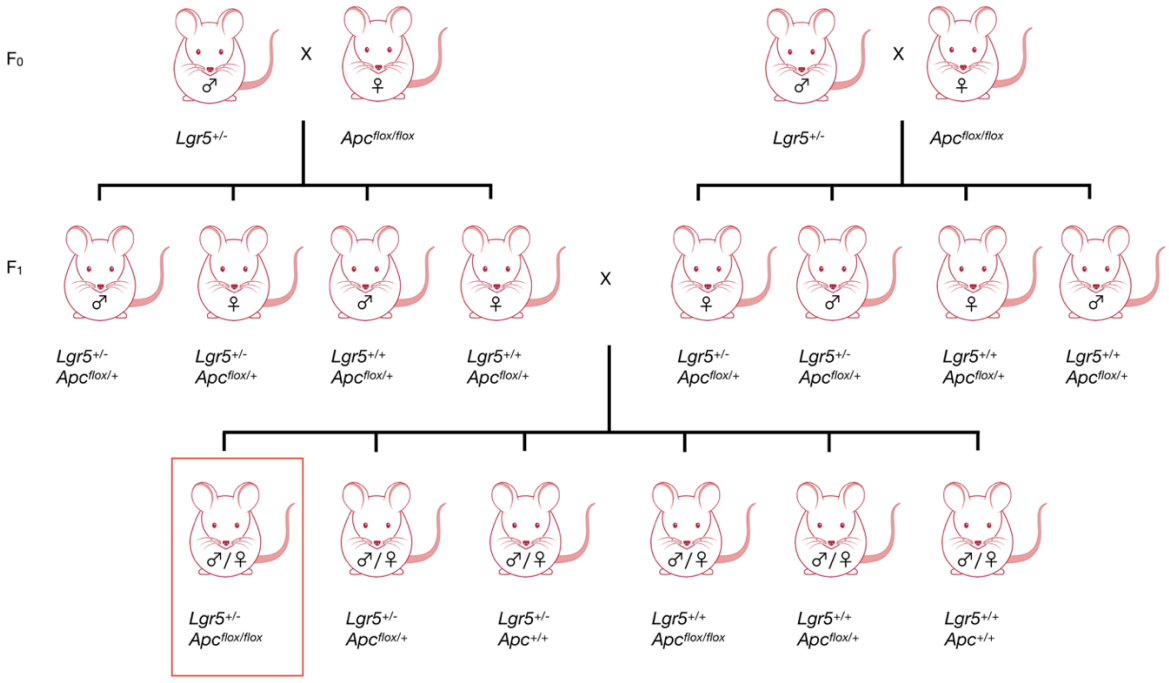

Figure 3-2. *Lgr5-EGFP-Ires-CreERT2* and *Apc*$^{flox/flox}$ mice breeding schedule. *Lgr5*$^{+/-}$ males were mated with *Apc*$^{flox/flox}$ females. Subsequent mating of males and females from the F_1 generation provided *Lgr5*$^{+/-}$/*Apc*$^{flox/flox}$ females (highlighted in red box) for use in generating experimental animals.

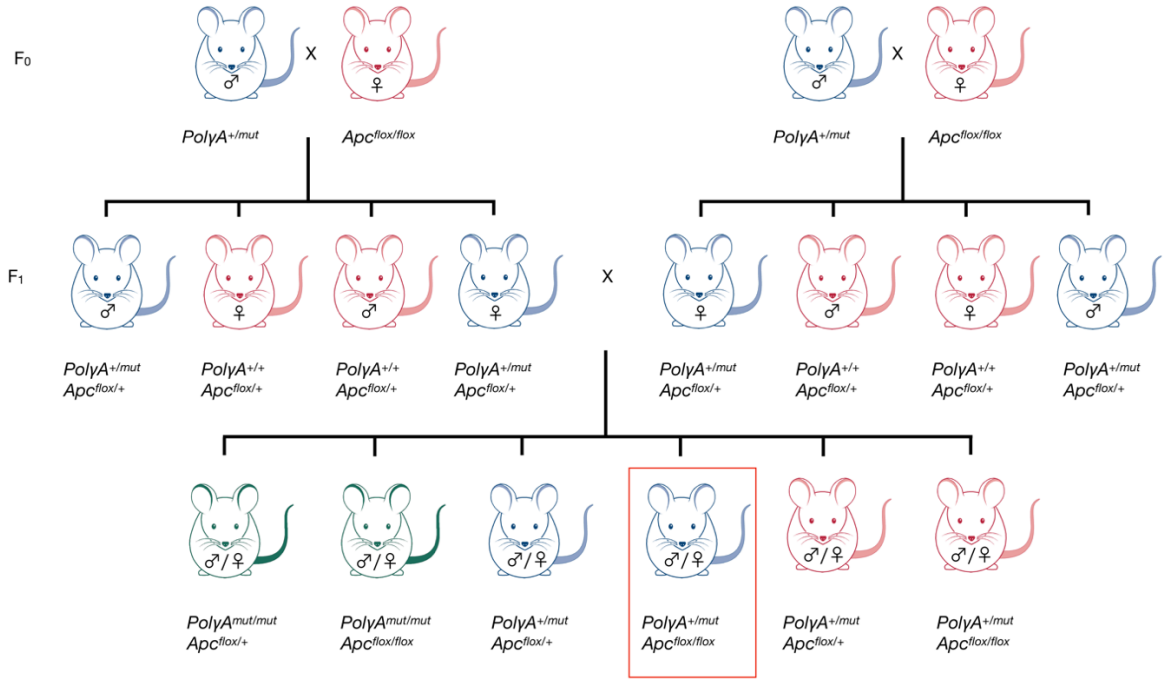

Figure 3-3. *PolγA*$^{+/mut}$ and *Apc*$^{flox/flox}$ breeding schedule. *PolγA*$^{+/mut}$ males were mated with *Apc*$^{flox/flox}$ females. Subsequent mating of males and females from the F_1 generation provided *PolγA*$^{+/mut}$ /*Apc*$^{flox/flox}$ males (highlighted in red box) for use in generating experimental animals.

3.3.1.3. Experimental animal generation

Generation of experimental animals was achieved by mating *PolγA*$^{+/mut}$/*Apc*$^{flox/flox}$ males and *Lgr5*$^{+/-}$/*Apc*$^{flox/flox}$ females. This cross generated control *PolγA*$^{+/+}$/*Lgr5*$^{+/-}$/*Apc*$^{flox/flox}$ and experimental *PolγA*$^{+/mut}$/*Lgr5*$^{+/-}$/*Apc*$^{flox/flox}$ F_1 animals. Mating *PolγA*$^{+/mut}$/*Lgr5*$^{+/-}$/*Apc*$^{flox/flox}$ and *PolγA*$^{+/mut}$/*Lgr5*$^{+/+}$/*Apc*$^{flox/flox}$ males and females from this generation produced *PolγA*$^{mut/mut}$/*Lgr5*$^{+/-}$/*Apc*$^{flox/flox}$ experimental animals. As mtDNA mutations in the germline are transmitted to offspring (Giles et al., 1980), 'control' *PolγA*$^{+/+}$ /*Lgr5*$^{+/-}$/*Apc*$^{flox/flox}$ animals from *PolγA*$^{+/mut}$ mothers (also generated in this cross) are not truly wild type and were not used experimentally. In order to minimise this transmission, control animals from the F_1 generation only were used as such. The generation of experimental animals is depicted in Figure 3-4.

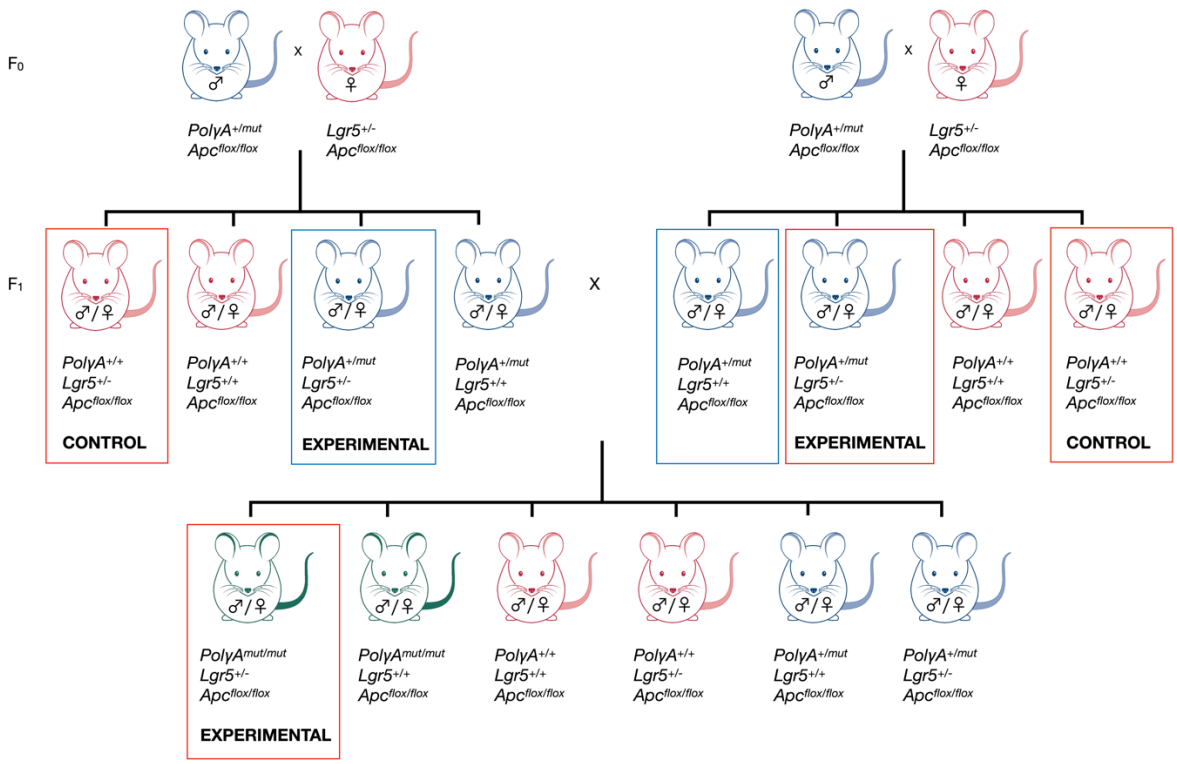

Figure 3-4. Breeding schedule depicting the mating of *PolyA*$^{+/mut}$/*Apc*$^{flox/flox}$ males with *Lgr5*$^{+/-}$/*Apc*$^{flox/flox}$ females. F_1 generation *PolyA*$^{+/+}$ /*Lgr5*$^{+/-}$/*Apc*$^{flox/flox}$ animals highlighted accordingly were used as experimental control animals. Crossing of F_1 generation animals highlighted in blue boxes permitted the generation of *PolyA*$^{mut/mut}$/ *Lgr5*$^{+/-}$/*Apc*$^{flox/flox}$ experimental animals. *PolyA*$^{+/mut}$ /*Lgr5*$^{+/-}$/*Apc*$^{flox/flox}$ experimental animals were obtained at the F_1 generation.

3.3.1.4. Experimental cohorts

In order to address different experimental objectives, several cohorts were established. Each of these cohorts are outlined in Table 3-1 alongside the rationale behind the development of each group.

Cohort	Tamoxifen induction dose	*PolγA* genotypes	Age at induction	Experiment endpoint	Rationale
Lifespan (6)	3mg, 2mg, 2mg, 2mg	*PolγA*$^{+/+}$ *PolγA*$^{+/mut}$ *PolγA*$^{mut/mut}$	6 months	Lifespan	To investigate whether mtDNA mutations decrease the lifespan of animals post *Apc* deletion.
Lifespan (12)	3mg, 2mg, 2mg, 2mg	*PolγA*$^{+/+}$ *PolγA*$^{+/mut}$	12 months	Lifespan	As above. No *PolγA*$^{mut/mut}$ animals included as systemic mitochondrial dysfunction limits survival of these mice to ~12 months of age (Trifunovic et al., 2004). Mosaic pattern of OXPHOS defects observed in *PolγA*$^{+/mut}$ mouse intestine allows for intra mouse comparison and control.
Day 23 (6)	3mg, 2mg, 2mg, 2mg	*PolγA*$^{+/+}$ *PolγA*$^{+/mut}$ *PolγA*$^{mut/mut}$	6 months	23 days post *Apc* deletion (median lifespan of *PolγA*$^{mut/mut}$ induced at 6 months of age)	All animals sacrificed at the same time point post *Apc* deletion to allow direct comparison of rate of tumour progression.
Day 23 (12)	3mg, 2mg, 2mg, 2mg	*PolγA*$^{+/+}$ *PolγA*$^{+/mut}$	12 months	23 days post *Apc* deletion	As above, omitting *PolγA*$^{mut/mut}$ animals.
Tamoxifen control	-	*PolγA*$^{+/+}$ *PolγA*$^{mut/mut}$	6 months	Lifespan	Assessment of the toxicity and potential effect on lifespan of the tamoxifen regime used to induce tumorigenesis in experimental animals.
Thymidine analogue	3mg, 2mg, 2mg, 2mg	*PolγA*$^{+/+}$ *PolγA*$^{mut/mut}$	6 months	16 days post *Apc* deletion	Thymidine analogue incorporation to explore cell cycle kinetics within adenomas of *PolγA*$^{+/+}$ versus *PolγA*$^{mut/mut}$ mice.

Table 3-1. Experimental cohorts used in this study.

3.3.2. Lifespan cohorts (6 and 12 months)

Mitochondrial OXPHOS dysfunction is not commonly observed in the intestine of normal ageing mice. By six months of age, both *PolγA*$^{mut/mut}$ and *PolγA*$^{+/mut}$ mice demonstrate significantly greater frequencies of COX deficient crypts when compared to wild type animals. Up to 60% of colonic crypts of *PolγA*$^{mut/mut}$ mice are COX deficient by the age of six months whereas only ~5% are COX deficient in *PolγA*$^{+/mut}$ mice of the same age (Baines et al., 2014). There is no evidence of COX deficiency in the colonic crypts of *PolγA*$^{+/+}$ mice at 6 months of age (Greaves et al., 2011). As such, *PolγA*$^{mut/mut}$ (n=23), *PolγA*$^{+/mut}$ (n=17) and *PolγA*$^{+/+}$ (n=15) mice were aged to six months before beginning the intraperitoneal tamoxifen regime for tumour induction. Intraperitoneal tamoxifen (T5648, Sigma Aldrich) was administered over the course of four days at a concentration of 10mg/ml in sunflower oil. Day one; 300µl (3mg), day two to four; 200µl (2mg) each day (2.2.5.).

By 12 months of age, a 40% loss of complex I (NDUFB8) and a 20% loss of complex IV (MTCO1) is reported in colonic crypts of *PolγA*$^{+/mut}$ mice (Stamp, 2015). A mosaic pattern of OXPHOS defects within these animals allows intra-mouse comparisons to be made while also providing internal controls. Furthermore, as *PolγA*$^{+/-}$ mice do not present with a premature ageing phenotype (Kujoth et al., 2005; Trifunovic et al., 2004) the systemic effects of the *PolγA* mutation on adenoma development in these animals is greatly reduced. As such, a further cohort of *PolγA*$^{+/mut}$ (n=14) and *PolγA*$^{+/+}$ (n=11) animals were aged to 12 months prior to tamoxifen induction. As described in 2.2.6 and presented in Table 2-2 all mice were monitored daily and clinical scores recorded until such scores dictated that they be humanely killed. Mice were euthanised using the Schedule 1 approved method of concussion of the brain followed by cervical dislocation (Animals Scientific Procedures Act, 1986).

3.3.2.1. Investigating the effect of mtDNA mutations on lifespan post-Apc deletion

In order to investigate the effect of age-related mitochondrial dysfunction on intestinal adenoma growth and ascertain if this has any impact on longevity following intestinal *Apc* deletion, survival analyses of experimental animals were carried out. All animals were aged to six months to allow an accumulation of *PolγA* mediated mtDNA mutations in $PolγA^{+/mut}$ and $PolγA^{mut/mut}$ mice prior to tamoxifen induction and *Apc* deletion. Survival curves of animals monitored are shown in Figure 3-5. $PolγA^{mut/mut}$ and $PolγA^{+/mut}$ animals showed clinical signs of deteriorating health much earlier than $PolγA^{+/+}$ wild type animals. When compared to $PolγA^{+/+}$ and $PolγA^{+/mut}$ mice, $PolγA^{mut/mut}$ mice have significantly shorter lifespans (P<0.0001, Mantel-Cox log rank test).

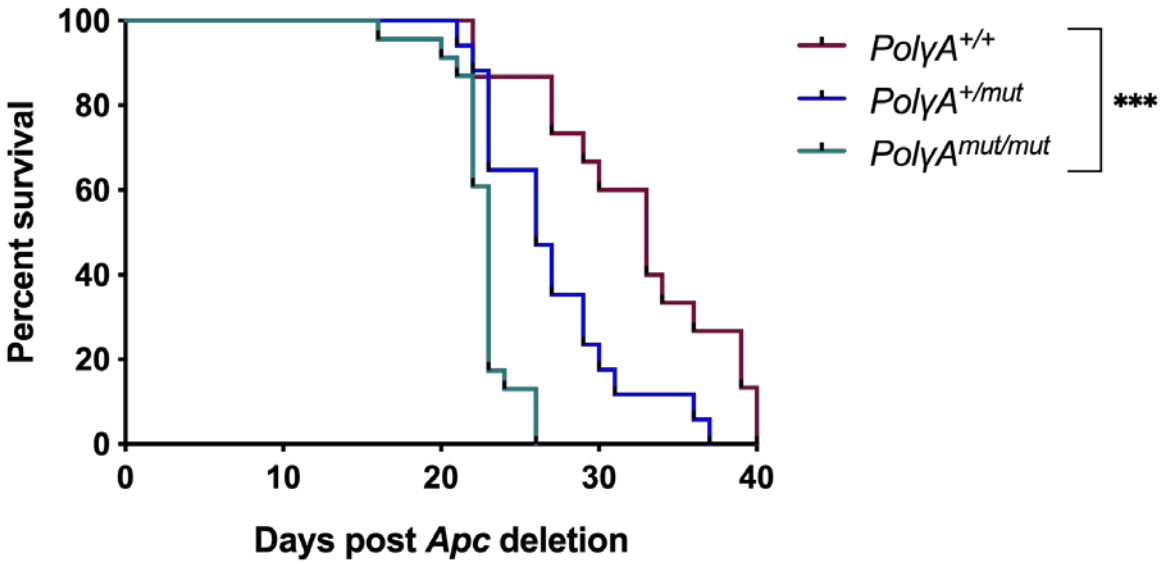

Figure 3-5. Kaplan-Meier survival curve depicting survival times of $PolγA^{+/+}$ (n=15), $PolγA^{+/mut}$ (n=17) and $PolγA^{mut/mut}$ (n=23) mice aged to 6 months prior to *Apc* deletion. $PolγA^{mut/mut}$ mice have significantly shorter lifespans in comparison to $PolγA^{+/+}$ and $PolγA^{+/mut}$ animals. Mantel-Cox log rank test P<0.0001.

Given that at 12 months of age, $PolγA^{+/mut}$ mice display colonic crypt respiratory chain deficiency comparable to 70-year-old human subjects (Stamp, 2015), in order to investigate the effect of this burden post-*Apc* deletion at a level comparable to humans, a survival analysis was carried out in $PolγA^{+/+}$ and $PolγA^{+/mut}$ mice aged to 12 months prior to *Apc* deletion. Survival curves of animals monitored are shown in Figure 3-6. $PolγA^{+/mut}$ mice aged

to 12 months prior to *Apc* deletion have significantly shorter lifespans post *Apc* deletion than *PolγA*$^{+/+}$ mice (P=0.0211, Mantel-Cox log rank test).

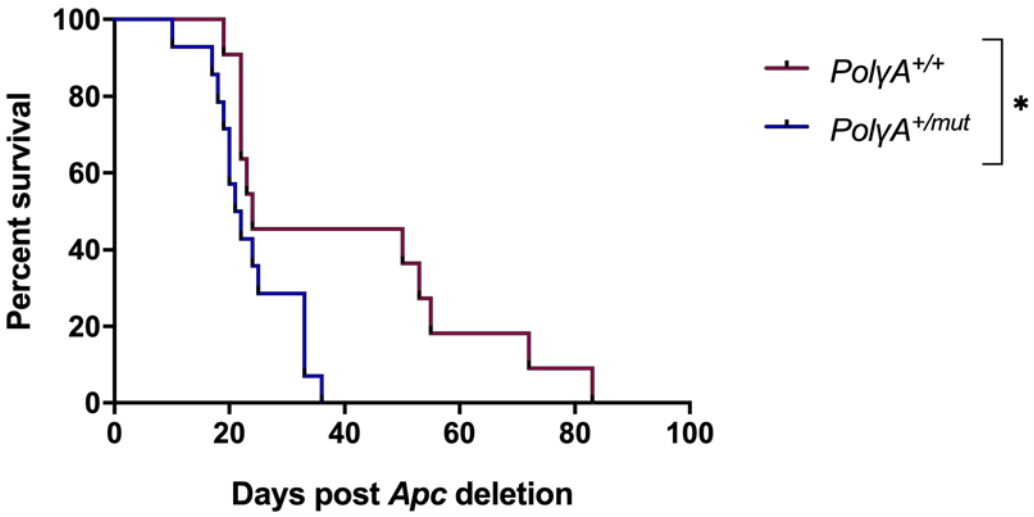

Figure 3-6. Kaplan-Meier survival curve depicting survival times of *PolγA*$^{+/+}$ mice (n=11) and *PolγA*$^{+/mut}$ (n=14) aged to 12 months prior to *Apc* deletion. *PolγA*$^{+/+}$ mice have significantly shorter lifespans in comparison to *PolγA*$^{+/mut}$ animals. Mantel-Cox log rank test, P=0.0211.

3.3.2.2. Investigating the effect of mtDNA mutations on body mass post-Apc deletion

Defined as a significant reduction in body weight resulting largely from the loss of adipose tissue and skeletal muscle, cancer cachexia is a co-morbid condition that affects the majority of cancer patients with advanced disease (Fearon et al., 2012). Cachexia as evidenced by unintentional weight loss is most common in intestinal cancer over all other cancer types (reviewed in Tan & Fearon, 2008). Weight loss can be used as an indicator of health in animal models, particularly in those of intestinal cancer where occlusion of the intestine may occur. As such, all experimental animals were weighed daily as part of their clinical monitoring protocol. Presented in Figure 3-7, weight loss is noted in all experimental groups from approximately ten days post *Apc* deletion. A significant negative correlation of mean body mass with time post *Apc* deletion is detected in each group (*PolγA*$^{+/+}$ r^2=0.6031, P<0.0001, *PolγA*$^{+/mut}$ r^2=0.1481, P=0.0187, *PolγA*$^{mut/mut}$ r^2=0.3088, P<0.0048, Pearson correlation analyses).

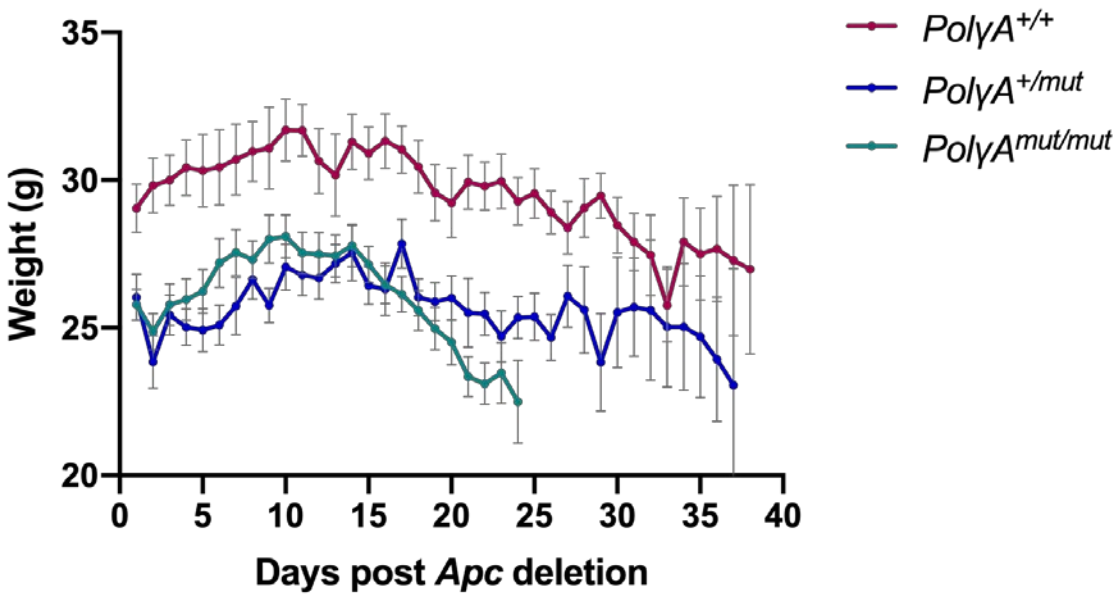

Figure 3-7. Mean body mass measurements of experimental animals following *Apc* deletion at six months of age. *PolyA*$^{+/+}$ (n=15), *PolyA*$^{+/mut}$ (n=15) and *PolyA*$^{mut/mut}$ (n=20). Weight was measured each day during and following the IP tamoxifen *Apc* deletion regime. Pearson correlation analyses detect a significant negative correlation in all groups. *PolyA*$^{+/+}$ r^2=0.6031, P<0.0001, *PolyA*$^{+/mut}$ r^2=0.1481, P=0.0187, *PolyA*$^{mut/mut}$ r^2=0.3088, P=0.0048. Mean body mass significantly decreases in all groups following tamoxifen induction of *Apc* deletion. Data are represented as mean ± SEM.

An initial drop in mean body mass from days 1 to 4 (*PolyA*$^{+/mut}$ and *PolyA*$^{mut/mut}$) was attributed to stress experienced by the animals caused by daily intraperitoneal injections during this time period. The subsequent steady increase in mean body mass would correlate with the removal of this stressor upon completion of the IP regime. This is not apparent within the *PolyA*$^{+/+}$group and may reflect a decreased intervention tolerance within the *PolyA*$^{mut/mut}$ and *PolyA*$^{+/mut}$ groups due to their phenotype. The exclusion of these initial 4 days post *Apc* deletion may allow a more appropriate analysis of weight loss as the effect of stress of the induction regime on this measure is removed. In fact, the correlation of body mass with days post *Apc* deletion is strengthened by this as evidenced by an increase in r^2 values in all groups (*PolyA*$^{+/+}$ r^2=0.7843, P<0.0001, *PolyA*$^{+/mut}$ r^2=0.3574, P=0.0002, *PolyA*$^{mut/mut}$ r^2=0.7052, P<0.0001, Pearson correlation analyses). Subsequent linear regression analysis followed by analysis of covariance allows the comparison of rates of weight loss from the point at which the induction regime stressor is removed. A significant slope deviation from zero is detected in all cases (*PolyA*$^{+/+}$ P<0.0001, *PolyA*$^{+/mut}$ P=0.0002, *PolyA*$^{mut/mut}$ P<0.0001, linear regression) while significant differences between slopes were detected in all comparisons (*PolyA*$^{+/+}$ versus *PolyA*$^{+/mut}$ P=0.0008, *PolyA*$^{+/+}$ versus *PolyA*$^{mut/mut}$ P=0.0011, *PolyA*$^{+/mut}$ versus *PolyA*$^{mut/mut}$ P<0.0001, analysis of covariance). These data are presented in Figure 3-8. The weight loss observed in our model post *Apc* deletion is

consistent with that seen in other mouse models of *Apc* deletion (Muller et al., 2009) and is likely due to the functional decline or blockage of the intestine as the adenomas grow in addition to a reduced intake as the condition of the animals deteriorates. This is exacerbated in *PolyA*$^{mut/mut}$ animals in comparison with *PolyA*$^{+/+}$ and *PolyA*$^{+/mut}$ mice following *Apc* deletion at 6 months of age.

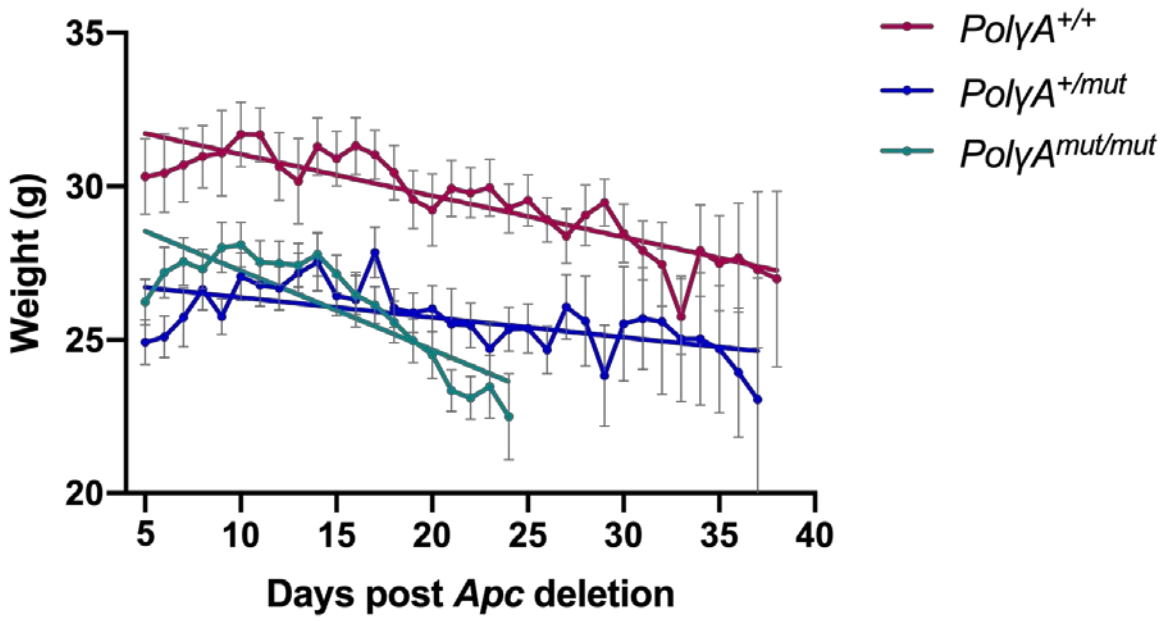

Figure 3-8. Correlation and linear regression analyses of mean body mass measurements over time from day 5 post *Apc* deletion. A significant negative correlation of body temperature with increasing time post *Apc* deletion is detected in all groups (*PolyA*$^{+/+}$ r^2=0.7843, P<0.0001, *PolyA*$^{+/mut}$ r^2=0.3574, P=0.0002, *PolyA*$^{mut/mut}$ r2=0.7052, P<0.0001, Pearson correlation analyses). Comparison of linear regression slopes detected a significant difference between all groups (*PolyA*$^{+/+}$ versus *PolyA*$^{+/mut}$ P=0.0008, *PolyA*$^{+/+}$ versus *PolyA*$^{mut/mut}$ P=0.0011, *PolyA*$^{+/mut}$ versus *PolyA*$^{mut/mut}$ P<0.0001, analysis of covariance). Error bars denote mean ±SEM.

3.3.2.3. Anaemia

In patients with FAP, as adenomas become larger and more numerous they may bleed, patients presenting with rectal bleeding and anaemia as a result (Half et al., 2009). Iron deficiency and anaemia are also common in colorectal cancer (Edna et al., 2012; Ludwig et al., 2004; Wilson et al., 2017), and their presence often associated with poor outcome (Ludwig et al., 2013; Zacharakis et al., 2010).

Anaemia is also a prominent clinical symptom in mouse models of intestinal cancer. By 2 months of age, heterozygous *Apc*^{Min} mice become anaemic with death occurring around 4

months of age. This is attributed to an extensive adenoma burden and secondary anaemia due to this burden (Moser et al., 1990). As such, as part of the clinical scoring of our cohort, all experimental animals were monitored for the appearance of pale extremities and blood in the stools. Within experimental groups in which *Apc* was deleted at 6 months of age (*PolγA*$^{+/+}$ (n=19), *PolγA*$^{+/mut}$ (n=24) and *PolγA*$^{mut/mut}$ (n=29)), 63.2% of *PolγA*$^{+/+}$, 75% of *PolγA*$^{+/mut}$ and 93.1% of *PolγA*$^{mut/mut}$ animals presented with pale extremities categorised as mild. Moderate paling of the extremities was identified in 26.3% of *PolγA*$^{+/+}$, 54.2% of *PolγA*$^{+/mut}$ and 41.4% of *PolγA*$^{mut/mut}$ animals at the clinical endpoint. Severe paling of the extremities was not observed in any *PolγA*$^{+/+}$ animals, however 4.2% of *PolγA*$^{+/mut}$ and 6.9% of *PolγA*$^{mut/mut}$ animals were observed as such at the clinical endpoint. No experimental animals presented with pale extremities at the point of *Apc* deletion. These data suggest that while anaemia develops in all genotypes following *Apc* deletion at 6 months of age, this symptom is exacerbated in the presence of both the heterozygous and homozygous *PolγA* mutation. The development of anaemia in *PolγA*$^{+/+}$ mice post *Apc* deletion in the absence of an mtDNA mutational background demonstrates that the intestinal pathology of the model alone also causes this symptom.

3.3.2.4. Temperature

As the appearance of pale extremities in our experimental cohort was a subjective observation, and an impairment of thermoregulation is associated with iron-deficiency anaemia in both animal (Dillmann et al., 1979) and human studies (Martinez-Torres et al., 1984), an objective measure of body temperature was used as an additional marker of anaemia in this study.

As part of daily clinical monitoring, body temperature was measured using subcutaneous RFID chips in all experimental animals. At the point of *Apc* deletion, a significant difference in body temperature was not detected between *PolγA*$^{+/+}$ and *PolγA*$^{+/mut}$ or between *PolγA*$^{+/+}$ and *PolγA*$^{mut/mut}$ (P=0.3301 and P=0.7391 respectively, one-way ANOVA with by Tukey's multiple comparisons test). However, a significantly greater experimental starting temperature was detected in *PolγA*$^{+/mut}$ mice in comparison with *PolγA*$^{mut/mut}$ animals (P=0.0075, one-way ANOVA with by Tukey's multiple comparisons test). As shown in Figure 3-9, *PolγA*$^{+/+}$, *PolγA*$^{+/mut}$ and *PolγA*$^{mut/mut}$ experimental groups demonstrate a significant

negative correlation of body temperature with increasing time post *Apc* deletion (*PolγA*$^{+/+}$ r^2=0.6325, P=0.0183, *PolγA*$^{+/mut}$ r^2=0.8325, P=0.0016, *PolγA*$^{mut/mut}$ r^2=0.7466, P=0.0265, Pearson correlation analyses). Linear regression analyses detect a significant slope deviation from zero in all cases (*PolγA*$^{+/+}$ P=0.0002, *PolγA*$^{+/mut}$ P<0.0001, *PolγA*$^{mut/mut}$ P<0.0001). Comparison of the slopes using an analysis of covariance detected a significant difference between *PolγA*$^{+/+}$ and *PolγA*$^{+/mut}$ (P=0.0140) and between *PolγA*$^{+/+}$ and *PolγA*$^{mut/mut}$ (P=0.0284). A significant difference was not detected and between *PolγA*$^{+/mut}$ and *PolγA*$^{mut/mut}$ (P=0.9669, analysis of covariance). This suggests that anaemia and impaired thermoregulation are exacerbated in *PolγA*$^{+/mut}$ and *PolγA*$^{mut/mut}$ mice in comparison to *PolγA*$^{+/+}$ animals following *Apc* deletion at 6 months of age.

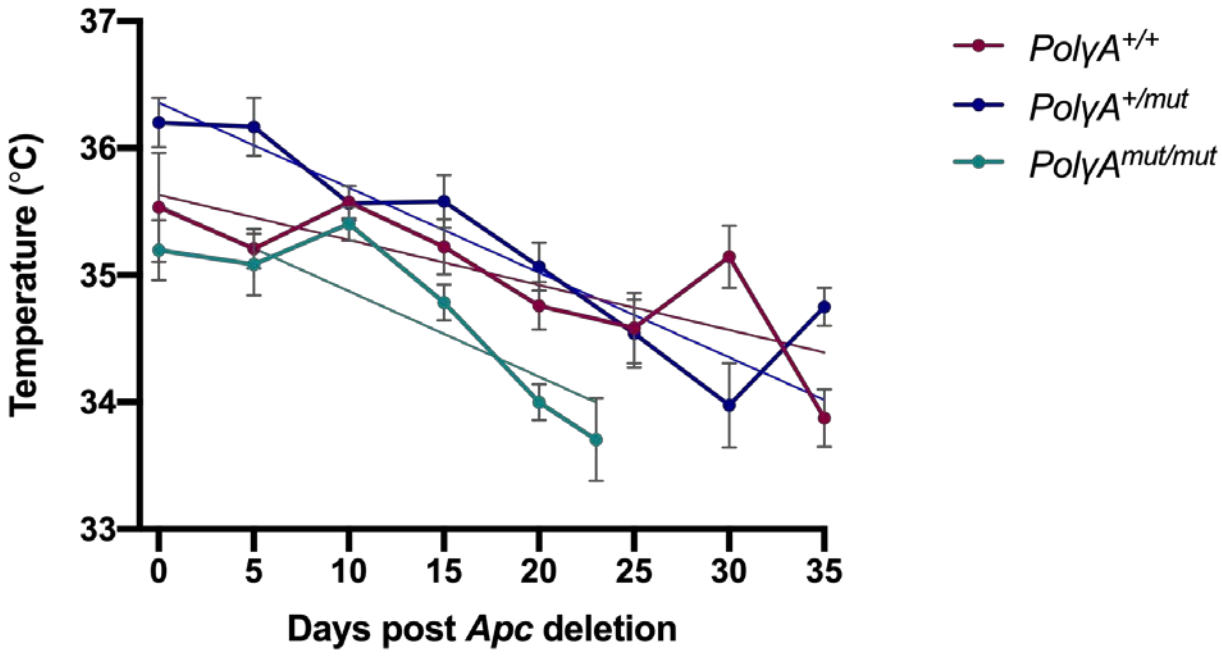

Figure 3-9. Body temperature as measured using subcutaneous RFID chips in *PolγA*$^{+/+}$ (n=19), *PolγA*$^{+/mut}$ (n=24) and *PolγA*$^{mut/mut}$ (n=29) at 0, 5, 10, 15, 20, 25, 30 and 35-days post *Apc* deletion. A significant negative correlation of body temperature with increasing time post *Apc* deletion is detected in all groups (*PolγA*$^{+/+}$ r^2=0.6325, P=0.0183, *PolγA*$^{+/mut}$ r^2=0.8325, P=0.0016, *PolγA*$^{mut/mut}$ r^2=0.7466, P=0.0265, Pearson correlation analyses). Comparison of linear regression slopes detected a significant difference between *PolγA*$^{+/+}$ and *PolγA*$^{+/mut}$ (P=0.0140, analysis of covariance) and between *PolγA*$^{+/+}$ and *PolγA*$^{mut/mut}$ (P=0.0284, analysis of covariance). A significant difference was not detected and between *PolγA*$^{+/mut}$ and *PolγA*$^{mut/mut}$ (P=0.9669, analysis of covariance). Error bars denote mean ±SEM.

As plotting the body temperature of experimental animals at precise time points does not necessarily reflect the condition of animals at that specific time, a more appropriate presentation of this data may be as an association with the clinical score of the mouse. With the deterioration of the condition of experimental animals, the cumulative clinical score of

each mouse increases taking multiple observations into account. Prior to the development of clinical symptoms (at cumulative clinical score zero), no significant difference is detected between the mean body temperature of the three experimental cohorts (*PolγA*$^{+/+}$ versus *PolγA*$^{+/mut}$; P=0.4111, *PolγA*$^{+/+}$ versus *PolγA*$^{mut/mut}$; P=0.9819, *PolγA*$^{+/mut}$ versus *PolγA*$^{mut/mut}$; P=0.4705, one-way ANOVA with by Tukey's multiple comparisons test in all instances). However, as clinical condition deteriorates, there is a significant negative correlation of mean body temperature with increasing clinical score in all three experimental groups post *Apc* deletion (*PolγA*$^{+/+}$ r_S=0.8411, p<0.0001, *PolγA*$^{+/mut}$ r_S=0.5377, both Spearman correlation analyses, *PolγA*$^{mut/mut}$ r^2=0.8944, p<0.0001, Pearson correlation analysis). This is presented in Figure 3-10. These data suggest that body temperature is a good measure of the condition of the animal. Linear regression analyses detect a significant slope deviation from zero in all cases (*PolγA*$^{+/+}$ P<0.0001, *PolγA*$^{+/mut}$ P<0.0001, *PolγA*$^{mut/mut}$ P<0.0001). Comparison of the slopes using an analysis of covariance detected a significant difference between *PolγA*$^{+/+}$ and *PolγA*$^{+/mut}$ (P=0.0280) and between *PolγA*$^{+/+}$ and *PolγA*$^{mut/mut}$ (P=0.0011). A significant difference was not detected between *PolγA*$^{+/mut}$ and *PolγA*$^{mut/mut}$ (P=0.4139, analysis of covariance). This suggests that the clinical deterioration is exacerbated in *PolγA*$^{+/mut}$ and *PolγA*$^{mut/mut}$ mice in comparison to *PolγA*$^{+/+}$ animals following *Apc* deletion at 6 months of age.

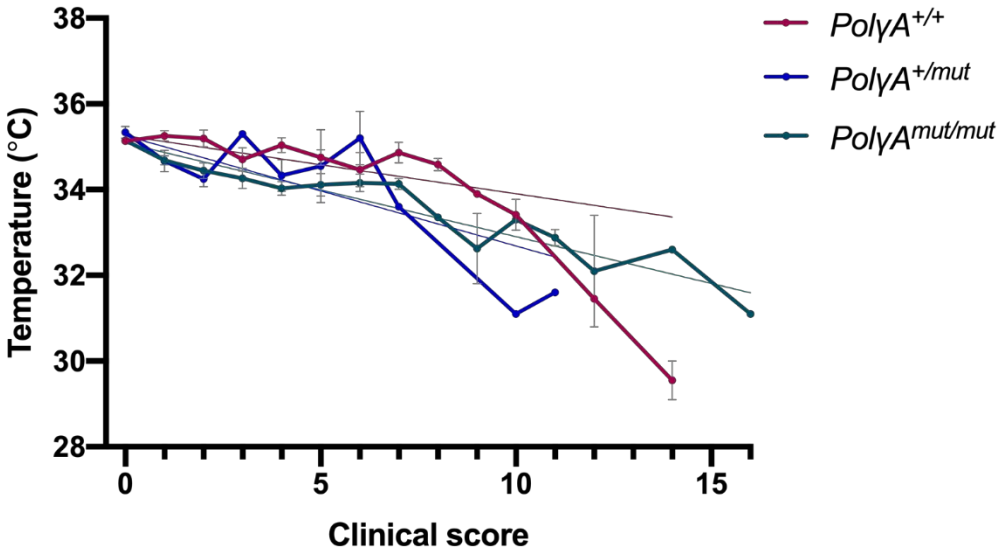

Figure 3-10. Correlation of mean body temperature with increasing clinical score. Observations in all three groups show a significant negative correlation. Spearman correlation analyses of *PolγA*$^{+/+}$ (n=15), r_S=0.8411, P<0.0001, *PolγA*$^{+/mut}$ (n=15), r_S=0.5377, P=0.0202. Pearson correlation analysis of *PolγA*$^{mut/mut}$ (n=19), r^2=0.8944, p<0.0001. Comparison of linear regression slopes detected a significant difference between *PolγA*$^{+/+}$ and *PolγA*$^{+/mut}$ (P=0.0280, analysis of covariance) and between *PolγA*$^{+/+}$ and *PolγA*$^{mut/mut}$ (P=0.0011, analysis of covariance). A significant difference was not detected between *PolγA*$^{+/mut}$ and *PolγA*$^{mut/mut}$ (P=0.4139, analysis of covariance). Error bars denote mean ±SEM.

3.3.2.5. Tamoxifen toxicity

Tamoxifen is a non-steroidal anti-oestrogen drug that has been widely used in the treatment of breast cancer. A strong hepatocarcinogenic effect of tamoxifen has been reported in the rat (Greaves et al., 1993; Williams et al., 1993), with such oestrogen receptor independent hepatic pathologies purported to be attributable in part to oxidative stress mediated by tamoxifen. Accordingly, this is of concern with regard to this study and others in which mitochondrial function is under scrutiny and unexpected experimental perturbation would confound results.

The tamoxifen control mouse cohort was set up in order to assess the toxicity and potential effect on lifespan of the tamoxifen regime used to induce tumorigenesis in experimental animals. Tamoxifen control animals are wild type *Lgr5* and as such do not express *creERT2*. Administration of tamoxifen to these animals does not induce the development of adenomas as seen in *Lgr5-creERT2* heterozygous animals. Ten *PolγA*$^{mut/mut}$ and ten *PolγA*$^{+/+}$ animals were aged to 6 months to allow the accumulation of mtDNA mutations before tamoxifen induction following the same 3mg, 2mg, 2mg, 2mg IP protocol administered to the lifespan cohort heterozygous for *Lgr5-CreERT2*. Animals were regularly monitored and humanely sacrificed upon the observation of three moderate or one severe clinical sign of ill health (Table 2-1). Lifespan data for tamoxifen control animals versus their *Lgr5-CreERT2* equivalents from the lifespan 6 cohort are shown in Figure 3-11 where both *PolγA*$^{+/+}$ and *PolγA*$^{mut/mut}$ tamoxifen control mice significantly outlive their adenomatous counterparts ($P=0.002$ and $P<0.0001$ respectively, Mantel-Cox log rank test in both instances). These data suggest that the tamoxifen induction regime alone does not negatively affect lifespan.

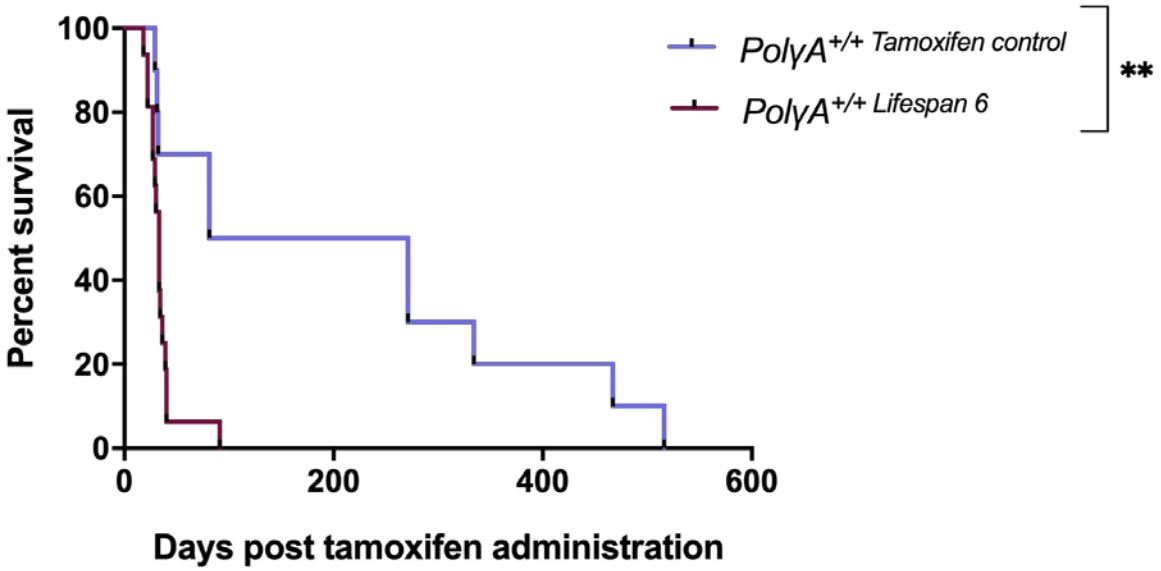

Figure 3-11 (A) Kaplan-Meier survival curve depicting survival times of *PolγA*$^{+/+}$ tamoxifen control mice and *Lgr5-CreERT2*/*PolγA*$^{+/+}$ mice. *PolγA*$^{+/+}$ tamoxifen control mice (n=10) are greatly outliving their *PolγA*$^{+/+}$ counterparts with *Lgr5-CreERT2* and associated adenomatous phenotype (n=16), P=0.002, Mantel-Cox log rank test.

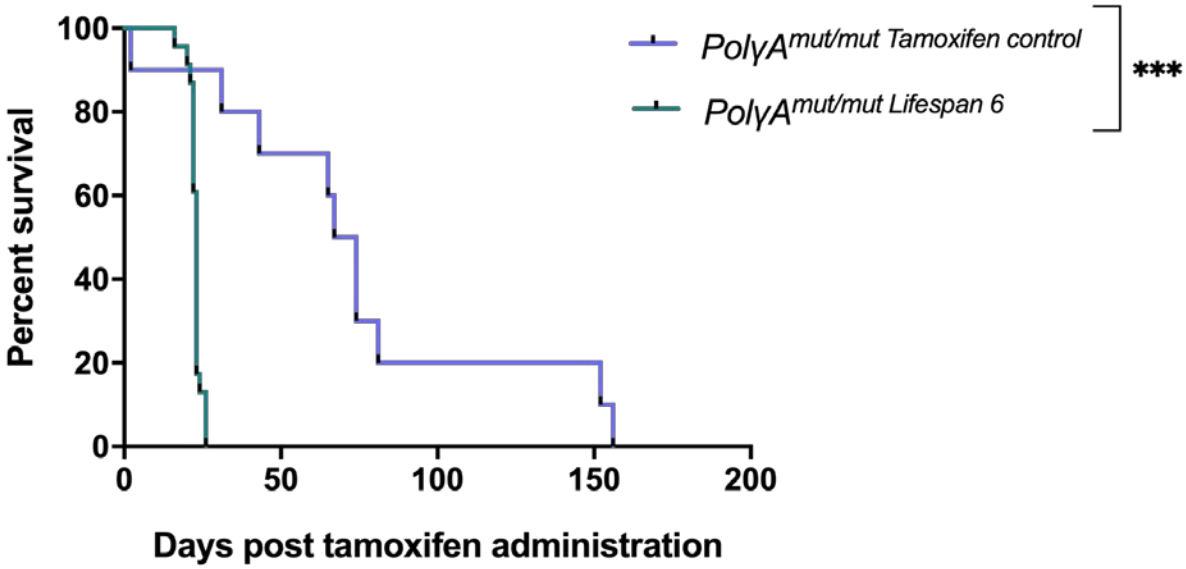

Figure 3-11 (B) Kaplan-Meier survival curve depicting survival times of *PolγA*$^{mut/mut}$ tamoxifen controls and *Lgr5-CreERT2*/ *PolγA*$^{mut/mut}$ mice. *PolγA*$^{mut/mut}$ tamoxifen controls (n=10) are significantly outliving their *PolγA*$^{mut/mut}$ /*Lgr5-creERT2* counterparts (n=23), P<0.0001, Mantel-Cox log rank test.

3.3.3. Day 23 6-month cohort

In order to directly compare rates of adenoma progression between *PolγA*$^{mut/mut}$, *PolγA*$^{+/mut}$, and *PolγA*$^{+/+}$ animals the 'Day 23' cohort was established. As previously, experimental animals were aged to either six or twelve months prior to tamoxifen induction, however all animals were all sacrificed at the same time point post induction. This ensured that in all cases, tumour initiation and progression was given the same amount of time, to allow direct comparisons of tumour growth between genotypes. The median survival time of *PolγA*$^{mut/mut}$ mice was 23 days, therefore this was chosen as the endpoint of this cohort. Intraperitoneal tamoxifen (T5648, Sigma Aldrich) was administered to each mouse over the course of four days at a concentration of 10mg/ml in sunflower oil. Day one; 300µl (3mg), day two to four; 200µl (2mg) each day (2.2.5.). All mice were monitored daily until the experiment end point. Mice were euthanised using the Schedule 1 approved method of concussion of the brain followed by cervical dislocation (Animals Scientific Procedures Act, 1986). Due to time constraints, further analysis focused only on animals in which *Apc* deletion was induced at six months of age.

3.3.3.1. Macroscopic adenoma burden quantification

In order to quantify and compare macroscopic adenoma burden, the intestines were removed from mice culled at 23 days post *Apc* deletion, flushed with 10% neutral buffered formalin, opened longitudinally and pinned out flat as intestinal whole mounts. Using a dissecting microscope, all visible adenomas were counted, and their areas measured throughout the entire intestine. Adenomas were included when they were a minimum of 1mm^2. In the event of multiple adenomas appearing to have merged together, the total area of the lesion was measured.

The quantification of macroscopic adenomas throughout the intestines of this cohort revealed a significantly greater total adenoma burden in the *PolγA*$^{mut/mut}$ mice (n=19) compared with the *PolγA*$^{+/mut}$ (n=12) and *PolγA*$^{+/+}$ (n=13) mice. The mean adenoma burden within *PolγA*$^{mut/mut}$ animals (434.1mm^2 ± 247) is twice that of mice heterozygous for the

PolyA mutation (197.7mm^2 ± 118.9) and almost 4.5 times the mean adenoma burden seen in wild type *PolyA*$^{+/+}$ animals (96.69mm^2 ± 41.94). This is shown in Figure 3-12.

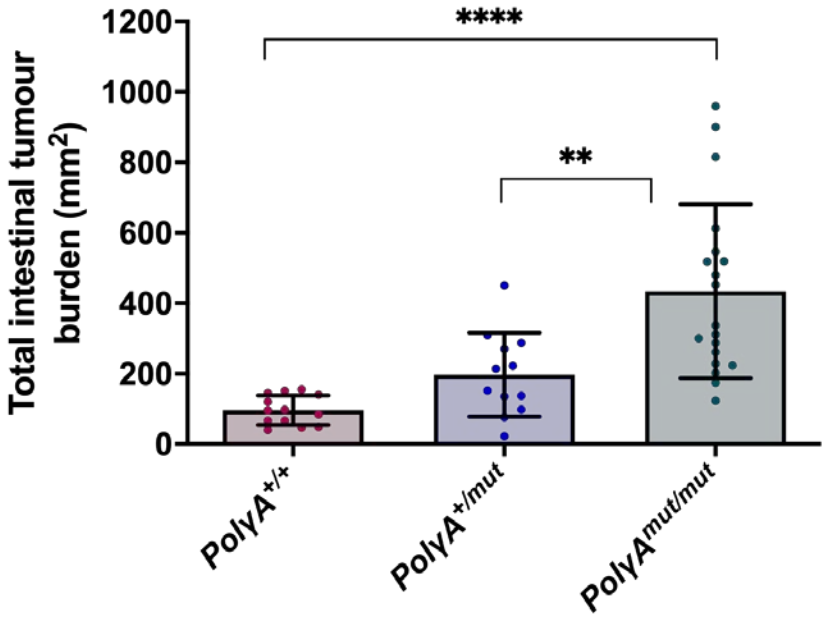

Figure 3-12. Total macroscopic intestinal adenoma burden of *PolyA*$^{+/+}$ (n=13), *PolyA*$^{+/mut}$ (n=12) and *PolyA*$^{mut/mut}$ (n=19) mice aged to 6 months prior to *Apc* deletion and culled 23 days later. *PolyA*$^{mut/mut}$ have a significantly greater adenoma burden than *PolyA*$^{+/mut}$ (P<0.01, one-way ANOVA followed by Tukey's multiple comparisons test) and *PolyA*$^{+/+}$ mice (P<0.0001, one-way ANOVA followed by Tukey's multiple comparisons test). Each data point represents one animal and error bars denote mean ±SD.

3.3.3.2. Microscopic adenoma burden quantification

Tamoxifen induced *Apc* deletion causes activation of the Wnt signalling system as described in 1.7.3. This results in the release of β-catenin from the cytoplasmic destruction complex. It is destabilised and moves to the nucleus where it activates transcription factors controlling cell proliferation. Beta catenin accumulates in both the cytoplasm and nucleus of cells in which *Apc* deletion has occurred. In order to microscopically quantify the adenoma burden within *PolyA*$^{mut/mut}$, *PolyA*$^{+/mut}$ and *PolyA*$^{+/+}$ mice aged to six months prior to adenoma induction and humanely killed 23 days later, intestinal tissues were harvested and processed as described in 2.2.7. and sections of colon and distal small intestine were labelled with anti-β-catenin as described in 2.2.9.1-2. The sections adjacent to those stained with anti-β-catenin were stained with H&E in order to determine if the tumour foci were indeed dysplastic. This was confirmed with the guidance of a histopathologist (Dr James Sampson, Consultant Histopathologist, Royal Victoria Infirmary, Newcastle). Following β-catenin immunohistochemistry, an intense nuclear and cytoplasmic expression of β-catenin was

seen in the adenomas as opposed to the cell margin demarcation observed in surrounding normal mucosa. A representative example of this is shown in Figure 3-13.

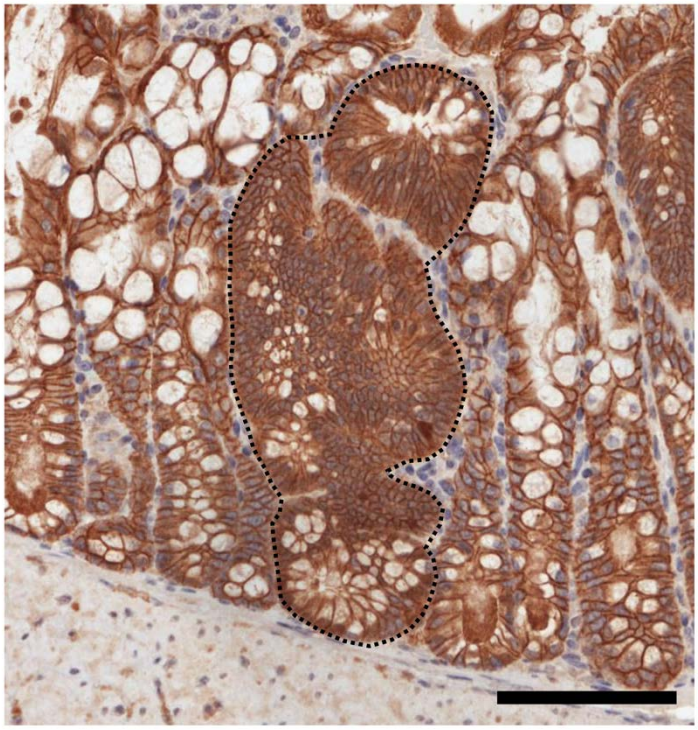

Figure 3-13. Pattern of beta catenin immunohistochemical labelling in the murine colonic mucosa. An intense nuclear and cytoplasmic expression of β-catenin can be seen in the adenomatous region highlighted by black dashed lines. Within the normal crypts adjacent to the adenoma, β-catenin labelling is diminished and is largely limited to the cytoplasm and demarcation of cell margins. Scale bar 100µm.

Sections were analysed as described in 2.2.12.1, measuring the area of each adenoma in addition to recording the frequency of adenomas per tissue section. Figures 3-14 and 3-15 show typical examples of beta catenin immunohistochemistry in colonic and small intestinal tissue sections respectively. As can be seen in the second and third columns, adenoma foci demonstrate a more intense staining pattern than that of the surrounding normal mucosa. Non-transformed cells have clear β- catenin demarcated cell margins, whereas the adenomata have a more widespread, increased level of β-catenin expression within the nucleus and cytoplasm with cell margins less clear.

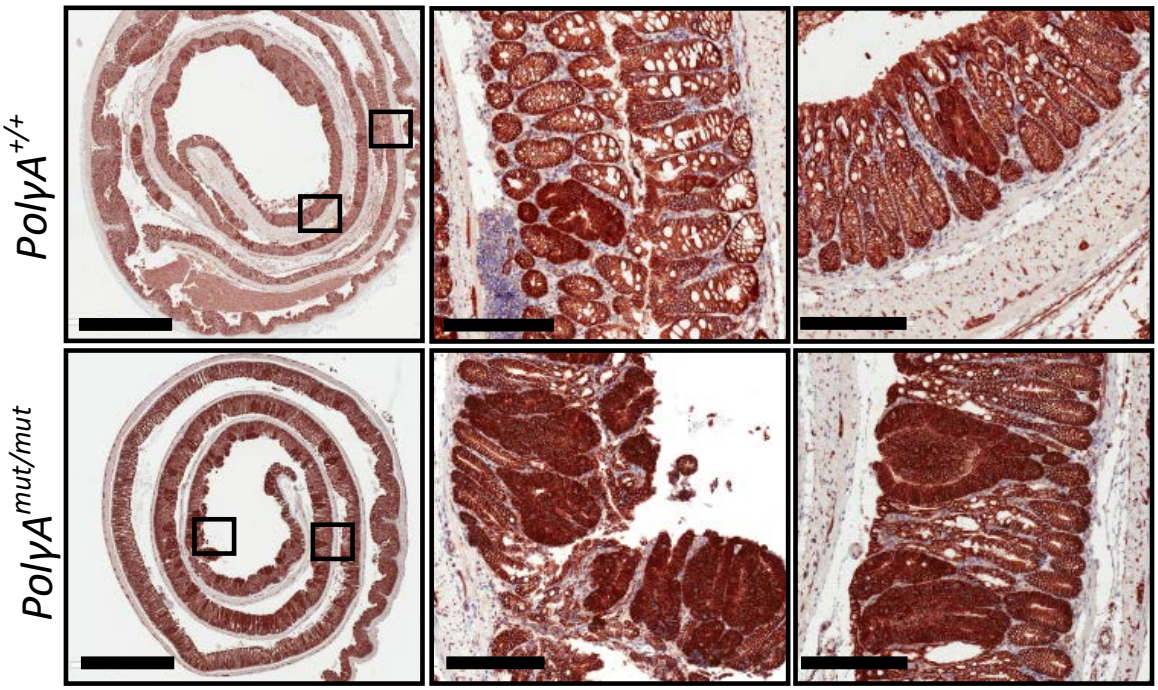

Figure 3-14. Beta catenin immunohistochemistry on colon tissue sections from *PolγA*$^{+/+}$ and *PolγA*$^{mut/mut}$ mice. Scale bars 3mm (first column) and 200µm (second and third columns). Areas demarcated by black boxes within the first column are shown at higher magnification in the second and third columns.

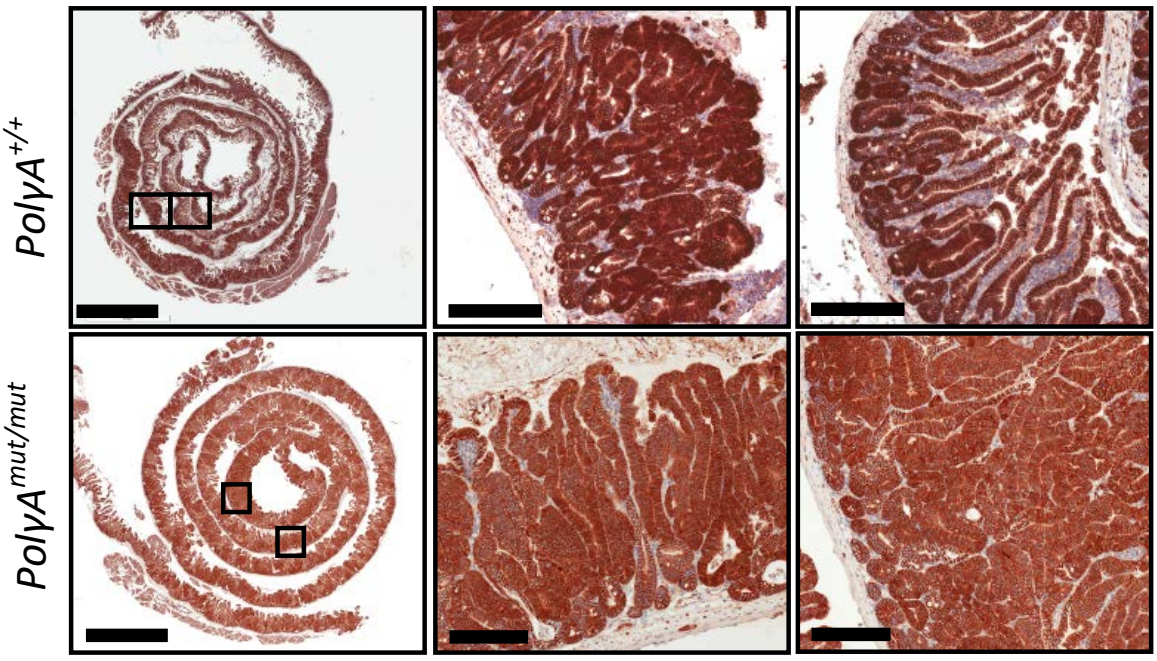

Figure 3-15. Beta catenin immunohistochemistry on small intestinal tissue sections from *PolγA*$^{+/+}$ and *PolγA*$^{mut/mut}$ mice. Scale bars 3mm (first column) and 200µm (second and third columns). Areas demarcated by black boxes within the first column are shown at higher magnification in the second and third columns.

Within the colon of *PolγA*$^{mut/mut}$ (n=19) and *PolγA*$^{+/+}$ (n=13) mice, the mean frequency of lesions was similar (128.237 ± 42.13 and 140.462 ± 83.16 respectively) with no significant difference detected between these two groups (P=0.8108, one-way ANOVA followed by Tukey's multiple comparisons test). Within the colons of *PolγA*$^{+/mut}$ (n=11) mice, the mean frequency of adenomas observed (60.36 ± 23.65) was significantly lower than in both the *PolγA*$^{mut/mut}$ and *PolγA*$^{+/+}$ colon (P=0.0062 and P=0.0027 respectively, one-way ANOVA with Tukey's multiple comparisons test). Within the small intestine of *PolγA*$^{+/+}$ (n=12) and *PolγA*$^{+/mut}$ (n=8) mice, the mean frequency of adenomas observed was similar (145.667 ± 50.53 and 151.125 ± 47.32 respectively) with no significant difference detected (P=0.9654, one-way ANOVA with Tukey's multiple comparisons test). However small intestinal sections from *PolγA*$^{mut/mut}$ mice (n=16) had a significantly greater mean frequency of adenomas per tissue section (201.3 ± 44.71) in comparison with *PolγA*$^{+/+}$ mice (P=0.0112, one-way ANOVA with Tukey's multiple comparisons test). These data are shown in Figure 3-16 A and D.

In the colon of *PolγA*$^{mut/mut}$ mice, the mean size of each adenoma (16125µm ± 6148) was significantly greater than that of the *PolγA*$^{+/+}$ animals (7063.27µm ± 6447) (P=0.0004, one-way ANOVA with Tukey's multiple comparisons test). Similarly, the mean *PolγA*$^{mut/mut}$ small intestinal adenoma size (72170.2µm ± 31710) was significantly greater than that of the *PolγA*$^{+/+}$ animals (37690.1µm ± 7321) (P=0.0008, one-way ANOVA with Tukey's multiple comparisons test). Mean adenoma size in the small intestine of *PolγA*$^{+/+}$ and *PolγA*$^{+/mut}$ mice was similar (37690.1µm ± 7321 and 40800.3µm ± 9094 respectively) and as such, mean small intestinal adenoma size in *PolγA*$^{mut/mut}$ mice was also significantly greater than that of *PolγA*$^{+/mut}$ mice animals (P=0.0070, one-way ANOVA with Tukey's multiple comparisons test). These data are shown in Figure 3-16 B and E.

In the colon of *PolγA*$^{mut/mut}$ mice, the mean adenoma burden represented as a percentage proportion of the tissue section area (8.424% ± 4.417) was significantly greater than that of the *PolγA*$^{+/+}$ animals (3.135% ± 2.129) (P=0.0003, one-way ANOVA followed by Tukey's multiple comparisons test). The mean adenoma burden in the colon of *PolγA*$^{+/+}$ and *PolγA*$^{+/mut}$ mice was similar (3.135% ± 2.129 and 3.458% ± 2.219 respectively) and as such, mean colonic adenoma burden in *PolγA*$^{mut/mut}$ mice was also significantly greater than that of *PolγA*$^{+/mut}$ mice animals (P=0.0010, one-way ANOVA followed by Tukey's multiple comparisons test). In the small intestine, a similar pattern was observed. The mean adenoma

burden represented as a percentage proportion of the small intestinal tissue section area in *PolγA*$^{mut/mut}$ mice (31.51% ± 13.57) was significantly greater than that of the *PolγA*$^{+/+}$ animals (18.47% ± 10.32) (P=0.0118, one-way ANOVA followed by Tukey's multiple comparisons test). The mean adenoma burden in the small intestine of *PolγA*$^{+/+}$ and *PolγA*$^{+/mut}$ mice was similar (18.47% ± 10.32 and 19.49% ± 4.896 respectively) and as such, mean small intestinal adenoma burden in *PolγA*$^{mut/mut}$ mice was also significantly greater than that of *PolγA*$^{+/mut}$ mice animals (P=0.0460, one-way ANOVA with Tukey's multiple comparisons test). These data are shown in Figure 3-16 C and F.

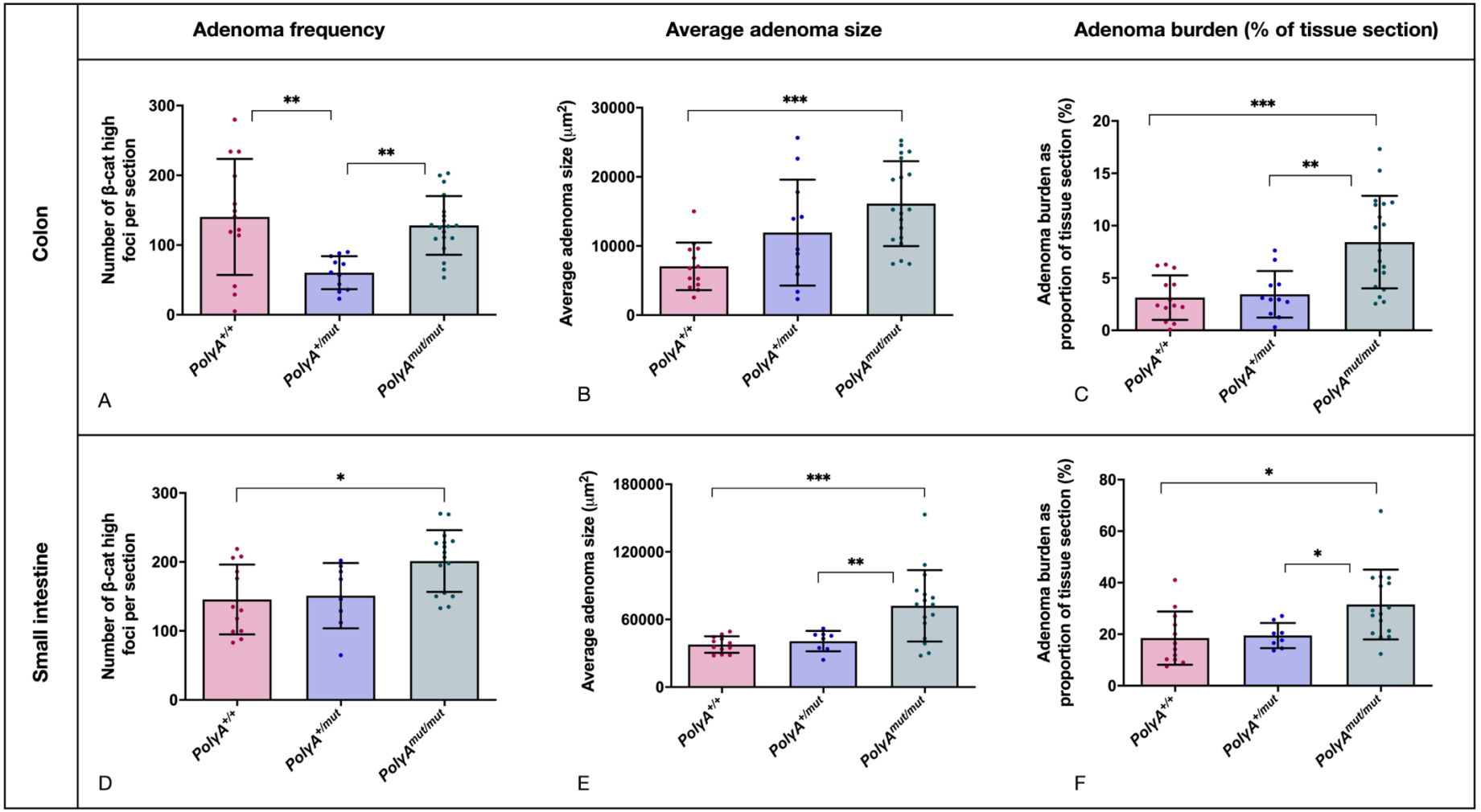

Figure 3-16. Quantification of the frequency of adenomas, mean adenoma size and total adenoma burden within the colon and small intestine of experimental animals. (A, B, C) Quantification of the frequency of adenomas, mean adenoma size and total adenoma burden within the colon of *PolyA*$^{+/+}$ (n=13), *PolyA*$^{+/mut}$ (n=11) and *PolyA*$^{mut/mut}$ (n=19) animals. (C, D, E) Quantification of the frequency of adenomas, mean adenoma size and total adenoma burden within the small intestine of *PolyA*$^{+/+}$ (n=12), *PolyA*$^{+/mut}$ (n=8) and *PolyA*$^{mut/mut}$ (n=16) animals. Each dot represents the mean of one mouse. Error bars ± SD. One-way ANOVA followed by Tukey's multiple comparison test; for all panels: * P<0.05, **P<0.01, ***P<0.001.

3.4. Discussion

As with many malignancies, age is a major risk factor for colorectal cancer. Over the decades, a multitude of evolutionary and molecular mechanisms have been proposed in order to further our understanding of the ageing process and the organismal functional decline with which it is associated. An accumulation of cellular damage which occurs in a time dependant fashion is generally considered to be fundamental to ageing, with the amalgamation of numerous processes leading to this damage (Kirkwood, 2005). In 2013, López-Otín and colleagues summarised these processes, thus describing nine hallmarks of ageing postulated to contribute to the manifestation of an ageing phenotype; mitochondrial dysfunction is one of these hallmarks (López-Otín et al., 2013). Metabolism has been implicated in the process of ageing since the turn of the century, at which time it was suggested that longevity was inversely proportional to metabolic rate (Rubner, 1883; Rubner, 1908). The free radical theory of ageing (Harman, 1956) and later the mitochondrial free radical theory of ageing (Harman, 1972) subsequently offered a mechanistic hypothesis proposing a role of mitochondria in ageing. Since that time, a myriad of reports has been published documenting the association of mitochondrial dysfunction with an ageing phenotype in multiple tissue types, with reports of increased levels of mitochondrial DNA deletions and point mutations in ageing tissues being described from the early 1990s. Cortopassi and Arnheim described the presence of a specific 4977 base pair deletion in the heart and brain of older individuals (Cortopassi & Arnheim, 1990). The mtDNA^{4977} 'common deletion' had previously only been associated with mitochondrial disorders such as Kearns-Sayre syndrome (KSS) and progressive external ophthalmoplegia (PEO). Similarly, frequencies of the point mutations responsible for the mitochondrial syndromes MERFF and MELAS (mt.8344A>G and mt.3243A>G) were also found to increase in an age-dependant manner in tissues such as the brain, heart and skeletal muscle (Munscher et al., 1993; Zhang et al., 1993). As such, these studies provided early experimental evidence in support of the importance of an accumulation of mitochondrial DNA mutations in normal ageing. The origin of clonally expanded mtDNA point mutations in ageing mitotic tissues is thought likely to be due to *Poly* mediated errors of mtDNA replication rather than by damage incurred as a result of oxidative stress (Greaves et al., 2014; Kennedy et al., 2013; Zheng et al., 2006) and the mechanism by which single mutated mtDNA species are able to expand to high levels of heteroplasmy and often homoplasmy in mitotic tissues is currently understood to be

initiated by mutational events that occur in early life. Owing to numerous rounds of mtDNA replication and random segregation of mitochondria as the cell divides, the mutated species are able to, by chance, become the dominant clone within that cell (Greaves et al., 2014). Furthermore, if mtDNA mutations are acquired within the long-lived stem cells that maintain mitotic tissues, these mutations will be propagated into the progeny of that cell resulting in mosaic patterns of clonal units demonstrating biochemical defects as the mutation reaches high levels of heteroplasmy.

With regard to the colon specifically, the exponential increase in mitochondrial dysfunction caused by clonally expanded pathogenic point mutations of the mitochondrial genome with increasing age has provided strong evidence supporting the role of these mutations in the ageing process (Taylor et al., 2003). Furthermore, the detection of somatic mtDNA mutations in human colorectal tumours (Ericson et al., 2012; He et al., 2010; Larman et al., 2012; Polyak et al., 1998) and their similarity to those found in the normal ageing colon suggests there may be a link between mitochondrial dysfunction of the ageing colon and colorectal carcinogenesis. Computer modelling studies also report the presence of observed homoplasmic mtDNA mutations in human tumours (Fliss et al., 2000; Polyak et al., 1998) as being plausibly generated via random mutagenesis and segregation of mtDNA molecules (Coller et al., 2001a). Since Warburg's initial observation that tumour cells favour glycolytic over oxidative energy production, even in the presence of oxygen (Warburg, 1956) it has become widely accepted that metabolism is altered within many types of malignancy (Hanahan & Weinberg, 2011). The primary concerns of the tumour are growth and proliferation, and a shift towards a more glycolytic metabolism assists in providing the anabolic requirements necessary for this growth to occur. With this in mind and given the similarities in mtDNA mutation spectrum and mechanisms of expansion within mutator mouse and human intestinal crypts and also in human intestinal tumours, it would be plausible to suggest that alterations in mitochondrial function that occur as a normal process of ageing are able to support malignant growth within those tissues should malignant transformation occur. Accordingly, the *PolγA* mutator mouse (Kujoth et al., 2005; Trifunovic et al., 2004) was selected as a model of accelerated mtDNA mutagenesis with a progeroid phenotype and crossed with the *Lgr5-EGFP-IREScreERT2/Apc*$^{flox/flox}$ inducible colorectal cancer mouse in order to further investigate this hypothesised link.

Tumorigenesis in our experimental cohort was achieved via the tamoxifen mediated *Lgr5+* stem cell specific activation of CreERT2 and subsequent deletion of *Apc.* With the complex pharmacological actions of tamoxifen in mind, it cannot be assumed that this regimen is without consequence. As previously mentioned, the hepatotoxic effect of tamoxifen has been described with regards to its use as an anti-cancer agent and also in relation to its use in tamoxifen-induced gene knockout studies (Greaves et al., 1993; Hammad et al., 2018; Williams et al., 1993). Less well explored is the effect of tamoxifen on the gastrointestinal tract. However, one study reports a striking disruption of the gastric mucosa in normal mice administered with a 3-day 5mg/20g tamoxifen regime. Within 3 days, a dramatic loss of gastric parietal cells was observed as was an increase in stem/progenitor cell proliferation alongside the metaplasia of zymogenic chief cells (Huh et al., 2012). A single 3mg/20g dose elicited similar results in the stomach, however by 3 weeks, gastric histology had returned to almost normal. Highly relevant to this study was the finding of no small or large intestinal changes in mice treated with tamoxifen when compared to those that were not (Huh et al., 2012). Interestingly, an earlier study by the same group attributed this gastric phenotype to a genotoxicity caused by the Cre recombinase rather than the activating tamoxifen (Huh et al., 2010). This phenomenon has also been described by Bohin and colleagues, whereby the group use a *Villin-CreERT2* mouse model to demonstrate an impaired capacity of CreERT2 activated intestinal stem cells to regenerate following an irradiation challenge compared to those in which CreERT2 was absent (Bohin et al., 2018). The group rule out tamoxifen alone as the mediator of this damage and attribute the regeneration defect to the off-target action of activated Cre recombinase at cryptic *LoxP* sites other than the target *LoxP* at which cleavage has been engineered to occur. Importantly, this genotoxicity is resolved by 7 days post–tamoxifen treatment. Furthermore, the defect in *Lgr5-CreERT2* mice was not as pronounced as observed in *Villin-CreERT2* animals. As villin is expressed throughout the entire intestinal epithelium, CreERT2 toxicity may potentially affect additional cell populations such as facultative stem cells involved in the regeneration response. As only *Lgr5+* stem cells contain the *CreERT2* transgene in our experiments, this may therefore reduce the proportion of cells involved in crypt regeneration which are exposed to CreERT2 toxicity. Nonetheless, this study and those also discussed highlight the importance of appropriate controls when using a tamoxifen activated CreERT2 system.

Clinical monitoring of experimental animals post *Apc* deletion characterised a phenotype in which weight loss, anaemia and a decreasing body temperature present as condition of the animals deteriorates. A decline in mutator mouse weight from 6 months of age is also reported in other studies (Kim et al., 2019; Kujoth et al., 2005; Shabalina et al., 2017; Trifunovic et al., 2004). In comparing our short window of weight monitoring (~40 days) to the extended period of body mass monitoring by Trifunovic *et al*. (~9 months) it would seem that weight loss is more pronounced in our model. Over a 3-week period from 24 to 27 weeks of age, mean body weight of Trifunovic *PolγA*$^{mut/mut}$ mice dropped approximately 1g from ~29g to 28g. Over the same period of time, mean body mass of our *PolγA*$^{mut/mut}$ mice dropped 2.4g from 25.7g to 23.3g, over twice the weight loss of the Trifunovic mouse. It is clear that this additional intestinal pathology in our model exacerbates the weight loss already characteristic of the mutator mouse from 6 months of age.

Also characteristic of the *PolγA* mutator mouse model is a prominent, limiting anaemia attributed to a requirement of mitochondrial function for the appropriate differentiation of haematological stem cells (Norddahl et al., 2011). With this in mind it may be surmised that in this study, the reduced longevity of *PolγA*$^{+/mut}$ and *PolγA*$^{mut/mut}$ experimental animals in comparison to *PolγA*$^{+/+}$ mice is a direct result of this pathology. However, anaemia is also frequently observed in colorectal cancer patients and has been associated with poor prognosis and increased risk of mortality (Mörner et al., 2017; Zhen et al., 2012). While blood loss via tumour haemorrhage into the bowel is a major cause of anaemia seen in colorectal cancer, additional mechanisms are also at play such as the release of inflammatory cytokines from an activated immune system and their subsequent effect on iron absorption and erythropoiesis (Väyrynen et al., 2018) . Nutritional deficits and malabsorption can also lead to iron deficiency, this mechanism potentially being particularly relevant in mouse models due to the preponderance of adenomas being preferentially located in the small intestine, the major site of iron absorption. As a subjective measure of anaemia in this study, the appearance of pale extremities was monitored in all experimental animals. Although severe paling was not noted in any *PolγA*$^{+/+}$ mice, observations of this symptom at a mild level were made in 63.2% of *PolγA*$^{+/+}$ mice and 26.3% of *PolγA*$^{+/+}$ mice at a moderate level. Furthermore, pale extremities were not noted in any experimental animals at the point of *Apc* deletion at six months of age whereas 63.2% of *PolγA*$^{+/+}$, 75% of *PolγA*$^{+/mut}$ and 93.1% of *PolγA*$^{mut/mut}$ animals exhibited this symptom at the end point. These

data strongly suggest that the anaemia observed in all experimental cohorts develops as adenoma burden increases following *Apc* deletion. Although anaemia as a result of the *PolγA* mutator phenotype alone is acknowledged, the presence of this symptom in the absence of an mtDNA mutator phenotype in conjunction with the significantly greater adenoma burden observed in *PolγA*$^{mut/mut}$ animals suggests that the intestinal pathology and thus the anaemia exacerbated by this burden significantly contributes to mortality.

Secondary to the anaemia observed in all experimental groups is a decreasing body temperature or impaired thermoregulation, significantly detected in all groups as their physical condition deteriorates. Following a deviation below the range of thermoneutrality, the secretion of the thyroid hormones triiodothyronine (T_3) and thyroxine (T_4) form part of the obligatory or chemical thermogenesis response which globally increases the rate of cellular respiration and ATP production (reviewed in Rosenzweig & Volpe, 1999). Heat is generated as a by-product of mitochondrial oxidative phosphorylation raising the organismal metabolic rate above basal. The first two steps of thyroid hormone synthesis are catalysed by an iron-dependant thyroid peroxidase (TPO) (reviewed in Dunn & Dunn, 2001) and as such, iron deficiency anaemia is associated with both an impaired thyroid metabolism and diminished thermoregulatory capacity (Beard et al., 1984; Beard et al., 1990). Accordingly, temperature was used as an objective measure of anaemia in this study. An additional thermoregulatory response in mammals also involves iron and mitochondria. Known as adaptive or non-shivering thermogenesis, this response takes place within the mitochondria of brown adipose tissue (BAT) (Cannon & Nedergaard, 2004; Rothwell & Stock, 1997; Smith & Roberts, 1964) and centralises around the unique expression of mitochondrial uncoupling protein-1 (UCP-1) within this tissue. The association of UCP-1 with the mitochondria of brown fat deposits was first described in the 1970s (Heaton et al., 1978; Ricquier & Kader, 1976), and while other members of the UCP family are expressed in multiple tissue types, UCP-1 is expressed exclusively in brown adipocyte mitochondria (Cannon et al., 1982). Mitochondrial uncoupling proteins reside on the inner mitochondrial membrane. Essentially, they function as proton transporters shuttling H^+ ions back into the mitochondrial matrix after their generation by the electron transport chain. Where this role is normally reserved for ATP synthase and facilitates the production of ATP, UCPs 'uncouple' the generation of ATP from oxidative phosphorylation, instead using the proton motive force to generate heat (Cannon & Nedergaard, 2004). Adaptive thermogenesis is stimulated by the sympathetic

nervous system but also has an absolute requirement for thyroid hormone (Ribeiro et al., 2001). Additionally, the more potent thyroid hormone T_3 directly stimulates UCP-1 gene expression (Guerra et al., 1996; Rabelo et al., 1995). Given the anaemic phenotype of both the *PolγA* mutator and intestinal cancer models, aberrant thermoregulation in our cohort is unsurprising. As mitochondrial abundance is of importance and oxidative phosphorylation is a prerequisite to UCP-1 uncoupling and heat generation, it would follow suit that mitochondria dysfunctional in their oxidative phosphorylation capacity would also display thermogenic defects. Indeed, it has been shown that *PolγA*$^{mut/mut}$ generate much less heat than their wild-type counterparts, with the expression of thermogenic genes such as *Ucp1* being reduced in young (2.5-month-old) *PolγA*$^{mut/mut}$ when compared to *PolγA*$^{+/+}$ mice (Wall et al., 2015). With this in mind, it may be proposed that the *PolγA*$^{mut/mut}$ genotype with associated anaemia and thermoregulatory defect is responsible for the shortened lifespan of these animals in comparison to *PolγA*$^{+/+}$ mice. However, as is the case with review of the subjective measures of anaemia, a review of the data regarding the objective of measure of temperature also implicates the intestinal pathology as the major limiting factor in our model. Although at the experimental start point, a significantly greater experimental starting temperature was detected in *PolγA*$^{+/mut}$ mice in comparison with *PolγA*$^{mut/mut}$ animals, no difference in starting temperature was observed between *PolγA*$^{+/+}$ and *PolγA*$^{+/mut}$ or between *PolγA*$^{+/+}$ and *PolγA*$^{mut/mut}$ animals. This suggests that while the anaemic and thermoregulatory defects associated with the *PolγA* mutator phenotype are acknowledged, no evidence of these pathologies is noted at the experimental start point. As a significant negative correlation of temperature over time post *Apc* deletion was detected in all groups, including the *PolγA*$^{+/+}$ group, this suggests that the intestinal pathology alone is sufficient to cause prominent anaemic and defective thermoregulatory symptoms in experimental animals. Furthermore, the detection of significant differences between linear regression slopes of *PolγA*$^{+/+}$ animals in comparison to both *PolγA*$^{+/mut}$ and *PolγA*$^{mut/mut}$ mice confirms an exacerbation of these symptoms in the presence of age-related mtDNA mutation accumulation. This is supported by the correlation of mean body temperature with increasing clinical score in which mean body temperature in association with clinical deterioration decreases at a significantly greater rate per clinical score unit in both *PolγA*$^{+/mut}$ and *PolγA*$^{mut/mut}$ mice in comparison to *PolγA*$^{+/+}$ animals. As a significantly greater adenoma burden is observed within the *PolγA*$^{mut/mut}$ colon and small intestine in comparison to *PolγA*$^{+/+}$ and *PolγA*$^{+/mut}$ mice, the intestinal pathology as opposed to the systemic effects of

the *PolγA* mutator phenotype is further implicated in eliciting the clinical decline of experimental animals post *Apc* deletion.

With regard to adenoma frequency in the colon, there are significantly fewer adenomata observed in *PolγA*$^{+/mut}$ mice when compared to both the *PolγA*$^{+/+}$ and *PolγA*$^{mut/mut}$ animals. In the small intestine, there are significantly fewer adenomata observed in *PolγA*$^{+/+}$ animals when compared to *PolγA*$^{mut/mut}$ mice. As adenomas were manually selected, this method of selection is liable to subjectivity. Particularly within the small intestine where the largest adenomas are observed, distinguishing discrete adenomas from one another presented with some difficulty and may therefore account for the variation with regard to adenoma frequency between animals. Alternatively, this variation may suggest that adenomagenesis may be impaired in the *PolγA*$^{+/mut}$ colon or *PolγA*$^{+/+}$ small intestine due to the differences in genotype. However, it is understood that due to random silencing of the mutant *Lgr5-eGFP-IRES-CreERT2* allele, expression of *CreERT2* and thus *Apc* excision is variegated or mosaic (Barker et al., 2007; Schuijers et al., 2014) and the observation made here in relation to a lower adenoma frequency in *PolγA*$^{+/mut}$ mouse colon and *PolγA*$^{+/+}$ small intestine may be a result of this phenomenon. Despite the variation in colonic adenoma frequency in experimental animals, mean adenoma size within *PolγA*$^{mut/mut}$ mice is significantly greater than is observed in *PolγA*$^{+/+}$ animals. In the case of colonic adenoma burden, a significantly greater adenomatous burden is observed in *PolγA*$^{mut/mut}$ mice in comparison to both *PolγA*$^{+/mut}$ and *PolγA*$^{+/+}$ animals. In the small intestine, mean adenoma size and mean adenoma burden are significantly greater in *PolγA*$^{mut/mut}$ mice when compared to *PolγA*$^{+/mut}$ and *PolγA*$^{+/+}$ animals. Taken together, these data suggest that a growth advantage is provided by the *PolγA*$^{mut/mut}$ genotype resulting in a more substantial adenoma burden within this group. With reference to the clinical data, it is apparent that this greater burden causes a more rapid deterioration of the condition of the *PolγA*$^{mut/mut}$ group in comparison the *PolγA*$^{+/mut}$ and *PolγA*$^{+/+}$ groups culminating in their reduced survival.

3.5. Conclusion

In this chapter I have described the generation of and further characterised a novel mouse model combining the two pathologies of age-related mitochondrial dysfunction and intestinal cancer. A model of mtDNA mutation accumulation with an ageing phenotype is provided by the *PolγA* mutator mouse (Kujoth et al., 2005; Trifunovic et al., 2004) which at six months of age demonstrates respiratory chain dysfunction in around 60% of colonic crypts (Baines et al., 2014). As such, in order to investigate the potential effect that mitochondrial dysfunction may have on tumour growth and development, mice are aged to six months prior to tamoxifen induced *Apc* deletion which initiates adenomagenesis. The intestinal cancer phenotype is provided by the *Lgr5-EGFP-IRES-creERT2- Apc*$^{flox/flox}$ mouse (Barker et al., 2009) in which numerous microadenomas form throughout the intestine and colon. This is recapitulated in our model, however clinically, a deterioration in health as evidenced primarily by anaemia, impaired thermoregulation and weight loss is exacerbated in mice with mitochondrial dysfunction compared to those without, significantly reducing their lifespan. Analysis of the size and total adenoma burden in the colon and small intestine at the same time points revealed a significantly greater colonic and small intestinal adenoma burden with larger average adenoma size in the *PolγA*$^{mut/mut}$ mice suggesting accelerated adenoma growth. It is therefore hypothesised that mitochondrial dysfunction caused by an accumulation of somatic mtDNA mutations promotes the progression of intestinal adenomas.

3.6. Future work – pilot studies

3.6.1. Reduced tamoxifen dosage cohorts

The tamoxifen induced *Apc* deletion regimen for experimental animals thus far followed a 3mg, 2mg, 2mg, and 2mg dosage pattern with one IP dose on each consecutive day. Lifespan was significantly reduced due to the rapid development of intestinal adenomas, particularly in *PolγA*$^{mut/mut}$ animals, thus preventing the observation of advanced stages of disease. It was proposed that lifespan may be extended by reducing the initial rapid adenoma accumulation with a lower dose of tamoxifen, potentially allowing the observation of more advanced disease stages such as the progression to carcinoma or metastases as seen in human

patients. Animals in the 2mg tamoxifen cohort were aged to 6 months prior to administration of a single 2mg IP dose of tamoxifen. Clinical monitoring was carried out as per previous cohorts and animals were humanely sacrificed when necessary to do so. Data for this cohort describes a significantly shorter survival of *PolγA*$^{mut/mut}$ animals when compared to *PolγA*$^{+/mut}$ and *PolγA*$^{+/+}$ mice (P=0.0010, Mantel-Cox log rank test). This is presented in Figure 3-17**.**

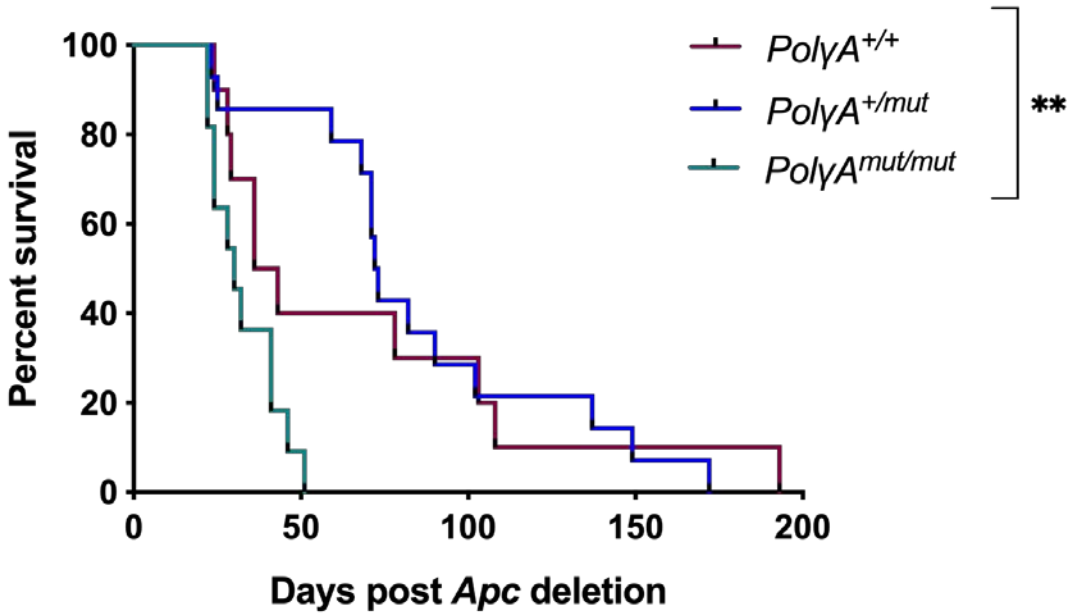

Figure 3-17. Kaplan-Meier survival curve depicting survival times of 2mg tamoxifen dosage *PolγA*$^{+/+}$ (n=10), *PolγA*$^{+/mut}$ (n=14) and *PolγA*$^{mut/mut}$ mice (n=11) aged to 6 months prior to *Apc* deletion. *PolγA*$^{mut/mut}$ mice have significantly shorter lifespans in comparison to *PolγA*$^{+/+}$ and *PolγA*$^{+/mut}$ animals. Mantel-Cox log rank test P=0.0017.

As hypothesised, lifespan was extended with the reduction of the initiating tamoxifen dosage. An increase in the median survival time post *Apc* deletion was observed in all three experimental groups, the greatest increase being observed in the *PolγA*$^{+/mut}$ group in which the median survival of 26 days became 72.5 days survival post *Apc* deletion with the reduced tamoxifen induction dosage.

In order to ascertain whether a longer lifespan facilitated the progression of adenomas to a more advanced phenotype, sections were cut from the paraffin embedded colons and distal small intestines of these mice. Sections were stained with H&E and sample images were assessed by Dr Simon Buczacki, Clinician Scientist & Honorary Consultant Colorectal Surgeon,

CRUK, Cambridge. Example H&E micrographs of *PolγA*$^{+/+}$ and *PolγA*$^{+/mut}$ small intestinal adenomas are presented in Figure 3-18.

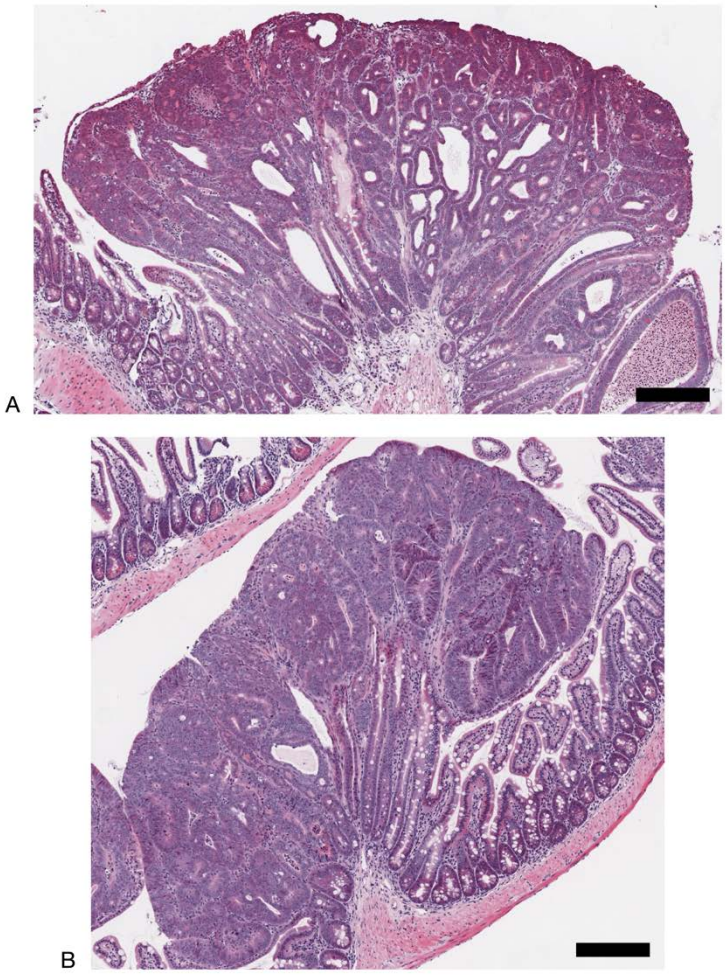

Figure 3-18. H&E labelling of small intestinal adenomas from animals administered with 2mg tamoxifen (A) H&E labelling of a small intestinal adenoma from a *PolγA*$^{+/+}$ animal at 103 days post *Apc* deletion. (B) H&E labelling of a small intestinal adenoma from a *PolγA*$^{+/mut}$ animal at 149 days post *Apc* deletion. Scale bars 200µm.

Despite the observation that adenomas appear to be taking on a more traditional appearance, lesions are maintaining a glandular structure without disruption of the basement membrane or desmoplastic stromal reaction. This casts doubt upon the hypothesis that this experimental cohort may demonstrate more advanced stages of disease, however given the extended lifespan and adenomatous morphology with a reduced initiating dose of tamoxifen further cohorts are currently under investigation. Single initiating tamoxifen dosages of 0.5, 1 and 1.5mg have been administered to *PolγA*$^{+/+}$, *PolγA*$^{+/mut}$ and *PolγA*$^{mut/mut}$ animals at six months of age. It is anticipated that the reduced level of Cre recombination in these animals may further permit the extension of lifespan and disease progression.

3.6.2. Apc heterozygote cohort

In many cases of human colorectal cancer, one mutated allele of *APC* is inherited with a mutational event later in life facilitating loss of the second allele. In an attempt to recapitulate this human situation and assess whether the presence of mitochondrial dysfunction facilitates the loss of the second copy of *APC*, a cohort of animals heterozygous for the Apc^{flox} gene were established. Fermentation of glucose into lactate in favour of utilising oxidative phosphorylation facilitates the generation of anabolic products required for a tumour mass to proliferate. In extracts of normal intestinal tissue from $Apc^{Min/+}$ mice, elevated lactate levels were reported when compared to tissue from wild type animals. Additionally, levels in metabolites such as the phosphocoline/glycerophosphocoline ratio (PC/GPC), were reported to be significantly greater in lamina propria tissues of $Apc^{Min/+}$ versus wild type animals (Backshall et al., 2009). The authors suggest a metabolic difference between these groups of animals based upon their differing levels of functional Apc may constitute a permissive tumorigenic environment, or 'field cancerisation', leading to loss of *Apc* heterozygosity and adenoma formation. Additionally, the potential increase in mitochondrial generation of reactive oxygen species as a result of the *PolγA* mutation may affect loss of *Apc* heterozygosity. Although of a less persistent and less extensive nature, DNA damage caused by oxidative stress is also reported to affect nuclear, in addition to mitochondrial DNA (Yakes & Van Houten, 1997). A cohort of animals heterozygous for the Apc^{flox} gene was therefore established in order to recapitulate the human situation and assess whether mitochondrial dysfunction caused by *PolγA* mutation facilitates loss of the second copy of *Apc*.

A longer disease course was predicted in this cohort due to the excision of only one copy of *Apc* at induction. To allow for this, experimental animals were induced at 4 months of age as opposed to six. With some animals surviving beyond 13 months post tamoxifen induction, this was chosen as the experimental endpoint for $PolγA^{+/+}$ (n=9) and $PolγA^{+/mut}$ (n=9) animals. $PolγA^{mut/mut}$ animals were not included in this cohort due to their shorter lifespan not permitting the longer disease course required to observe a somatic loss of heterozygosity. Macroscopic tumour burden data from the entire intestine of experimental animals is shown in Figure 3-19.

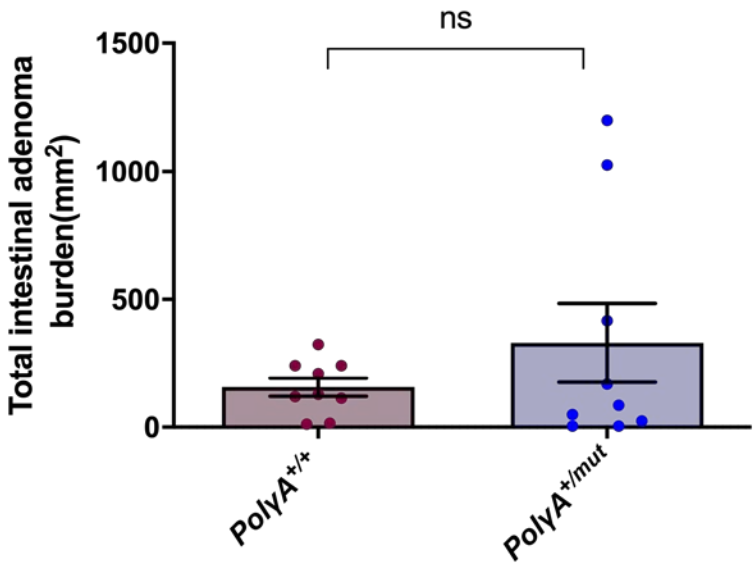

Figure 3-19. Total intestinal macroscopic adenoma burden from *PolγA*$^{+/+}$ (n=9) and *PolγA*$^{+/mut}$ (n=9) *Apc* heterozygote mice. No significant difference was detected between mean adenoma burden of these groups (P=0.2878, unpaired t test).

No significant difference was detected between the means of the two groups (P=0.00265, unpaired t test) and although this suggests mitochondrial dysfunction is not contributing to loss of *Apc* heterozygosity, all tissues require further histological analysis.

Chapter 4. Assessment of mitochondrial dysfunction within adenomas and normal non-transformed crypts of the murine colon and small intestine

4.1. Introduction

4.1.1. Mitochondrial dysfunction in ageing and cancer

Advancing age is a major risk factor for malignant transformation and the development of cancer. As such, over 50% of neoplasms occur in individuals over the age of 70 (Siegel et al., 2015). Similarly, as organisms age, the efficiency of mitochondrial oxidative phosphorylation is impaired and alterations in mitochondrial morphology and abundance are observed (Shigenaga et al., 1994). The development of perturbations in mitochondrial function are common to both pathologies and consequently lead to a hypothesised link between an age-associated mitochondrial dysfunction and tumorigenesis.

Ample evidence exists documenting the accumulation of somatic mtDNA mutations in ageing human post-mitotic tissues such as the brain and skeletal muscle (Brierley et al., 1998; Corral-Debrinski et al., 1992) and in numerous replicative tissues (Fellous et al., 2009; McDonald et al., 2008; Taylor et al., 2003). The mechanisms by which these mutations accumulate have historically been attributed to ROS mediated mtDNA damage and Polγ mediated replication errors and as such the causative effect of mtDNA mutation accumulation with regard to ageing has been investigated with the use of the *PolγA* mutator mouse (Kujoth et al., 2005; Trifunovic et al., 2004). Specifically, in the in the colon, clonal expansion of early life acquired somatic mtDNA mutations has been shown to diminish mitochondrial oxidative phosphorylation with advancing age in both humans and mice (Baines et al., 2014; Greaves et al., 2014; Taylor et al., 2003). This has been demonstrated using a dual histochemical assay to demonstrate cytochrome *c* oxidase (COX) and succinate dehydrogenase (SDH) enzymatic activity. In this assay diaminobenzidine (DAB) acts as an electron donor resulting in a brown insoluble compound deposition at the location of COX or complex IV activity; cells with no COX

activity are labelled blue upon subsequent incubation in media to demonstrate SDH activity. Using this assay, it has been shown that the proportion of COX-deficient colonic crypts exponentially increases with age in humans (Taylor et al., 2003). Single crypt and single cell mtDNA sequencing analyses confirmed that clonally expanded mtDNA mutations were the underlying cause of the COX deficiency in these crypts. In addition to fully COX deficient crypts, partially deficient colonic crypts are observed using this histochemical technique. The three-dimensional reconstruction of COX/SDH labelled serial sections revealed ribbons of COX deficient cells which emanate from the crypt base right up to the apex (Taylor et al., 2003). This represents the transmission of mtDNA defects from the parent stem cell harbouring these defects to the progeny of that parent cell which subsequently migrate along the crypt axis and COX deficiency is preserved. Sequencing of the mtDNA of individual cells within these ribbons confirmed that they had a common clonal ancestor. These analyses demonstrated that colonic stem cells accumulate pathogenic mtDNA mutations with age.

The relationship between cancer and mitochondrial dysfunction spans almost 100 years from the initial observations of Warburg detailing the glycolytic phenotype favoured by tumour cells (Warburg, 1927; Warburg, 1956), to the current understanding that mitochondrial function extends beyond that of energy and anabolic precursor provision and is intricately linked to numerous facets of cancer biology. Following appropriate stimuli, mitochondria are crucial in orchestrating apoptosis; a process staunchly evaded by tumour cells by a number of means (reviewed in Lopez & Tait, 2015). Mitochondrial ROS have been linked to the promotion of invasion and metastases (Ishikawa et al., 2008) as has the regulation of mitochondrial dynamics (Zhao et al., 2013b). Furthermore, the recent Pan-Cancer Analysis of Whole Genomes (PCAWG) Consortium reported a marked enrichment of truncating mtDNA mutations in colorectal, kidney and thyroid cancers with an associated upregulation of mTOR and TNFα signalling. The activation of such oncogenic signalling pathways further implicates the role of mtDNA mutations in cancer development, and a link with ageing is corroborated by the observation that the detection of somatic mtDNA mutations at the highest levels of heteroplasmy positively correlate with age (Yuan et al., 2020). The selective enrichment of these somatic mtDNA mutations is also proposed as an alternative mechanism by

which they are able to reach high levels of heteroplasmy within the tumours, additionally indicating a physiological advantage provided by the mutations themselves (Yuan et al., 2020).

4.2. Aims of study

In the previous chapter I demonstrated that mice with mitochondrial dysfunction caused by an accumulation of somatic mtDNA mutations harbour a significantly greater colonic and small intestinal adenoma burden than those without. In this chapter I wanted to fully characterise the extent of mitochondrial dysfunction within the colon and small intestine of experimental animals compared with controls. In this chapter I aimed to;

1. Quantify the expression of mitochondrial oxidative phosphorylation complexes I, III, IV and V within the colonic and small intestinal adenomas of *PolγA*$^{+/+}$ and *PolγA*$^{mut/mut}$ mice culled at 23 days following *Apc* deletion at six months age.

2. Quantify OXPHOS protein expression in *PolγA*$^{+/mut}$ experimental animal colonic and small intestinal adenomas compared with those of *PolγA*$^{+/+}$ mice culled at 23 days following *Apc* deletion at six months age.

3. Utilise the mosaic pattern of OXHPOS normal and OXPHOS deficient adenomas within *PolγA*$^{+/mut}$ experimental animals to investigate any correlation between OXPHOS protein levels and adenoma size within individual mice.

4. Investigate the effect of *Apc* deletion on expression of mitochondrial OXPHOS proteins by comparing their levels within colonic and small intestinal adenomas to those of normal non-transformed crypts within the same mice.

4.3. Results

4.3.1. Quantification of mitochondrial OXPHOS protein levels in intestinal adenomas following Apc deletion in 6-month-old PolγA$^{mut/mut}$ and PolγA$^{+/+}$ mice

With the exception of complex II, each of the complexes of the mitochondrial OXPHOS system are encoded in part by the mitochondrial genome, part by the nuclear genome. As such, mutations in the mitochondrial genome should only directly affect complexes I, III, IV and V protein expression. To investigate the effect of the *PolγA* mutation on the intestinal tissues, the quadruple immunofluorescence assay developed within the group was used. This method has been optimised for diagnostic purposes to reliably and robustly quantify the levels of key OXPHOS proteins thus defining biochemical phenotypes in genetically-defined primary mitochondrial myopathies (Rocha et al., 2015). Initially developed to quantify complex I and IV protein abundance, the method was adapted for this study to include the labelling of the UQCRFS1 subunit of complex III and the ATPB subunit of complex V in addition to NDUFB8 of complex I and MTCO1 of complex IV. Due to the addition of anti-UQCRFS1 and anti-ATPB to the assay, and the availability of antibody isotypes, the technique was further modified with the labelling of two adjacent serial sections in order to accommodate all antibodies. The first section was labelled with anti-NDUFB8 and anti-UQCRFS1 and the second with anti-MTCO1 and anti-ATPB. Anti-VDAC1 was initially used as a mitochondrial mass marker, however punctate labelling was not observed, therefore this was replaced and labelling re-optimised using a rabbit anti-TOMM20 as a mitochondrial mass marker. The immunofluorescent assay protocol is outlined in 2.2.11.3. Colonic and small intestinal tissue samples were labelled, and fluorescent micrographs of adenomas acquired using a Nikon A1R inverted point scanning confocal microscope. Confocal images were analysed using Image J software (NIH). Adenomas were selected as regions of interest (ROI) and fluorophore mean intensity values recorded for each channel before their use in generation of z score plots as described in 2.2.12.4. In the colon, a minimum of 20 adenomas were manually identified from *PolγA*$^{mut/mut}$ (n=9) and *PolγA*$^{+/+}$ (n=9) mice culled at 23 days post *Apc* deletion. Example immunofluorescent panels are presented in Figures 4-1 and 4-2.

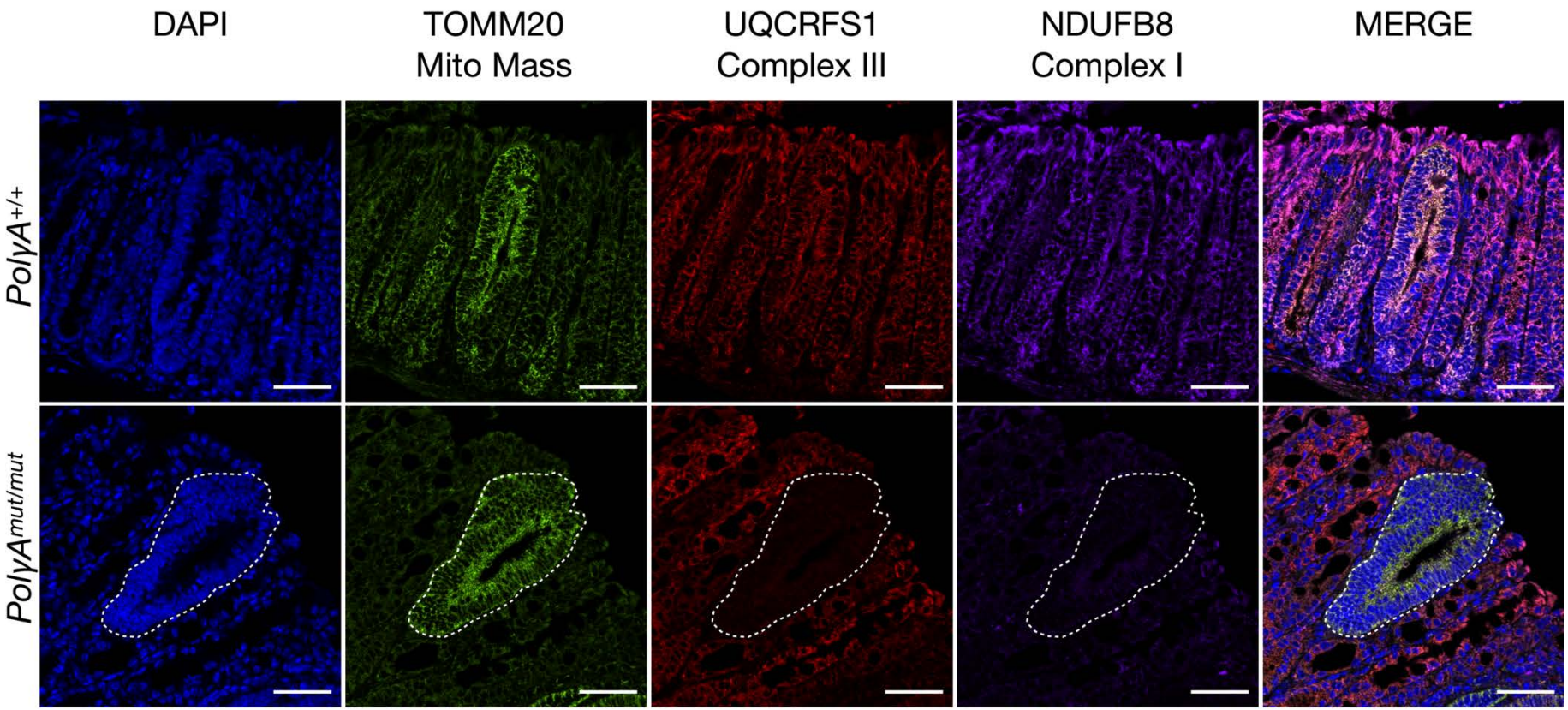

Figure 4-1. Immunofluorescent labelling of mitochondrial OXPHOS protein expression within the *PolγA*$^{+/+}$ and *PolγA*$^{mut/mut}$ colon 23 days after *Apc* deletion. A Hoescht counterstain labels nuclei, AlexaFluor 488 labels anti-TOMM20 primary antibody, AlexaFluor 647 labels anti-NDUFB8 and AlexaFluor 546 labels anti-UQCRFS1. The white dashed line highlights a *PolγA*$^{mut/mut}$ adenoma deficient in complex I and complex III. Scale bars 50µm.

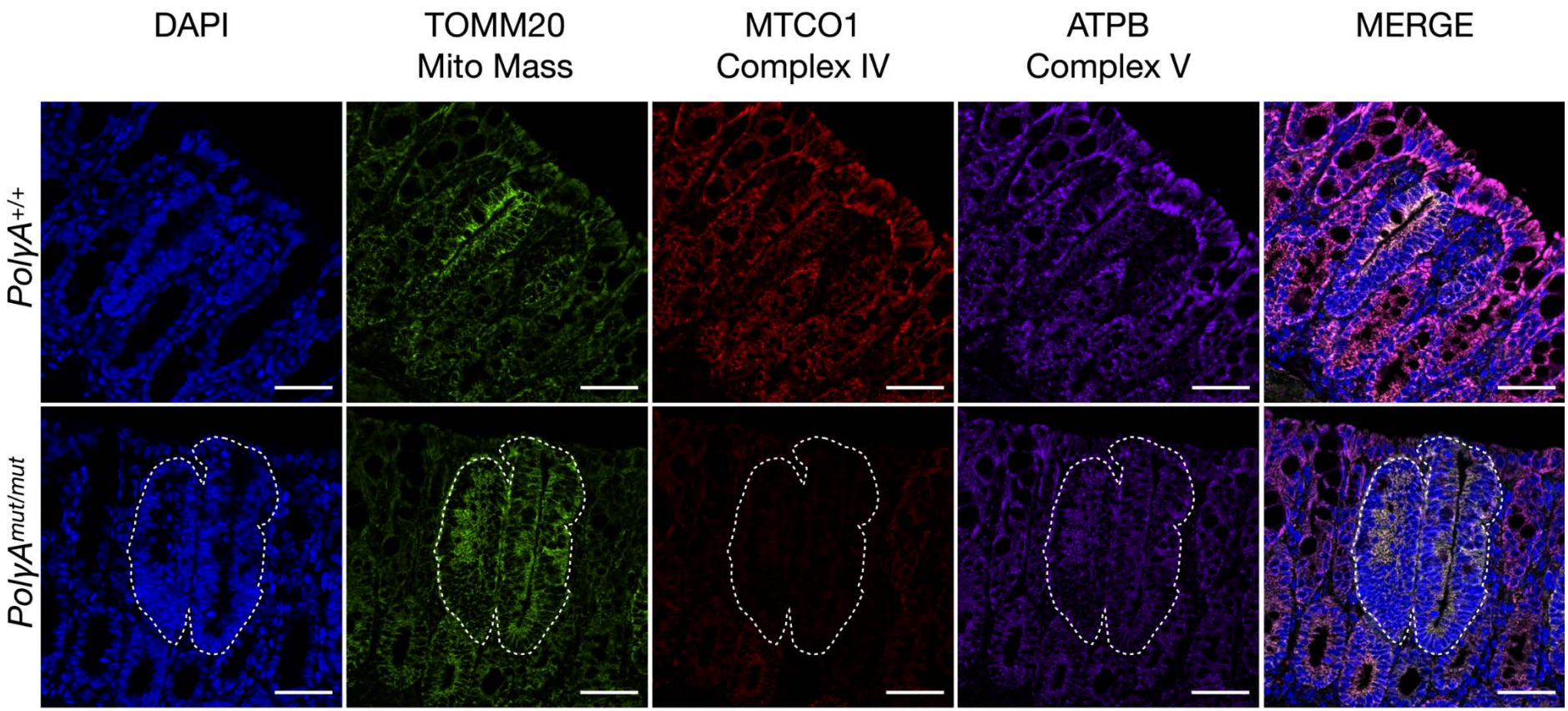

Figure 4-2. Immunofluorescent labelling of mitochondrial OXPHOS protein expression within the *PolγA*$^{+/+}$ and *PolγA*$^{mut/mut}$ colon 23 days after *Apc* deletion. A Hoescht counterstain labels nuclei, AlexaFluor 488 labels anti-TOMM20 primary antibody, AlexaFluor 647 labels anti-MTCO1 and AlexaFluor 546 labels anti-ATPB. The white dashed line highlights a *PolγA*$^{mut/mut}$ adenoma deficient in complex IV. Scale bars 50µm.

All *PolγA*$^{+/+}$ colonic adenomas were found to express normal levels of all OXPHOS proteins investigated, with the exception of one isolated adenoma demonstrating an intermediate positive expression of UQCRFS1. In contrast only 36.06% and 18.75% of *PolγA*$^{mut/mut}$ colonic adenomas demonstrate a normal level of MTCO1 and NDUFB8 respectively when compared to *PolγA*$^{+/+}$ colonic adenomas (Figure 4-3).

With regard to MTCO1, 63.95% of *PolγA*$^{mut/mut}$ colonic adenomas demonstrate a reduced level of protein expression (15.87% intermediate positive, 22.12% intermediate negative and 25.96% negative) when compared to *PolγA*$^{+/+}$ adenomas. With regard to NDUFB8, 81.25% of *PolγA*$^{mut/mut}$ colonic adenomas demonstrate a reduced level of protein expression (27.88% intermediate positive, 37.5% intermediate negative and 15.87% negative) in comparison to *PolγA*$^{+/+}$ adenomas. Some reduction in expression of UQCRFS1 is detected in *PolγA*$^{mut/mut}$ colonic adenomas (10.58% intermediate positive, 5.77% intermediate negative and 6.25% negative) however the remaining 77.4% retain a normal UQCRFS1 expression when compared to *PolγA*$^{+/+}$ adenomas. The majority of *PolγA*$^{mut/mut}$ colonic adenomas (96.15%) retain normal expression of the ATPB subunit of complex V with 3.85% categorised as demonstrating intermediate positive expression. Importantly, it is noted that OXPHOS protein defects are not visibly associated with a loss of mitochondrial mass. The maintenance of TOMM20 expression and indeed an often-increased expression of TOMM20 in regions of adenoma suggests that the observed deficiencies are due to defects in the OXPHOS proteins themselves and not merely as a result of fewer numbers of mitochondria. These data suggest that defects in mitochondrial oxidative phosphorylation, specifically that of complex I and complex IV may promote the growth of colonic adenomas following *Apc* deletion.

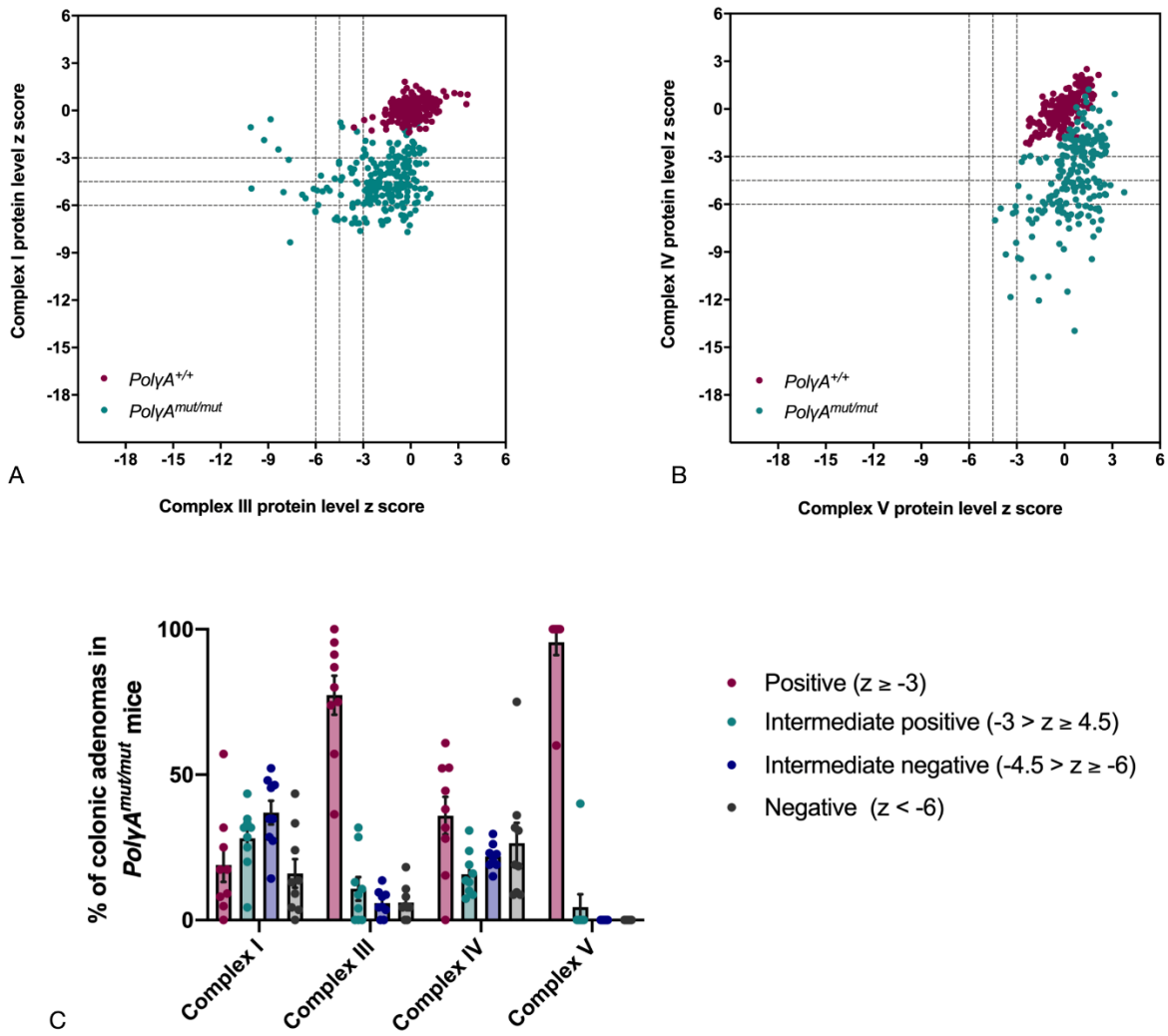

Figure 4-3. Dot plots showing z scores calculated following quantification of mitochondrial OXPHOS protein levels in colonic adenomas of *PolγA*$^{+/+}$ (n=9) and *PolγA*$^{mut/mut}$ (n=9) mice. (A) Z score plot depicting complex I and III levels. (B) Z score plot depicting complex IV and V levels. (C) Categorical analysis of OXPHOS protein levels in *PolγA*$^{mut/mut}$ colonic adenomas (error bars denote mean ±SEM).

A minimum of 20 adenomas from the small intestines of *PolγA*$^{+/+}$ (n=10) mice and *PolγA*$^{mut/mut}$ (n=9) were identified and imaged in the same manner as per the colon. As part of an MRes project, *PolγA*$^{+/+}$ (n=5) and *PolγA*$^{mut/mut}$ (n=5) were labelled and analysed by Matthew Hunt. Example immunofluorescent panels are presented in Figures 4-4 and 4-5.

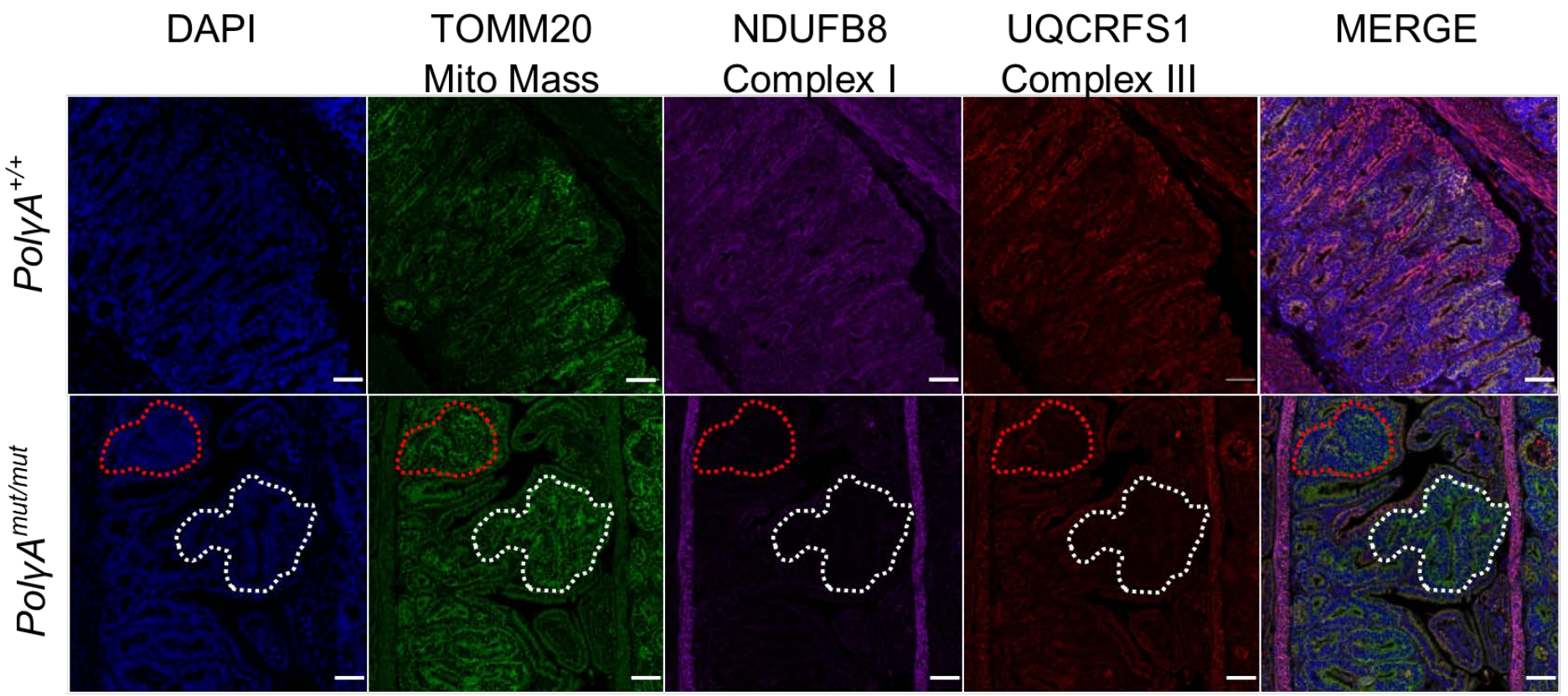

Figure 4-4. Immunofluorescent labelling of mitochondrial OXPHOS protein expression within the *PolγA*$^{+/+}$ and *PolγA*$^{mut/mut}$ small intestine 23 days after *Apc* deletion. A Hoescht counterstain labels nuclei, AlexaFluor 488 labels anti-TOMM20 primary antibody, AlexaFluor 647 labels anti-NDUFB8 and AlexaFluor 546 labels anti-UQCRFS1. The white dashed line highlights a *PolγA*$^{mut/mut}$ adenoma deficient in both complex I and complex III. The red dashed line highlights a *PolγA*$^{mut/mut}$ adenoma deficient in complex I with some retention of complex III expression. Scale bars 50µm.

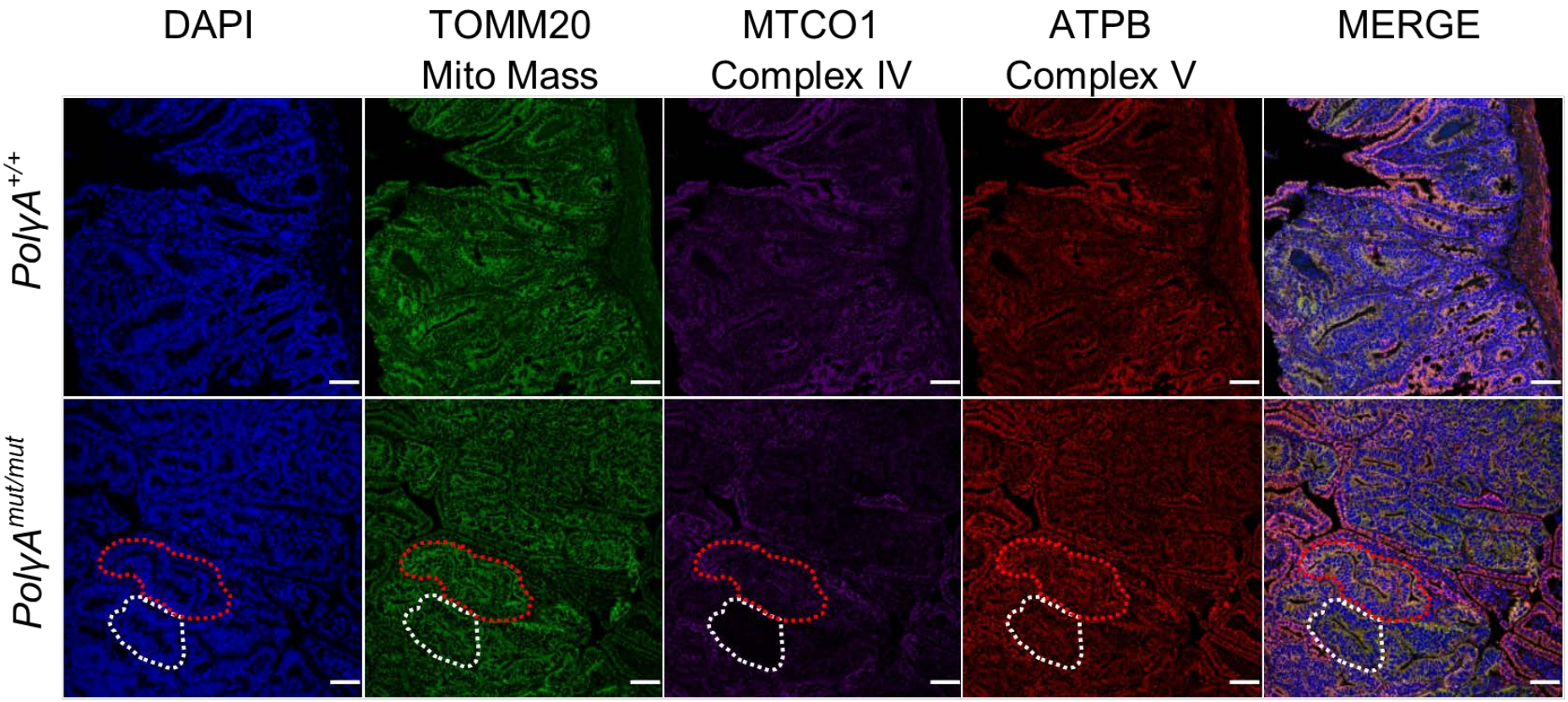

Figure 4-5. Immunofluorescent labelling of mitochondrial OXPHOS protein expression within the *PolγA*$^{+/+}$ and *PolγA*$^{mut/mut}$ small intestine 23 days after *Apc* deletion. A Hoescht counterstain labels nuclei, AlexaFluor 488 labels anti-TOMM20 primary antibody, AlexaFluor 647 labels anti-MTCO1 and AlexaFluor 546 labels anti-ATPB. The white dashed line highlights a *PolγA*$^{mut/mut}$ adenoma deficient in complex IV. The red dashed line highlights a *PolγA*$^{mut/mut}$ adenoma with retained complex IV and V expression. Scale bars 50µm

In the small intestine, all *PolγA*$^{+/+}$ adenomas analysed were found to express normal levels of each OXPHOS protein investigated. In the *PolγA*$^{mut/mut}$ small intestine however, 100% of adenomas demonstrate reduced levels of NDUFB8 protein expression. 80.86% were categorised as negative in their expression of NDUFB8, 14.35% categorised as intermediate negative and 4.78% categorised as intermediate positive. With regard to MTCO1, 37.63% of *PolγA*$^{mut/mut}$ small intestinal adenomas demonstrate a reduction in expression of protein (26.29% intermediate positive, 5.15% intermediate negative and 6.19% negative) while the remaining 62.37% retained MTCO1 expression. A reduction of UQCRFS1 expression is noted in 9.1% of *PolγA*$^{mut/mut}$ compared to *PolγA*$^{+/+}$ adenomas (7.18% intermediate positive, 1.44% intermediate negative, 0.48% negative) while ATPB expression is retained in all *PolγA*$^{mut/mut}$ adenomas. Interestingly, a slight shift towards increased levels of ATPB expression above those of the *PolγA*$^{+/+}$ adenomas is observed in *PolγA* $^{mut/mut}$ adenomas (Figure 4-6).

Collectively, OXPHOS protein expression analysis of experimental animal colonic and small intestinal adenomas demonstrates an extensive reduction in the levels of expression of the complex I subunit NDUFB8 in *PolγA*$^{mut/mut}$ compared to *PolγA*$^{+/+}$ adenomas. This is more pronounced in the small intestine where all *PolγA* $^{mut/mut}$ adenomas display reduced protein expression. Minimal UQCRFS1 (complex III) is detected in each compartment and ATPB (complex V) expression is retained throughout. Although MTCO1 (complex IV) expression is reduced in *PolγA*$^{mut/mut}$ adenomas in both the colon and small intestine, this defect is more prominent in the colon where 63.95% of *PolγA*$^{mut/mut}$ colonic adenomas demonstrate a reduced level of protein expression in comparison with 37.63% of *PolγA*$^{mut/mut}$ small intestinal adenomas. This observation may imply that the loss of MTCO1 protein is better tolerated within the colon than the small intestine and therefore persists.

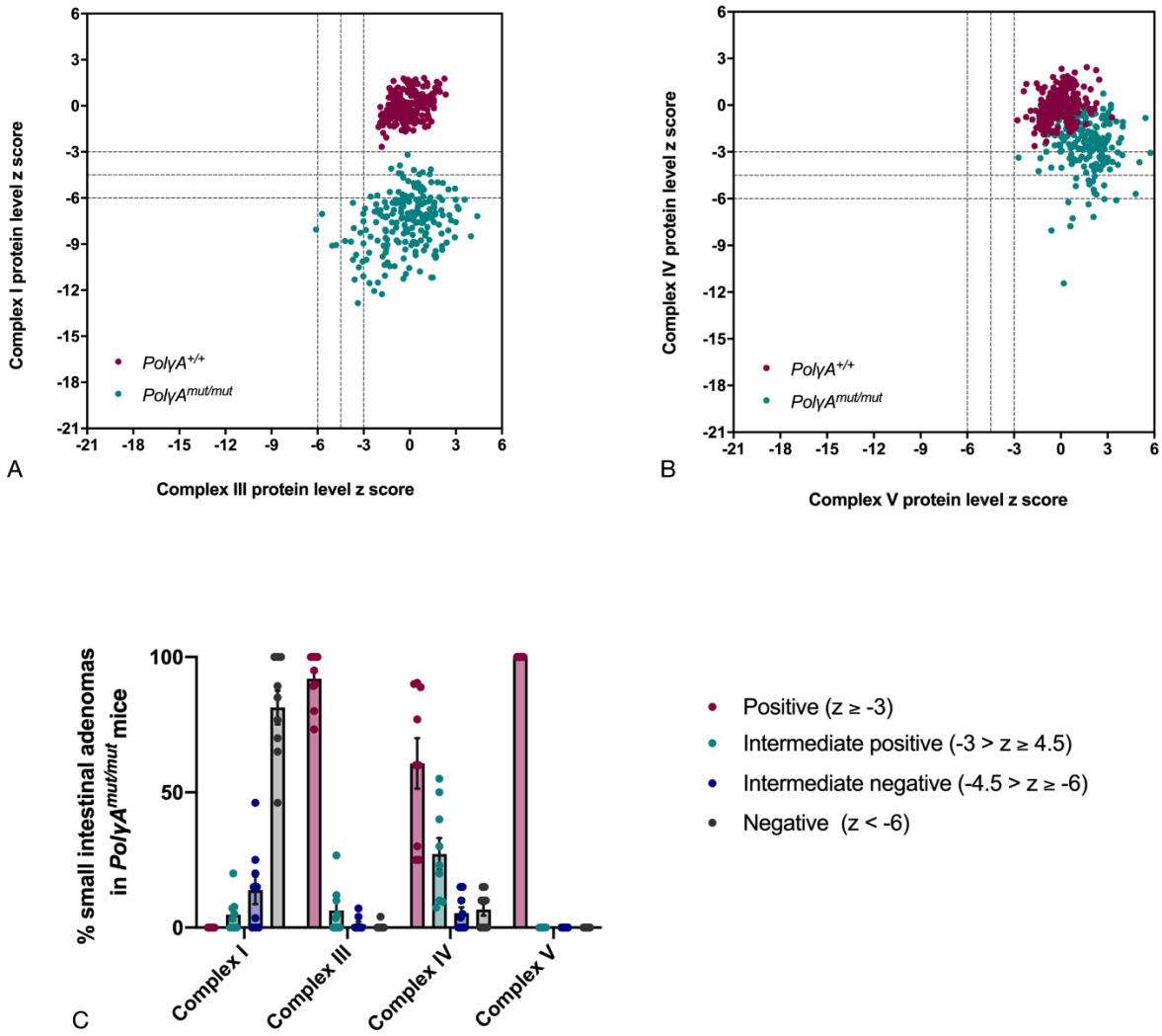

Figure 4-6. Dot plots showing z scores calculated following quantification of mitochondrial OXPHOS protein levels in small intestinal adenomas of *PolγA*$^{+/+}$ (n=10) and *PolγA*$^{mut/mut}$ (n=9) mice. (A) Z score plot depicting complex I and III levels. (B) Z score plot depicting complex IV and V levels. (C) Categorical analysis of OXPHOS protein levels in *PolγA*$^{mut/mut}$ small intestinal adenomas (error bars denote mean ±SEM).

4.3.2. Quantification of mitochondrial OXPHOS protein levels in Intestinal adenomas following Apc deletion in 6-month-old PolγA$^{+/mut}$ and PolγA$^{+/+}$ mice

The frequency of COX deficiency within the colonic crypts of 6-month-old *PolγA*$^{+/mut}$ mice is markedly lower than that of 6-month-old *PolγA* $^{mut/mut}$ animals at 5% and 60% respectively (Baines et al., 2014). In contrast to *PolγA*$^{mut/mut}$ colon in which OXPHOS defects are extensive, the assessment of *PolγA*$^{+/mut}$ tissues in which there is a mosaic pattern of OXHPOS normal and OXPHOS deficient crypts or adenomas allows intra-mouse comparisons to be made using the OXPHOS normal crypts as internal controls. As results of the previous section identified defects in complex I and complex IV as most prominent in *PolγA*$^{mut/mut}$ colonic and small intestinal adenomas, in order to assess the degree of mitochondrial OXPHOS protein defects within the adenomas of mice heterozygous for the *PolγA* mutation, the immunofluorescence assay was adjusted accordingly. Antibodies targeting ATPB and UQCRFS1 were omitted, and an immunofluorescent assay using antibodies targeting NDUFB8, MTCO1 and TOMM20 was carried out on the colonic and intestinal samples of an additional subset of 6-month-old *PolγA*$^{+/mut}$ and *PolγA*$^{+/+}$ mice all humanely sacrificed at 23 days post *Apc* deletion. Fluorescent micrographs of adenomas were acquired in the same manner as previously described, with manual identification of a minimum of 15 adenomas from the colons of *PolγA*$^{+/mut}$ (n=5) and *PolγA*$^{+/+}$ (n=4) mice culled at 23 days post *Apc* deletion. Similarly, a minimum of 15 adenomas from the small intestines of *PolγA*$^{+/mut}$ (n=4) and *PolγA*$^{+/+}$ (n=4) mice were identified and imaged as such. Confocal images were analysed using Image J software (NIH). Adenomas were selected as regions of interest (ROI) and fluorophore mean intensity values recorded for each channel.

Levels of OXPHOS protein expression within *PolγA*$^{+/mut}$ colonic adenomas are not reduced to the same degree as seen in *PolγA* $^{mut/mut}$ mice (Figure 4-7). In the colon, 18.71% of *PolγA*$^{+/mut}$ adenomas demonstrate reduced levels of NDUFB8 and 19.43% display reduced levels of MTCO1, compared with 81.25% for NDUFB8 and 63.95% for MTCO1 in *PolγA* $^{mut/mut}$ colonic adenomas. Levels of OXPHOS proteins within *PolγA*$^{+/mut}$ colonic adenomas are significantly lower than in *PolγA*$^{+/+}$ colonic adenomas sampled in which all adenomas with the exception of one, express NDUFB8 and MTCO1 within a normal range (Figure 4-8).

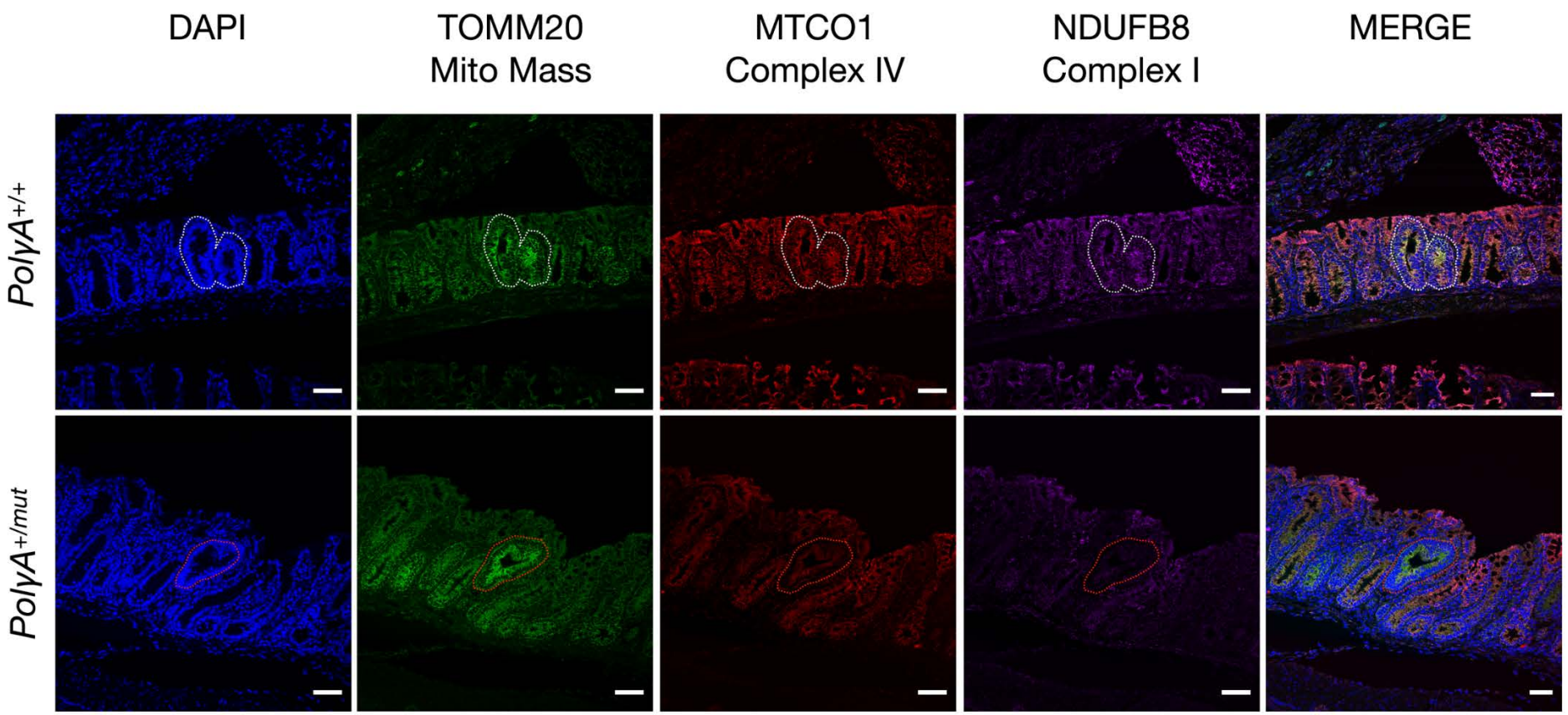

Figure 4-7. Immunofluorescent labelling of mitochondrial OXPHOS protein expression within the *PolγA*$^{+/+}$ and *PolγA*$^{+/mut}$ colon 23 days after *Apc* deletion. A Hoescht counterstain labels nuclei, AlexaFluor 488 labels anti-TOMM20 primary antibody, AlexaFluor 546 labels anti-MTCO1 and AlexaFluor 647 labels anti-NDUFB8. The white dashed line highlights a *PolγA*$^{+/+}$ adenoma with retained complex IV and I expression. The red dashed line highlights a *PolγA*$^{+/mut}$ region of adenoma demonstrating reduced levels of complex IV and I. Scale bars 50µm.

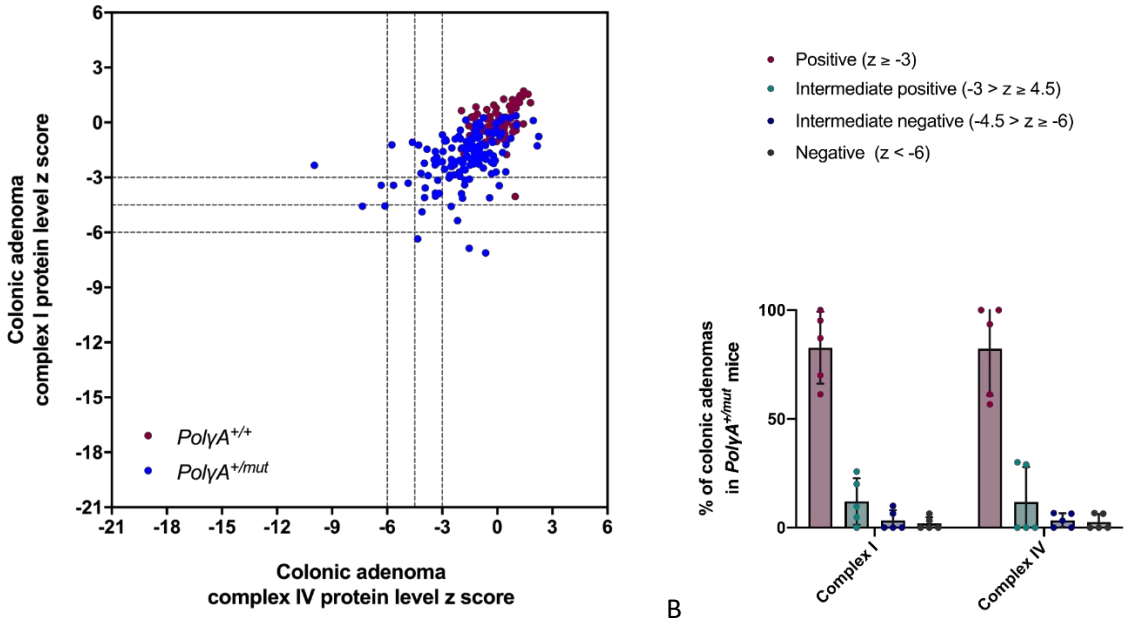

Figure 4-8. Dot plot showing z scores calculated following quantification of mitochondrial OXPHOS protein levels in colonic adenomas of *PolγA*$^{+/+}$ and *PolγA*$^{+/mut}$ mice. (A) Z score plot depicting complex I and IV levels in colonic adenomas of *PolγA*$^{+/+}$ (n=4) and *PolγA*$^{+/mut}$ (n=4) mice. (B) Categorical analysis of adenoma OXPHOS protein levels in *PolγA*$^{+/mut}$ (n=4) colonic adenomas (error bars denote mean ±SEM).

In the small intestine, no MTCO1 defect was observed in *PolγA*$^{+/+}$ adenomas, however 92.59% of *PolγA*$^{+/mut}$ adenomas sampled demonstrated a reduced level of NDUFB8 (35.8% intermediate positive, 39.51% intermediate negative and 17.28% negative). As expected, this does not reach the same level of NDUFB8 deficiency as observed within the *PolγA* $^{mut/mut}$ small intestine; 80.86% of *PolγA* $^{mut/mut}$ small intestinal adenomas were classified as NDUFB8 negative in comparison to 17.28% of *PolγA*$^{+/mut}$ small intestinal adenomas (Figure 4-10). Example immunofluorescent panels of the *PolγA*$^{+/+}$ and *PolγA*$^{+/mut}$ small intestine are presented in Figure 4-9.

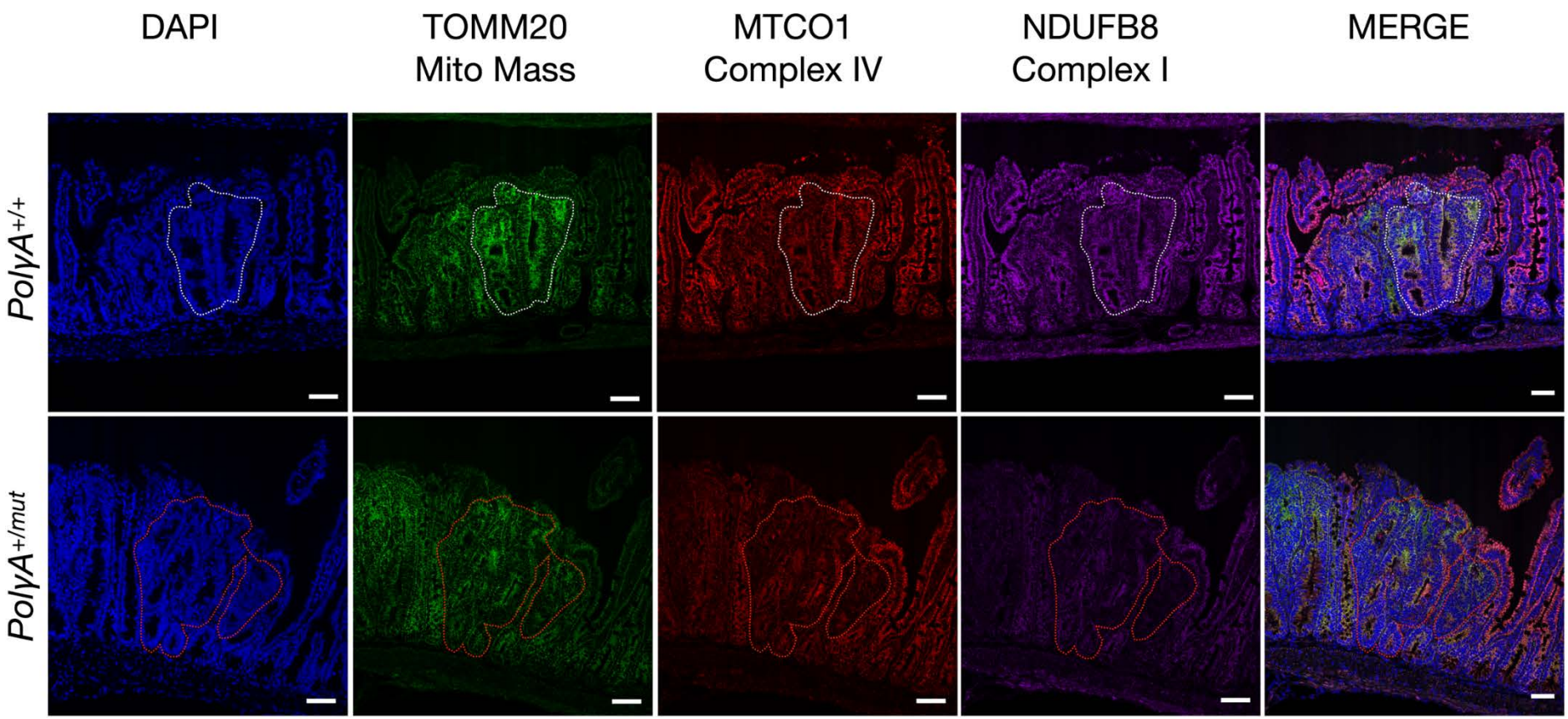

Figure 4-9. Immunofluorescent labelling of mitochondrial OXPHOS protein expression within the *PolγA*$^{+/+}$ and *PolγA*$^{+/mut}$ small intestine 23 days after *Apc* deletion. A Hoescht counterstain labels nuclei, AlexaFluor 488 labels anti-TOMM20 primary antibody, AlexaFluor 546 labels anti-MTCO1 and AlexaFluor 647 labels anti-NDUFB8. The white dashed line highlights a *PolγA*$^{+/+}$ adenoma with retained complex IV and I expression. The red dashed line highlights a *PolγA*$^{+/mut}$ region of adenoma demonstrating reduced levels of complex IV and I. Scale bars 50µ

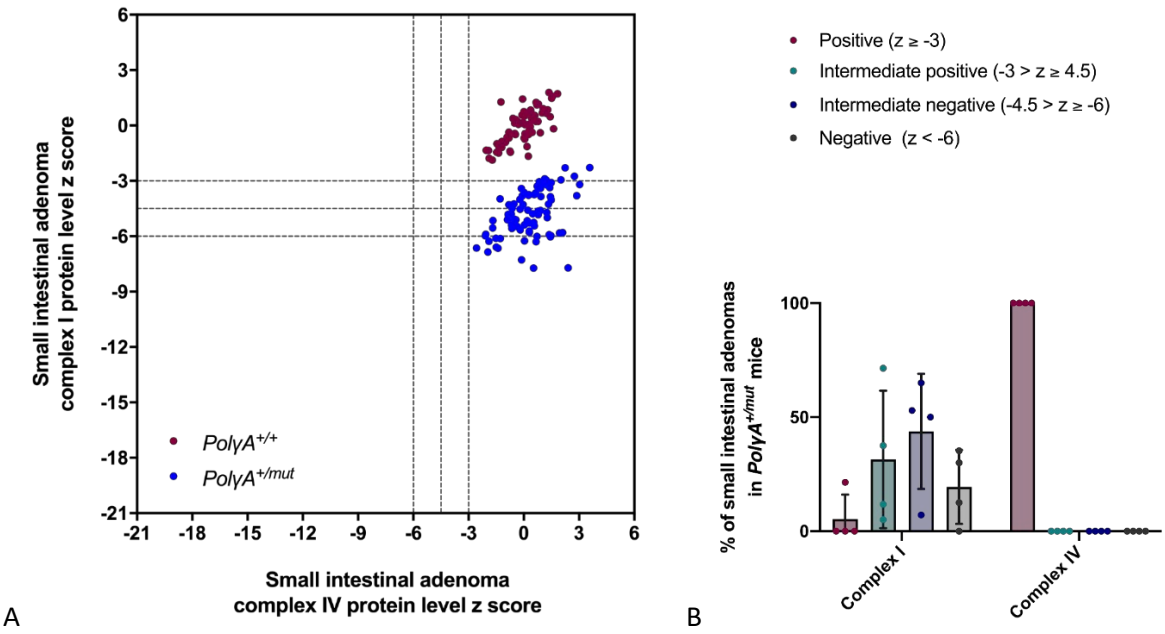

Figure 4-10. Dot plot showing z scores calculated following quantification of mitochondrial OXPHOS protein levels in small intestinal adenomas of *PolγA*$^{+/+}$ and *PolγA*$^{+/mut}$ mice. (A) Z score plot depicting complex I and IV levels in small intestinal adenomas of *PolγA*$^{+/+}$ (n=4) and *PolγA*$^{+/mut}$ (n=5) mice. (B) Categorical analysis of adenoma OXPHOS protein levels in *PolγA*$^{+/mut}$ (n=4) small intestinal adenomas (error bars denote mean ±SEM).

Using the *PolγA*$^{+/mut}$ mouse in which a more mosaic pattern of OXPHOS deficiency is observed, this analysis aimed to ascertain if adenoma size was associated with a defect of either MTCO1 or NDUFB8 in favour of the other. In order to investigate the potentially differing contribution of each defect to adenoma growth, a further analysis was undertaken in which adenoma size was correlated to the level of expression of MTCO1 and NDUFB8 in individual adenomas. As discussed in chapter 3, differentiating small intestinal adenomas from one another at the microscopic level was challenging. As colonic adenoma size could be more accurately quantified, only adenomas of the colon were included in this analysis. The surface area of each *PolγA*$^{+/mut}$ colonic adenoma included in the OXPHOS protein level analysis was measured using Image J software generating a pixels^2 value which was plotted against adenoma NDUFB8 and MTCO1 mean intensity individually. NDUFB8 and MTCO1 mean intensities were expressed as a ratio to TOMM20 expression, thus accounting for variability in mitochondrial mass between adenomas. Data were not normally distributed therefore a Spearman non-parametric correlation analysis was used.

Adenoma size correlation with MTCO1 and NDUFB8 protein expression demonstrates a weak but significant negative correlation in both cases (MTCO1 r_S=-0.1744, P=0.0415; NDUFB8 r_S=-0.3150, P=0.0002). This suggests that a larger adenoma size in the *PolγA*$^{+/mut}$ colon is associated with lower levels of expression of both MTCO1 and NDUFB8 protein. The strength of each correlation, as described by Spearman's correlation coefficient (r_S) however, designates a slightly stronger correlation of adenoma size with NDUFB8 expression than that of MTCO1. This is indicated by the larger numeric value of r_S NDUFB8 (-0.3150) compared to r_S MTCO1 (-0.1744) (Figure 4-11).

A

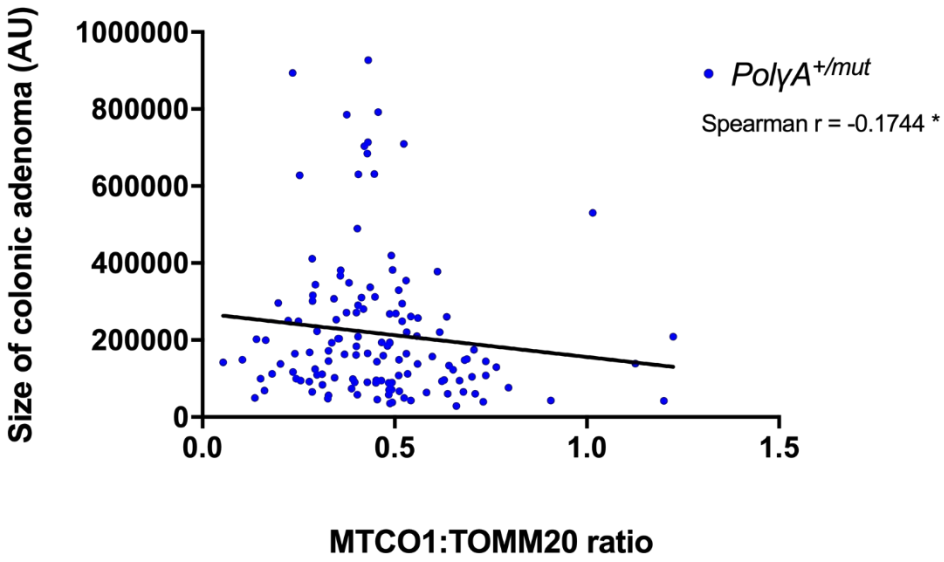

B

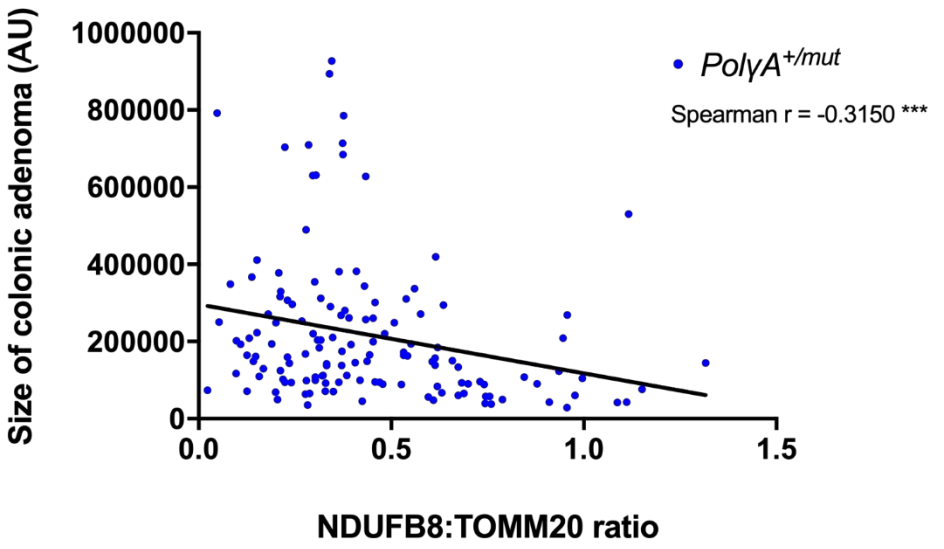

Figure 4-11. Correlation of OXPHOS protein levels with colonic adenoma size in *PolγA*$^{+/mut}$ mice. (A) Correlation of colonic adenoma size in *PolγA*$^{+/mut}$ mice (n=5) with MTCO1 mean fluorescent intensity normalised to that of TOMM20. Spearman's rank non-parametric correlation analysis indicates a weak negative correlation (r_S=-0.1744, P=0.0415). (B) Correlation of colonic adenoma size in *PolγA*$^{+/mut}$ (n=5) mice with NDUFB8 mean fluorescent intensity normalised to that of TOMM20. Spearman's rank non-parametric correlation analysis indicates a moderately stronger negative correlation (r_S=-0.3150, P=0.0002).

In order to investigate the relationship between colonic adenoma size and OXPHOS protein abundance across a greater range of protein levels, colonic adenomas from *PolγA*$^{+/+}$ (n=4) and *PolγA* $^{mut/mut}$ (n=5) mice were analysed in the same manner as per *PolγA*$^{+/mut}$ colonic adenomas; the surface area of each *PolγA*$^{+/+}$ and *PolγA*$^{+/mut}$ colonic adenoma was measured using Image J software generating a pixels^2 value with the simultaneous acquisition of NDUFB8 and MTCO1 mean intensity values.

The inclusion of size and OXPHOS protein expression data obtained from colonic adenomas of *PolγA*$^{+/+}$ and *PolγA*$^{mut/mut}$ mice strengthened the correlation of adenoma size with expression of MTCO1 and NDUFB8 protein. This is evidenced by an increase in the numeric values of r_s in both cases. A weak correlation as denoted by an r_S value of -0.2608 is observed in the MTCO1 analysis, however a moderately strong relationship between adenoma size and NDUFB8 protein expression is indicated by an r_S value of -0.4569 (Figure 4-12). These data suggest complex I deficiency is the predominant driver of the increased rate of adenoma growth. However, it should be noted that adenomas were not categorised into solely MTCO1 or NDUFB8 deficient groups, a factor which may influence the interpretation of the data. For example, a subset of relatively large adenomas deficient in both MTCO1 and NDUFB8 would lead to the strengthening of the correlation between adenoma size and the deficiency of both proteins without assessing the contribution of each individual defect. The further delineation of adenomas into solely MTCO1 or NDUFB8 deficient groups would therefore assist in defining the correlation between protein deficiency and adenoma size

A

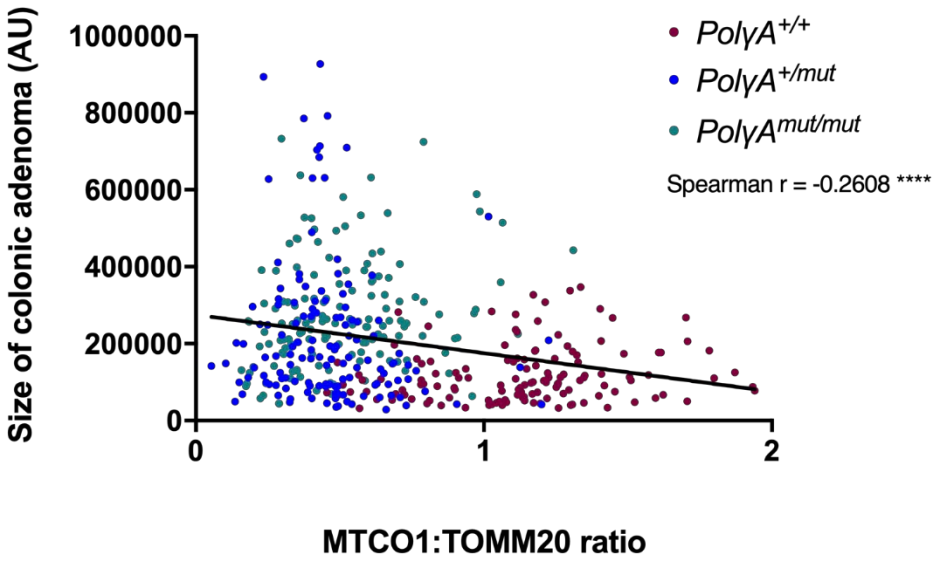

B

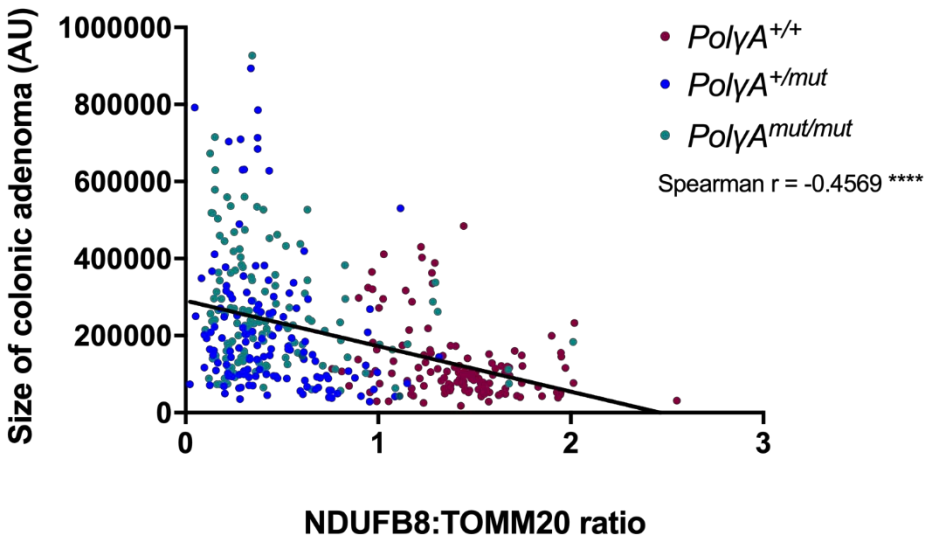

Figure 4-12. Correlation of OXPHOS protein levels with colonic adenoma size in *PolγA*$^{+/+}$, *PolγA*$^{+/mut}$ and *PolγA*$^{mut/mut}$ mice. (A) Correlation of colonic adenoma size in *PolγA*$^{+/+}$ (n=4), *PolγA*$^{+/mut}$ (n=5) and *PolγA*$^{mut/mut}$ (n=5) mice with MTCO1 mean fluorescent intensity normalised to that of TOMM20. Spearman's rank non-parametric correlation analysis indicates a weak negative correlation (r_S=-0.2608, P=<0.0001). (B) Correlation of colonic adenoma size in *PolγA*$^{+/+}$ (n=4), *PolγA*$^{+/mut}$ (n=5) and *PolγA*$^{mut/mut}$ (n=5) mice with NDUFB8 mean fluorescent intensity normalised to that of TOMM20. Spearman's rank non-parametric correlation analysis indicates a moderate negative correlation (r_S=-0.4569, P=0.0002).

4.3.3. Quantification of OXPHOS protein levels intestinal adenomas compared with non-transformed mucosa in 6-month-old PolγA$^{mut/mut}$ and PolγA$^{+/+}$ mice

Whilst undertaking the analysis of OXPHOS protein levels within the adenomas of the *PolγA$^{mut/mut}$*, *PolγA$^{+/mut}$* and *PolγA$^{+/+}$* colon and small intestine, it was noted that *PolγA$^{+/+}$* adenomas also appeared to display lower levels of OXPHOS proteins, in comparison to adjacent normal non-transformed crypts, suggesting that *Apc* loss alone is sufficient to initiate metabolic remodelling in terms of OXPHOS protein expression levels. This was formally investigated by quantifying OXPHOS protein levels in the non-transformed crypts from *PolγA$^{+/+}$* and *PolγA$^{mut/mut}$* colon and small intestine. A minimum of 17 crypts from *PolγA$^{+/+}$* (n=9) and *PolγA$^{mut/mut}$* (n=7) were selected as regions of interest and fluorophore mean intensity values recorded for each channel as previously carried out in the adenoma analysis. Using the non-transformed *PolγA$^{+/+}$* crypts as the control population from which z scores were derived, additional plots were created and included all areas sampled (*PolγA$^{+/+}$* normal crypts and adenomas, *PolγA$^{mut/mut}$* normal crypts and adenomas) for both the colon and small intestine. In the colon, all *PolγA$^{+/+}$* non-transformed normal crypts express levels of NFUFB8, UQCRFS1, MTCO1 and ATPB within a normal range. In the small intestine, OXPHOS protein levels within *PolγA$^{+/+}$* non-transformed normal crypts are also categorised as normal with the exception of two crypts demonstrating a reduced level of NDUFB8. Within *PolγA$^{+/+}$* colonic and small intestinal adenomas, reductions in the expression levels of OXPHOS protein subunits in comparison with those of *PolγA$^{+/+}$* non-transformed normal crypts are observed, suggesting a programmed downregulation of these proteins following *Apc* deletion. With regard to *PolγA$^{mut/mut}$* non-transformed normal colonic and small intestinal crypts, reductions in OXPHOS protein levels are observed in comparison with *PolγA$^{+/+}$* non-transformed normal crypts as expected. Further reductions are noted with regard to the comparison of OXPHOS protein levels in *PolγA$^{mut/mut}$* colonic and small intestinal adenomas with those of *PolγA$^{mut/mut}$* non-transformed normal colonic and small intestinal crypts. These observations suggest that while a programmed OXPHOS protein downregulation in response to *Apc* deletion is observed in the *PolγA$^{+/+}$* colon and intestine, this mechanism is accelerated in *PolγA$^{mut/mut}$* animals (Figure 4-13).

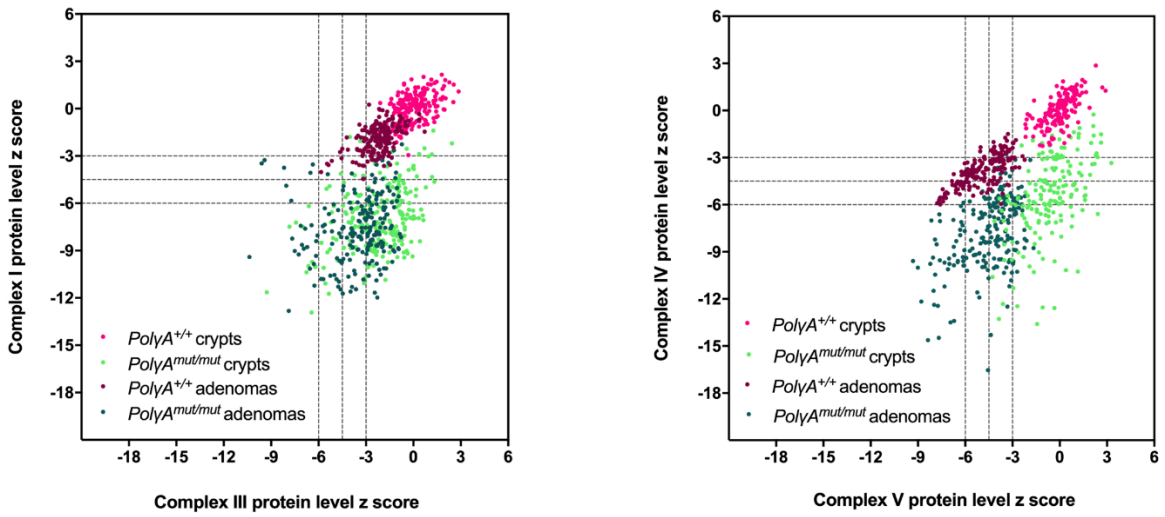

A Colon

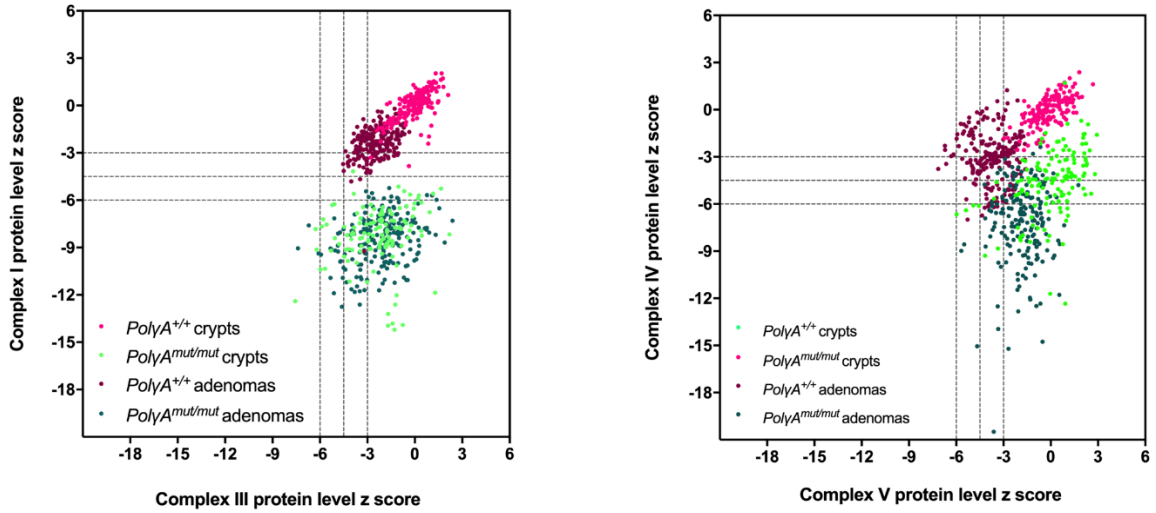

B Small intestine

Figure 4-13. Dot plots showing z scores calculated following quantification of mitochondrial OXPHOS protein levels in colonic and small intestinal adenomas of *PolγA*$^{+/+}$ and *PolγA*$^{mut/mut}$ mice (A) Dot plots showing z scores calculated following quantification of mitochondrial OXPHOS protein levels in colonic adenomas of *PolγA*$^{+/+}$ and *PolγA*$^{mut/mut}$ mice (n=9 per genotype) and normal non-transformed crypts of *PolγA*$^{+/+}$ mice (n=9 in complex I and III analysis, n=6 in complex IV and V analysis) and *PolγA*$^{mut/mut}$ mice (n=9 in complex I and III analysis, n=7 in complex IV and V analysis). (B) Dot plots showing z scores calculated following quantification of mitochondrial OXPHOS protein levels in small intestinal adenomas from *PolγA*$^{+/+}$ (n=10) and *PolγA*$^{mut/mut}$ mice (n=9) and non-transformed crypts of *PolγA*$^{+/+}$ (n=5) and *PolγA*$^{mut/mut}$ (n=4) mice.

In order to directly compare the expression levels of individual proteins in each compartment and investigate the effect of *Apc* loss alone on OXPHOS protein expression, raw mean intensity values were plotted and analysed. Raw mean intensity analysis of fluorophore labelled anti-TOMM20 indicates that in comparison to normal non-transformed crypts of the colon and small intestine, both *PolγA*$^{+/+}$ and *PolγA*$^{mut/mut}$ adenomas demonstrate an increase in mitochondrial mass (Figures 4-14 A and 4-15 A, P<0.0001 in all instances, one-way ANOVA with Tukey's multiple comparisons test). With regard to mitochondrial OXPHOS proteins, a significant decrease in the expression of each subunit investigated was seen in both colonic and small intestinal adenomas of *PolγA*$^{+/+}$ adenomas compared to *PolγA*$^{+/+}$ normal non-transformed crypts (P<0.0001 in all instances, one-way ANOVA with Tukey's multiple comparisons test).

Although mean mitochondrial mass is significantly higher in *PolγA*$^{mut/mut}$ colonic and small intestinal adenomas compared to normal non-transformed crypts, individual OXPHOS protein subunits demonstrate different patterns of expression. As may be expected in tissues in which there are already pronounced deficiencies of complex I or NDUFB8, following *Apc* deletion, no significant differences were detected in the expression levels of NDUFB8 in *PolγA*$^{mut/mut}$ colonic and small intestinal adenomas compared to normal non-transformed crypts (Figures 4-14 B and 5-15 B; P>0.05, one-way ANOVA with Tukey's multiple comparisons test). With regard to the UQCRFS1 subunit of complex III, no difference is detected between the expression in *PolγA*$^{mut/mut}$ colonic and small intestinal adenomas versus normal crypts (Figures 4-14 C and 4-15 C; P>0.05, one-way ANOVA with Tukey's multiple comparisons test). Mean intensity values representing the expression of the MTCO1 subunit of complex IV and ATPB subunit of complex V are both shown to be significantly decreased in *PolγA*$^{mut/mut}$ colonic and small intestinal adenomas in comparison to normal non-transformed crypts in both compartments (Figures 4-14 D; P<0.05 and E P<0.001, 4-15 D and E; P<0.001, one-way ANOVA with Tukey's multiple comparisons test in all instances). Together these data suggest that with regard to mitochondrial mass and mitochondrial OXPHOS subunit expression, significant metabolic remodelling is occurring in response to *Apc* deletion within the *PolγA*$^{+/+}$ and *PolγA*$^{mut/mut}$ intestinal tract.

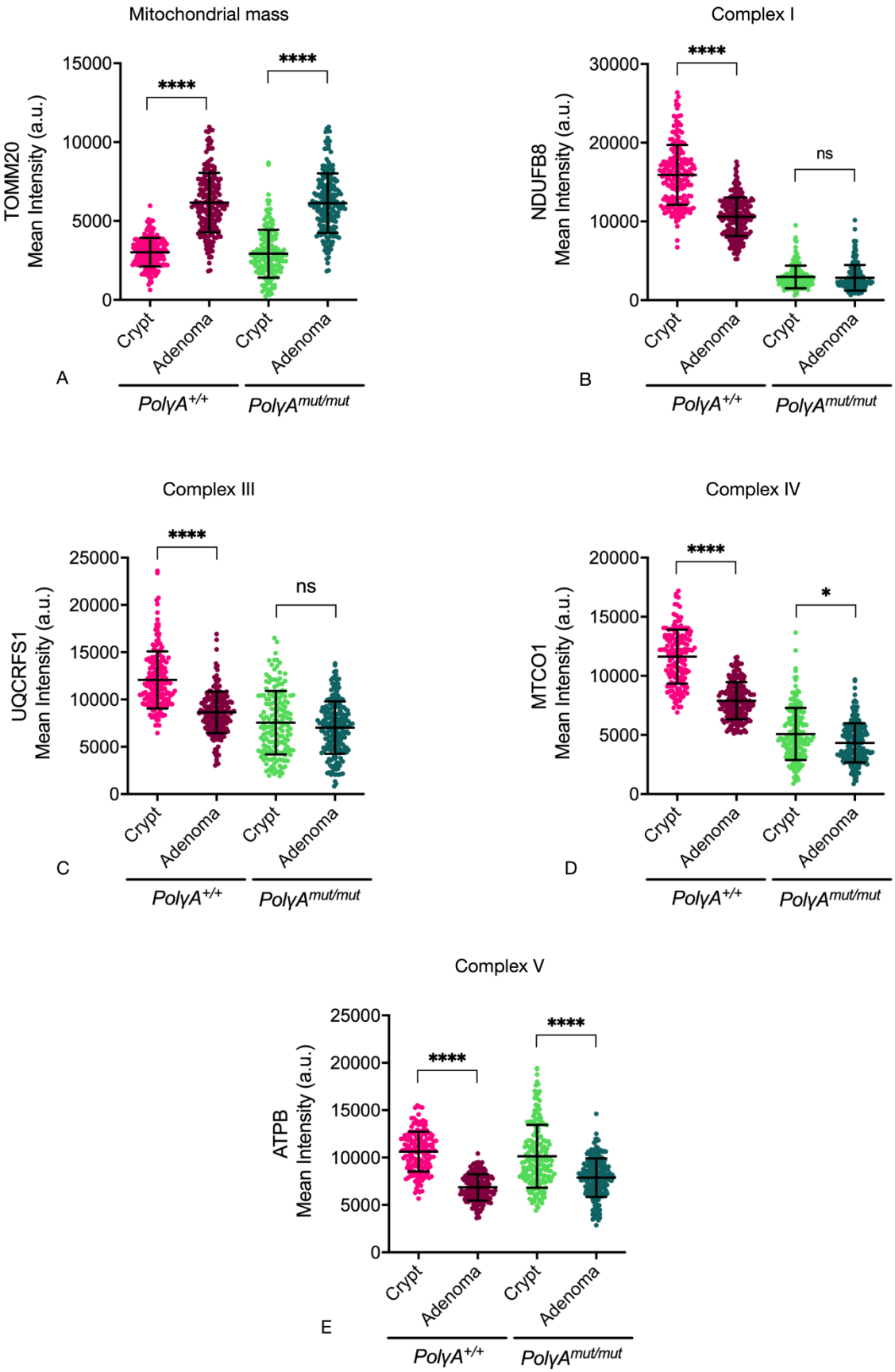

Figure 4-14. Raw mean intensity values for individual mitochondrial OXPHOS protein subunits and TOMM20 as a marker of mitochondrial mass within the *PolγA*$^{+/+}$ and *PolγA*$^{mut/mut}$ colon. Each dot represents a single crypt or adenoma. Error bars denote mean ±SD. Data were analysed using a one-way ANOVA with Tukey's multiple comparison test. All P values are: * p<0.05, **p<0.01, ***p<0.001, ****p<0.0001.

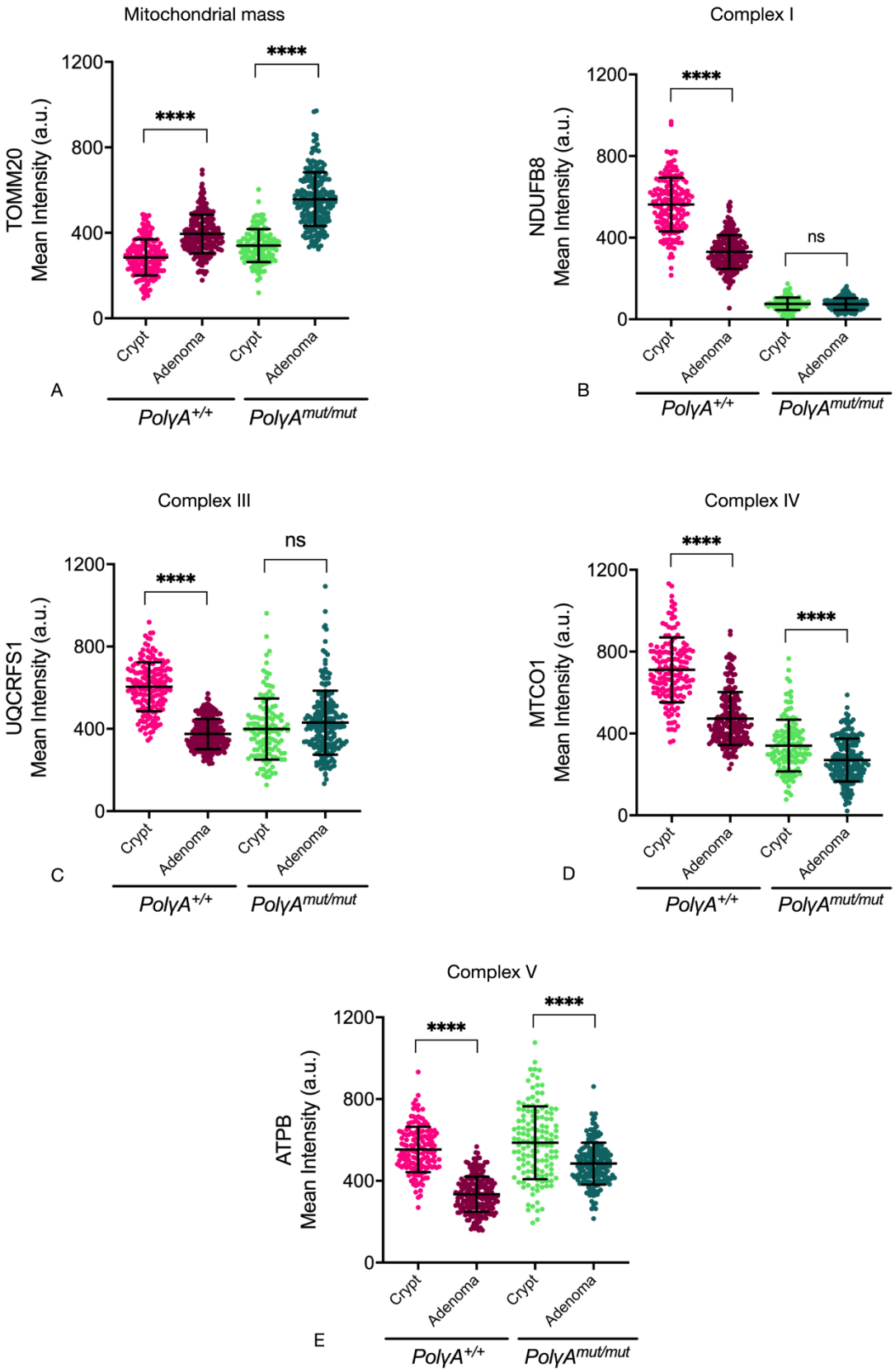

Figure 4-15. Raw mean intensity values for individual mitochondrial OXPHOS protein subunits and TOMM20 as a marker of mitochondrial mass within the *PolγA*$^{+/+}$ and *PolγA*$^{mut/mut}$ small intestine. Each dot represents a single crypt or adenoma. Error bars denote mean ±SD. Data were analysed using a one-way ANOVA with Tukey's multiple comparison test. All P values are: * p<0.05, **p<0.01, ***p<0.001, ****p<0.0001.

4.4. Discussion

Since the initial observations of Otto Warburg, in which a tumour specific preference for glycolytic metabolism even in the presence of oxygen was described, altered metabolism has been fundamentally associated with cancer (Warburg, 1927; Warburg, 1956). Despite the energetic inefficiency of 'aerobic glycolysis' versus mitochondrial oxidative phosphorylation, much evidence in favour of the Warburg Effect is in existence today and glycolysis remains a primary metabolic phenotype amongst cancers (Hu et al., 2013). Although heterogeneous between different malignancies, mitochondrial oxidative phosphorylation is also commonly found to be down regulated in human neoplasms (Gaude & Frezza, 2016); a pathology common to numerous ageing human tissues. With regard to the human colon specifically, defective oxidative phosphorylation is ascribed to an age-related expansion of somatic mtDNA point mutations (Greaves et al., 2010; Greaves et al., 2014; Taylor et al., 2003) and as such the contribution of age-related mtDNA mutations to the pathogenesis of colorectal cancer is investigated therein.

The previous chapter detailed the development of a mouse model in which an age-related accumulation of *PolγA* mediated mtDNA mutations was established prior to the intestinal *Lgr5* stem cell specific deletion of *Apc* at six months of age. The development of a significantly greater intestinal adenoma burden resulting in shortened lifespan in mice with age-related mitochondrial dysfunction compared with those without suggests that a permissive environment conducive to increased adenoma growth may be created by age-related mitochondrial dysfunction. Indeed, permissive changes in mitochondrial function have been described within the normal human pre-malignant colorectal mucosa. An increased mitochondrial copy number and expression of genes governing mitochondrial fission and fusion, DRP1 and OPA1 respectively, have been reported as significantly increased in patients harbouring precancerous lesions elsewhere in the colon when compared to control patients. Also increased in patients compared to controls was expression of the uncoupling protein, UCP2 (Cruz et al., 2017). Unlike the structurally similar UCP1, the uncoupling activity of UCP2 remains elusive. Instead, UCP2 has been shown to play a more prominent role in metabolic regulation by diverting TCA cycle intermediates away from mitochondrial oxidative metabolism towards biosynthetic processes (Vozza et al., 2014). Facilitating the development of a Warburg-like metabolic environment, such changes

are likely attributable to multiple components such as disorders of metabolic dysregulation including diabetes and obesity, chronic inflammation and hypoxia, all of which can contribute to metabolic perturbations (reviewed in Seth Nanda et al., 2020). Representing another potential contributor is the age-associated decline in mitochondrial function, which with specific regard to the impact of age-related mtDNA mutations on oxidative phosphorylation, may also encourage a Warburg-like environment by virtue of its dysfunction.

Presented in this chapter is a thorough analysis of the expression of mitochondrial oxidative phosphorylation complex subunits within the colon and small intestine of mice following *Lgr5* stem cell specific *Apc* deletion. The genotypes of *PolγA*$^{mut/mut}$, *PolγA*$^{+/mut}$ and *PolγA*$^{+/+}$ mice predispose animals to high, intermediate and negligible levels of mtDNA mutation respectively with the resultant intestinal phenotypes having been extensively characterised and compared to that of normal ageing humans (Baines et al., 2014). The aim of this study was to quantify the levels of OXPHOS defects within the adenomas of the *PolγA*$^{mut/mut}$ and *PolγA*$^{+/mut}$ mice, both of which display a significantly greater adenoma burden compared to *PolγA*$^{+/+}$ mice. At each stage of the analysis, the prevailing OXPHOS defect in *PolγA*$^{mut/mut}$ and *PolγA*$^{+/mut}$ mice occurs in complex I of the respiratory chain. As the largest of the mitochondrial oxidative phosphorylation protein complexes, also occupying the largest proportion of the mitochondrial genome, simple probability dictates that random mutational events affecting mtDNA are most likely to occur within complex I genes. The main function of complex I is to catalyse the transfer of electrons from TCA cycle and fatty acid oxidation generated NADH to ubiquinone while simultaneously translocating four protons from the mitochondrial matrix into the intermembrane space (Wikström, 1984). In addition to the proton translocation by complexes III and IV, this creates the electrochemical gradient necessary for ATP synthesis (Mitchell, 1961). The generation of reactive oxygen species is also an important function of complex I and it is considered the primary source of mitochondrial ROS (St-Pierre et al., 2002). This occurs when errant electrons reduce oxygen as it gains access to the flavin moiety of the NADH binding site or the ubiquinone binding site, producing the superoxide anion (O_2^-) (Hirst et al., 2008). At a cellular level, complex I is thus involved in maintaining cellular redox and ROS balance which have implications for survival and proliferation, in addition to the role it plays in energetic and metabolic control.

Recent decades have seen numerous reports of mtDNA defects in multiple cancer subtypes, however no clear consensus has been decided upon with regard to the tumour promoting (Kim et al., 2016) or tumour supressing (Iommarini et al., 2014) functions these mutations may confer. It is becoming apparent that while mtDNA mutations alone are insufficient to initiate neoplastic transformation, the specific location, species and heteroplasmy of mutation with regard to mitochondrially encoded complex I proteins can mediate different effects within the tumour setting.

An important event in tumour progression is the stabilisation of hypoxia inducible factor (HIF-1α). As its name suggests, HIF-1α mediates the activation of a response by which tumour cells adapt to the reduced availability of oxygen. The expression of glycolytic genes is upregulated (Semenza et al., 1994), pyruvate dehydrogenase kinase expression prevents the entry of acetyl-coA into the TCA cycle (Kim et al., 2006) and mitochondrial oxygen consumption is downregulated (Papandreou et al., 2006). Each of these events converge to inhibit mitochondrial aerobic respiration and promote a glycolytic Warburg-like phenotype, however a requirement for mitochondrial complex I has been shown in this context (Calabrese et al., 2013). Regulating the stability of HIF-1α are the prolyl hydroxylase enzymes (PHDs), which in turn are regulated by levels of the TCA intermediates α-ketoglutarate (α-KG) and succinate (SA) (Selak et al., 2005). As NADH accumulation inhibits the activity of α-ketoglutarate dehydrogenase of the TCA cycle (Bunik et al., 1990), defective complex I function can perturb the α-KG/SA ratio in favour of α-KG negatively affecting the hypoxic response. In osteosarcoma cell lines in which a homoplasmic m.3571insC mutation in the *MT-ND1* gene disabled complex I activity, restoration of enzyme activity via allotopic expression of wild-type *ND1* rescued the disturbed α-KG/SA ratio and HIF-1α destabilisation observed in mutant cells (Calabrese et al., 2013). Also demonstrated by the same group; homoplasmic *ND1* mutations conferring a milder effect on complex I activity (m.3460G>A/*MT-ND1*) did not induce HIF1α destabilisation or inhibit tumour growth as was the case with severe complex I mutations (Iommarini et al., 2014). Accordingly, these observations have led to the understanding that while defects that exert mild effects on complex I may have little or no impact on tumorigenicity, those that are severe may in fact be detrimental to tumour growth. This may seem somewhat contradictory to the findings described in this work in which severe complex I defects are observed in the intestinal adenomas of *PolγA*$^{mut/mut}$ mice. However, the continued progression of complex I deficient

osteosarcoma and colorectal carcinoma cell lines in nude mouse xenografts over time despite a reduction in HIF-1α stabilisation suggests an activation of adaptive mechanisms (Kurelac et al., 2019). It is well understood that components of the tumour microenvironment can greatly influence tumorigenicity and also the response to therapeutics (reviewed in Binnewies et al., 2018). Indeed, complex I and HIF-1α deficient xenografts displayed stroma-associated angiogenesis with an increased infiltration of pro-tumorigenic tumour associated macrophages at both 10- and 30-days post-transplantation. The elimination of macrophages from complex I deficient colon carcinoma xenografts substantially reduced xenograft growth in nude mice. Furthermore, the transduction of complex I deficient osteosarcoma cells with a constitutively expressed HIF-1α vector reduced the frequency of tumour associated macrophages in xenografts, thus implicating complex I deficiency associated HIF-1α destabilisation as the mechanism by which they are recruited (Kurelac et al., 2019). Although this work was conducted with the use of NDUFS3 deficient cell lines, this does not necessarily absolve mitochondrially encoded complex I defects of similar pro-tumorigenic adaptations. In-depth fluorescence-activated cell sorting (FACS) analysis of our *PolγA*$^{+/+}$ and *PolγA*$^{mut/mut}$ mouse immune cell population has not detected any significant differences in the small intestinal immune cell microenvironment between genotypes prior to *Apc* deletion (Smith et al., 2020). However future investigations must include the analysis of key microenvironment components in experimental animals in which adenomagenesis has been induced in order to ascertain the effect the immune microenvironment may have on tumour growth. Interestingly, a recent study in which growth screens at 21%, 5%, and 1% oxygen tensions were used to identify gene sets with relative fitness defects in high or low oxygen revealed genes encoding complex I as 'selectively essential' (Jain et al., 2020). Using CRISPR-Cas9 mediated knockouts of nuclear encoded subunits of mitochondrial complex I in human embryonic kidney cells, it was demonstrated that in conditions of very low oxygen (1%), complex I mutants grew equally as well as complex I competent cells (Jain et al., 2020). While hypoxia may indeed be therapeutic in complex I deficient mitochondrial disease models in that low oxygen delivery can improve cellular fitness (Jain et al., 2019; Jain et al., 2016), in oxygen-deprived tumours, particularly in the intestine in which oxygen levels are already physiologically low, complex I deficiency may inadvertently promote tumour cell fitness by virtue of its 'buffering' by hypoxia (Jain et al., 2020).

Additional mutations in mitochondrially encoded complex I genes have been investigated and further mechanisms with regard to tumour promotion described. The Akt growth and survival promoting pathway was reportedly activated by aberrant ROS production in human cell lines harbouring a heteroplasmic frameshift m.12417insA/*MT-ND5* mutation leading to enhanced tumorigenesis (Sharma et al., 2011). Similarly, *ND6* nonsense and missense mutations in lung adenocarcinoma cell line cybrids also activate the Akt pathway in a ROS-dependant manner (Yuan et al., 2015). In the same study, a significant correlation between missense and nonsense *ND6* mutations and pathological grade, tumour stage and lymph node metastasis were reported in human lung adenocarcinoma samples. Furthermore, the migratory distance of the lung adenocarcinoma cell line cybrids was significantly further in those with *ND6* nonsense and missense mutations suggesting the promotion of migration and invasion by these mutations (Yuan et al., 2015). The induction of epithelial-to-mesenchymal transition (EMT) is an important step in the progression of epithelial-derived carcinomas in achieving dissemination to distant sites via metastasis (reviewed in Tsai & Yang, 2013). Correlated with a poor prognosis, the upregulation of EMT is also associated with downregulation of OXPHOS in multiple cancer types (Gaude & Frezza, 2016). With specific regard to complex I defects, albeit nuclear encoded, the reduced expression NDUFB8 has been implicated in EMT as highly invasive breast carcinoma cells display reduced levels of this protein in comparison to cells with a weakly invasive phenotype (Lunetti et al., 2019). At this point it would be pertinent to mention that while NDUFB8 is not a requirement of complex I enzyme activity, it is integral to its assembly and also to supercomplex formation with complex III (Lunetti et al., 2019). While mutations in mitochondrial complex I genes *ND1*, *ND2* and *ND6* genes can severely affect complex I assembly (Gorman et al., 2015; Kirby et al., 2004; Ugalde et al., 2007; Ugalde et al., 2003) and potentially expression of NDUFB8, mutations in *ND3* and *ND5* may affect complex I assembly in varying degrees (McFarland et al., 2004; Shanske et al., 2008). Defects in these genes may therefore remain undetected by immunofluorescent techniques targeting NDUFB8 as utilised in this study. In the absence of commercially available antibodies against mitochondrially encoded complex I subunits this does represent a limitation of the study.

Complex IV, also known as cytochrome c oxidase, represents the final, rate limiting enzyme of the mitochondrial respiratory chain. In the current study, the expression of complex IV, specifically the mitochondrially encoded MTCO1 (COXI) subunit has been shown to be

reduced in expression within intestinal adenomas of *PolγA*$^{mut/mut}$ and *PolγA*$^{+/mut}$ mice compared to *PolγA*$^{+/+}$ animals and also in *PolγA*$^{+/+}$ intestinal adenomas compared to non-transformed crypts. An increased risk of ovarian cancer has been associated with mutations in the *COXI* (*MTCO1*) gene (Permuth-Wey et al., 2011) as has an increased tumorigenicity in prostate cancer cybrids (Petros et al., 2005). Furthermore, the recent Pan-Cancer Analysis of Whole Genomes (PCAWG) Consortium report *COXI* as the most frequently mutated mtDNA protein-encoding gene in breast, cervical and bladder cancers (Yuan et al., 2020). With regard to nuclear encoded subunits of complex IV, the converse upregulation of and tumour promoting activity of these proteins has been reported in several cancer types (Bini et al., 1997; Fu et al., 2006; Wu et al., 2000). Indeed, in a lymphoblastic leukaemia cell line overexpressing the anti-apoptotic Bcl-2 protein involved in tumour evasion of apoptosis, exposure to oxidative stress leads to a Bcl-2 mediated enhanced translocation of the nuclear-encoded COX5a subunit to the mitochondria resulting in enhanced COX activity (Chen & Pervaiz, 2010). shRNA mediated knockdown of nuclear encoded complex IV subunits COX4i1 and COX5b however, has been shown to elicit a glycolytic metabolic shift, reduced membrane potential and to induce invasive and anchorage independent growth characteristics in myoblasts (Srinivasan et al., 2016).

As has been described in relation to complex I, the location of specific mutations and thus the protein subunit they affect can have differing consequences in the tumour setting. In addition, the cooperation of mitochondrial function with classical driver mutation mediated tumorigenicity such as in *KRAS* driven lung adenocarcinoma (Weinberg et al., 2010) adds a further layer of complexity. As such it is becoming apparent that a great metabolic heterogeneity exists among different tumour types and the contribution of OXPHOS function to tumorigenicity cannot be generalised. Despite the increasing interest in targeting mitochondrial oxidative phosphorylation as a cancer therapy, a further consideration to be made lies with the observation that many tumours exhibit a metabolic intra-tumoral heterogeneity. A glycolytic tumour bulk phenotype with small populations of cancer stem cells reliant on mitochondrial oxidative phosphorylation has been described within several tumour types including pancreatic, colonic and ovarian cancers (Pastò et al., 2014; Song et al., 2015; Viale et al., 2014; Ye et al., 2011). With hindsight, the inclusion of an anti-GFP antibody within the immunofluorescent cocktail used in this study in order to label the *Lgr5+* stem cell population within intestinal adenomas would have been extremely useful in

visualising the extent of such metabolic heterogeneity in this study. This represents an avenue that may benefit from future investigation.

4.5. Future work

Given that the tumour microenvironment plays an important role in the progression of malignancies (reviewed in Hanahan & Weinberg, 2011), this represents an area which requires investigation with regard to *Apc* deficient adenoma growth within the intestine of *PolγA* mutator mice. The contributions of numerous components of the tumour microenvironment for example immune cells and mesenchymal cells such as cancer associated fibroblasts (CAFs) and adipocytes may be as equally influenced by age-related mitochondrial dysfunction as the tumour cells themselves. Although in-depth FACS analysis of *PolγA*$^{+/+}$ and *PolγA*$^{mut/mut}$ mouse immune cell populations did not detect any significant differences in the small intestinal immune cell microenvironment between genotypes prior to *Apc* deletion, this does not reflect any changes that may occur following transformation as a result of tumour-secreted factors and metabolites. Accordingly, FACS analysis or immunohistochemical investigation of *PolγA*$^{+/+}$ and *PolγA*$^{mut/mut}$ intestinal tissues primarily focusing on the major immune cell populations as per (Smith et al., 2020) would be extremely useful in investigating any microenvironmental changes associated with age-related mitochondrial dysfunction.

4.6. Conclusion

In conjunction with results of the previous chapter in which a greater intestinal adenoma burden is observed in animals with age-associated mtDNA mutations compared to those without, data presented here confirms that mitochondrial dysfunction is indeed present within adenomas and as such may contribute to the promotion of adenoma growth in these animals. A prominent defect in complex I of the mitochondrial electron transport chain is observed in *PolγA*$^{mut/mut}$ compared to *PolγA*$^{+/+}$ adenomas of both the colon and small intestine. As the largest of the mitochondrial oxidative phosphorylation protein complexes, also occupying the largest proportion of the mitochondrial genome, simple probability predicts that random mutational events affecting mtDNA are most likely to occur within

complex I genes. Furthermore, the subsequent loss of complex I protein may be better tolerated than a loss of complex III or complex V, defects of which are infrequently observed within *PolγA*$^{mut/mut}$ adenomas.

Although the mtDNA mutational burden observed in the *PolγA*$^{mut/mut}$ intestine is significantly greater than that observed in the natural course of ageing in the human intestine, the same defect is observed in *PolγA*$^{+/mut}$ adenomas in which a similar mtDNA mutation load has been reported in *PolγA*$^{+/mut}$ mice at 18 months and humans at 70 years (Baines et al., 2014). Despite undergoing investigation at an earlier point at which the mtDNA mutational burden is of a lesser amplitude, early dysplastic adenomatous lesions in these mice also demonstrate reduced expression of mitochondrial complex I. Furthermore, a significant negative association between the expression of NDUFB8 used as marker of complex I, and the size of adenomas is observed in the *PolγA*$^{+/mut}$ colon. The additional observation that in comparison to non-transformed crypts, *PolγA*$^{+/+}$ adenomas also demonstrate reduced levels of complex I and to a lesser degree complex IV, suggests that the down regulation of OXPHOS components occurs as a tumour promoting mechanism in the absence of pre-existing mitochondrial oxidative phosphorylation defects. This is supported by the work of Pate et al., in which a shift towards a glycolytic metabolism is promoted by Wnt/β-catenin mediated transcriptional activation of pyruvate dehydrogenase kinase 1 (PDHK1) and a resultant inhibition of pyruvate flux to mitochondrial respiration in colorectal cancer cells (Pate et al., 2014). Although the specific mechanisms by which adenoma growth is promoted in our *PolγA*$^{mut/mut}$ and *PolγA*$^{+/mut}$ adenomas remains to be elucidated, data presented here suggests that these mechanisms are enhanced by age-associated mtDNA mutation induced mitochondrial dysfunction.

Chapter 5. Quantification of cell proliferation and apoptosis in adenomas of the murine colon and small intestine

5.1. Introduction

5.1.1. Proliferation and apoptosis in cancer

Despite the extensive heterogeneity observed between and within cancers of all denominations, there are fundamental characteristics which are common to all. The escape of tumour cells from the normal constraints that regulate cell growth and division permits the unchecked proliferation that is a basic requirement for malignant growth. Equally in order to survive, tumour cells must evade the cellular mechanisms which, in response to the numerous stresses of malignant growth, are in place to facilitate their removal. Sustaining proliferative growth and resisting cell death are therefore two critical hallmarks of cancer (reviewed in Hanahan & Weinberg, 2011).

In order to maintain growth and progress through the cell cycle, there are various means by which tumour cells can manipulate growth factor signalling to their advantage. Firstly, they may upregulate the expression of cell surface growth factor receptors, thus increasing their sensitivity to mitogenic signalling. Epidermal growth factor receptor (EGFR) is one such receptor tyrosine kinase that has been well characterised and is frequently upregulated in lung and breast cancer and glioblastoma. EGFR activation in cancer is often attributed to genetic lesions which increase gene or protein expression (Lee et al., 2006; Red Brewer et al., 2013), however tumour cells may also produce EGFR ligands themselves, further potentiating their own growth via autocrine signalling (Wilson et al., 2012). Activating mutations within signal transduction pathways downstream of growth factor receptors represent another avenue by which tumour growth may be constitutively activated. The Ras-Raf-ERK mitogen activated protein kinase (MAPK) and PI3K-Akt-mTOR pathways are two such systems which when dysregulated by the acquisition of activating mutations in pathway intermediates results in enhanced cellular proliferation and survival in many cancer types (Davies et al., 2002; Samuels et al., 2004) . Increases in proliferative signalling in cancer cells may also occur when negative feedback systems which usually function to inhibit signalling in the presence of sufficient activated protein are disabled. For example, despite the

preservation of the negative feedback program in BRAF V600E mutant malignant melanoma, these cells are resistant to feedback inhibition and transcriptional output of the Ras-Raf-ERK pathway is enhanced (Pratilas et al., 2009). Conversely, the therapeutic targeting of effector proteins such as mTORC1 in the PI3K-Akt-mTOR pathway may paradoxically lead to increased activation of the system as existing negative feedback is removed (Tabernero et al., 2008). Finally, tumour derived cytokines and miRNA containing microvesicles can induce the conversion of normal fibroblasts into cancer associated fibroblasts (CAFs) (Albrengues et al., 2015; Pang et al., 2015). The reciprocal production of cytokines, chemokines and growth factors by CAFs can thus promote growth but can additionally support invasion and metastases (Duda et al., 2010; Erez et al., 2010; Kuchnio et al., 2015) .

In the process of malignant growth, tumour cells encounter numerous stressors such as increased DNA damage, hypoxia and nutrient deprivation. Under normal circumstances, as the impact of these stressors reaches a critical threshold, 'stressed' cells are eliminated as apoptotic pathways are triggered. The survival of cancer cells therefore is impacted heavily by their ability to evade or supress such apoptotic signalling (reviewed in Evan & Vousden, 2001). There are two apoptotic signalling pathways that are well conserved between different species of animal and represent the predominant routes by which cell death is programmed. Known as death receptors, cell surface pro-apoptotic proteins including Fas (also known as CD95 or APO1), the tumour necrosis factor (TNF) receptors and the TNF-related apoptosis inducing ligand (TRAIL) receptors, relay apoptotic signals and mediate cell death in response to extrinsic ligand binding (Itoh et al., 1991; Smith et al., 1994; Wiley et al., 1995). This represents the extrinsic pathway while within the cell, mitochondria act in response to death signals such as DNA damage, oncogene activation or withdrawal of growth factors leading to apoptosis via the intrinsic pathway (reviewed in Wang & Youle, 2009). Critical to both pathways are a group of protease enzymes known as caspases which once activated, proteolytically cleave cellular components facilitating the deconstruction of the cell. Synthesised as latent molecules, their cleavage results in their activation and is usually carried out by upstream caspases. The primary initiating caspase of the extrinsic apoptotic pathway is caspase 8, while that of the intrinsic pathway is caspase 9 (Li et al., 1997; Muzio et al., 1996). Ultimately, both primary initiators result in the activation of a core group of effector caspases; caspase-3, caspase-7, and indirectly caspase-6 which induce

plasma membrane blebbing, cell body shrinkage, DNA fragmentation and consequent cell death (Fernandes-Alnemri et al., 1996; Srinivasula et al., 1998; Stennicke et al., 1998) .

The mechanisms by which tumour cells evade the apoptotic machinery are diverse and involve the dysregulation of both extrinsic and intrinsic components. The increased expression of decoy death receptors which compete for death ligand binding and thus reduce apoptotic signalling have been described with regard to Fas (Pitti et al., 1998) and TRAIL mediated mechanisms (Marsters et al., 1997; Pan et al., 1997; Sheridan et al., 1997). Similarly, expression of key oncogenes such as *Ras* have been shown to down regulate the expression of death receptors (Fenton et al., 1998). Downstream of death receptor activation, the degradation of the key initiator caspase of the extrinsic apoptotic pathway; caspase 8, has been described in a colorectal cancer cell line further promoting apoptotic resistance (Zhang et al., 2005). Within the intrinsic pathway, caspase 9 activation is preceded by pro-apoptotic Bcl-2 family member mediated promotion of mitochondrial outer membrane permeability (MOMP) facilitating the release of cytochrome *c* (Li et al., 1997). As MOMP is considered the point of no return with regards cell death, the prevention of this phenotype via the upregulation of anti-apoptotic and down-regulation of pro-apoptotic Bcl-2 proteins, has been frequently described in cancer (reviewed in Campbell & Tait, 2018). As for the extrinsic pathway and degradation of caspase 8, the inhibition of caspase 9 within the intrinsic pathway also mediates apoptosis evasion in cancer cells. As cytochrome *c* is released from the mitochondria, it binds and activates the apoptotic protease activating factor-1 (Apaf-1) forming the caspase 9 cleaving apoptosome. Diminished functioning of Apaf-1 has been described in terms of its allelic loss in human pancreatic cancer (Kimura et al., 1998), its epigenetic modification and transcriptional silencing in metastatic melanoma (Soengas et al., 2001) with post-translational phosphorylation of Apaf-1 also being described as an inhibitory mechanism (Deming et al., 2004; Martin et al., 2005b). First discovered in baculoviral genomes, the inhibition of apoptosis (IAP) family of proteins (Birnbaum et al., 1994; Crook et al., 1993), particularly X-linked XIAP can perturb apoptosis by binding to and inhibiting caspases 9, 7 and 3 (Deveraux et al., 1998; Deveraux et al., 1997; Roy et al., 1997). Additional human IAP family members such as melanoma inhibitor of apoptosis (ML-IAP) have less potent caspase inhibiting activity than XIAP, however they exert their anti-apoptotic effects by sequestering second mitochondria-derived activator of caspase (SMAC) which is released from the mitochondria concomitantly with cytochrome *c.* This prevents

SMAC from inhibiting XIAP and accordingly apoptosis is attenuated (Vucic et al., 2005). Many human IAP family members are overexpressed in numerous cancers, thus representing an important means by which apoptotic evasion is achieved in malignant tissues (reviewed in Fulda & Vucic, 2012).

5.2. Aims of study

It has been established that age-associated mitochondrial dysfunction is associated with a greater adenoma burden within the colon and small intestine of *PolγA*$^{mut/mut}$ compared to *PolγA*$^{+/+}$ mice. In order to investigate the underlying cause of this, the aim of this study was to quantify the opposing processes of proliferation and apoptosis within intestinal adenomas. When injected intraperitoneally into the mouse, thymidine analogues incorporate into the DNA of cells during S phase of the cell cycle. Subsequent immunofluorescent labelling of these analogues allows the quantification of the number of cells which have replicated from the time of injection to the time of death. Using a double labelling method with two different thymidine analogues administered at specific time points, the specific objectives of this study were as follows.

1. To identify the sub-population of *Lgr5+* stem cells within *PolγA*$^{mut/mut}$ and *PolγA*$^{+/+}$ colonic and intestinal adenomas using an anti-EGFP marker.
2. To quantify, within colonic and small intestinal adenomas:
    a. The frequency of cells which have divided within 28 hours using an anti-CldU marker.
    b. The frequency of newly divided cells using an anti-IdU marker.
    c. The frequency of cells which have re-entered the cell cycle as identified by colocalisation of anti-CldU and -IdU markers.
3. To quantify the frequencies of apoptotic cells within *PolγA*$^{mut/mut}$ and *PolγA*$^{+/+}$ colonic and intestinal adenomas using anti-cleaved caspase 3 immunohistochemistry.

5.3. Results

As described in section 2.2.10, *PolγA*$^{mut/mut}$ (n=5) and *PolγA*$^{+/+}$ (n=5) mice were administered with two different thymidine analogues by intraperitoneal (IP) injection at timed intervals. Administration of IP CldU at two specific time points on the 15th day post *Apc* deletion facilitated exposure to this analogue for a period of 24 hours prior to administration of the second thymidine analogue. Cells that have replicated and synthesised DNA during these 24 hours will incorporate CldU, detectable with an anti-CldU primary antibody. On the 16th day post *Apc* deletion, mice were administered with a single dose of the second analogue; IdU before humane sacrifice four hours later. Incorporation of IdU into the newly synthesised DNA of replicating cells and subsequent labelling with an anti-IdU antibody allows the quantification of cells that have re-entered the cell cycle in the four hours prior to their death. As the clinical condition of experimental animals had been monitored in detail in previous studies, it was deemed that a cull date for this study must be earlier than the previously used 23 days post *Apc* deletion. At 23 days post *Apc* deletion, the condition of *PolγA*$^{mut/mut}$ animals had deteriorated considerably and it would be unethical to subject mice to a series of intraperitoneal injections at this stage. Microadenomas become visible within the *Lgr5-EGFP-Ires-CreERT2*/*Apc*$^{flox/flox}$ colon at around 14 days post *Apc* deletion, with the small intestine bearing slightly larger adenomas at this time point (Barker et al., 2009). As such, to ensure adenoma growth while minimising distress to animals, 15 days post *Apc* deletion was chosen as an appropriate time point to administer thymidine analogues. As described in section 2.2.11.2, colonic and small intestinal sections from *PolγA*$^{mut/mut}$ and *PolγA*$^{+/+}$ mice were immunofluorescently labelled in order to identify replicating cells in which CldU and IdU had been incorporated. For each mouse, 20 colonic and 20 small intestinal adenomas were manually identified, and immunofluorescent images acquired using a Zeiss AxioImager M1 fluorescent microscope. Example micrographs of typical labelling in the colon and small intestine are presented in Figures 5-1 and 5-2 respectively. Small intestinal section labelling and quantification was carried out by Matthew Hunt as part of an MRes project.

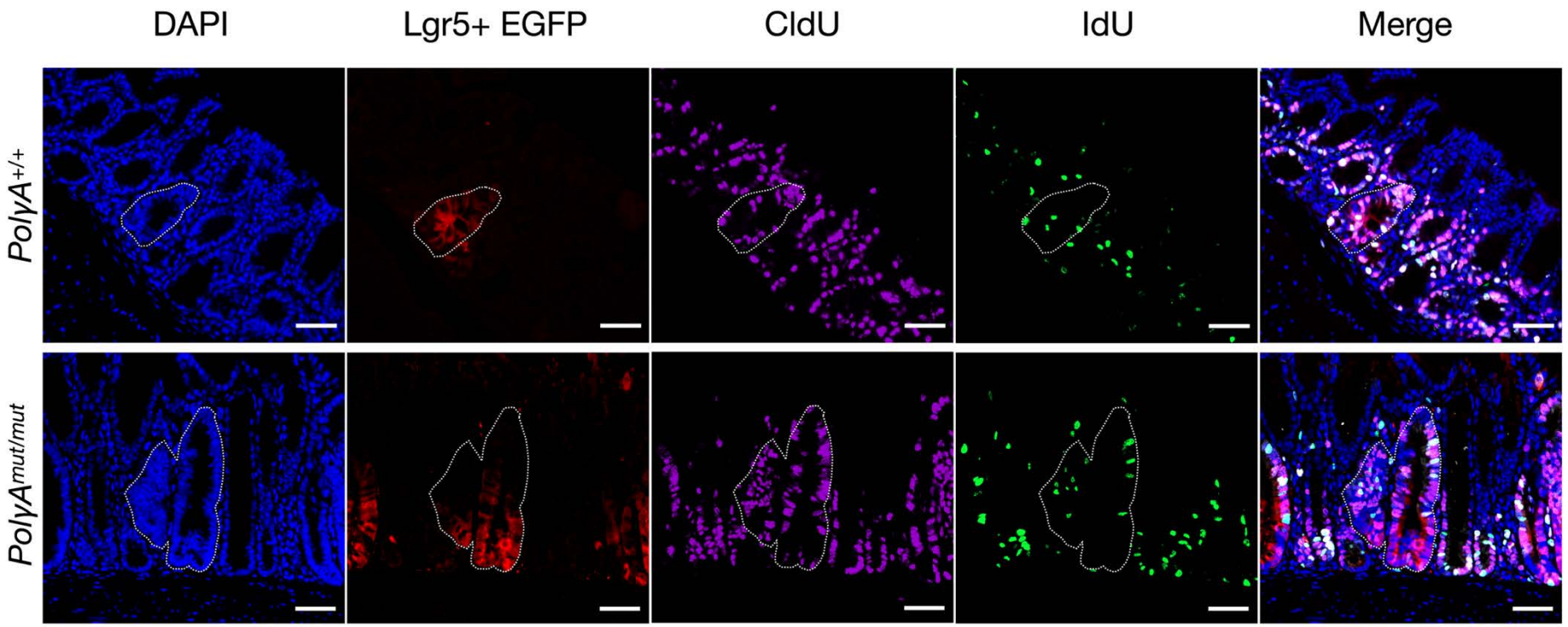

Figure 5-1. Immunofluorescent identification of double thymidine analogue incorporation within colonic adenomas of *PolyA*$^{+/+}$ and *PolyA*$^{mut/mut}$ mice. A Hoescht counterstain labels nuclei, AlexaFluor 546 labels anti-EGFP targeted against the EGFP construct of *Lgr5+* cells, AlexaFluor 647 labels anti-CldU identifying cells which have replicated once in the 24 hour period following initial administration, AlexaFluor 488 labels anti-IdU primary antibody identifying cells which have replicated once in the 4 hour period prior to death. The final panel shows a merge of all channels in which colocalisation of both analogues is identified by a yellow/white colouration. This identifies cells which have re-entered the cell cycle within the 28 hours prior to death. The white dashed line highlights regions of adenoma in each panel. Scale bars 50µm.

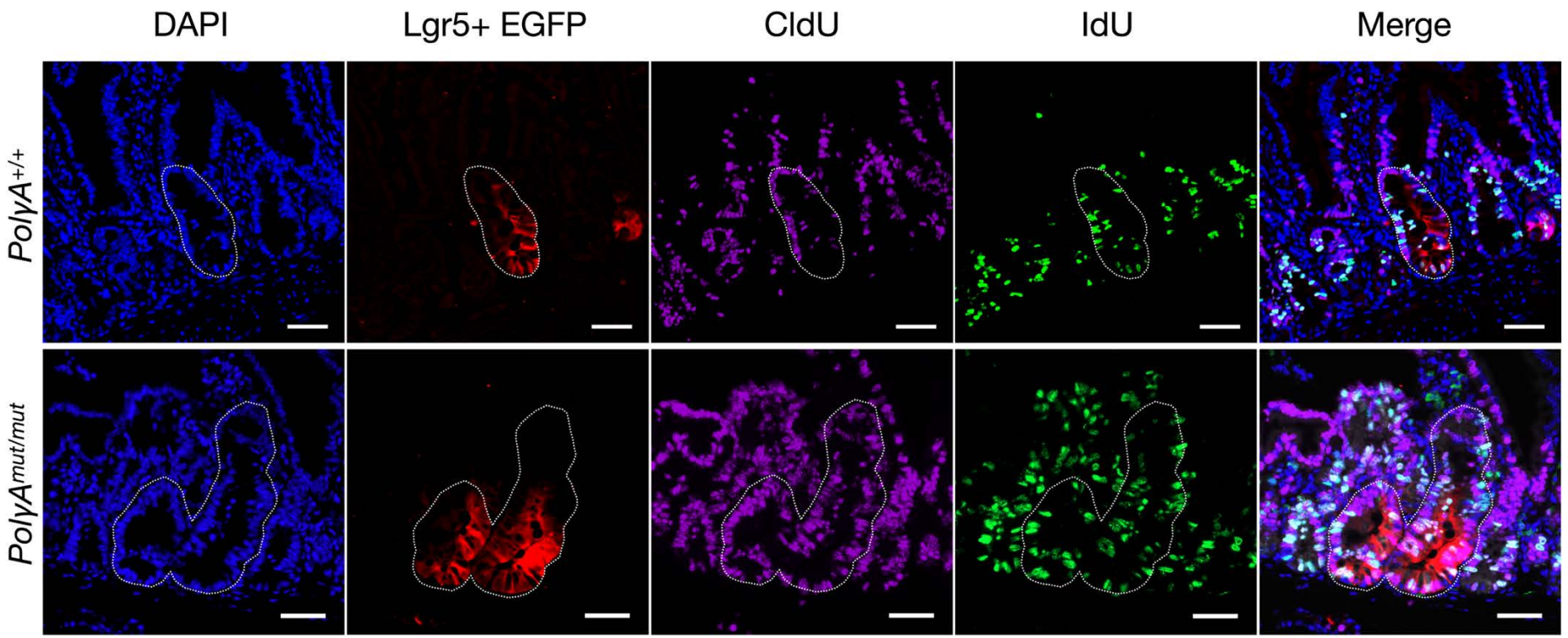

Figure 5-2. Immunofluorescent identification of double thymidine analogue incorporation within small intestinal adenomas of *PolyA*$^{+/+}$ and *PolyA*$^{mut/mut}$ mice. A Hoescht counterstain labels nuclei, AlexaFluor 546 labels anti-EGFP targeted against the EGFP construct of *Lgr5+* cells, AlexaFluor 647 labels anti-CldU identifying cells which have replicated once in the 24 hour period following initial administration, AlexaFluor 488 labels anti-IdU primary antibody identifying cells which have replicated once in the 4 hour period prior to death. The final panel shows a merge of all channels in which colocalisation of both analogues is identified by a yellow/white colouration. This identifies cells which have re-entered the cell cycle within the 28 hours prior to death. The white dashed line highlights regions of adenoma in each panel. Scale bars 50µm.

5.3.1. Adenoma size quantification

A significant difference in adenoma size between *PolγA*$^{mut/mut}$ and *PolγA*$^{+/+}$ mice at 23 days post *Apc* deletion was observed in previous studies. In order to confirm that this difference was still seen at the earlier cull date of 16 days post *Apc* deletion, total nuclei in each colonic and small intestinal adenoma were identified with the use of a Hoescht nuclear counterstain and manually quantified. In both the colon and small intestine, *PolγA*$^{mut/mut}$ adenomas are significantly larger than those of *PolγA*$^{+/+}$ mice at 16 days post *Apc* deletion (P<0.01, Mann-Whitney U test, Figure 5-3). Pre-existing data supported a prediction in the direction of a difference between samples, therefore a one-tailed test was used.

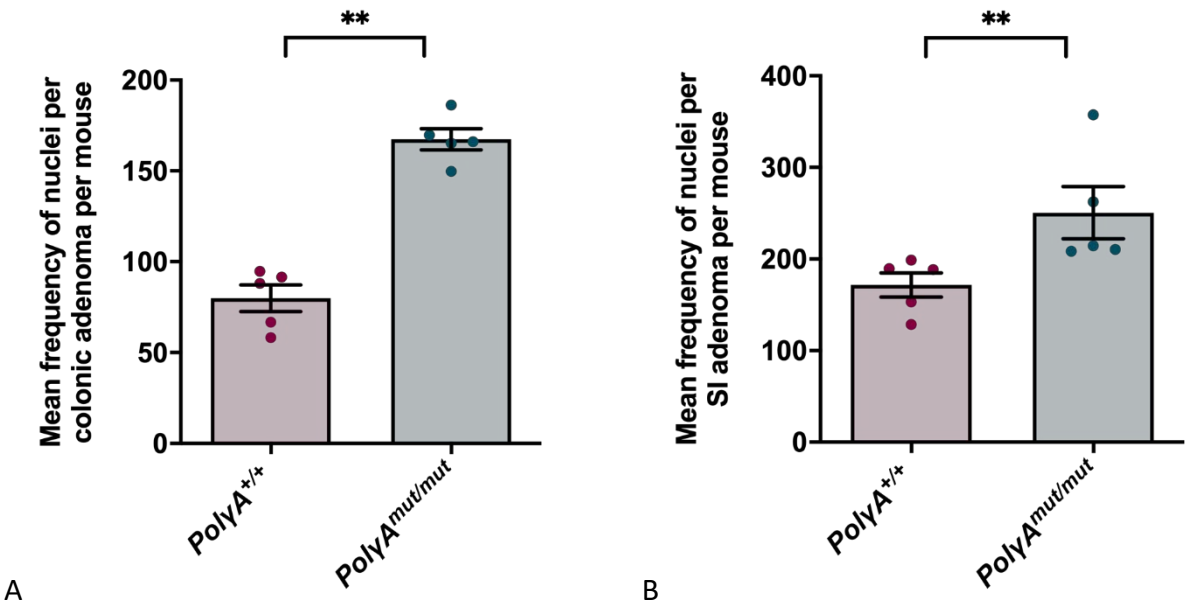

Figure 5-3. Mean frequencies of nuclei within colonic and small intestinal adenomas of thymidine analogue labelled *PolγA*$^{+/+}$ and *PolγA*$^{mut/mut}$ mice. At 16 days post *Apc* deletion, adenomas within the colon (A) and small intestine (B) of *PolγA*$^{mut/mut}$ mice (n=5 in all groups) are significantly larger than those observed in *PolγA*$^{+/+}$ mice animals (P<0.01, one-tailed Mann-Whitney U test). Each dot represents the mean frequency of cells per adenoma in one animal. Error bars denote mean ± SEM.

5.3.2. Adenoma proliferation characterisation

Within each adenoma, the frequency of cells incorporating only CldU, only IdU, and cells incorporating both analogues together were manually quantified. This respectively identified cells which have replicated once within the 24 hours following initial CldU administration, once within the four hours prior to death, and cells which have re-entered the cell cycle during the 28-hour period of thymidine analogue administration. The frequencies of cells incorporating one or both thymidine analogues were significantly greater within both the colonic and small intestinal adenomas of *PolγA*$^{mut/mut}$ in comparison with *PolγA*$^{+/+}$ mice ($P<0.001$, linear mixed effect model, Figure 5-4). The use of a linear mixed effect model quantifies the effect of genotype on frequency of cells per group whilst accounting for the variation between individual animals which is included as a random effect. *PolγA*$^{mut/mut}$ adenomas are significantly more proliferative than their *PolγA*$^{+/+}$ counterparts.

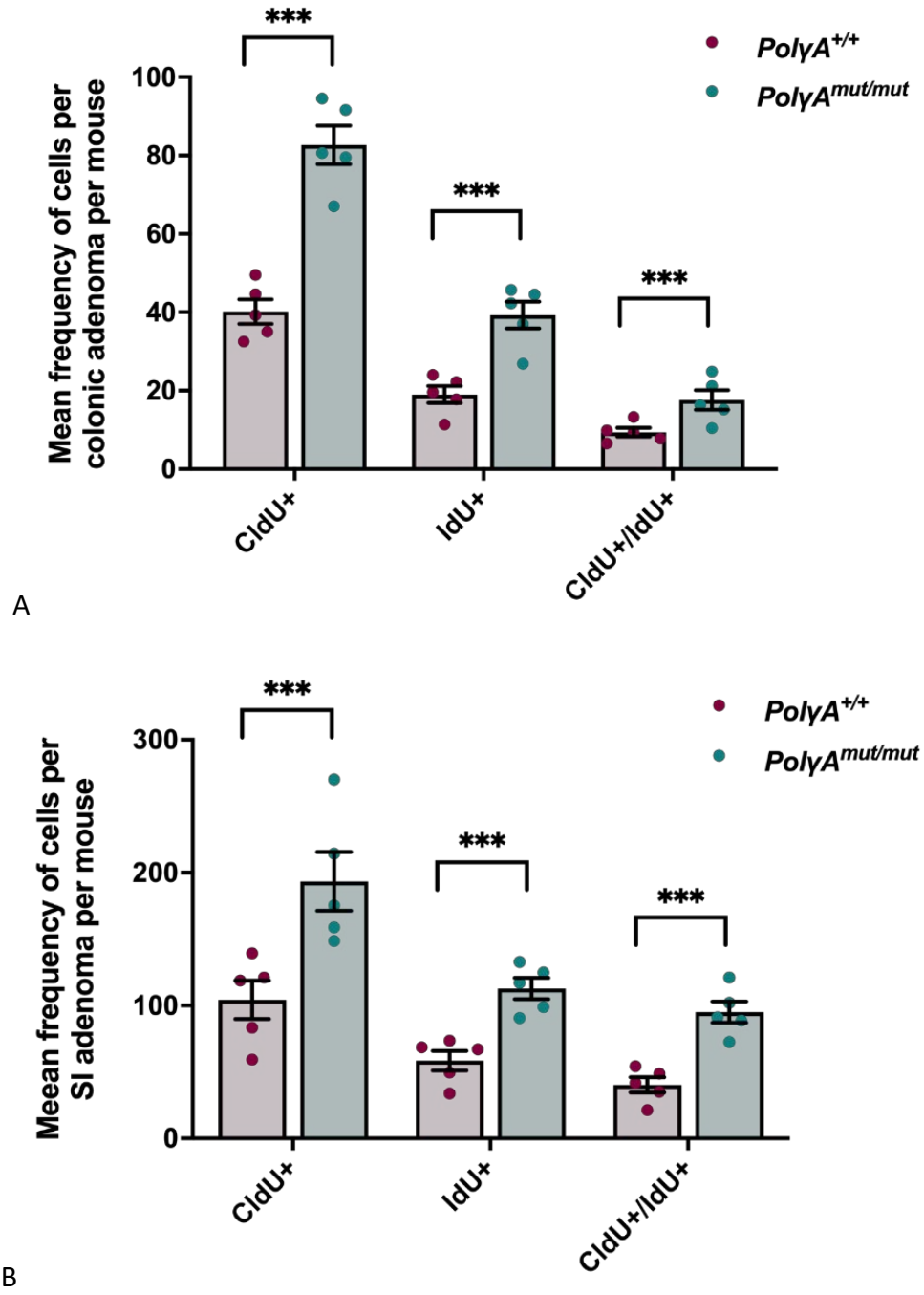

Figure 5-4. Quantification of the frequency of thymidine analogue incorporation in all cells of colonic and small intestinal adenomas of *PolγA*$^{+/+}$ and *PolγA*$^{mut/mut}$ mice (n=5 in all groups). (A) colon, (B) small intestine. Each dot represents the mean frequency of cells per adenoma in one animal. *PolγA*$^{mut/mut}$ adenomas are significantly more proliferative than those of *PolγA*$^{+/+}$ mice (P<0.001, linear mixed effect model). Error bars denote mean ± SEM.

5.3.3. Lgr5+ stem cell proliferation characterisation

A primary antibody against the EGFP component of the *Lgr5-EGFP-Ires-CreERT2* construct allowed *Lgr5+* stem cells to be identified and quantified. As the cells of origin of the intestinal adenomas of the mice, a difference in the frequencies of *Lgr5+* stem cells between the *PolγA*$^{mut/mut}$ and *PolγA*$^{+/+}$ groups could represent a factor which may contribute to the difference in adenoma burden observed. As in the previous section, the frequency of cells incorporating only CldU, only IdU, and cells incorporating both analogues together were manually quantified. In this analysis, only EGFP+ *Lgr5+* cells were included, thus characterising the proliferative capacity of the stem cell compartment.

Within adenomas of the *PolγA*$^{mut/mut}$ colon and small intestine, *Lgr5+* stem cells are significantly more numerous than within *PolγA*$^{+/+}$ adenomas (P<0.001, linear mixed effect model, Figure 5-5). However, a significant difference with regard to the proliferative rate of *Lgr5+* cells is detected only within the small intestine. In the colon, no significant difference of single or double thymidine analogue incorporation is detected, indicating that while *PolγA*$^{mut/mut}$ colonic adenomas harbour a greater number of *Lgr5+* stem cells, these cells are no more proliferative than their wild type counterparts (Figure 5-5A, linear mixed effect model). In addition to the significantly greater frequency of *Lgr5+* stem cells within *PolγA*$^{mut/mut}$ small intestinal adenomas, this population demonstrates a significantly greater degree of single and double thymidine analogue incorporation than the *PolγA*$^{+/+}$ *Lgr5+* population (P<0.001, linear mixed effect model). In summary, at 16 days post *Apc* deletion, *Lgr5+* stem cells are more abundant in both colonic and small intestinal *PolγA*$^{mut/mut}$ adenomas in comparison to *PolγA*$^{+/+}$ adenomas, however this population is more proliferative only in the small intestine.

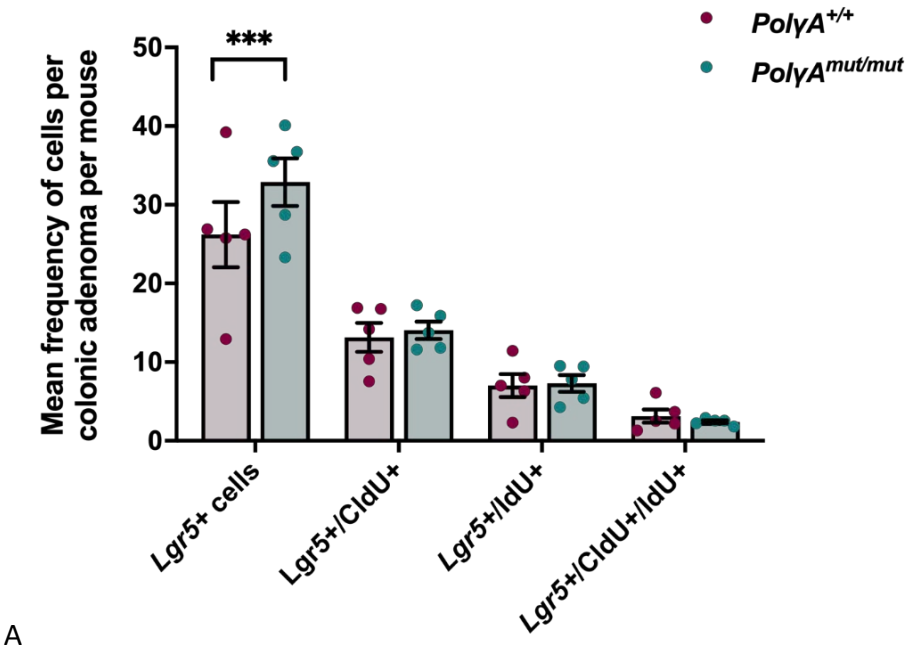

A

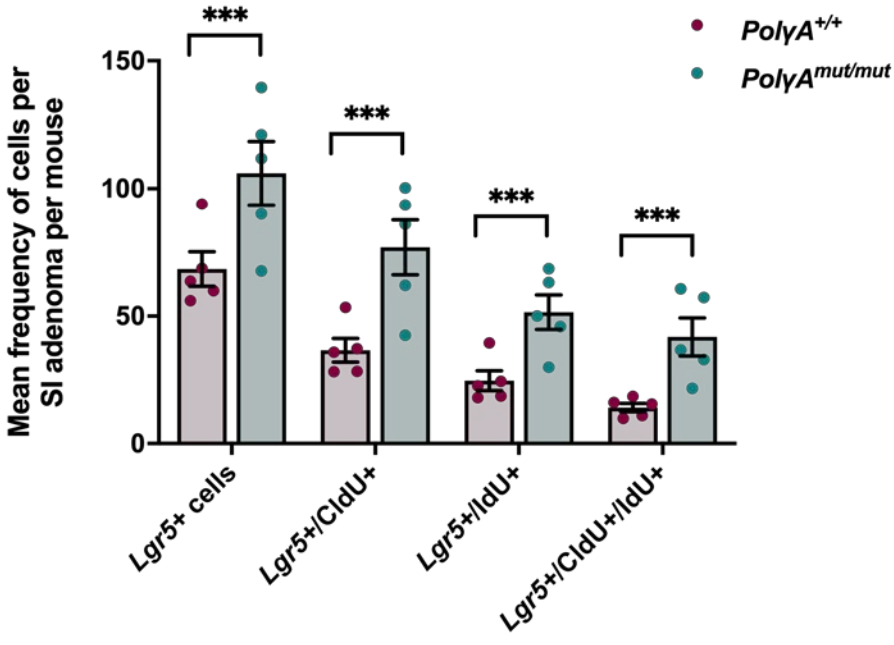

B

Figure 5-5. Quantification of the frequency of thymidine analogue incorporation in *Lgr5+* cells of colonic and small intestinal adenomas of *PolγA*$^{+/+}$ and *PolγA*$^{mut/mut}$ mice (n=5 in all groups). (A) colon, (B) small intestine. Each dot represents the mean frequency of cells per adenoma in one animal. Within the small intestine (B), the *Lgr5+* stem cell population of *PolγA*$^{mut/mut}$ adenomas is significantly more abundant and significantly more proliferative than that of *PolγA*$^{+/+}$ adenomas (P<0.001, linear mixed effect model). Within the colon (A), the *Lgr5+* stem cell population of *PolγA*$^{mut/mut}$ adenomas is significantly more abundant than that of *PolγA*$^{+/+}$ adenomas (P<0.001, linear mixed effect model). Error bars denote mean ± SEM.

5.3.4. Adenoma apoptotic index

In cells undergoing apoptosis, the inactive proenzyme caspase 3 is cleaved into two smaller fragments which re-associate to form an active caspase enzyme. This enzyme, in its active state, activates other caspases and appropriate targets within the apoptotic cell. Immunohistochemistry using an antibody against the larger (17 kDa) cleaved fragment of caspase 3 allows identification and quantification of apoptotic cells. Sections from the colon of *PolγA*$^{mut/mut}$ (n=7) and *PolγA*$^{+/+}$ (n=9) experimental animals culled at 23 days post *Apc* deletion were labelled, and a minimum of 10 randomly selected adenomas from each section imaged using bright field microscopy on a Zeiss AxioImager M1 microscope. Similarly, small intestinal sections from *PolγA*$^{mut/mut}$ (n=9) and *PolγA*$^{+/+}$ (n=9) 23 days post *Apc* deletion were labelled with anti-cleaved caspase 3 and imaged in the same manner. Total number of nuclei per foci and the number of cleaved caspase 3 (CC3) positive cells per foci were manually counted using Zen 2 Lite software (Zeiss). Example micrographs showing typical labelling within *PolγA*$^{+/+}$ and *PolγA*$^{mut/mut}$ colonic and small intestinal adenomas are shown in Figure 5-6 (A). In both the colon and small intestine *PolγA*$^{mut/mut}$ adenomas harbour a significantly smaller proportion of apoptotic cells per foci than those of the *PolγA*$^{+/+}$ animals ($P<0.05$ and $P<0.001$ for the colon and small intestine respectively, linear mixed effect model, Figure 5-6 (B).

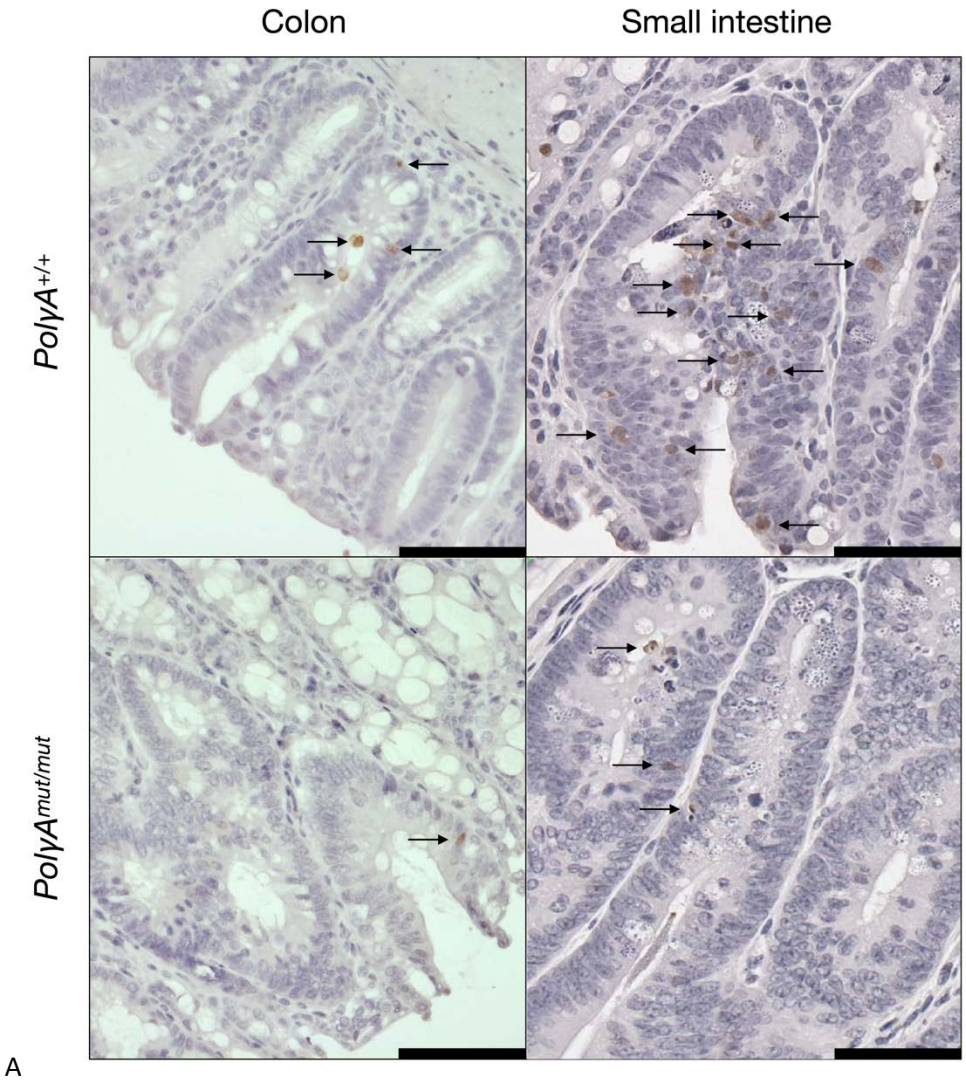

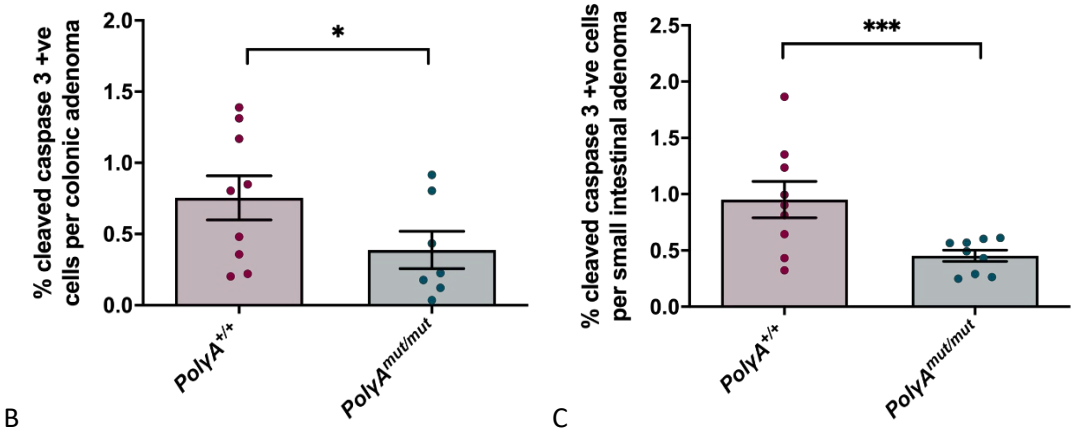

Figure 5-6. Cleaved caspase 3 immunohistochemical labelling and quantification of apoptotic cells within *PolγA*$^{+/+}$ and *PolγA*$^{mut/mut}$ colonic and small intestinal adenomas (A) CC3 immunohistochemical labelling within *PolγA*$^{+/+}$ and *PolγA*$^{mut/mut}$ colonic and small intestinal adenomas. CC3 positive cells are highlighted with black arrows. Scale bars colon; 100µm, scale bars small intestine; 60µm. (B, C) Quantification of apoptotic cells in colonic and small intestinal adenomas identified using cleaved caspase 3 immunohistochemistry in mice 23 days post *Apc* deletion. (B) The proportion of apoptotic cells per adenoma is significantly smaller in the colon of *PolγA*$^{mut/mut}$ (n=7) compared to *PolγA*$^{+/+}$ (n=9) mice (P<0.05, linear mixed effect model). (C) The proportion of apoptotic cells per adenoma is significantly greater in the small intestine of *PolγA*$^{mut/mut}$ (n=9) compared to *PolγA*$^{+/+}$ (n=9) mice (P<0.001, linear mixed effect model). Each data point represents the mean of multiple measurements taken from >10 adenomas in one animal. Error bars denote mean ±SEM.

5.4. Discussion

Results presented in this chapter have characterised the proliferative and apoptotic indices of colonic and small intestinal adenomas within mice with and without pre-existing *PolγA* mediated mitochondrial dysfunction. Double thymidine analogue labelling of mice revealed a significantly greater rate of replication in *PolγA*$^{mut/mut}$ colonic and intestinal adenomas when compared to *PolγA*$^{+/+}$ animals. The identification of the sub-population of *Lgr5+* stem cells within adenomas allowed the proliferative index of this compartment to be investigated independently and while in the small intestine *Lgr5+* stem cells were found to be significantly more proliferative within *PolγA*$^{mut/mut}$ versus *PolγA*$^{+/+}$ adenomas, this significance was not observed within the colon. In the colon, although *PolγA*$^{mut/mut}$ adenomas in their entirety demonstrated enhanced proliferation in comparison to *PolγA*$^{+/+}$ adenomas, this was not reflected in the *Lgr5+* stem cell compartment and as such suggests differing contributions to adenoma growth derived from each cellular compartment.

In contrast to the stochastic tumour theory in which all cells possess the potential to initiate and propagate a tumour, the cancer stem cell theory describes a tumour as originating from a small subpopulation of stem cells; the cancer stem cells (Bonnet & Dick, 1997). These subgroups of cells are capable of long-term self-renewal and can differentiate into multiple cell types (Reya et al., 2001). They generate progeny cancer cells responsible for maintaining the tumour mass, are largely resistant to conventional chemo and radiotherapies and bear specific molecular markers. According to this theory, it is the cancer stem cell population that drives tumour progression. Cell division is either symmetrical, with a division giving rise to daughter stem cells, or asymmetrical with a division giving rise to one daughter stem cell and one progenitor cell with the ability to differentiate but with limited proliferative capacity. This gives rise to a tumour in which there is a hierarchical organisation, descended from the proliferative cancer stem cell compartment, much like the tissue from which the tumour is derived. It may be however, that the stochastic and stem cell theories are not entirely independent of one another. With genomic instability and an altered microenvironment, the progeny of the cancer stem cells may be subject to additional mutagenesis events bestowing them with tumorigenic potential transforming them into new cells of origin. Indeed, a normal tissue response to injury sees the de-differentiation of committed small intestine secretory cells back to a proliferative stem cell state (Buczacki et

al., 2013; van Es et al., 2012). Within the tumour microenvironment, it has also been demonstrated that an increase in inflammatory signalling, namely NF-κB also induces de-differentiation in non-stem cells of the intestine, causing them to acquire stem-like proliferative qualities (Schwitalla et al., 2013). Additionally, a recent study in a colorectal cancer mouse model demonstrates that while fundamental to tumour initiation, *Lgr5+* cells are not essential for tumour maintenance. Ablation of *Lgr5+* cells resulted in a less efficient tumour growth, but a growth, nonetheless, maintained by proliferative *Lgr5-* cells (de Sousa e Melo et al., 2017). With these findings in mind, consideration of the proliferative data taken from the colonic adenomas of *PolγA*$^{mut/mut}$ and *PolγA*$^{+/+}$mice may suggest that while imperative in adenoma initiation in this model, the growth and progression of colonic adenomas may not be entirely dependent on the *Lgr5+* stem cell compartment.

Within the small intestine, an important contribution from stem-cell supportive Paneth cells may be relevant. In addition to the secretion of the growth factors EGF and TGFα, and the Wnt and Notch signalling ligands Wnt3 and Dll4 respectively, Paneth cells also produce antimicrobial peptides involved in host defence and immunity. As such, Paneth cells are regarded as important regulators of stem cell function (Sato et al., 2011b). In normal small intestinal crypts, Rodriguez-Colman et al. report the reliance of crypt base Paneth cells on a glycolytic metabolism with their inhibition preventing organoid growth. Conversely, a primarily oxidative metabolic phenotype was observed in *Lgr5+* stem cells with inhibition of mitochondrial activity impairing the growth of intestinal organoids (Rodríguez-Colman et al., 2017). Similarly, in comparison with intestinal organoids derived from wild type mice, those derived from *PolγA*$^{mut/mut}$ animals demonstrate limited growth (Fox et al., 2012). This suggests that both cell types and metabolic signatures support normal stem cell function and crypt development, however the reliance of organoid *Lgr5+* cells on an oxidative metabolism may represent an artefact of culture as *in vivo*, *PolγA*$^{mut/mut}$ crypts are clearly maintained by *Lgr5+* cells despite their impaired oxidative phosphorylation (Fox et al., 2012). With reference to colorectal cancer, Rodríguez-Colman et al propose a scenario in which cells comprising the tumour bulk favour a glycolytic, Warburg-like metabolism with the *Lgr5+* stem cells relying on OXPHOS. With regard to observations made in this chapter, the mitochondrial dysfunction seen in the adenomas of *PolγA*$^{mut/mut}$ animals may therefore be contributing to the increased proliferation of the *Lgr5+* progeny: the tumour bulk, via an enhanced use of glycolytic metabolic pathways. The *Lgr5+* stem cells themselves may exhibit

increased rates of proliferation within the small intestine as a result of the additional support they receive from the Paneth cells. Although *Apc* deletion abrogates the *Lgr5+* requirement for exogenous Wnt, a recent study has identified Paneth cells as important modulators of immune escape in colorectal cancer. The indoleamine-2,3-dioxygenase-1 (IDO1) tryptophan degrading enzyme was found to be expressed extensively within the Paneth cells of Apc^{Min} murine adenomas with IDO1+ Paneth cells also being identified in human CRC. Via the depletion of tryptophan and generation of the immune-suppressive metabolite kynurenine, IDO1 facilitates the cell cycle arrest of cytotoxic CD8+ T-lymphocytes and promotes immune suppressive regulatory T cell (Treg) differentiation. Accordingly, the ablation of IDO1 via the deletion of the IDO1 regulatory transcription factor *Stat1* resulted in smaller tumours with increased frequencies of CD8+ T cells and reduced numbers of infiltrating Treg cells in Apc^{Min} mice (Pflügler et al., 2020). Additionally, in the context of inflammatory bowel disorders, Paneth cell specific mitochondrial dysfunction has recently been reported as central to the development of ileitis with Paneth cell abnormalities linked to de-differentiation (Jackson et al., 2020). Given the links between ageing, inflammation and tumorigenesis, Paneth cell mitochondrial dysfunction may represent an important mechanism by which adenoma growth is promoted within the $PolyA^{mut/mut}$ small intestine.

The loss of *Apc* has profound implications for intestinal crypt homeostasis and pathology. A key component of the Wnt signalling pathway which regulates intestinal stem cell self-renewal, *Apc* loss results in constitutive activation of a transcriptional complex that another critical Wnt pathway component; β-catenin forms with transcription factor 4 (Tcf-4) (Korinek et al., 1997). Several targets of the β-catenin-Tcf-4 transcription complex have been identified, one of which, the proto-oncogene *c-myc* has been established as the critical driver of the proliferative phenotype associated with *Apc* loss in the murine intestine (Sansom et al., 2007). Since early observations that Myc overexpression facilitated the growth of fibroblasts even in the absence of mitogenic stimulus (Armelin et al., 1984), the growth promoting activities of the transcription factor such as cell-cycle progression, promotion and differentiation inhibition have been extensively characterised. Paradoxically, in addition to the growth promoting capacity of Myc, a strong induction of apoptosis is also associated with Myc overexpression (Askew et al., 1991; Evan et al., 1992; Neiman et al., 1991; Wyllie et al., 1987). The mechanisms by which Myc regulates apoptosis include activation of the p53 tumour suppressor protein (Hermeking & Eick, 1994; Wagner et al.,

1994), the disruption of the balance of pro and anti-apoptotic effectors in favour of pro-apoptotic components such as Bax (Dansen et al., 2006; Juin et al., 2002; Soucie et al., 2001) and the inhibition of anti-apoptotic mediators such as Bcl-2, Bcl-xL and Bag-1 (Eischen et al., 2001a; Eischen et al., 2001b; Zhang et al., 2011). Myc can also augment cellular sensitivity to receptor conveyed death signals (Klefstrom et al., 1994), however tumour cells have evolved mechanisms by which Myc mediated apoptosis can be evaded. For example, Myc upregulation is commonly associated with anti-apoptotic Bcl-2 family member upregulation in human cancers (Beroukhim et al., 2010). Additionally, the abundance of Myc protein and the cellular environment in terms of growth factor availability or the methylation/acetylation status of Myc target DNA binding sites can reportedly influence Myc activity (Askew et al., 1991; Fernandez et al., 2003; Guccione et al., 2006). Although mitochondrial dysfunction in terms of defective oxidative phosphorylation has been associated with increased levels of apoptosis (Kujoth et al., 2005; Wang et al., 2001), in the malignant context of oncogene activation, diminished oxidative phosphorylation may have differing consequences. Indeed, in mtDNA deficient p^0 143B osteosarcoma cell lines in which Myc expression is reportedly high (Chen et al., 2018), the absence of functional oxidative phosphorylation and ensuing reduction in inner mitochondrial membrane potential ($\Delta\psi m$) was associated with the reduced activation of caspase 3 and an enhanced resistance to staurosporine induced apoptosis (Dey & Moraes, 2000). Similarly, a reduced apoptotic index was demonstrated in cybrids harbouring pathogenic mitochondrial complex V *mATP6* mutations *in vitro* and also *in vivo* in tumours derived from mutant cybrid transplantation in comparison to those bearing wild type mtDNA (Shidara et al., 2005). Furthermore, in tumours derived from cybrids harbouring a heteroplasmic complex I *ND5* frameshift mutation, an increased tumorigenicity coupled with an enhanced apoptotic resistance is observed in comparison to tumours derived from cybrids bearing a homoplasmic level of the same mutation. Mechanistically, increased levels of mitochondrial ROS in heteroplasmic mutants are proposed as a means by which tumour survival is augmented in these clones (Park et al., 2009). Further studies by the same group using the aforementioned heteroplasmic *ND5* mutant cybrids revealed a significantly increased level of Akt protein phosphorylation; a component of the potent PI3K-Akt pro-survival pathway which is frequently hyperactivated in human cancer (reviewed in Altomare & Testa, 2005). Again, attributed to increased ROS levels induced by complex I dysfunction, Akt activation resulted in the upregulation of transcription of the anti-apoptotic mediators Bcl-xL and myeloid cell leukaemia 1 (Mcl1) and

a transcriptional downregulation of pro-apoptotic proteins such as Bad, caspase-9 and FOXO1 (Sharma et al., 2011). Importantly, the introduction of the yeast NADH quinone oxidoreductase (*NDI1*) gene into mutant *ND5* heteroplasmic cybrids restored complex I function and reversed the enhanced tumorigenicity observed in the original complex I defective cells. Regarding the response to anti-cancer agents, mitochondrial oxidative phosphorylation defects, particularly those involving complex I, have been shown to modulate the apoptotic response to several chemotherapeutic agents. Following treatment with the DNA-damaging agents etoposide and doxorubicin, caspase activation was significantly reduced in a complex I deficient cell line in comparison to wild type cells. In contrast, administration with the histone deacetylase inhibitor apicidin enhanced caspase activation in both complex I and grossly OXPHOS deficient cells in comparison to wild type cells (Yadav et al., 2015). A significantly increased mitochondrial ROS production in wild type cells following etoposide and apicidin treatment with a mechanistic link to cytochrome *c* release and apoptosis is also described. Interestingly however, the authors attribute the reduced apoptosis in complex I deficient cells following anti-cancer agent treatment in part to a reduction in mitochondrial ROS elicited by OXPHOS dysfunction. Given the prominent complex I defect, and reduced apoptosis levels seen in our *PolγA*$^{mut/mut}$ intestinal adenomas in comparison to *PolγA*$^{+/+}$ adenomas this mechanism may benefit from further investigation.

5.5. Future work

With regard to the *Lgr5+* stem cell compartment of the intestine specifically, in which adenomagenesis is initiated in our model, a significantly greater proliferative rate was detected only in the small intestine of *PolγA*$^{mut/mut}$ in comparison to *PolγA*$^{+/+}$ mice. This may reflect an immunomodulatory function elicited by resident Paneth cells as recently described (Pflügler et al., 2020), a function which may be affected by an age-related mitochondrial dysfunction. This reinforces the requirement for further investigation in this area. The specific labelling of Paneth cells using lysozyme markers for example in conjunction with an immune cell marker panel as suggested in 4.5. would be extremely useful in investigation of the contribution of age-related mitochondrial dysfunction to the tumour immune response. With regard to the reduced apoptotic frequency within *PolγA*$^{mut/mut}$ adenomas, the mechanism by which this is facilitated remains unknown. Studies which indicate an increase in ROS production by complex I deficient cells as mechanistically important in diminishing

apoptosis (Park et al., 2009; Sharma et al., 2011) in addition to the involvement of mitochondrial ROS in the apoptotic response to anti-cancer agents indicate a key role for these species. The labelling of adenoma organoids with the fluorescent marker mitoSOX in order to assess ROS levels with additional experiments investigating the effect of ROS scavengers on survival and/or apoptosis may shed light on the underlying mechanisms inhibiting apoptosis in *PolγA*$^{mut/mut}$ adenomas.

5.6. Conclusion

In conclusion, this chapter presents quantification of the apoptotic and proliferative indices of colonic and small intestinal *Apc*-Wnt driven adenomas in mice harbouring age-related *PolγA* induced mitochondrial dysfunction in comparison to those which do not. Using a double-thymidine analogue labelling technique followed by fluorescent microscopic analysis, both colonic and small intestinal *PolγA*$^{mut/mut}$ adenomas demonstrate a significantly greater replicative rate in comparison to their *PolγA*$^{+/+}$ counterparts. *Lgr5+* stem cells are significantly more numerous in *PolγA*$^{mut/mut}$ versus *PolγA*$^{+/+}$ adenomas with a significantly greater rate of replication identified within the *Lgr5+* stem cell compartment of the *PolγA*$^{mut/mut}$ small intestine. With the use of cleaved caspase 3 immunohistochemistry, apoptosis within *PolγA*$^{mut/mut}$ colonic and small intestinal adenomas is shown to be a significantly less frequent event in comparison to *PolγA*$^{+/+}$ adenomas. Together, the investigations undertaken in this chapter suggest that age-related mitochondrial dysfunction promotes an accelerated proliferation and reduced apoptosis in intestinal adenomas in our mouse model.

Chapter 6. Investigating the mechanisms by which mitochondrial dysfunction promotes adenoma growth

6.1. Introduction

Data presented thus far have shown that when intestinal adenomas are genetically induced on a background of a high mtDNA mutation rate due to a homozygous or heterozygous mutation in the mitochondrial DNA *PolγA* gene (*PolγA*$^{mut/mut}$*;Lgr5-EGFP-IREScreERT2;Apc*$^{flox/flox}$), this significantly shortens lifespan in comparison to control *PolγA*$^{+/+}$*/Lgr5-EGFP-IREScreERT2/Apc*$^{flox/flox}$ mice. This is due to a significantly greater total adenoma burden, resulting from significantly higher rates of cell proliferation and lower levels of apoptosis in both the colon and small intestine of *PolγA*$^{mut/mut}$ when compared to *PolγA*$^{+/+}$ mice. Furthermore, immunofluorescent analysis of mitochondrial respiratory chain enzyme expression revealed that 85% of small intestinal and 55% of colonic adenomas in *PolγA*$^{mut/mut}$ mice were categorised as negative or intermediate negative in their expression of the complex I subunit NDUFB8 with minimal respiratory chain enzyme deficiency seen in *PolγA*$^{+/+}$ adenomas. These data suggest that an age-related accumulation of mtDNA mutations may promote the growth of adenomas within the intestine. In order to investigate the underlying mechanisms by which mitochondrial dysfunction may prime the intestinal tissue prior to tumour development, RNA sequencing analysis was performed by Dr Julia Whitehall on small intestinal crypt samples from *PolγA*$^{mut/mut}$ and *PolγA*$^{+/+}$ mice in which *Apc* deletion had not been induced.

As the majority of adenomas occur at the distal end of the small intestine, a small sample of this tissue was removed from 6-month-old *PolγA*$^{mut/mut}$ (n=4) and *PolγA*$^{+/+}$ (n=4) mice at dissection. Small intestinal crypts were isolated from stromal tissue as described by Sato et al (Sato et al., 2009). RNA was extracted from crypt pellets and RNA integrity (RIN) scores analysed. Samples of RNA were then sent for total RNA Sequencing at The Genomics Core Facility, Institute of Genetic Medicine, Newcastle University.

Following library preparation, the NextSeq 500 system (Illumina) was used to analyse all samples at a depth of 16 million 75 bp single reads per sample. All samples were quality assessed, genome aligned, and subsequent differential gene expression analysis carried out

by Fiona Robertson, Bioinformatician, Newcastle University. The quantity of each transcript was denoted by a fragments per kilobase of transcript per million mapped reads (FPKM) value and log transformed. An adjusted *p*-value of <0.05 was applied to identify significantly differentially expressed genes in non-transformed small intestinal crypts from 6-month-old *PolγA*$^{mut/mut}$ compared with *PolγA*$^{+/+}$ mice (Figure 6-1). A cut off of -2> to >2 log2 fold change was applied before submitting differentially expressed gene lists to the Enrichr web-based enrichment tool (Chen et al., 2013; Kuleshov et al., 2016) in order to align gene signatures with biological functions. The highest-ranking pathways included those relating to serine synthesis and one-carbon metabolism. Table 6-1 presents the identification of these pathways alongside participating genes (*Phgdh, Psat1, Psph, Mthfd2 and Aldh1l2*) found to be significantly upregulated within the small intestinal crypts of *PolγA*$^{mut/mut}$ mice. As mitochondrial dysfunction has been shown to promote glutathione synthesis via the upregulation of *de novo* serine synthesis (Nikkanen et al., 2016) and cancer cells rely on exogenous serine uptake and *de novo* synthesis to provide them with the one-carbon units essential for their growth and proliferation (reviewed in Newman & Maddocks, 2017), these genes became the focus of the next stages of investigation.

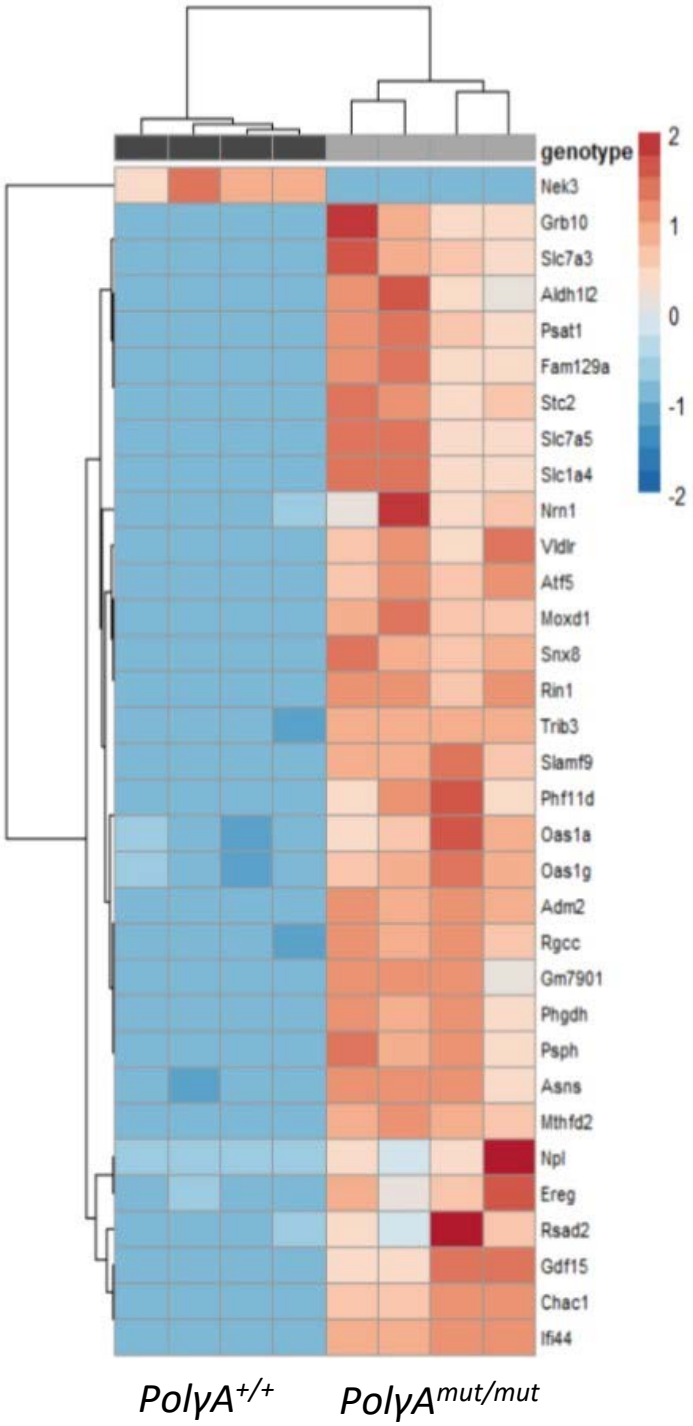

Figure 6-1. Heat map of differentially expressed genes in non-transformed small intestinal crypts from 6-month-old *PolγA*$^{+/+}$ (n=4) compared with *PolγA*$^{mut/mut}$ (n=4) mice. Scale bar represents log2 (FPKM+1) values with positive values in red highlighting upregulation and negative values in blue highlighting downregulation. Courtesy of Julia Whitehall.

Pathway	Genes
Glycine, serine and threonine metabolism_Homo sapiens_hsa00260	PHGDH; PSAT1; PSPH
One carbon pool by folate_Homo sapiens_hsa00670	MTHFD2; ALDH1L2
Biosynthesis of amino acids_Homo sapiens_hsa01230	PHGDH; PSAT1; PSPH
Carbon metabolism_Homo sapiens_hsa01200	PHGDH; PSAT1; PSPH
Aminoacyl-tRNA biosynthesis_Homo sapiens_hsa00970	
Metabolic pathways_Homo sapiens_hsa01100	
Non-alcoholic fatty liver disease (NAFLD)_Homo sapiens_hsa04932	
Selenocompound metabolism_Homo sapiens_hsa00450	
Cysteine and methionine metabolism_Homo sapiens_hsa00270	
Alanine, aspartate and glutamate metabolism_Homo sapiens_hsa00250	

Table 6-1. Gene set enrichment analysis identifying pathways associated with differentially expressed genes in non-transformed small intestinal crypts from 6-month-old *PolγA*$^{+/+}$ (n=4) compared with *PolγA*$^{mut/mut}$ (n=4) mice. Genes were mapped to the KEGG pathway database (2016) using the Enrichr web-based enrichment tool.

6.1.1. Serine and one carbon metabolism

One carbon metabolism encompasses a network of metabolic processes that facilitate the generation of one-carbon units (also known as methyl groups) that fuel biosynthetic reactions, epigenetic regulation, redox defence and amino acid homeostasis (reviewed in Ducker & Rabinowitz, 2017). Integral to one-carbon metabolism are the folate and methionine cycles which depend on folate molecules to accept and transfer the one-carbon units they require. One-carbon molecules can be obtained from several dietary sources, however in humans the main one-carbon group donor is the non-essential amino acid serine (Davis et al., 2004).

A number of different transporters can facilitate the uptake of exogenous serine; however, it may also be synthesised by the cell via the diversion of glycolytic or gluconeogenic carbon into the *de novo* serine synthesis pathway (SSP) (Snell, 1984). The serine synthesis pathway is catalysed by three enzymes. The first, and rate-limiting enzyme of the pathway is phosphoglycerate dehydrogenase (PHGDH) which catalyses the NAD^+ dependant oxidation of the glycolytic (or gluconeogenic) intermediate 3-phosphoglycerate (3PG) generating NADH and 3-phosphohydroxypyruvate (3PHP). Phosphoserine aminotransferase 1 (PSAT1) is the second enzyme of the pathway and catalyses the glutamate dependant transamination

of 3PHP generating α-ketoglutarate (αKG) and 3-phosphoserine (3PSer). The final enzyme, phosphoserine phosphatase (PSPH) catalyses the hydrolysis of 3PSer synthesising serine. Regulation of the SSP is achieved with the convergence of multiple feedback mechanisms. Serine itself acts as an inhibitor of PSPH in mammals (Neuhaus & Byrne, 1960) and also allosterically activates the M2 isoform of pyruvate kinase (PKM2). PKM2 catalyses the final step of glycolysis, thus its activation decreases the availability of upstream glycolytic intermediates such as 3PG that feeds into the SSP, inhibiting it accordingly (Ye et al., 2012). A depletion of intracellular serine is detected by the eukaryotic initiation factor 2, α subunit (eIF2α) kinase, GCN2 which in turn phosphorylates eIF2α leading to increased translation of activating transcription factor 4 (ATF4). The expression of all three enzymes of the SSP are induced by ATF4 and the pathway positively regulated as such (Ye et al., 2012).

As previously mentioned, serine is the main donor of one-carbon units to the folate cycle. Folates are a group of molecules function as carriers of one carbon units and although diverse, they share three core structural units. A polyglutamate tail which can vary in length is required for retention of the molecule within the cell, and a pteridine ring and para-aminobenzoic acid (PABA) linker function together to bind one-carbon units. Folates can be synthesised by most bacteria, plants and yeast however they must be ingested in the diet of animals (reviewed in Ducker & Rabinowitz, 2017). In order to enter the folate cycle, folates must be in the biologically active reduced form, tetrahydrofolate (THF). The donation of a one-carbon unit, typically from serine, generates glycine and 5,10-methylene-THF in which the 1C group is covalently bound to the 5-position nitrogen atom on the pteridine ring and the 10-position nitrogen atom on the PABA linker of THF (reviewed in Ducker & Rabinowitz, 2017). This reaction is catalysed by serine hydroxymethyltransferase 1 (SHMT1) in the cytoplasm, but in vertebrates occurs preferentially within the mitochondria, catalysed by serine hydroxymethyltransferase 2 (SHMT2) (Yoshida & Kikuchi, 1970). Also localised within the mitochondria is the glycine cleavage system, a series of enzymes that catalyse the removal of one carbon units from glycine (Kikuchi, 1973).

Once the 1C unit is bound to THF and 5,10-methylene-THF has been generated, the molecule can interconvert between different redox states, these reactions being catalysed by methylenetetrahydrofolate dehydrogenase 1 (MTHFD1) in the cytoplasm and MTHFD2/2L/1L in the mitochondria. The fate of one-carbon units depends on the folate

species from which it is derived, with each redox state supporting different biosynthetic processes. The synthesis of purines requires 10-formyl-THF, the most oxidised 1C folate, which can also be derived from formate. *De novo* purine synthesis from 10-formyl-THF is catalysed by groups of enzymes which form cytoplasmic clusters named purinosomes (An et al., 2008; Zhao et al., 2013a). Although not located within the mitochondria, purinosomes are close in proximity to them and share a functional relationship with mitochondria. ATP and formate which are produced by mitochondrial folate metabolism are required for purine synthesis, similarly the products of purine synthesis are required for the synthesis of mitochondrial DNA (Chan et al., 2018). 10-formyl-THF is also required to formylate the mitochondrial $tRNA^{Met}$ generating fMet-$tRNA^{Met}$, a critical component of the mitochondrial DNA translation initiation machinery (Tucker et al., 2011).

The generation of the most reduced 1C folate, 5-methyl-THF from 5,10- methylene-THF is catalysed by methylene tetrahydrofolate reductase (MTHFR). The subsequent consumption of 5-methyl-THF by methionine synthase (MTR) in a vitamin B12 dependant manner permits the re-methylation of homocysteine to form methionine. It is at this point that the folate cycle intersects with the methionine cycle allowing the transfer of 1C units necessary for key members of this pathway namely S-adenosylmethionine (SAM) and S-adenosylhomocysteine (SAH), to facilitate vital epigenetic modification and methylation reactions. SAM is the primary mammalian methyl donor (Finkelstein, 1990), responsible for supplying 1C units to the methyltransferases that undertake these processes, and its ratio with SAH has been shown to affect their interaction with and hence the activity of these enzymes (Mentch et al., 2015). The hydrolysis of SAH into homocysteine and adenosine completes the methionine cycle and in tissues such as the liver, kidney, pancreas, intestine and brain, homocysteine can enter the transsulphuration pathway (Finkelstein, 2007) facilitating the biosynthesis of the antioxidant glutathione (Beatty & Reed, 1980). Figure 6-2 depicts the systems described.

As folates laden with one-carbon units are unable to cross the mitochondrial membrane, one-carbon metabolism is compartmentalised to the mitochondria and cytoplasm with each region possessing distinct enzymes as described. The mitochondrial membrane is permeable to serine, glycine and formate, and these molecules link the two compartments (reviewed in Tibbetts & Appling, 2010). Although the pathway preferentially proceeds in one direction,

with the production of formate in the mitochondria, both compartments can exhibit bidirectionality relevant to the changing metabolic requirements of the cell. Thus, the serine synthesis pathway, one carbon cycle and methionine and transsulphuration pathways converge to support numerous biosynthetic and regulatory processes with mitochondria playing a pivotal role.

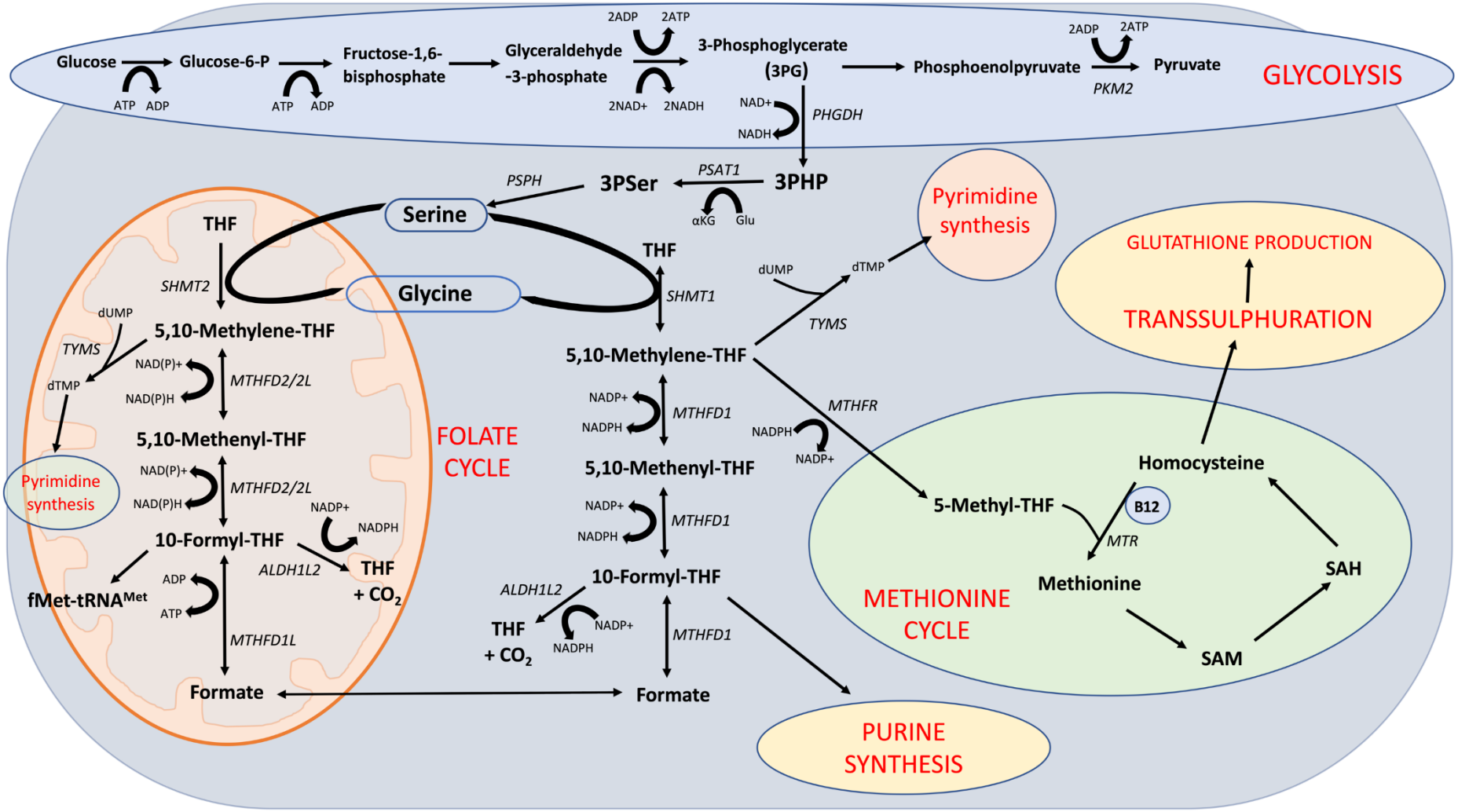

Figure 6-2. Schematic depicting central carbon metabolic pathways and their compartmentalisation. The diversion of glycolytic intermediates into the *de novo* serine synthesis pathway provides one carbon units for mitochondrial and cytoplasmic one carbon folate metabolism. Branching from the folate cycle are the methionine and transsulphuration pathways in addition to purine and pyrimidine synthesis.

6.2. Aims of study

Previous work carried out by Dr Julia Whitehall revealed an upregulation of a particular set of genes within the small intestinal crypt transcriptome of 6-month-old *PolγA*$^{mut/mut}$ compared to *PolγA*$^{+/+}$ mice in the absence of an adenomatous pathology. Specifically, these genes were involved in the uptake, biosynthesis and metabolism of the amino acid serine. Quantitative RT-PCR carried out by Dr Whitehall subsequently validated the findings elucidated by RNA sequencing in both normal non-transformed crypts and adenomas extracted from *PolγA*$^{mut/mut}$ and *PolγA*$^{+/+}$ mice, however the levels of these enzymes at the protein level *in vivo* remained unknown. Furthermore, these molecular analyses were limited to the small intestine of experimental animals with the pathology, if any, in the colon also remaining unknown. Finally, of paramount importance was investigating the potential translation of findings in the mouse model to humans. In this chapter I aimed to:

1. Investigate if changes in gene expression detected by RNA Seq and q-PCR translate into changes at the protein level in the colon and small intestine.
2. Ascertain if these proteins are upregulated in response to an age-related accumulation of OXPHOS defects in the small intestine and colon of the *PolγA*$^{mut/mut}$ and *PolγA*$^{+/+}$ mice.
3. Investigate whether changes in gene expression and protein levels in response to OXPHOS deficiency observed in the mouse are directly translatable to the human colonic epithelium.

6.3. Results

6.3.1. Serine synthesis pathway and one-carbon cycle enzyme immunohistochemistry

RNA sequencing analysis of normal non-transformed small intestinal crypts from *PolγA*$^{mut/mut}$ and *PolγA*$^{+/+}$ mice revealed an upregulation of genes involved in pathways relating to serine synthesis, serine uptake and one-carbon metabolism (*Phgdh, Psat1, Psph, Mthfd2, Slc1a4 and Aldh1l2*). In order to confirm RNA sequencing results at the protein level and evaluate the expression of these proteins in the adenoma setting, immunohistochemistry using antibodies targeting several of the proteins encoded by these genes was carried out on tissue sections of colon and small intestine from animals in which tumorigenesis had been induced via *Apc* deletion. Sections from *PolγA*$^{mut/mut}$ (n=4) and *PolγA*$^{+/+}$ (n=4) mice humanely sacrificed at 23 days post *Apc* deletion were labelled with anti-PHGDH, anti-PSAT1 and anti-MTHFD2 as described in 2.2.9.4. Representative immunohistochemistry images showing in situ levels of SSP proteins in the non-transformed normal mucosa and adenomas of the colon and small intestine are shown in Figures 6-3 and 6-4 respectively.

As can be seen in Figure 6-3 (A) and Figure 6-4 (A), in comparison to *PolγA*$^{+/+}$ mice, the expression levels of PHGDH, PSAT1 and MTHFD2 proteins are increased in the normal crypt compartments of both the colon and small intestine of *PolγA*$^{mut/mut}$ mice. Similarly, as presented in Figure 6-3 (B) and Figure 6-4 (B), colonic and small intestinal adenomas from *PolγA*$^{mut/mut}$ mice display an upregulation of PHGDH, PSAT1 and MTHFD2 in comparison to *PolγA*$^{+/+}$ adenomas. The expression of PHGDH and PSAT1 proteins appear marginally raised in the adenomas of *PolγA*$^{+/+}$ mice when compared to *PolγA*$^{+/+}$ normal mucosa, however the adenomas of *PolγA*$^{mut/mut}$ mice demonstrate a clear increased expression of these proteins when compared to all tissue compartments from all mice. These observations suggest an association of *PolγA*$^{mut/mut}$ induced intestinal crypt mitochondrial dysfunction with an upregulation of *de novo* serine synthesis and the mitochondrial folate cycle in these crypts. This confirms results of RNA sequencing analysis at the protein level.

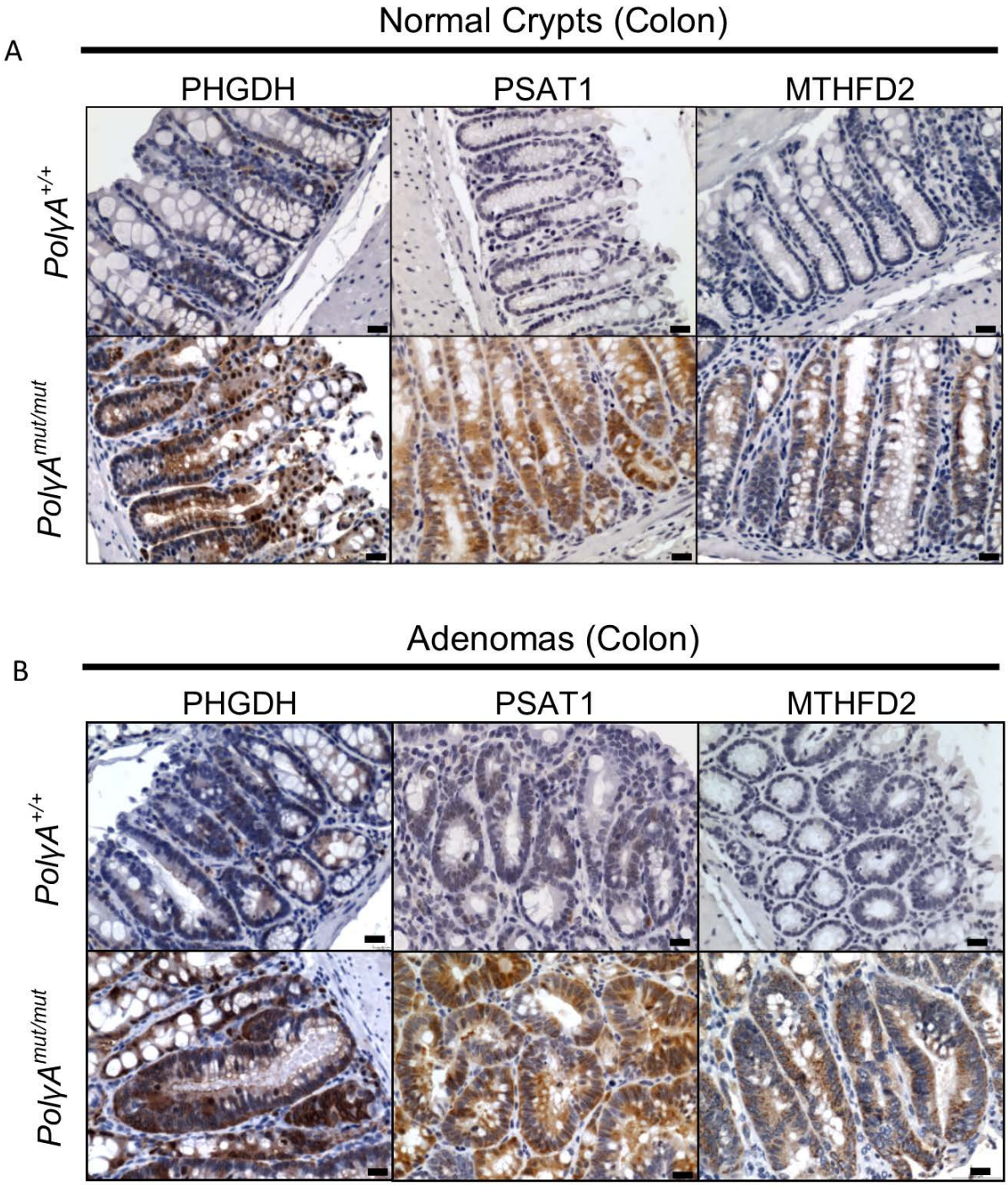

Figure 6-3. Immunohistochemistry showing in situ levels of SSP proteins in the non-transformed normal mucosa and adenomas from the colons of *PolγA*$^{+/+}$ and *PolγA*$^{mut/mut}$ mice. (A) normal mucosa, (B) adenomas. Representative images are shown, n=4 mice per group analysed. Scale bars 100µm.

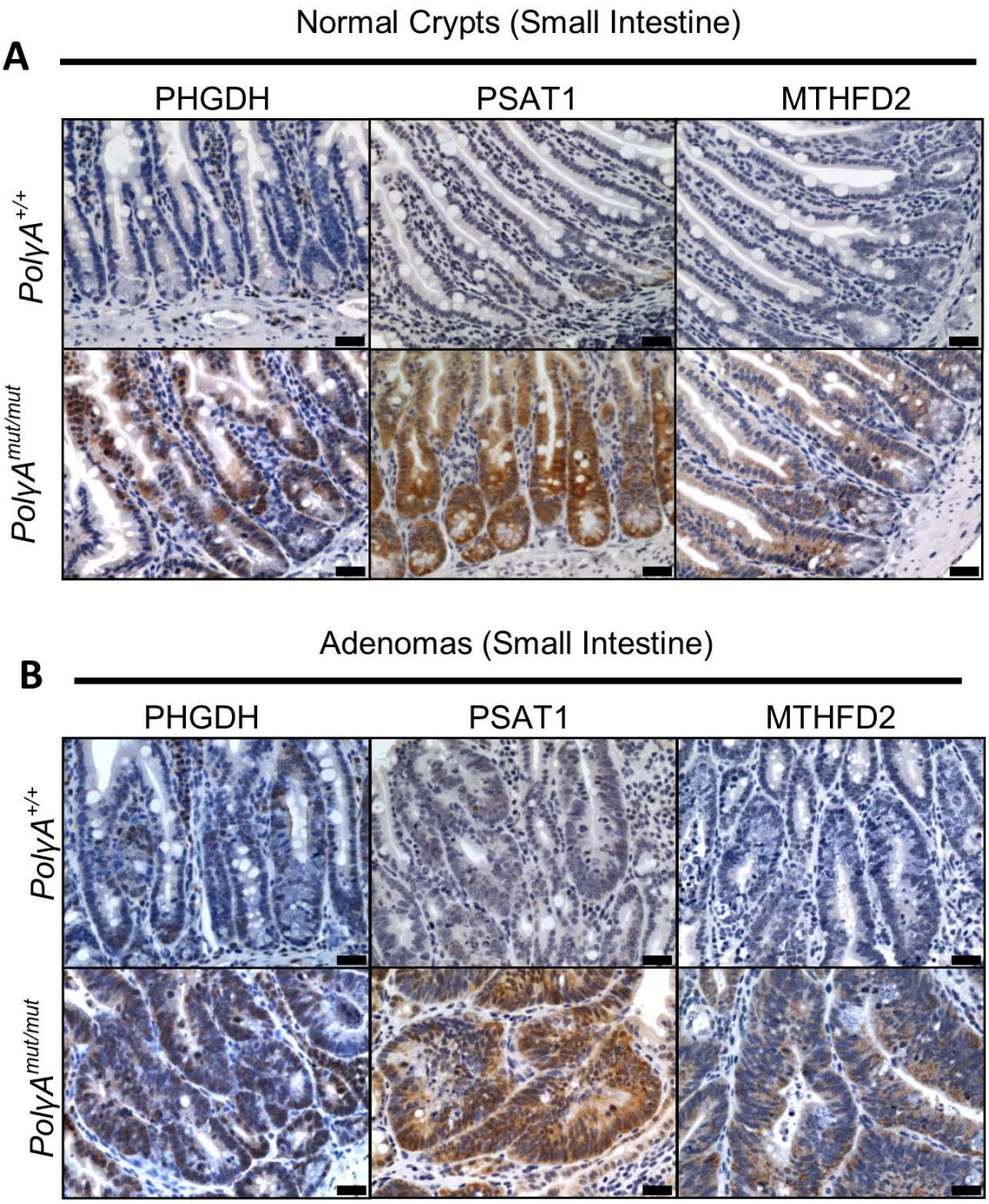

Figure 6-4. Immunohistochemistry showing in situ levels of SSP proteins in the non-transformed normal mucosa and adenomas from the small intestines of *PolγA*$^{+/+}$ and *PolγA*$^{mut/mut}$ mice. (A) normal mucosa, (B) adenomas. Representative images are shown, n=4 mice per group analysed. Scale bars 100µm.

6.3.2. Serine synthesis pathway and one-carbon cycle enzyme immunofluorescence in non-transformed mouse colon and small intestine

In light of the results of the previous section in which serine synthesis pathway enzymes were found to be upregulated in the normal non-transformed intestinal crypts of *PolγA*$^{mut/mut}$ mice, it was hypothesised that if this was a response to the age-related accumulation of OXPHOS deficiency observed in the *PolγA*$^{mut/mut}$ mice (Baines et al., 2014), an age-related increase in the expression of SSP enzymes would also be observed in the normal non-transformed intestine. In order to investigate this, serial sections from the colon and small intestine of *PolγA*$^{+/+}$ and *PolγA*$^{mut/mut}$ mice at 1, 3, 6, 9 and 12-months of age were labelled with antibodies against PHGDH, PSAT1 and MTHFD2 with one antibody per section. For each age group, *PolγA*$^{+/+}$ (n=3) and *PolγA*$^{mut/mut}$ (n=3) mice were labelled according to the protocol outlined in 2.2.11.4.1. Quantification of SSP/one-carbon cycle enzyme protein levels was carried out as described in 2.2.12.5.1. Supporting the hypothesis that SSP/one-carbon cycle enzymes are upregulated in response to an age-related accumulation of OXPHOS defects in *PolγA*$^{mut/mut}$ mice, a clear age-related increase in SSP/one-carbon cycle enzyme protein levels are observed within the normal non-transformed crypts of the colon and small intestine of *PolγA*$^{mut/mut}$ mice. This is in contrast to normal crypts of *PolγA*$^{+/+}$ mice in which an absence of mitochondrial dysfunction abrogates the upregulation response. Representative immunofluorescent images taken from *PolγA*$^{+/+}$ and *PolγA*$^{mut/mut}$ colon samples are shown in Figures 6-5 to 6-7. Representative immunofluorescent images taken from *PolγA*$^{+/+}$ and *PolγA*$^{mut/mut}$ small intestinal samples are shown in Figures 6-8 to 6-10.

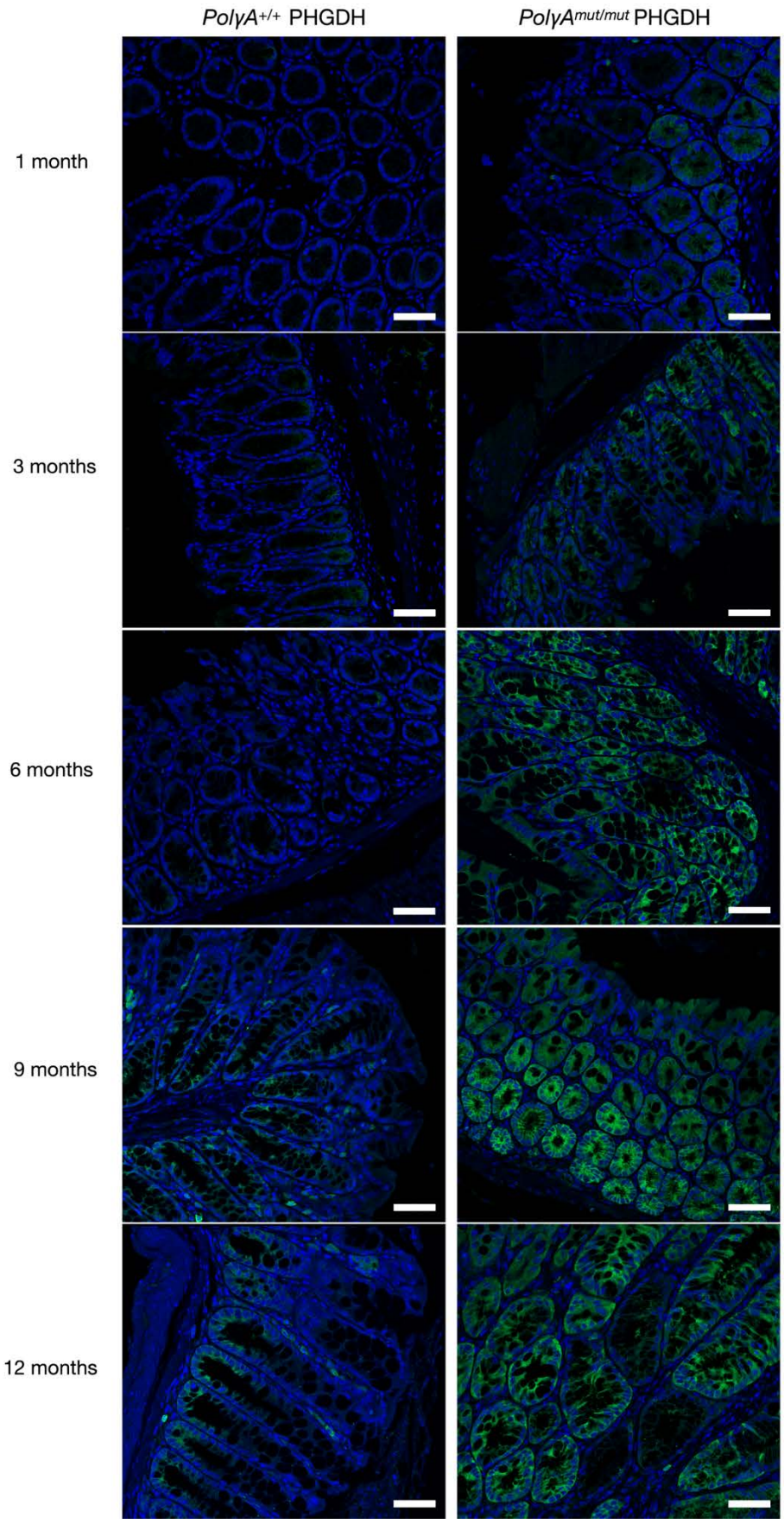

Figure 6-5. Representative immunofluorescent images depicting the levels of PHGDH within 1, 3, 6, 9 and 12-month-old *PolγA*$^{+/+}$ and *PolγA*$^{mut/mut}$ normal non-transformed colonic crypts. Scale bars 50μm.

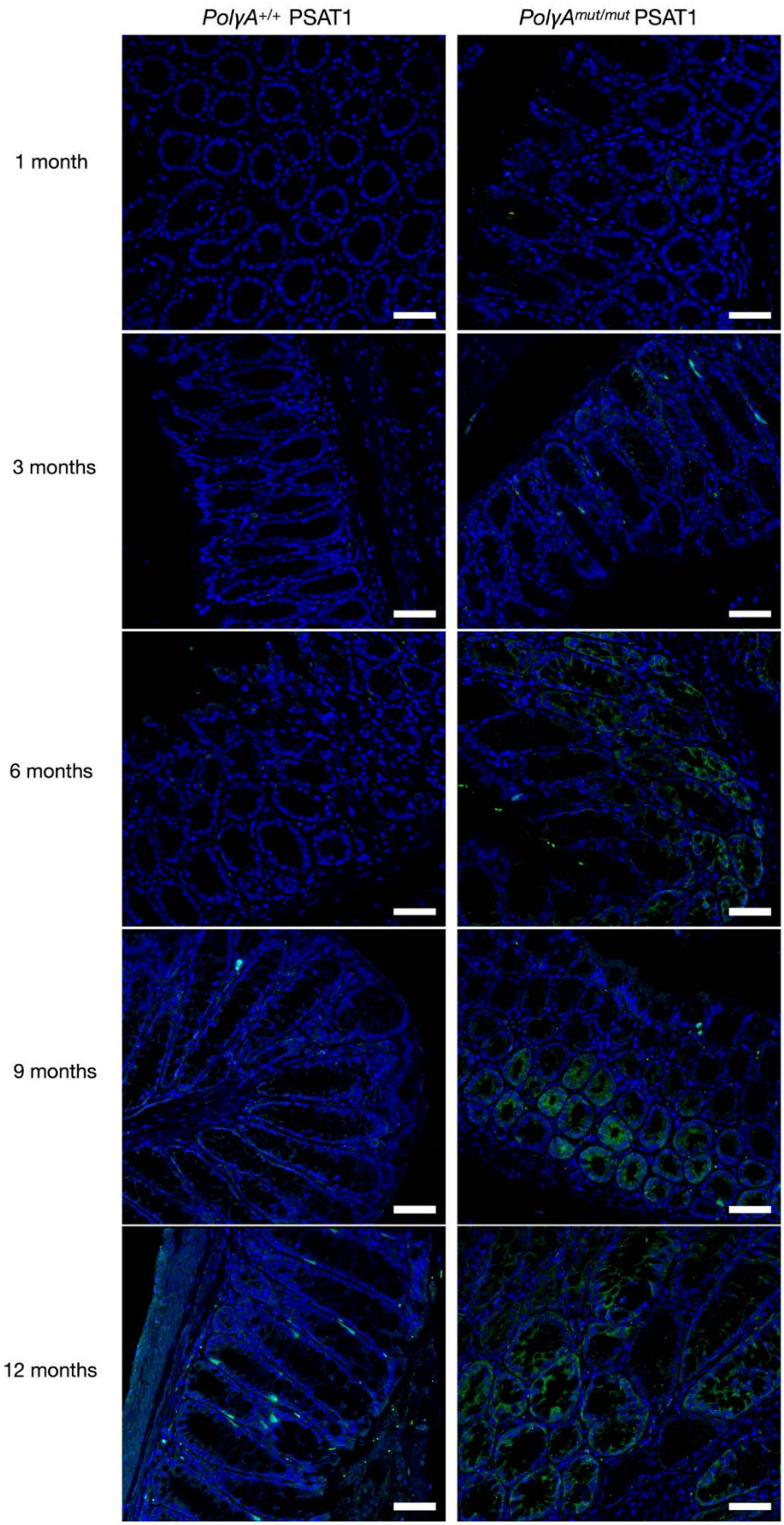

Figure 6-6. Representative immunofluorescent images depicting the levels of PSAT1 within 1, 3, 6, 9 and 12-month-old *PolγA*$^{+/+}$ and *PolγA*$^{mut/mut}$ normal non-transformed colonic crypts. Scale bars 50μm.

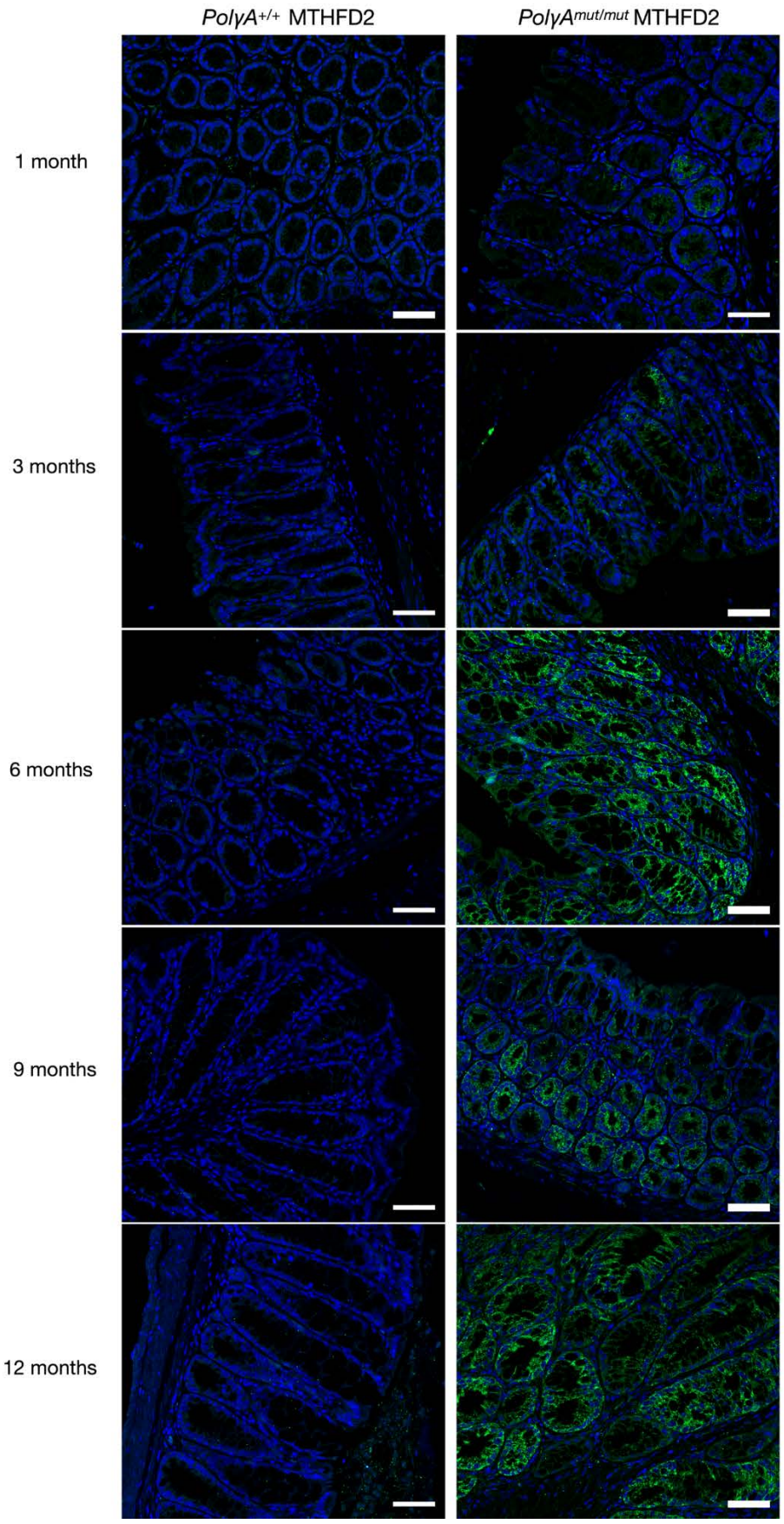

Figure 6-7. Representative immunofluorescent images depicting the levels of MTHFD2 within 1, 3, 6, 9 and 12-month-old *PolγA*$^{+/+}$ and *PolγA*$^{mut/mut}$ normal non-transformed colonic crypts. Scale bars 50μm.

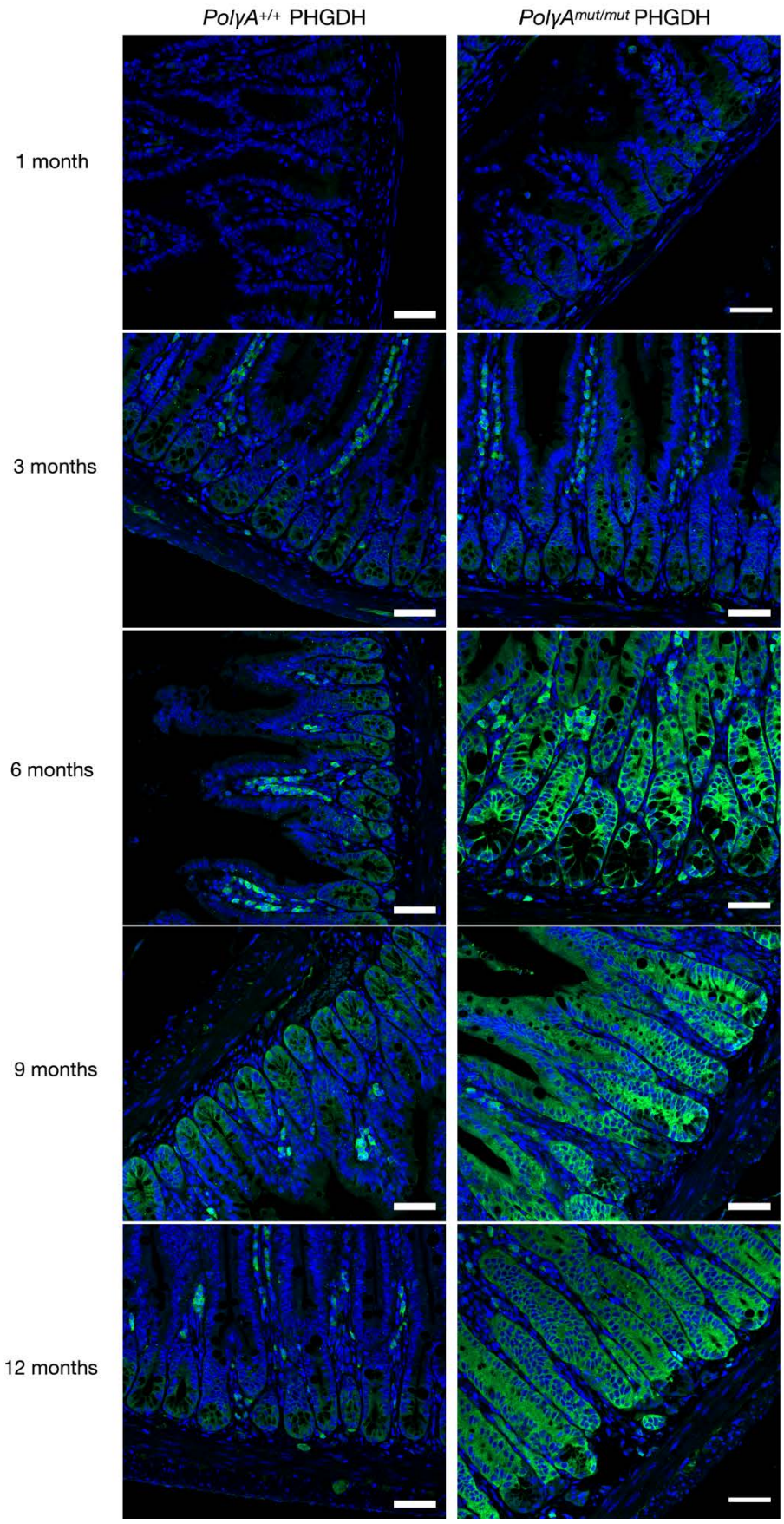

Figure 6-8. Representative immunofluorescent images depicting the levels of PHGDH within 1, 3, 6, 9 and 12-month-old *PolγA*$^{+/+}$ and *PolγA*$^{mut/mut}$ normal non-transformed small intestinal crypts. Scale bars 50μm.

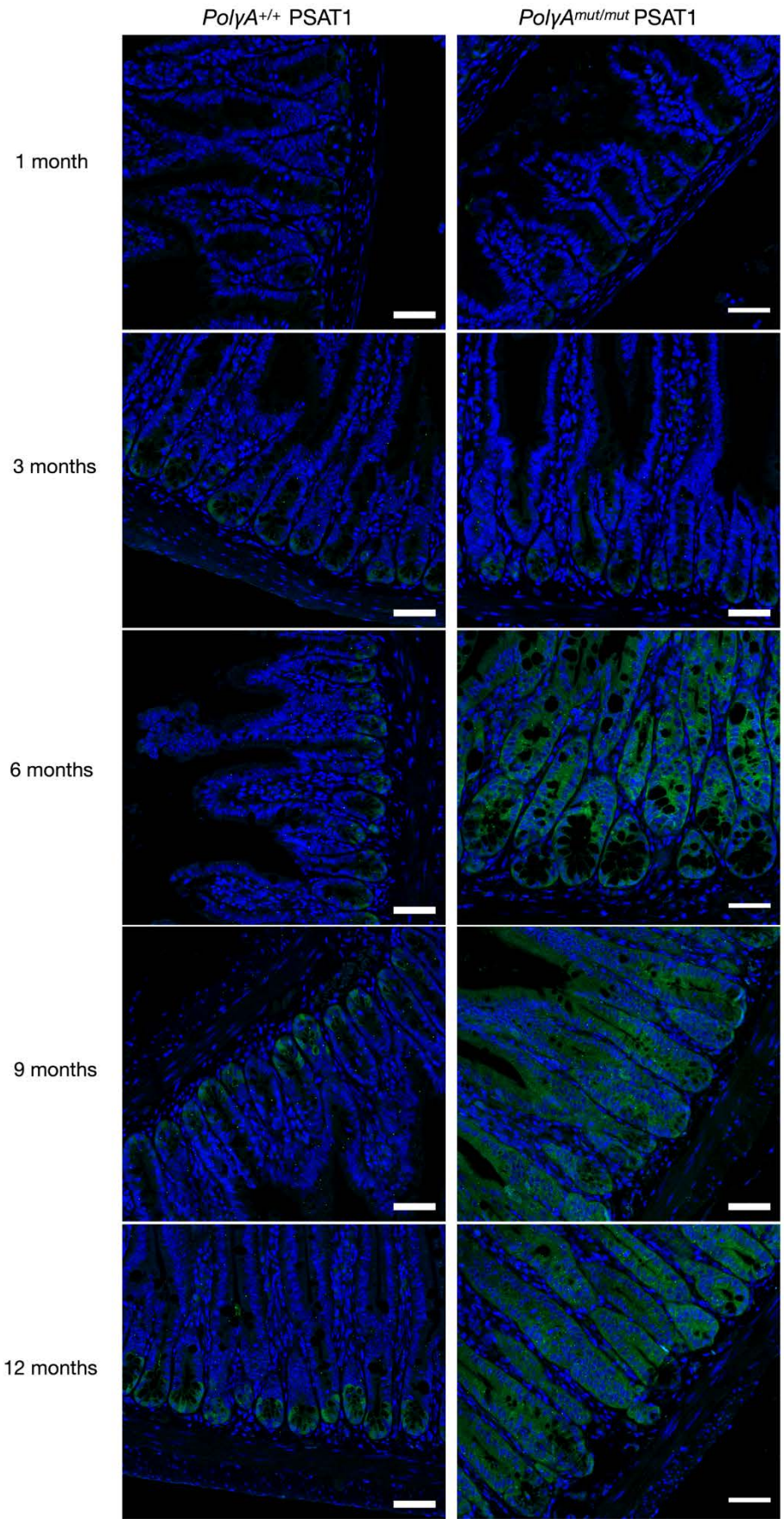

Figure 6-9. Representative immunofluorescent images depicting the levels of PSAT1 within 1, 3, 6, 9 and 12-month-old *PolγA*$^{+/+}$ and *PolγA*$^{mut/mut}$ normal non-transformed small intestinal crypts. Scale bars 50μm.

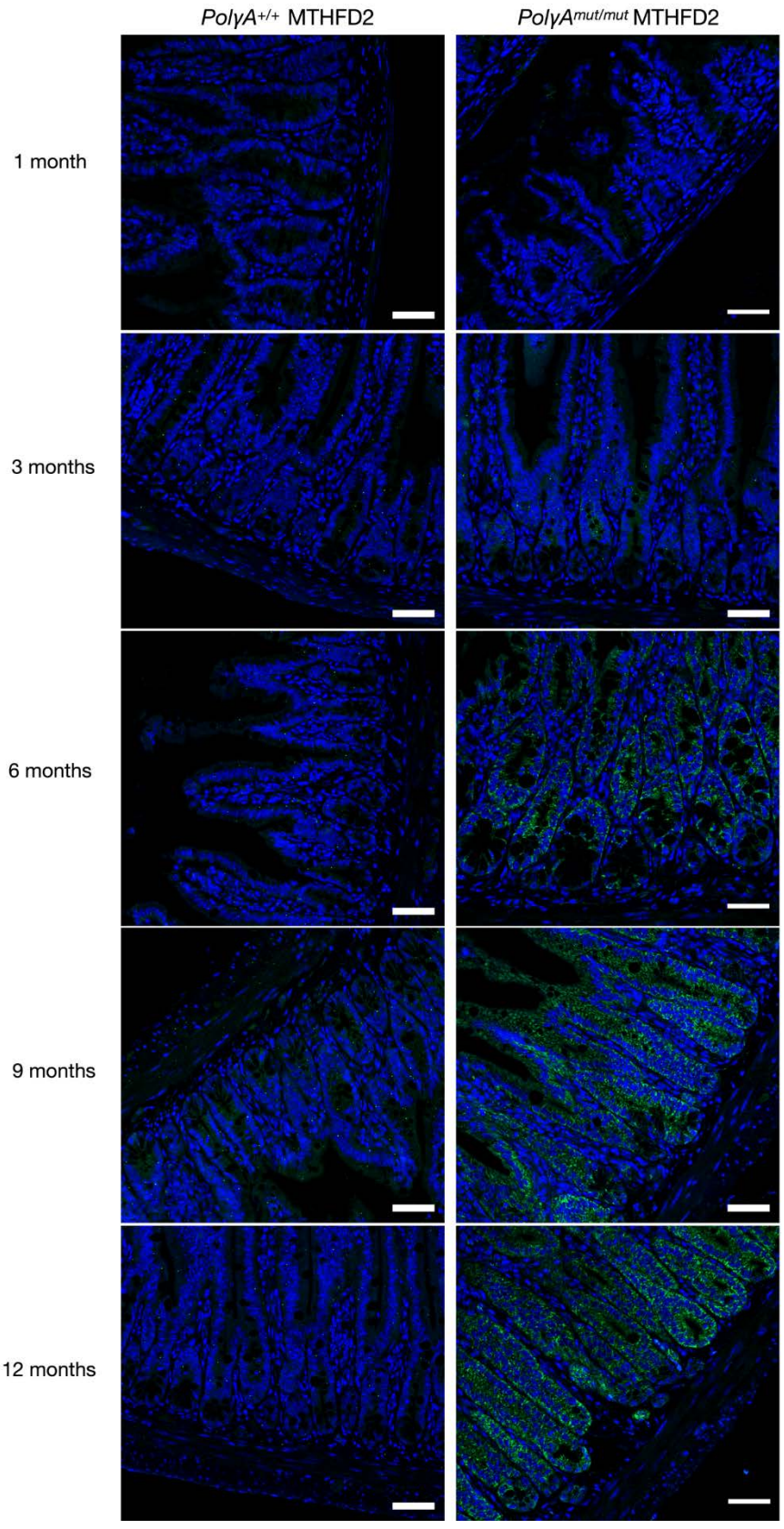

Figure 6-10. Representative immunofluorescent images depicting the levels of MTHFD2 within 1, 3, 6, 9 and 12-month-old *PolγA*$^{+/+}$ and *PolγA*$^{mut/mut}$ normal non-transformed small intestinal crypts. Scale bars 50μm.

Within the colon, linear regression analyses detect a significant deviation from zero with regard to expression levels of all three enzymes in both *PolγA*$^{+/+}$ and *PolγA*$^{mut/mut}$ normal crypts with increasing age (Figure 6-11) (*PolγA*$^{+/+}$ PHGDH P=0.0025, PSAT1 P=0.0066, MTHFD2 P=0.0028, *PolγA*$^{mut/mut}$ PHGDH P<0.0001, PSAT1 P<0.0001, MTHFD2 P<0.0001, linear regression). Despite the apparent increase in expression levels of each enzyme in both *PolγA*$^{+/+}$ and *PolγA*$^{mut/mut}$ normal colonic mucosa, the comparison of regression slopes between genotypes detects a significant difference between these slopes (PHGDH P<0.0001, PSAT1 P<0.0001, MTHFD2 P=0.0005, analysis of covariance). This suggests that the rate of increase in expression of PHGDH, PSAT1 and MTHFD2 over time is greater within *PolγA*$^{mut/mut}$ colonic crypts in comparison with those of *PolγA*$^{+/+}$ mice.

Similarly, within the small intestine, linear regression analyses detect a significant deviation from zero with regard to expression levels of all three enzymes in both *PolγA*$^{+/+}$ and *PolγA*$^{mut/mut}$ normal crypts with increasing age (Figure 6-12) (*PolγA*$^{+/+}$ PHGDH P=0.0014, PSAT1 P=0.0169, MTHFD2 P=0.0005, *PolγA*$^{mut/mut}$ PHGDH P<0.0001, PSAT1 P=0.0002, MTHFD2 P<0.0001, linear regression). As is demonstrated within the colon, upon comparison of regression slopes, a significantly greater rate of increase in the expression level of each enzyme over time is observed in *PolγA*$^{mut/mut}$ small intestinal crypts compared with those of *PolγA*$^{+/+}$ mice (PHGDH P=0.0004, PSAT1 P=0.0023, MTHFD2 <0.0001, analysis of covariance). These data confirm that key enzymes of the *de novo* serine synthesis pathway and mitochondrial one carbon cycle are upregulated in response to age-related mtDNA mutation induced mitochondrial dysfunction within the murine colon and small intestine.

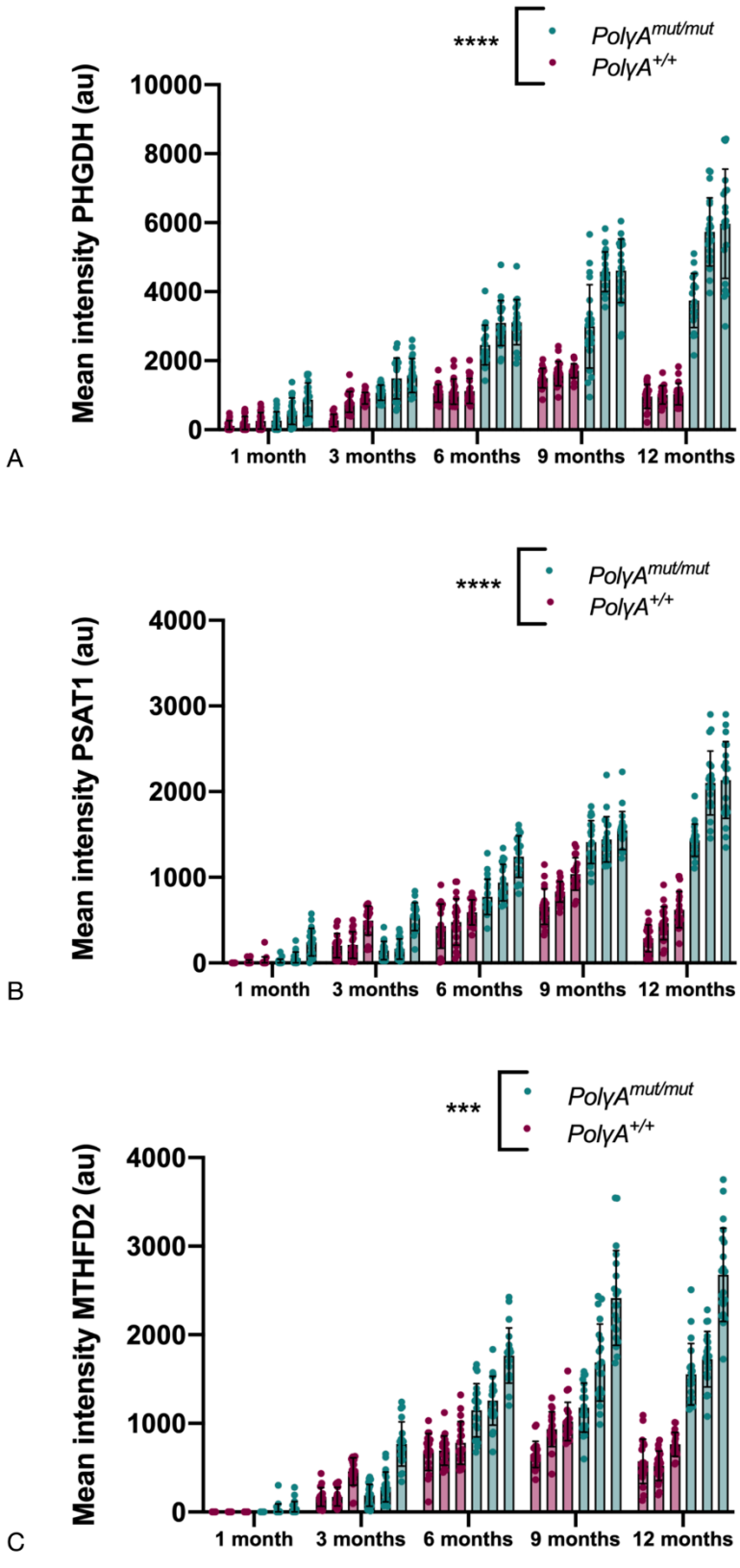

Figure 6-11. Quantification of the expression levels of PHGDH, PSAT1 and MTHFD2 in normal non-transformed colonic crypts of *PolγA*$^{+/+}$ and *PolγA*$^{mut/mut}$ mice of increasing ages (n=3 mice per genotype per age group). (A) PHGDH, (B) PSAT1, (C) MTHFD2. Each dot represents an individual crypt (n=20 crypts per mouse). Error bars denote mean ±SD. Expression levels of all three enzymes increase at a significantly greater rate in *PolγA*$^{mut/mut}$ normal crypts compared to *PolγA*$^{mut/mut}$ normal crypts (****P<0.0001, ***P<0.001, **P<0.01, linear regression and analysis of covariance).

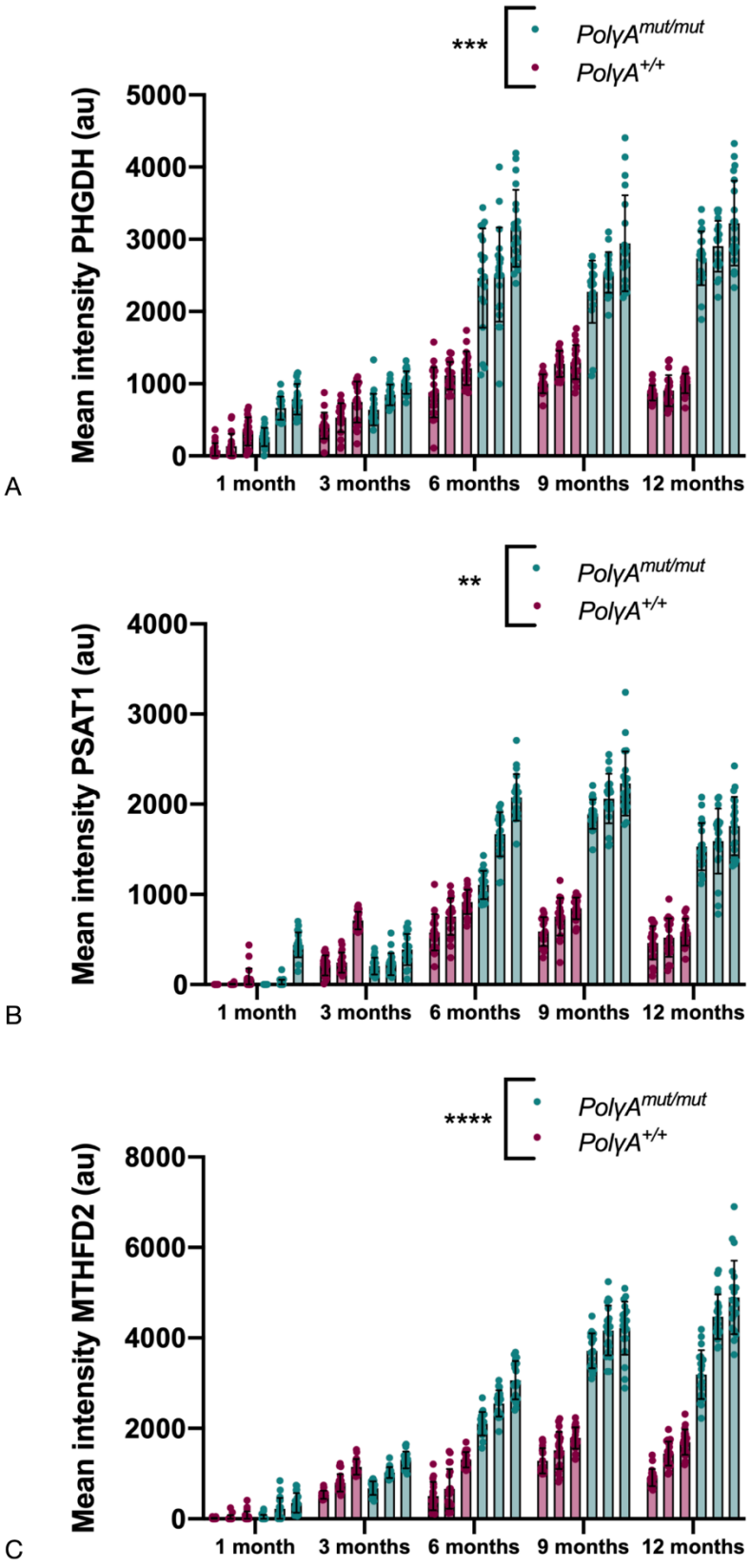

Figure 6-12. Quantification of the expression levels of PHGDH, PSAT1 and MTHFD2 in normal non-transformed small intestinal crypts of *PolγA*$^{+/+}$ and *PolγA*$^{mut/mut}$ mice of increasing ages (n=3 mice per genotype per age group). (A) PHGDH, (B) PSAT1, (C) MTHFD2. Each dot represents an individual crypt (n=20 crypts per mouse). Error bars denote mean ±SD. Expression of PHGDH increases at a significantly greater rate in *PolγA*$^{mut/mut}$ normal crypts compared to *PolγA*$^{mut/mut}$ normal crypts (***P<0.001, linear regression and analysis of covariance).

6.3.3. Serine synthesis pathway enzyme and mitochondrial OXPHOS protein immunofluorescence in human colon

In order to assess whether findings in the mouse model were translatable to humans, levels of PHGDH, PSAT1 and MTHFD2 in individual crypts from normal human colon samples were quantified using immunofluorescence. These levels were correlated with the levels of expression of mitochondrial OXPHOS subunit proteins, also quantified using immunofluorescence. 4µm serial sections were taken from multiple biopsies (where available) of normal colonic mucosa taken from 12 patients who had undergone either surgical colorectal tumour resection or polyp removal. The first section was labelled with antibodies against NDUFB8, MTCO1 and PHGDH. The second section was labelled with antibodies against NDUFB8, MTCO1 and TOMM20 in order to quantify OXPHOS proteins and categorise individual crypts as OXPHOS positive or deficient based on their Z-scores. The third and fourth serial sections were labelled with antibodies against NDUFB8, MTCO1 and one of either anti-PSAT1 or anti-MTHFD2. Using antibodies against NDUFB8 and MTCO1 in all serial sections assisted with the identification of the same crypts across all sections and also confirmed that expression of OXPHOS proteins was maintained throughout all sections. Sections were labelled according to the protocols outlined in 2.2.11.4.2., and imaged and analysed as detailed in section 2.2.12.5.2.

6.3.3.1. Categorisation of OXPHOS deficiency in normal human colonic crypts

As described in section 2.2.12.5.2., sections labelled with antibodies against OXPHOS components were analysed using Zen Lite microscope software (Zeiss). An example micrograph showing typical labelling is presented in Figure 6-13.

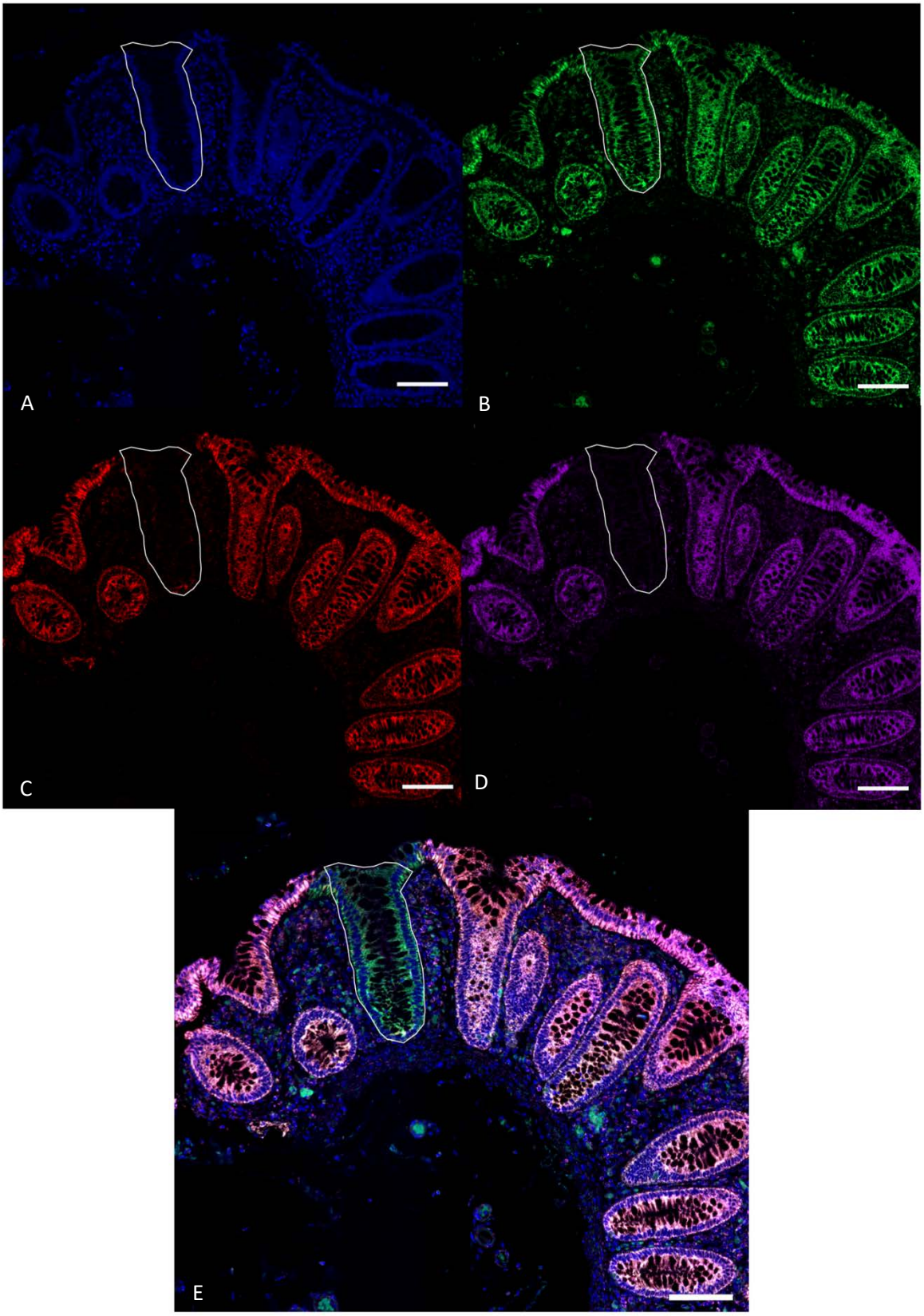

Figure 6-13. Example micrograph of OXPHOS subunit labelling in normal human colon. (A) Nuclei are labelled with Hoescht nucleic acid counterstain. (B) Anti-TOMM20 with Alexa Fluor488 conjugated secondary antibody labels mitochondria providing a measure of mitochondrial mass. (C) The MTCO1 subunit of mitochondrial complex IV is labelled with the use of an Alexa Fluor 546 conjugated secondary antibody. (D) The NDUFB8 subunit of mitochondrial complex I is labelled with an Alexa Fluor 647 conjugated secondary antibody. (E) Merge of all channels. Scale bars 100μm. A single crypt deficient in both MTCO1 and NDUFB8 is highlighted by the white line.

Colonic crypts with visually apparent reductions in the expression either NDUFB8 or MTCO1 or both proteins were categorised as OXPHOS deficient, whilst those displaying normal levels of these proteins were categorised as OXPHOS normal. All visually deficient crypts were selected and at least an equal number of normal crypts were selected per section. As such a method of analysis may be subjective, the generation of Z-score plots was used to confirm (or refute) the manual categorisation. Furthermore, expression of individual proteins was highly variable between patients, therefore Z-score generation facilitated standardisation of data and Z-score plots were generated as described in 2.2.12.4 and are presented with one plot per patient in Figures 6-14 and 6-15.

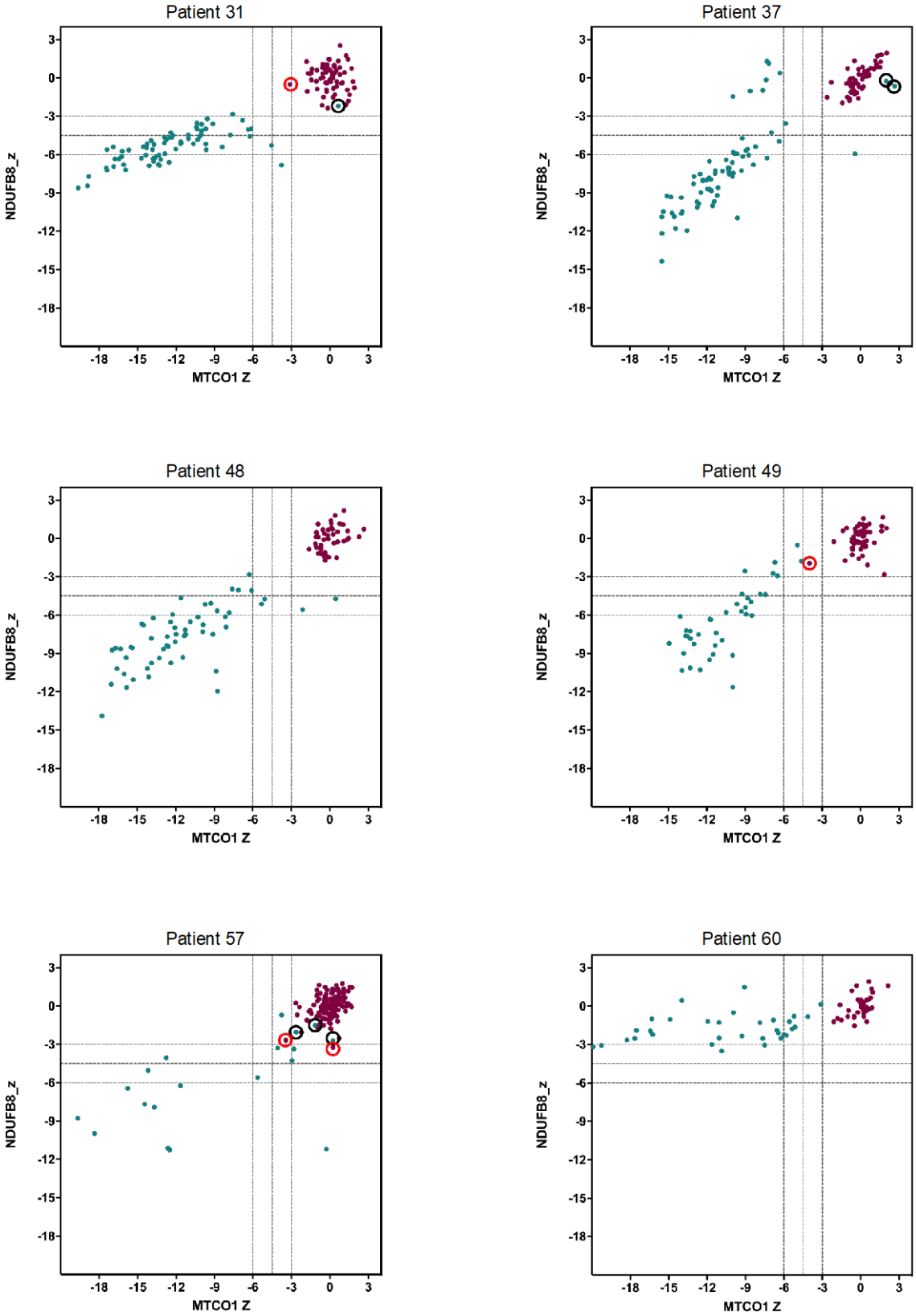

Figure 6-14. Z score plots generated in order to categorise normal human colonic crypts as OXPHOS normal or deficient in either NDUFB8 subunit of mitochondrial complex I or MTCO1 subunit of mitochondrial complex IV. Z-scores were calculated based on the control population (crypts expressing no visual deficiency of any protein) and all crypts thus categorised as normal ($z > -3$), intermediate positive ($-4.5 \leq z < -3.0$), intermediate negative ($-6 \leq z < -4.5$) and negative ($z < -6$) for each protein. Each dot represents an individual crypt. Black circles denote visually deficient crypts re-categorised as normal, red circles denote visually normal crypts re-categorised as deficient.

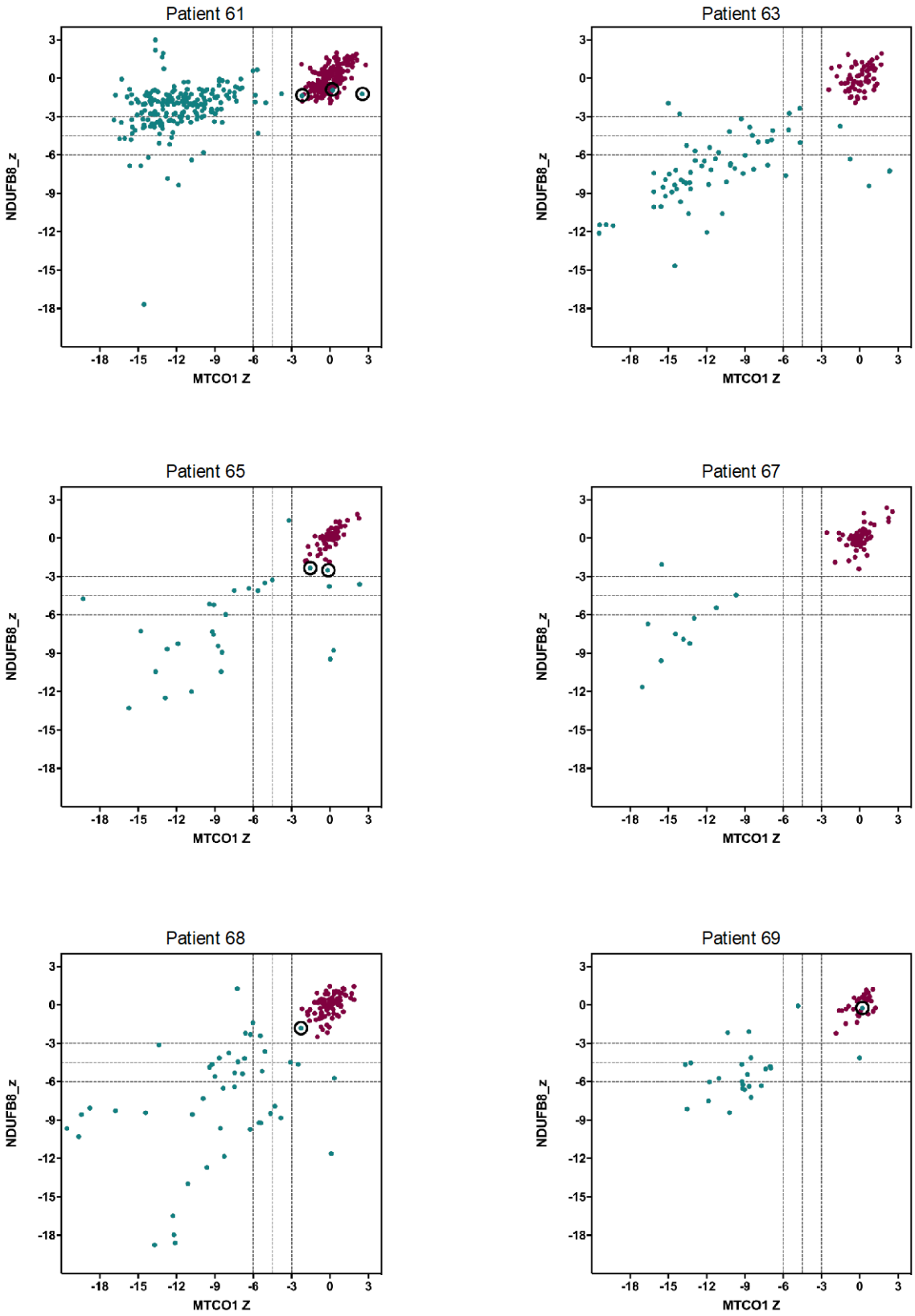

Figure 6-15. Z score plots generated in order to categorise normal human colonic crypts as OXPHOS normal or deficient in either NDUFB8 subunit of mitochondrial complex I or MTCO1 subunit of mitochondrial complex IV. Z-scores were calculated based on the control population (crypts expressing no visual deficiency of any protein) and all crypts thus categorised as normal ($z > -3$), intermediate positive ($-4.5 \leq z < -3.0$), intermediate negative ($-6 \leq z < -4.5$) and negative ($z < -6$) for each protein. Each dot represents an individual crypt. Black circles denote visually deficient crypts re-categorised as normal, red circles denote visually normal crypts re-categorised as deficient.

The frequency of OXPHOS deficient crypts in patient biopsies varied from n=10 in patient 67 up to n=202 in patient 61. Interestingly, at 60 years of age, patient 67 represents one of the youngest patients in the cohort with the fewest OXPHOS deficient crypts while patient 61 with the highest frequency of OXPHOS deficient crypts, represents the oldest patient in the cohort at 85 years of age. This is consistent with previously published findings (Greaves et al., 2012; Taylor et al., 2003). Similarly, the presence of a greater extent of complex IV than complex I deficiency is also supported by previous work (Greaves et al., 2010). In all patients, the proportion of OXPHOS deficient crypts categorised as MTCO1 negative was greater than the proportion categorised as NDUFB8 negative. No significant difference was detected between the mean frequencies of OXPHOS deficient crypts observed in male (63.5 ± 59.47) versus female (41.5 ± 23.57) patients (P=0.6828, unpaired Mann Whitney U test).

6.3.3.2. Correlation of serine synthesis pathway enzyme expression with OXPHOS status in normal human colonic crypts

Following the quantification of OXPHOS subunit proteins and categorisation of normal human crypts as OXPHOS normal or deficient, correlation of OXPHOS status with expression of PHGDH, PSAT1 and MTHFD2 expression was achieved by analysing the remaining serial sections. These three sections had been labelled with antibodies against one of the aforementioned SSP/1C enzymes in conjunction with antibodies targeting the NDUFB8 subunit of mitochondrial complex I and the MTCO1 subunit of mitochondrial complex IV. OXPHOS subunit labelling was used as a guide to map the same crypts across all serial sections and thus correlate SSP enzyme expression with OXPHOS status. As described in section 2.2.12.5.2., all sections were imaged using a Celldiscoverer 7 fluorescent microscope (Zeiss) and analysed using Zen lite microscope software (Zeiss). Example micrographs of representative labelling are presented in Figures 6-16, 6-17 and 6-18. The results of the analyses are presented in Figures 6-19, 6-20 and 6-21 for PHGDH, PSAT1 and MTHFD2 expression respectively.

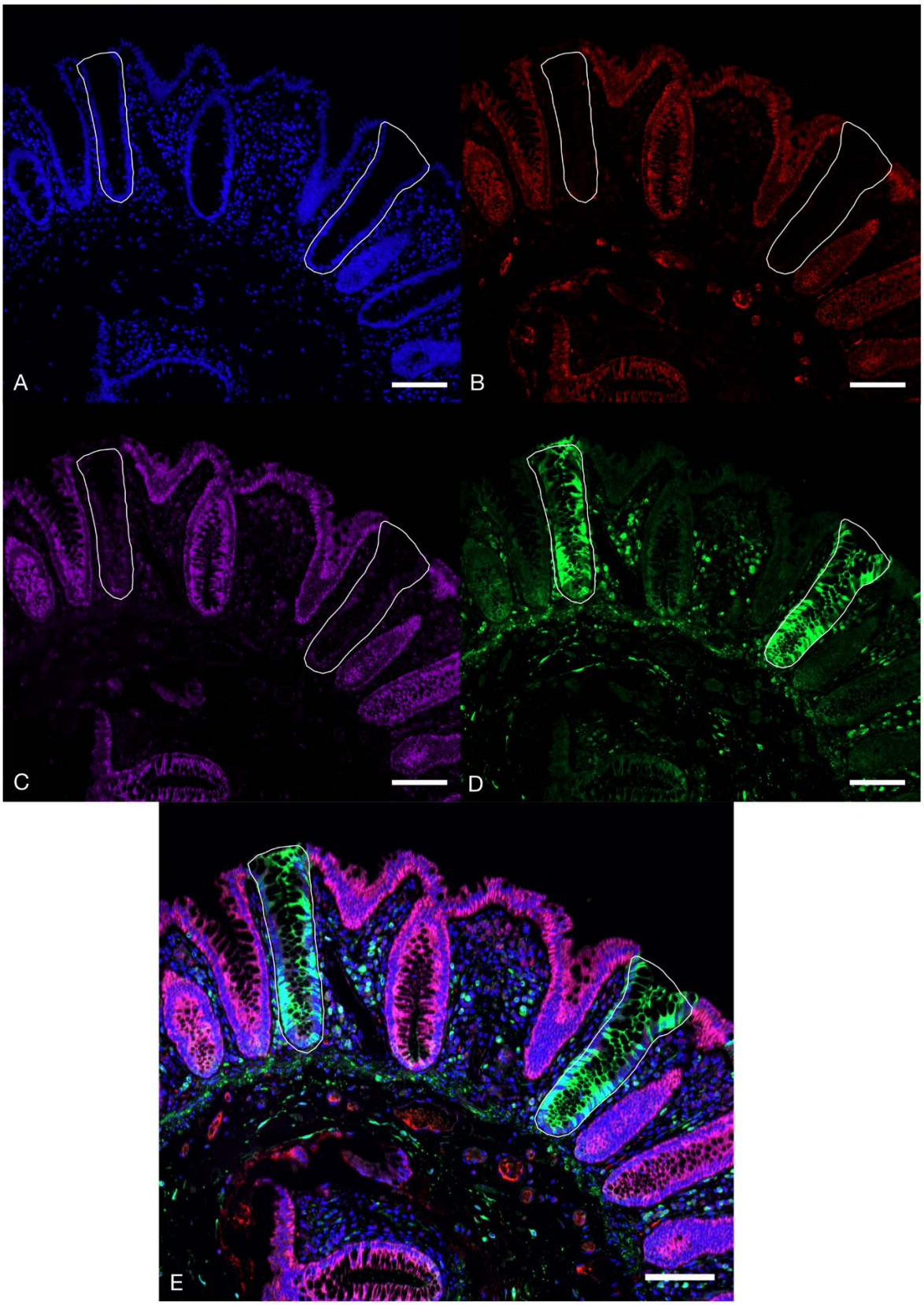

Figure 6-16. Example micrograph of PHGDH and OXPHOS subunit labelling in normal human colon. (A) Nuclei are labelled with Hoescht nucleic acid counterstain. (B) The MTCO1 subunit of mitochondrial complex IV is labelled with the use of an Alexa Fluor 546 conjugated secondary antibody. (C) The NDUFB8 subunit of mitochondrial complex I is labelled with an Alexa Fluor 647 conjugated secondary antibody. (D) PHGDH protein is visualised with an Alexa Fluor 488 conjugated secondary antibody (E) Merge of all channels. Scale bars 100μm. Two crypts deficient in both MTCO1 and NDUFB8 are highlighted by the white lines.

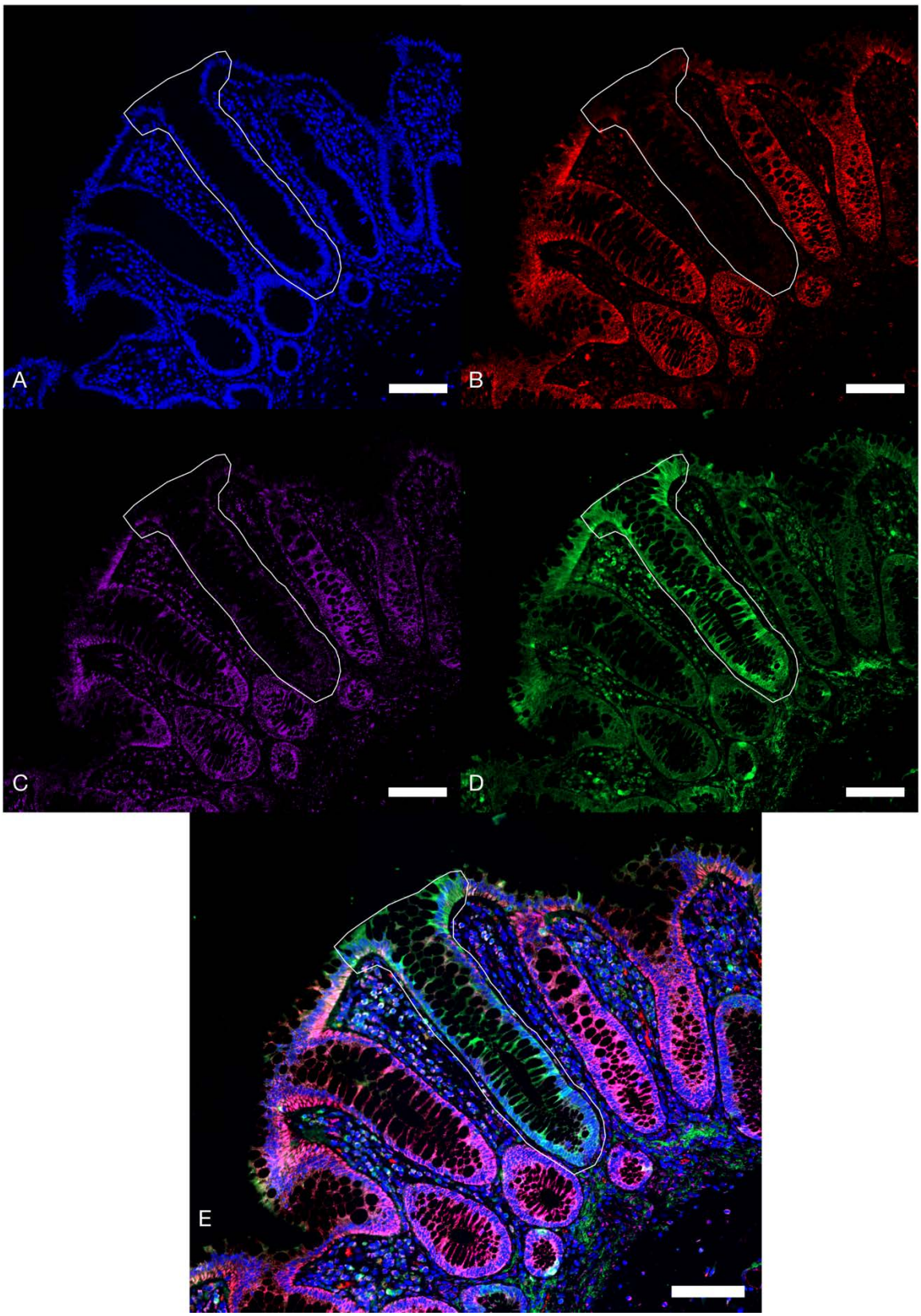

Figure 6-17. Example micrograph of PSAT1 and OXPHOS subunit labelling in normal human colon. (A) Nuclei are labelled with Hoescht nucleic acid counterstain. (B) The MTCO1 subunit of mitochondrial complex IV is labelled with the use of an Alexa Fluor 546 conjugated secondary antibody. (C) The NDUFB8 subunit of mitochondrial complex I is labelled with an Alexa Fluor 647 conjugated secondary antibody. (D) PSAT1 protein is visualised with an Alexa Fluor 488 conjugated secondary antibody (E) Merge of all channels. Scale bars 100μm. One crypt deficient in both MTCO1 and NDUFB8 is highlighted by the white line.

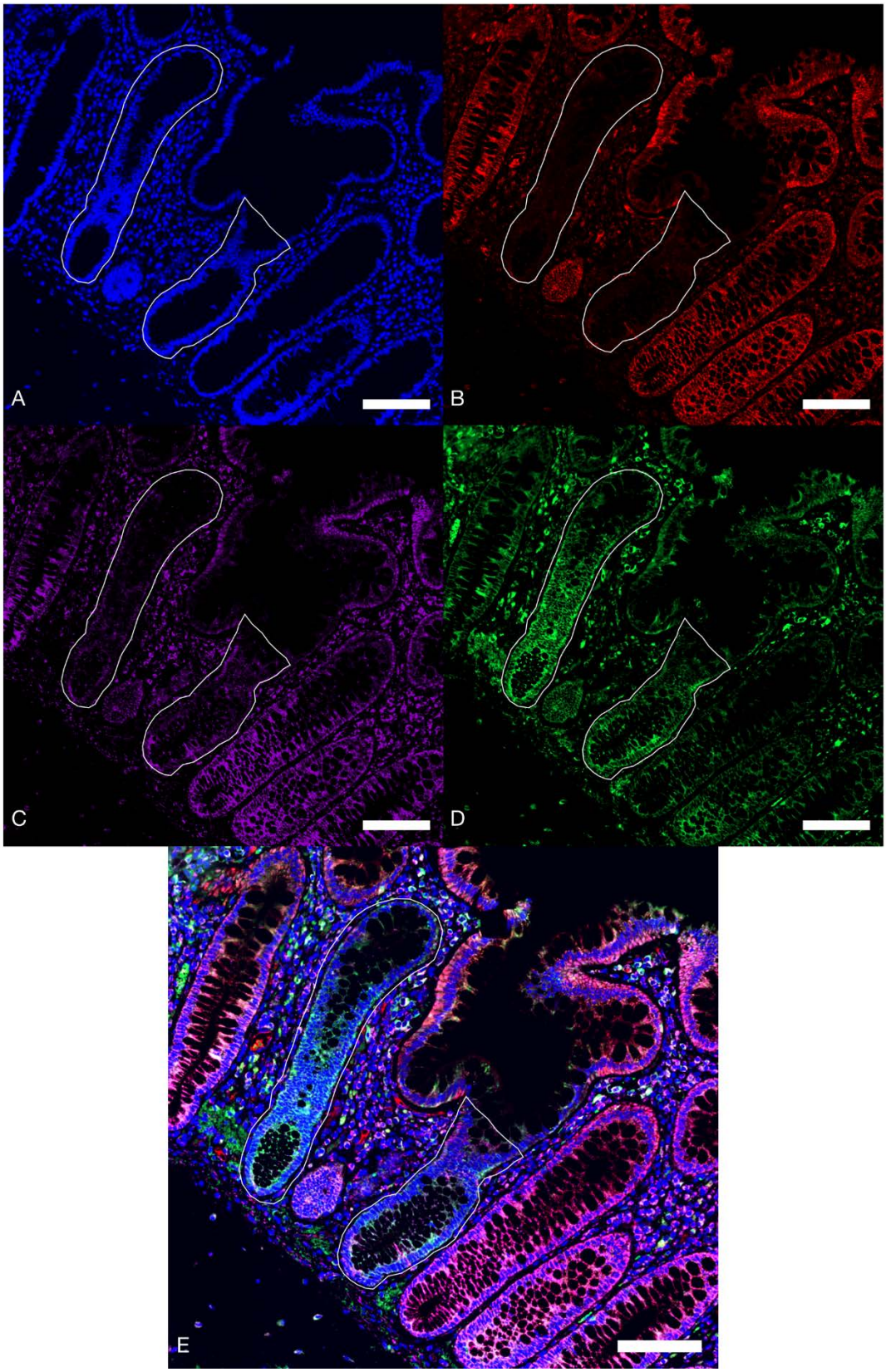

Figure 6-18. Example micrograph of MTHFD2 and OXPHOS subunit labelling in normal human colon. (A) Nuclei are labelled with Hoescht nucleic acid counterstain. (B) The MTCO1 subunit of mitochondrial complex IV is labelled with the use of an Alexa Fluor 546 conjugated secondary antibody. (C) The NDUFB8 subunit of mitochondrial complex I is labelled with an Alexa Fluor 647 conjugated secondary antibody. (D) MTHFD2 protein is visualised with an Alexa Fluor 488 conjugated secondary antibody (E) Merge of all channels. Scale bars 100μm. Two crypts deficient in both MTCO1 and NDUFB8 are highlighted by the white lines.

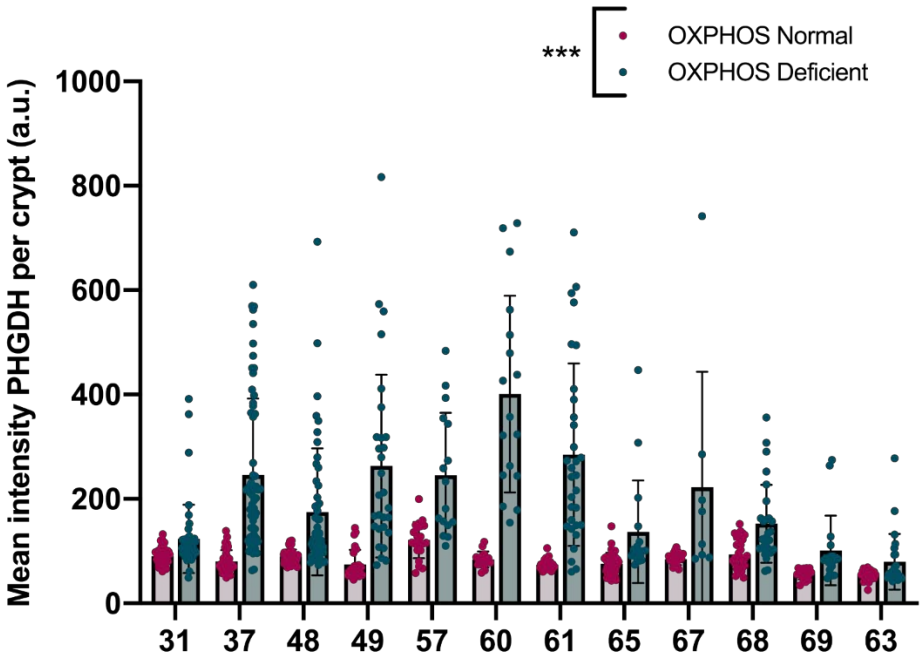

Figure 6-19. Quantification of the expression levels of PHGDH in non-transformed human OXPHOS normal and OXPHOS deficient crypts (n=12 patients). Each dot represents an individual crypt. Error bars denote mean ±SD. Levels of PHGDH expression are significantly greater in OXPHOS deficient compared to OXPHOS normal crypts. P<0.001, linear mixed effect model.

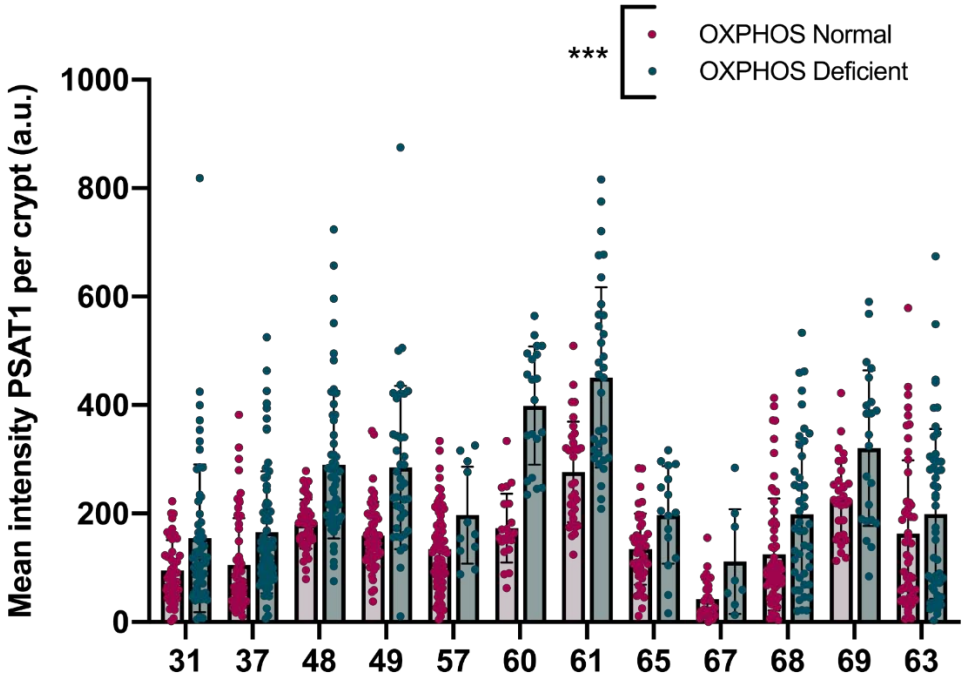

Figure 6-20. Quantification of the expression levels of PSAT1 in non-transformed human OXPHOS normal and OXPHOS deficient crypts (n=12 patients). Each dot represents an individual crypt. Error bars denote mean ±SD. Levels of PSAT1 expression are significantly greater in OXPHOS deficient compared to OXPHOS normal crypts. P<0.001, linear mixed effect model.

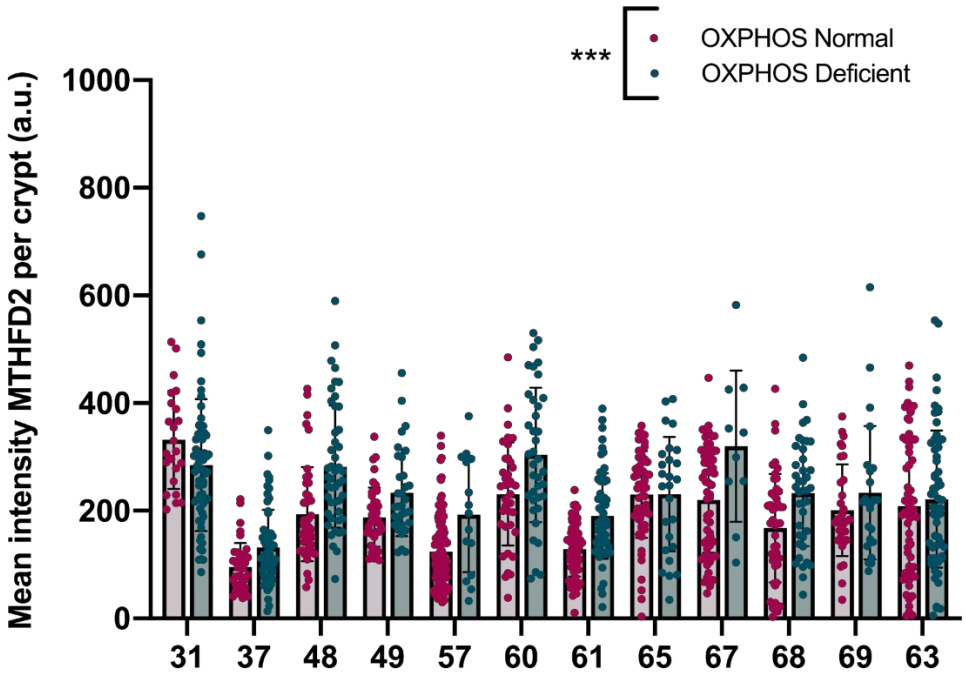

Figure 6-21. Quantification of the expression levels of MTHFD2 in non-transformed human OXPHOS normal and OXPHOS deficient crypts (n=12 patients). Each dot represents an individual crypt. Error bars denote mean ±SD. Levels of MTHFD2 expression are significantly greater in OXPHOS deficient compared to OXPHOS normal crypts. P<0.001, linear mixed effect model.

As shown by the immunofluorescent assay and linear mixed effect model, levels of all three enzymes were significantly higher in crypts with OXPHOS defects than those with normal OXPHOS protein expression within the normal ageing human colon. On a patient-by-patient basis applying multiple t-tests with a Holm-Sidak multiple comparisons p value adjustment, the expression of PHGDH is significantly greater in OXPHOS deficient versus OXPHOS normal crypts in all patients investigated. With regard to PSAT1 expression, all patients with the exception of patient 63 demonstrate a significantly greater expression of PSAT1 in OXPHOS deficient crypts compared to OXPHOS normal. With regard to MTHFD2 expression, eight out of twelve patients demonstrate a significantly increased MTHFD2 expression in OXPHOS deficient versus OXPHOS normal crypts also detected using a multiple t-test analysis with Holm-Sidak multiple comparisons p value adjustment. In the PHGDH analysis, three patients (37, 60 and 61) present with particularly significant expression of this enzyme in OXPHOS deficient versus OXPHOS normal crypts. At 85 years of age at the time of sampling, patient 61 is the oldest subject within the sample group by ten years and as such may represent a colonic crypt population in which longevity may have permitted the clonal expansion of early life acquired somatic mtDNA mutations to a greater level than may be observed in younger patients (Baines et al., 2014; Greaves et al., 2014) correspondingly eliciting a greater upregulation of PHGDH expression. Patient 60, which also represents the patient with the

most significant upregulation of PSAT1, interestingly displays a pattern of OXPHOS deficiency in which a complex IV defect is extensive whereas complex I expression is largely retained. The majority of OXPHOS deficient crypts (86.8%) demonstrate a normal expression of NDUFB8 ($z > -3$) and 13.2 % show minimal NDUFB8 protein loss and are categorised intermediate positive expression of NDUFB8 ($-4.5 \leq z < -3.0$). No crypts are categorised as intermediate negative or as negative for NDUFB8 expression ($-6 \leq z < -4.5$, $z < -6$ respectively). Similarly, patient 61 presents with 97.03% of OXPHOS deficient crypts as complex IV (MTCO1) negative ($z < -6$) whereas only 3.47% are categorised as complex I (NDUFB8) negative, 3.47% categorised as complex I intermediate negative ($-6 \leq z < -4.5$), 19.8% are complex I intermediate positive and the remaining 73.26% are categorised as complex I normal ($z > -3$). Ostensibly this may suggest a stronger association of serine synthesis pathway upregulation with complex IV deficiency as opposed to complex I deficiency in human colonic crypts, however, an induction of PHGDH expression of equal magnitude is also observed in patient 37 in which complex I deficiency is almost as extensive as that of complex IV (83.7% deficient crypts are complex I deficient, 98.39% deficient crypts are complex IV deficient). More likely, such observations reflect the typical pattern of OXPHOS deficiency within the ageing human colon, in that an isolated complex I deficiency is much less frequent than an isolated complex IV defect, with crypts deficient in multiple complexes being most commonly observed (Greaves et al., 2010). Taken together the results of these analyses suggest that the *de novo* serine synthesis pathway and mitochondrial one carbon cycle are both upregulated in normal aged human crypts expressing OXPHOS deficiency.

6.4. Discussion

As a result of molecular investigations carried out by Dr Julia Whitehall, a subset of differentially expressed transcripts was highlighted as being upregulated in the normal non-transformed small intestinal crypts of *PolγA*$^{mut/mut}$ versus *PolγA*$^{+/+}$ mice. Quantitative RT-PCR carried out by Dr Whitehall subsequently validated the expression of these transcripts (*Phgdh, Psat1, Psph, Mthfd2, Slc1a4 and Aldh1l2)* at the gene level detecting significantly increased levels of expression ($P<0.0005$) of all genes in *PolγA*$^{mut/mut}$ non-transformed small intestinal crypts versus those extracted from *PolγA*$^{+/+}$ mice. An immunohistochemical assay

targeting PHGDH, PSAT1 and MTHFD2 was applied to *PolγA*$^{mut/mut}$ and *PolγA*$^{+/+}$ colonic and small intestinal sections in which adenomagenesis had been induced at 6 months of age and animals culled at 23 days post induction. Representative images presented in Figures 6-3 and 6-4 depict an increased abundance of these proteins within both the normal crypt and adenoma compartments of *PolγA*$^{mut/mut}$ in comparison to *PolγA*$^{+/+}$ mice. These observations are supported by reports of increased *Psat1* (and *Psph*) mRNA levels in intestinal tissue from intestinal cancer model *Vil1-creER;Apc*$^{fl/fl}$ mice when compared to non-transformed mucosa in wild type animals (Maddocks et al., 2017). An increase in *Phgdh* levels was not detected in *Vil1-creER; Apc*$^{fl/fl}$ adenomas until the addition of a *Kras*^{G12D} mutation generating *Vil1-creER; Apc*$^{fl/f}$*; Kras*$^{G12D/+}$ mice, however the addition of this mutant allele enhanced the expression of SSP enzymes to a much greater extent. Again, this supports observations made here in which the addition of a potential accelerator mutation in the form of *PolγA*$^{mut/mut}$ serves to further amplify SSP enzyme expression.

It was hypothesised that an age-related mitochondrial dysfunction driven upregulation of the serine synthesis and mitochondrial one carbon metabolism pathways may provide the *PolγA*$^{mut/mut}$ intestine with an advantageous, pro-oncogenic environment should a transforming event such as the loss of *Apc* subsequently occur. To address this hypothesis, an ageing series of *PolγA*$^{mut/mut}$ and *PolγA*$^{+/+}$ mice were immunofluorescently labelled with antibodies against PHGDH, PSAT1 and MTHFD2. Analysis of both colonic and small intestinal crypts revealed a significant age-related increase in these proteins in response to increasing levels of OXPHOS deficiency in *PolγA*$^{mut/mut}$, an effect that was notably diminished in *PolγA*$^{+/+}$ intestinal crypts in which no OXPHOS deficiency is observed. A similar analysis with the addition of antibodies against mitochondrial OXPHOS components applied to normal non-transformed human colonic biopsies demonstrated a supporting pattern in which each SSP/one-carbon enzyme was shown to be upregulated in OXPHOS deficient crypts in comparison to OXPHOS normal crypts.

Given that mitochondria are intricately involved in one-carbon metabolism, it comes as little surprise that perturbations of mitochondrial function have downstream effects on this pathway and those that branch from it. The ‘Deletor’ mouse models a late-onset mitochondrial myopathy with progressive respiratory chain dysfunction caused by a dominant mutation of the nuclear-encoded mtDNA helicase, Twinkle (Tyynismaa et al.,

2005). In humans, mutations of this type manifest as an adult-onset progressive external ophthalmoplegia (PEO) with multiple mtDNA deletions occurring as the role of Twinkle in the maintenance of the integrity of mtDNA is compromised (Spelbrink et al., 2001). In order to characterise the physiological consequences, gene expression profiles from the skeletal muscle of 20 to 24-month-old Deletor mice were examined by the same group that developed the model (Tyynismaa et al., 2010). The group identified the upregulation of several genes previously associated with an amino acid starvation response, including *Mthfd2* and *Psat1*, their respective protein products being involved in one-carbon metabolism and *de novo* serine synthesis. The finding that alongside other upregulated genes, the *Mthfd2* gene bears an amino acid response element that can bind stress-response linked transcription factor family members (ATFs), in addition to the observation that *Atf5* was also upregulated in Deletor mouse muscle supports the hypothesis that mitochondrial dysfunction may induce a starvation-like stress response. Furthermore, the restoration of previously elevated levels of *Atf4, Atf5, Mthfd2,* all three SSP enzymes and mitochondrial unfolded protein response (mtUPR) markers in Deletor mouse muscle after treatment with the mTORC1 inhibitor rapamycin suggests that the mTORC1 pathway, a key regulator of protein synthesis, cell proliferation and autophagy, regulates this response (Khan et al., 2017; Saxton & Sabatini, 2017). Further investigations of Deletor skeletal muscle subsequently revealed an upregulated serine synthesis pathway with increased flux to the transsulphuration pathway resulting in increased glutathione synthesis. Levels of folate cycle intermediates were also affected, with Deletor skeletal muscle demonstrating significantly increased levels of certain species. A decreased level of formate, the end-product of the folate cycle and substrate for purine synthesis was also detected, suggesting an increased demand for purines in the model. Indeed, dNTP pools were found to be increased and imbalanced in the Deletor skeletal muscle. Interestingly, the same analysis performed in a mouse model bearing a recessive rather than dominant Twinkle mutation resulting in a phenotype of mtDNA depletion as opposed to multiple mtDNA deletions (infantile onset spinocerebellar ataxia – IOSCA) demonstrated the opposite effect on dNTP pools. Homology modelling proposed a mechanism of replisome stalling in the Deletor mouse driving increased dNTP synthesis, and a mechanism of increased NTP hydrolysis in the IOSCA mouse depleting dNTP pools. Human IOSCA and mitochondrial myopathy patients also showed evidence of metabolic remodelling, corroborating observations taken from the mouse models (Nikkanen et al., 2016).

Also, in humans, in a cellular model of mitochondrial DNA depletion, Bao and colleagues describe a strikingly similar scenario in which all SSP enzymes were upregulated in response to mtDNA depletion which was reversed by the inhibition of ATF4 (Bao et al., 2016). Mitochondrial folate metabolism was also impaired, with the generation of reduced folate species being favoured. The oxidation of folates requires NAD+ and as mitochondrial inhibition or dysfunction limits the availability of mitochondrial NAD+, it is proposed that a redox imbalance drives the impairment of mitochondrial folate metabolism. Branching from reduced folate species, an upregulation of the transsulphuration pathway was also inferred by transcriptional activation of transsulphuration genes and a significant decrease in cellular homocysteine. A low level of homocysteine remethylation to methionine suggested the conversion of homocysteine to cysteine by transsulphuration as being the dominant pathway (Bao et al., 2016). Patient derived cells harbouring pathogenic mutations of mitochondrial complex I also show altered glutathione levels, specifically a significant reduction in the ratio between reduced and oxidised glutathione (GSH/GSSG) further supporting the role that mitochondrial dysfunction has in the remodelling of folate metabolism and pathways that branch from it (Ni et al., 2019).

In order to adapt to stressors such as nutrient deprivation or an accumulation of unfolded proteins within the endoplasmic reticulum, cellular pathways have evolved which are now highly conserved means by which to combat such stress. Aberrations of mtDNA expression, present in both *PolγA*$^{mut/mut}$ mice and aged human tissues in which somatic mtDNA mutations have accumulated over time are able to induce stress responses in affected tissues. The first such mitochondria-specific response to be described; the mitochondrial unfolded protein response (UPR^{mt}) was characterised in cultured mammalian cells elicited by the expression of a mutant form of the mitochondrial matrix protein, ornithine transcarbamylase (OTC). An accumulation of mutant unfolded protein within the mitochondrial matrix reportedly resulted in the transcriptional upregulation of nuclear genes encoding mitochondrial stress proteins (Zhao et al., 2002). Further characterised in the *Caenorhabditis elegans* nematode worm, proteotoxic stress drives the relocation of stress activated transcription factor S1 (ATFS-1) from the mitochondria to the nucleus where amino acid response element (AARE) containing promoters are transcriptionally activated by ATFS-1. The subsequent transcription of mitochondrial heat shock proteins (HSPs), proteases and chaperones promote the folding or clearance of abnormal proteins, activating the stress

response (Haynes et al., 2013; Haynes et al., 2007). Analogous to ATFS-1 in the nematode worm are the ATF transcription factors 3-5 in mammals which, when subjected to stresses derived from mtDNA expression defects also initiate a transcriptional response driven by the induction of AARE-regulated genes. Unlike in the worm, the stress response activated by ATFs in mammals drives a minimal UPR^{mt} response and is instead characterised by the remodelling of multiple metabolic pathways, namely serine, glutathione, and purine biosynthesis. Described in the Deletor mouse model of late-onset mitochondrial myopathy with muscle specific remodelling of serine synthesis and one carbon metabolism (Nikkanen et al., 2016; Tyynismaa et al., 2010), this collective response has been termed the mitochondrial integrated stress response (ISR^{mt}) and is controlled by mTORC1 (Khan et al., 2017).

Coinciding with the appearance of COX deficient muscle fibres at around 12 months of age, the first stage of the ISR^{mt} is defined by a strong induction of transcription of *Fgf21, Mthfd2* and *Gdf15.* Fibroblast growth factor 21 (FGF21), is a circulating hormone-like cytokine with roles in the regulation of lipid metabolism and the fasting response (Badman et al., 2007; Kharitonenkov et al., 2005). Although primarily produced by the liver (Nishimura et al., 2000), FGF21 is also secreted from adipose tissue (Muise et al., 2008) and from the muscle of both mice and humans with muscle-manifesting mitochondrial disorders leading to its identification as a useful biomarker of myopathic mitochondrial diseases (Davis et al., 2013; Suomalainen et al., 2011; Tyynismaa et al., 2010). A member of the transforming growth factor-β (TGFβ) family; growth differentiation factor 15 (GDF15) is a cytokine that although elevated in several conditions such as cardiovascular disease (Wollert et al., 2017), cancer and chronic inflammation (Breit et al., 2011), it is also elevated in the circulation of mitochondrial disease patients and as such, like FGF21 , GDF15 has been identified as a mitochondrial disease biomarker (Davis et al., 2016; Yatsuga et al., 2015).

Following the initial transcriptional program of the ISR^{mt}, the metabolic phase of the response initiates at around 15 months of age in Deletor mice (Forsström et al., 2019).This involves the activation of serine synthesis pathway genes *Phgdh* and *Psat1* in addition to further elevation of mTORC1 and enhanced induction of *Atf5* which increases steadily from the initial ISR^{mt}. The induction of *Atf3* and *Atf4* begins to increase from this stage with an elevation in glucose uptake and transsulphuration in affected tissues. The final stage of the

ISR^{mt} in Deletor muscle is characterised by a mild UPR^{mt} response as shown by a slight increase in heat shock protein and protease expression between 21 and 24 months of age. The ISR^{mt} is shown to be conserved in human patients with mitochondrial myopathy caused by either single or multiple mtDNA deletions. RNA sequencing carried out on patient muscle biopsies demonstrated an increased level of *FGF21, MTHFD2, GDF15, PHGDH, PSAT1* and *ATF5* with the identification of additional upregulated transcripts namely *SHMT2, DDIT, ASNS and TRIB3.* Interestingly, this gene set bears a strong resemblance to significantly upregulated transcripts within non-transformed small intestinal crypts from our own 6-month-old *PolγA$^{mut/mut}$* mice. Our analysis did not detect an upregulation of *Shmt2 or Ddit* however all other transcripts correlate (*Atf5*, *Trib3, Phgdh, Psat1, Asns, Mthfd*2 and *Gdf15*), with one particularly notable absence; that of the master regulator of the ISR^{mt}; *Fgf21.* Given that increased serum levels of FGF21 are most strongly associated with muscle manifesting defects of mtDNA translation or maintenance (Lehtonen et al., 2016), it would seem appropriate that a muscle specific marker is absent from intestinal tissue. Furthermore, the induction of ISR^{mt} components and corresponding metabolic pathways in FGF21 knock out mouse embryonic fibroblasts with pharmacologically induced mtDNA translation defects demonstrates that while intrinsic to the ISR^{mt} in skeletal muscle, FGF21 is not an absolute requirement for the response in other cell types (Forsström et al., 2019).

Also, intriguingly absent from our upregulated gene set is *Atf4,* which Forsström et al report as a requirement for the ISR^{mt} in dividing cells. Here, the silencing of ATF4 using siRNA abrogates the expression of ATF3, CTH, PHGDH, MTHFD2, GDF15, and FGF21 in human fibroblasts. Numerous other works also report the central role of ATF4 in regulation of integrated stress responses and as such it is considered a master regulator (Harding et al., 2003; Rutkowski & Kaufman, 2003). ATF4 mRNA is ubiquitously expressed, however in response to stressors, expression of ATF4 protein is largely under translational control (Harding et al., 2000). Increased levels of ATF4 protein have thus been shown to occur without a corresponding elevation of mRNA following cAMP activation in hippocampal neurons (Harding et al., 2000; Yukawa et al., 1999) somewhat explaining the absence of differentially expressed levels of ATF4 mRNA in our analysis. In addition to genes identified as ATF4 dependant by Forsström et al., further members of our upregulated gene set on are reportedly dependent on ATF4. Following amino acid deprivation, *Atf4$^{-/-}$* mouse embryonic fibroblasts fail to upregulate *Asns, Trib3, Mthfd2*, and *Atf5* (Huggins et al., 2015). The

similarity of significantly upregulated transcripts in normal non-transformed *PolγA*$^{mut/mut}$ intestinal crypts to those which are upregulated in known responses to cellular stresses suggests the induction of an integrated stress response initiated by *PolγA* mediated mitochondrial dysfunction in our cohort. An age-related increase in the expression of serine synthesis and mitochondrial one carbon cycle enzymes in the normal non-transformed intestine of *PolγA*$^{mut/mut}$ mice as demonstrated using immunofluorescence supports the association of this pathway with an age-related accumulation of mtDNA mutations. This is also shown in normal ageing OXPHOS deficient human colonic crypts, however further investigations particularly in human tissues are warranted in order to ascertain the involvement of key mediators of the ISR^{mt} and thus the validity of a mechanistically analogous response in mitotic tissues. Interestingly, recent work carried out in the fruit fly, *Drosophila melanogaster*, has described an over-proliferation of eye progenitor cells which is initiated following disruption of the electron transport chain. The reduced expression of the Cox7a subunit of complex IV induced a glycolytic Warburg-like metabolism and associated reduction in cellular pH. This in conjunction with an eIF2a-kinase PERK-ATF4 mediated stress response, also induced by the Cox7a defect increased cellular sensitivity to Notch signalling resulting in substantial over proliferation (Sorge et al., 2020). This work further supports the notion that a similar stress response may be relevant in the human intestine.

Real-time PCR was carried out on laser micro dissected adenomas from *PolγA*$^{mut/mut}$ and *PolγA*$^{+/+}$ mice in which adenomagenesis was induced at 6 months of age followed by humane sacrifice 23 days later. Significant increases in gene expression of *Phgdh*, *Psph*, *Mthfd2* and *Aldh1l2* were detected in *PolγA*$^{mut/mut}$ compared to *PolγA*$^{+/+}$ mice (Smith et al., 2020; Whitehall, 2019). A wealth of evidence exists in which these genes and the pathways their protein products participate in are implicated in cancer. The 1940s saw the advent of interest in the role of one-carbon metabolism in cancer with the observation that a dietary deficiency of folate reduced the frequency of malignant cells in children with acute leukaemia (Farber & Diamond, 1948). Administration of the folic acid antagonist aminopterin provided these patients with a temporary remission of their condition as a direct result of inhibition of the folate cycle. By competing for the folate binding site of dihydrofolate reductase (DHFR), the enzyme responsible for the synthesis of tetrahydrofolate (THF) from dietary folate, aminopterin effectively blocks the synthesis of THF and thus one-carbon metabolism (Osborn et al., 1958). Similarly, the discovery that tumours were able to

synthesise serine (and glycine) from glucose drew attention to the *de novo* serine synthesis pathway and its involvement in cancer several decades ago (Kit, 1955). Analysis of the activity of enzymes involved in this pathway subsequently revealed their upregulation in neoplastic tissues of animal models of disease (Davis et al., 1970; Knox et al., 1969; Snell, 1985), and since then, numerous studies have reported the overexpression of SSP enzymes in multiple tumour types with inhibition of growth facilitated by the inhibition or knockdown of the enzymes (Pacold et al., 2016; Possemato et al., 2011). Exogenous serine also plays an important role in tumour survival, its removal inducing stress and reducing proliferation of cancers in which the *de novo* SSP is not amplified (Labuschagne et al., 2014; Maddocks et al., 2013).

With regard to regulation of the SSP and folate cycle in cancer, several oncogenes and tumour suppressors have been associated with the upregulation of these pathways. All three SSP enzymes are amplified by oncogenic cMYC, a transcription factor often aberrantly expressed in cancer (Sun et al., 2015). PHGDH expression has also been found to be positively regulated by the tumour associated transcription factors nuclear transcription factor Y (NFY) and specificity protein 1 (SP1) (Jun et al., 2008) and by the receptor tyrosine kinase oncogene HER2 in breast cancer cells (Bollig-Fischer et al., 2011). SSP enzyme expression is also regulated by epigenetic modifiers which have been shown to be elevated in multiple cancers. SSP enzyme transcription is promoted in a number of different human cancer cell lines by G9A, a H3K9 methyltransferase (Ding et al., 2013) while in Ewing sarcoma cell lines, the inhibition of the overexpressed histone methyltransferase MLL1 and scaffolding protein menin reduced the expression of SSP genes with confirmation of the requirement for the pathway being demonstrated by a reduced viability of PHGDH knock-down xenograft tumours in nude mice (Svoboda et al., 2018). Folate cycle enzymes have also been shown to be regulated by oncogenes and tumour suppressors, for example an enhanced expression of MTHFD2 is associated with activating *KRAS* mutations in non-small cell lung cancer (NSCLC) cell lines (Moran et al., 2014).

The loss of the p53 tumour suppressor, a common event in many human cancers, is largely associated with the gain of a proliferative advantage due to the role of the wild-type protein in the induction of senescence and cell death. Accompanying this proliferative advantage, however, is the loss of the metabolic plasticity that wild type p53 provides under conditions

of stress. Indeed, the depletion of serine from media reduced the proliferation and viability of $p53^{-/-}$ HCT116 cells more so than $p53^{+/+}$ cells (Maddocks et al., 2013). The mechanism by which $p53^{+/+}$ cells were able to adapt to serine starvation was attributed to the induction of p21, a mediator of cell cycle arrest which also facilitates the inhibition of nucleotide synthesis and the shunting of serine derived one-carbon units into glutathione production. Without the induction of this pathway and the subsequent production of glutathione, $p53^{-/-}$ cells are unable to detoxify increases in intracellular ROS associated with serine deprivation stress. Conversely, the loss of the tumour suppressor protein kinase C zeta type (PKCζ) augments the ability of colon cancer cell lines to resist glucose deprivation stress (Ma et al., 2013). Mechanistically, these cells demonstrate reduced levels of AMPK and associated autophagy and also maintain levels of mTOR in contrast to cells in which PKCζ is present and the converse is observed. Furthermore, it was noted that PKCζ deficient cells consumed more glutamine than controls and that ^{13}C-glutamine labelling followed the utilisation of this glutamine into the serine synthesis pathway. The subsequent gene expression analysis of SSP enzymes revealed that expression of PHGDH and PSAT1 was significantly greater in PKCζ deficient cells. These observations were corroborated in an *Apc*$^{Min/+}$ mouse model of intestinal cancer in which PKCζ deficiency promoted intestinal tumorigenesis (Ma et al., 2013). In support of these findings, Reina-Campos and colleagues describe a mouse model of prostate cancer in which tumorgenicity is enhanced by the deficiency of another atypical protein kinase C; protein kinase C lambda/iota (PKCλ/ι). PKCλ/ι deficiency was also associated with increased activation of mTOR and ATF4 and increased expression of *PHGDH*, *MTHFD2*, and *PSAT1* in prostate cancer cell lines (Reina-Campos et al., 2019).

The pyruvate kinase isoenzyme type-M2 (PKM2) which catalyses the final step of glycolysis is highly overexpressed in many tumour cells. While most adult tissues express the PKM1 isoform, tumour cells expressing the PKM2 isoform possess a proliferative advantage over those that do not as evidenced by xenograft models in which the PKM1 isoform grafts display a diminished tumour formation capacity (Christofk et al., 2008). A shift to the PKM2 isoform is required to drive the aerobic glycolysis favoured by tumour cells, however as the activity of PKM2 is regulated by the availability of serine, the metabolic remodelling it can facilitate extends beyond a simple glycolytic switch. In the absence of serine, PKM2 is inactive and as such the availability of glycolytic intermediates including the serine precursor 3PG increase in abundance. Indeed, by blocking the serine synthesis pathway, Ye and

colleagues demonstrate that under serine starvation, the proliferative advantage PKM2 colon carcinoma cells display results from increased flux through the SSP (Ye et al., 2012). Furthermore, the group demonstrate that in PKM1 cells, a reduction in mTOR activity and diminished proliferation is induced by serine starvation. In contrast, the activity of mTOR, a key oncogenic regulator of proliferation is maintained in PKM2 cells. As mTOR is reported to regulate the translation and stability of ATF4 mRNA (Park et al., 2017), and ATF4 increases the expression of all three SSP enzymes, it would appear that the PKM2 switch observed in many cancers has a key role in coordinating not only glycolysis but mTOR activation and serine synthesis.

As outlined in 6.1.1., serine and other amino acids donate one-carbon units to the folate and methionine cycles supporting methylation reactions and the synthesis of nucleotides, antioxidants and anabolic precursors. These processes are vital to cellular survival in general, however in the event of malignant transformation, the support of survival and proliferation becomes paramount to the growing tumour and these metabolic processes are rewired (reviewed in Hanahan & Weinberg, 2011). In order to replicate and proliferate, tumours require purine and pyrimidine nucleotides, both of which are synthesised using one-carbon units. As serine is a major one-carbon unit donor, the inhibition of its metabolism has been shown to negatively affect the synthesis of purine nucleotides when serine metabolism is inhibited via starvation (Labuschagne et al., 2014; Maddocks et al., 2016) or via deletion/knockdown of SHMT2, the mitochondrial enzyme responsible for the removal of 1C units from serine (Ducker et al., 2016; Kim et al., 2015). Accordingly, SHMT2 is often found to be upregulated in cancer (Jain et al., 2012; Lee et al., 2014). The synthesis of pyrimidine nucleotides is also reduced by the inhibition of serine metabolism, specifically via small molecule inhibition of PHGDH (Pacold et al., 2016). Following the 1C removal from serine and its conjugation to THF generating 5,10-methylene-THF, MTHFD2 facilitates the redox reactions that transfer 1C units through the mitochondrial folate cycle. MTHFD2 has also been shown to be amplified within multiple tumour types (Nilsson et al., 2014). Although its CRISPR-mediated knockout can be compensated for by the cytoplasmic folate pathway and addition of exogenous formate, the loss of MTHFD2 causes an accumulation of purine precursors which are static at the penultimate stage of synthesis due to a 10-formyl-THF deficiency caused by loss of MTHFD2 (Ducker et al., 2016).

A deficiency of purine nucleotides due to serine restriction has implications for cancer cells beyond that of the supply of building blocks for DNA and RNA synthesis. Maintenance of the methionine cycle relies on the generation of SAM from methionine using adenosine derived from ATP. ATP is synthesised *de novo* via the purine synthesis pathway using serine derived one-carbon units. If there is a paucity of serine derived carbon, *de novo* ATP synthesis is curtailed as is generation of SAM (Maddocks et al., 2016). As the primary mammalian methyl donor, SAM is critical in providing methyl groups for their transfer to metabolites, proteins, lipids, RNA and DNA, aberrations of the latter bearing significance in the development of cancer (reviewed in Kulis & Esteller, 2010).

Folate cycle reactions in the direction of 5,10-methylene-THF conversion to 10-formyl-THF generate NADPH from NADP+ in the cytoplasm catalysed by MTHFD1. Mitochondrial MTHFD2/2L catalyses the same reactions with the ability to use either NAD+ or NADP+ generating NADH and NADPH respectively, with an NAD+ cofactor being favoured by MTHFD2. The availability of these cofactors has far reaching consequences for the cell, in that they provide the reducing power required to drive the redox reactions essential to numerous biochemical, biosynthetic and metabolic pathways. The observation that folate flux through the mitochondria occurs at a rate in excess of that which is demanded for biosynthetic 1C delivery suggests that the concomitant production of NAD(P)H is an important function of the mitochondrial folate pathway (Ducker et al., 2016; Fan et al., 2014). In addition to the NADPH generated via the pentose phosphate pathway and malic enzyme, one-carbon metabolism contributes a significant proportion of this cofactor which can support lipogenesis and antioxidant defence, processes which are of particular importance in the highly proliferative, hostile malignant environment. Paradoxically, as many cancers overexpress the NAD+ dependant MTHFD2 which favours the 5,10-methylene-THF to 10-formyl-THF directionality of the folate cycle in the mitochondria, this would lead to consumption of NADPH as the reverse directionality is driven in the cytosol. The NADP+/NADPH ratio however may be restored by the activity of ALDH1L2 (aldehyde dehydrogenase 1 family member L2 or mitochondrial 10-formyl-THF dehydrogenase) which has also been reported to be overexpressed in cancer cell lines (Krupenko et al., 2010). ALDH1L2 catalyses the 'wasting' of one-carbon units from 10-formyl-THF releasing them as CO_2, regenerating THF and concomitantly generating NADPH. NADPH is required to reduce oxidised glutathione and as such the loss of *ALDH1L2* in HEK293 cells increases their

sensitivity to oxidative stress (Ducker et al., 2016). *Aldh1l2* is significantly upregulated in both the normal non-transformed intestinal crypts and adenomas of *PolγA*$^{mut/mut}$ mice in comparison to *PolγA*$^{+/+}$ (Whitehall, 2019) and as such may suggest the relevance of this mechanism in *PolγA*$^{mut/mut}$ oxidative stress defence. This is in agreement with the work of Meiser and colleagues, in which tumours of a more oxidative phenotype are associated with increased mitochondrial formate overflow; an alternate fate of mitochondrial 10-formyl-THF which due to its requirement for competent mitochondrial oxidative phosphorylation is hypothesised to be opposed in non-oxidative tumours (Meiser et al., 2018).

The implications of oxidative versus non-oxidative tumour types are further highlighted when considering the role of the mitochondrial folate cycle in the generation of another important reducing agent; NADH. Yang et al., describe a considerable contribution to the mitochondrial NADH pool as being mediated by serine catabolism via the mitochondrial folate cycle. An accumulation of NADH is toxic and as such under conditions which inhibit cellular respiration (thus reducing the utilisation of NADH by the electron transport chain), alternative mechanisms of NADH production such as TCA cycling, and *de novo* serine synthesis are inhibited. However, the mitochondrial folate cycle and key redox enzyme, MTHFD2 are unaffected by a high NADH/NAD+ ratio and serine catabolism by this route persists in the absence of evidence of product inhibition (Yang et al., 2020). Interestingly, in HCT116 colon cancer cells in which cellular respiration was inhibited by hypoxia or treatment with metformin, phenformin or rotenone, concurrent knock down of *MTHFD2* reduced the NADH/NAD+ ratio and as a result facilitated cell growth in these cells in comparison to respiration impaired cells in which MTHFD2 was retained (Yang et al., 2020). These observations are not in agreement with data presented here in which a defect of cellular respiration in the adenomas of *PolγA*$^{mut/mut}$ mice is associated with increased expression of serine synthesis and mitochondrial one carbon cycle enzymes hypothesised to facilitate their enhanced growth. The work of Yang et al., is also somewhat contradictory to others in which treatment with similar doses of metformin decrease the growth of *Vil1-creER; Apc*$^{fl/fl}$ organoids (Maddocks et al., 2017) and lung and adenocarcinoma cell lines (Gravel et al., 2014) which are deprived of serine. The actions of the biguanide anti-diabetic agent metformin are complex and include AMPK-dependent inactivation of mTORC1 exerting antiproliferative effects (Dowling et al., 2007; Zakikhani et al., 2006) and a similarly AMPK mediated inhibition of gluconeogenesis and induction of fatty acid oxidation and glucose

utilisation in the liver mechanistically driving the antidiabetic effects of the drug (Zhou et al., 2001). Furthermore, at low doses, metformin possesses antioxidant properties (Hou et al., 2010). With these complexities and the differences between acute pharmacological respiration inhibition in cultured cells and that of physiological systems at an organismal level in mind, it may be more biologically relevant to compare the findings the current work with those of the *in vivo* studies carried out by Yang et al. Although the contribution of serine to NADH was reported as elevated in NDUSF4 knockout mice compared to wild type animals, treatment with a dual SHMT1/2 inhibitor did not decrease NADH levels (Yang et al., 2020). Although evidently important in the systems described, the differences between this work and that of Yang et al., may represent differing mechanisms at play *in vivo* versus *in vitro* and also in acute pharmacological inhibition of cellular respiration as opposed to that associated with an age-related accumulation of mtDNA mutations. Prior to adenomagenesis, tissues within our experimental animals may have had sufficient time to adapt to an increasing NADH/NAD+ ratio and as such are less affected by this potentially toxic insult, perhaps with a shift towards reductive carboxylation contributing to their metabolic adaptation (Mullen et al., 2011).

Reductive carboxylation describes an alternative metabolic pathway, which in contrast to the canonical TCA which metabolises glucose and glutamine derived carbon in an oxidative manner, key reactions are reversed, and glutamine is used to generate TCA intermediates and acetyl-coA thus supporting lipid (Metallo et al., 2012), protein and nucleotide (Birsoy et al., 2015; Sullivan et al., 2015) synthesis reductively. In cells in which mitochondria have a normal oxidative capacity, glutamine is a major anaplerotic contributor thus facilitating the generation of biosynthetic precursors that branch from TCA intermediates (reviewed in DeBerardinis & Cheng, 2010). A continuous supply of biosynthetic precursors is essential to fuel the rapid growth of tumours, and an alternative reductive pathway that ensures this provision may be of particular importance in those tumours in which oxidative capacity may be compromised by defects of TCA enzymes or components of the mitochondrial electron transport chain (Mullen et al., 2011). Using metabolomics and stable isotope tracing in an osteosarcoma sarcoma cell line containing a mutation in the complex III *cytb* gene it was demonstrated that reductive carboxylation first requires the oxidation of alpha ketoglutarate (αKG) by αKG dehydrogenase generating NADH. The formation of NADPH from NADH by nicotinamide nucleotide transhydrogenase (NNT) reduces the NADP+/NADPH

ratio driving the reverse reductive reaction of NADPH-dependant isocitrate dehydrogenases 1 and 2 (IDH1 and IDH2) in the cytosol and mitochondria respectively (Mullen et al., 2014; Mullen et al., 2011). Moreover, the generation of NADPH by this means in addition to that generated by the oxidation of isocitrate by IDH2 in the mitochondria has been shown to reduce mitochondrial ROS (Jiang et al., 2016). Further evidence for the role of the NAD+/NADH ratio in supporting reductive carboxylation is taken from the use of mitochondrially targeted zinc-finger nucleases (mtZFNs) in creating isogenic cell lines with different levels of m.8993T>G heteroplasmy. Those with the highest levels of heteroplasmy demonstrated a reduced oxygen consumption rate, a lower NAD+/NADH ratio and a corresponding increased activation of cytosolic reductive carboxylation (Gaude et al., 2018). *In silico* modelling of the pathway noted a significant contribution of the activity of the cytosolic malate-aspartate shuttle enzyme malate dehydrogenase 1 (MDH1) to ATP generation suggesting an additional link to glycolysis. Indeed, hydrogen tracing of GAPDH derived NADH to cytosolic malate provided evidence that the glycolytic GAPDH is redox linked to the malate generating, NADH dependant *MDH1* (Gaude et al., 2018).

Support for the potential involvement of reductive carboxylation in our model comes from a functional metabolomic analysis carried out at the metabolomics facility at the Beatson Institute, Glasgow (Smith et al., 2020; Whitehall, 2019). *Ex vivo* small intestinal adenoma organoids from *PolγA*$^{+/+}$/*Lgr5-creER*/*Apc*$^{fl/fl}$ and *PolγA*$^{mut/mut}$/*Lgr5-creER*/*Apc*$^{fl/fl}$ were grown in $^{13}C_6$- labelled glucose and intra and extra cellular metabolites measured using high performance liquid chromatography-mass spectrometry (HPLC-MS). Firstly, an increased level of unlabelled αKG in *PolγA*$^{mut/mut}$ versus *PolγA*$^{+/+}$ adenomas suggests the derivation of this metabolite from a source other than glucose, potentially glutamine for reductive carboxylation. An increased NAD+/NADH ratio in *PolγA*$^{mut/mut}$ versus *PolγA*$^{+/+}$ adenoma organoids may suggest the increased activity of cytosolic NAD+ generating *MDH1.* The decreased levels of labelled citrate M+2, fumarate M+2 and malate M+2 in *PolγA*$^{mut/mut}$ versus *PolγA*$^{+/+}$ adenoma organoids does imply an impaired oxidative TCA turning, however it may also suggest an increased utilisation of these intermediates for example the use of citrate to generate acetyl-CoA and oxaloacetate for the synthesis of lipids and nucleotides (via aspartate) respectively. In order to investigate this further the tracing of labelled glutamine as opposed to glucose is required. Metabolite measurement at different time

points providing a flux analysis would assist greatly in elucidating the contribution of reductive carboxylation of glutamine in *PolγA*$^{mut/mut}$ adenomas.

6.5. Future work

Although *de novo* serine synthesis and mitochondrial folate enzyme quantification was carried out in the ageing human colon, limitations of this study are that the same analyses have not yet been performed in human carcinomas. An obvious next step is to investigate the patterns of OXPHOS dysfunction within the matched tumour biopsies from our patient cohort and correlate findings with the expression of serine and one carbon metabolism enzymes. Furthermore, the delineation of OXPHOS deficient crypts in the normal human colon samples into complex specific deficiencies may help in assigning an association of the upregulation of serine and one carbon metabolism with a defect of a particular OXPHOS protein. Additionally, the study may benefit from a quantitative analysis of the expression of these enzymes in our animal model as only a subjective immunohistochemical analysis has been performed in a small number of experimental animals thus far. With regard to the mechanism by which mitochondrial dysfunction may lead to the metabolic remodelling reported, it would be particularly interesting to investigate the involvement of mTORC1 signalling and mediators of the ISR^{mt} in both human tissues and those from our mouse model, potentially identifying a response in dividing tissues analogous to that which has been described post-mitotically.

As the overriding aim of biomedical research is to gain insights into the pathophysiology of disease with the view to ameliorating the conditions in question, the feasibility of therapeutically targeting identified vulnerabilities is of great importance. As evidence of the upregulation of the *de novo* serine synthesis and mitochondrial folate cycle pathways has been identified in association with an increased adenoma burden in our mouse model, a logical next step would be to examine the effect of pharmacologically inhibiting these pathways *in vivo*. The PHGDH inhibitor NCT-503 has been demonstrated to reduce the growth and increase necrosis of PHGDH-dependant xenograft breast tumours in mice, also inducing the consumption of one carbon units to regenerate serine from glycine. This subsequently reduces the availability of one carbon units required to synthesise purines and dTMP which may impair the growth of PHGDH-dependant tumours Importantly, NCT 503

appears to be well tolerated by the animal model and no weight loss was associated with administration (Pacold et al., 2016). Two further compounds; PKUMDL-WQ-2101 and PKUMDL-WQ-2201 have been reported to supress the growth of the same xenograft breast cancer line used by Pacold et al, by allosterically inhibiting PHGDH (Wang et al., 2017).

6.6. Conclusion

Following molecular investigations carried out by Dr Julia Whitehall, a subset of differentially expressed transcripts was identified as upregulated in the normal non-transformed small intestinal crypts of *PolγA*$^{mut/mut}$ versus *PolγA*$^{+/+}$ mice. These transcripts, relating to serine biosynthesis and uptake and mitochondrial folate metabolism were subsequently validated at the protein level *in vivo* and correspondingly shown to be upregulated in the normal non-transformed crypts and adenomas of *PolγA*$^{mut/mut}$ in comparison to *PolγA*$^{+/+}$ animals in both the colon and small intestine. With the use of a quantitative immunofluorescent assay, an age-related increase in the expression of each enzyme was also demonstrated in the ageing *PolγA*$^{mut/mut}$ non-transformed intestinal and colonic epithelium. This was not found to be as pronounced in the *PolγA*$^{+/+}$ epithelium suggesting that an age-related increase in the accumulation of somatic mtDNA mutations may drive this metabolic remodelling, possibly as part of a mitochondrial stress response. In the ageing human colon, the same metabolic remodelling was associated with OXPHOS deficient crypts also evidenced by a quantitative immunofluorescent assay. The importance of serine and one-carbon metabolism in the support of tumour growth and survival is well documented and findings described here may represent a protective cellular response to age-related mitochondrial dysfunction which, in the event of malignant transformation, provides those cells with a marked metabolic advantage over those in which mitochondrial function is retained.

Chapter 7. Final discussion

The overriding aim of this thesis was to investigate the effect of age-related mtDNA mutations on intestinal tumour development. This was achieved through the generation and characterisation of a novel mouse model of intestinal cancer in which *PolγA* mediated mtDNA mutation accumulation preceded the intestinal stem cell specific deletion of *Apc*. In mice harbouring both heterozygous and homozygous *PolγA* mutations and intermediate and high levels of age-related mitochondrial dysfunction respectively, the intestinal adenoma burden was found to be significantly larger in comparison with control $PolγA^{+/+}$ animals. Immunofluorescent labelling and quantification of mitochondrial OXPHOS proteins revealed a prominent complex I defect within $PolγA^{+/mut}$ and $PolγA^{mut/mut}$ adenomas in comparison with controls. Furthermore, double thymidine analogue labelling of experimental animals with subsequent immunofluorescent labelling of these analogues identified a significantly greater rate of cell replication within $PolγA^{mut/mut}$ intestinal adenomas in comparison with controls. Coupled with a reduced apoptotic index within $PolγA^{mut/mut}$ intestinal adenomas as detected using immunohistochemical methods, accelerated adenoma growth in $PolγA^{mut/mut}$ mice resulted in a significantly greater adenoma burden and decreased survival in comparison with $PolγA^{+/+}$ mice. Further investigations into molecular pathways perturbed in response to age-related mitochondrial OXPHOS defects in the mouse model were carried out by Dr Julia Whitehall and revealed an upregulation of transcripts encoding enzymes involved in serine biosynthesis, uptake and mitochondrial folate metabolism (Whitehall, 2019). Within the current work, these findings were validated in both mice and humans as demonstrated by increased levels of the enzymes PHGDH, PSAT1 and MTHFD2 within OXPHOS deficient intestinal crypts. The importance of serine and one carbon metabolism in cancer cells is well established, with these pathways being vital to the provision of nucleotides, antioxidants and anabolic precursors essential to maximal tumour growth (reviewed in Newman & Maddocks, 2017). Furthermore, the upregulation of these pathways in response to mitochondrial dysfunction (Bao et al., 2016; Nikkanen et al., 2016; Tyynismaa et al., 2010) supports the work presented in this thesis which collectively proposes that age-related mitochondrial dysfunction causes metabolic remodelling that in the event of a transforming mutation such as loss of *Apc*, contributes to accelerated intestinal adenoma growth. Presented in Figure 7-1 is a schematic depicting the hypothesised mechanism by which mtDNA mutations and OXPHOS defects contribute to tumorigenesis.

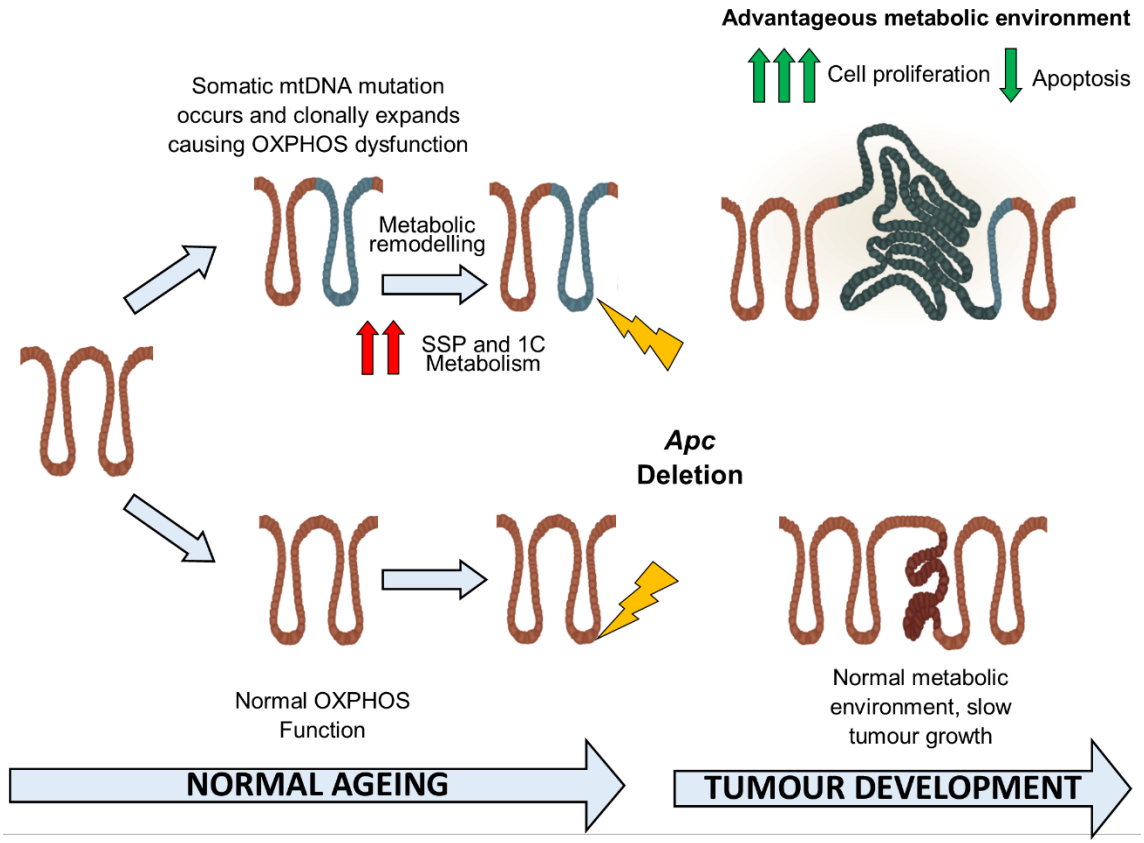

Figure 7-1. Schematic depicting the hypothesised mechanism by which mtDNA mutations and OXPHOS defects contribute to tumorigenesis.

Interestingly, the preservation of and indeed expansion of mtDNA mutations within intestinal crypts only applies to somatically acquired defects. In the instance of inherited mtDNA mutations, the opposite occurs, and these mutations are lost from replicating tissues with increasing age. Loss of the m.3243A>G mutation is observed in the blood (de Laat et al., 2012; Grady et al., 2018; Rahman et al., 2001) and epithelial tissues (Frederiksen et al., 2006; Olsson et al., 2001). With regard to the gastrointestinal tract specifically, loss of this mutation over time has been demonstrated in the oesophagus, stomach, and the small and large intestine (Su et al., 2018). Despite an absence of published work investigating the incidence of colorectal cancer in patients with inherited pathogenic mtDNA mutations, the differences observed with regard to the behaviour of inherited and age-associated somatic mtDNA mutations over time suggests that mitochondrial disease patients are not at increased risk of CRC. The loss of OXPHOS deficient cells in these patients would also be associated with the loss of any metabolic advantage and as such, it is surmised that the mechanism proposed in this thesis is only applicable with respect to somatically acquired mtDNA mutations.

As is the case with any experimental investigation there are limitations to this work; firstly, with regard to the *PolγA* mutator mouse model. As discussed in Chapter 3, the systemic effects of the *PolγA* mutation are extensive. While the characterisation of our *PolγA*/*Lgr5*$^{+/-}$/*Apc*$^{flox/flox}$ experimental animals and adenoma burden quantification implicated the significantly greater intestinal adenoma burden within *PolγA*$^{mut/mut}$ mice as the primary limiting pathology, the whole-body effect of the *PolγA* mutation cannot be excluded. Although in-depth FACS analysis of *PolγA*$^{+/+}$ and *PolγA*$^{mut/mut}$ mouse immune cell populations did not detect any significant differences in the small intestinal immune cell microenvironment between genotypes prior to *Apc* deletion (Smith et al., 2020), the impact of the *PolγA* mutation on cells comprising the tumour microenvironment has not been investigated within this work. Given the role inflammation in both the initiation of colitis associated colorectal cancer (Ekbom et al., 1990) and the promotion of sporadic CRC (Kojima et al., 2004), the enhancement of a pro-inflammatory response following immune stimulation as has been described within the *PolγA*$^{mut/mut}$ model (Logan et al., 2014) may represent an additional mechanism by which adenoma growth is promoted within the *PolγA*$^{mut/mut}$ intestine. Despite the similarity in mtDNA mutation gene location between *PolγA*$^{+/mut}$ mice and ageing humans (mutations are randomly distributed throughout the genome in both species), a significantly greater frequency of transversion mutations are observed in *PolγA*$^{+/mut}$ COX deficient crypts when compared with human COX deficient crypts (Baines et al., 2014). The majority of mutations in both species are transitions, however a predominance of C>T transitions is observed in the mutator mouse in comparison to the G>A prevalence within ageing crypts. Additionally, 10% of mutational changes within human COX deficient crypts comprise insertions/deletions whereas no such changes are identified in *PolγA*$^{+/mut}$ counterparts (Baines et al., 2014; Greaves et al., 2012). In addition to the observation that mtDNA mutations are accumulated at a significantly greater rate within *PolγA*$^{mut/mut}$ animals in comparison to humans (Khrapko et al., 2006), these considerations suggest the requirement for a more refined model in which to assess the contribution of age-related mtDNA mutation accumulations in intestinal adenoma growth.

In order to circumvent the limitation regarding the mutational spectrum associated with the *PolγA* mutator model, alternative models have been developed. The mito-APOBEC1 *Drosophila* model utilises the cytidine deaminase APOBEC1 (Apolipoprotein B (apoB) mRNA editing catalytic polypeptide 1) to specifically induce C:G>T:A transition mutations within the

mitochondrial genome (Andreazza et al., 2019). The usual physiological function of the APOBEC1 enzyme is ApoB mRNA editing via the catalysis of the deamination of cytosine to uracil residues. When targeted to the mitochondria, APOBEC1 induces C>U deamination within single stranded DNA, suggested to be exposed during the replication or transcription of the mitochondrial genome. In the absence of uracil repair by uracil-DNA glycosylase, subsequent replication pairs an adenine base with uracil, resulting in the C:G>T:A transition point mutation and associated mitochondrial dysfunction in the absence of deletions or DNA depletion (Andreazza et al., 2019). As this mutational profile is consistent with that of human ageing, the development of a similar system in the mouse would assist in improving the recapitulation of age-related mtDNA mutation accumulation in our model.

The use of an additional cytidine deaminase in mitochondrial genome editing has recently been described. In contrast to the single-stranded DNA activity of the APOBEC1 model, the so-named DddA bacterial cytidine deaminase catalyses this reaction within double-stranded DNA and has been engineered to allow base editing within specific mtDNA genes (Mok et al., 2020). In order to avoid the cell toxicity associated with intact DddA, the protein was split in half. By fusion with transcription activator-like effector array (TALE) proteins, each half was targeted to neighbouring DNA target sites where reconstitution of the protein facilitated cytidine deaminase activity and C:G>T:A transition mutation formation. In association with a mitochondrial targeting sequence (MTS) and a glycosylase inhibitor (UGI) to prevent uracil repair by uracil glycosylase, the split-DddA and TALE protein fusion (collectively termed DdCBE) was specifically targeted to mitochondrially encoded complex I genes. In comparison with control cells treated with inactive DdCBE, cells in which DdCBE was targeted to the *ND4* gene demonstrated reduced levels of oxidative phosphorylation and reduced complex I assembly and activity (Mok et al., 2020). Given the prominent complex I defect observed within intestinal adenomas in our model, the ability to specifically induce mutations homologous to those acquired during normal ageing within mitochondrial genes encoding complex I subunits would greatly enhance future studies. In the absence of such techniques in the mouse at present, the induction of specific mtDNA mutations into intestinal organoids would present the opportunity to assess the response of complex I deficient adenomas to small molecule inhibitors of serine synthesis enzymes and evaluate the potential therapeutic intervention accordingly.

The maintained growth of *PolγA*$^{mut/mut}$ derived intestinal organoids in comparison with the impaired growth the *PolγA*$^{+/+}$ organoids upon withdrawal of serine demonstrates the functional significance of the upregulation of serine synthesis pathway and mitochondrial one carbon cycle enzymes in adenoma growth (Whitehall, 2019). While the advantage of the *PolγA*$^{mut/mut}$ genotype and ensuing metabolic remodelling has been ascertained with regard to adenoma growth, the specific cellular outputs of the pathway have not been ascertained in this work. The use of additional dynamic metabolic flux analyses of adenoma organoids at multiple time points following ^{13}C carbon labelling would assist greatly in identifying which SSP cellular outputs are required. Additionally, the mass spectrometric analysis of specific folate cycle intermediates within both *PolγA*$^{+/+}$ and *PolγA*$^{mut/mut}$ derived intestinal organoids would assist in providing this information. For example, as the folate intermediate which donates 1C units to the methionine cycle and methylation reactions, an abundance of this cofactor would indicate a flux in this direction. Similarly, an increased level of 5,10-methenyl-THF and 10-formyl-THF would indicate flow in the direction of purine synthesis. The final outputs of each of these pathways may also be interrogated. As described by Maddocks and colleagues, by feeding cells with labelled serine followed by DNA and RNA isolation, nucleic acid hydrolysis and analysis by LCMS, the contribution of serine to methyl cytosine and methyl adenine labelling was assessed (Maddocks et al., 2016). This method may also be applied to our intestinal adenoma organoids as could the measurement of dNTP pools in order to investigate differences in purine and pyrimidine synthesis between *PolγA*$^{+/+}$ and *PolγA*$^{mut/mut}$ groups. The analysis of dNTP pools involves the DNA polymerase-catalysed incorporation of endogenous and radiolabelled dNTPs into a DNA template with the amount of resultant radioactivity indicating endogenous dNTP levels (Martí et al., 2012). Finally, while the HPLC-MS measurement of metabolites extracted from adenoma organoids following ^{13}C carbon labelling would assist in providing a measure of glutathione levels and thus activation of the transsulphuration pathway, additional measures of the activity of this pathway may be achieved with the quantification of hydrogen sulphide (H_2S) levels. As a by-product of transsulphuration, the measurement of H_2S levels either by HPLC with fluorescence detection or with mass spectrometric measurement of dissociated organoid cell extracts following the reaction with the thiol-specific monobromobimane may facilitate in providing a measure of activity this pathway (Shen et al., 2015). While western blot analysis of transsulphuration pathway enzymes would also provide a measure of pathway activation within adenoma organoids, immunohistochemical or immunofluorescent

interrogation of these enzymes within intestinal tissue sections would also be informative. The identification of the specific cellular requirements mediated by the upregulation of serine biosynthesis and mitochondrial one carbon metabolism in *PolγA*$^{mut/mut}$ adenomas may ultimately reveal metabolic vulnerabilities which could be exploited therapeutically.

While the effect of age-related mtDNA mutation and OXPHOS dysfunction in pre-malignant adenomatous lesions has been described within this study, the consequences of mitochondrial dysfunction at subsequent stages of the adenoma-carcinoma sequence is unknown. Interestingly, a recent study utilising existing exome sequencing data reported a significantly greater survival in 344 stage 1-3 colorectal cancer patients harbouring truncating mtDNA mutations or non-truncating, non-synonymous mutations in comparison to wild-type samples (Gorelick et al., 2020). Truncating mutations affecting complex I were reported in approximately 20% of cases and those affecting the remaining respiratory chain complexes accounted for roughly 5% of cases. The enrichment of truncating variants affecting complex I in this dataset supports work presented in this thesis in that complex I defects provide a phenotype advantageous to adenoma growth, however the survival data presented by Gorelick et al. subsequently questions that advantage at advanced adenoma-carcinoma sequence stages. Accordingly, further investigation is required, and the current work would benefit greatly from the analysis of a large cohort of human CRC samples in which the quantification of OXPHOS defects could be correlated with clinical phenotypes. In contrast to conventional immunofluorescent analyses, imaging mass cytometry (IMC) techniques utilise the conjugation of rare earth metals to antibodies of interest in place of fluorophores. This abrogates the limitations associated with fluorophore spectral overlap allowing a greater number of proteins to be investigated simultaneously. Antibody labelling followed by high resolution laser ablation and mass cytometry facilitates the quantification of target protein levels within single tissue sections (Giesen et al., 2014). The application of this technique to human CRC sections would allow simultaneous OXPHOS protein and SSP enzyme quantification without the requirement for serial sections as utilised in the current study. Alongside clinical data, this would allow the assessment of both the presence and impact of OXPHOS defects and SSP upregulation at later stages of colorectal cancer. Furthermore, the technique has been optimised at a single cell level within muscle biopsy sections within our department and has been found to generate results comparable to immunofluorescent analysis (Warren et al., 2020).

In tandem with the investigation of CRC samples at advanced stages, the use of additional transgenic mouse lines in which the progression from adenoma to adenocarcinoma and metastatic disease can be recapitulated would greatly improve this work by providing a model in which the impact of OXPHOS defects at each of these stages can be investigated. As described by Jackstadt et al., the enterocyte specific *VillinCre*^{ER} activation of *Kras*$^{G12D/+}$ and deletion of *Trp53*$^{fl/fl}$ in the presence or absence of *Apc*$^{fl/+}$ has been shown to model intestinal adenocarcinoma and invasive intestinal adenocarcinoma respectively in the mouse (Jackstadt et al., 2019). Furthermore, the addition of *Rosa26* mediated Notch1 receptor activation (*Rosa26*$^{N1icd/+}$) to the invasive adenocarcinoma model facilitates the development of metastases to the lymph nodes, lungs, liver, and/or diaphragm via transforming growth factor (TGF) β-dependent neutrophil recruitment (Jackstadt et al., 2019). As per experimental animals described in the current work, the accumulation of *PolγA* mediated mtDNA mutation accumulation prior to tamoxifen mediated intestinal tumorigenesis would allow the effect of age-related OXPHOS dysfunction on these advanced models to be observed. Alternatively, the use of a tetracycline/doxycycline (Tet-on/Tet-off) expression system (Gossen & Bujard, 1992) to temporospatially control the expression of nuclear genome encoded mitochondrial complex I subunits may provide another possible model. However, the off-target effects of this system must be considered as impaired mitochondrial translation and consequently respiratory function in addition to UPR^{mt} activation has been described as a result of the administration of tetracyclines in several models (Clark-Walker & Linnane, 1966; Houtkooper et al., 2013; Moullan et al., 2015).

As the overriding aim of biomedical research is to develop an understanding of the pathology in question, with a view to improving the prognosis of affected patients via therapeutic intervention and/or prevention, the implications of the current work on such interventions must be considered. Obesity is a well-known risk factor for colorectal cancer, and in comparison with the non-obese, obese patients harbour greater frequencies of OXPHOS deficient colonic crypts (Breininger, 2019). Often associated with obesity is a metabolic syndrome characterised by insulin resistance, hypertension and dyslipidaemia (Reaven, 1988). Given the chronic inflammatory component associated with metabolic syndrome, this obesity related disorder may increase mtDNA mutagenesis and thus the development of OXPHOS dysfunction. The management of weight may therefore reduce the

frequency of OXPHOS deficient crypts and accordingly impede the development of an advantageous metabolic phenotype should malignant transformation occur.

With regard to the prominent complex I defect observed within colonic and small intestinal adenomas within this study, it may be surmised that a reduced oxidation of NADH to NAD+ leads to a redox imbalance which if addressed may impair tumorigenicity. Declining levels of NAD+ with ageing have been shown to induce a pseudohypoxic state driven by the accumulation of HIF-1α. Notably, this phenotype was compared to a Warburg-like metabolism which was alleviated by NAD+ repletion (Gomes et al., 2013). Similarly, the oral administration of an NAD+ precursor, nicotinamide riboside (NR) to mitochondrial myopathy mice delayed early and late-stage disease progression via the induction of mitochondrial biogenesis in skeletal muscle and brown adipose tissue (Khan et al., 2014). The administration of another NAD+ precursor, nicotinamide mononucleotide (NMN) has also been shown to normalise the NAD+ redox imbalance, lower HIF1a accumulation and extend the lifespan of complex I deficient *Ndufs4* knock out mice (Lee et al., 2019). While treatment with NAD+ precursors has reportedly increased animal survival and inhibited tumour progression and metastases in xenograft models of breast cancer (Santidrian et al., 2013), the overexpression of nicotinamide mononucleotide adenylyl transferase 2 (NMNAT2), the final enzyme in the cytosolic NAD+ salvage synthesis pathway has been shown to correlate with stage and invasive depth of colorectal cancer (Cui et al., 2016; Qi et al., 2018). As such, an increased cellular NAD+ is associated with tumour progression and many enzymes of the NAD+ synthesis pathway have been assessed with regard to their application as anti-cancer agents. It would be very interesting to assess whether the administration of NAD+ precursors prior to *Apc* deletion in our experimental animals has any impact upon OXPHOS dysfunction and tumour burden.

In terms of treatment as opposed to prevention, in addition to the documented inhibition of cancer growth with SSP enzyme inhibition or knockdown in multiple tumour types (Pacold et al., 2016; Possemato et al., 2011), an interest in MTHFD2 inhibitors as anti-cancer agents is emerging. Selective inhibition or knockdown of *MTHFD2* has been shown to impair tumour growth in xenograft mouse models of CRC and reduce tumorigenesis and stem like properties in lung cancer cells (Ju et al., 2019; Nishimura et al., 2019). Additionally, Mthfd2 has recently been shown to maintain the pluripotency of mouse stem cells in part via its

indirect interaction with mitochondrial complex III maintaining *Uqcrc2* expression and oxidative phosphorylation (Yue et al., 2020). Interestingly, within our cohort, complex III protein levels remain largely unchanged between *PolγA*$^{mut/mut}$ normal non transformed crypts and adenomas. Although not significant, a slight increase in raw mean expression of *Uqcrfs1* is observed within *PolγA*$^{mut/mut}$ small intestinal adenomas in comparison with *PolγA*$^{mut/mut}$ normal crypts (Figure 4.15 C). Given the recent report that the oxidation of ubiquinol by complex III is necessary for the growth of osteosarcoma cells (Martínez-Reyes et al., 2020), this may represent a vulnerability which may be targeted therapeutically. The determination of patient tumour biopsy OXPHOS status in concert with SSP enzyme levels may therefore assist in predicting patient response to a particular treatment regimen, enhancing stratification and personalised medicine thus improving prognosis for CRC patients.

7.1. Concluding remarks

This thesis has presented the characterisation of a novel mouse model of intestinal cancer in which *PolγA* mediated mtDNA mutation accumulation preceded the intestinal stem cell specific deletion of *Apc*. The resultant adenomas within *PolγA*$^{mut/mut}$ animals displayed a prominent complex I defect in addition to a larger size driven by accelerated cell proliferation and reduced apoptosis in comparison with controls. Aided by the identification of a *PolγA*$^{mut/mut}$ transcriptomic and metabolic signature (Whitehall, 2019), the development of a permissive upregulation of the *de novo* serine synthesis pathway within both mouse and human OXPHOS deficient crypts prior to tumorigenesis was described. This work highlights a potential metabolic vulnerability of OXPHOS deficient colorectal tumours which upon further investigation may assist in the development of therapeutic regimens that target this vulnerability thus improving patient prognosis.

Appendices

7.2. Appendix A - Mice used in study

7.2.1. Lifespan and Day 23 mice

Mouse ID	Genotype	Date of birth	Date of death	Age at Cre induction (months)	Culled after Cre induction (days)	Sex
LPA 390	*PolyA$^{+/+}$/Lgr5creER/Apc$^{flox/flox}$*	5.12.2013	30.7.2014	6.9	30	Male
LPA 398	*PolyA$^{+/+}$/Lgr5creER/Apc$^{flox/flox}$*	28.12.2013	27.7.2014	6.1	27	Male
LPA 442	*PolyA$^{+/+}$/Lgr5creER/Apc$^{flox/flox}$*	30.1.2014	6.9.2014	5.9	39	Male
LPA 479	*PolyA$^{+/+}$/Lgr5creER/Apc$^{flox/flox}$*	2.3.2014	16.9.2014	5.8	22	Male
LPA 480	*PolyA$^{+/+}$/Lgr5creER/Apc$^{flox/flox}$*	2.3.2014	3.10.2014	5.8	39	Male
LPA 547	*PolyA$^{+/+}$/Lgr5creER/Apc$^{flox/flox}$*	9.7.2014	7.2.2015	6.2	27	Male
LPA 578	*PolyA$^{+/+}$/Lgr5creER/Apc$^{flox/flox}$*	22.9.2014	4.5.2015	6.2	36	Male
LPA 588	*PolyA$^{+/+}$/Lgr5creER/Apc$^{flox/flox}$*	9.9.2014	1.5.2015	6.7	33	Male
LPA 590	*PolyA$^{+/+}$/Lgr5creER/Apc$^{flox/flox}$*	9.9.2014	7.5.2015	6.7	40	Male
LPA 606	*PolyA$^{+/+}$/Lgr5creER/Apc$^{flox/flox}$*	2.10.2014	15.5.2015	6.4	33	Female
LPA 609	*PolyA$^{+/+}$/Lgr5creER/Apc$^{flox/flox}$*	1.10.2014	16.5.2015	6.4	34	Male
LPA 610	*PolyA$^{+/+}$/Lgr5creER/Apc$^{flox/flox}$*	1.10.2014	4.5.2015	6.4	22	Male
LPA 650	*PolyA$^{+/+}$/Lgr5creER/Apc$^{flox/flox}$*	24.10.2014	2.6.2015	6.6	23	Male
LPA 658	*PolyA$^{+/+}$/Lgr5creER/Apc$^{flox/flox}$*	26.10.2014	2.6.2015	6.5	23	Female
LPA 663	*PolyA$^{+/+}$/Lgr5creER/Apc$^{flox/flox}$*	7.11.2014	2.6.2015	6.1	23	Male
LPA 675	*PolyA$^{+/+}$/Lgr5creER/Apc$^{flox/flox}$*	29.11.2014	23.6.2015	6.1	23	Female
LPA 693	*PolyA$^{+/+}$/Lgr5creER/Apc$^{flox/flox}$*	10.11.2014	2.6.2015	6.0	23	Female
LPA 694	*PolyA$^{+/+}$/Lgr5creER/Apc$^{flox/flox}$*	10.11.2014	2.6.2015	6.0	23	Female
LPA 763	*PolyA$^{+/+}$/Lgr5creER/Apc$^{flox/flox}$*	20.12.2014	17.7.2015	6.1	23	Male
LPA 768	*PolyA$^{+/+}$/Lgr5creER/Apc$^{flox/flox}$*	22.12.2014	14.7.2015	6.0	23	Female
LPA 769	*PolyA$^{+/+}$/Lgr5creER/Apc$^{flox/flox}$*	22.12.2014	14.7.2015	6.0	23	Female
LPA 770	*PolyA$^{+/+}$/Lgr5creER/Apc$^{flox/flox}$*	22.12.2014	14.7.2015	6.0	23	Female
LPA 1089	*PolyA$^{+/+}$/Lgr5creER/Apc$^{flox/flox}$*	22.7.2015	16.2.2016	6.2	23	Male
LPA 1090	*PolyA$^{+/+}$/Lgr5creER/Apc$^{flox/flox}$*	22.7.2015	22.2.2016	6.2	29	Male
LPA 1257	*PolyA$^{+/+}$/Lgr5creER/Apc$^{flox/flox}$*	22.3.2016	28.10.2016	6.2	33	Male
LPA 1265	*PolyA$^{+/+}$/Lgr5creER/Apc$^{flox/flox}$*	30.3.2016	4.11.2016	5.9	40	Male
LPA 444	*PolyA$^{+/+}$/Lgr5creER/Apc$^{flox/flox}$*	30.1.2014	8.6.2015	14.0	72	Female

LPA 447	*PolyA$^{+/+}$/Lgr5creER/Apc$^{flox/flox}$*	30.1.2014	19.3.2015	14.0	83	Female
LPA 456	*PolyA$^{+/+}$/Lgr5creER/Apc$^{flox/flox}$*	2.2.2014	21.4.2015	13.9	22	Female
LPA 513	*PolyA$^{+/+}$/Lgr5creER/Apc$^{flox/flox}$*	13.5.2014	2.7.2015	12.0	53	Male
LPA 515	*PolyA$^{+/+}$/Lgr5creER/Apc$^{flox/flox}$*	13.5.2014	29.6.2015	12.0	50	Male
LPA 518	*PolyA$^{+/+}$/Lgr5creER/Apc$^{flox/flox}$*	22.5.2014	24.7.2015	12.4	55	Female
LPA 632	*PolyA$^{+/+}$/Lgr5creER/Apc$^{flox/flox}$*	16.10.2014	2.11.2015	11.9	22	Female
LPA 636	*PolyA$^{+/+}$/Lgr5creER/Apc$^{flox/flox}$*	16.10.2014	2.11.2015	11.9	22	Female
LPA 691	*PolyA$^{+/+}$/Lgr5creER/Apc$^{flox/flox}$*	10.11.2014	2.12.2015	12.0	24	Male
LPA 737	*PolyA$^{+/+}$/Lgr5creER/Apc$^{flox/flox}$*	16.12.2014	23.1.2016	12.7	19	Female
LPA 741	*PolyA$^{+/+}$/Lgr5creER/Apc$^{flox/flox}$*	16.12.2014	27.1.2016	12.7	23	Female
LPA 714	*PolyA$^{+/mut}$/Lgr5creER/Apc$^{flox/flox}$*	4.12.2014	26.6.2015	5.9	26	Female
LPA 716	*PolyA$^{+/mut}$/Lgr5creER/Apc$^{flox/flox}$*	4.12.2014	23.6.2015	5.9	23	Female
LPA 720	*PolyA$^{+/mut}$/Lgr5creER/Apc$^{flox/flox}$*	28.11.2014	7.7.2015	6.1	37	Female
LPA 721	*PolyA$^{+/mut}$/Lgr5creER/Apc$^{flox/flox}$*	28.11.2014	26.6.2015	6.1	26	Female
LPA 738	*PolyA$^{+/mut}$/Lgr5creER/Apc$^{flox/flox}$*	16.12.2014	14.7.2015	6.2	23	Female
LPA 743	*PolyA$^{+/mut}$/Lgr5creER/Apc$^{flox/flox}$*	16.12.2014	20.7.2015	6.2	39	Female
LPA 749	*PolyA$^{+/mut}$/Lgr5creER/Apc$^{flox/flox}$*	12.12.2014	20.7.2015	6.3	29	Female
LPA 764	*PolyA$^{+/mut}$/Lgr5creER/Apc$^{flox/flox}$*	20.12.2014	22.7.2015	6.1	31	Male
LPA 783	*PolyA$^{+/mut}$/Lgr5creER/Apc$^{flox/flox}$*	1.1.2015	19.7.2015	5.9	21	Female
LPA 785	*PolyA$^{+/mut}$/Lgr5creER/Apc$^{flox/flox}$*	1.1.2015	21.7.2015	5.9	23	Female
LPA 786	*PolyA$^{+/mut}$/Lgr5creER/Apc$^{flox/flox}$*	1.1.2015	28.7.2015	5.9	30	Female
LPA 787	*PolyA$^{+/mut}$/Lgr5creER/Apc$^{flox/flox}$*	1.1.2015	4.8.2015	6.4	23	Female
LPA 789	*PolyA$^{+/mut}$/Lgr5creER/Apc$^{flox/flox}$*	11.1.2015	7.8.2015	6.0	26	Male
LPA 793	*PolyA$^{+/mut}$/Lgr5creER/Apc$^{flox/flox}$*	11.1.2015	8.8.2015	6.0	27	Male
LPA 794	*PolyA$^{+/mut}$/Lgr5creER/Apc$^{flox/flox}$*	11.1.2015	17.8.2015	6.0	36	Male
LPA 795	*PolyA$^{+/mut}$/Lgr5creER/Apc$^{flox/flox}$*	11.1.2015	8.8.2015	6.0	27	Male
LPA 803	*PolyA$^{+/mut}$/Lgr5creER/Apc$^{flox/flox}$*	11.1.2015	4.8.2015	6.0	23	Female
LPA 849	*PolyA$^{+/mut}$/Lgr5creER/Apc$^{flox/flox}$*	20.2.2015	8.9.2015	5.9	23	Male
LPA 1295	*PolyA$^{+/mut}$/Lgr5creER/Apc$^{flox/flox}$*	12.4.2016	7.11.2016	6.2	22	Female
LPA 1268	*PolyA$^{+/mut}$/Lgr5creER/Apc$^{flox/flox}$*	12.4.2016	8.11.2016	6.2	23	Male
LPA 1290	*PolyA$^{+/mut}$/Lgr5creER/Apc$^{flox/flox}$*	21.4.2016	8.11.2016	5.9	23	Male
LPA 1882	*PolyA$^{+/mut}$/Lgr5creER/Apc$^{flox/flox}$*	24.10.2017	16.5.2018	6.0	23	Female
LPA 1886	*PolyA$^{+/mut}$/Lgr5creER/Apc$^{flox/flox}$*	24.10.2017	16.5.2018	6.0	23	Male
LPA 1889	*PolyA$^{+/mut}$/Lgr5creER/Apc$^{flox/flox}$*	21.10.2017	16.5.2018	6.1	23	Female
LPA 323	*PolyA$^{+/mut}$/Lgr5creER/Apc$^{flox/flox}$*	2.11.2013	29.1.2015	14.1	18	Female
LPA 341	*PolyA$^{+/mut}$/Lgr5creER/Apc$^{flox/flox}$*	30.10.2013	28.1.2015	14.2	17	Female
LPA 439	*PolyA$^{+/mut}$/Lgr5creER/Apc$^{flox/flox}$*	2.1.2014	29.3.2015	14.2	20	Female
LPA 587	*PolyA$^{+/mut}$/Lgr5creER/Apc$^{flox/flox}$*	9.9.2014	9.10.2015	12.4	19	Female

LPA 613	*PolγA$^{+/mut}$/Lgr5creER/Apc$^{flox/flox}$*	16.10.2014	7.11.2015	12.1	20	Female
LPA 619	*PolγA$^{+/mut}$/Lgr5creER/Apc$^{flox/flox}$*	14.10.2014	17.11.2015	12.0	36	Male
LPA 624	*PolγA$^{+/mut}$/Lgr5creER/Apc$^{flox/flox}$*	14.10.2014	1.11.2015	12.0	21	Female
LPA 625	*PolγA$^{+/mut}$/Lgr5creER/Apc$^{flox/flox}$*	13.10.2014	4.11.2015	12.0	24	Female
LPA 626	*PolγA$^{+/mut}$/Lgr5creER/Apc$^{flox/flox}$*	13.10.2014	22.12.2015	12.0	71	Female
LPA 631	*PolγA$^{+/mut}$/Lgr5creER/Apc$^{flox/flox}$*	13.10.2014	5.11.2015	12.0	25	Male
LPA 643	*PolγA$^{+/mut}$/Lgr5creER/Apc$^{flox/flox}$*	18.10.2014	20.11.2015	12.1	33	Male
LPA 644	*PolγA$^{+/mut}$/Lgr5creER/Apc$^{flox/flox}$*	18.10.2014	20.11.2015	12.1	33	Male
LPA 645	*PolγA$^{+/mut}$/Lgr5creER/Apc$^{flox/flox}$*	18.10.2014	20.11.2015	12.1	33	Male
LPA 660	*PolγA$^{+/mut}$/Lgr5creER/Apc$^{flox/flox}$*	5.11.2014	18.11.2015	12.2	10	Male
LPA 282	*PolγA$^{mut/mut}$/Lgr5creER/Apc$^{flox/flox}$*	19.8.2013	24.5.2014	8.3	26	Male
LPA 433	*PolγA$^{mut/mut}$/Lgr5creER/Apc$^{flox/flox}$*	2.1.2014	23.7.2014	5.9	23	Male
LPA 471	*PolγA$^{mut/mut}$/Lgr5creER/Apc$^{flox/flox}$*	20.2.2014	10.9.2014	6.2	16	Male
LPA 612	*PolγA$^{mut/mut}$/Lgr5creER/Apc$^{flox/flox}$*	16.10.2014	8.5.2015	5.9	26	Male
LPA 615	*PolγA$^{mut/mut}$/Lgr5creER/Apc$^{flox/flox}$*	14.10.2014	5.5.2015	6.0	23	Male
LPA 618	*PolγA$^{mut/mut}$/Lgr5creER/Apc$^{flox/flox}$*	14.10.2014	5.5.2015	6.0	23	Male
LPA 630	*PolγA$^{mut/mut}$/Lgr5creER/Apc$^{flox/flox}$*	13.10.2014	5.5.2015	6.0	23	Male
LPA 639	*PolγA$^{mut/mut}$/Lgr5creER/Apc$^{flox/flox}$*	18.10.2014	6.5.2015	5.8	24	Female
LPA 647	*PolγA$^{mut/mut}$/Lgr5creER/Apc$^{flox/flox}$*	18.10.2014	8.5.2015	5.8	26	Male
LPA 648	*PolγA$^{mut/mut}$/Lgr5creER/Apc$^{flox/flox}$*	18.10.2014	5.5.2015	5.8	23	Male
LPA 672	*PolγA$^{mut/mut}$/Lgr5creER/Apc$^{flox/flox}$*	11.11.2014	2.6.2015	6.0	23	Female
LPA 709	*PolγA$^{mut/mut}$/Lgr5creER/Apc$^{flox/flox}$*	28.11.2014	22.6.2015	6.1	22	Female
LPA 713	*PolγA$^{mut/mut}$/Lgr5creER/Apc$^{flox/flox}$*	4.12.2014	23.6.2015	5.9	23	Female
LPA 723	*PolγA$^{mut/mut}$/Lgr5creER/Apc$^{flox/flox}$*	28.11.2014	22.6.2015	6.1	22	Female
LPA 731	*PolγA$^{mut/mut}$/Lgr5creER/Apc$^{flox/flox}$*	28.11.2014	23.6.2015	6.1	23	Male
LPA 746	*PolγA$^{mut/mut}$/Lgr5creER/Apc$^{flox/flox}$*	12.12.2014	14.7.2015	6.3	23	Male
LPA 774	*PolγA$^{mut/mut}$/Lgr5creER/Apc$^{flox/flox}$*	1.1.2015	20.7.2015	5.9	22	Male
LPA 775	*PolγA$^{mut/mut}$/Lgr5creER/Apc$^{flox/flox}$*	1.1.2015	21.7.2015	5.9	23	Male
LPA 784	*PolγA$^{mut/mut}$/Lgr5creER/Apc$^{flox/flox}$*	1.1.2015	19.7.2015	5.9	21	Female
LPA 791	*PolγA$^{mut/mut}$/Lgr5creER/Apc$^{flox/flox}$*	11.1.2015	4.8.2015	6.0	23	Male
LPA 799	*PolγA$^{mut/mut}$/Lgr5creER/Apc$^{flox/flox}$*	11.1.2015	4.8.2015	6.0	23	Female
LPA 848	*PolγA$^{mut/mut}$/Lgr5creER/Apc$^{flox/flox}$*	20.2.2015	7.9.2015	5.9	22	Male
LPA 864	*PolγA$^{mut/mut}$/Lgr5creER/Apc$^{flox/flox}$*	4.3.2015	26.9.2015	6.2	20	Male
LPA 875	*PolγA$^{mut/mut}$/Lgr5creER/Apc$^{flox/flox}$*	6.3.2015	29.9.2015	6.1	23	Male
LPA 949	*PolγA$^{mut/mut}$/Lgr5creER/Apc$^{flox/flox}$*	24.4.2015	9.11.2015	5.9	22	Female
LPA 1068	*PolγA$^{mut/mut}$/Lgr5creER/Apc$^{flox/flox}$*	11.7.2015	1.2.2016	6.1	22	Male
LPA 1074	*PolγA$^{mut/mut}$/Lgr5creER/Apc$^{flox/flox}$*	11.7.2015	2.2.2016	6.1	23	Female
LPA 1180	*PolγA$^{mut/mut}$/Lgr5creER/Apc$^{flox/flox}$*	3.11.2015	25.5.2016	6.0	23	Male

7.2.2. Thymidine analogue labelled mice

Mouse ID	Genotype	Date of birth	Date of death	Age at Cre induction (months)	Culled after Cre induction (days)	Sex
LPA 1101	*PolγA$^{+/+}$/Lgr5creER/Apc$^{flox/flox}$*	13.8.2015	8.3.2016	6.4	16	Male
LPA 1102	*PolγA$^{+/+}$/Lgr5creER/Apc$^{flox/flox}$*	13.8.2015	8.3.2016	6.4	16	Male
LPA 1184	*PolγA$^{+/+}$/Lgr5creER/Apc$^{flox/flox}$*	14.12.2015	6.7.2016	6.3	16	Male
LPA 1196	*PolγA$^{+/+}$/Lgr5creER/Apc$^{flox/flox}$*	22.11.2015	7.6.2016	6.0	16	Male
LPA 1197	*PolγA$^{+/+}$/Lgr5creER/Apc$^{flox/flox}$*	22.11.2015	7.6.2016	6.0	16	Male
LPA 1115	*PolγA$^{mut/mut}$/Lgr5creER/Apc$^{flox/flox}$*	21.8.2015	8.3.2016	6.1	16	Female
LPA 1125	*PolγA$^{mut/mut}$/Lgr5creER/Apc$^{flox/flox}$*	29.8.2015	8.3.2016	5.8	16	Male
LPA 1176	*PolγA$^{mut/mut}$/Lgr5creER/Apc$^{flox/flox}$*	13.12.2015	6.7.2016	6.3	16	Male
LPA 1284	*PolγA$^{mut/mut}$/Lgr5creER/Apc$^{flox/flox}$*	2.5.2016	15.11.2016	6.0	16	Male
LPA 1285	*PolγA$^{mut/mut}$/Lgr5creER/Apc$^{flox/flox}$*	2.5.2016	15.11.2016	6.0	16	Male

7.2.3. 2mg tamoxifen mice

Mouse ID	Genotype	Date of birth	Date of death	Age at Cre induction (months)	Culled after Cre induction (days)	Sex
LPA 1185	*PolγA$^{+/+}$/Lgr5creER/Apc$^{flox/flox}$*	14.12.2015	3.10.2016	6.3	103	Female
LPA 1311	*PolγA$^{+/+}$/Lgr5creER/Apc$^{flox/flox}$*	3.5.2016	27.1.2017	6.2	78	Female
LPA 1374	*PolγA$^{+/+}$/Lgr5creER/Apc$^{flox/flox}$*	19.6.2016	30.6.2017	6.0	193	Male
LPA 1376	*PolγA$^{+/+}$/Lgr5creER/Apc$^{flox/flox}$*	19.6.2016	17.1.2017	6.0	28	Male
LPA 1377	*PolγA$^{+/+}$/Lgr5creER/Apc$^{flox/flox}$*	19.6.2016	6.4.2017	6.0	108	Male
LPA 1360	*PolγA$^{+/+}$/Lgr5creER/Apc$^{flox/flox}$*	30.6.2016	10.3.2017	6.0	36	Male
LPA 1647	*PolγA$^{+/+}$/Lgr5creER/Apc$^{flox/flox}$*	7.11.2016	20.6.2017	6.0	43	Male
LPA 1737	*PolγA$^{+/+}$/Lgr5creER/Apc$^{flox/flox}$*	16.3.2017	6.11.2017	6.8	29	Male
LPA 1786	*PolγA$^{+/+}$/Lgr5creER/Apc$^{flox/flox}$*	30.5.2017	15.1.2018	6.4	36	Male
LPA 1790	*PolγA$^{+/+}$/Lgr5creER/Apc$^{flox/flox}$*	30.5.2017	3.1.2018	6.4	24	Male
LPA 1288	*PolγA$^{+/mut}$/Lgr5creER/Apc$^{flox/flox}$*	2.5.2016	28.2.2017	6.0	102	Female
LPA 1312	*PolγA$^{+/mut}$/Lgr5creER/Apc$^{flox/flox}$*	22.5.2016	16.2.2017	5.6	68	Female
LPA 1314	*PolγA$^{+/mut}$/Lgr5creER/Apc$^{flox/flox}$*	3.5.2016	20.1.2017	6.3	71	Female
LPA 1316	*PolγA$^{+/mut}$/Lgr5creER/Apc$^{flox/flox}$*	3.5.2016	31.1.2017	6.3	82	Female

LPA 1321	*PolγA$^{+/mut}$/Lgr5creER/Apc$^{flox/flox}$*	22.5.2016	26.4.2017	6.3	149	Male
LPA 1473	*PolγA$^{+/mut}$/Lgr5creER/Apc$^{flox/flox}$*	8.8.2016	2.5.2017	5.9	90	Male
LPA 1564	*PolγA$^{+/mut}$/Lgr5creER/Apc$^{flox/flox}$*	25.9.2016	10.8.2017	6.0	137	Female
LPA 1565	*PolγA$^{+/mut}$/Lgr5creER/Apc$^{flox/flox}$*	25.9.2016	5.6.2017	6.0	71	Male
LPA 1566	*PolγA$^{+/mut}$/Lgr5creER/Apc$^{flox/flox}$*	25.9.2016	14.9.2017	6.0	172	Male
LPA 1567	*PolγA$^{+/mut}$/Lgr5creER/Apc$^{flox/flox}$*	25.9.2016	2.6.2017	6.0	68	Male
LPA 1584	*PolγA$^{+/mut}$/Lgr5creER/Apc$^{flox/flox}$*	10.10.2016	20.6.2017	6.0	72	Female
LPA 1618	*PolγA$^{+/mut}$/Lgr5creER/Apc$^{flox/flox}$*	18.10.2016	10.5.2017	6.0	23	Male
LPA 1843	*PolγA$^{+/mut}$/Lgr5creER/Apc$^{flox/flox}$*	31.7.2017	2.3.2018	6.0	25	Male
LPA 1848	*PolγA$^{+/mut}$/Lgr5creER/Apc$^{flox/flox}$*	31.7.2017	19.4.2018	6.0	73	Female
LPA 1341	*PolγA$^{mut/mut}$/Lgr5creER/Apc$^{flox/flox}$*	16.6.2016	30.1.2017	6.2	41	Female
LPA 1345	*PolγA$^{mut/mut}$/Lgr5creER/Apc$^{flox/flox}$*	18.6.2016	30.1.2017	6.1	41	Female
LPA 1408	*PolγA$^{mut/mut}$/Lgr5creER/Apc$^{flox/flox}$*	28.7.2016	6.3.2017	6.2	32	Female
LPA 1421	*PolγA$^{mut/mut}$/Lgr5creER/Apc$^{flox/flox}$*	1.8.2016	22.2.2017	6.0	24	Female
LPA 1475	*PolγA$^{mut/mut}$/Lgr5creER/Apc$^{flox/flox}$*	8.8.2016	23.3.2017	6.0	46	Male
LPA 1569	*PolγA$^{mut/mut}$/Lgr5creER/Apc$^{flox/flox}$*	22.9.2016	9.5.2017	5.9	51	Male
LPA 1588	*PolγA$^{mut/mut}$/Lgr5creER/Apc$^{flox/flox}$*	10.10.2016	3.5.2017	6.0	24	Female
LPA 1544	*PolγA$^{mut/mut}$/Lgr5creER/Apc$^{flox/flox}$*	14.9.2016	19.4.2017	6.2	31	Male
LPA 1831	*PolγA$^{mut/mut}$/Lgr5creER/Apc$^{flox/flox}$*	9.7.2017	2.2.2018	6.1	22	Male
LPA 1835	*PolγA$^{mut/mut}$/Lgr5creER/Apc$^{flox/flox}$*	9.7.2017	2.2.2018	6.1	22	Male
LPA 1851	*PolγA$^{mut/mut}$/Lgr5creER/Apc$^{flox/flox}$*	12.7.2017	13.2.2018	6.0	28	Female

7.2.4. Apc heterozygote mice

Mouse ID	Genotype	Date of birth	Date of death	Age at Cre induction (months)	Culled after Cre induction (days)	Sex
LPA 1128	*PolγA$^{+/+}$/Lgr5creER/Apc$^{flox/+}$*	4.9.2015	3.2.2017	4.1	396	Male
LPA 1130	*PolγA$^{+/+}$/Lgr5creER/Apc$^{flox/+}$*	4.9.2015	9.1.2017	4.1	371	Male
LPA 1140	*PolγA$^{+/+}$/Lgr5creER/Apc$^{flox/+}$*	4.9.2015	9.2.2017	4.1	402	Female
LPA 1143	*PolγA$^{+/+}$/Lgr5creER/Apc$^{flox/+}$*	4.9.2015	9.2.2017	4.1	402	Female
LPA 1145	*PolγA$^{+/+}$/Lgr5creER/Apc$^{flox/+}$*	8.9.2015	9.2.2017	3.9	402	Male
LPA 1148	*PolγA$^{+/+}$/Lgr5creER/Apc$^{flox/+}$*	8.9.2015	9.2.2017	3.9	402	Female
LPA 1191	*PolγA$^{+/+}$/Lgr5creER/Apc$^{flox/+}$*	2.12.2015	22.5.2017	4.3	407	Female
LPA 1192	*PolγA$^{+/+}$/Lgr5creER/Apc$^{flox/+}$*	2.12.2015	22.5.2017	4.3	407	Female
LPA 1417	*PolγA$^{+/+}$/Lgr5creER/Apc$^{flox/+}$*	27.7.2016	10.10.2017	4.3	310	Male

LPA 1137	*PolγA$^{+/mut}$/Lgr5creER/Apc$^{flox/+}$*	4.9.2015	9.2.2017	4.1	402	Female
LPA 1138	*PolγA$^{+/mut}$/Lgr5creER/Apc$^{flox/+}$*	4.9.2015	9.2.2017	4.1	402	Female
LPA 1147	*PolγA$^{+/mut}$/Lgr5creER/Apc$^{flox/+}$*	8.9.2015	26.7.2016	3.9	569	Male
LPA 1190	*PolγA$^{+/mut}$/Lgr5creER/Apc$^{flox/+}$*	2.12.2015	22.5.2017	4.3	407	Female
LPA 1411	*PolγA$^{+/mut}$/Lgr5creER/Apc$^{flox/+}$*	30.7.2016	10.1.2018	4.2	402	Female
LPA 1437	*PolγA$^{+/mut}$/Lgr5creER/Apc$^{flox/+}$*	1.8.2016	10.1.2018	4.2	402	Female
LPA 1455	*PolγA$^{+/mut}$/Lgr5creER/Apc$^{flox/+}$*	1.8.2016	23.10.2017	4.2	323	Male
LPA 1655	*PolγA$^{+/mut}$/Lgr5creER/Apc$^{flox/+}$*	25.11.2016	14.5.2018	3.8	421	Male
LPA 1657	*PolγA$^{+/mut}$/Lgr5creER/Apc$^{flox/+}$*	25.11.2016	14.2.2018	3.8	332	Male

7.2.5. Ageing mouse series – SSP enzyme expression

Mouse ID	Genotype	Date of birth	Date of death	Age at death (months)	Sex
POLG 2205	*PolγA$^{+/+}$*	5.4.2019	8.5.2019	1.1	Female
POLG 2206	*PolγA$^{+/+}$*	5.4.2019	8.5.2019	1.1	Female
POLG 2207	*PolγA$^{+/+}$*	5.4.2019	8.5.2019	1.1	Female
POLG 205	*PolγA$^{+/+}$*	9.4.2013	9.7.2013	2.9	Female
POLG 206	*PolγA$^{+/+}$*	9.4.2013	9.7.2013	2.9	Female
POLG 208	*PolγA$^{+/+}$*	9.4.2013	9.7.2013	2.9	Female
POLG 203	*PolγA$^{+/+}$*	21.11.12	3.6.13	6.34	Female
POLG 138	*PolγA$^{+/+}$*	21.5.12	20.11.12	6.01	Female
POLG 140	*PolγA$^{+/+}$*	21.5.12	20.11.12	6.01	Female
POLG 1168	*PolγA$^{+/+}$*	15.9.2016	28.3.2017	6.4	Female
POLG 1171	*PolγA$^{+/+}$*	15.9.2016	29.3.2017	6.4	Female
POLG 95	*PolγA$^{+/+}$*	10.4.2012	15.1.2013	9.2	Female
POLG 96	*PolγA$^{+/+}$*	10.4.2012	15.1.2013	9.2	Female
POLG 201	*PolγA$^{+/+}$*	21.8.2012	3.6.13	9.4	Female
POLG 202	*PolγA$^{+/+}$*	21.8.2012	3.6.13	9.4	Female
POLG 08	*PolγA$^{+/+}$*	13.9.2011	5.10.2012	12.75	Female
POLG 94	*PolγA$^{+/+}$*	10.4.2012	9.4.2013	11.96	Female
POLG 210	*PolγA$^{+/+}$*	21.8.2012	20.08.2013	11.96	Female
POLG 1180	*PolγA$^{+/+}$*	8.9.2016	12.9.2017	12.2	Male
POLG 2187	*PolγA$^{mut/mut}$*	17.3.2019	14.4.2019	0.99	Female
POLG 2211	*PolγA$^{mut/mut}$*	18.4.2019	16.5.2019	0.92	Male
POLG 2214	*PolγA$^{mut/mut}$*	18.4.2019	16.5.2019	0.92	Female
POLG 215	*PolγA$^{mut/mut}$*	19.6.2013	17.9.2013	3.29	Female
POLG 220	*PolγA$^{mut/mut}$*	21.6.2013	17.9.2013	2.89	Female
POLG 221	*PolγA$^{mut/mut}$*	26.6.2013	17.9.2013	2.89	Female
LPA 134	*PolγA$^{mut/mut}$*	21.1.2013	9.4.2013	2.53	Female

POLG 126	*PolγA*$^{mut/mut}$	17.5.2012	20.11.2012	6.14	Female
POLG 129	*PolγA*$^{mut/mut}$	15.5.2012	20.11.2012	6.21	Female
POLG 150	*PolγA*$^{mut/mut}$	20.6.2012	15.1.2013	6.87	Female
POLG 194	*PolγA*$^{mut/mut}$	10.12.2012	18.6.2013	6.21	Female
POLG 73	*PolγA*$^{mut/mut}$	2.4.2012	30.1.2013	9.95	Female
POLG 115	*PolγA*$^{mut/mut}$	24.4.2012	30.1.2013	9.23	Female
POLG 118	*PolγA*$^{mut/mut}$	24.4.2012	30.1.2013	9.23	Female
POLG 161	*PolγA*$^{mut/mut}$	17.8.2012	21.5.2013	9.1	Female
POLG 199	*PolγA*$^{mut/mut}$	6.6.2012	9.4.2013	10.09	Female
POLG 63	*PolγA*$^{mut/mut}$	2.4.2012	9.4.2013	12.22	Female
POLG 74	*PolγA*$^{mut/mut}$	2.4.2012	9.4.2013	12.22	Female
POLG 78	*PolγA*$^{mut/mut}$	2.4.2012	9.4.2013	12.22	Female
POLG 88	*PolγA*$^{mut/mut}$	2.4.2012	9.4.2013	12.22	Female

nature cancer

ARTICLES

https://doi.org/10.1038/s43018-020-00112-5

Check for updates

Age-associated mitochondrial DNA mutations cause metabolic remodeling that contributes to accelerated intestinal tumorigenesis

Anna L. M. Smith[1,2,10], Julia C. Whitehall[1,2,10], Carla Bradshaw[1,2], David Gay[3,4], Fiona Robertson[1,5], Alasdair P. Blain[1,5], Gavin Hudson[1,2], Angela Pyle[1,2], David Houghton[1,5], Matthew Hunt[1,5], James N. Sampson[1,5], Craig Stamp[1,2], Grace Mallett[5], Shoba Amarnath[5], Jack Leslie[6], Fiona Oakley[6], Laura Wilson[7], Angela Baker[1,5], Oliver M. Russell[1,5], Riem Johnson[1,5], Claire A. Richardson[5], Bhavana Gupta[1,2], Iain McCallum[5], Stuart A. C. McDonald[8], Seamus Kelly[5], John C. Mathers[9], Rakesh Heer[7], Robert W. Taylor[1,5], Neil D. Perkins[2], Doug M. Turnbull[1,5], Owen J. Sansom[3,4] and Laura C. Greaves[1,2]✉

Oxidative phosphorylation (OXPHOS) defects caused by somatic mitochondrial DNA mutations increase with age in human colorectal epithelium and are prevalent in colorectal tumors, but whether they actively contribute to tumorigenesis remains unknown. Here we demonstrate that mitochondrial DNA mutations causing OXPHOS defects are enriched during the human adenoma/carcinoma sequence, suggesting that they may confer a metabolic advantage. To test this, we deleted the tumor suppressor *Apc* in OXPHOS-deficient intestinal stem cells in mice. The resulting tumors were larger than in control mice due to accelerated cell proliferation and reduced apoptosis. We show that both normal crypts and tumors undergo metabolic remodeling in response to OXPHOS deficiency by upregulating the de novo serine synthesis pathway. Moreover, normal human colonic crypts upregulate the serine synthesis pathway in response to OXPHOS deficiency before tumorigenesis. Our data show that age-associated OXPHOS deficiency causes metabolic remodeling that can functionally contribute to accelerated intestinal cancer development.

Fundamental changes in the cellular metabolism of tumor cells were first observed in 1956 by Otto Warburg, who showed that tumor cells preferentially utilize glycolysis for ATP production over mitochondrial oxidative phosphorylation (OXPHOS)[1,2]. This was termed aerobic glycolysis, or the Warburg effect. Warburg suggested that a key event in carcinogenesis was injury to the respiratory machinery, and subsequent analysis of mitochondrial function showed that OXPHOS was frequently downregulated in many tumors[3]. This shift to glycolysis results in less efficient production of ATP, but has been shown to confer selective advantages during oncogenesis via other mitochondrial processes such as resistance to apoptosis[4], diversion of glycolytic intermediates into pathways required for cellular biomass production via one-carbon metabolism[5], and reactive oxygen species (ROS) production[6].

Defects in the OXPHOS system are also a common feature in a number of human aging tissues[7–10]. The colorectal epithelium is particularly susceptible to the accumulation of crypts deficient in complexes I and IV[11–13], with an average of 15% of crypts being OXPHOS deficient at the age of 70 years[13]. The underlying causes of the OXPHOS defects in the aging colonic epithelium are somatic mutations of the mitochondrial DNA (mtDNA). Human mtDNA is a circular, multicopy genome of ~16.6 kilobases that is found within the mitochondrial matrix and encodes 13 essential subunits of the OXPHOS system, together with 22 transfer RNAs and two ribosomal RNAs, to support the synthesis of mtDNA-encoded proteins within the organelle. As there are multiple copies of mtDNA in individual cells, mutant and wild-type mtDNA can co-exist in a situation termed heteroplasmy, or all copies can be the same, termed homoplasmy. Most mtDNA mutations are functionally recessive; somatic mtDNA mutations must clonally expand to high levels of heteroplasmy within an individual cell before a defect in the OXPHOS system becomes manifest[14]. The downstream metabolic consequences of such mutations in the rapidly proliferating colonic epithelial cells are largely unknown, although studies of other proliferative cell lines taken from patients with primary mtDNA disease have shown evidence of metabolic rewiring similar to that of cancer cells as a compensatory response to promote cell survival[15]. mtDNA mutations at very high levels of heteroplasmy, or homoplasmy, have also been detected in a number of tumor types[16], including in 60–70% of colorectal cancers[17–19]. In silico predictions have suggested that

[1]Wellcome Centre for Mitochondrial Research, Newcastle University, Newcastle upon Tyne, UK. [2]Biosciences Institute, Newcastle University, Newcastle upon Tyne, UK. [3]Cancer Research UK Beatson Institute, Glasgow, UK. [4]Institute of Cancer Sciences, University of Glasgow, Glasgow, UK. [5]Translational and Clinical Research Institute, Newcastle University, Newcastle upon Tyne, UK. [6]Newcastle Fibrosis Research Group, Biosciences Institute, Newcastle upon Tyne, UK. [7]Newcastle Cancer Centre, Translational and Clinical Research Institute, Newcastle University, Newcastle upon Tyne, UK. [8]Centre for Tumour Biology, Barts Cancer Institute, Queen Mary University of London, London, UK. [9]Human Nutrition Research Centre, Population Health Sciences Institute, Newcastle University, Newcastle upon Tyne, UK. [10]These authors contributed equally: Anna L. M. Smith, Julia C. Whitehall.
✉e-mail: laura.greaves@ncl.ac.uk

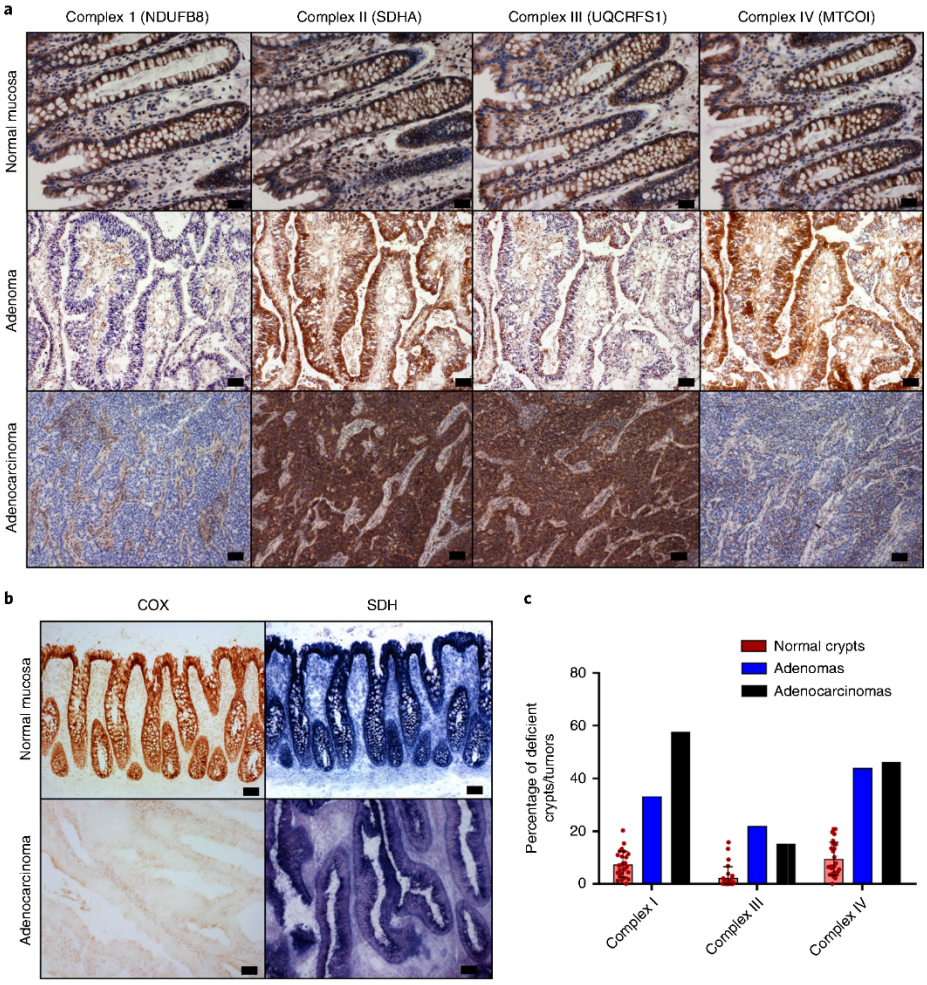

Fig. 1 | OXPHOS subunit IHC and histochemical analysis of human colorectal adenomas and adenocarcinomas. a, IHC was performed on 26 adenocarcinoma samples and patient-matched normal mucosa and nine colonic adenoma samples. Representative images show OXPHOS subunit expression in normal mucosa (CSC024), an adenoma (AD07) and an adenocarcinoma (CSC024). **b**, COX and SDH histochemistry was performed on the same samples as in **a**. Representative images of normal colonic mucosa and adenocarcinoma from CRC009 are shown. **c**, Quantification of the mean percentage of normal crypts per subject with defects in the specified OXPHOS subunits (each dot represents the mean percentage of OXPHOS-deficient crypts in each subject; $n = 26$ subjects; error bars are s.e.m.) and the percentage of adenomas ($n = 9$) and adenocarcinomas ($n = 26$) analyzed with defects in the specified OXPHOS subunits. Scale bars, 20 μm (**a**) and 50 μm (**b**).

mtDNA mutations that are likely to be detrimental to OXPHOS function are particularly enriched in colorectal tumors[16]. Age is the biggest risk factor for colorectal cancer development[20], and given the fact that pathogenic mtDNA mutations are a common feature of both normal aging colorectal crypts and colorectal tumors, we wanted to address the question of whether age-related mtDNA mutations are playing a role in colorectal cancer development.

Results

We hypothesized that if age-related mtDNA mutations present in non-transformed colonic epithelium[13,21] contribute to colorectal cancer development, a similar spectrum of mtDNA mutations (and downstream mitochondrial OXPHOS deficiency) would be present and enriched in colorectal tumors. To investigate this, we assessed mitochondrial OXPHOS subunit protein levels and enzyme activities in nine adenomatous polyps and 26 adenocarcinomas and their patient-matched normal mucosa (Fig. 1a,b). We performed in situ immunohistochemistry (IHC) analysis to ensure we only analyzed the epithelial compartment without contamination by muscle, stromal or immune cells or the non-transformed mucosa. Four out of nine (44%) of the adenomas and 18 out of 26 (69%) of the adenocarcinomas had decreased levels, or absence, of one or more OXPHOS subunits and/or loss of histochemical cytochrome *c* oxidase (COX) reactivity (Fig. 1 and Supplementary Table 1) compared with an average of 10% of normal crypts (Fig. 1c). Sequencing of the mtDNA of laser microdissected tumor epithelium, and either patient-matched normal mucosa or stromal tissue from the tumor section (to provide the germline mitochondrial genotype of each subject), detected tumor-specific, clonally expanded mtDNA point mutations in four out of nine adenomas and 22 out of 26

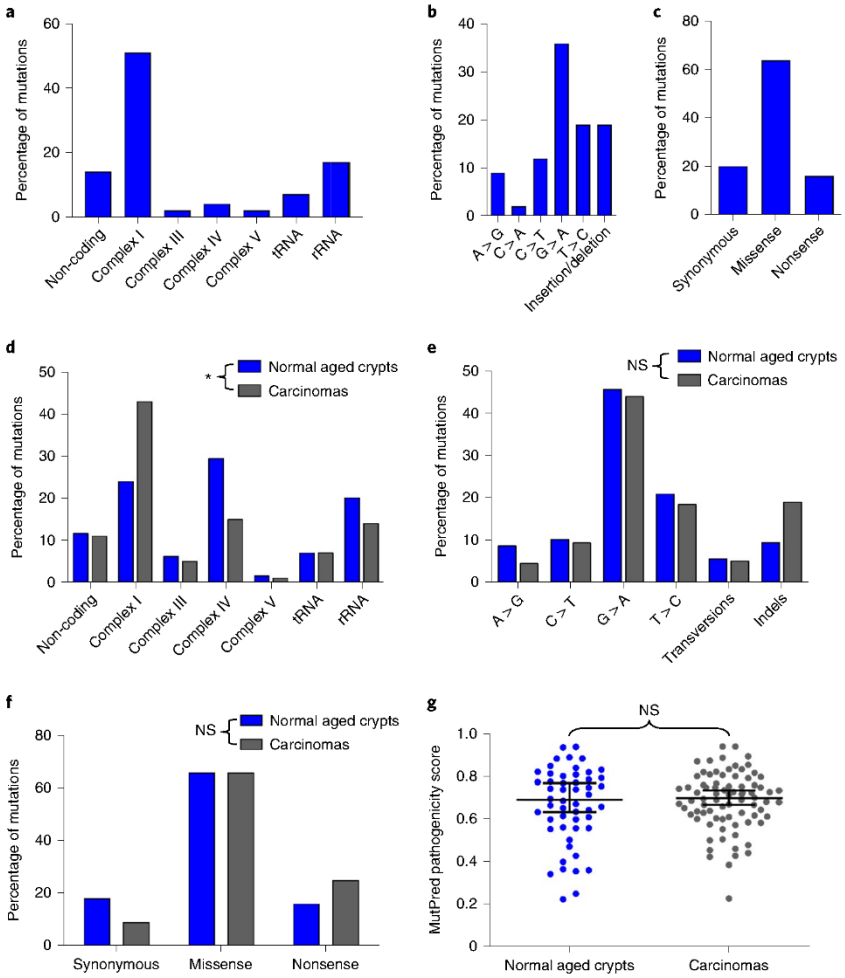

Fig. 2 | Analysis of mtDNA mutations detected in 26 colorectal adenocarcinomas compared with normal aged crypts. a–c, Location (**a**), type (**b**) and consequences (**c**) of mtDNA mutations detected in colorectal adenocarcinomas in this study ($n=41$ mutations). rRNA, ribosomal RNA; tRNA, transfer RNA. **d–f**, Comparison of the location (**d**), types (**e**) and functional consequences (**f**) of mtDNA mutations in previously published normal crypts ($n=129$ mutations) and adenocarcinomas[11,13,21,23] ($n=182$ mutations). There was a significant difference in the location of the mtDNA mutations in adenocarcinomas compared with normal aged crypts ($P=0.0123$; chi-squared analysis (**d**)), but no significant differences were detected in the types of mutations ($P=0.2264$; chi-squared analysis (**e**)) or the predicted functional consequences ($P=0.1504$; chi-squared analysis (**f**)). NS, not significant. **g**, Comparison of MutPred pathogenicity scores for missense mutations in protein-encoding genes in normal aging crypts ($n=52$ mutations) and adenocarcinomas ($n=80$ mutations). Statistical significance was determined by two-tailed Mann–Whitney *U*-test ($P=0.8138$; medians ± 95% confidence intervals are shown). $^*P<0.05$.

adenocarcinomas (47 mutations in total) (Supplementary Table 2 and Fig. 2). Of the 22 OXPHOS-deficient tumors, 18 had one or more mtDNA mutations at high levels of heteroplasmy correlating with the IHC profile (Supplementary Table 2). mtDNA mutations detected in tumors with normal OXPHOS protein levels were either present at <50% heteroplasmy or were known polymorphic variants predicted not to affect OXPHOS[14]. This highlights the fact that mtDNA mutations are functionally recessive and must reach high levels of heteroplasmy before an OXPHOS defect will become manifest. In four of the tumors with OXPHOS defects, mtDNA mutations were not detected, similar to our previous analyses of normal crypts[13], suggesting that nuclear factors can also contribute to age-related OXPHOS deficiency. Combining the mtDNA mutations detected in the human adenocarcinomas here with those published by others[17–19,22] (Supplementary Table 3), we observed a similar mtDNA mutation spectrum in tumors and normal aging colonic crypts[11,13,21,23] (Supplementary Table 4 and Fig. 2), with the only significant difference being a higher proportion of complex I subunit mutations in the tumors (Fig. 2d, $P=0.0123$). Given the similarities between the mutational spectrum and OXPHOS defects in normal crypts and tumors, and the very high prevalence of OXPHOS defects in the tumors, we hypothesized that pre-existing OXPHOS defects in normal crypts may provide a selective metabolic advantage during tumorigenesis.

To test this hypothesis, we crossed an inducible intestinal tumor mouse model (*Lgr5-creER;Apc*$^{fl/fl}$)[24] with a model of accelerated mtDNA mutagenesis (*PolgA*$^{mut/mut}$)[25,26] (Extended Data Fig. 1a). By 6 months of age, the *PolgA*$^{mut/mut}$ mice have a high frequency of intestinal crypts with OXPHOS dysfunction caused by clonally

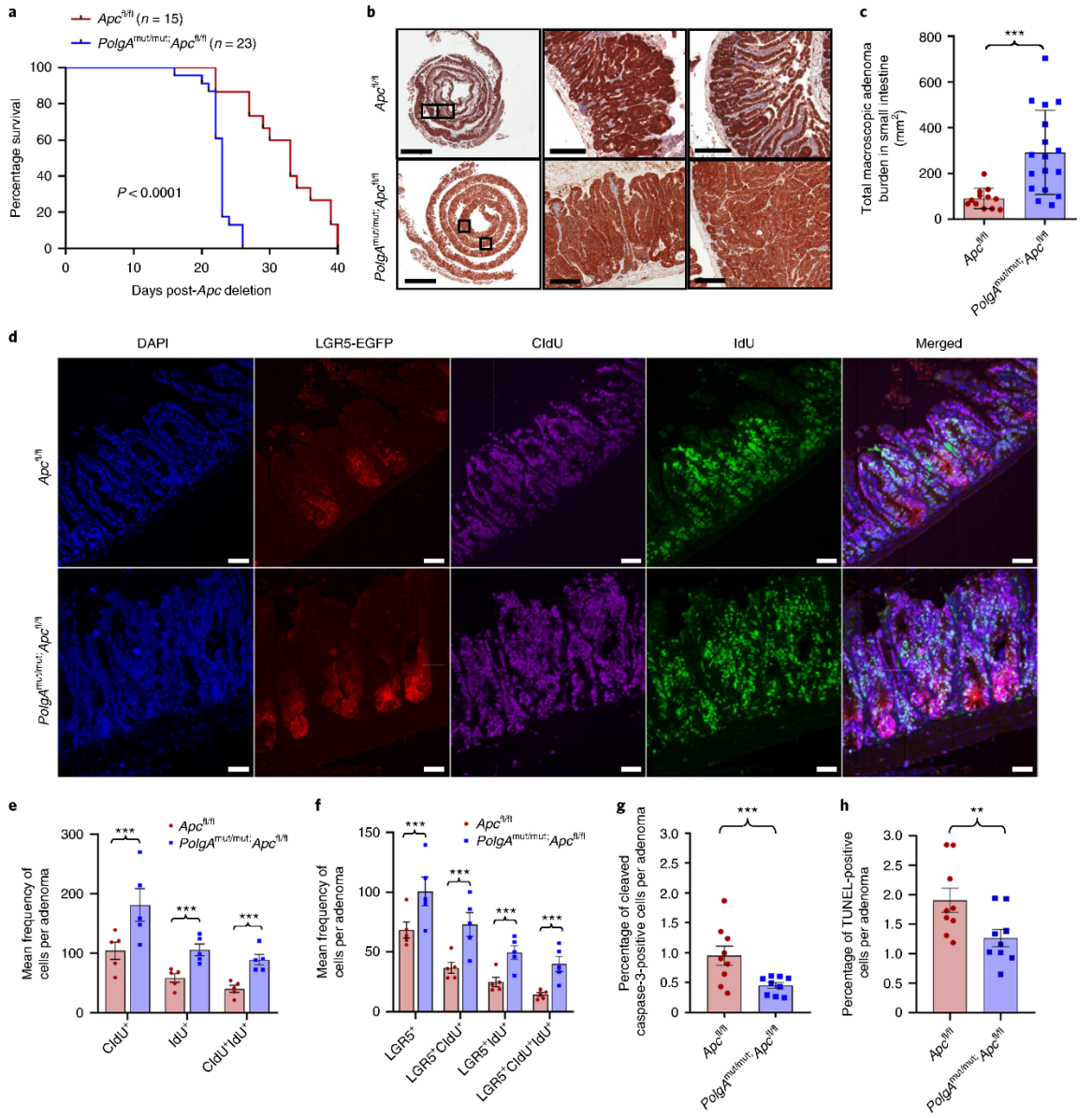

Fig. 3 | *PolgA*$^{mut/mut}$;*Apc*$^{fl/fl}$ mice have a reduced lifespan and enhanced tumor growth due to accelerated cell proliferation and reduced apoptosis compared with *Apc*$^{fl/fl}$ mice. a, Kaplan–Meier survival curve showing survival times post-*Apc* deletion (two-sided Mantel–Cox (log-rank) test; $P < 0.0001$; n = number of mice). **b**, β-catenin IHC on small intestinal sections. Scale bars, 3 mm (first column) and 200 µm (second and third columns). IHC was performed on *PolgA*$^{mut/mut}$;*Apc*$^{fl/fl}$ ($n = 17$) and *Apc*$^{fl/fl}$ ($n = 12$) mice 23 d post-*Apc* deletion. Representative images are shown. **c**, Tumor burden in the small intestines of *PolgA*$^{mut/mut}$;*Apc*$^{fl/fl}$ ($n = 17$) and *Apc*$^{fl/fl}$ ($n = 12$) mice 23 d post-*Apc* deletion (unpaired, two-tailed t-test; error bars show s.d.; $P = 0.0010$). **d**, Immunoflourescence images showing LGR5$^+$ cells and cells that had incorporated CldU and IdU. Scale bars, 50 µm. Immunofluorescence was performed on $n = 5$ mice per group and representative images are shown. **e**,**f**, Quantification of the frequency of thymidine analog incorporation in all cells per adenoma (**e**) and LGR5$^+$ cells per adenoma per mouse (**f**) ($n = 5$ mice per group with 20 adenomas analyzed per mouse; two-sided linear mixed-effects regression model with mouse ID as a random effect; $P < 0.001$ in all comparisons). **g**,**h**, Apoptotic cells were identified and quantified using cleaved caspase-3 IHC (**g**) and TUNEL labeling (**h**) in mice 23 d post-*Apc* deletion ($n = 9$ mice per group with a minimum of ten adenomas analyzed per mouse; two-sided linear mixed-effects regression model with mouse ID as a random effect; $P < 0.001$ for cleaved caspase-3; $P = 0.008$ for TUNEL; mean percentages of apoptotic cells per adenoma per mouse are shown ± s.e.m). $^{**}P < 0.01$; $^{***}P < 0.001$.

expanded mtDNA mutations[27]. Furthermore, modeling studies support a similar mechanism of clonal expansion of mtDNA mutations through random genetic drift with age in intestinal crypts of *PolgA*$^{mut/mut}$ mice[27] and humans[28]. Intestinal tumors were induced in *PolgA*$^{mut/mut}$;*Lgr5-creER*;*Apc*$^{fl/fl}$ (hereafter denoted *PolgA*$^{mut/mut}$;*Apc*$^{fl/fl}$) and *Lgr5-creER*;*Apc*$^{fl/fl}$ (hereafter denoted *Apc*$^{fl/fl}$) mice by tamoxifen activation of the Cre recombinase at 6 months of age. *PolgA*$^{mut/mut}$;*Apc*$^{fl/fl}$ mice had a significantly shorter lifespan than *Apc*$^{fl/fl}$ mice, with median survival times post-*Apc* deletion of 23 and 33 d, respectively (Fig. 3a, $P<0.0001$). We confirmed that the dose of the inducing agent tamoxifen was not toxic when given to mice that did not express Cre recombinase (Extended Data Fig. 1b). To compare tumor growth rates, *Apc* deletion was induced in *PolgA*$^{mut/mut}$;*Apc*$^{fl/fl}$ and *Apc*$^{fl/fl}$ mice at 6 months of age, and all mice were killed 23 d later (the median lifespan of the *PolgA*$^{mut/mut}$;*Apc*$^{fl/fl}$ line). The total tumor burden in the small intestine of *PolgA*$^{mut/mut}$;*Apc*$^{fl/fl}$ mice was significantly higher than in *Apc*$^{fl/fl}$ mice (Fig. 3b,c, $P=0.0010$). β-catenin IHC showed no significant difference in the number of microscopic β-catenin^{high} foci in the colon between the two groups (Extended Data Fig. 1c,d, $P=0.7444$). However, foci in *PolgA*$^{mut/mut}$;*Apc*$^{fl/fl}$ mice were almost twice the size of those in *Apc*$^{fl/fl}$ mice (Extended Data Fig. 1e, $P<0.0001$). These data suggest that mitochondrial dysfunction in intestinal epithelial cells of *PolgA*$^{mut/mut}$;*Apc*$^{fl/fl}$ mice promotes tumor cell growth after transformation by *Apc* deletion.

To investigate the underlying cause of the increased tumor size in the *PolgA*$^{mut/mut}$;*Apc*$^{fl/fl}$ mice, we compared proliferation rates of all cells in the adenomas, and specifically in the leucine-rich repeat-containing G protein-coupled receptor 5-positive (LGR5^{+}) stem cells, from both groups of animals using multiple thymidine analog labeling (Fig. 3d). We noted a significantly higher frequency of cells incorporating 5-chloro-2′-deoxyuridine (CldU) and 5-iodo-2′-deoxyuridine (IdU), both individually and together, in adenomas of the small intestine (Fig. 3e, $P<0.001$ in all cases) and colon (Extended Data Fig. 1f, $P<0.001$ in all cases) of the *PolgA*$^{mut/mut}$;*Apc*$^{fl/fl}$ mice. Incorporation of both thymidine analogs identifies cells that have divided twice within the 28 h period, providing evidence that the cells are proliferating faster in *PolgA*$^{mut/mut}$;*Apc*$^{fl/fl}$ adenomas. In the small intestine, both the frequency of LGR5^{+} cells per adenoma and their levels of thymidine analog incorporation were significantly higher in the *PolgA*$^{mut/mut}$;*Apc*$^{fl/fl}$ mice compared with the *Apc*$^{fl/fl}$ mice, indicative of a higher proliferative index (Fig. 3f, $P<0.001$ in all cases). Despite an increase in LGR5^{+} stem cells in colonic adenomas (Extended Data Fig. 1g, $P<0.001$, no significant differences in LGR5^{+} stem cell proliferation rates were noted (Extended Data Fig. 1g). Using cleaved caspase-3 IHC and terminal deoxynucleotidyl transferase (TdT)-mediated dUTP nick end (TUNEL) labeling, we detected a significantly lower frequency of apoptotic cells in adenomas from the *PolgA*$^{mut/mut}$;*Apc*$^{fl/fl}$ mice in both the small intestine (Fig. 3g,h, $P<0.001$ for cleaved caspase 3 and $P=0.008$ for TUNEL) and colon (Extended Data Fig. 1h,i, $P=0.0092$ for cleaved caspase 3 and $P=0.002$ for TUNEL). These data suggest that mitochondrial dysfunction leads to increased cell proliferation and decreased apoptosis, resulting in accelerated tumor growth.

Next, we investigated the pattern of OXPHOS deficiency in intestinal adenomas from *PolgA*$^{mut/mut}$;*Apc*$^{fl/fl}$ and *Apc*$^{fl/fl}$ mice using quantitative quadruple immunofluorescence[29] (Fig. 4a–e and Extended Data Fig. 2a–e). OXPHOS proteins were normalized to the mitochondrial mass marker TOMM20, with *Apc*$^{fl/fl}$ adenomas acting as controls. In the small intestine, >85% of *PolgA*$^{mut/mut}$;*Apc*$^{fl/fl}$ adenomas were classified as NADH:ubiquinone oxidoreductase subunit B8 (NDUFB8; complex I) deficient, whereas mitochondrially encoded cytochrome *c* oxidase I (MTCO1; complex IV) and ubiquinol–cytochrome *c* reductase, Rieske iron-sulfur polypeptide 1 (UQCRFS1; complex III) labeling only revealed minimal deficiency (Fig. 4e). Similar patterns of OXPHOS deficiency were detected in colonic adenomas (Extended Data Fig. 2e). To determine whether *Apc* deletion affected mitochondrial OXPHOS protein abundance, we compared normal (non-recombined) small intestine and colonic mucosa of the *PolgA*$^{mut/mut}$;*Apc*$^{fl/fl}$ and *Apc*$^{fl/fl}$ mice with the adenomas (Fig. 4f and Extended Data Fig. 2f–h). In both tissues, mitochondrial density increased significantly following *Apc* deletion in both mouse models ($P<0.0001$ all cases). There were no significant differences in NDUFB8 or UQCRFS1 between the crypts and adenomas of the *PolgA*$^{mut/mut}$;*Apc*$^{fl/fl}$ mice in both small intestine and colon, but MTCO1 and ATP synthase subunit beta (ATPB) levels were significantly lower in the adenomas (MTCO1, $P<0.0001$ in the small intestine and $P=0.007$ in the colon; ATPB, $P<0.0001$ in both tissues). In the *Apc*$^{fl/fl}$ mice, OXPHOS proteins were significantly lower in the adenomas than in the normal mucosa in both colon and small intestine ($P<0.0001$ in all cases), supporting previous studies showing Wnt-mediated downregulation of mitochondrial OXPHOS as a tumor-promoting mechanism[30]. Our data suggest that this mechanism is accelerated in *PolgA*$^{mut/mut}$;*Apc*$^{fl/fl}$ mice.

To investigate whether somatic mtDNA mutations were responsible for the OXPHOS deficiencies in the mice, individual adenomas were laser microdissected from *PolgA*$^{mut/mut}$;*Apc*$^{fl/fl}$ and *Apc*$^{fl/fl}$ mice and the mtDNA was sequenced. *PolgA*$^{mut/mut}$;*Apc*$^{fl/fl}$ adenomas harbored an average of 13–14 variants present at 30–70% heteroplasmy (Supplementary Table 5), whereas in *Apc*$^{fl/fl}$ adenomas, none were detected at >5%. The mutational spectrum was consistent with the random mutagenesis model previously described in colonic crypts of the *PolgA*$^{mut/+}$ mice[27] (Extended Data Fig. 3). Unlike our human dataset, no homoplasmic mtDNA variants were detected; however, this is not unexpected given the age of the mice and the predictions of the time required for an mtDNA variant to reach homoplasmy[27]. These data strongly infer that multiple heteroplasmic clonally expanded mtDNA mutations are the underlying cause of the OXPHOS defects detected in *PolgA*$^{mut/mut}$;*Apc*$^{fl/fl}$ adenomas.

Next, we used RNA sequencing (RNA-Seq) to investigate the mechanism by which OXPHOS dysfunction in the normal aging

Fig. 4 | Small intestinal adenomas from *PolgA*$^{mut/mut}$;*Apc*$^{fl/fl}$ mice are deficient in mitochondrial complex I, but the majority retain expression of subunits of complexes III, IV and V. a,c, Immunofluorescence was performed to quantify levels of OXPHOS proteins on $n=9$ *PolgA*$^{mut/mut}$;*Apc*$^{fl/fl}$ mice and $n=10$ *Apc*$^{fl/fl}$ mice. Representative images are shown. Scale bars, 50 µm. In **a**, white dashed lines show an adenoma region deficient in complexes I and III and red dashed lines highlight deficiency in complex I only. In **c**, white dashed lines show an adenoma region deficient in complex IV and red dashed lines show normal complex IV. **b,d**, Dot plots showing relative *Z* scores for complexes I and III (**b**) and IV and V (**d**), calculated following quantification of mitochondrial OXPHOS protein levels in adenomas from *PolgA*$^{mut/mut}$;*Apc*$^{fl/fl}$ ($n=9$) and *Apc*$^{fl/fl}$ ($n=10$) mice using the method described in ref. [29] ($n=20$ adenomas quantified per mouse). The dashed lines indicate *Z* scores of −3, −4.5 and −6, which are used in the categorical analsyis of OXPHOS protein levels in **e**. **e**, Categorical analysis of OXPHOS protein levels in *PolgA*$^{mut/mut}$;*Apc*$^{fl/fl}$ ($n=9$) mice. Data points show individual mice ± s.d. **f**, Dot plots showing raw densitometry values for mitochondrial protein levels. For the adenomas, $n=9$ *PolgA*$^{mut/mut}$;*Apc*$^{fl/fl}$ and $n=10$ *Apc*$^{fl/fl}$ mice with 20 adenomas analyzed per mouse. For the normal crypts, $n=5$ mice were analyzed per group with a minimum of 13 crypts quantified per mouse. Statistical significance was determined by one-way ANOVA with Tukey's post-hoc test. *P* values for within-genotype comparisons between normal crypts and adenomas were as follows: TOMM20: $P<0.0001$ (*Apc*$^{fl/fl}$); $P<0.0001$ (*PolgA*$^{mut/mut}$;*Apc*$^{fl/fl}$); NDUFB8: $P<0.0001$ (*Apc*$^{fl/fl}$); $P=0.9995$ (*PolgA*$^{mut/mut}$;*Apc*$^{fl/fl}$); UQCRFS1: $P<0.0001$ (*Apc*$^{fl/fl}$); $P=0.1302$ (*PolgA*$^{mut/mut}$;*Apc*$^{fl/fl}$), MTCO1: $P<0.0001$ (*Apc*$^{fl/fl}$); $P=0.0001$ (*PolgA*$^{mut/mut}$;*Apc*$^{fl/fl}$); ATPB: $P<0.0001$ (*Apc*$^{fl/fl}$); $P<0.0001$ (*PolgA*$^{mut/mut}$;*Apc*$^{fl/fl}$). ***$P<0.001$. Error bars show s.e.m.

intestinal epithelium accelerates tumor development. Normal epithelial crypts from the distal end of the small intestine (where the majority of adenomas occur) were isolated from 6-month-old *PolgA*$^{mut/mut}$ and *PolgA*$^{+/+}$ mice. Comparison of differentially expressed genes revealed that the most significantly upregulated genes (*Phgdh*, *Psat1*, *Psph*, *Mthfd2*, *Slc1a4* and *Aldh1l2*) were

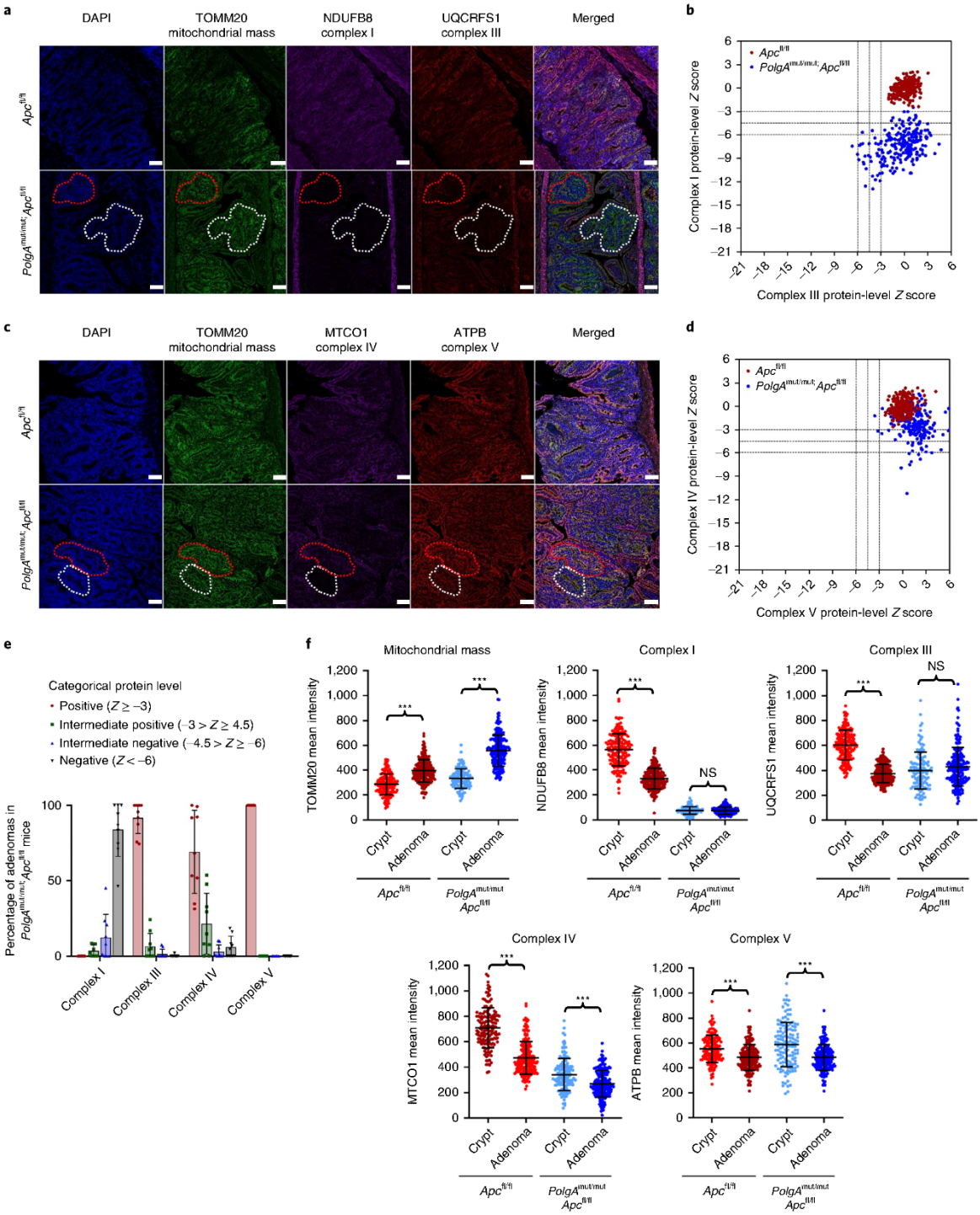

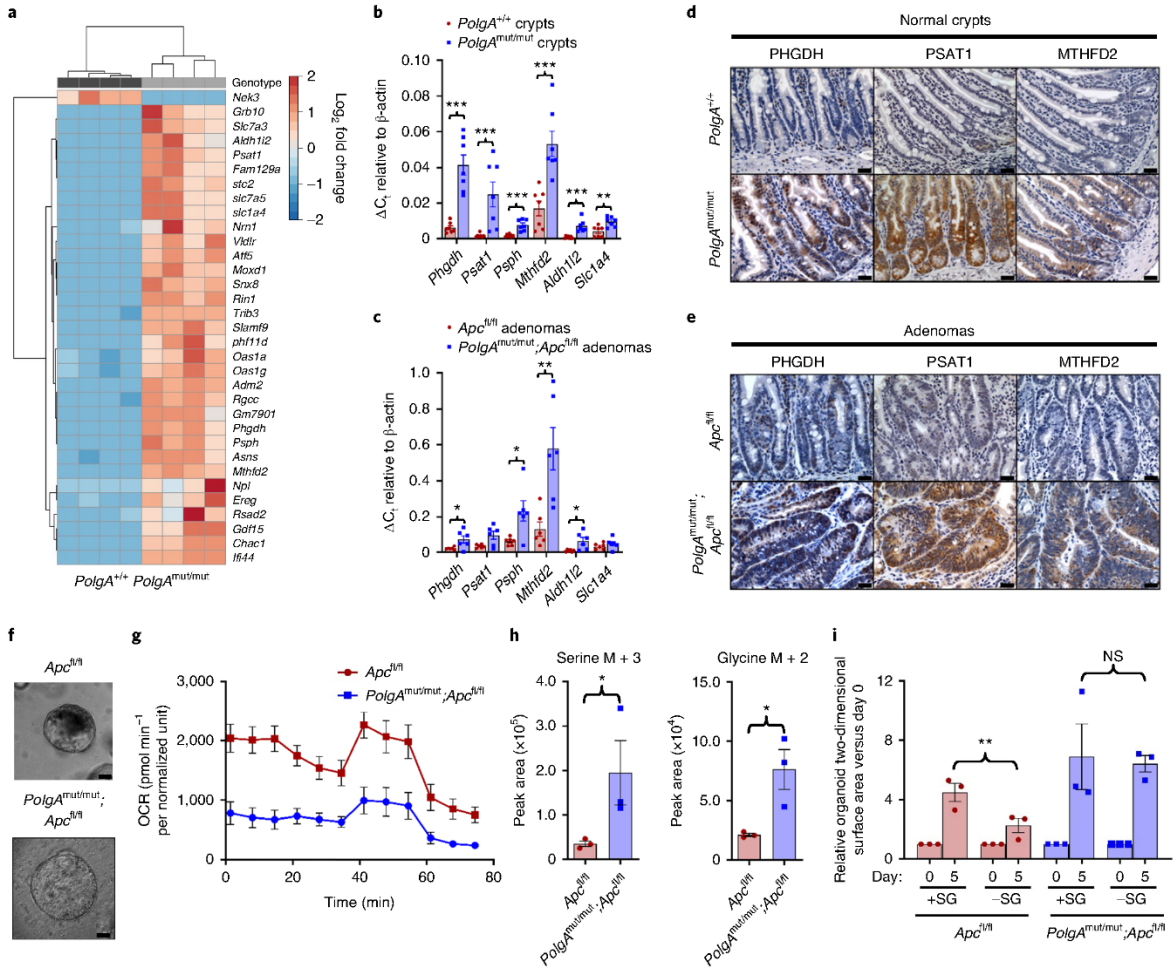

Fig. 5 | Mitochondrial OXPHOS dysfunction causes upregulation of denovo serine synthesis in both non-transformed crypts and adenomas from mice. **a**, Heat map showing differential gene expression in non-transformed crypt homogenates from the small intestines of $PolgA^{+/+}$ and $PolgA^{mut/mut}$ mice ($n=4$ mice per group). **b**, Mean relative expression of the SSP genes by RT-PCR that were identified to be upregulated by RNA-Seq analysis in normal crypts ($n=7$ mice per group; one-way Mann–Whitney *U*-test; $P=0.0003$ for all genes except *Slc1a4*, where $P=0.0035$; error bars show s.e.m.). **c**, Mean relative expression of the SSP genes by RT-PCR that were identified to be upregulated by RNA-Seq analysis in laser microdissected adenomas ($n=6$ mice per group; one-way Mann–Whitney *U*-test; *P* values as follows: $P=0.0325$ (*Phgdh*); $P=0.066$ (*Psat1*); $P=0.0130$ (*Psph*); $P=0.0043$ (*Mthfd2*); $P=0.0130$ (*Aldh1l2*), $P=0.1548$ (*Slc1a4*); error bars show s.e.m.). **d**,**e**, IHC images showing in situ levels of SSP proteins in the non-transformed normal small intestinal mucosa (**d**) and adenomas (**e**). IHC was performed on $n=4$ mice per genotype and representative images are shown. Scale bars, 50 µm. **f**, Organoids were generated from $n=3$ $PolgA^{mut/mut};Apc^{fl/fl}$ and $n=3$ $Apc^{fl/fl}$ mice. Representative images of adenoma organoids are shown. Scale bars, 100 µm. **g**, OCRs measured by Seahorse analysis in adenoma organoids ($n=3$ mice per genotype; $n=8$ technical replicates per mouse; means ± s.e.m per mouse are shown). **h**, Quantification of major mass isotopomers detected in adenoma organoids following growth in the presence of $^{13}C_6$ glucose for 24 h. ^{13}C labeling is shown as M+3 (serine) or M+2 (glycine) ($n=3$ mice per group with $n=3$ technical replicates performed per mouse; one-way unpaired *t*-test; $P=0.0143$ for labeled serine and $P=0.0151$ for labeled glycine; data are means per mouse ± s.e.m). **i**, Quantification of the growth of adenoma organoids in medium with (+SG) or without (−SG) serine and glycine for 5 d. Data are normalized to organoid area on day 0. Mean organoid sizes per mouse relative to day 0 ± s.e.m are shown ($n=3$ mice per group; unpaired, two-tailed *t*-test; $P=0.0021$ for $Apc^{fl/fl}$; $P=0.4140$ for $PolgA^{mut/mut};Apc^{fl/fl}$). $^*P<0.05$; $^{**}P<0.01$; $^{***}P<0.001$.

involved in pathways relating to serine biosynthesis, uptake and metabolism (Fig. 5a and Supplementary Table 6). These data were confirmed by quantitative reverse-transcriptase PCR (qRT-PCR; Fig. 5b, $P=0.0003$ for all genes except *Slc1a4*, where $P=0.0035$). RNA extracted from laser microdissected adenoma tissue from the small intestine of both groups of animals showed significant upregulation of *Phgdh*, *Psph*, *Mthfd2* and *Aldh1l2* in the adenomas from $PolgA^{mut/mut};Apc^{fl/fl}$ mice (Fig. 5c, $P=0.0325$ (*Phgdh*), $P=0.0130$ (*Psph*), $P=0.0043$ (*Mthfd2*), $P=0.0130$ (*Aldh1l2*)). These findings were confirmed at the protein level for phosphoglycerate dehydrogenase (PHGDH), phosphoserine aminotransferase 1 (PSAT1) and methylenetetrahydrofolate dehydrogenase (NADP+ dependent) 2, methenyltetrahydrofolate cyclohydrolase (MTHFD2) by IHC in the small intestine (Fig. 5d,e) and colon (Extended Data Fig. 4a,b).

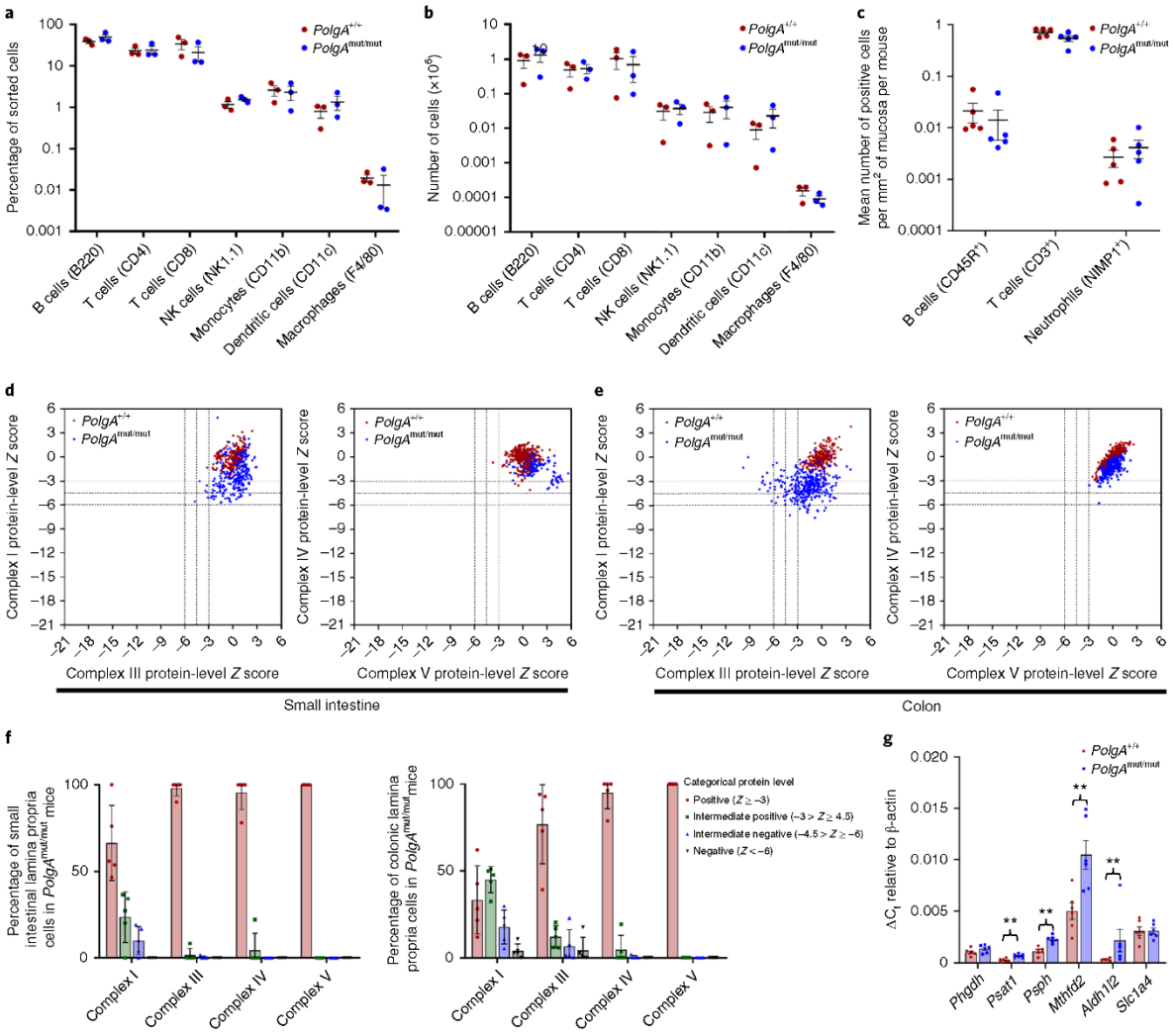

Fig. 6 | Characterization of the immune microenvironment in the lamina propria of the small intestine of *PolgA*$^{mut/mut}$ and *PolgA*$^{+/+}$ mice at 6 months of age, before tumor induction. a,**b**, Immune cell infiltration within the distal third of the small intestine was analyzed by flow cytometry. Relative proportions (**a**) and absolute numbers (**b**) of each cell type are shown. No significant differences were found between the two groups ($n=3$ mice per group; one-way ANOVA with Tukey's post-hoc test). NK, natural killer. **c**, Mean frequency of B cells, T cells and neutrophils per mm^2 of small intestinal epithelium, as quantified by IHC ($n=5$ mice per group). No significant differences were detected by one-way ANOVA with Tukey's post-hoc test. **d**,**e**, Dot plots showing *Z* scores, for complex 1 versus complex III (left) and complex IV versus complex V (right), calculated following quantification of mitochondrial OXPHOS protein levels in small groups of lamina propria cells in the small intestine (**d**) and colon (**e**) of *PolgA*$^{mut/mut}$ and *PolgA*$^{+/+}$ mice ($n=5$ mice per group; a minimum of 50 areas per mouse were analyzed). **f**, Categorical analysis of OXPHOS protein levels in the small intestine (left) and colon (right) of *PolgA*$^{mut/mut}$ mice ($n=5$ mice per group). **g**, Relative expression of the SSP genes in the lamina propria of the small intestine by RT-PCR that had been identified to be upregulated by RNA-Seq analysis in the crypts ($n=6$ mice per group; one-way Mann–Whitney *U*-test). *P* values are as follows: $P=0.1201$ (*Phgdh*); $P=0.0043$ (*Psat1*); $P=0.0011$ (*Psph*); $P=0.0043$ (*Mthfd2*); $P=0.0022$ (*Aldh1l2*); $P=0.500$ (*Slc1a4*). Mean values per mouse ± s.e.m are shown. $^{**}P<0.01$.

Supporting the hypothesis that these proteins are upregulated in response to age-related accumulation of OXPHOS defects in the *PolgA*$^{mut/mut}$ mice, we observed an age-related increase in serine synthesis pathway (SSP) protein levels in the normal small intestine crypts of *PolgA*$^{mut/mut}$ mice between 1 and 12 months of age (Extended Data Fig. 5).

We investigated the functional consequences of changes in gene expression and protein levels in the *PolgA*$^{mut/mut}$;*Apc*$^{fl/fl}$ adenomas by generating in vitro adenoma organoids from mice from the two groups (Fig. 5f). We were unable to investigate this in non-transformed normal small intestinal organoids as it has been shown previously (as is our own experience) that these do not grow from the *PolgA*$^{mut/mut}$ mice in vitro[31]. The baseline oxygen consumption rate (OCR) was lower in organoids derived from *PolgA*$^{mut/mut}$;*Apc*$^{fl/fl}$ adenomas compared with *Apc*$^{fl/fl}$ adenomas, confirming that in vivo OXPHOS defects were manifest in the in vitro model (Fig. 5g).

Following growth in $^{13}C_6$-labeled glucose for 24h, we found that labeled serine (M+3) and glycine (M+2) (derived from the labeled glucose through the SSP) were significantly higher in *PolgA*$^{mut/mut}$; *Apc*$^{fl/fl}$ organoids, indicating increased rates of de novo serine synthesis (Fig. 5h, $P=0.0143$ (serine), $P=0.0151$ (glycine)). No significant differences were observed in the levels of labeled glucose per se, suggesting equal uptake, nor were there differences in the levels of unlabeled (M+0) serine or glycine (Extended Data Fig. 6a). Growth rates in the absence of serine and glycine (−SG) were significantly impaired in the *Apc*$^{fl/fl}$ organoids ($P=0.0021$), whereas *PolgA*$^{mut/mut}$; *Apc*$^{fl/fl}$ organoids maintained their growth (Fig. 5i, $P=0.4140$), suggesting that complex I deficiency induces the SSP, conferring a significant growth advantage to adenomas. Next, we investigated the effect of the biguanide metformin, which has been shown to inhibit complex I[32,33], on the growth of *Apc*$^{fl/fl}$ organoids. There was a notable increase in organoid growth rate when they were dosed with metformin compared with vehicle controls (Extended Data Fig. 6b), confirming that pharmacological inhibition of complex I can also enhance adenoma organoid growth[34].

Since the *PolgA*$^{mut/mut}$ model is a whole body knock-in, we evaluated changes in the intestinal immune microenvironment at 6 months of age before tumor induction to determine any contribution to accelerated tumor growth. In-depth fluorescence-activated cell sorting (FACS) analysis of immune cell types in the distal end of the small intestine revealed no significant differences between either the proportions or the absolute numbers of the sorted immune cells between the two groups (Fig. 6a,b and Supplementary Fig. 1). This was confirmed in a subset of immune cells by IHC (Fig. 6c). Furthermore, in contrast with our crypt data, we detected little evidence of OXPHOS deficiency within the lamina propria of *PolgA*$^{mut/mut}$ mice; 66% of small intestinal cells showed normal NDUFB8 levels while 95% had normal MTCO1 levels (Fig. 6d–f). Gene expression studies revealed significant upregulation of *Psat1*, *Psph*, *Mthfd2* and *Aldh1l2*, but not *Phgdh* (Fig. 6g, $P=0.0043$ (*Psat1*), $P=0.0011$ (*Psph*), $P=0.0043$ (*Mthfd2*), $P=0.0022$ (*Aldh1l2*)), providing evidence that there is mitochondrial dysfunction and metabolic remodeling in the epithelial tissue microenvironment, but this is less marked than in epithelial cells.

Our mouse experiments have provided evidence that mitochondrial OXPHOS dysfunction can induce metabolic remodeling in the mouse small intestine and colon. Finally, it was important to see whether these findings were translatable to humans. We tested this by quantifying levels of PHGDH, PSAT1 and MTHFD2 in individual OXPHOS-normal and OXPHOS-deficient crypts from aged human samples by immunofluorescence. Levels of all three enzymes were significantly higher in crypts with OXPHOS defects than those with normal OXPHOS function (Fig. 7a–d, $P<0.0001$ for all enzymes), suggesting that normal aged human crypts expressing OXPHOS deficiency upregulate the de novo SSP as a pro-survival mechanism.

Discussion

Our data show that age-related mitochondrial OXPHOS dysfunction caused by mtDNA mutations in both humans and mice causes metabolic remodeling in intestinal epithelial cells, with specific upregulation of the de novo SSP, and the mouse model shows that this provides a metabolically favorable environment for tumor growth (Fig. 7e). Our human mtDNA sequencing data show that mtDNA mutations are not a requirement for tumorigenesis as they were not present in all adenocarcinomas studied, highlighting diverse mitochondrial genetic heterogeneity between tumors. In addition, the specific mtDNA mutation and its level of heteroplasmy are important determinants of whether an mtDNA mutation is actively contributing to a favorable metabolic phenotype for the tumor or whether it is simply a passenger mutation. Only those mtDNA mutations that are present both at functionally important sites and at a high enough level of heteroplasmy to cause OXPHOS defects result in a favorable metabolic shift, which, as we have shown in the mouse, can accelerate tumor cell growth. We believe that it is the biochemical change rather than the mutational event per se providing the advantage. In contrast, mtDNA mutations that are present at low levels of heteroplasmy, or ones that do not cause a biochemical defect, fall into the passenger mutation category and examples of these were also detected in our study.

The pathways we show to be upregulated in OXPHOS-deficient crypts in both our human and mouse data are well recognized as being critical for biomass production during tumor growth[34]. It is well accepted that only a small proportion of human adenomas go on to become adenocarcinomas[35] and that the larger the adenoma the higher the risk of carcinogenesis[36]. Therefore, the selective advantage of OXPHOS dysfunction for tumor growth, acting in synergy with nuclear DNA mutations, would be reflected in their increasing prevalence in clinically detectable large adenomas and adenocarcinomas, which is in line with our data. Although our mouse data specifically identified the contribution of pre-existing mtDNA mutations to tumorigenesis, it is also possible that tumor cells can acquire new mtDNA mutations that randomly clonally expand to high levels of heteroplasmy in individual cells during the tumorigenic process. If these mutations cause an OXPHOS defect, together with the associated favorable metabolic phenotype, those cells may outcompete others and become dominant within the tumor. Additional data to support a pro-tumorigenic role for pathogenic mtDNA mutations can be found in a recent pan-cancer analysis of mtDNA by the Pancancer Analysis of Whole Genomes Consortium[16]. This study showed selective enrichment of truncating mtDNA mutations in the protein-encoding genes at high levels of heteroplasmy (>60%), specifically in colorectal cancers. This was not seen in most other cancer types, with the authors suggesting that these mtDNA mutations could have oncogenic effects by altering signaling pathways[16].

In the normal aging intestine, this metabolic shift in response to OXPHOS deficiency may represent a response to mitochondrial stress, particularly if there are increased mitochondrial ROS levels; diversion of glucose through the SSP to increase glutathione production to help detoxify mitochondrial ROS is documented in mitochondrial disease models[37]. In addition, mitochondrial ROS play a significant role as signaling molecules in LGR5$^+$ stem cell

Fig. 7 | Mitochondrial OXPHOS dysfunction causes upregulation of de novo serine synthesis in normal aging human colonic crypts. a, Immunoflourescent images showing co-labeling of OXPHOS proteins and SSP enzymes in normal human colonic epithelium. CI (Complex I), CIV (Complex IV). White dashed lines highlight crypts that are NDUFB8 and MTCO1 deficient and have upregulation of PHGDH, PSAT1 or MTHFD2. Scale bars, 50 µm. Immunofluorescence was performed for each antibody on $n=12$ human samples. Representative images are shown. **b–d**, Quantification of the levels of PHGDH (**b**), PSAT1 (**c**) and MTHFD2 (**d**) in individual human crypts. Every OXPHOS-deficient crypt on the section was quantified, and OXPHOS-normal crypts on the same section were randomly sampled. In **b**, the numbers of crypts analyzed from left to right are: $n=45$, 46, 40, 62, 43, 50, 28, 29, 21, 16, 16, 17, 33, 31, 41, 17, 20, 8, 32, 27, 15, 17, 24 and 24. In **c**, the numbers of crypts analyzed from left to right are: $n=47$, 57, 58, 70, 44, 56, 54, 39, 73, 11, 21, 20, 33, 33, 39, 16, 30, 8, 61, 45, 31, 22, 51 and 49. In **d**, the numbers of crypts analyzed from left to right are: $n=23$, 67, 40, 61, 44, 47, 42, 32, 108, 15, 37, 38, 59, 60, 58, 26, 62, 10, 48, 40, 31, 24, 60 and 59. Error bars show means ± s.d. Data were analyzed using a two-sided linear mixed-effects regression model with mouse ID as a random effect. $P<0.0001$ in all comparisons. e, Schematic showing the hypothesized mechanism by which mtDNA mutations and OXPHOS defects contribute to tumorigenesis. ***$P<0.001$.

maintenance and crypt differentiation, highlighting the importance of maintaining the required ROS levels for normal crypt cell homeostasis[38,39]. Through its role as a precursor for the synthesis of nucleic acids, proteins and lipids, as well as antioxidants, serine is critical to support metabolic processes for cellular growth and survival in cancer development[40]. Therefore, the apparently protective cellular response to OXPHOS deficiency during aging may provide a distinct metabolic advantage for tumor growth when those cells are transformed. The OXPHOS deficiency observed in our mouse model provoked a similar metabolic response (that is, resistance to serine starvation due to upregulation of the SSP) to that seen in a model with activating *Kras* mutations in the presence of *Apc* deletion[34].

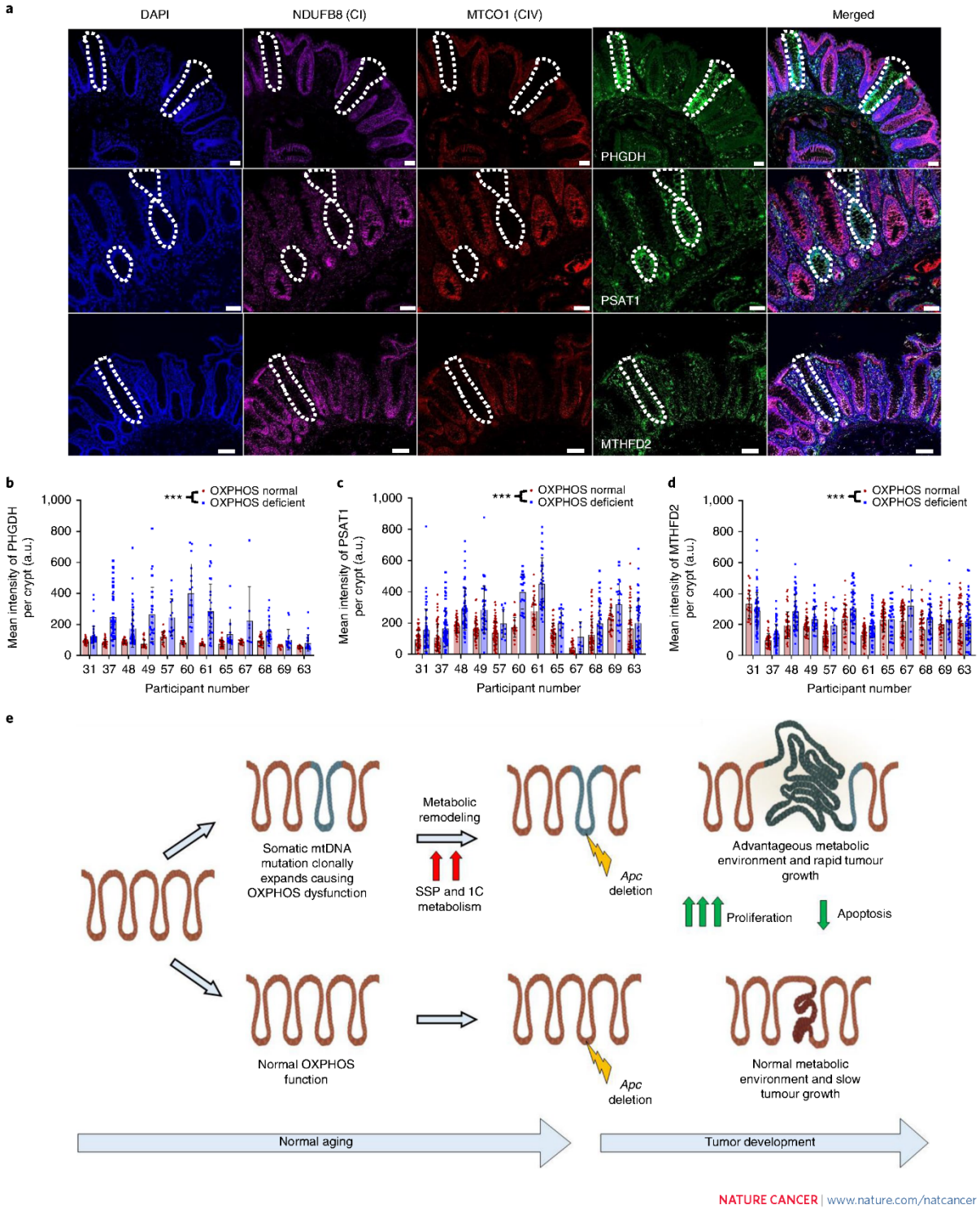

Furthermore, metabolic rewiring has been shown to occur in gliomas containing oncogenic *IDH1* mutations in response to oxidative stress, suggesting that mechanisms to maintain cellular redox balance are important for cancer cell survival[41]. Although we found no significant differences in either the absolute numbers or proportions of immune cell types in our model, we found evidence of low-level OXPHOS defects and a compensatory increase in SSP gene expression in cells of the lamina propria. Therefore, in addition to definitive evidence of the cell intrinsic effect of OXPHOS defects on tumor cell growth, it is possible that the aged microenvironment also plays a role.

We stress that our observations do not indicate that mtDNA-driven OXPHOS deficiency alone is able to initiate cancer as *PolgA*$^{mut/mut}$ mice do not have a higher tumor incidence compared with age-matched wild-type controls[25,26]. Rather, we hypothesize that age-related mtDNA mutations act synergistically with driver mutations, which are present in ~1% of normal crypts in middle-aged individuals[42], providing an advantageous metabolic environment during the pervasive process of neoplastic change during the colorectal adenoma–carcinoma sequence[35]. This hypothesis is supported by evidence of an increasing frequency of mtDNA mutations and OXPHOS defects from normal aged human crypts to adenoma to carcinoma.

A logical question arising from our studies is whether there is an increased incidence of colorectal cancer in patients with inherited pathogenic mtDNA mutations causing mitochondrial disease. Although there are no published studies addressing this question, in our clinical experience, we see no evidence to suggest that the patients have an increased incidence of cancer over their lifetime. However, a number of studies have shown that there is rapid loss of inherited pathogenic mtDNA mutations in human replicating tissues with age[43–48]. This is supported by similar findings in mouse models of inherited mtDNA disease[49,50]. Specifically looking at data from the gut, this loss of inherited mtDNA mutations results in the frequency of crypts with OXPHOS defects being similar to age-matched controls[18,51]. We currently do not understand the mechanism by which this selective loss is happening; however, loss of OXPHOS-deficient cells from the rapidly proliferating tissues would mean that any metabolic advantage for cancer cells would also be lost. This could explain why these patients do not appear to be at a higher risk of cancer. These observations suggest that inherited and age-associated somatic mtDNA mutations are behaving differently, highlighting the value of using the *PolgA*$^{mut/mut}$ mouse model in our study to model the aging human phenotype.

In conclusion, we propose that age-related mitochondrial OXPHOS defects can contribute to accelerated intestinal cancer cell growth and survival through upregulation of serine biosynthetic pathways. Metabolic pathways are attractive targets for therapeutic intervention, and the inherent reliance on the SSP in intestinal tumors with OXPHOS defects may make them selectively vulnerable to SSP inhibition and worthy of future investigation.

Methods

Patients and samples. Normal colonic epithelial and colorectal adenocarcinoma tissue was obtained from 26 patients undergoing surgical resection for a histopathologically graded adenocarcinoma diagnosis and from nine patients undergoing surgery for the removal of adenomatous polyps (age range: 52–82 years; 20 male; 15 female). Informed written consent was obtained before surgery and samples were coded to maintain confidentiality. This project was approved by the Joint Ethics Committee of Newcastle and North Tyneside Health Authority (2001/188) and the London–Stanmore National Research Ethics Committee (11/LO/1613).

Genetically engineered mouse models. *Lgr5-EGFP-IRES-creERT2*, *Apc*$^{fl/fl}$ (ref. [24]) and *PolgA*$^{+/mut}$ (ref. [25]) mice were cross-bred to generate *PolgA*$^{mut/mut}$;*Lgr5-creER*;*Apc*$^{fl/fl}$ and *Lgr5-creER*;*Apc*$^{fl/fl}$ mice, as shown in Extended Data Fig. 1. Mice were maintained on a C57BL/6 background, both sexes were used and researchers were blinded to genotypes. Mice were housed in single-sex cages at 20 ± 2 °C under a 12 h light/12 h dark photoperiod with the lights on at 07:00. All animal work was carried out in line with the Animals (Scientific Procedures) Act 1986 and the EU Directive 2010 in compliance with the UK Home Office (PPL P3052AD70) and the Newcastle University Animal Welfare Ethical Review Board (AWERB 425). Both sexes were used in all experiments (except RNA-Seq, for which all mice were female) and all mice were 6 months old unless otherwise stated.

COX/succinate dehydrogenase (SDH) histochemistry. Human colon samples were mounted for sectioning and frozen in isopentane pre-cooled to −190 °C in liquid nitrogen. Cryostat sections (12 µm) were cut onto glass slides and COX/SDH histochemistry was performed as previously described[13].

OXPHOS subunit IHC (human samples). Sections of 10 µm were cut from all samples described above and air dried for 1 h at room temperature. IHC was performed as previously described[11] using the antibodies complex I NDUFB8 (1:50), complex II SDHA (1:1,000), complex III UQCRFS1 (1:1,000) and complex IV MTCO1 (1:1,000) combined with a polymer detection system (Menarini Diagnostics). Protein levels were qualitatively scored in tumors compared with patient-matched colonic epithelium by two independent scorers (+++ normal levels, ++ intermediate levels, + low levels, – absence of protein). For adenoma samples, patient-matched normal epithelium was not available; therefore, we compared the samples with at least five samples of normal epithelium from the adenocarcinoma cohort. All normal crypts on each tissue section were analyzed (mean: 243 per section; range: 43–769).

DNA isolation from tumor epithelium and normal tissue. Human colon tumor samples or murine small intestinal adenomas were mounted for sectioning and frozen in isopentane pre-cooled to −190 °C in liquid nitrogen. Cryostat sections (20 µm) were mounted on polyethylene naphthalate membrane slides (Leica Microsystems). Sections were subjected to SDH histochemistry followed by ethanol dehydration and were then air dried for 1 h. Areas of tumor epithelium were cut into sterile 0.5-ml PCR tubes using a Zeiss PALM microdissection system and lysed as previously described[13]. DNA was extracted from whole tissue from matched normal colon using an EZ1 DNA extraction system (Qiagen).

Human mtDNA sequencing. The entire mtDNA sequence was determined from the adenocarcinoma tissue and matched normal colon. mtDNA was PCR amplified and sequenced using the ABI 3130xl Genetic Analyzer system with ABI 3130 Data Collection Software version 4 and analyzed as previously described using SeqScape software version 2.6 (ref. [13]). Human adenoma tissue was sequenced as previously described[52].

Mouse mtDNA sequencing. mtDNA was PCR amplified in two overlapping 9-kilobase fragments using the primer sets 1628F (5′-AGAAAGCGTTCAAGCT CAAC-3′) and 10737R (5′-CCATGAAGCGTCTAAGGTGTG-3′) and 10059F (5′-ACCATCTTAGTTTTCGCAGC-3′ and 2315R (5′-CACTTTGACTTGTAAG TCTAGG-3′) (numbers correspond to NC_005089.1). The PCR parameters were: an initial denaturation at 94 °C for 10 min followed by 30 cycles of denaturation at 94 °C for 20 s, primer annealing at 68 °C for 20 s, extension for 9 min at 68 °C and a final extension at 72 °C for 5 min. PCR products were purified and sequenced on an MiSeq system (Illumina) using MiSeq control software, and bioinformatics analysis was performed as previously described[52], with the exception that the mouse mtDNA reference sequence was used (NC_005089.1 and MM10). The software used in the bioinformatics analysis was as follows: BWA version 0.7, SAMtools version 0.1.18, Picard version 1.85, VarScan version 2.3.8, LoFreq version 0.6.1, ANNOVAR version 529 and Haplogrep version 2.

Tamoxifen induction. *PolgA*$^{mut/mut}$;*Lgr5-creER*;*Apc*$^{fl/fl}$ and *Lgr5-creER*;*Apc*$^{fl/fl}$ mice aged 6 months were injected intraperitoneally with four doses of tamoxifen in sunflower oil at 10 mg ml^{-1} over four consecutive days (300, 200, 200 and 200 µl).

Scoring of macroscopic adenomas. Mice were culled 23 d post-tamoxifen administration. Their intestines were removed, flushed with 10% neutral-buffered formalin, opened up and pinned out as intestinal whole mounts. Using a dissecting microscope, intestinal adenomas (minimum: 1 mm × 1 mm) were counted and their areas were measured. For fused adenomas, the total area was measured. For comparative analysis between *PolgA*$^{mut/mut}$;*Apc*$^{fl/fl}$ ($n = 17$) and *Apc*$^{fl/fl}$ ($n = 12$) mice, the total sum of the adenomatous area was calculated. Adenomas were counted blind by two independent scorers.

IHC. Sections (4 µm) were de-paraffinized and rehydrated as standard. Antigen retrieval was performed by pressure cooking in either 1 mM EDTA pH 8.0 (β-catenin, CD3 and OXPHOS antibodies) or 10 mM sodium citrate pH 6.0 (PSAT1, PHGDH, MTHFD2, cleaved caspase-3, CD45R and neutrophil) for 20 min. Standard IHC was performed using the following antibodies: rabbit anti-β-catenin (1:1,000), anti-MTHFD2 (1:600), anti-PSAT1 (1:600), anti-PHGDH (1:4,000), anti-cleaved caspase-3 (1:35), rat anti-CD45R (1:200), anti-CD3 (1:100) and anti-neutrophil (1:100). Rabbit primary antibodies were visualized using the EnVision Anti-Rabbit HRP Polymer Kit (Dako), per the manufacturer's instructions. Rat primary antibodies were detected and visualized using goat

anti-IgG:Biotin and a HRP-conjugated ABC kit (Vector Laboratories). All IHC slides were imaged using the Aperio virtual pathology system (Leica Microsystems) and analyzed using Aperio ImageScope version 12.4.

Immunofluorescence. Sections were prepared and antigen retrieval performed as for IHC. Sections were incubated in primary antibodies at 4 °C overnight. The primary antibodies used were: anti-NDUFB8 (1:50), anti-UQCRFS1 (1:100), anti-MTCO1 (1:100), anti-ATPB (1:100), anti-TOMM20 (1:100), anti-IdU (1:100), anti-BrdU (1:100), anti-GFP biotin (1:100), anti-MTHFD2 (mouse: 1:300; human: 1:90), anti-PSAT1 (mouse: 1:300; human: 1:90) and anti-PHGDH (mouse: 1:2,000; human: 1:300). Sections were washed in 1× Tris-buffered saline with 0.1% Tween 20 and incubated in secondary antibodies for 2 h at room temperature. Secondary antibodies (all diluted 1:200 unless otherwise stated) were: goat anti-mouse IgG1 biotin, goat anti-mouse IgG2b-546, goat anti-rabbit IgG-488, goat anti-mouse IgG2a-546, goat anti-mouse IgG1-647, donkey anti-mouse IgG-488 (1:150), donkey anti-rat IgG-Cy5, streptavidin-546 and donkey anti-rabbit-750. Sections were then washed. For anti-NDUFB8, sections were also incubated in tertiary antibody: streptavidin-647 for 2 h at room temperature. All sections were stained with Hoechst 33342 (Invitrogen).

TUNEL labeling. TUNEL labeling was performed using an In Situ Cell Death Detection kit (Merck; 11684817910) per the manufacturer's standard protocol with the following exceptions: the enzyme solution was diluted 1:40 in TUNEL dilution buffer (Merck; 11966006001) and the convertor POD was diluted 1:2 in phosphate-buffered saline (PBS).

OXPHOS protein quantification, image analysis and *Z* score generation (mice). Sections were imaged using a Nikon A1R inverted confocal microscope and were analyzed using ImageJ software (NIH). Adenomas ($n=9$ *PolgA*$^{mut/mut}$;*Lgr5-creER*;*Apc*$^{fl/fl}$ mice per group; $n=10$ *Lgr5-creER*;*Apc*$^{fl/fl}$ mice per group; minimum of 20 crypts per mouse), normal crypts ($n=5$ mice per group; minimum of ten crypts per mouse) or small areas of lamina propria containing approximately 5–10 stromal cells ($n=5$ mice per group; minimum of 50 areas per mouse) were selected as regions of interest and fluorophore mean intensity values were recorded for each channel. Values were background corrected by subtracting the mean intensity of a no primary control from the regions of interest mean. *Z* scores were generated using in-house software (available at http://mito.ncl.ac.uk/immuno/), as previously described[29].

OXPHOS/SSP protein quantification, image analysis and *Z* score generation (humans). OXPHOS and OXPHOS/SSP immunofluorescence was performed as above on four serial sections per subject ($n=12$). The first section was labeled with antibodies against NDUFB8, MTCO1 and TOMM20. OXPHOS proteins were quantified and crypts were categorized as OXPHOS positive or deficient based on their *Z* scores. The second to fourth sections were labeled with antibodies against NDUFB8, MTCO1 and one of either PHGDH, PSAT1 or MTHFD2. The same crypts were identified in all serial sections and levels of SSP enzymes were quantified. Data were binned into OXPHOS normal or OXPHOS deficient and SSP enzyme protein levels were compared. Every OXPHOS-deficient crypt on the section was quantified (range: $n=8$–108) and OXPHOS-normal crypts on the same section were randomly selected based on the 4′,6-diamidino-2-phenylindole (DAPI) channel and quantified.

Thymidine analog labeling, immunofluorescence and analysis. At 16 d post-*Apc* deletion, mice ($n=5$ per group) were injected with 300 µl CldU (C6891; Sigma–Aldrich) 28 and 20 h before death. At 4 h before death, mice were injected with 300 µl IdU (I7125; Sigma–Aldrich). Immunofluorescence was performed as above. Twenty adenomas per mouse were manually identified and imaged using a Zeiss Axio Imager M1 fluorescence microscope. Zeiss ZEN Lite (Blue Edition) was used to quantify cells labeled with a single antibody and cells in which co-localization of >1 antibody was observed.

Scoring of β-catenin^{high} foci. Two serial sections were taken for scoring β-catenin^{high} foci; the first was subjected to β-catenin IHC and the adjacent section was subjected to standard hematoxylin and eosin staining, as previously described[13]. β-catenin^{high} foci were scored as clusters of cells that showed increases in both nuclear and cytoplasmic β-catenin compared with surrounding cells. Hematoxylin and eosin sections were used to confirm the dysplastic nature of the cells. Areas of β-catenin^{high} cell clusters were measured, with cells being classed as belonging to the same cluster or foci if there were no normal crypts separating them. Sections were scored blind by two people independently.

Scoring of apoptotic cells. Apoptotic cells were labeled in colon and small intestine tissue sections from $n=9$ mice per group using two methods: cleaved caspase-3 IHC and TUNEL assay. For the small intestine, $n=9$ mice were analyzed per assay per group. For the colon, $n=7$ *PolgA*$^{mut/mut}$;*Lgr5-creER*;*Apc*$^{fl/fl}$ mice and $n=9$ *Lgr5-creER*;*Apc*$^{fl/fl}$ mice were analyzed per group using cleaved caspase-3 IHC and $n=9$ mice per group were analyzed for the TUNEL assay. A minimum of ten adenomas were analyzed per mouse. Apoptotic cells were counted and presented as the percentage of total nuclei in the adenoma.

Quantification of CD3$^+$, CD45R$^+$ and NIMP1$^+$ cells. Small intestine sections from $n=5$ *PolgA*$^{mut/mut}$ and *PolgA*$^{+/+}$ mice underwent IHC as above to identify CD3$^+$, CD45R$^+$ and NIMP1$^+$ cells. Ten random ×20 magnification images were taken per section and the number of positive cells per field of view were counted. The total area of epithelium was measured and the frequency of positive cells per mm^2 was calculated. Areas containing Peyer's patches were excluded.

Small intestinal crypt and stromal RNA extraction. Small intestine crypts were isolated from the stroma from the distal small intestine as previously described[53]. Crypt pellets and stromal pellets were flash frozen in liquid nitrogen and stored at −80 °C. RNA was extracted using the RNeasy Mini Kit with DNase (Qiagen) using the manufacturer's protocol. Sample RNA integrity scores were analyzed on a 2100 Bioanlyzer (Agilent) using the RNA 600 Nanokit and 2100 Expert software version B02.9.

RNA-Seq. Crypt RNA from *Polg*$^{mut/mut}$ ($n=4$) and *PolgA*$^{+/+}$ ($n=4$) mice with an RNA integrity score of >7.0 (range: 7.5–9.2) were used in differential gene expression analysis. Crypt messenger RNA (mRNA) libraries were prepared using the TruSeq Stranded mRNA library kit (Illumina). Samples were analyzed using the NextSeq 500 system (Illumina) with 16 million 75-base pair single reads per sample. All samples were quality assessed using FASTQC version 0.11.7, before processing in accordance with the protocol in refs. [54–57] using StringTie version 1.3.4 and Ballgown version 3.8. Alignment and annotation used the Hisat2 mm10 genome build (Hisat2 version 2.1.0) and the Ensembl GTF version GRCm38.92, respectively. The resultant gene lists were then submitted to Enrichr webserver[58,59] to obtain ontology information.

Small intestine adenoma RNA extraction. The distal small intestine was extracted from 6-month-old *PolgA*$^{mut/mut}$;*Lgr5-creER*;*Apc*$^{fl/fl}$ and *Lgr5-creER*;*Apc*$^{fl/fl}$ mice at 23 d post-tamoxifen induction. Tissue was flushed with PBS, opened longitudinally and rolled up, followed by freezing in isopentane cooled to −190 °C in liquid nitrogen. Small intestine tissue sections (15 µM) were cut on polyethylene naphthalate membrane slides. Sections were fixed in 75% ethanol and stained in 1% cresyl violet acetate (in 50% ethanol). Sections were dehydrated in a graded ethanol series and air dried for 5 min. Laser microdissection of adenomas was performed using the Zeiss PALM microdissection system. Adenoma RNA was isolated using the RNeasy Micro kit with DNase (Qiagen).

qRT-PCR. A High-Capacity cDNA Reverse Transcription Kit (Applied Biosystems) was used to reverse transcribe RNA from crypt, stromal and adenoma samples. qRT-PCR was performed in triplicate using validated TaqMan assays for *Phgdh*, *Psat1*, *Psph*, *Mtirfd2*, *Aldh1l2* and *Slc1a4* with TaqMan Universal PCR Master Mix (Applied Biosystems) on the Applied Biosystems StepOnePlus Real-Time PCR system. In total, 14 crypt samples ($n=7$ per group), 12 stromal samples ($n=6$ per group) and 12 adenoma samples ($n=6$ per group) were analyzed by StepOne Software version 2.1. The comparative C_t method was used with *Actb* mRNA as a reference to generate ΔC_t values in Microsoft Excel 2016.

Adenoma organoid generation. *Lgr5-creER*;*Apc*$^{fl/fl}$ and *PolgA*$^{mut/mut}$;*Lgr5-creER*;*Apc*$^{fl/fl}$ mice were induced with tamoxifen across 4 d (3, 2, 2 and 2 mg) at 6 months and small intestine adenomas were isolated ~3 weeks after induction. Organoids were generated and maintained as previously described[34].

Growth analysis in SG medium. Adenoma cultures from *Apc*$^{fl/fl}$ ($n=3$) and *PolgA*$^{mut/mut}$;*Apc*$^{fl/fl}$ ($n=3$) mice were collected in PBS, pelleted and resuspended in 50% Matrigel (vol/vol) in PBS in a 96-well plate. Amino acid-free Advanced DMEM/F-12 (Life Technologies) was reconstituted with the appropriate concentrations of amino acids. Cultures were grown in complete (+SG) or serine and glycine free (−SG) medium for 5 d at 37 °C and 5% CO_2, with the media refreshed after 3 d. Images of four points per well were taken every 2 h using Incucyte ZOOM (Essen BioScience) equipped with their Dual Color Filter Cube (4459) and a Nikon 10× objective, using Incucyte ZOOM 2018A (version 20181.1.6628.28170) software. Organoid two-dimensional areas on day 0 and day 5 were measured using ImageJ version 1.51.

Mitochondrial functional assay. The XF Cell Mito Stress Test Kit (Seahorse Bioscience) was performed using the adenoma organoids. One day before the assay, 96-well plates were prepared with Matrigel as previously described[60]. Intestinal adenoma cultures from *Apc*$^{fl/fl}$ ($n=3$) and *PolgA*$^{mut/mut}$;*Apc*$^{fl/fl}$ mice ($n=3$) were collected 3 d post-seeding, pooled, washed and pelleted. Pellets were resuspended in Mito XF medium. The Mito Stress Test was performed per the manufacturer's standard protocol on a Seahorse XF96 Extracellular Flux analyzer. Data were collected using Agilent Seahorse Wave software version 2.4. Following analysis, organoids were fixed in 10% neutral-buffered formalin for 30 min at room temperature. Formalin was then removed and the plates were left to air dry overnight. Organoids were incubated in cresyl violet at room temperature for 30 min, then washed in dH_2O overnight followed by incubation in 10 mM acetic acid on a shaker at room temperature for 30 min. The optical intensity was measured at 562 nm and read-outs were used to normalize OCR measurements.

Metabolomics analysis. Organoid cultures were plated in technical triplicates in 24-well plates and 3 d post-seeding the medium was changed to include $^{13}C_6$-labeled glucose (Cambridge Isotope Laboratories) minus HEPES and nystatin. Samples were prepared and underwent liquid chromatography–mass spectrometry (LC-MS) as previously described[54]. Metabolite peak areas were determined using Thermo TraceFinder (version 3.2). Commercial standards of all metabolites detected had been previously analyzed on this LC-MS system with the pHLIC column. ^{13}C labeling patterns were determined by measuring peak areas for the accurate mass of each isotopolog of many metabolites. Metabolite levels were normalized to total cell protein. The LC-MS protocol was adapted from ref. [61].

Complex I inhibition of adenoma organoids with metformin. Adenoma organoids from *Apc*$^{fl/fl}$ mice ($n=3$) were washed in PBS, resuspended in 100 µl CellTracker Green CMFDA (1:200 in media) and incubated at 37°C for 10 min. Afterwards, the cells were pelleted, washed and resuspended in Matrigel, then seeded in 96-well plates, and complete media was added. Cells were imaged on a Zeiss LSM 800 confocal microscope at 2.5× magnification to generate 1-mm-thick Z-stacks of 25 slices. Organoids were then dosed with 0–500 µM metformin in dimethyl sulfoxide (three technical replicates per dose per mouse). On the fifth day, organoids were stained with DAPI (1:200), washed and imaged as above. Images were stitched using ZEN version 2.6 and channels were deconvolved using Huygens Software version 18.04. Surfaces were created in Imaris version 9.0 using the CellTracker or DAPI labeling. A threshold of >200,000 µm^3 was applied and the volumetric size of organoids on day 5 was normalized to day 1.

FACS analysis of small intestinal lymphocytes. Lamina propria lymphocytes were extracted from 6-month-old *PolgA*$^{+/+}$ and *PolgA*$^{mut/mut}$ mice ($n=3$ per genotype) as follows: small intestines were extracted, cleared of mesentery, fat and Peyer's patches, cut into pieces and washed in Hank's balanced salt solution without calcium and magnesium. Intraepithelial lymphocytes were removed by agitation for 15 min in Hank's balanced salt solution with 20 mM HEPES and 2% fetal calf serum. The remaining tissue was digested in serum-free medium containing Liberase TL (250 µg ml^{-1}; Roche) and 0.05% DNase I (Roche) for 15 min. Lamina propria lymphocytes were separated from epithelial cells by centrifugation in 40% Percoll and cell pellets were collected.

Lymphocytes were washed once with PBS and then stained with LIVE/DEAD stain (Invitrogen; 34961) for 30 min at 40°C. Cells were then washed once with PBS and labeled with the following cell-surface antibodies: CD4, CD8, CD45R/B220, NK1.1, CD11b, CD11c, F4/80 and Class II (anti-mouse I-A/I-E). Cells were analyzed using LSR II (FACSDiva version 8 software) and FlowJo version 10 software.

Statistics and reproducibility. Statistical comparisons for survival data were performed using GraphPad Prism (version 8.3.1) software using a Mantel–Cox (log-rank) test. Unpaired *t*-tests and Mann–Whitney *U*-tests were performed using GraphPad Prism (version 8.3.1). Where no predication was made about the direction of a potential difference, two-tailed tests were used (for example, Fig. 3c). Where pre-existing data supported a prediction in the direction of a difference between samples, a one-tailed *t*-test was used (for example, Fig. 5b,c). Where multiple comparisons were made, one-way analysis of variance (ANOVA) was calculated using GraphPad Prism (version 8.3.1), followed by Tukey's post-hoc test (for example, Fig. 4f). Linear mixed-effects models were employed to compare the tumor sizes, cell proliferation apoptotic and immune cell (IHC) frequencies for each group (for example, Fig. 3e–h). This allowed variation between individual mice and sample location to be accounted for as random effects within the model structure. Tumor data were logged to approximate a normal distribution. For analysis of organoids following metformin dosing, estimation graphics for observed organoid sizes were displayed on Gardner–Altman plots[62]. This allows the distribution of the mean difference to be observed though bootstrapping[63], generating a robust sampling-error curve with a 95% confidence interval. Analysis was conducted using the R programming language (code available on request)[64] (R Studio version 3.4.0). In all figures where the data shown are the means per mouse or human of multiple measurements, error bars represent s.e.m. Where they are a single data point per mouse or human, error bars represent s.d. All *P* values are: $^*P<0.05$; $^{**}P<0.01$; $^{***}P<0.001$.

Sample sizes were chosen based on previous studies and our experience using these models, which had shown robust statistical power. No statistical methods were used to predetermine sample size. All experiments were successfully replicated. For the mouse studies, a minimum of four mice were used; organoid cultures were generated from three different animals; and a minimum of three independent cultures per mouse were used in each experiment. All mouse and organoid work was replicated in at least two independent experiments. For the IHC or immunofluorescence experiments, preliminary staining was performed on $n=3$–5 samples, then optimized staining was performed on the entire cohort (minimum $n=3$ biological replicates (for example, three murine or human samples) per experiment) at the same time. Image analysis was performed at the same time for each experiment. Mouse experiments were not randomized; animals were allocated to experimental groups based on their genotype. Investigators were blinded to the genotypes of the animals during the experiments and data analysis.

Reporting Summary. Further information on research design is available in the Nature Research Reporting Summary linked to this article.

Data availability

RNA-Seq and DNA next-generation sequencing data have been deposited in the Sequence Read Archive under BioProject accession code PRJNA645504. All other data supporting the findings of this study are available from the corresponding author upon reasonable request. Source data are provided with this paper.

Code availability

Code used to generate the mitochondrial OXPHOS Zscores and dot pots is freely available at http://mito.ncl.ac.uk/immuno/. The R programming code used in the linear regression mixed-effects modeling is available upon request.

Received: 5 June 2020; Accepted: 5 August 2020;
Published online: 21 September 2020

References

1. Warburg, O. On the origin of cancer cells. *Science* **123**, 309–314 (1956).
2. Warburg, O. On respiratory impairment in cancer cells. *Science* **124**, 269–270 (1956).
3. Pedersen, P. L. Tumor mitochondria and the bioenergetics of cancer cells. *Prog. Exp. Tumor Res.* **22**, 190–274 (1978).
4. Marchetti, P. et al. Mitochondrial permeability transition is a central coordinating event of apoptosis. *J. Exp. Med.* **184**, 1155–1160 (1996).
5. Rosenzweig, A., Blenis, J. & Gomes, A. P. Beyond the Warburg effect: how do cancer cells regulate one-carbon metabolism? *Front. Cell Dev. Biol.* https://doi.org/10.3389/fcell.2018.00090 (2018).
6. Diebold, L. & Chandel, N. S. Mitochondrial ROS regulation of proliferating cells. *Free Radic. Biol. Med.* **100**, 86–93 (2016).
7. Bender, A. et al. High levels of mitochondrial DNA deletions in substantia nigra neurons in aging and Parkinson disease. *Nat. Genet.* **38**, 515–517 (2006).
8. Fellous, T. G. et al. Locating the stem cell niche and tracing hepatocyte lineages in human liver. *Hepatology* **49**, 1655–1663 (2009).
9. Muller-Hocker, J. Cytochrome-*c*-oxidase deficient cardiomyocytes in the human heart—an age-related phenomenon. A histochemical ultracytochemical study. *Am. J. Pathol.* **134**, 1167–1173 (1989).
10. Muller-Hocker, J. Cytochrome *c* oxidase deficient fibres in the limb muscle and diaphragm of man without muscular disease: an age-related alteration. *J. Neurol. Sci.* **100**, 14–21 (1990).
11. Greaves, L. C. et al. Defects in multiple complexes of the respiratory chain are present in ageing human colonic crypts. *Exp. Gerontol.* **45**, 573–579 (2010).
12. Greaves, L. C. et al. Clonal expansion of early to mid-life mitochondrial DNA point mutations drives mitochondrial dysfunction during human ageing. *PLoS Genet.* **10**, e1004620 (2014).
13. Taylor, R. W. et al. Mitochondrial DNA mutations in human colonic crypt stem cells. *J. Clin. Invest.* **112**, 1351–1360 (2003).
14. Lightowlers, R. N., Chinnery, P. F., Turnbull, D. M. & Howell, N. Mammalian mitochondrial genetics: heredity, heteroplasmy and disease. *Trends Genet.* **13**, 450–455 (1997).
15. Bao, X. R. et al. Mitochondrial dysfunction remodels one-carbon metabolism in human cells. *eLife* **5**, e10575 (2016).
16. Yuan, Y. et al. Comprehensive molecular characterization of mitochondrial genomes in human cancers. *Nat. Genet.* **52**, 342–352 (2020).
17. He, Y. et al. Heteroplasmic mitochondrial DNA mutations in normal and tumour cells. *Nature* **464**, 610–614 (2010).
18. Larman, T. C. et al. Spectrum of somatic mitochondrial mutations in five cancers. *Proc. Natl Acad. Sci. USA* **109**, 14087–14091 (2012).
19. Polyak, K. et al. Somatic mutations of the mitochondrial genome in human colorectal tumours. *Nat. Genet.* **20**, 291–293 (1998).
20. *Bowel Cancer Statistics* (CRUK); http://www.cancerresearchuk.org/health-professional/cancer-statistics/statistics-by-cancer-type/bowel-cancer (accessed March 2020).
21. Greaves, L. C. et al. Comparison of mitochondrial mutation spectra in ageing human colonic epithelium and disease: absence of evidence for purifying selection in somatic mitochondrial DNA point mutations. *PLoS Genet.* **8**, e1003082 (2012).
22. Ericson, N. G. et al. Decreased mitochondrial DNA mutagenesis in human colorectal cancer. *PLoS Genet.* **8**, e1002689 (2012).
23. Greaves, L. C. et al. Mitochondrial DNA mutations are established in human colonic stem cells, and mutated clones expand by crypt fission. *Proc. Natl Acad. Sci. USA* **103**, 714–719 (2006).
24. Barker, N. et al. Crypt stem cells as the cells-of-origin of intestinal cancer. *Nature* **457**, 608–611 (2009).
25. Kujoth, G. C. et al. Mitochondrial DNA mutations, oxidative stress, and apoptosis in mammalian aging. *Science* **309**, 481–484 (2005).
26. Trifunovic, A. et al. Premature ageing in mice expressing defective mitochondrial DNA polymerase. *Nature* **429**, 417–423 (2004).

27. Baines, H. L. et al. Similar patterns of clonally expanded somatic mtDNA mutations in the colon of heterozygous mtDNA mutator mice and ageing humans. *Mech. Ageing Dev.* **139**, 22–30 (2014).
28. Stamp, C. et al. Predominant asymmetrical stem cell fate outcome limits the rate of niche succession in human colonic crypts. *EBioMedicine* **31**, 166–173 (2018).
29. Rocha, M. C. et al. A novel immunofluorescent assay to investigate oxidative phosphorylation deficiency in mitochondrial myopathy: understanding mechanisms and improving diagnosis. *Sci. Rep.* **5**, 15037 (2015).
30. Pate, K. T. et al. Wnt signaling directs a metabolic program of glycolysis and angiogenesis in colon cancer. *EMBO J.* **33**, 1454–1473 (2014).
31. Fox, R. G., Magness, S., Jujoth, G. C., Prolla, T. A. & Maeda, N. Mitochondrial DNA polymerase editing mutation, $Polg^{D257A}$, disturbs stem-progenitor cell cycling in the small intestine and restricts excess fat absorption. *Am. J. Physiol. Gastrointest. Liver Physiol.* **302**, G914–G924 (2012).
32. El-Mir, M. Y. et al. Dimethylbiguanide inhibits cell respiration via an indirect effect targeted on the respiratory chain complex I. *J. Biol. Chem.* **275**, 223–228 (2000).
33. Owen, M. R., Doran, E. & Halestrap, A. P. Evidence that metformin exerts its anti-diabetic effects through inhibition of complex 1 of the mitochondrial respiratory chain. *Biochem. J.* **348**, 607–614 (2000).
34. Maddocks, O. D. K. et al. Modulating the therapeutic response of tumours to dietary serine and glycine starvation. *Nature* **544**, 372–376 (2017).
35. Fearon, E. R. & Vogelstein, B. A genetic model for colorectal tumorigenesis. *Cell* **61**, 759–767 (1990).
36. Winawer, S. J. et al. Colorectal cancer screening: clinical guidelines and rationale. *Gastroenterology* **112**, 594–642 (1997).
37. Nikkanen, J. et al. Mitochondrial DNA replication defects disturb cellular dNTP pools and remodel one-carbon metabolism. *Cell Metab.* **23**, 635–648 (2016).
38. Rodriguez-Colman, M. J. et al. Interplay between metabolic identities in the intestinal crypt supports stem cell function. *Nature* **543**, 424–427 (2017).
39. Stringari, C. et al. Metabolic trajectory of cellular differentiation in small intestine by Phasor Fluorescence Lifetime Microscopy of NADH. *Sci. Rep.* **2**, 568 (2012).
40. Yang, M. & Vousden, K. H. Serine and one-carbon metabolism in cancer. *Nat. Rev. Cancer* **16**, 650–662 (2016).
41. Hollinshead, K. E. R. et al. Oncogenic *IDH1* mutations promote enhanced proline synthesis through PYCR1 to support the maintenance of mitochondrial redox homeostasis. *Cell Rep.* **22**, 3107–3114 (2018).
42. Lee-Six, H. et al. The landscape of somatic mutation in normal colorectal epithelial cells. *Nature* **574**, 532–537 (2019).
43. De Laat, P. et al. Clinical features and heteroplasmy in blood, urine and saliva in 34 Dutch families carrying the m.3243A>G mutation. *J. Inherit. Metab. Dis.* **35**, 1059–1069 (2012).
44. Frederiksen, A. L. et al. Tissue specific distribution of the 3243A→G mtDNA mutation. *J. Med. Genet.* **43**, 671–677 (2006).
45. Grady, J. P. et al. mtDNA heteroplasmy level and copy number indicate disease burden in m.3243A>G mitochondrial disease. *EMBO Mol. Med.* https://doi.org/10.15252/emmm.201708262 (2018).
46. Olsson, C. et al. The level of the mitochondrial mutation A3243G decreases upon ageing in epithelial cells from individuals with diabetes and deafness. *Eur. J. Hum. Genet.* **9**, 917–921 (2001).
47. Rahman, S., Poulton, J., Marchington, D. & Suomalainen, A. Decrease of 3243 A>G mtDNA mutation from blood in MELAS syndrome: a longitudinal study. *Am. J. Hum. Genet.* **68**, 238–240 (2001).
48. Su, T. et al. Inherited pathogenic mitochondrial DNA mutations and gastrointestinal stem cell populations. *J. Pathol.* **246**, 427–432 (2018).
49. Filograna, R. et al. Modulation of mtDNA copy number ameliorates the pathological consequences of a heteroplasmic mtDNA mutation in the mouse. *Sci. Adv.* **5**, eaav9824 (2019).
50. Kauppila, J. H. K. et al. A phenotype-driven approach to generate mouse models with pathogenic mtDNA mutations causing mitochondrial disease. *Cell Rep.* **16**, 2980–2990 (2016).
51. Betts, J. et al. Gastrointestinal tract involvement associated with the 3243A>G mitochondrial DNA mutation. *Neurology* **70**, 1290–1292 (2008).
52. Coxhead, J. et al. Somatic mtDNA variation is an important component of Parkinson's disease. *Neurobiol. Aging* **38**, 217.e1–217.e6 (2016).
53. Sato, T. et al. Single Lgr5 stem cells build crypt–villus structures in vitro without a mesenchymal niche. *Nature* **459**, 262–265 (2009).
54. Pertea, M., Kim, D., Pertea, G. M., Leek, J. T. & Salzberg, S. L. Transcript-level expression analysis of RNA-seq experiments with HISAT, StringTie and Ballgown. *Nat. Protocols* **11**, 1650–1667 (2016).
55. Pertea, M. et al. StringTie enables improved reconstruction of a transcriptome from RNA-seq reads. *Nat. Biotechnol.* **33**, 290–295 (2015).
56. Frazee, A. C. et al. Ballgown bridges the gap between transcriptome assembly and expression analysis. *Nat. Biotechnol.* **33**, 243–246 (2015).
57. Kim, D., Langmead, B. & Salzberg, S. L. HISAT: a fast spliced aligner with low memory requirements. *Nat. Methods* **12**, 357–360 (2015).
58. Chen, E. Y. et al. Enrichr: interactive and collaborative HTML5 gene list enrichment analysis tool. *BMC Bioinformatics* **14**, 128 (2013).
59. Kuleshov, M. V. et al. Enrichr: a comprehensive gene set enrichment analysis web server 2016 update. *Nucleic Acids Res.* **44**, W90–W97 (2016).
60. Fan, Y. Y. et al. A bioassay to measure energy metabolism in mouse colonic crypts, organoids, and sorted stem cells. *Am. J. Physiol. Gastrointest. Liver Physiol.* **309**, G1–G9 (2015).
61. Gonzalez, P. S. et al. Mannose impairs tumour growth and enhances chemotherapy. *Nature* **563**, 719–723 (2018).
62. Ho, J., Tumkaya, T., Aryal, S., Choi, H. & Claridge-Chang, A. Moving beyond *P* values: data analysis with estimation graphics. *Nat. Methods* **16**, 565–566 (2019).
63. Efron, B. & Tibshirani, R. J. *An Introduction to the Bootstrap* (CRC Press, 1994).
64. R Development Core Team *R: A Language and Environment for Statistical Computing* (R Foundation for Statistical Computing, 2018).
65. Ross, J. M. et al. Germline mitochondrial DNA mutations aggravate ageing and can impair brain development. *Nature* **501**, 412–415 (2013).

Acknowledgements

We thank T. Prolla (University of Wisconsin, Washington, United States) for donating the $PolgA^{+/mut}$ mice. We thank C. Alston for assistance with the analysis of mtDNA mutations and staff at the Newcastle University Comparative Biology Centre for animal husbandry. This work was supported by the Wellcome Centre for Mitochondrial Research (203105/Z/16/Z), Newcastle University Centre for Ageing and Vitality (supported by the Biotechnology and Biological Sciences Research Council, Engineering and Physical Sciences Research Council, Economic and Social Research Council and Medical Research Council (MR/L016354/1)), UK NIHR Biomedical Research Centre Age and Age Related Diseases award (to the Newcastle upon Tyne Hospitals NHS Foundation Trust) and NC3Rs (to C.A.R.; NC/K500513/1). O.J.S. is supported by Cancer Research UK grants (A25045, A17196, A12481 and A21139). O.J.S. and D.G. were supported by ERC starting grant 311301 awarded to O.J.S. F.O. is supported by the Medical Research Council (MR/R023026/1). J.L. is supported by Cancer Research UK (C18342/A23390).

Author contributions

L.C.G., C.B., C.S. and C.A.R. performed the breeding and phenotypic analyses of mice. A.L.M.S., D.H., M.H., J.N.S. and A.B. performed the histology, IHC, immunofluorescence and analysis of mouse and human samples. L.C.G., O.M.R., R.J. and B.G. performed the sequencing and histological analysis of human samples. S.A.C.M., I.M., S.K. and J.C.M. collected and processed the human samples. J.C.W. performed the molecular biology and cell culture experiments. G.H. and A.P. performed the sequencing and bioinformatics analyses of the mouse and human adenomas. Flow cytometric immunophenotyping of the small intestine was carried out by S.A. and G.M. J.L. and F.O. performed the immune cell IHC. L.W. carried out the imaging and analysis of the immune cell IHC. F.R. performed the statistical analysis of the RNA-Seq data. A.P.B. performed the statistical analysis of the experimental data. D.G., J.C.W. and O.J.S. performed the metabolomics analyses and analyzed the data. L.C.G., R.W.T., R.H., D.M.T., N.D.P. and O.J.S. conceived of the ideas, designed the experiments and interpreted the data. All authors contributed to writing and revising the paper.

Competing interests

F.O. is a director of Fibrofind. J.L. and F.O. are shareholders in Fibrofind. The other authors declare no competing interests.

Additional information

Extended data is available for this paper at https://doi.org/10.1038/s43018-020-00112-5.

Supplementary information is available for this paper at https://doi.org/10.1038/s43018-020-00112-5.

Correspondence and requests for materials should be addressed to L.C.G.

Reprints and permissions information is available at www.nature.com/reprints.

Publisher's note Springer Nature remains neutral with regard to jurisdictional claims in published maps and institutional affiliations.

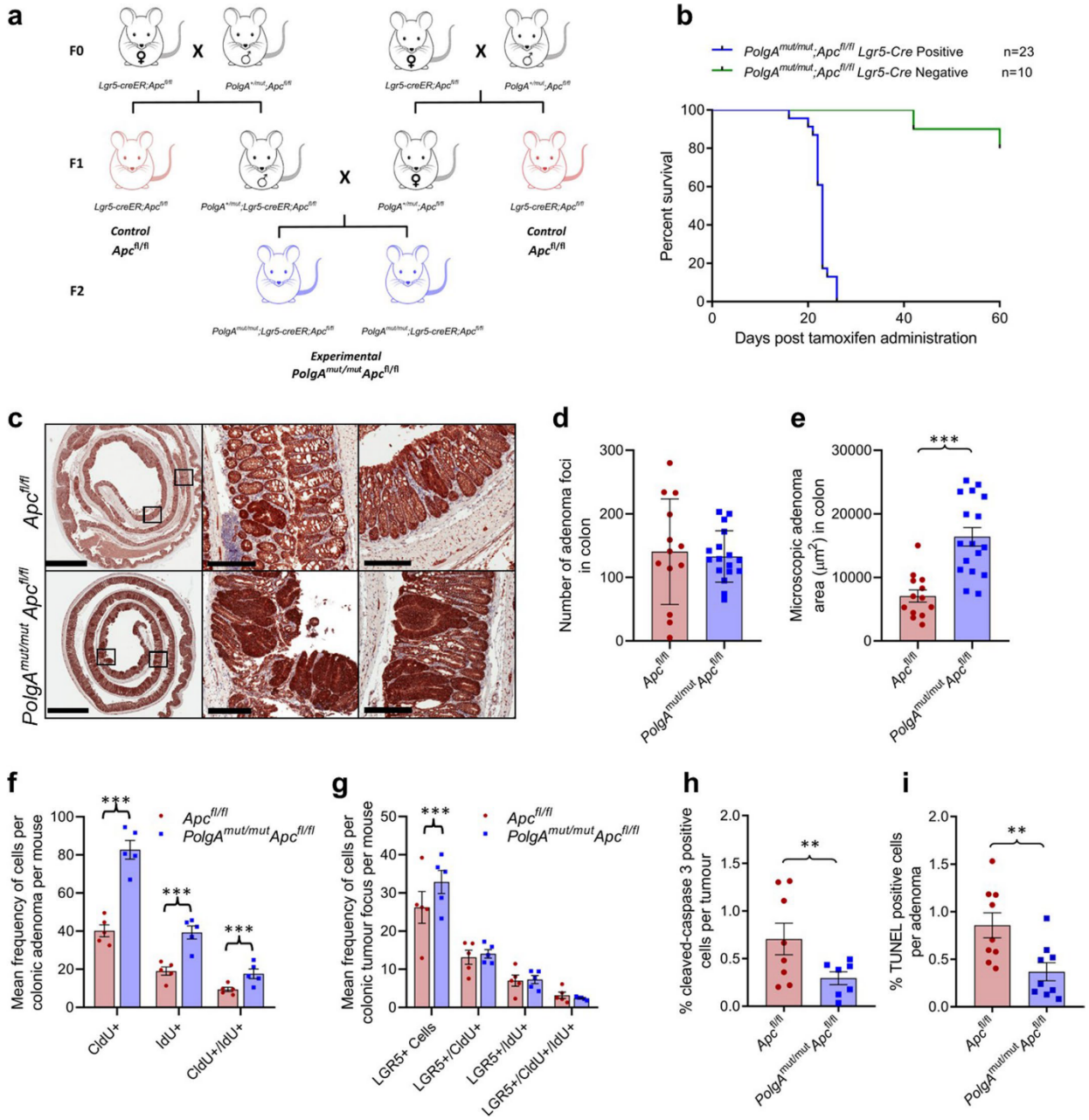

Extended Data Fig. 1 | Generation of *PolgA*$^{mut/mut}$*;Lgr5-creER;Apc*$^{fl/fl}$ and *Lgr5-creER;Apc*$^{fl/fl}$ mice and analysis of colonic adenomas. a: Breeding scheme. MtDNA mutations can be transmitted down the maternal germline[55] therefore it was essential that only *Lgr5-creER;Apc*$^{fl/fl}$ (red) mice from a wild-type *PolgA* mother used as controls. **b**: Kaplan-Meier survival curve showing survival time following tamoxifen administration in *PolgA*$^{mut/mut}$ mice. Survival to clinical endpoint or experimental endpoint of 60 days is shown, 'n' = number of mice. **c**: β-Catenin immunohistochemistry was performed on colon sections from n = 17 *PolgA*$^{mut/mut}$*;Apc*$^{fl/fl}$ mice and n = 13 *Apc*$^{fl/fl}$ mice. Representative images are shown (scale bars 3 mm (first column) and 200 µm). **d**: Frequency of adenomas in the colon 23 days post-*Apc* deletion (unpaired, two tailed, t-test, p = 0.7444), n = 17 *PolgA*$^{mut/mut}$*;Apc*$^{fl/fl}$ mice and n = 13 *Apc*$^{fl/fl}$ mice, data are mean ±s.d. **e**: Mean adenoma size in the colon in n = 17 *PolgA*$^{mut/mut}$*;Apc*$^{fl/fl}$ mice and n = 13 *Apc*$^{fl/fl}$ mice 23 days post-*Apc* deletion. All adenomas on a section were quantified ranging from 5 to 280, mean per mouse ± s.e.m are shown. Two-sided linear mixed effect regression model with mouse ID as a random effect, $P < 0.0001$. **f-g**: Quantification of the frequency of thymidine analogue incorporation in all cells per colonic adenoma (**f**) and LGR5 + cells per colon adenoma per mouse (**g**). n = 5 mice per group with 18 adenomas analysed per mouse. Mean frequency per adenoma per mouse ± s.e.m is shown. Two-sided linear mixed effect regression model with mouse ID as a random effect, $P < 0.001$. **h**, **i**: Apoptotic cells were quantified using (**h**) cleaved caspase 3 (CC3) immunohistochemistry n = 7 *PolgA*$^{mut/mut}$*;Apc*$^{fl/fl}$ mice and n = 9 *Apc*$^{fl/fl}$ mice and (**i**) TUNEL labelling (n = 9 mice per group) in mice 23 days post-*Apc* deletion. A minimum of 10 adenomas were analysed per mouse, mean percentage of apoptotic cells per adenoma per mouse ±s.e.m is shown. Two-sided linear mixed effect regression model with mouse ID as a random effect, CC3 $P = 0.0092$, TUNEL $P = 0.002$. * $P < 0.05$, ** $P < 0.01$, *** $P < 0.001$.

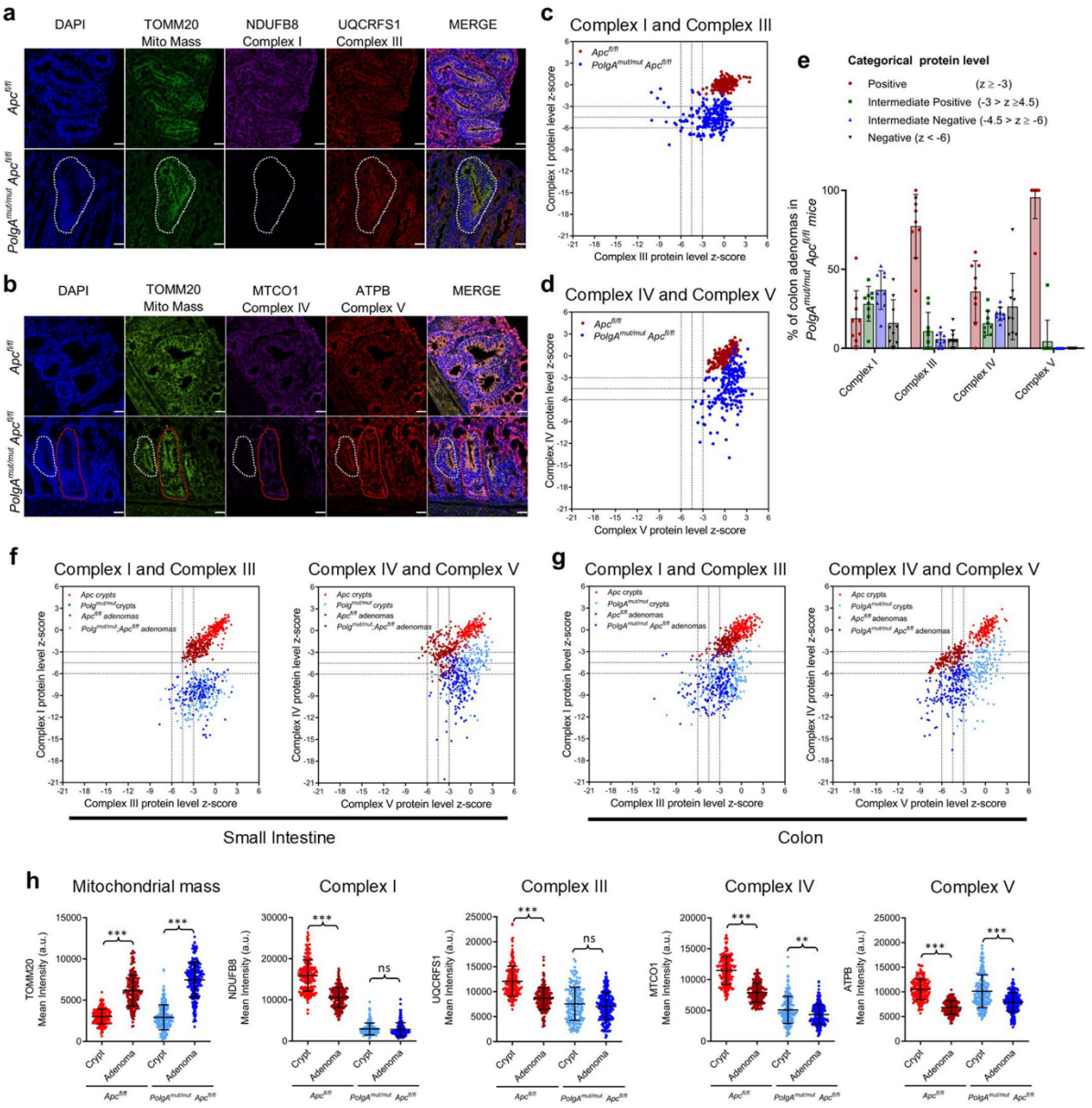

Extended Data Fig. 2 | Colonic adenomas from *PolgA*$^{mut/mut}$;*Apc*$^{fl/fl}$ mice are deficient in mitochondrial complex I, but the majority retain expression of subunits of complexes III, IV and V. a, **b**: Immunofluorescence was performed to quantify levels of OXPHOS proteins in n = 9 *PolgA*$^{mut/mut}$;*Apc*$^{fl/fl}$ mice and n = 9 *Apc*$^{fl/fl}$ mice. Representative images are shown. Scale bars 50 µm. An adenoma deficient in complex I is highlighted by the white dashed line in **a**. The white dashed line highlights an adenoma deficient in complex IV, and red dashed line shows one with normal complex IV in **b**-**d**: dot plots showing Z-scores calculated following quantification of mitochondrial OXPHOS protein levels in adenomas from n = 9 *PolgA*$^{mut/mut}$;*Apc*$^{fl/fl}$ and n = 9 *Apc*$^{fl/fl}$ mice with 20 adenomas quantified per mouse. **e**: Categorical analysis of OXPHOS protein levels in *PolgA*$^{mut/mut}$;*Apc*$^{fl/fl}$ (n = 9) and *Apc*$^{fl/fl}$ (n = 9) mice, error bars show mean ±s.d. **f**, **g**: dot plots showing Z-scores calculated following quantification of mitochondrial OXPHOS protein levels in normal crypts and adenomas in the small intestine (**f**) and the colon (**g**). **f**: For the adenomas: n = 9 *PolgA*$^{mut/mut}$;*Apc*$^{fl/fl}$ and n = 10 *Apc*$^{fl/fl}$ mice were analysed with 20 adenomas quantified per mouse. For the normal crypts, n = 5 mice were analysed with a minimum of 13 crypts quantified per mouse. **g**: For the colonic adenomas: n = 9 mice per group were analysed with a minimum of 20 adenomas quantified per mouse. For the normal crypts, n = 6 *Apc*$^{fl/fl}$ mice and n = 7 *PolgA*$^{mut/mut}$;*Apc*$^{fl/fl}$ mice were analysed with a minimum of 22 crypts quantified per mouse. **h** Dot plots showing raw densitometry values for mitochondrial protein levels in the colon (n numbers same as in **g**, error bars are s.d.). One-way ANOVA with Tukey's post-test. *P* values for within genotype comparisons between normal crypts and adenomas were as follows: TOMM20: *Apc*$^{fl/fl}$ $P < 0.0001$, *PolgA*$^{mut/mut}$;*Apc*$^{fl/fl}$ $P < 0.0001$, NDUFB8: *Apc*$^{fl/fl}$ $P < 0.0001$, *PolgA*$^{mut/mut}$;*Apc*$^{fl/fl}$ $P = 0.9761$, UQCRFS1: *Apc*$^{fl/fl}$ $P < 0.0001$, *PolgA*$^{mut/mut}$;*Apc*$^{fl/fl}$ $P = 0.2901$, MTCO1: *Apc*$^{fl/fl}$ $P < 0.0001$, *PolgA*$^{mut/mut}$;*Apc*$^{fl/fl}$ $P = 0.007$, ATPB: *Apc*$^{fl/fl}$ $P < 0.0001$, *PolgA*$^{mut/mut}$;*Apc*$^{fl/fl}$ $P < 0.0001$. For all panels: * $P < 0.05$, ** $P < 0.01$, *** $P < 0.001$.

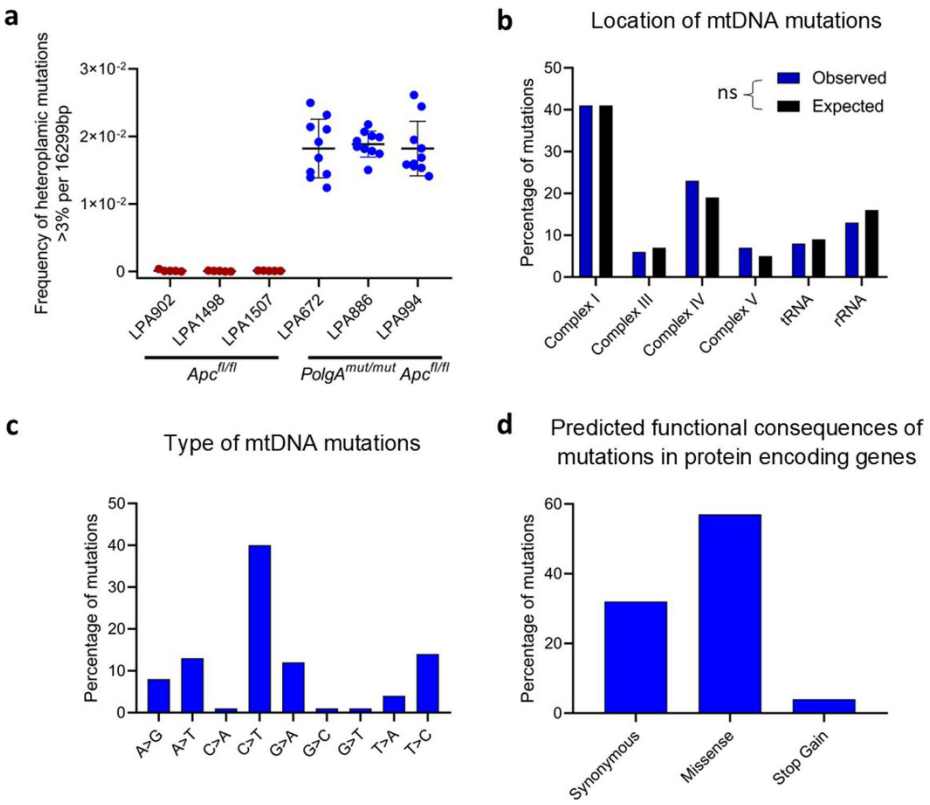

Extended Data Fig. 3 | Analysis of mitochondrial DNA (mtDNA) mutations detected in individual small intestinal adenomas from *PolgA*$^{mut/mut}$;*Apc*$^{fl/fl}$ and *Apc*$^{fl/fl}$ mice. a: The frequency of heteroplasmic variants >3% detected in adenomas from *PolgA*$^{mut/mut}$;*Apc*$^{fl/fl}$ (n = 3 mice per group and n = 10 adenomas per mouse) and *Apc*$^{fl/fl}$ mice (n = 3 mice per group, n = 5 adenomas per mouse), mean ±s.d. are shown. **b–d**: Analysis of mtDNA variants present at >30% heteroplasmy in individual adenomas from *PolgA*$^{mut/mut}$;*Apc*$^{fl/fl}$ mice (n = 413 mtDNA mutations in total). For location (**b**), expected values were calculated based on the proportion of the mitochondrial genome taken up by each gene category and observed and expected values compared using Chi-squared analysis. No significant deviation from the expected frequencies was detected ($P = 0.4744$).

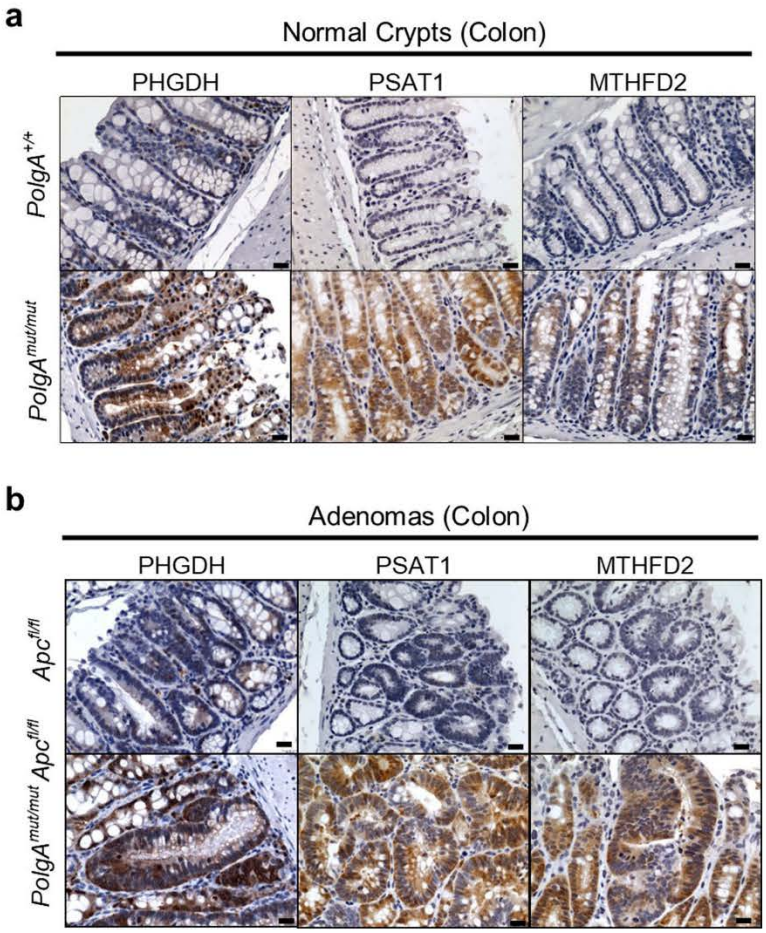

Extended Data Fig. 4 | Mitochondrial OXPHOS dysfunction causes upregulation of denovo serine synthesis *in vivo* in the mouse colon. Immunohistochemistry images showing in situ levels of SSP proteins in the non-transformed normal colonic mucosa (**a**) and adenomas (**b**) of *PolgA*$^{+/+}$ and *PolgA*$^{mut/mut}$ mice. Immunohistochemistry was performed on n = 4 mice per group. Representative images are shown. Scale bars 50 µm.

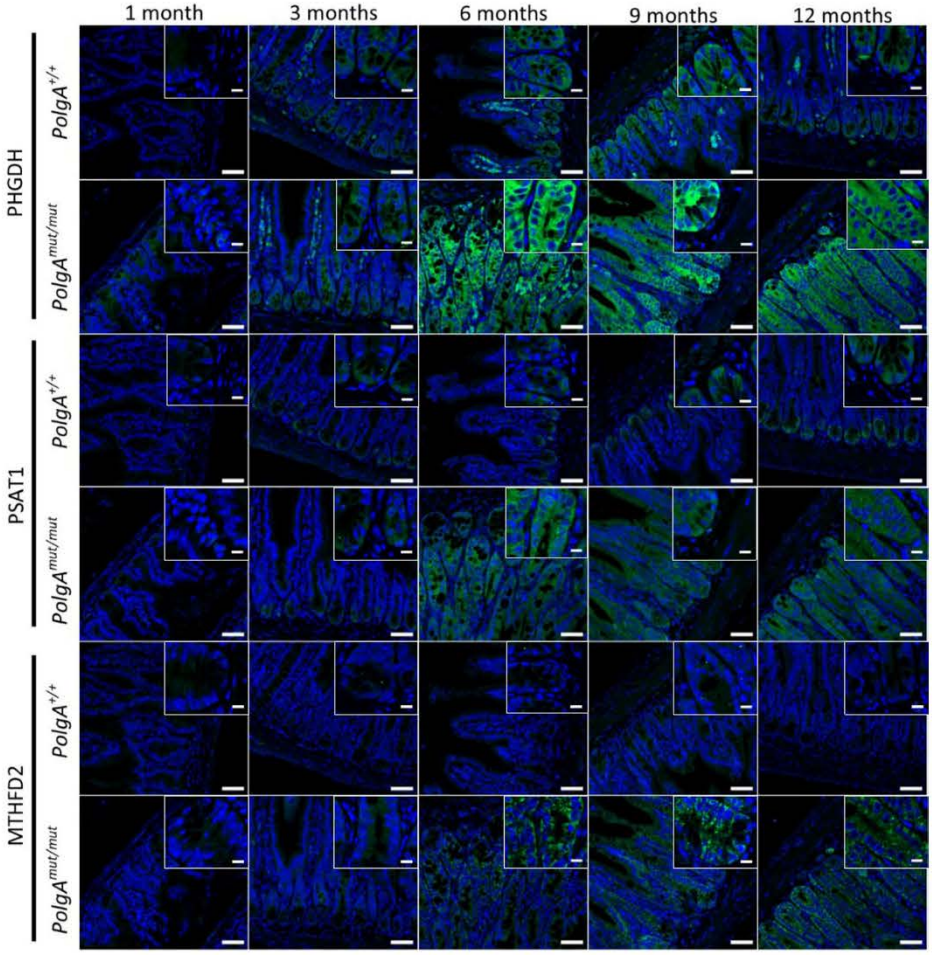

Extended Data Fig. 5 | Immunofluorescent images showing the levels of PHGDH, PSAT1 and MTHFD2 in *PolgA*$^{+/+}$ and *PolgA*$^{mut/mut}$ mice from 1–12 months of age. Immunofluorescence was performed on n = 3 mice per group at each time point. Representative images are shown. Scale bars 50 μm.

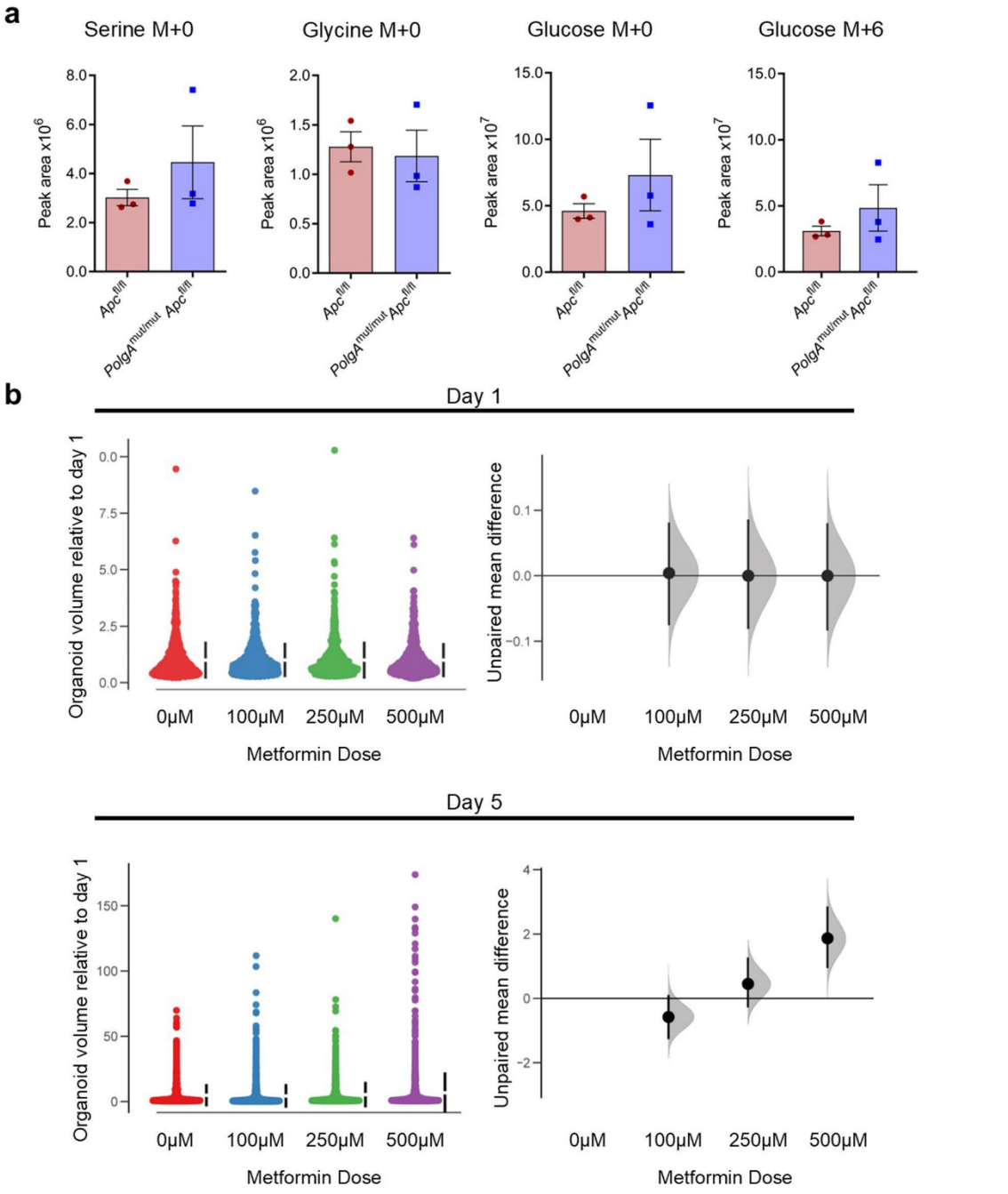

Extended Data Fig. 6 | Quantification of major mass isotopomers following growth of adenoma organoids in $^{13}C_6$-glucose and adenoma organoid growth in to the presence of metformin. a: Quantification of major mass isotopomers following growth in the presence of $^{13}C_6$-glucose for 24 h. ^{13}C labelling is shown as M + 6 (glucose) and M + 0 denotes no labelling. No significant differences were found between organoids from *Apc*$^{fl/fl}$ mice compared with *PolgA*$^{mut/mut}$;*Apc*$^{fl/fl}$ mice by one-tailed unpaired t-test. n = 3 mice per group with 3 technical replicates performed per mouse. Error bars show s.e.m. **b**: A shared group estimation plot comparing the effect of metformin on the volume of individual adenoma organoids generated from *Apc*$^{fl/fl}$ mice (n = 3) on days 1 and 5 post seeding. Volume data are normalised to day 1. On day 1 the numbers of organoids measured were: 0 μM: n = 739, 100 μM: n = 796, 250 μM: n = 711, 500 μM: n = 652. On day 5 the numbers of organoids measured were: 0 μM: n = 1060, 100 μM: n = 1515, 250 μM: n = 1088, 500 μM: n = 1431. Bootstrap estimation of group mean differences (circle) and 95% confidence intervals (vertical bars) are plotted as a sampling distribution.

nature research

Corresponding author(s): Laura Greaves

Last updated by author(s): Jul 16, 2020

Reporting Summary

Nature Research wishes to improve the reproducibility of the work that we publish. This form provides structure for consistency and transparency in reporting. For further information on Nature Research policies, see Authors & Referees and the Editorial Policy Checklist.

Statistics

For all statistical analyses, confirm that the following items are present in the figure legend, table legend, main text, or Methods section.

n/a	Confirmed
☐	☒ The exact sample size (*n*) for each experimental group/condition, given as a discrete number and unit of measurement
☐	☒ A statement on whether measurements were taken from distinct samples or whether the same sample was measured repeatedly
☐	☒ The statistical test(s) used AND whether they are one- or two-sided *Only common tests should be described solely by name; describe more complex techniques in the Methods section.*
☒	☐ A description of all covariates tested
☐	☒ A description of any assumptions or corrections, such as tests of normality and adjustment for multiple comparisons
☐	☒ A full description of the statistical parameters including central tendency (e.g. means) or other basic estimates (e.g. regression coefficient) AND variation (e.g. standard deviation) or associated estimates of uncertainty (e.g. confidence intervals)
☐	☒ For null hypothesis testing, the test statistic (e.g. *F*, *t*, *r*) with confidence intervals, effect sizes, degrees of freedom and *P* value noted *Give P values as exact values whenever suitable.*
☒	☐ For Bayesian analysis, information on the choice of priors and Markov chain Monte Carlo settings
☒	☐ For hierarchical and complex designs, identification of the appropriate level for tests and full reporting of outcomes
☒	☐ Estimates of effect sizes (e.g. Cohen's *d*, Pearson's *r*), indicating how they were calculated

Our web collection on statistics for biologists contains articles on many of the points above.

Software and code

Policy information about availability of computer code

Data collection	ABI3130 Data Collection Software v4 MiSeq control software v3.1 2100 Expert Software vB02.9 StepOne Software v2.1 FACS Diva v8 Aperio ImageScope v12.4 Thermotrace Finder v3.2 IncuCyte ZOOM 2018A v20181.1.6628.28170 Zen 2 (Blue Edition) Seahorse Wave Analyser v2.4
Data analysis	SeqScape V2.6 BWA v0.7. Samtools v0.1.18 Picard v1.85 VarScan v2.3.8 LoFreq v0.6.1 ANNOVAR v529 Haplogrep v2 FASTQC v0.11.7 Stringtie v.1.3.4 Hisat2 v.2.1.0 Ballgown v3.8 Enrichr webserver (2016 update) Ensembl GTF v.GRCm38.92

Aperio ImageScope v12.4
Zen 2 (Blue Edition)
Seahorse Wave Analyser v2.4
Graphpad Prism v8.3.1
FlowJo v10
StepOne Software v2.1
Imaris v9.0
Huygens v18.04
Zen v2.6
ImageJ v1.51
R Studio v3.4.0
Microsoft Excel 2016

For manuscripts utilizing custom algorithms or software that are central to the research but not yet described in published literature, software must be made available to editors/reviewers. We strongly encourage code deposition in a community repository (e.g. GitHub). See the Nature Research guidelines for submitting code & software for further information.

Data

Policy information about availability of data

All manuscripts must include a data availability statement. This statement should provide the following information, where applicable:

- Accession codes, unique identifiers, or web links for publicly available datasets
- A list of figures that have associated raw data
- A description of any restrictions on data availability

RNA and DNA sequencing data has been deposited in the Sequence Read Archive under Bioproject accession code PRJNA645504. Raw data is provided for Figures 1c, 2d-g, 3a,c,e-h, 4c-f, 5b,c, g-i, 6a-g, 7b-d and for Extended Data Figures 1b, d-i, 2c-h, 3a-d, 6b. All other data supporting the findings of this study are available from the corresponding author on reasonable request.

Field-specific reporting

Please select the one below that is the best fit for your research. If you are not sure, read the appropriate sections before making your selection.

☒ Life sciences ☐ Behavioural & social sciences ☐ Ecological, evolutionary & environmental sciences

For a reference copy of the document with all sections, see nature.com/documents/nr-reporting-summary-flat.pdf

Life sciences study design

All studies must disclose on these points even when the disclosure is negative.

Sample size	No statistical methods were used to predetermine sample size. Sample sizes were chosen based on previous studies which had shown robust statistical power.
Data exclusions	No data were excluded
Replication	No statistical methods were used to predetermine sample size. Sample sizes were chosen based on previous studies which had shown robust statistical power. All experiments were successfully replicated. For mouse studies a minimum of 4 mice were used, and organoid cultures were generated from 3 different animals and a minimum of 4 independent cultures per mouse used in each experiment. All mouse and organoid work was replicated in at least 2 independent experiments. For IHC or IF experiments, preliminary staining was performed on n=3-5 samples then optimised staining performed on the entire cohort (minimum n=3 biological replicates (e.g. 3 mice or human samples) per experiment) at the same time. Image analysis was performed at the same time for each experiment.
Randomization	Mouse were not randomized, animals were allocated to experimental groups based on their genotype
Blinding	Investigators were blinded to the genotypes of the animals during the experiments and data analysis.

Reporting for specific materials, systems and methods

We require information from authors about some types of materials, experimental systems and methods used in many studies. Here, indicate whether each material, system or method listed is relevant to your study. If you are not sure if a list item applies to your research, read the appropriate section before selecting a response.

Materials & experimental systems

n/a	Involved in the study
☐	☒ Antibodies
☒	☐ Eukaryotic cell lines
☒	☐ Palaeontology
☐	☒ Animals and other organisms
☐	☒ Human research participants
☒	☐ Clinical data

Methods

n/a	Involved in the study
☒	☐ ChIP-seq
☐	☒ Flow cytometry
☒	☐ MRI-based neuroimaging

Antibodies

Antibodies used

Rabbit anti-β-Catenin (ab6302, Abcam), 1:1000
mouse anti-IdU [Clone 32D8.D9] (ab181664, Abcam), 1:100
rat anti-BrdU [Clone BU1/75 (ICR1] (NB-500-169, Novus Biologicals), 1:100
goat anti-GFP biotin [polyclonal] (ab6658, Abcam), 1:100
rabbit anti-MTHFD2 [polyclonal] (ab151447, Abcam), mouse IHC: 1:600, mouse IF:1:300, human IF: 1:90
rabbit anti-PSAT1 [polyclonal] (NBP1-32920, Novus Biologicals) mouse IHC: 1:600, mouse IF:1:300, human IF: 1:90
rabbit anti-PHGDH [polyclonal](HPA021241, Sigma Aldrich), mouse IHC: 1:4000, mouse IF:1:2000 human IF: 1:300
donkey anti-mouse IgG (H+L) secondary antibody, Alexa Fluor 488 conjugated (A21202, Invitrogen) 1:150
Cy5-conjugated AffiniPure donkey anti-rat IgG (H&L) secondary antibody (712-175-153, Jackson Immuno Research), 1:200
streptavidin, Alexa Fluor 546 conjugated secondary antibody (S11225, Invitrogen), 1:200
donkey anti-rabbit IgG (H&L) Alexa Fluor 750 conjugated secondary antibody (ab175728, Abcam), 1:200
mouse anti-NDUFB8 [clone 20E9DH10C12] (ab110242, Abcam), 1:50
mouse anti-UQCRFS1 [clone 5A5] (ab14746, Abcam), 1:100
rabbit anti-TOMM20 [clone EPR15581-39] (ab186734, Abcam), 1:100
mouse anti-MTCO1 antibody [clone 1D6E1A8] (ab14705, Abcam), 1:100
mouse anti-ATPB antibody [clone 3D5] (ab14730, Abcam), 1:100
mouse anti-SDHA [2E3GC12FB2AE2] (ab14715, Abcam), 1:100
goat anti-mouse IgG1 cross adsorbed secondary antibody biotin-XX (A10519, Invitrogen), 1:200
goat anti-mouse IgG2b cross-adsorbed secondary antibody, Alexa Fluor 546 (A21143, Invitrogen), 1:200
goat anti-rabbit IgG (H+L) cross-adsorbed secondary antibody, Alexa Fluor 488 (A11008, Invitrogen), 1:200
goat anti-mouse IgG2a cross-adsorbed secondary antibody, Alexa Fluor 546 (A21133, Invitrogen), 1:200
goat anti-mouse IgG1 cross-adsorbed secondary antibody, Alexa Fluor 647 (A21240, Invitrogen), 1:200
goat anti-rabbit IgG (H+L) cross-adsorbed secondary antibody, Alexa Fluor 488 (A11008, Invitrogen), 1:200
streptavidin, Alexa Fluor 647 conjugate (S32357, Invitrogen), 1:200
rabbit anti-cleaved caspase 3 [polyclonal] (AB3623 Merck Millipore), 1:35
rat anti-CD45R [clone RA3-6B2] (ab64100, Abcam), 1:200
rat Anti-Neutrophil [clone NIMP-R14] (ab2557 Abcam), 1:100
rat anti-CD3 [clone CD3-12] (MCA1477 BioRad], 1:100
rat-anti CD4 [clone: RM4-5] (BioLegend 100536), 1:200
rat-anti CD8 [clone: 53-6.7] (BioLegend 100737), 1:200
rat-anti-CD45R/B220 [clone: RA3-6B2[(BioLegend 103235), 1:200
rat-anti NK1.1[clone: PK136] (BioLegend 108737), 1:200
rat-anti CD11b [clone: M1/70] (BioLegend 101237) 1:200
Armenian hamster anti-CD11c [clone: N418] (BioLegend 117309), 1:200
rat anti-F4/80 (clone: BM8) [BioLegend 123107], 1:200
rat anti-Class II [anti-mouse I-A/I-E; clone: M5/114.15.2] (BioLegend 107645), 1:200

Validation

All primary antibodies used were commercially available and validated by the manufacturers and have been extensively used in previous publications. Links to the manufacturer's websites that contain relevant citations are below. No primary antibody controls were included in all experiments to check for non-specific activity of primary antibodies. Cellular localization of the antibody labeling was confirmed to be as predicted e.g. anti-IdU and anti-cleaved caspase 3 showed nuclear labelling and the mitochondrial OXPHOS antibodies showed cytoplasmic labeling.

Rabbit anti-β-Catenin (ab6302, Abcam); https://www.abcam.com/beta-catenin-antibody-ab6302-references.html#top-0
mouse anti-IdU (ab181664, Abcam); https://www.abcam.com/idu-antibody-32d8d9-ab181664.html
rat anti-BrdU (NB-500-169, Novus Biologicals); https://www.novusbio.com/products/bromodeoxyuridine-brdu-antibody-bu1-75-icr1-_nb500-169#reviews-publications
goat anti-GFP biotin (ab6658, Abcam); https://www.abcam.com/gfp-antibody-biotin-ab6658-references.html#top-0
rabbit anti-MTHFD2 (ab151447, Abcam), https://www.abcam.com/mthfd2-antibody-ab151447-references.html#top-0
rabbit anti-PSAT1 (NBP1-32920, Novus Biologicals), https://www.novusbio.com/products/psat1-antibody_nbp1-32920#reviews-publications
rabbit anti-PHGDH (HPA021241, Sigma Aldrich), https://www.sigmaaldrich.com/catalog/product/sigma/hpa021241?lang=en&region=GB
mouse anti-NDUFB8 (ab110242, Abcam), https://www.abcam.com/ndufb8-antibody-20e9dh10c12-ab110242-references.html#top-0
mouse anti-UQCRFS1 (ab14746, Abcam), https://www.abcam.com/uqcrfs1--risp-antibody-5a5-ab14746-references.html#top-0
mouse anti-TOMM20 (ab186734, Abcam); https://www.abcam.com/tomm20-antibody-epr15581-39-mitochondrial-marker-

ab186734-references.html#top-0
mouse anti-MTCO1 antibody (ab14705, Abcam), https://www.abcam.com/mtco1-antibody-1d6e1a8-ab14705-references.html#top-0
mouse anti-ATPB antibody (ab14730, Abcam), https://www.abcam.com/atpb-antibody-3d5-mitochondrial-marker-ab14730-references.html#top-0
mouse anti-SDHA (ab14715, Abcam) https://www.abcam.com/sdha-antibody-2e3gc12fb2ae2-ab14715-references.html
rabbit anti-cleaved caspase 3 (AB3623 Merck Millipore) http://www.merckmillipore.com/GB/en/product/Anti-Caspase-3-Antibody-active-cleaved-form,MM_NF-AB3623
rat anti-CD45 (ab64100, Abcam) https://www.abcam.com/cd45r-antibody-ra3-6b2-ab64100.html
rat Anti-Neutrophil antibody [NIMP-R14] (ab2557 Abcam) https://www.abcam.com/neutrophil-antibody-nimp-r14-ab2557.html
rat anti-CD3 (MCA1477 BioRad) https://www.bio-rad-antibodies.com/monoclonal/human-cd3-antibody-cd3-12-mca1477.html?f=purified

rat anti-CD4 (clone: RM4-5) (BioLegend 100536) https://www.biolegend.com/en-us/products/alexa-fluor-700-anti-mouse-cd4-antibody-3386
rat anti-CD8 (clone: 53-6.7) (BioLegend 100737) https://www.biolegend.com/en-us/products/brilliant-violet-421-anti-mouse-cd8a-antibody-7138
rat anti-CD45R/B220 (clone: RA3-6B2) (BioLegend 103235) https://www.biolegend.com/en-us/products/percp-cyanine5-5-anti-mouse-human-cd45r-b220-antibody-4267
rat anti-NK1.1(clone: PK136) (BioLegend 108737) https://www.biolegend.com/en-us/products/brilliant-violet-510-anti-mouse-nk-1-1-antibody-8615
rat anti-CD11b (clone: M1/70) (BioLegend 101237) https://www.biolegend.com/en-us/products/brilliant-violet-605-anti-mouse-human-cd11b-antibody-7637
Armenian hamster anti-CD11c (clone: N418) (BioLegend 117309) https://www.biolegend.com/en-us/products/apc-anti-mouse-cd11c-antibody-1813
rat anti-F4/80 (clone: BM8) (BioLegend 123107) https://www.biolegend.com/en-us/products/fitc-anti-mouse-f4-80-antibody-4067
rat anti-Class II (anti-mouse I-A/I-E; clone: M5/114.15.2) (BioLegend 107645) https://www.biolegend.com/en-us/products/brilliant-violet-785-anti-mouse-i-a-i-e-antibody-12087

Animals and other organisms

Policy information about studies involving animals; ARRIVE guidelines recommended for reporting animal research

Laboratory animals	Lgr5-EGFP-IRES-creERT2, Apcfl/fl15 and PolgAmut/mut mice were all on a C57Bl6/J background The majority mice were 6 months old, except the experiments looking at SSP enzyme expression in an ageing series of PolgAmut/mut and PolgA+/+ mice where they were between 1 and 12 months old. Both males and females were used in the study. Mice were housed in single sex cages at 20 ± 2°C under a 12 hr light/12 hr dark photoperiod with lights on at 07:00 hr.
Wild animals	The study did not involve wild animals
Field-collected samples	The study did not involve animals collected from the field
Ethics oversight	All animal experiments were conducted in compliance with the UK Home Office (PPL P3052AD70) and the Newcastle University Animal Welfare Ethical Review Board (AWERB 425).

Note that full information on the approval of the study protocol must also be provided in the manuscript.

Human research participants

Policy information about studies involving human research participants

Population characteristics	Human patients with a histopathologically confirmed adenoma or adenocarcinoma were included in the study. Age range 52-82, 20 Male, 15 Female
Recruitment	All patients with histopathologically confirmed adenocarcinoma (any grade) or adenoma within a defined time frame were recruited to the study. Informed written consent was obtained prior to surgery and samples were coded to maintain confidentiality. Patients were undergoing scheduled surgery regardless of their participation in the study, therefore we do not anticipate any self-selection bias.
Ethics oversight	This project was approved by the Joint Ethics Committee of Newcastle and North Tyneside Health Authority (2001/188) and the National Research Ethics Committee London-Stanmore (11/LO/1613).

Note that full information on the approval of the study protocol must also be provided in the manuscript.

Flow Cytometry

Plots

Confirm that:

☒ The axis labels state the marker and fluorochrome used (e.g. CD4-FITC).

☒ The axis scales are clearly visible. Include numbers along axes only for bottom left plot of group (a 'group' is an analysis of identical markers).

☒ All plots are contour plots with outliers or pseudocolor plots.

☒ A numerical value for number of cells or percentage (with statistics) is provided.

Methodology

Sample preparation	Lamina propria lymphocytes were extracted from 6-month old PolgA+/+ and PolgAmut/mut mice (n=3/genotype) as follows: SIs were extracted, cleared of mesentery, fat and Peyers Patches, cut into pieces and washed in HBSS without calcium and magnesium. Intraepithelial lymphocytes were removed by agitation for 15min in HBSS with 20mM HEPES and 2% FCS. The remaining tissue was digested in serum free medium containing Liberase TL (250µg/ml; Roche) and 0.05% DNase I (Roche) for 15min. Lamina propria lymphocytes were separated from epithelial cells by centrifugation in 40% Percoll and cell pellets collected. Lymphocytes were washed once with PBS and then stained with LIVE/Dead stain (Invitrogen 34961) for 30 min at 40oC. Cells were then washed once with PBS and stained with surface antibodies as follows; CD4 (clone: RM4-5, BioLegend, 10053), CD8 (clone: 53-6.7, BioLegend, 100737), CD45R/B220 (clone: RA3-6B2, BioLegend, 103235), NK1.1(clone: PK136, BioLegend, 108737), CD11b, clone: M1/70, BioLegend, 101237), CD11c (clone: N418, BioLegend, 117309), F4/80 (clone: BM8, BioLegend, 123107), Class II (anti-mouse I-A/I-E; clone: M5/114.15.2, BioLegend, 107645), Cells were analysed using LSRII (FACS DIVA v8)and by FlowJo v10 software.
Instrument	Fortessa X20 system
Software	DIVA software v8, analysis package is FlowJo v10
Cell population abundance	Cells were not flow sorted. Frequency analysis was performed in single cell suspensions from bulk population from small intestine.
Gating strategy	The gating strategy is as follows: Lymphocyte gate was first applied to gate out debris. From this gate, a second gate was derived to exclude dead cells using the LIVE/DEAD marker. From this gate, the frequency of T (CD4, CD8), B cells (B220) and NK cells was analysed as shown in the top panel of the figure. In order to determine the frequency of myeloid cells such as macrophages, monocytes and dendritic cells, the following gating strategy was used. From the LIVE/DEAD gate, frequency of class II positive cells was determined. A gate was drawn on class II positive cells and from this gate the frequency of DCs (CD11c), monocytes (CD11b) and macrophages (F4/80) was determined.

☒ Tick this box to confirm that a figure exemplifying the gating strategy is provided in the Supplementary Information.

Chapter 8. Bibliography

Aberle, H., Bauer, A., Stappert, J., Kispert, A., & Kemler, R. (1997). beta-catenin is a target for the ubiquitin-proteasome pathway. *Embo j, 16*(13), 3797-3804. doi:10.1093/emboj/16.13.3797

Acín-Pérez, R., Bayona-Bafaluy, M. P., Fernández-Silva, P., Moreno-Loshuertos, R., Pérez-Martos, A., Bruno, C., . . . Enríquez, J. A. (2004). Respiratory complex III is required to maintain complex I in mammalian mitochondria. *Mol Cell, 13*(6), 805-815. doi:10.1016/s1097-2765(04)00124-8

Ahlqvist, K. J., Leoncini, S., Pecorelli, A., Wortmann, S. B., Ahola, S., Forsström, S., . . . Suomalainen, A. (2015). MtDNA mutagenesis impairs elimination of mitochondria during erythroid maturation leading to enhanced erythrocyte destruction. *Nature Communications, 6*(1), 6494. doi:10.1038/ncomms7494

Albrengues, J., Bertero, T., Grasset, E., Bonan, S., Maiel, M., Bourget, I., . . . Gaggioli, C. (2015). Epigenetic switch drives the conversion of fibroblasts into proinvasive cancer-associated fibroblasts. *Nature Communications, 6*(1), 10204. doi:10.1038/ncomms10204

Alexander, C., Votruba, M., Pesch, U. E., Thiselton, D. L., Mayer, S., Moore, A., . . . Wissinger, B. (2000). OPA1, encoding a dynamin-related GTPase, is mutated in autosomal dominant optic atrophy linked to chromosome 3q28. *Nat Genet, 26*(2), 211-215. doi:10.1038/79944

Alexander, P. G., Roseweir, A. K., Pennel, K. A. F., van Wyk, H. C., Powell, A., McMillan, D. C., . . . Park, J. H. (2020). The Glasgow Microenvironment Score associates with prognosis and adjuvant chemotherapy response in colorectal cancer. *British journal of cancer*. doi:10.1038/s41416-020-01168-x

Almuhaideb, A., Papathanasiou, N., & Bomanji, J. (2011). 18F-FDG PET/CT imaging in oncology. *Annals of Saudi medicine, 31*(1), 3-13. doi:10.4103/0256-4947.75771

Alonso, A., Martin, P., Albarran, C., Aguilera, B., Garcia, O., Guzman, A., . . . Sancho, M. (1997). Detection of somatic mutations in the mitochondrial DNA control region of colorectal and gastric tumors by heteroduplex and single-strand conformation analysis. *Electrophoresis, 18*(5), 682-685. doi:10.1002/elps.1150180504

Alston, C. L., Lowe, J., Turnbull, D. M., Maddison, P., & Taylor, R. W. (2010). A novel mitochondrial tRNAGlu (MTTE) gene mutation causing chronic progressive external

ophthalmoplegia at low levels of heteroplasmy in muscle. *J Neurol Sci, 298*(1-2), 140-144. doi:10.1016/j.jns.2010.08.014

Altmann, R. (1894). *Die Elementarorganismen und ihre Beziehungen zu den Zellen*: Veit.

Altomare, D. A., & Testa, J. R. (2005). Perturbations of the AKT signaling pathway in human cancer. *Oncogene, 24*(50), 7455-7464. doi:10.1038/sj.onc.1209085

An, R., Wilms, E., Masclee, A. A. M., Smidt, H., Zoetendal, E. G., & Jonkers, D. (2018). Age-dependent changes in GI physiology and microbiota: time to reconsider? *Gut, 67*(12), 2213-2222. doi:10.1136/gutjnl-2017-315542

An, S., Kumar, R., Sheets, E. D., & Benkovic, S. J. (2008). Reversible Compartmentalization of de Novo Purine Biosynthetic Complexes in Living Cells. *Science, 320*(5872), 103. doi:10.1126/science.1152241

Anderson, S., Bankier, A. T., Barrell, B. G., de Bruijn, M. H. L., Coulson, A. R., Drouin, J., . . . Young, I. G. (1981). Sequence and organization of the human mitochondrial genome. *Nature, 290*(5806), 457-465. doi:10.1038/290457a0

André, T., Boni, C., Navarro, M., Tabernero, J., Hickish, T., Topham, C., . . . de Gramont, A. (2009). Improved overall survival with oxaliplatin, fluorouracil, and leucovorin as adjuvant treatment in stage II or III colon cancer in the MOSAIC trial. *J Clin Oncol, 27*(19), 3109-3116. doi:10.1200/jco.2008.20.6771

Andreazza, S., Samstag, C. L., Sanchez-Martinez, A., Fernandez-Vizarra, E., Gomez-Duran, A., Lee, J. J., . . . Whitworth, A. J. (2019). Mitochondrially-targeted APOBEC1 is a potent mtDNA mutator affecting mitochondrial function and organismal fitness in Drosophila. *Nat Commun, 10*(1), 3280. doi:10.1038/s41467-019-10857-y

Antonicka, H., Sasarman, F., Nishimura, T., Paupe, V., & Shoubridge, E. A. (2013). The mitochondrial RNA-binding protein GRSF1 localizes to RNA granules and is required for posttranscriptional mitochondrial gene expression. *Cell Metab, 17*(3), 386-398. doi:10.1016/j.cmet.2013.02.006

Armelin, H. A., Armelin, M. C., Kelly, K., Stewart, T., Leder, P., Cochran, B. H., & Stiles, C. D. (1984). Functional role for c-myc in mitogenic response to platelet-derived growth factor. *Nature, 310*(5979), 655-660. doi:10.1038/310655a0

Arnold, M., Rutherford, M. J., Bardot, A., Ferlay, J., Andersson, T. M., Myklebust, T., . . . Bray, F. (2019). Progress in cancer survival, mortality, and incidence in seven high-income countries 1995-2014 (ICBP SURVMARK-2): a population-based study. *Lancet Oncol, 20*(11), 1493-1505. doi:10.1016/s1470-2045(19)30456-5

Asin-Cayuela, J., Schwend, T., Farge, G., & Gustafsson, C. M. (2005). The human mitochondrial transcription termination factor (mTERF) is fully active in vitro in the non-phosphorylated form. *J Biol Chem, 280*(27), 25499-25505. doi:10.1074/jbc.M501145200

Askew, D. S., Ashmun, R. A., Simmons, B. C., & Cleveland, J. L. (1991). Constitutive c-myc expression in an IL-3-dependent myeloid cell line suppresses cell cycle arrest and accelerates apoptosis. *Oncogene, 6*(10), 1915-1922.

Attene-Ramos, M. S., Nava, G. M., Muellner, M. G., Wagner, E. D., Plewa, M. J., & Gaskins, H. R. (2010). DNA damage and toxicogenomic analyses of hydrogen sulfide in human intestinal epithelial FHs 74 Int cells. *Environ Mol Mutagen, 51*(4), 304-314. doi:10.1002/em.20546

Attisano, L., & Tuen Lee-Hoeflich, S. (2001). The Smads. *Genome Biology, 2*(8), reviews3010.3011. doi:10.1186/gb-2001-2-8-reviews3010

Backshall, A., Alferez, D., Teichert, F., Wilson, I. D., Wilkinson, R. W., Goodlad, R. A., & Keun, H. C. (2009). Detection of metabolic alterations in non-tumor gastrointestinal tissue of the Apc(Min/+) mouse by (1)H MAS NMR spectroscopy. *J Proteome Res, 8*(3), 1423-1430. doi:10.1021/pr800793w

Badman, M. K., Pissios, P., Kennedy, A. R., Koukos, G., Flier, J. S., & Maratos-Flier, E. (2007). Hepatic Fibroblast Growth Factor 21 Is Regulated by PPARα and Is a Key Mediator of Hepatic Lipid Metabolism in Ketotic States. *Cell Metab, 5*(6), 426-437. doi:https://doi.org/10.1016/j.cmet.2007.05.002

Baines, H. L., Stewart, J. B., Stamp, C., Zupanic, A., Kirkwood, T. B., Larsson, N. G., . . . Greaves, L. C. (2014). Similar patterns of clonally expanded somatic mtDNA mutations in the colon of heterozygous mtDNA mutator mice and ageing humans. *Mech Ageing Dev, 139*, 22-30. doi:10.1016/j.mad.2014.06.003

Baker, S. J., Fearon, E. R., Nigro, J. M., Hamilton, S. R., Preisinger, A. C., Jessup, J. M., . . . Vogelstein, B. (1989). Chromosome 17 deletions and p53 gene mutations in colorectal carcinomas. *Science, 244*(4901), 217-221. doi:10.1126/science.2649981

Baker, S. J., Markowitz, S., Fearon, E. R., Willson, J. K., & Vogelstein, B. (1990a). Suppression of human colorectal carcinoma cell growth by wild-type p53. *Science, 249*(4971), 912-915. doi:10.1126/science.2144057

Baker, S. J., Preisinger, A. C., Jessup, J. M., Paraskeva, C., Markowitz, S., Willson, J. K., . . . Vogelstein, B. (1990b). p53 gene mutations occur in combination with 17p allelic deletions as late events in colorectal tumorigenesis. *Cancer Res, 50*(23), 7717-7722.

Balaban, R. S., Nemoto, S., & Finkel, T. (2005). Mitochondria, oxidants, and aging. *Cell, 120*(4), 483-495. doi:10.1016/j.cell.2005.02.001

Balsa, E., Marco, R., Perales-Clemente, E., Szklarczyk, R., Calvo, E., Landázuri, M. O., & Enríquez, J. A. (2012). NDUFA4 is a subunit of complex IV of the mammalian electron transport chain. *Cell Metab, 16*(3), 378-386. doi:10.1016/j.cmet.2012.07.015

Baltimore, D. (1970). Viral RNA-dependent DNA Polymerase: RNA-dependent DNA Polymerase in Virions of RNA Tumour Viruses. *Nature, 226*(5252), 1209-1211. doi:10.1038/2261209a0

Ban, T., Ishihara, T., Kohno, H., Saita, S., Ichimura, A., Maenaka, K., . . . Ishihara, N. (2017). Molecular basis of selective mitochondrial fusion by heterotypic action between OPA1 and cardiolipin. *Nat Cell Biol, 19*(7), 856-863. doi:10.1038/ncb3560

Bao, X. R., Ong, S.-E., Goldberger, O., Peng, J., Sharma, R., Thompson, D. A., . . . Mootha, V. K. (2016). Mitochondrial dysfunction remodels one-carbon metabolism in human cells. *Elife, 5*, e10575. doi:10.7554/eLife.10575

Barker, N., Ridgway, R. A., van Es, J. H., van de Wetering, M., Begthel, H., van den Born, M., . . . Clevers, H. (2009). Crypt stem cells as the cells-of-origin of intestinal cancer. *Nature, 457*(7229), 608-611. doi:10.1038/nature07602

Barker, N., van Es, J. H., Kuipers, J., Kujala, P., van den Born, M., Cozijnsen, M., . . . Clevers, H. (2007). Identification of stem cells in small intestine and colon by marker gene Lgr5. *Nature, 449*(7165), 1003-1007. doi:10.1038/nature06196

Batlle, E., & Clevers, H. (2017). Cancer stem cells revisited. *Nat Med, 23*(10), 1124-1134. doi:10.1038/nm.4409

Baulies, A., Angelis, N., Foglizzo, V., Danielsen, E. T., Patel, H., Novellasdemunt, L., . . . Li, V. S. W. (2020). The Transcription co-Repressors MTG8 and MTG16 Regulate Exit of Intestinal Stem Cells From Their Niche and Differentiation into Enterocyte vs Secretory Lineages. *Gastroenterology*. doi:10.1053/j.gastro.2020.06.012

Beard, J., Green, W., Miller, L., & Finch, C. (1984). Effect of iron-deficiency anemia on hormone levels and thermoregulation during cold exposure. *Am J Physiol, 247*(1 Pt 2), R114-119. doi:10.1152/ajpregu.1984.247.1.R114

Beard, J. L., Borel, M. J., & Derr, J. (1990). Impaired thermoregulation and thyroid function in iron-deficiency anemia. *Am J Clin Nutr, 52*(5), 813-819. doi:10.1093/ajcn/52.5.813

Beatty, P. W., & Reed, D. J. (1980). Involvement of the cystathionine pathway in the biosynthesis of glutathione by isolated rat hepatocytes. *Archives of Biochemistry and Biophysics, 204*(1), 80-87. doi:https://doi.org/10.1016/0003-9861(80)90009-0

Becht, E., de Reyniès, A., Giraldo, N. A., Pilati, C., Buttard, B., Lacroix, L., . . . Fridman, W. H. (2016). Immune and Stromal Classification of Colorectal Cancer Is Associated with Molecular Subtypes and Relevant for Precision Immunotherapy. *Clin Cancer Res, 22*(16), 4057-4066. doi:10.1158/1078-0432.Ccr-15-2879

Beckman, K. B., & Ames, B. N. (1997). Oxidative decay of DNA. *J Biol Chem, 272*(32), 19633-19636. doi:10.1074/jbc.272.32.19633

Behrens, J., von Kries, J. P., Kühl, M., Bruhn, L., Wedlich, D., Grosschedl, R., & Birchmeier, W. (1996). Functional interaction of β-catenin with the transcription factor LEF-1. *Nature, 382*(6592), 638-642. doi:10.1038/382638a0

Belitzer, V., & Tsybakova, E. (1939). The mechanism of phosphorylation associated with respiration. *Biochimiya, 4*, 516-534.

Bell, E. L., Klimova, T. A., Eisenbart, J., Moraes, C. T., Murphy, M. P., Budinger, G. R., & Chandel, N. S. (2007). The Qo site of the mitochondrial complex III is required for the transduction of hypoxic signaling via reactive oxygen species production. *J Cell Biol, 177*(6), 1029-1036. doi:10.1083/jcb.200609074

Bender, A., Krishnan, K. J., Morris, C. M., Taylor, G. A., Reeve, A. K., Perry, R. H., . . . Turnbull, D. M. (2006). High levels of mitochondrial DNA deletions in substantia nigra neurons in aging and Parkinson disease. *Nat Genet, 38*(5), 515-517. doi:10.1038/ng1769

Berg, J. M., Tymoczko, J. L., & Stryer, L. (2012). Biochemistry/Jeremy M. Berg, John L. Tymoczko, Lubert Stryer; with Gregory J. Gatto, Jr. In: New York: WH Freeman.

Berk, A. J., & Clayton, D. A. (1974). Mechanism of mitochondrial DNA replication in mouse L-cells: Asynchronous replication of strands, segregation of circular daughter molecules, aspects of topology and turnover of an initiation sequence. *J Mol Biol, 86*(4), 801-824. doi:https://doi.org/10.1016/0022-2836(74)90355-6

Bernardes de Jesus, B., Vera, E., Schneeberger, K., Tejera, A. M., Ayuso, E., Bosch, F., & Blasco, M. A. (2012). Telomerase gene therapy in adult and old mice delays aging and increases longevity without increasing cancer. *EMBO molecular medicine, 4*(8), 691-704. doi:10.1002/emmm.201200245

Beroukhim, R., Mermel, C. H., Porter, D., Wei, G., Raychaudhuri, S., Donovan, J., . . . Meyerson, M. (2010). The landscape of somatic copy-number alteration across human cancers. *Nature, 463*(7283), 899-905. doi:10.1038/nature08822

Bhargava, K., & Spremulli, L. L. (2005). Role of the N- and C-terminal extensions on the activity of mammalian mitochondrial translational initiation factor 3. *Nucleic Acids Res, 33*(22), 7011-7018. doi:10.1093/nar/gki1007

Bianchi, M. S., Bianchi, N. O., & Bailliet, G. (1995). Mitochondrial DNA mutations in normal and tumor tissues from breast cancer patients. *Cytogenet Cell Genet, 71*(1), 99-103. doi:10.1159/000134072

Bini, L., Magi, B., Marzocchi, B., Arcuri, F., Tripodi, S., Cintorino, M., . . . Tosi, P. (1997). Protein expression profiles in human breast ductal carcinoma and histologically normal tissue. *Electrophoresis, 18*(15), 2832-2841. doi:10.1002/elps.1150181519

Binnewies, M., Roberts, E. W., Kersten, K., Chan, V., Fearon, D. F., Merad, M., . . . Krummel, M. F. (2018). Understanding the tumor immune microenvironment (TIME) for effective therapy. *Nat Med, 24*(5), 541-550. doi:10.1038/s41591-018-0014-x

Birnbaum, M. J., Clem, R. J., & Miller, L. K. (1994). An apoptosis-inhibiting gene from a nuclear polyhedrosis virus encoding a polypeptide with Cys/His sequence motifs. *Journal of virology, 68*(4), 2521-2528. doi:10.1128/JVI.68.4.2521-2528.1994

Birsoy, K., Wang, T., Chen, W. W., Freinkman, E., Abu-Remaileh, M., & Sabatini, D. M. (2015). An Essential Role of the Mitochondrial Electron Transport Chain in Cell Proliferation Is to Enable Aspartate Synthesis. *Cell, 162*(3), 540-551. doi:10.1016/j.cell.2015.07.016

Bleau, C., Karelis, A. D., St-Pierre, D. H., & Lamontagne, L. (2015). Crosstalk between intestinal microbiota, adipose tissue and skeletal muscle as an early event in systemic low-grade inflammation and the development of obesity and diabetes. *Diabetes Metab Res Rev, 31*(6), 545-561. doi:10.1002/dmrr.2617

Bleazard, W., McCaffery, J. M., King, E. J., Bale, S., Mozdy, A., Tieu, Q., . . . Shaw, J. M. (1999). The dynamin-related GTPase Dnm1 regulates mitochondrial fission in yeast. *Nat Cell Biol, 1*(5), 298-304. doi:10.1038/13014

Bodnar, A. G., Ouellette, M., Frolkis, M., Holt, S. E., Chiu, C. P., Morin, G. B., . . . Wright, W. E. (1998). Extension of life-span by introduction of telomerase into normal human cells. *Science, 279*(5349), 349-352. doi:10.1126/science.279.5349.349

Bogenhagen, D. F., Rousseau, D., & Burke, S. (2008). The layered structure of human mitochondrial DNA nucleoids. *J Biol Chem, 283*(6), 3665-3675. doi:10.1074/jbc.M708444200

Bohin, N., Carlson, E. A., & Samuelson, L. C. (2018). Genome Toxicity and Impaired Stem Cell Function after Conditional Activation of CreERT2 in the Intestine. *Stem Cell Reports, 11*(6), 1337-1346. doi:https://doi.org/10.1016/j.stemcr.2018.10.014

Bohnsack, M. T., & Sloan, K. E. (2018). The mitochondrial epitranscriptome: the roles of RNA modifications in mitochondrial translation and human disease. *Cell Mol Life Sci, 75*(2), 241-260. doi:10.1007/s00018-017-2598-6

Bolden, A., Noy, G. P., & Weissbach, A. (1977). DNA polymerase of mitochondria is a gamma-polymerase. *J Biol Chem, 252*(10), 3351-3356.

Bollig-Fischer, A., Dewey, T. G., & Ethier, S. P. (2011). Oncogene activation induces metabolic transformation resulting in insulin-independence in human breast cancer cells. *PloS one, 6*(3), e17959. doi:10.1371/journal.pone.0017959

Bonnet, D., & Dick, J. E. (1997). Human acute myeloid leukemia is organized as a hierarchy that originates from a primitive hematopoietic cell. *Nat Med, 3*(7), 730-737. doi:10.1038/nm0797-730

Botteri, E., Iodice, S., Bagnardi, V., Raimondi, S., Lowenfels, A. B., & Maisonneuve, P. (2008). Smoking and colorectal cancer: a meta-analysis. *Jama, 300*(23), 2765-2778. doi:10.1001/jama.2008.839

Bouaoun, L., Sonkin, D., Ardin, M., Hollstein, M., Byrnes, G., Zavadil, J., & Olivier, M. (2016). TP53 Variations in Human Cancers: New Lessons from the IARC TP53 Database and Genomics Data. Version R20. *Hum Mutat, 37*(9), 865-876. doi:10.1002/humu.23035

Boulay, J. L., Mild, G., Lowy, A., Reuter, J., Lagrange, M., Terracciano, L., . . . Rochlitz, C. (2002). SMAD4 is a predictive marker for 5-fluorouracil-based chemotherapy in patients with colorectal cancer. *British journal of cancer, 87*(6), 630-634. doi:10.1038/sj.bjc.6600511

Boutin, A. T., Liao, W.-T., Wang, M., Hwang, S. S., Karpinets, T. V., Cheung, H., . . . DePinho, R. A. (2017). Oncogenic Kras drives invasion and maintains metastases in colorectal cancer. *Genes & development, 31*(4), 370-382. doi:10.1101/gad.293449.116

Braidy, N., Guillemin, G. J., Mansour, H., Chan-Ling, T., Poljak, A., & Grant, R. (2011). Age related changes in NAD+ metabolism oxidative stress and Sirt1 activity in wistar rats. *PloS one, 6*(4), e19194. doi:10.1371/journal.pone.0019194

Bray, F., Ferlay, J., Soerjomataram, I., Siegel, R. L., Torre, L. A., & Jemal, A. (2018). Global cancer statistics 2018: GLOBOCAN estimates of incidence and mortality worldwide for 36 cancers in 185 countries. *CA Cancer J Clin, 68*(6), 394-424. doi:10.3322/caac.21492

Breit, S. N., Johnen, H., Cook, A. D., Tsai, V. W. W., Mohammad, M. G., Kuffner, T., . . . Brown, D. A. (2011). The TGF-β superfamily cytokine, MIC-1/GDF15: A pleotrophic cytokine with roles in inflammation, cancer and metabolism. *Growth Factors, 29*(5), 187-195. doi:10.3109/08977194.2011.607137

Bretscher, A., & Weber, K. (1979). Villin: the major microfilament-associated protein of the intestinal microvillus. *Proc Natl Acad Sci U S A, 76*(5), 2321-2325.

Bridwell-Rabb, J., Fox, N. G., Tsai, C. L., Winn, A. M., & Barondeau, D. P. (2014). Human frataxin activates Fe-S cluster biosynthesis by facilitating sulfur transfer chemistry. *Biochemistry, 53*(30), 4904-4913. doi:10.1021/bi500532e

Brierley, E. J., Johnson, M. A., Lightowlers, R. N., James, O. F., & Turnbull, D. M. (1998). Role of mitochondrial DNA mutations in human aging: implications for the central nervous system and muscle. *Ann Neurol, 43*(2), 217-223. doi:10.1002/ana.410430212

Brijwani, N., Jain, M., Dhandapani, M., Zahed, F., Mukhopadhyay, P., Biswas, M., . . . Thiyagarajan, S. (2017). Rationally co-targeting divergent pathways in KRAS wild-type colorectal cancers by CANscript technology reveals tumor dependence on Notch and Erbb2. *Sci Rep, 7*(1), 1502. doi:10.1038/s41598-017-01566-x

Brown, K., Xie, S., Qiu, X., Mohrin, M., Shin, J., Liu, Y., . . . Chen, D. (2013). SIRT3 reverses aging-associated degeneration. *Cell Rep, 3*(2), 319-327. doi:10.1016/j.celrep.2013.01.005

Brzezniak, L. K., Bijata, M., Szczesny, R. J., & Stepien, P. P. (2011). Involvement of human ELAC2 gene product in 3' end processing of mitochondrial tRNAs. *RNA Biol, 8*(4), 616-626. doi:10.4161/rna.8.4.15393

Buczacki, S. J., Zecchini, H. I., Nicholson, A. M., Russell, R., Vermeulen, L., Kemp, R., & Winton, D. J. (2013). Intestinal label-retaining cells are secretory precursors expressing Lgr5. *Nature, 495*(7439), 65-69. doi:10.1038/nature11965

Bunik, V. I., Buneeva, O. A., & Gomazkova, V. S. (1990). Change in alpha-ketoglutarate dehydrogenase cooperative properties due to dihydrolipoate and NADH. *FEBS Lett, 269*(1), 252-254. doi:10.1016/0014-5793(90)81166-l

Burgart, L. J., Zheng, J., Shu, Q., Strickler, J. G., & Shibata, D. (1995). Somatic mitochondrial mutation in gastric cancer. *Am J Pathol, 147*(4), 1105-1111.

Burkholder, T., Foltz, C., Karlsson, E., Linton, C. G., & Smith, J. M. (2012). Health Evaluation of Experimental Laboratory Mice. *Current protocols in mouse biology, 2*, 145-165. doi:10.1002/9780470942390.mo110217

Cadenas, E., Boveris, A., Ragan, C. I., & Stoppani, A. O. (1977). Production of superoxide radicals and hydrogen peroxide by NADH-ubiquinone reductase and ubiquinol-cytochrome c reductase from beef-heart mitochondria. *Arch Biochem Biophys, 180*(2), 248-257. doi:10.1016/0003-9861(77)90035-2

Cadet, J., Berger, M., Douki, T., & Ravanat, J. L. (1997). Oxidative damage to DNA: formation, measurement, and biological significance. *Rev Physiol Biochem Pharmacol, 131*, 1-87. doi:10.1007/3-540-61992-5_5

Cai, S., Li, Y., Ding, Y., Chen, K., & Jin, M. (2014). Alcohol drinking and the risk of colorectal cancer death: a meta-analysis. *Eur J Cancer Prev, 23*(6), 532-539. doi:10.1097/cej.0000000000000076

Cai, Y. C., Bullard, J. M., Thompson, N. L., & Spremulli, L. L. (2000). Interaction of mitochondrial elongation factor Tu with aminoacyl-tRNA and elongation factor Ts. *J Biol Chem, 275*(27), 20308-20314. doi:10.1074/jbc.M001899200

Calabrese, C., Iommarini, L., Kurelac, I., Calvaruso, M. A., Capristo, M., Lollini, P.-L., . . . Porcelli, A. M. (2013). Respiratory complex I is essential to induce a Warburg profile in mitochondria-defective tumor cells. *Cancer & Metabolism, 1*(1), 11. doi:10.1186/2049-3002-1-11

Campbell, K. J., & Tait, S. W. G. (2018). Targeting BCL-2 regulated apoptosis in cancer. *Open Biol, 8*(5). doi:10.1098/rsob.180002

Cannon, B., Hedin, A., & Nedergaard, J. (1982). Exclusive occurrence of thermogenin antigen in brown adipose tissue. *FEBS Lett, 150*(1), 129-132. doi:10.1016/0014-5793(82)81319-7

Cannon, B., & Nedergaard, J. (2004). Brown adipose tissue: function and physiological significance. *Physiol Rev, 84*(1), 277-359. doi:10.1152/physrev.00015.2003

Cantatore, P., & Attardi, G. (1980). Mapping of nascent light and heavy strand transcripts on the physical map of HeLa cell mitochondrial DNA. *Nucleic Acids Res, 8*(12), 2605-2625. doi:10.1093/nar/8.12.2605

Cantó, C., Gerhart-Hines, Z., Feige, J. N., Lagouge, M., Noriega, L., Milne, J. C., . . . Auwerx, J. (2009). AMPK regulates energy expenditure by modulating NAD+ metabolism and SIRT1 activity. *Nature, 458*(7241), 1056-1060. doi:10.1038/nature07813

Cao, L., Shitara, H., Horii, T., Nagao, Y., Imai, H., Abe, K., . . . Yonekawa, H. (2007). The mitochondrial bottleneck occurs without reduction of mtDNA content in female mouse germ cells. *Nat Genet, 39*(3), 386-390. doi:10.1038/ng1970

Cao, Y. L., Meng, S., Chen, Y., Feng, J. X., Gu, D. D., Yu, B., . . . Gao, S. (2017). MFN1 structures reveal nucleotide-triggered dimerization critical for mitochondrial fusion. *Nature, 542*(7641), 372-376. doi:10.1038/nature21077

Capaldi, R. A. (1990). STRUCTURE AND FUNCTION OF CYTOCHROME c OXIDASE. *Annual Review of Biochemistry, 59*(1), 569-596. doi:10.1146/annurev.bi.59.070190.003033

Carmon, K. S., Gong, X., Lin, Q., Thomas, A., & Liu, Q. (2011). R-spondins function as ligands of the orphan receptors LGR4 and LGR5 to regulate Wnt/beta-catenin signaling. *Proc Natl Acad Sci U S A, 108*(28), 11452-11457. doi:10.1073/pnas.1106083108

Carragher, L. A. S., Snell, K. R., Giblett, S. M., Aldridge, V. S. S., Patel, B., Cook, S. J., . . . Pritchard, C. A. (2010). V600EBraf induces gastrointestinal crypt senescence and promotes tumour progression through enhanced CpG methylation of p16INK4a. *EMBO molecular medicine, 2*(11), 458-471. doi:10.1002/emmm.201000099

Carroll, J., Fearnley, I. M., Skehel, J. M., Shannon, R. J., Hirst, J., & Walker, J. E. (2006). Bovine complex I is a complex of 45 different subunits. *J Biol Chem, 281*(43), 32724-32727. doi:10.1074/jbc.M607135200

Caspary, W. F. (1992). Physiology and pathophysiology of intestinal absorption. *Am J Clin Nutr, 55*(1 Suppl), 299s-308s. doi:10.1093/ajcn/55.1.299s

Cavalli, L. R., Varella-Garcia, M., & Liang, B. C. (1997). Diminished tumorigenic phenotype after depletion of mitochondrial DNA. *Cell Growth Differ, 8*(11), 1189-1198.

Chan, C. Y., Pedley, A. M., Kim, D., Xia, C., Zhuang, X., & Benkovic, S. J. (2018). Microtubule-directed transport of purine metabolons drives their cytosolic transit to mitochondria. *Proc Natl Acad Sci U S A, 115*(51), 13009-13014. doi:10.1073/pnas.1814042115

Chandel, N. S., Maltepe, E., Goldwasser, E., Mathieu, C. E., Simon, M. C., & Schumacker, P. T. (1998). Mitochondrial reactive oxygen species trigger hypoxia-induced transcription. *Proc Natl Acad Sci U S A, 95*(20), 11715-11720. doi:10.1073/pnas.95.20.11715

Chang, C. R., & Blackstone, C. (2007). Cyclic AMP-dependent protein kinase phosphorylation of Drp1 regulates its GTPase activity and mitochondrial morphology. *J Biol Chem, 282*(30), 21583-21587. doi:10.1074/jbc.C700083200

Chang, D. D., & Clayton, D. A. (1984). Precise identification of individual promoters for transcription of each strand of human mitochondrial DNA. *Cell, 36*(3), 635-643. doi:10.1016/0092-8674(84)90343-x

Chen, D., Zhao, Z., Huang, Z., Chen, D.-C., Zhu, X.-X., Wang, Y.-Z., . . . Jiang, Y.-Z. (2018). Super enhancer inhibitors suppress MYC driven transcriptional amplification and tumor progression in osteosarcoma. *Bone Research, 6*(1), 11. doi:10.1038/s41413-018-0009-8

Chen, E. Y., Tan, C. M., Kou, Y., Duan, Q., Wang, Z., Meirelles, G. V., . . . Ma'ayan, A. (2013). Enrichr: interactive and collaborative HTML5 gene list enrichment analysis tool. *BMC Bioinformatics, 14*, 128. doi:10.1186/1471-2105-14-128

Chen, Z. X., & Pervaiz, S. (2010). Involvement of cytochrome c oxidase subunits Va and Vb in the regulation of cancer cell metabolism by Bcl-2. *Cell Death Differ, 17*(3), 408-420. doi:10.1038/cdd.2009.132

Cheng, H., & Leblond, C. P. (1974). Origin, differentiation and renewal of the four main epithelial cell types in the mouse small intestine. V. Unitarian Theory of the origin of the four epithelial cell types. *Am J Anat, 141*(4), 537-561. doi:10.1002/aja.1001410407

Chinnery, P. F., DiMauro, S., Shanske, S., Schon, E. A., Zeviani, M., Mariotti, C., . . . Turnbull, D. M. (2004). Risk of developing a mitochondrial DNA deletion disorder. *Lancet, 364*(9434), 592-596. doi:10.1016/s0140-6736(04)16851-7

Chinnery, P. F., Elliott, H. R., Hudson, G., Samuels, D. C., & Relton, C. L. (2012). Epigenetics, epidemiology and mitochondrial DNA diseases. *Int J Epidemiol, 41*(1), 177-187. doi:10.1093/ije/dyr232

Chinnery, P. F., Howell, N., Lightowlers, R. N., & Turnbull, D. M. (1997). Molecular pathology of MELAS and MERRF. The relationship between mutation load and clinical phenotypes. *Brain, 120 (Pt 10)*, 1713-1721. doi:10.1093/brain/120.10.1713

Chinnery, P. F., & Samuels, D. C. (1999). Relaxed replication of mtDNA: A model with implications for the expression of disease. *American journal of human genetics, 64*(4), 1158-1165. doi:10.1086/302311

Cho, S. W., Kim, S., Kim, J. M., & Kim, J. S. (2013). Targeted genome engineering in human cells with the Cas9 RNA-guided endonuclease. *Nat Biotechnol, 31*(3), 230-232. doi:10.1038/nbt.2507

Chomyn, A., Cleeter, M. W., Ragan, C. I., Riley, M., Doolittle, R. F., & Attardi, G. (1986). URF6, last unidentified reading frame of human mtDNA, codes for an NADH dehydrogenase subunit. *Science, 234*(4776), 614-618. doi:10.1126/science.3764430

Chomyn, A., Mariottini, P., Cleeter, M. W., Ragan, C. I., Matsuno-Yagi, A., Hatefi, Y., . . . Attardi, G. (1985). Six unidentified reading frames of human mitochondrial DNA encode components of the respiratory-chain NADH dehydrogenase. *Nature, 314*(6012), 592-597. doi:10.1038/314592a0

Christofk, H. R., Vander Heiden, M. G., Harris, M. H., Ramanathan, A., Gerszten, R. E., Wei, R., . . . Cantley, L. C. (2008). The M2 splice isoform of pyruvate kinase is important for cancer metabolism and tumour growth. *Nature, 452*(7184), 230-233. doi:10.1038/nature06734

Cipolat, S., de Brito, O. M., Dal Zilio, B., & Scorrano, L. (2004). OPA1 requires mitofusin 1 to promote mitochondrial fusion. *Proc Natl Acad Sci U S A, 101*(45), 15927. doi:10.1073/pnas.0407043101

Clark-Walker, G. D., & Linnane, A. W. (1966). In vivo differentiation of yeast cytoplasmic and mitochondrial protein synthesis with antibiotics. *Biochem Biophys Res Commun, 25*(1), 8-13. doi:10.1016/0006-291x(66)90631-0

Clarke, M. F., Dick, J. E., Dirks, P. B., Eaves, C. J., Jamieson, C. H., Jones, D. L., . . . Wahl, G. M. (2006). Cancer stem cells--perspectives on current status and future directions: AACR Workshop on cancer stem cells. *Cancer Res, 66*(19), 9339-9344. doi:10.1158/0008-5472.Can-06-3126

Clevers, H. (2016). Modeling Development and Disease with Organoids. *Cell, 165*(7), 1586-1597. doi:https://doi.org/10.1016/j.cell.2016.05.082

Coller, H. A., Khrapko, K., Bodyak, N. D., Nekhaeva, E., Herrero-Jimenez, P., & Thilly, W. G. (2001a). High frequency of homoplasmic mitochondrial DNA mutations in human tumors can be explained without selection. *Nature Genetics, 28*(2), 147-150. doi:10.1038/88859

Coller, H. A., Khrapko, K., Bodyak, N. D., Nekhaeva, E., Herrero-Jimenez, P., & Thilly, W. G. (2001b). High frequency of homoplasmic mitochondrial DNA mutations in human

tumors can be explained without selection. *Nat Genet, 28*(2), 147-150. doi:10.1038/88859

Conboy, I. M., Conboy, M. J., Wagers, A. J., Girma, E. R., Weissman, I. L., & Rando, T. A. (2005). Rejuvenation of aged progenitor cells by exposure to a young systemic environment. *Nature, 433*(7027), 760-764. doi:10.1038/nature03260

Cong, L., Ran, F. A., Cox, D., Lin, S., Barretto, R., Habib, N., . . . Zhang, F. (2013). Multiplex Genome Engineering Using CRISPR/Cas Systems. *Science, 339*(6121), 819. doi:10.1126/science.1231143

Corral-Debrinski, M., Horton, T., Lott, M. T., Shoffner, J. M., Beal, M. F., & Wallace, D. C. (1992). Mitochondrial DNA deletions in human brain: regional variability and increase with advanced age. *Nat Genet, 2*(4), 324-329. doi:10.1038/ng1292-324

Cortopassi, G. A., & Arnheim, N. (1990). Detection of a specific mitochondrial DNA deletion in tissues of older humans. *Nucleic Acids Res, 18*(23), 6927-6933. doi:10.1093/nar/18.23.6927

Crakes, K. R., Santos Rocha, C., Grishina, I., Hirao, L. A., Napoli, E., Gaulke, C. A., . . . Dandekar, S. (2019). PPARα-targeted mitochondrial bioenergetics mediate repair of intestinal barriers at the host–microbe intersection during SIV infection. *Proceedings of the National Academy of Sciences, 116*(49), 24819-24829. doi:10.1073/pnas.1908977116

Cribbs, J. T., & Strack, S. (2007). Reversible phosphorylation of Drp1 by cyclic AMP-dependent protein kinase and calcineurin regulates mitochondrial fission and cell death. *EMBO Rep, 8*(10), 939-944. doi:10.1038/sj.embor.7401062

Crook, N. E., Clem, R. J., & Miller, L. K. (1993). An apoptosis-inhibiting baculovirus gene with a zinc finger-like motif. *J Virol, 67*(4), 2168-2174. doi:10.1128/jvi.67.4.2168-2174.1993

Cruz, M. D., Ledbetter, S., Chowdhury, S., Tiwari, A. K., Momi, N., Wali, R. K., . . . Roy, H. K. (2017). Metabolic reprogramming of the premalignant colonic mucosa is an early event in carcinogenesis. *Oncotarget, 8*(13), 20543-20557. doi:10.18632/oncotarget.16129

Cui, C., Qi, J., Deng, Q., Chen, R., Zhai, D., & Yu, J. (2016). Nicotinamide Mononucleotide Adenylyl Transferase 2: A Promising Diagnostic and Therapeutic Target for Colorectal Cancer. *BioMed research international, 2016*, 1804137. doi:10.1155/2016/1804137

Cummings, J. H. (1975). The Colon: Absorptive, Secretory and Metabolic Functions. *Digestion, 13*(4), 232-240. doi:10.1159/000197712

D'Aurelio, M., Gajewski, C. D., Lin, M. T., Mauck, W. M., Shao, L. Z., Lenaz, G., . . . Manfredi, G. (2004). Heterologous mitochondrial DNA recombination in human cells. *Hum Mol Genet, 13*(24), 3171-3179. doi:10.1093/hmg/ddh326

Dalerba, P., Dylla, S. J., Park, I.-K., Liu, R., Wang, X., Cho, R. W., . . . Clarke, M. F. (2007). Phenotypic characterization of human colorectal cancer stem cells. *Proceedings of the National Academy of Sciences, 104*(24), 10158. doi:10.1073/pnas.0703478104

Dang, L., White, D. W., Gross, S., Bennett, B. D., Bittinger, M. A., Driggers, E. M., . . . Su, S. M. (2009). Cancer-associated IDH1 mutations produce 2-hydroxyglutarate. *Nature, 462*(7274), 739-744. doi:10.1038/nature08617

Dansen, T. B., Whitfield, J., Rostker, F., Brown-Swigart, L., & Evan, G. I. (2006). Specific Requirement for Bax, Not Bak, in Myc-induced Apoptosis and Tumor Suppression in Vivo. *Journal of Biological Chemistry, 281*(16), 10890-10895. doi:10.1074/jbc.M513655200

Davies, H., Bignell, G. R., Cox, C., Stephens, P., Edkins, S., Clegg, S., . . . Futreal, P. A. (2002). Mutations of the BRAF gene in human cancer. *Nature, 417*(6892), 949-954. doi:10.1038/nature00766

Davis, H., Irshad, S., Bansal, M., Rafferty, H., Boitsova, T., Bardella, C., . . . Leedham, S. J. (2015). Aberrant epithelial GREM1 expression initiates colonic tumorigenesis from cells outside the stem cell niche. *Nat Med, 21*(1), 62-70. doi:10.1038/nm.3750

Davis, J. L., Fallon, H. J., & Morris, H. P. (1970). Two Enzymes of Serine Metabolism in Rat Liver and Hepatomas. *Cancer Res, 30*(12), 2917-2920.

Davis, R. L., Liang, C., Edema-Hildebrand, F., Riley, C., Needham, M., & Sue, C. M. (2013). Fibroblast growth factor 21 is a sensitive biomarker of mitochondrial disease. *Neurology, 81*(21), 1819. doi:10.1212/01.wnl.0000436068.43384.ef

Davis, R. L., Liang, C., & Sue, C. M. (2016). A comparison of current serum biomarkers as diagnostic indicators of mitochondrial diseases. *Neurology, 86*(21), 2010-2015. doi:10.1212/WNL.0000000000002705

Davis, S. R., Stacpoole, P. W., Williamson, J., Kick, L. S., Quinlivan, E. P., Coats, B. S., . . . Gregory, J. F., 3rd. (2004). Tracer-derived total and folate-dependent homocysteine remethylation and synthesis rates in humans indicate that serine is the main one-

carbon donor. *Am J Physiol Endocrinol Metab, 286*(2), E272-279. doi:10.1152/ajpendo.00351.2003

de Brito, O. M., & Scorrano, L. (2008). Mitofusin 2 tethers endoplasmic reticulum to mitochondria. *Nature, 456*(7222), 605-610. doi:10.1038/nature07534

de Grey, A. D. (1997). A proposed refinement of the mitochondrial free radical theory of aging. *Bioessays, 19*(2), 161-166. doi:10.1002/bies.950190211

de Laat, P., Koene, S., van den Heuvel, L. P. W. J., Rodenburg, R. J. T., Janssen, M. C. H., & Smeitink, J. A. M. (2012). Clinical features and heteroplasmy in blood, urine and saliva in 34 Dutch families carrying the m.3243A > G mutation. *Journal of Inherited Metabolic Disease, 35*(6), 1059-1069. doi:10.1007/s10545-012-9465-2

de Lau, W., Barker, N., Low, T. Y., Koo, B. K., Li, V. S., Teunissen, H., . . . Clevers, H. (2011). Lgr5 homologues associate with Wnt receptors and mediate R-spondin signalling. *Nature, 476*(7360), 293-297. doi:10.1038/nature10337

de Sousa e Melo, F., Kurtova, A. V., Harnoss, J. M., Kljavin, N., Hoeck, J. D., Hung, J., . . . de Sauvage, F. J. (2017). A distinct role for Lgr5+ stem cells in primary and metastatic colon cancer. *Nature, 543*(7647), 676-680. doi:10.1038/nature21713

De Sousa E Melo, F., Wang, X., Jansen, M., Fessler, E., Trinh, A., de Rooij, L. P. M. H., . . . Vermeulen, L. (2013). Poor-prognosis colon cancer is defined by a molecularly distinct subtype and develops from serrated precursor lesions. *Nat Med, 19*(5), 614-618. doi:10.1038/nm.3174

DeBerardinis, R. J., & Cheng, T. (2010). Q's next: the diverse functions of glutamine in metabolism, cell biology and cancer. *Oncogene, 29*(3), 313-324. doi:10.1038/onc.2009.358

Deming, P. B., Schafer, Z. T., Tashker, J. S., Potts, M. B., Deshmukh, M., & Kornbluth, S. (2004). Bcr-Abl-mediated protection from apoptosis downstream of mitochondrial cytochrome c release. *Molecular and cellular biology, 24*(23), 10289-10299. doi:10.1128/mcb.24.23.10289-10299.2004

Desbats, M. A., Giacomini, I., Prayer-Galetti, T., & Montopoli, M. (2020). Metabolic Plasticity in Chemotherapy Resistance. *Front Oncol, 10*, 281. doi:10.3389/fonc.2020.00281

Deveraux, Q. L., Roy, N., Stennicke, H. R., Van Arsdale, T., Zhou, Q., Srinivasula, S. M., . . . Reed, J. C. (1998). IAPs block apoptotic events induced by caspase-8 and cytochrome c by direct inhibition of distinct caspases. *Embo j, 17*(8), 2215-2223. doi:10.1093/emboj/17.8.2215

Deveraux, Q. L., Takahashi, R., Salvesen, G. S., & Reed, J. C. (1997). X-linked IAP is a direct inhibitor of cell-death proteases. *Nature, 388*(6639), 300-304. doi:10.1038/40901

Dey, R., & Moraes, C. T. (2000). Lack of oxidative phosphorylation and low mitochondrial membrane potential decrease susceptibility to apoptosis and do not modulate the protective effect of Bcl-x(L) in osteosarcoma cells. *J Biol Chem, 275*(10), 7087-7094. doi:10.1074/jbc.275.10.7087

Diaz, F., Fukui, H., Garcia, S., & Moraes, C. T. (2006). Cytochrome c oxidase is required for the assembly/stability of respiratory complex I in mouse fibroblasts. *Molecular and cellular biology, 26*(13), 4872-4881. doi:10.1128/mcb.01767-05

Dienstmann, R., Mason, M. J., Sinicrope, F. A., Phipps, A. I., Tejpar, S., Nesbakken, A., . . . Guinney, J. (2017). Prediction of overall survival in stage II and III colon cancer beyond TNM system: a retrospective, pooled biomarker study. *Annals of oncology : official journal of the European Society for Medical Oncology, 28*(5), 1023-1031. doi:10.1093/annonc/mdx052

Dillmann, E., Johnson, D. G., Martin, J., Mackler, B., & Finch, C. (1979). Catecholamine elevation in iron deficiency. *Am J Physiol, 237*(5), R297-300. doi:10.1152/ajpregu.1979.237.5.R297

Ding, J., Li, T., Wang, X., Zhao, E., Choi, J.-H., Yang, L., . . . Ding, H.-F. (2013). The histone H3 methyltransferase G9A epigenetically activates the serine-glycine synthesis pathway to sustain cancer cell survival and proliferation. *Cell Metab, 18*(6), 896-907. doi:10.1016/j.cmet.2013.11.004

Dobson, P. F., Dennis, E. P., Hipps, D., Reeve, A., Laude, A., Bradshaw, C., . . . Greaves, L. C. (2020). Mitochondrial dysfunction impairs osteogenesis, increases osteoclast activity, and accelerates age related bone loss. *Scientific Reports, 10*(1), 11643. doi:10.1038/s41598-020-68566-2

Donohoe, D. R., Garge, N., Zhang, X., Sun, W., O'Connell, T. M., Bunger, M. K., & Bultman, S. J. (2011). The microbiome and butyrate regulate energy metabolism and autophagy in the mammalian colon. *Cell Metab, 13*(5), 517-526. doi:10.1016/j.cmet.2011.02.018

Dowling, R. J. O., Zakikhani, M., Fantus, I. G., Pollak, M., & Sonenberg, N. (2007). Metformin Inhibits Mammalian Target of Rapamycin–Dependent Translation Initiation in Breast Cancer Cells. *Cancer Res, 67*(22), 10804. doi:10.1158/0008-5472.CAN-07-2310

Drasar, B. S., & Irving, D. (1973). Environmental factors and cancer of the colon and breast. *British journal of cancer, 27*(2), 167-172. doi:10.1038/bjc.1973.20

Drost, J., van Jaarsveld, R. H., Ponsioen, B., Zimberlin, C., van Boxtel, R., Buijs, A., . . . Clevers, H. (2015). Sequential cancer mutations in cultured human intestinal stem cells. *Nature, 521*(7550), 43-47. doi:10.1038/nature14415

Du, L., Wang, H., He, L., Zhang, J., Ni, B., Wang, X., . . . Chen, Q. (2008). CD44 is of functional importance for colorectal cancer stem cells. *Clin Cancer Res, 14*(21), 6751-6760. doi:10.1158/1078-0432.Ccr-08-1034

Duchen, M. R. (2000). Mitochondria and calcium: from cell signalling to cell death. *J Physiol, 529 Pt 1*(Pt 1), 57-68. doi:10.1111/j.1469-7793.2000.00057.x

Ducker, G. S., Chen, L., Morscher, R. J., Ghergurovich, J. M., Esposito, M., Teng, X., . . . Rabinowitz, J. D. (2016). Reversal of Cytosolic One-Carbon Flux Compensates for Loss of the Mitochondrial Folate Pathway. *Cell Metab, 23*(6), 1140-1153. doi:10.1016/j.cmet.2016.04.016

Ducker, G. S., & Rabinowitz, J. D. (2017). One-Carbon Metabolism in Health and Disease. *Cell Metab, 25*(1), 27-42. doi:10.1016/j.cmet.2016.08.009

Duda, D. G., Duyverman, A. M., Kohno, M., Snuderl, M., Steller, E. J., Fukumura, D., & Jain, R. K. (2010). Malignant cells facilitate lung metastasis by bringing their own soil. *Proc Natl Acad Sci U S A, 107*(50), 21677-21682. doi:10.1073/pnas.1016234107

Dukes, C. E. (1932). The classification of cancer of the rectum. *The Journal of Pathology and Bacteriology, 35*(3), 323-332. doi:https://doi.org/10.1002/path.1700350303

Dunn, J. T., & Dunn, A. D. (2001). Update on intrathyroidal iodine metabolism. *Thyroid, 11*(5), 407-414. doi:10.1089/105072501300176363

Edna, T. H., Karlsen, V., Jullumstro, E., & Lydersen, S. (2012). Prevalence of anaemia at diagnosis of colorectal cancer: assessment of associated risk factors. *Hepatogastroenterology, 59*(115), 713-716. doi:10.5754/hge11479

Eischen, C. M., Packham, G., Nip, J., Fee, B. E., Hiebert, S. W., Zambetti, G. P., & Cleveland, J. L. (2001a). Bcl-2 is an apoptotic target suppressed by both c-Myc and E2F-1. *Oncogene, 20*(48), 6983-6993. doi:10.1038/sj.onc.1204892

Eischen, C. M., Woo, D., Roussel, M. F., & Cleveland, J. L. (2001b). Apoptosis triggered by Myc-induced suppression of Bcl-X(L) or Bcl-2 is bypassed during lymphomagenesis. *Molecular and cellular biology, 21*(15), 5063-5070. doi:10.1128/MCB.21.15.5063-5070.2001

Ekbom, A., Helmick, C., Zack, M., & Adami, H. O. (1990). Ulcerative colitis and colorectal cancer. A population-based study. *N Engl J Med, 323*(18), 1228-1233. doi:10.1056/nejm199011013231802

Ekstrand, M. I., Terzioglu, M., Galter, D., Zhu, S., Hofstetter, C., Lindqvist, E., . . . Larsson, N.-G. (2007). Progressive parkinsonism in mice with respiratory-chain-deficient dopamine neurons. *Proc Natl Acad Sci U S A, 104*(4), 1325-1330. doi:10.1073/pnas.0605208103

Elabd, C., Cousin, W., Upadhyayula, P., Chen, R. Y., Chooljian, M. S., Li, J., . . . Conboy, I. M. (2014). Oxytocin is an age-specific circulating hormone that is necessary for muscle maintenance and regeneration. *Nat Commun, 5*, 4082. doi:10.1038/ncomms5082

Elliott, H. R., Samuels, D. C., Eden, J. A., Relton, C. L., & Chinnery, P. F. (2008). Pathogenic mitochondrial DNA mutations are common in the general population. *American journal of human genetics, 83*(2), 254-260. doi:10.1016/j.ajhg.2008.07.004

Elmore, S. (2007). Apoptosis: A Review of Programmed Cell Death. *Toxicol Pathol, 35*(4), 495-516. doi:10.1080/01926230701320337

Elson, J. L., Samuels, D. C., Turnbull, D. M., & Chinnery, P. F. (2001). Random intracellular drift explains the clonal expansion of mitochondrial DNA mutations with age. *American journal of human genetics, 68*(3), 802-806. doi:10.1086/318801

Engels, W. R., Johnson-Schlitz, D. M., Flores, C., White, L., & Preston, C. (2007). A Third Link connecting Aging with Double Strand Break Repair. *Cell Cycle, 6*(2), 131-135. doi:10.4161/cc.6.2.3758

Erez, N., Truitt, M., Olson, P., Arron, S. T., & Hanahan, D. (2010). Cancer-Associated Fibroblasts Are Activated in Incipient Neoplasia to Orchestrate Tumor-Promoting Inflammation in an NF-kappaB-Dependent Manner. *Cancer Cell, 17*(2), 135-147. doi:10.1016/j.ccr.2009.12.041

Ericson, N. G., Kulawiec, M., Vermulst, M., Sheahan, K., O'Sullivan, J., Salk, J. J., & Bielas, J. H. (2012). Decreased mitochondrial DNA mutagenesis in human colorectal cancer. *PLoS Genet, 8*(6), e1002689. doi:10.1371/journal.pgen.1002689

Evan, G. I., & Vousden, K. H. (2001). Proliferation, cell cycle and apoptosis in cancer. *Nature, 411*(6835), 342-348. doi:10.1038/35077213

Evan, G. I., Wyllie, A. H., Gilbert, C. S., Littlewood, T. D., Land, H., Brooks, M., . . . Hancock, D. C. (1992). Induction of apoptosis in fibroblasts by c-myc protein. *Cell, 69*(1), 119-128. doi:10.1016/0092-8674(92)90123-t

Evans, G. S., Flint, N., Somers, A. S., Eyden, B., & Potten, C. S. (1992). The development of a method for the preparation of rat intestinal epithelial cell primary cultures. *J Cell Sci, 101*(1), 219.

Falkenberg, M., Gaspari, M., Rantanen, A., Trifunovic, A., Larsson, N. G., & Gustafsson, C. M. (2002). Mitochondrial transcription factors B1 and B2 activate transcription of human mtDNA. *Nat Genet, 31*(3), 289-294. doi:10.1038/ng909

Fan, J., Ye, J., Kamphorst, J. J., Shlomi, T., Thompson, C. B., & Rabinowitz, J. D. (2014). Quantitative flux analysis reveals folate-dependent NADPH production. *Nature, 510*(7504), 298-302. doi:10.1038/nature13236

Farber, S., & Diamond, L. K. (1948). Temporary remissions in acute leukemia in children produced by folic acid antagonist, 4-aminopteroyl-glutamic acid. *N Engl J Med, 238*(23), 787-793. doi:10.1056/nejm194806032382301

Farge, G., Mehmedovic, M., Baclayon, M., van den Wildenberg, S. M., Roos, W. H., Gustafsson, C. M., . . . Falkenberg, M. (2014). In vitro-reconstituted nucleoids can block mitochondrial DNA replication and transcription. *Cell Rep, 8*(1), 66-74. doi:10.1016/j.celrep.2014.05.046

Faxén, K., Gilderson, G., Ädelroth, P., & Brzezinski, P. (2005). A mechanistic principle for proton pumping by cytochrome c oxidase. *Nature, 437*(7056), 286-289. doi:10.1038/nature03921

Fearnley, I. M., & Walker, J. E. (1986). Two overlapping genes in bovine mitochondrial DNA encode membrane components of ATP synthase. *Embo j, 5*(8), 2003-2008.

Fearon, E. R., & Vogelstein, B. (1990). A genetic model for colorectal tumorigenesis. *Cell, 61*(5), 759-767. doi:10.1016/0092-8674(90)90186-i

Fearon, Kenneth C. H., Glass, David J., & Guttridge, Denis C. (2012). Cancer Cachexia: Mediators, Signaling, and Metabolic Pathways. *Cell Metab, 16*(2), 153-166. doi:https://doi.org/10.1016/j.cmet.2012.06.011

Feil, R., Brocard, J., Mascrez, B., LeMeur, M., Metzger, D., & Chambon, P. (1996). Ligand-activated site-specific recombination in mice. *Proceedings of the National Academy of Sciences, 93*(20), 10887. doi:10.1073/pnas.93.20.10887

Feil, R., Wagner, J., Metzger, D., & Chambon, P. (1997). Regulation of Cre recombinase activity by mutated estrogen receptor ligand-binding domains. *Biochem Biophys Res Commun, 237*(3), 752-757. doi:10.1006/bbrc.1997.7124

Fellous, T. G., Islam, S., Tadrous, P. J., Elia, G., Kocher, H. M., Bhattacharya, S., . . . Alison, M. R. (2009). Locating the stem cell niche and tracing hepatocyte lineages in human liver. *Hepatology, 49*(5), 1655-1663. doi:10.1002/hep.22791

Fenton, R. G., Hixon, J. A., Wright, P. W., Brooks, A. D., & Sayers, T. J. (1998). Inhibition of Fas (CD95) Expression and Fas-mediated Apoptosis by Oncogenic Ras. *Cancer Res, 58*(15), 3391.

Fernandes-Alnemri, T., Armstrong, R. C., Krebs, J., Srinivasula, S. M., Wang, L., Bullrich, F., . . . Litwack, G. (1996). In vitro activation of CPP32 and Mch3 by Mch4, a novel human apoptotic cysteine protease containing two FADD-like domains. *Proceedings of the National Academy of Sciences, 93*(15), 7464-7469.

Fernandez, P. C., Frank, S. R., Wang, L., Schroeder, M., Liu, S., Greene, J., . . . Amati, B. (2003). Genomic targets of the human c-Myc protein. *Genes Dev, 17*(9), 1115-1129. doi:10.1101/gad.1067003

Figueroa, M. E., Abdel-Wahab, O., Lu, C., Ward, P. S., Patel, J., Shih, A., . . . Melnick, A. (2010). Leukemic IDH1 and IDH2 mutations result in a hypermethylation phenotype, disrupt TET2 function, and impair hematopoietic differentiation. *Cancer Cell, 18*(6), 553-567. doi:10.1016/j.ccr.2010.11.015

Finkelstein, J. D. (1990). Methionine metabolism in mammals. *The Journal of Nutritional Biochemistry, 1*(5), 228-237. doi:https://doi.org/10.1016/0955-2863(90)90070-2

Finkelstein, J. D. (2007). Metabolic regulatory properties of S-adenosylmethionine and S-adenosylhomocysteine. *Clin Chem Lab Med, 45*(12), 1694-1699. doi:10.1515/cclm.2007.341

Fiorini, E., Veghini, L., & Corbo, V. (2020). Modeling Cell Communication in Cancer With Organoids: Making the Complex Simple. *Front Cell Dev Biol, 8*, 166. doi:10.3389/fcell.2020.00166

Fisher, R. P., & Clayton, D. A. (1985). A transcription factor required for promoter recognition by human mitochondrial RNA polymerase. Accurate initiation at the heavy- and light-strand promoters dissected and reconstituted in vitro. *J Biol Chem, 260*(20), 11330-11338.

Fliss, M. S., Usadel, H., Caballero, O. L., Wu, L., Buta, M. R., Eleff, S. M., . . . Sidransky, D. (2000). Facile Detection of Mitochondrial DNA Mutations in Tumors and Bodily Fluids. *Science, 287*(5460), 2017. doi:10.1126/science.287.5460.2017

Fonseca, T. B., Sánchez-Guerrero, Á., Milosevic, I., & Raimundo, N. (2019). Mitochondrial fission requires DRP1 but not dynamins. *Nature, 570*(7761), E34-e42. doi:10.1038/s41586-019-1296-y

Forsström, S., Jackson, C. B., Carroll, C. J., Kuronen, M., Pirinen, E., Pradhan, S., . . . Suomalainen, A. (2019). Fibroblast Growth Factor 21 Drives Dynamics of Local and Systemic Stress Responses in Mitochondrial Myopathy with mtDNA Deletions. *Cell Metab, 30*(6), 1040-1054.e1047. doi:https://doi.org/10.1016/j.cmet.2019.08.019

Forsyth, C. B., Shannon, K. M., Kordower, J. H., Voigt, R. M., Shaikh, M., Jaglin, J. A., . . . Keshavarzian, A. (2011). Increased intestinal permeability correlates with sigmoid mucosa alpha-synuclein staining and endotoxin exposure markers in early Parkinson's disease. *PloS one, 6*(12), e28032. doi:10.1371/journal.pone.0028032

Foury, F., & Lahaye, A. (1987). Cloning and sequencing of the PIF gene involved in repair and recombination of yeast mitochondrial DNA. *Embo j, 6*(5), 1441-1449.

Fox, N. G., Yu, X., Feng, X., Bailey, H. J., Martelli, A., Nabhan, J. F., . . . Han, S. (2019). Structure of the human frataxin-bound iron-sulfur cluster assembly complex provides insight into its activation mechanism. *Nat Commun, 10*(1), 2210. doi:10.1038/s41467-019-09989-y

Fox, R. G., Magness, S., Kujoth, G. C., Prolla, T. A., & Maeda, N. (2012). Mitochondrial DNA polymerase editing mutation, PolgD257A, disturbs stem-progenitor cell cycling in the small intestine and restricts excess fat absorption. *Am J Physiol Gastrointest Liver Physiol, 302*(9), G914-924. doi:10.1152/ajpgi.00402.2011

Franceschi, C., Bonafè, M., Valensin, S., Olivieri, F., De Luca, M., Ottaviani, E., & De Benedictis, G. (2000). Inflamm-aging. An evolutionary perspective on immunosenescence. *Annals of the New York Academy of Sciences, 908*, 244-254. doi:10.1111/j.1749-6632.2000.tb06651.x

Franco-Obregón, A., & Gilbert, J. A. (2017). The Microbiome-Mitochondrion Connection: Common Ancestries, Common Mechanisms, Common Goals. *mSystems, 2*(3). doi:10.1128/mSystems.00018-17

Frank, S., Gaume, B., Bergmann-Leitner, E. S., Leitner, W. W., Robert, E. G., Catez, F., . . . Youle, R. J. (2001). The role of dynamin-related protein 1, a mediator of mitochondrial fission, in apoptosis. *Dev Cell, 1*(4), 515-525. doi:10.1016/s1534-5807(01)00055-7

Fre, S., Huyghe, M., Mourikis, P., Robine, S., Louvard, D., & Artavanis-Tsakonas, S. (2005). Notch signals control the fate of immature progenitor cells in the intestine. *Nature, 435*(7044), 964-968. doi:10.1038/nature03589

Frederiksen, A. L., Andersen, P. H., Kyvik, K. O., Jeppesen, T. D., Vissing, J., & Schwartz, M. (2006). Tissue specific distribution of the 3243A->G mtDNA mutation. *J Med Genet, 43*(8), 671-677. doi:10.1136/jmg.2005.039339

Friedman, J. R., Lackner, L. L., West, M., DiBenedetto, J. R., Nunnari, J., & Voeltz, G. K. (2011). ER tubules mark sites of mitochondrial division. *Science, 334*(6054), 358-362. doi:10.1126/science.1207385

Frolova, L. Y., Tsivkovskii, R. Y., Sivolobova, G. F., Oparina, N. Y., Serpinsky, O. I., Blinov, V. M., . . . Kisselev, L. L. (1999). Mutations in the highly conserved GGQ motif of class 1 polypeptide release factors abolish ability of human eRF1 to trigger peptidyl-tRNA hydrolysis. *Rna, 5*(8), 1014-1020. doi:10.1017/s135583829999043x

Fu, W.-n., Shang, C., Huang, D.-f., Xu, Z.-m., Sun, X.-h., & Sun, K.-l. (2006). Average-12.9 chromosome imbalances coupling with 15 differential expression genes possibly involved in the carcinogenesis, progression and metastasis of supraglottic laryngeal squamous cell cancer. *Zhonghua yi xue yi chuan xue za zhi = Zhonghua yixue yichuanxue zazhi = Chinese journal of medical genetics, 23*(1), 7-11.

Fukui, H., & Moraes, C. T. (2009). Mechanisms of formation and accumulation of mitochondrial DNA deletions in aging neurons. *Human Molecular Genetics, 18*(6), 1028-1036. doi:10.1093/hmg/ddn437

Fulda, S., & Vucic, D. (2012). Targeting IAP proteins for therapeutic intervention in cancer. *Nat Rev Drug Discov, 11*(2), 109-124. doi:10.1038/nrd3627

Fuller, S. D., Capaldi, R. A., & Henderson, R. (1979). Structure of cytochrome c oxidase in deoxycholate-drived two-dimensional crystals. *J Mol Biol, 134*(2), 305-327. doi:10.1016/0022-2836(79)90037-8

Fuste, J. M., Wanrooij, S., Jemt, E., Granycome, C. E., Cluett, T. J., Shi, Y., . . . Falkenberg, M. (2010). Mitochondrial RNA polymerase is needed for activation of the origin of light-strand DNA replication. *Mol Cell, 37*(1), 67-78. doi:10.1016/j.molcel.2009.12.021

Galati, D., Srinivasan, S., Raza, H., Prabu, S. K., Hardy, M., Chandran, K., . . . Avadhani, N. G. (2009). Role of nuclear-encoded subunit Vb in the assembly and stability of cytochrome c oxidase complex: implications in mitochondrial dysfunction and ROS production. *Biochem J, 420*(3), 439-449. doi:10.1042/bj20090214

Galon, J., Costes, A., Sanchez-Cabo, F., Kirilovsky, A., Mlecnik, B., Lagorce-Pagès, C., . . . Pagès, F. (2006). Type, density, and location of immune cells within human colorectal tumors predict clinical outcome. *Science, 313*(5795), 1960-1964. doi:10.1126/science.1129139

Galon, J., Mlecnik, B., Bindea, G., Angell, H. K., Berger, A., Lagorce, C., . . . Pagès, F. (2014). Towards the introduction of the 'Immunoscore' in the classification of malignant tumours. *J Pathol, 232*(2), 199-209. doi:10.1002/path.4287

Gandre-Babbe, S., & van der Bliek, A. M. (2008). The novel tail-anchored membrane protein Mff controls mitochondrial and peroxisomal fission in mammalian cells. *Mol Biol Cell, 19*(6), 2402-2412. doi:10.1091/mbc.E07-12-1287

Garnett, M. J., & Marais, R. (2004). Guilty as charged: B-RAF is a human oncogene. *Cancer Cell, 6*(4), 313-319. doi:https://doi.org/10.1016/j.ccr.2004.09.022

Gaude, E., & Frezza, C. (2016). Tissue-specific and convergent metabolic transformation of cancer correlates with metastatic potential and patient survival. *Nature Communications, 7*, 13041-13041. doi:10.1038/ncomms13041

Gaude, E., Schmidt, C., Gammage, P. A., Dugourd, A., Blacker, T., Chew, S. P., . . . Frezza, C. (2018). NADH Shuttling Couples Cytosolic Reductive Carboxylation of Glutamine with Glycolysis in Cells with Mitochondrial Dysfunction. *Mol Cell, 69*(4), 581-593.e587. doi:10.1016/j.molcel.2018.01.034

Giannakis, M., Hodis, E., Jasmine Mu, X., Yamauchi, M., Rosenbluh, J., Cibulskis, K., . . . Garraway, L. A. (2014). RNF43 is frequently mutated in colorectal and endometrial cancers. *Nat Genet, 46*(12), 1264-1266. doi:10.1038/ng.3127

Giannoni, E., Buricchi, F., Raugei, G., Ramponi, G., & Chiarugi, P. (2005). Intracellular reactive oxygen species activate Src tyrosine kinase during cell adhesion and anchorage-dependent cell growth. *Molecular and cellular biology, 25*(15), 6391-6403. doi:10.1128/mcb.25.15.6391-6403.2005

Giesen, C., Wang, H. A., Schapiro, D., Zivanovic, N., Jacobs, A., Hattendorf, B., . . . Bodenmiller, B. (2014). Highly multiplexed imaging of tumor tissues with subcellular resolution by mass cytometry. *Nat Methods, 11*(4), 417-422. doi:10.1038/nmeth.2869

Giles, R. E., Blanc, H., Cann, H. M., & Wallace, D. C. (1980). Maternal inheritance of human mitochondrial DNA. *Proc Natl Acad Sci U S A, 77*(11), 6715-6719. doi:10.1073/pnas.77.11.6715

Gomes, A. P., Price, N. L., Ling, A. J., Moslehi, J. J., Montgomery, M. K., Rajman, L., . . . Sinclair, D. A. (2013). Declining NAD(+) induces a pseudohypoxic state disrupting nuclear-mitochondrial communication during aging. *Cell, 155*(7), 1624-1638. doi:10.1016/j.cell.2013.11.037

Gorelick, A. N., Kim, M., Chatila, W. K., La, K., Hakimi, A. A., Taylor, B. S., . . . Reznik, E. (2020). Respiratory complex and tissue lineage drive mutational patterns in the tumor mitochondrial genome. *bioRxiv*, 2020.2008.2018.256362. doi:10.1101/2020.08.18.256362

Gorman, G. S., Blakely, E. L., Hornig-Do, H.-T., Tuppen, H. A. L., Greaves, L. C., He, L., . . . Taylor, R. W. (2015). Novel MTND1 mutations cause isolated exercise intolerance, complex I deficiency and increased assembly factor expression. *Clinical science (London, England : 1979), 128*(12), 895-904. doi:10.1042/cs20140705

Goss, K. H., & Groden, J. (2000). Biology of the Adenomatous Polyposis Coli Tumor Suppressor. *Journal of Clinical Oncology, 18*(9), 1967-1979. doi:10.1200/JCO.2000.18.9.1967

Gossen, M., & Bujard, H. (1992). Tight control of gene expression in mammalian cells by tetracycline-responsive promoters. *Proc Natl Acad Sci U S A, 89*(12), 5547-5551. doi:10.1073/pnas.89.12.5547

Goto, Y., Nonaka, I., & Horai, S. (1990). A mutation in the tRNA(Leu)(UUR) gene associated with the MELAS subgroup of mitochondrial encephalomyopathies. *Nature, 348*(6302), 651-653. doi:10.1038/348651a0

Grady, J. P., Pickett, S. J., Ng, Y. S., Alston, C. L., Blakely, E. L., Hardy, S. A., . . . McFarland, R. (2018). mtDNA heteroplasmy level and copy number indicate disease burden in m.3243A>G mitochondrial disease. *EMBO molecular medicine, 10*(6), e8262. doi:10.15252/emmm.201708262

Graff, R. E., Möller, S., Passarelli, M. N., Witte, J. S., Skytthe, A., Christensen, K., . . . Hjelmborg, J. B. (2017). Familial Risk and Heritability of Colorectal Cancer in the Nordic Twin Study of Cancer. *Clin Gastroenterol Hepatol, 15*(8), 1256-1264. doi:10.1016/j.cgh.2016.12.041

Gravel, S.-P., Hulea, L., Toban, N., Birman, E., Blouin, M.-J., Zakikhani, M., . . . Pollak, M. (2014). Serine Deprivation Enhances Antineoplastic Activity of Biguanides. *Cancer Res, 74*(24), 7521. doi:10.1158/0008-5472.CAN-14-2643-T

Gray, H., & Wong, T. W. (1992). Purification and identification of subunit structure of the human mitochondrial DNA polymerase. *Journal of Biological Chemistry, 267*(9), 5835-5841.

Greaves, L. C., Barron, M. J., Campbell-Shiel, G., Kirkwood, T. B., & Turnbull, D. M. (2011). Differences in the accumulation of mitochondrial defects with age in mice and humans. *Mech Ageing Dev, 132*(11-12), 588-591. doi:10.1016/j.mad.2011.10.004

Greaves, L. C., Barron, M. J., Plusa, S., Kirkwood, T. B., Mathers, J. C., Taylor, R. W., & Turnbull, D. M. (2010). Defects in multiple complexes of the respiratory chain are present in ageing human colonic crypts. *Exp Gerontol, 45*(7-8), 573-579. doi:10.1016/j.exger.2010.01.013

Greaves, L. C., Elson, J. L., Nooteboom, M., Grady, J. P., Taylor, G. A., Taylor, R. W., . . . Turnbull, D. M. (2012). Comparison of mitochondrial mutation spectra in ageing human colonic epithelium and disease: absence of evidence for purifying selection in somatic mitochondrial DNA point mutations. *PLoS Genet, 8*(11), e1003082. doi:10.1371/journal.pgen.1003082

Greaves, L. C., Nooteboom, M., Elson, J. L., Tuppen, H. A. L., Taylor, G. A., Commane, D. M., . . . Turnbull, D. M. (2014). Clonal expansion of early to mid-life mitochondrial DNA point mutations drives mitochondrial dysfunction during human ageing. *PLoS Genet, 10*(9), e1004620-e1004620. doi:10.1371/journal.pgen.1004620

Greaves, L. C., Preston, S. L., Tadrous, P. J., Taylor, R. W., Barron, M. J., Oukrif, D., . . . McDonald, S. A. (2006). Mitochondrial DNA mutations are established in human colonic stem cells, and mutated clones expand by crypt fission. *Proc Natl Acad Sci U S A, 103*(3), 714-719. doi:10.1073/pnas.0505903103

Greaves, P., Goonetilleke, R., Nunn, G., Topham, J., & Orton, T. (1993). Two-year carcinogenicity study of tamoxifen in Alderley Park Wistar-derived rats. *Cancer Res, 53*(17), 3919-3924.

Greber, B. J., Bieri, P., Leibundgut, M., Leitner, A., Aebersold, R., Boehringer, D., & Ban, N. (2015). Ribosome. The complete structure of the 55S mammalian mitochondrial ribosome. *Science, 348*(6232), 303-308. doi:10.1126/science.aaa3872

Gregorieff, A., Pinto, D., Begthel, H., Destrée, O., Kielman, M., & Clevers, H. (2005). Expression pattern of Wnt signaling components in the adult intestine. *Gastroenterology, 129*(2), 626-638. doi:10.1016/j.gastro.2005.06.007

Greider, C. W., & Blackburn, E. H. (1985). Identification of a specific telomere terminal transferase activity in Tetrahymena extracts. *Cell, 43*(2 Pt 1), 405-413. doi:10.1016/0092-8674(85)90170-9

Griparic, L., Kanazawa, T., & van der Bliek, A. M. (2007). Regulation of the mitochondrial dynamin-like protein Opa1 by proteolytic cleavage. *The Journal of Cell Biology, 178*(5), 757-764. doi:10.1083/jcb.200704112

Groden, J., Thliveris, A., Samowitz, W., Carlson, M., Gelbert, L., Albertsen, H., . . . White, R. (1991). Identification and characterization of the familial adenomatous polyposis coli gene. *Cell, 66*(3), 589-600. doi:https://doi.org/10.1016/0092-8674(81)90021-0

Gross, N. J., & Rabinowitz, M. (1969). Synthesis of new strands of mitochondrial and nuclear deoxyribonucleic acid by semiconservative replication. *Journal of Biological Chemistry, 244*(6), 1563-1566.

Gu, J., Wu, M., Guo, R., Yan, K., Lei, J., Gao, N., & Yang, M. (2016). The architecture of the mammalian respirasome. *Nature, 537*(7622), 639-643. doi:10.1038/nature19359

Guccione, E., Martinato, F., Finocchiaro, G., Luzi, L., Tizzoni, L., Dall' Olio, V., . . . Amati, B. (2006). Myc-binding-site recognition in the human genome is determined by chromatin context. *Nat Cell Biol, 8*(7), 764-770. doi:10.1038/ncb1434

Guerra, C., Roncero, C., Porras, A., Fernández, M., & Benito, M. (1996). Triiodothyronine induces the transcription of the uncoupling protein gene and stabilizes its mRNA in fetal rat brown adipocyte primary cultures. *Journal of Biological Chemistry, 271*(4), 2076-2081.

Guinney, J., Dienstmann, R., Wang, X., de Reyniès, A., Schlicker, A., Soneson, C., . . . Tejpar, S. (2015). The consensus molecular subtypes of colorectal cancer. *Nat Med, 21*(11), 1350-1356. doi:10.1038/nm.3967

Guliaeva, N. A., Kuznetsova, E. A., & Gaziev, A. I. (2006). [Proteins associated with mitochondrial DNA protect it against the action of X-rays and hydrogen peroxide]. *Biofizika, 51*(4), 692-697.

Günthert, U., Hofmann, M., Rudy, W., Reber, S., Zöller, M., Haussmann, I., . . . Herrlich, P. (1991). A new variant of glycoprotein CD44 confers metastatic potential to rat carcinoma cells. *Cell, 65*(1), 13-24. doi:10.1016/0092-8674(91)90403-l

Gyllensten, U., Wharton, D., Josefsson, A., & Wilson, A. C. (1991). Paternal inheritance of mitochondrial DNA in mice. *Nature, 352*(6332), 255-257. doi:10.1038/352255a0

Hagerhall, C. (1997). Succinate: quinone oxidoreductases. Variations on a conserved theme. *Biochim Biophys Acta, 1320*(2), 107-141. doi:10.1016/s0005-2728(97)00019-4

Halberg, R. B., Katzung, D. S., Hoff, P. D., Moser, A. R., Cole, C. E., Lubet, R. A., . . . Dove, W. F. (2000). Tumorigenesis in the multiple intestinal neoplasia mouse: redundancy of negative regulators and specificity of modifiers. *Proc Natl Acad Sci U S A, 97*(7), 3461-3466. doi:10.1073/pnas.050585597

Half, E., Bercovich, D., & Rozen, P. (2009). Familial adenomatous polyposis. *Orphanet journal of rare diseases, 4*, 22-22. doi:10.1186/1750-1172-4-22

Hammad, S., Othman, A., Meyer, C., Telfah, A., Lambert, J., Dewidar, B., . . . Dooley, S. (2018). Confounding influence of tamoxifen in mouse models of Cre recombinase-induced gene activity or modulation. *Arch Toxicol, 92*(8), 2549-2561. doi:10.1007/s00204-018-2254-4

Hanahan, D., & Weinberg, R. A. (2011). Hallmarks of cancer: the next generation. *Cell, 144*(5), 646-674. doi:10.1016/j.cell.2011.02.013

Hao, H. X., Xie, Y., Zhang, Y., Charlat, O., Oster, E., Avello, M., . . . Cong, F. (2012). ZNRF3 promotes Wnt receptor turnover in an R-spondin-sensitive manner. *Nature, 485*(7397), 195-200. doi:10.1038/nature11019

Haque, M. E., & Spremulli, L. L. (2008). Roles of the N- and C-terminal domains of mammalian mitochondrial initiation factor 3 in protein biosynthesis. *J Mol Biol, 384*(4), 929-940. doi:10.1016/j.jmb.2008.09.077

Haramis, A. P., Begthel, H., van den Born, M., van Es, J., Jonkheer, S., Offerhaus, G. J., & Clevers, H. (2004). De novo crypt formation and juvenile polyposis on BMP inhibition in mouse intestine. *Science, 303*(5664), 1684-1686. doi:10.1126/science.1093587

Harding, H. P., Novoa, I., Zhang, Y., Zeng, H., Wek, R., Schapira, M., & Ron, D. (2000). Regulated Translation Initiation Controls Stress-Induced Gene Expression in Mammalian Cells. *Mol Cell, 6*(5), 1099-1108. doi:https://doi.org/10.1016/S1097-2765(00)00108-8

Harding, H. P., Zhang, Y., Zeng, H., Novoa, I., Lu, P. D., Calfon, M., . . . Ron, D. (2003). An Integrated Stress Response Regulates Amino Acid Metabolism and Resistance to Oxidative Stress. *Mol Cell, 11*(3), 619-633. doi:https://doi.org/10.1016/S1097-2765(03)00105-9

Hardwick, J. C., Van Den Brink, G. R., Bleuming, S. A., Ballester, I., Van Den Brande, J. M., Keller, J. J., . . . Peppelenbosch, M. P. (2004). Bone morphogenetic protein 2 is

expressed by, and acts upon, mature epithelial cells in the colon. *Gastroenterology, 126*(1), 111-121. doi:10.1053/j.gastro.2003.10.067

Harley, C. B., Futcher, A. B., & Greider, C. W. (1990). Telomeres shorten during ageing of human fibroblasts. *Nature, 345*(6274), 458-460. doi:10.1038/345458a0

Harley, C. B., Vaziri, H., Counter, C. M., & Allsopp, R. C. (1992). The telomere hypothesis of cellular aging. *Exp Gerontol, 27*(4), 375-382. doi:https://doi.org/10.1016/0531-5565(92)90068-B

Harman, D. (1956). Aging: a theory based on free radical and radiation chemistry. *J Gerontol, 11*(3), 298-300. doi:10.1093/geronj/11.3.298

Harman, D. (1972). The biologic clock: the mitochondria? *J Am Geriatr Soc, 20*(4), 145-147. doi:10.1111/j.1532-5415.1972.tb00787.x

Hart, R. W., & Setlow, R. B. (1974). Correlation between deoxyribonucleic acid excision-repair and life-span in a number of mammalian species. *Proc Natl Acad Sci U S A, 71*(6), 2169-2173. doi:10.1073/pnas.71.6.2169

Hatefi, Y. (1985). The mitochondrial electron transport and oxidative phosphorylation system. *Annu Rev Biochem, 54*, 1015-1069. doi:10.1146/annurev.bi.54.070185.005055

Hauswirth, W. W., & Laipis, P. J. (1982). Mitochondrial DNA polymorphism in a maternal lineage of Holstein cows. *Proceedings of the National Academy of Sciences, 79*(15), 4686. doi:10.1073/pnas.79.15.4686

Hawkins, N. J., Bariol, C., & Ward, R. L. (2002). The serrated neoplasia pathway. *Pathology, 34*(6), 548-555.

Hayashi, J., Ohta, S., Kikuchi, A., Takemitsu, M., Goto, Y., & Nonaka, I. (1991). Introduction of disease-related mitochondrial DNA deletions into HeLa cells lacking mitochondrial DNA results in mitochondrial dysfunction. *Proc Natl Acad Sci U S A, 88*(23), 10614-10618. doi:10.1073/pnas.88.23.10614

Hayflick, L., & Moorhead, P. S. (1961). The serial cultivation of human diploid cell strains. *Exp Cell Res, 25*, 585-621. doi:10.1016/0014-4827(61)90192-6

Haynes, C. M., Fiorese, C. J., & Lin, Y.-F. (2013). Evaluating and responding to mitochondrial dysfunction: the mitochondrial unfolded-protein response and beyond. *Trends in Cell Biology, 23*(7), 311-318. doi:10.1016/j.tcb.2013.02.002

Haynes, C. M., Petrova, K., Benedetti, C., Yang, Y., & Ron, D. (2007). ClpP Mediates Activation of a Mitochondrial Unfolded Protein Response in C. elegans. *Developmental Cell, 13*(4), 467-480. doi:https://doi.org/10.1016/j.devcel.2007.07.016

He, D., Wu, H., Xiang, J., Ruan, X., Peng, P., Ruan, Y., . . . Li, B. (2020). Gut stem cell aging is driven by mTORC1 via a p38 MAPK-p53 pathway. *Nature Communications, 11*(1), 37. doi:10.1038/s41467-019-13911-x

He, J., Cooper, H. M., Reyes, A., Di Re, M., Sembongi, H., Litwin, T. R., . . . Holt, I. J. (2012). Mitochondrial nucleoid interacting proteins support mitochondrial protein synthesis. *Nucleic Acids Res, 40*(13), 6109-6121. doi:10.1093/nar/gks266

He, T. C., Sparks, A. B., Rago, C., Hermeking, H., Zawel, L., da Costa, L. T., . . . Kinzler, K. W. (1998). Identification of c-MYC as a target of the APC pathway. *Science, 281*(5382), 1509-1512. doi:10.1126/science.281.5382.1509

He, X. C., Zhang, J., Tong, W. G., Tawfik, O., Ross, J., Scoville, D. H., . . . Li, L. (2004). BMP signaling inhibits intestinal stem cell self-renewal through suppression of Wnt-beta-catenin signaling. *Nat Genet, 36*(10), 1117-1121. doi:10.1038/ng1430

He, Y., Wu, J., Dressman, D. C., Iacobuzio-Donahue, C., Markowitz, S. D., Velculescu, V. E., . . . Papadopoulos, N. (2010). Heteroplasmic mitochondrial DNA mutations in normal and tumour cells. *Nature, 464*(7288), 610-614. doi:10.1038/nature08802

Heaton, G. M., Wagenvoord, R. J., Kemp, A., Jr., & Nicholls, D. G. (1978). Brown-adipose-tissue mitochondria: photoaffinity labelling of the regulatory site of energy dissipation. *Eur J Biochem, 82*(2), 515-521. doi:10.1111/j.1432-1033.1978.tb12045.x

Heidelberger, C., Chaudhuri, N. K., Danneberg, P., Mooren, D., Griesbach, L., Duschinsky, R., . . . Scheiner, J. (1957). Fluorinated Pyrimidines, A New Class of Tumour-Inhibitory Compounds. *Nature, 179*(4561), 663-666. doi:10.1038/179663a0

Heinemann, V., von Weikersthal, L. F., Decker, T., Kiani, A., Vehling-Kaiser, U., Al-Batran, S. E., . . . Stintzing, S. (2014). FOLFIRI plus cetuximab versus FOLFIRI plus bevacizumab as first-line treatment for patients with metastatic colorectal cancer (FIRE-3): a randomised, open-label, phase 3 trial. *Lancet Oncol, 15*(10), 1065-1075. doi:10.1016/s1470-2045(14)70330-4

Heitzler, P., Bourouis, M., Ruel, L., Carteret, C., & Simpson, P. (1996). Genes of the Enhancer of split and achaete-scute complexes are required for a regulatory loop between Notch and Delta during lateral signalling in Drosophila. *Development, 122*(1), 161.

Heldin, C. H., Miyazono, K., & ten Dijke, P. (1997). TGF-beta signalling from cell membrane to nucleus through SMAD proteins. *Nature, 390*(6659), 465-471. doi:10.1038/37284

Henle, E. S., Luo, Y., Gassmann, W., & Linn, S. (1996). Oxidative damage to DNA constituents by iron-mediated fenton reactions. The deoxyguanosine family. *J Biol Chem, 271*(35), 21177-21186.

Herbers, E., Kekäläinen, N. J., Hangas, A., Pohjoismäki, J. L., & Goffart, S. (2019). Tissue specific differences in mitochondrial DNA maintenance and expression. *Mitochondrion, 44*, 85-92. doi:10.1016/j.mito.2018.01.004

Hermeking, H., & Eick, D. (1994). Mediation of c-Myc-induced apoptosis by p53. *Science, 265*(5181), 2091. doi:10.1126/science.8091232

Hillen, H. S., Morozov, Y. I., Sarfallah, A., Temiakov, D., & Cramer, P. (2017). Structural Basis of Mitochondrial Transcription Initiation. *Cell, 171*(5), 1072-1081.e1010. doi:10.1016/j.cell.2017.10.036

Hinchliffe, P., & Sazanov, L. A. (2005). Organization of iron-sulfur clusters in respiratory complex I. *Science, 309*(5735), 771-774. doi:10.1126/science.1113988

Hinkle, P. C., Butow, R. A., Racker, E., & Chance, B. (1967). Partial resolution of the enzymes catalyzing oxidative phosphorylation. XV. Reverse electron transfer in the flavin-cytochrome beta region of the respiratory chain of beef heart submitochondrial particles. *J Biol Chem, 242*(22), 5169-5173.

Hirst, J., King, M. S., & Pryde, K. R. (2008). The production of reactive oxygen species by complex I. *Biochem Soc Trans, 36*(Pt 5), 976-980. doi:10.1042/bst0360976

Ho, T. T., Warr, M. R., Adelman, E. R., Lansinger, O. M., Flach, J., Verovskaya, E. V., . . . Passegué, E. (2017). Autophagy maintains the metabolism and function of young and old stem cells. *Nature, 543*(7644), 205-210. doi:10.1038/nature21388

Höhn, P., Gabbert, H., & Wagner, R. (1978). Differentiation and aging of the rat intestinal mucosa. II. Morphological, enzyme histochemical and disc electrophoretic aspects of the aging of the small intestinal mucosa. *Mech Ageing Dev, 7*, 217-226. doi:https://doi.org/10.1016/0047-6374(78)90068-4

Hollander, D., & Tarnawski, H. (1985). Aging-Associated Increase in Intestinal Absorption of Macromolecules. *Gerontology, 31*(3), 133-137. doi:10.1159/000212694

Holmes, J. B., Akman, G., Wood, S. R., Sakhuja, K., Cerritelli, S. M., Moss, C., . . . Holt, I. J. (2015). Primer retention owing to the absence of RNase H1 is catastrophic for

mitochondrial DNA replication. *Proc Natl Acad Sci U S A, 112*(30), 9334-9339. doi:10.1073/pnas.1503653112

Holt, I. J., Harding, A. E., & Morgan-Hughes, J. A. (1988). Deletions of muscle mitochondrial DNA in patients with mitochondrial myopathies. *Nature, 331*(6158), 717-719. doi:10.1038/331717a0

Holt, I. J., Lorimer, H. E., & Jacobs, H. T. (2000). Coupled leading- and lagging-strand synthesis of mammalian mitochondrial DNA. *Cell, 100*(5), 515-524. doi:10.1016/s0092-8674(00)80688-1

Holzmann, J., Frank, P., Löffler, E., Bennett, K. L., Gerner, C., & Rossmanith, W. (2008). RNase P without RNA: identification and functional reconstitution of the human mitochondrial tRNA processing enzyme. *Cell, 135*(3), 462-474. doi:10.1016/j.cell.2008.09.013

Hori, Y. S., Kuno, A., Hosoda, R., & Horio, Y. (2013). Regulation of FOXOs and p53 by SIRT1 modulators under oxidative stress. *PloS one, 8*(9), e73875.

Horton, T. M., Petros, J. A., Heddi, A., Shoffner, J., Kaufman, A. E., Graham, S. D., Jr., . . . Wallace, D. C. (1996). Novel mitochondrial DNA deletion found in a renal cell carcinoma. *Genes Chromosomes Cancer, 15*(2), 95-101. doi:10.1002/(sici)1098-2264(199602)15:2<95::Aid-gcc3>3.0.Co;2-z

Hou, J. K., Abraham, B., & El-Serag, H. (2011). Dietary intake and risk of developing inflammatory bowel disease: a systematic review of the literature. *Am J Gastroenterol, 106*(4), 563-573. doi:10.1038/ajg.2011.44

Hou, X., Song, J., Li, X.-N., Zhang, L., Wang, X., Chen, L., & Shen, Y. H. (2010). Metformin reduces intracellular reactive oxygen species levels by upregulating expression of the antioxidant thioredoxin via the AMPK-FOXO3 pathway. *Biochemical and Biophysical Research Communications, 396*(2), 199-205. doi:https://doi.org/10.1016/j.bbrc.2010.04.017

Houghton, D., Stewart, C. J., Stamp, C., Nelson, A., Aj Ami, N. J., Petrosino, J. F., . . . Greaves, L. C. (2018). Impact of Age-Related Mitochondrial Dysfunction and Exercise on Intestinal Microbiota Composition. *The journals of gerontology. Series A, Biological sciences and medical sciences, 73*(5), 571-578. doi:10.1093/gerona/glx197

Houtkooper, R. H., Mouchiroud, L., Ryu, D., Moullan, N., Katsyuba, E., Knott, G., . . . Auwerx, J. (2013). Mitonuclear protein imbalance as a conserved longevity mechanism. *Nature, 497*(7450), 451-457. doi:10.1038/nature12188

Hu, J., Locasale, J. W., Bielas, J. H., O'Sullivan, J., Sheahan, K., Cantley, L. C., . . . Vitkup, D. (2013). Heterogeneity of tumor-induced gene expression changes in the human metabolic network. *Nature Biotechnology, 31*(6), 522-529. doi:10.1038/nbt.2530

Huang, E. H., Hynes, M. J., Zhang, T., Ginestier, C., Dontu, G., Appelman, H., . . . Boman, B. M. (2009). Aldehyde dehydrogenase 1 is a marker for normal and malignant human colonic stem cells (SC) and tracks SC overpopulation during colon tumorigenesis. *Cancer Res, 69*(8), 3382-3389. doi:10.1158/0008-5472.Can-08-4418

Huang, R., Xu, Y., Wan, W., Shou, X., Qian, J., You, Z., . . . Lippincott-Schwartz, J. (2015). Deacetylation of nuclear LC3 drives autophagy initiation under starvation. *Mol Cell, 57*(3), 456-466.

Hudson, B., & Vinograd, J. (1967). Catenated circular DNA molecules in HeLa cell mitochondria. *Nature, 216*(5116), 647-652. doi:10.1038/216647a0

Huff, J. (2015). The Airyscan detector from ZEISS: confocal imaging with improved signal-to-noise ratio and super-resolution. *Nature methods, 12*(12), i-ii.

Huggins, C. J., Mayekar, M. K., Martin, N., Saylor, K. L., Gonit, M., Jailwala, P., . . . Johnson, P. F. (2015). C/EBPγ Is a Critical Regulator of Cellular Stress Response Networks through Heterodimerization with ATF4. *Molecular and cellular biology, 36*(5), 693-713. doi:10.1128/MCB.00911-15

Huh, W. J., Khurana, S. S., Geahlen, J. H., Kohli, K., Waller, R. A., & Mills, J. C. (2012). Tamoxifen Induces Rapid, Reversible Atrophy, and Metaplasia in Mouse Stomach. *Gastroenterology, 142*(1), 21-24.e27. doi:https://doi.org/10.1053/j.gastro.2011.09.050

Huh, W. J., Mysorekar, I. U., & Mills, J. C. (2010). Inducible activation of Cre recombinase in adult mice causes gastric epithelial atrophy, metaplasia, and regenerative changes in the absence of "floxed" alleles. *American journal of physiology. Gastrointestinal and liver physiology, 299*(2), G368-G380. doi:10.1152/ajpgi.00021.2010

Hung, K. E., Maricevich, M. A., Richard, L. G., Chen, W. Y., Richardson, M. P., Kunin, A., . . . Kucherlapati, R. (2010). Development of a mouse model for sporadic and metastatic colon tumors and its use in assessing drug treatment. *Proceedings of the National Academy of Sciences, 107*(4), 1565. doi:10.1073/pnas.0908682107

Hunte, C., Zickermann, V., & Brandt, U. (2010). Functional modules and structural basis of conformational coupling in mitochondrial complex I. *Science, 329*(5990), 448-451. doi:10.1126/science.1191046

Iborra, F. J., Kimura, H., & Cook, P. R. (2004). The functional organization of mitochondrial genomes in human cells. *BMC Biol, 2*, 9. doi:10.1186/1741-7007-2-9

Ichijo, H., Nishida, E., Irie, K., ten Dijke, P., Saitoh, M., Moriguchi, T., . . . Gotoh, Y. (1997). Induction of apoptosis by ASK1, a mammalian MAPKKK that activates SAPK/JNK and p38 signaling pathways. *Science, 275*(5296), 90-94. doi:10.1126/science.275.5296.90

Indra, A. K., Warot, X., Brocard, J., Bornert, J. M., Xiao, J. H., Chambon, P., & Metzger, D. (1999). Temporally-controlled site-specific mutagenesis in the basal layer of the epidermis: comparison of the recombinase activity of the tamoxifen-inducible Cre-ER(T) and Cre-ER(T2) recombinases. *Nucleic Acids Res, 27*(22), 4324-4327. doi:10.1093/nar/27.22.4324

Iommarini, L., Kurelac, I., Capristo, M., Calvaruso, M. A., Giorgio, V., Bergamini, C., . . . Porcelli, A. M. (2014). Different mtDNA mutations modify tumor progression in dependence of the degree of respiratory complex I impairment. *Hum Mol Genet, 23*(6), 1453-1466. doi:10.1093/hmg/ddt533

Ionov, Y., Peinado, M. A., Malkhosyan, S., Shibata, D., & Perucho, M. (1993). Ubiquitous somatic mutations in simple repeated sequences reveal a new mechanism for colonic carcinogenesis. *Nature, 363*(6429), 558-561. doi:10.1038/363558a0

Isaacs, J. S., Jung, Y. J., Mole, D. R., Lee, S., Torres-Cabala, C., Chung, Y. L., . . . Neckers, L. (2005). HIF overexpression correlates with biallelic loss of fumarate hydratase in renal cancer: novel role of fumarate in regulation of HIF stability. *Cancer Cell, 8*(2), 143-153. doi:10.1016/j.ccr.2005.06.017

Ishihara, N., Eura, Y., & Mihara, K. (2004). Mitofusin 1 and 2 play distinct roles in mitochondrial fusion reactions via GTPase activity. *J Cell Sci, 117*(Pt 26), 6535-6546. doi:10.1242/jcs.01565

Ishihara, T., Ban-Ishihara, R., Maeda, M., Matsunaga, Y., Ichimura, A., Kyogoku, S., . . . Ishihara, N. (2015). Dynamics of mitochondrial DNA nucleoids regulated by mitochondrial fission is essential for maintenance of homogeneously active mitochondria during neonatal heart development. *Molecular and cellular biology, 35*(1), 211-223. doi:10.1128/MCB.01054-14

Ishikawa, K., Takenaga, K., Akimoto, M., Koshikawa, N., Yamaguchi, A., Imanishi, H., . . . Hayashi, J. (2008). ROS-generating mitochondrial DNA mutations can regulate tumor cell metastasis. *Science, 320*(5876), 661-664. doi:10.1126/science.1156906

Ito, K., Hirao, A., Arai, F., Takubo, K., Matsuoka, S., Miyamoto, K., . . . Suda, T. (2006). Reactive oxygen species act through p38 MAPK to limit the lifespan of hematopoietic stem cells. *Nat Med, 12*(4), 446-451. doi:10.1038/nm1388

Itoh, N., Yonehara, S., Ishii, A., Yonehara, M., Mizushima, S., Sameshima, M., . . . Nagata, S. (1991). The polypeptide encoded by the cDNA for human cell surface antigen Fas can mediate apoptosis. *Cell, 66*(2), 233-243. doi:10.1016/0092-8674(91)90614-5

Jackson, D. N., Panopoulos, M., Neumann, W. L., Turner, K., Cantarel, B. L., Thompson-Snipes, L., . . . Theiss, A. L. (2020). Mitochondrial dysfunction during loss of prohibitin 1 triggers Paneth cell defects and ileitis. *Gut*. doi:10.1136/gutjnl-2019-319523

Jackstadt, R., van Hooff, S. R., Leach, J. D., Cortes-Lavaud, X., Lohuis, J. O., Ridgway, R. A., . . . Sansom, O. J. (2019). Epithelial NOTCH Signaling Rewires the Tumor Microenvironment of Colorectal Cancer to Drive Poor-Prognosis Subtypes and Metastasis. *Cancer Cell, 36*(3), 319-336.e317. doi:10.1016/j.ccell.2019.08.003

Jain, I. H., Calvo, S. E., Markhard, A. L., Skinner, O. S., To, T. L., Ast, T., & Mootha, V. K. (2020). Genetic Screen for Cell Fitness in High or Low Oxygen Highlights Mitochondrial and Lipid Metabolism. *Cell, 181*(3), 716-727.e711. doi:10.1016/j.cell.2020.03.029

Jain, I. H., Zazzeron, L., Goldberger, O., Marutani, E., Wojtkiewicz, G. R., Ast, T., . . . Mootha, V. K. (2019). Leigh Syndrome Mouse Model Can Be Rescued by Interventions that Normalize Brain Hyperoxia, but Not HIF Activation. *Cell Metab, 30*(4), 824-832.e823. doi:10.1016/j.cmet.2019.07.006

Jain, I. H., Zazzeron, L., Goli, R., Alexa, K., Schatzman-Bone, S., Dhillon, H., . . . Mootha, V. K. (2016). Hypoxia as a therapy for mitochondrial disease. *Science, 352*(6281), 54-61. doi:10.1126/science.aad9642

Jain, M., Nilsson, R., Sharma, S., Madhusudhan, N., Kitami, T., Souza, A. L., . . . Mootha, V. K. (2012). Metabolite profiling identifies a key role for glycine in rapid cancer cell proliferation. *Science (New York, N.Y.), 336*(6084), 1040-1044. doi:10.1126/science.1218595

Jang, Y. C., Pérez, V. I., Song, W., Lustgarten, M. S., Salmon, A. B., Mele, J., . . . Richardson, A. (2009). Overexpression of Mn superoxide dismutase does not increase life span in mice. *The journals of gerontology. Series A, Biological sciences and medical sciences, 64*(11), 1114-1125. doi:10.1093/gerona/glp100

Jang, Y. Y., & Sharkis, S. J. (2007). A low level of reactive oxygen species selects for primitive hematopoietic stem cells that may reside in the low-oxygenic niche. *Blood, 110*(8), 3056-3063. doi:10.1182/blood-2007-05-087759

Janssen, K. P., Alberici, P., Fsihi, H., Gaspar, C., Breukel, C., Franken, P., . . . Robine, S. (2006). APC and Oncogenic KRAS Are Synergistic in Enhancing Wnt Signaling in Intestinal Tumor Formation and Progression. *Gastroenterology, 131*(4), 1096-1109. doi:https://doi.org/10.1053/j.gastro.2006.08.011

Jasperson, K. W., Tuohy, T. M., Neklason, D. W., & Burt, R. W. (2010). Hereditary and familial colon cancer. *Gastroenterology, 138*(6), 2044-2058. doi:10.1053/j.gastro.2010.01.054

Jass, J. R., Baker, K., Zlobec, I., Higuchi, T., Barker, M., Buchanan, D., & Young, J. (2006). Advanced colorectal polyps with the molecular and morphological features of serrated polyps and adenomas: concept of a 'fusion' pathway to colorectal cancer. *Histopathology, 49*(2), 121-131. doi:10.1111/j.1365-2559.2006.02466.x

Jensen, J., Pedersen, E. E., Galante, P., Hald, J., Heller, R. S., Ishibashi, M., . . . Madsen, O. D. (2000). Control of endodermal endocrine development by Hes-1. *Nat Genet, 24*(1), 36-44. doi:10.1038/71657

Jensen, P. K. (1966). Antimycin-insensitive oxidation of succinate and reduced nicotinamide-adenine dinucleotide in electron-transport particles. I. pH dependency and hydrogen peroxide formation. *Biochim Biophys Acta, 122*(2), 157-166. doi:10.1016/0926-6593(66)90057-9

Jiang, L., Shestov, A. A., Swain, P., Yang, C., Parker, S. J., Wang, Q. A., . . . DeBerardinis, R. J. (2016). Reductive carboxylation supports redox homeostasis during anchorage-independent growth. *Nature, 532*(7598), 255-258. doi:10.1038/nature17393

Jiang, Y., Qian, X., Shen, J., Wang, Y., Li, X., Liu, R., . . . Lu, Z. (2015). Local generation of fumarate promotes DNA repair through inhibition of histone H3 demethylation. *Nat Cell Biol, 17*(9), 1158-1168. doi:10.1038/ncb3209

Jinek, M., Chylinski, K., Fonfara, I., Hauer, M., Doudna, J. A., & Charpentier, E. (2012). A Programmable Dual-RNA–Guided DNA Endonuclease in Adaptive Bacterial Immunity. *Science, 337*(6096), 816. doi:10.1126/science.1225829

Jinek, M., East, A., Cheng, A., Lin, S., Ma, E., & Doudna, J. (2013). RNA-programmed genome editing in human cells. *Elife, 2*, e00471. doi:10.7554/eLife.00471

Jouaville, L. S., Pinton, P., Bastianutto, C., Rutter, G. A., & Rizzuto, R. (1999). Regulation of mitochondrial ATP synthesis by calcium: Evidence for a long-term metabolic priming.

Proceedings of the National Academy of Sciences, 96(24), 13807. doi:10.1073/pnas.96.24.13807

Jourdain, A. A., Koppen, M., Rodley, C. D., Maundrell, K., Gueguen, N., Reynier, P., . . . Martinou, J. C. (2015). A mitochondria-specific isoform of FASTK is present in mitochondrial RNA granules and regulates gene expression and function. *Cell Rep, 10*(7), 1110-1121. doi:10.1016/j.celrep.2015.01.063

Jourdain, A. A., Koppen, M., Wydro, M., Rodley, C. D., Lightowlers, R. N., Chrzanowska-Lightowlers, Z. M., & Martinou, J. C. (2013). GRSF1 regulates RNA processing in mitochondrial RNA granules. *Cell Metab, 17*(3), 399-410. doi:10.1016/j.cmet.2013.02.005

Ju, H. Q., Lu, Y. X., Chen, D. L., Zuo, Z. X., Liu, Z. X., Wu, Q. N., . . . Xu, R. H. (2019). Modulation of Redox Homeostasis by Inhibition of MTHFD2 in Colorectal Cancer: Mechanisms and Therapeutic Implications. *J Natl Cancer Inst, 111*(6), 584-596. doi:10.1093/jnci/djy160

Juin, P., Hunt, A., Littlewood, T., Griffiths, B., Swigart, L. B., Korsmeyer, S., & Evan, G. (2002). c-Myc functionally cooperates with Bax to induce apoptosis. *Molecular and cellular biology, 22*(17), 6158-6169. doi:10.1128/mcb.22.17.6158-6169.2002

Jun, D. Y., Park, H. S., Lee, J. Y., Baek, J. Y., Park, H. K., Fukui, K., & Kim, Y. H. (2008). Positive regulation of promoter activity of human 3-phosphoglycerate dehydrogenase (PHGDH) gene is mediated by transcription factors Sp1 and NF-Y. *Gene, 414*(1-2), 106-114. doi:10.1016/j.gene.2008.02.018

Jurk, D., Wilson, C., Passos, J. F., Oakley, F., Correia-Melo, C., Greaves, L., . . . von Zglinicki, T. (2014). Chronic inflammation induces telomere dysfunction and accelerates ageing in mice. *Nat Commun, 2*, 4172. doi:10.1038/ncomms5172

Kaiser, J. C., Meckbach, R., & Jacob, P. (2014). Genomic instability and radiation risk in molecular pathways to colon cancer. *PloS one, 9*(10), e111024.

Kalia, R., Wang, R. Y.-R., Yusuf, A., Thomas, P. V., Agard, D. A., Shaw, J. M., & Frost, A. (2018). Structural basis of mitochondrial receptor binding and constriction by DRP1. *Nature, 558*(7710), 401-405. doi:10.1038/s41586-018-0211-2

Kamata, H., Honda, S., Maeda, S., Chang, L., Hirata, H., & Karin, M. (2005). Reactive oxygen species promote TNFalpha-induced death and sustained JNK activation by inhibiting MAP kinase phosphatases. *Cell, 120*(5), 649-661. doi:10.1016/j.cell.2004.12.041

Kambara, T., Simms, L. A., Whitehall, V. L., Spring, K. J., Wynter, C. V., Walsh, M. D., . . . Leggett, B. A. (2004). BRAF mutation is associated with DNA methylation in serrated polyps and cancers of the colorectum. *Gut, 53*(8), 1137-1144. doi:10.1136/gut.2003.037671

Kamerkar, S. C., Kraus, F., Sharpe, A. J., Pucadyil, T. J., & Ryan, M. T. (2018). Dynamin-related protein 1 has membrane constricting and severing abilities sufficient for mitochondrial and peroxisomal fission. *Nat Commun, 9*(1), 5239. doi:10.1038/s41467-018-07543-w

Katajisto, P., Döhla, J., Chaffer, C. L., Pentinmikko, N., Marjanovic, N., Iqbal, S., . . . Sabatini, D. M. (2015). Stem cells. Asymmetric apportioning of aged mitochondria between daughter cells is required for stemness. *Science (New York, N.Y.), 348*(6232), 340-343. doi:10.1126/science.1260384

Kaufman, B. A., Durisic, N., Mativetsky, J. M., Costantino, S., Hancock, M. A., Grutter, P., & Shoubridge, E. A. (2007). The mitochondrial transcription factor TFAM coordinates the assembly of multiple DNA molecules into nucleoid-like structures. *Mol Biol Cell, 18*(9), 3225-3236. doi:10.1091/mbc.e07-05-0404

Kauppila, J. H. K., Bonekamp, N. A., Mourier, A., Isokallio, M. A., Just, A., Kauppila, T. E. S., . . . Larsson, N. G. (2018). Base-excision repair deficiency alone or combined with increased oxidative stress does not increase mtDNA point mutations in mice. *Nucleic Acids Res, 46*(13), 6642-6669. doi:10.1093/nar/gky456

Keelan, M., Walker, K., & Thomson, A. (1985). Intestinal morphology, marker enzymes and lipid content of brush border membranes from rabbit jejunum and ileum: effect of aging. *Mech Ageing Dev, 31*(1), 49-68.

Kennedy, S. R., Salk, J. J., Schmitt, M. W., & Loeb, L. A. (2013). Ultra-sensitive sequencing reveals an age-related increase in somatic mitochondrial mutations that are inconsistent with oxidative damage. *PLoS Genet, 9*(9), e1003794. doi:10.1371/journal.pgen.1003794

Kerr, E. M., Gaude, E., Turrell, F. K., Frezza, C., & Martins, C. P. (2016). Mutant Kras copy number defines metabolic reprogramming and therapeutic susceptibilities. *Nature, 531*(7592), 110-113. doi:10.1038/nature16967

Khan, N. A., Auranen, M., Paetau, I., Pirinen, E., Euro, L., Forsström, S., . . . Suomalainen, A. (2014). Effective treatment of mitochondrial myopathy by nicotinamide riboside, a

vitamin B3. *EMBO molecular medicine, 6*(6), 721-731. doi:10.1002/emmm.201403943

Khan, N. A., Nikkanen, J., Yatsuga, S., Jackson, C., Wang, L., Pradhan, S., . . . Suomalainen, A. (2017). mTORC1 Regulates Mitochondrial Integrated Stress Response and Mitochondrial Myopathy Progression. *Cell Metab, 26*(2), 419-428.e415. doi:https://doi.org/10.1016/j.cmet.2017.07.007

Kharbanda, S., Pandey, P., Schofield, L., Israels, S., Roncinske, R., Yoshida, K., . . . Kufe, D. (1997). Role for Bcl-xL as an inhibitor of cytosolic cytochrome C accumulation in DNA damage-induced apoptosis. *Proc Natl Acad Sci U S A, 94*(13), 6939-6942. doi:10.1073/pnas.94.13.6939

Kharitonenkov, A., Shiyanova, T. L., Koester, A., Ford, A. M., Micanovic, R., Galbreath, E. J., . . . Shanafelt, A. B. (2005). FGF-21 as a novel metabolic regulator. *J Clin Invest, 115*(6), 1627-1635. doi:10.1172/JCI23606

Khrapko, K., Kraytsberg, Y., De Grey, A. D. N. J., Vijg, J., & Schon, E. A. (2006). Does premature aging of the mtDNA mutator mouse prove that mtDNA mutations are involved in natural aging? *Aging cell, 5*(3), 279-282. doi:10.1111/j.1474-9726.2006.00209.x

Kikuchi, G. (1973). The glycine cleavage system: composition, reaction mechanism, and physiological significance. *Mol Cell Biochem, 1*(2), 169-187. doi:10.1007/bf01659328

Kim, D., Fiske, B. P., Birsoy, K., Freinkman, E., Kami, K., Possemato, R. L., . . . Sabatini, D. M. (2015). SHMT2 drives glioma cell survival in ischaemia but imposes a dependence on glycine clearance. *Nature, 520*(7547), 363-367. doi:10.1038/nature14363

Kim, H.-R., Wheeler, M. A., Wilson, C. M., Iida, J., Eng, D., Simpson, M. A., . . . Bullard, K. M. (2004). Hyaluronan facilitates invasion of colon carcinoma cells in vitro via interaction with CD44. *Cancer Res, 64*(13), 4569-4576.

Kim, H., Komiyama, T., Inomoto, C., Kamiguchi, H., Kajiwara, H., Kobayashi, H., . . . Terachi, T. (2016). Mutations in the Mitochondrial ND1 Gene Are Associated with Postoperative Prognosis of Localized Renal Cell Carcinoma. *International journal of molecular sciences, 17*(12), 2049. doi:10.3390/ijms17122049

Kim, I., & Lemasters, J. J. (2011). Mitophagy selectively degrades individual damaged mitochondria after photoirradiation. *Antioxidants & redox signaling, 14*(10), 1919-1928. doi:10.1089/ars.2010.3768

Kim, J. W., Tchernyshyov, I., Semenza, G. L., & Dang, C. V. (2006). HIF-1-mediated expression of pyruvate dehydrogenase kinase: a metabolic switch required for cellular adaptation to hypoxia. *Cell Metab, 3*(3), 177-185. doi:10.1016/j.cmet.2006.02.002

Kim, K. A., Kakitani, M., Zhao, J., Oshima, T., Tang, T., Binnerts, M., . . . Tomizuka, K. (2005). Mitogenic influence of human R-spondin1 on the intestinal epithelium. *Science, 309*(5738), 1256-1259. doi:10.1126/science.1112521

Kim, M.-J., Haroon, S., Chen, G.-D., Ding, D., Wanagat, J., Liu, L., . . . Someya, S. (2019). Increased burden of mitochondrial DNA deletions and point mutations in early-onset age-related hearing loss in mitochondrial mutator mice. *Exp Gerontol, 125*, 110675. doi:https://doi.org/10.1016/j.exger.2019.110675

Kimura, M., Furukawa, T., Abe, T., Yatsuoka, T., Youssef, E. M., Yokoyama, T., . . . Horii, A. (1998). Identification of Two Common Regions of Allelic Loss in Chromosome Arm 12q in Human Pancreatic Cancer. *Cancer Res, 58*(11), 2456.

Kinzler, K. W., Nilbert, M. C., Su, L. K., Vogelstein, B., Bryan, T. M., Levy, D. B., . . . et al. (1991). Identification of FAP locus genes from chromosome 5q21. *Science, 253*(5020), 661-665. doi:10.1126/science.1651562

Kirby, D. M., McFarland, R., Ohtake, A., Dunning, C., Ryan, M. T., Wilson, C., . . . Taylor, R. W. (2004). Mutations of the mitochondrial ND1 gene as a cause of MELAS. *J Med Genet, 41*(10), 784-789. doi:10.1136/jmg.2004.020537

Kirichok, Y., Krapivinsky, G., & Clapham, D. E. (2004). The mitochondrial calcium uniporter is a highly selective ion channel. *Nature, 427*(6972), 360-364. doi:10.1038/nature02246

Kirkwood, T. B. (2008). Understanding ageing from an evolutionary perspective. *J Intern Med, 263*(2), 117-127. doi:10.1111/j.1365-2796.2007.01901.x

Kirkwood, T. B. L. (1977). Evolution of ageing. *Nature, 270*(5635), 301-304. doi:10.1038/270301a0

Kirkwood, T. B. L. (2005). Understanding the Odd Science of Aging. *Cell, 120*(4), 437-447. doi:https://doi.org/10.1016/j.cell.2005.01.027

Kit, S. (1955). The Biosynthesis of Free Glycine and Serine by Tumors. *Cancer Res, 15*(11), 715.

Klefstrom, J., Västrik, I., Saksela, E., Valle, J., Eilers, M., & Alitalo, K. (1994). c-Myc induces cellular susceptibility to the cytotoxic action of TNF-alpha. *Embo j, 13*(22), 5442-5450.

Klintrup, K., Mäkinen, J. M., Kauppila, S., Väre, P. O., Melkko, J., Tuominen, H., . . . Mäkinen, M. J. (2005). Inflammation and prognosis in colorectal cancer. *Eur J Cancer, 41*(17), 2645-2654. doi:10.1016/j.ejca.2005.07.017

Knekt, P., Jarvinen, R., Dich, J., & Hakulinen, T. (1999). Risk of colorectal and other gastro-intestinal cancers after exposure to nitrate, nitrite and N-nitroso compounds: a follow-up study. *Int J Cancer, 80*(6), 852-856. doi:10.1002/(sici)1097-0215(19990315)80:6<852::aid-ijc9>3.0.co;2-s

Knox, W. E., Herzfeld, A., & Hudson, J. (1969). Phosphoserine phosphatase distribution in normal and neoplastic rat tissues. *Archives of Biochemistry and Biophysics, 132*(2), 397-403. doi:https://doi.org/10.1016/0003-9861(69)90381-6

Kojima, M., Morisaki, T., Sasaki, N., Nakano, K., Mibu, R., Tanaka, M., & Katano, M. (2004). Increased nuclear factor-kB activation in human colorectal carcinoma and its correlation with tumor progression. *Anticancer Res, 24*(2b), 675-681.

Kolesar, J. E., Safdar, A., Abadi, A., MacNeil, L. G., Crane, J. D., Tarnopolsky, M. A., & Kaufman, B. A. (2014). Defects in mitochondrial DNA replication and oxidative damage in muscle of mtDNA mutator mice. *Free Radical Biology and Medicine, 75*, 241-251. doi:https://doi.org/10.1016/j.freeradbiomed.2014.07.038

Koo, B. K., Spit, M., Jordens, I., Low, T. Y., Stange, D. E., van de Wetering, M., . . . Clevers, H. (2012). Tumour suppressor RNF43 is a stem-cell E3 ligase that induces endocytosis of Wnt receptors. *Nature, 488*(7413), 665-669. doi:10.1038/nature11308

Korhonen, J. A., Gaspari, M., & Falkenberg, M. (2003). TWINKLE Has 5' -> 3' DNA helicase activity and is specifically stimulated by mitochondrial single-stranded DNA-binding protein. *J Biol Chem, 278*(49), 48627-48632. doi:10.1074/jbc.M306981200

Korhonen, J. A., Pham, X. H., Pellegrini, M., & Falkenberg, M. (2004). Reconstitution of a minimal mtDNA replisome in vitro. *Embo j, 23*(12), 2423-2429. doi:10.1038/sj.emboj.7600257

Korinek, V., Barker, N., Moerer, P., van Donselaar, E., Huls, G., Peters, P. J., & Clevers, H. (1998). Depletion of epithelial stem-cell compartments in the small intestine of mice lacking Tcf-4. *Nature Genetics, 19*(4), 379-383. doi:10.1038/1270

Korinek, V., Barker, N., Morin, P. J., van Wichen, D., de Weger, R., Kinzler, K. W., . . . Clevers, H. (1997). Constitutive transcriptional activation by a beta-catenin-Tcf complex in APC-/- colon carcinoma. *Science, 275*(5307), 1784-1787. doi:10.1126/science.275.5307.1784

Koshiba, T., Detmer, S. A., Kaiser, J. T., Chen, H., McCaffery, J. M., & Chan, D. C. (2004). Structural basis of mitochondrial tethering by mitofusin complexes. *Science, 305*(5685), 858-862. doi:10.1126/science.1099793

Kosinski, C., Li, V. S., Chan, A. S., Zhang, J., Ho, C., Tsui, W. Y., . . . Chen, X. (2007). Gene expression patterns of human colon tops and basal crypts and BMP antagonists as intestinal stem cell niche factors. *Proc Natl Acad Sci U S A, 104*(39), 15418-15423. doi:10.1073/pnas.0707210104

Kowald, A., Dawson, M., & Kirkwood, T. B. (2014). Mitochondrial mutations and ageing: can mitochondrial deletion mutants accumulate via a size based replication advantage? *J Theor Biol, 340*, 111-118. doi:10.1016/j.jtbi.2013.09.009

Kowald, A., & Kirkwood, T. B. L. (2014). Transcription could be the key to the selection advantage of mitochondrial deletion mutants in aging. *Proc Natl Acad Sci U S A, 111*(8), 2972-2977. doi:10.1073/pnas.1314970111

Kowald, A., & Kirkwood, T. B. L. (2018). Resolving the Enigma of the Clonal Expansion of mtDNA Deletions. *Genes (Basel), 9*(3). doi:10.3390/genes9030126

Krupenko, N. I., Dubard, M. E., Strickland, K. C., Moxley, K. M., Oleinik, N. V., & Krupenko, S. A. (2010). ALDH1L2 is the mitochondrial homolog of 10-formyltetrahydrofolate dehydrogenase. *J Biol Chem, 285*(30), 23056-23063. doi:10.1074/jbc.M110.128843

Kruse, B., Narasimhan, N., & Attardi, G. (1989). Termination of transcription in human mitochondria: identification and purification of a DNA binding protein factor that promotes termination. *Cell, 58*(2), 391-397. doi:10.1016/0092-8674(89)90853-2

Kucherlapati, M. H., Lee, K., Nguyen, A. A., Clark, A. B., Hou, H., Jr., Rosulek, A., . . . Edelmann, W. (2010). An Msh2 conditional knockout mouse for studying intestinal cancer and testing anticancer agents. *Gastroenterology, 138*(3), 993-1002.e1001. doi:10.1053/j.gastro.2009.11.009

Kuchnio, A., Moens, S., Bruning, U., Kuchnio, K., Cruys, B., Thienpont, B., . . . Carmeliet, P. (2015). The Cancer Cell Oxygen Sensor PHD2 Promotes Metastasis via Activation of Cancer-Associated Fibroblasts. *Cell Rep, 12*(6), 992-1005. doi:10.1016/j.celrep.2015.07.010

Kuebler, J. P., Wieand, H. S., O'Connell, M. J., Smith, R. E., Colangelo, L. H., Yothers, G., . . . Wolmark, N. (2007). Oxaliplatin combined with weekly bolus fluorouracil and leucovorin as surgical adjuvant chemotherapy for stage II and III colon cancer: results from NSABP C-07. *J Clin Oncol, 25*(16), 2198-2204. doi:10.1200/jco.2006.08.2974

Kühl, I., Miranda, M., Posse, V., Milenkovic, D., Mourier, A., Siira, S. J., . . . Larsson, N.-G. (2016). POLRMT regulates the switch between replication primer formation and gene expression of mammalian mtDNA. *Science Advances, 2*(8), e1600963. doi:10.1126/sciadv.1600963

Kujoth, G. C., Hiona, A., Pugh, T. D., Someya, S., Panzer, K., Wohlgemuth, S. E., . . . Prolla, T. A. (2005). Mitochondrial DNA Mutations, Oxidative Stress, and Apoptosis in Mammalian Aging. *Science, 309*(5733), 481. doi:10.1126/science.1112125

Kukat, C., Davies, K. M., Wurm, C. A., Spåhr, H., Bonekamp, N. A., Kühl, I., . . . Larsson, N. G. (2015). Cross-strand binding of TFAM to a single mtDNA molecule forms the mitochondrial nucleoid. *Proc Natl Acad Sci U S A, 112*(36), 11288-11293. doi:10.1073/pnas.1512131112

Kukat, C., Wurm, C. A., Spåhr, H., Falkenberg, M., Larsson, N.-G., & Jakobs, S. (2011). Super-resolution microscopy reveals that mammalian mitochondrial nucleoids have a uniform size and frequently contain a single copy of mtDNA. *Proceedings of the National Academy of Sciences, 108*(33), 13534. doi:10.1073/pnas.1109263108

Kuleshov, M. V., Jones, M. R., Rouillard, A. D., Fernandez, N. F., Duan, Q., Wang, Z., . . . Ma'ayan, A. (2016). Enrichr: a comprehensive gene set enrichment analysis web server 2016 update. *Nucleic Acids Res, 44*(W1), W90-97. doi:10.1093/nar/gkw377

Kulis, M., & Esteller, M. (2010). DNA methylation and cancer. *Adv Genet, 70*, 27-56. doi:10.1016/b978-0-12-380866-0.60002-2

Kurelac, I., Iommarini, L., Vatrinet, R., Amato, L. B., De Luise, M., Leone, G., . . . Gasparre, G. (2019). Inducing cancer indolence by targeting mitochondrial Complex I is potentiated by blocking macrophage-mediated adaptive responses. *Nature Communications, 10*(1), 903. doi:10.1038/s41467-019-08839-1

Labrousse, A. M., Zappaterra, M. D., Rube, D. A., & van der Bliek, A. M. (1999). C. elegans dynamin-related protein DRP-1 controls severing of the mitochondrial outer membrane. *Mol Cell, 4*(5), 815-826. doi:10.1016/s1097-2765(00)80391-3

Labuschagne, Christiaan F., van den Broek, Niels J. F., Mackay, Gillian M., Vousden, Karen H., & Maddocks, Oliver D. K. (2014). Serine, but Not Glycine, Supports One-Carbon Metabolism and Proliferation of Cancer Cells. *Cell Rep, 7*(4), 1248-1258. doi:https://doi.org/10.1016/j.celrep.2014.04.045

Lane, D. P., & Crawford, L. V. (1979). T antigen is bound to a host protein in SV40-transformed cells. *Nature, 278*(5701), 261-263. doi:10.1038/278261a0

Lang, G. A., Iwakuma, T., Suh, Y. A., Liu, G., Rao, V. A., Parant, J. M., . . . Lozano, G. (2004). Gain of function of a p53 hot spot mutation in a mouse model of Li-Fraumeni syndrome. *Cell, 119*(6), 861-872. doi:10.1016/j.cell.2004.11.006

Lapuente-Brun, E., Moreno-Loshuertos, R., Acín-Pérez, R., Latorre-Pellicer, A., Colás, C., Balsa, E., . . . Enríquez, J. A. (2013). Supercomplex assembly determines electron flux in the mitochondrial electron transport chain. *Science, 340*(6140), 1567-1570. doi:10.1126/science.1230381

Larman, T. C., DePalma, S. R., Hadjipanayis, A. G., Protopopov, A., Zhang, J., Gabriel, S. B., . . . Seidman, J. G. (2012). Spectrum of somatic mitochondrial mutations in five cancers. *Proc Natl Acad Sci U S A, 109*(35), 14087-14091. doi:10.1073/pnas.1211502109

Larsson, N. G., Eiken, H. G., Boman, H., Holme, E., Oldfors, A., & Tulinius, M. H. (1992a). Lack of transmission of deleted mtDNA from a woman with Kearns-Sayre syndrome to her child. *American journal of human genetics, 50*(2), 360-363.

Larsson, N. G., Tulinius, M. H., Holme, E., Oldfors, A., Andersen, O., Wahlström, J., & Aasly, J. (1992b). Segregation and manifestations of the mtDNA tRNA(Lys) A-->G(8344) mutation of myoclonus epilepsy and ragged-red fibers (MERRF) syndrome. *American journal of human genetics, 51*(6), 1201-1212.

Larsson, N. G., Wang, J., Wilhelmsson, H., Oldfors, A., Rustin, P., Lewandoski, M., . . . Clayton, D. A. (1998). Mitochondrial transcription factor A is necessary for mtDNA maintenance and embryogenesis in mice. *Nat Genet, 18*(3), 231-236. doi:10.1038/ng0398-231

Le, D. T., Uram, J. N., Wang, H., Bartlett, B. R., Kemberling, H., Eyring, A. D., . . . Diaz, L. A., Jr. (2015). PD-1 Blockade in Tumors with Mismatch-Repair Deficiency. *N Engl J Med, 372*(26), 2509-2520. doi:10.1056/NEJMoa1500596

Lee, C. F., Caudal, A., Abell, L., Nagana Gowda, G. A., & Tian, R. (2019). Targeting NAD(+) Metabolism as Interventions for Mitochondrial Disease. *Scientific Reports, 9*(1), 3073-3073. doi:10.1038/s41598-019-39419-4

Lee, G. Y., Haverty, P. M., Li, L., Kljavin, N. M., Bourgon, R., Lee, J., . . . Neve, R. M. (2014). Comparative oncogenomics identifies PSMB4 and SHMT2 as potential cancer driver genes. *Cancer Res, 74*(11), 3114-3126. doi:10.1158/0008-5472.Can-13-2683

Lee, J. C., Vivanco, I., Beroukhim, R., Huang, J. H., Feng, W. L., DeBiasi, R. M., . . . Mellinghoff, I. K. (2006). Epidermal growth factor receptor activation in glioblastoma through

novel missense mutations in the extracellular domain. *PLoS Med, 3*(12), e485. doi:10.1371/journal.pmed.0030485

Lee, S. R., Yang, K. S., Kwon, J., Lee, C., Jeong, W., & Rhee, S. G. (2002). Reversible inactivation of the tumor suppressor PTEN by H2O2. *J Biol Chem, 277*(23), 20336-20342. doi:10.1074/jbc.M111899200

Legros, F., Lombès, A., Frachon, P., & Rojo, M. (2002). Mitochondrial fusion in human cells is efficient, requires the inner membrane potential, and is mediated by mitofusins. *Mol Biol Cell, 13*(12), 4343-4354. doi:10.1091/mbc.e02-06-0330

Lehtonen, J. M., Forsström, S., Bottani, E., Viscomi, C., Baris, O. R., Isoniemi, H., . . . Suomalainen, A. (2016). FGF21 is a biomarker for mitochondrial translation and mtDNA maintenance disorders. *Neurology, 87*(22), 2290-2299. doi:10.1212/WNL.0000000000003374

Lei, N. Y., Jabaji, Z., Wang, J., Joshi, V. S., Brinkley, G. J., Khalil, H., . . . Martin, M. G. (2014). Intestinal subepithelial myofibroblasts support the growth of intestinal epithelial stem cells. *PloS one, 9*(1), e84651. doi:10.1371/journal.pone.0084651

Levine, A. J., & Oren, M. (2009). The first 30 years of p53: growing ever more complex. *Nature Reviews Cancer, 9*, 749. doi:10.1038/nrc2723

Lewis, K. N., Andziak, B., Yang, T., & Buffenstein, R. (2013). The naked mole-rat response to oxidative stress: just deal with it. *Antioxidants & redox signaling, 19*(12), 1388-1399. doi:10.1089/ars.2012.4911

Li, J., Kogan, M., Knight, S. A., Pain, D., & Dancis, A. (1999). Yeast mitochondrial protein, Nfs1p, coordinately regulates iron-sulfur cluster proteins, cellular iron uptake, and iron distribution. *J Biol Chem, 274*(46), 33025-33034. doi:10.1074/jbc.274.46.33025

Li, P., Nijhawan, D., Budihardjo, I., Srinivasula, S. M., Ahmad, M., Alnemri, E. S., & Wang, X. (1997). Cytochrome c and dATP-Dependent Formation of Apaf-1/Caspase-9 Complex Initiates an Apoptotic Protease Cascade. *Cell, 91*(4), 479-489. doi:10.1016/S0092-8674(00)80434-1

Li, Y., Huang, T.-T., Carlson, E. J., Melov, S., Ursell, P. C., Olson, J. L., . . . Epstein, C. J. (1995). Dilated cardiomyopathy and neonatal lethality in mutant mice lacking manganese superoxide dismutase. *Nature Genetics, 11*(4), 376-381. doi:10.1038/ng1295-376

Li, Y., Park, J. S., Deng, J. H., & Bai, Y. (2006). Cytochrome c oxidase subunit IV is essential for assembly and respiratory function of the enzyme complex. *Journal of bioenergetics and biomembranes, 38*(5-6), 283-291. doi:10.1007/s10863-006-9052-z

Liao, H. X., & Spremulli, L. L. (1990). Identification and initial characterization of translational initiation factor 2 from bovine mitochondria. *J Biol Chem, 265*(23), 13618-13622.

Lichtenstein, P., Holm, N. V., Verkasalo, P. K., Iliadou, A., Kaprio, J., Koskenvuo, M., . . . Hemminki, K. (2000). Environmental and heritable factors in the causation of cancer--analyses of cohorts of twins from Sweden, Denmark, and Finland. *N Engl J Med, 343*(2), 78-85. doi:10.1056/nejm200007133430201

Lightowlers, R. N., Chinnery, P. F., Turnbull, D. M., & Howell, N. (1997). Mammalian mitochondrial genetics: heredity, heteroplasmy and disease. *Trends in Genetics, 13*(11), 450-455. doi:https://doi.org/10.1016/S0168-9525(97)01266-3

Lim, S. E., Longley, M. J., & Copeland, W. C. (1999). The Mitochondrial p55 Accessory Subunit of Human DNA Polymerase γ Enhances DNA Binding, Promotes Processive DNA Synthesis, and Confers N-Ethylmaleimide Resistance. *Journal of Biological Chemistry, 274*(53), 38197-38203. doi:10.1074/jbc.274.53.38197

Linzer, D. I., & Levine, A. J. (1979). Characterization of a 54K dalton cellular SV40 tumor antigen present in SV40-transformed cells and uninfected embryonal carcinoma cells. *Cell, 17*(1), 43-52. doi:10.1016/0092-8674(79)90293-9

Liou, G. Y., Döppler, H., DelGiorno, K. E., Zhang, L., Leitges, M., Crawford, H. C., . . . Storz, P. (2016). Mutant KRas-Induced Mitochondrial Oxidative Stress in Acinar Cells Upregulates EGFR Signaling to Drive Formation of Pancreatic Precancerous Lesions. *Cell Rep, 14*(10), 2325-2336. doi:10.1016/j.celrep.2016.02.029

Litonin, D., Sologub, M., Shi, Y., Savkina, M., Anikin, M., Falkenberg, M., . . . Temiakov, D. (2010). Human mitochondrial transcription revisited: only TFAM and TFB2M are required for transcription of the mitochondrial genes in vitro. *J Biol Chem, 285*(24), 18129-18133. doi:10.1074/jbc.C110.128918

Liu, L., & Rando, T. A. (2011). Manifestations and mechanisms of stem cell aging. *J Cell Biol, 193*(2), 257-266. doi:10.1083/jcb.201010131

Liu, V. W., Shi, H. H., Cheung, A. N., Chiu, P. M., Leung, T. W., Nagley, P., . . . Ngan, H. Y. (2001). High incidence of somatic mitochondrial DNA mutations in human ovarian carcinomas. *Cancer Res, 61*(16), 5998-6001.

Liu, X., Kim, C. N., Yang, J., Jemmerson, R., & Wang, X. (1996). Induction of apoptotic program in cell-free extracts: requirement for dATP and cytochrome c. *Cell, 86*(1), 147-157. doi:10.1016/s0092-8674(00)80085-9

Logan, A., Shabalina, I. G., Prime, T. A., Rogatti, S., Kalinovich, A. V., Hartley, R. C., . . . Murphy, M. P. (2014). In vivo levels of mitochondrial hydrogen peroxide increase with age in mtDNA mutator mice. *Aging cell, 13*(4), 765-768. doi:10.1111/acel.12212

Longley, M. J., Ropp, P. A., Lim, S. E., & Copeland, W. C. (1998). Characterization of the Native and Recombinant Catalytic Subunit of Human DNA Polymerase γ: Identification of Residues Critical for Exonuclease Activity and Dideoxynucleotide Sensitivity. *Biochemistry, 37*(29), 10529-10539. doi:10.1021/bi980772w

López-Otín, C., Blasco, M. A., Partridge, L., Serrano, M., & Kroemer, G. (2013). The hallmarks of aging. *Cell, 153*(6), 1194-1217. doi:10.1016/j.cell.2013.05.039

Lopez, J., & Tait, S. W. G. (2015). Mitochondrial apoptosis: killing cancer using the enemy within. *British journal of cancer, 112*(6), 957-962. doi:10.1038/bjc.2015.85

Loschen, G., Azzi, A., Richter, C., & Flohé, L. (1974). Superoxide radicals as precursors of mitochondrial hydrogen peroxide. *FEBS Lett, 42*(1), 68-72. doi:10.1016/0014-5793(74)80281-4

Loschen, G., Flohé, L., & Chance, B. (1971). Respiratory chain linked H(2)O(2) production in pigeon heart mitochondria. *FEBS Lett, 18*(2), 261-264. doi:10.1016/0014-5793(71)80459-3

Losón, O. C., Song, Z., Chen, H., & Chan, D. C. (2013). Fis1, Mff, MiD49, and MiD51 mediate Drp1 recruitment in mitochondrial fission. *Mol Biol Cell, 24*(5), 659-667. doi:10.1091/mbc.E12-10-0721

Lu, C., Ward, P. S., Kapoor, G. S., Rohle, D., Turcan, S., Abdel-Wahab, O., . . . Thompson, C. B. (2012). IDH mutation impairs histone demethylation and results in a block to cell differentiation. *Nature, 483*(7390), 474-478. doi:10.1038/nature10860

Ludwig, H., Müldür, E., Endler, G., & Hübl, W. (2013). Prevalence of iron deficiency across different tumors and its association with poor performance status, disease status and anemia. *Annals of oncology : official journal of the European Society for Medical Oncology, 24*(7), 1886-1892. doi:10.1093/annonc/mdt118

Ludwig, H., Van Belle, S., Barrett-Lee, P., Birgegard, G., Bokemeyer, C., Gascon, P., . . . Schrijvers, D. (2004). The European Cancer Anaemia Survey (ECAS): a large, multinational, prospective survey defining the prevalence, incidence, and treatment of anaemia in cancer patients. *Eur J Cancer, 40*(15), 2293-2306. doi:10.1016/j.ejca.2004.06.019

Lunetti, P., Di Giacomo, M., Vergara, D., De Domenico, S., Maffia, M., Zara, V., . . . Ferramosca, A. (2019). Metabolic reprogramming in breast cancer results in distinct mitochondrial bioenergetics between luminal and basal subtypes. *Febs j, 286*(4), 688-709. doi:10.1111/febs.14756

Luo, S., Valencia, C. A., Zhang, J., Lee, N. C., Slone, J., Gui, B., . . . Huang, T. (2018). Biparental Inheritance of Mitochondrial DNA in Humans. *Proc Natl Acad Sci U S A, 115*(51), 13039-13044. doi:10.1073/pnas.1810946115

Lynch, H. T., Shaw, M. W., Magnuson, C. W., Larsen, A. L., & Krush, A. J. (1966). Hereditary factors in cancer. Study of two large midwestern kindreds. *Arch Intern Med, 117*(2), 206-212.

Ma, J., & Spremulli, L. L. (1996). Expression, purification, and mechanistic studies of bovine mitochondrial translational initiation factor 2. *J Biol Chem, 271*(10), 5805-5811. doi:10.1074/jbc.271.10.5805

Ma, L., Tao, Y., Duran, A., Llado, V., Galvez, A., Barger, J. F., . . . Moscat, J. (2013). Control of nutrient stress-induced metabolic reprogramming by PKCζ in tumorigenesis. *Cell, 152*(3), 599-611. doi:10.1016/j.cell.2012.12.028

Macpherson, A. J., Gatto, D., Sainsbury, E., Harriman, G. R., Hengartner, H., & Zinkernagel, R. M. (2000). A primitive T cell-independent mechanism of intestinal mucosal IgA responses to commensal bacteria. *Science, 288*(5474), 2222-2226. doi:10.1126/science.288.5474.2222

Maddocks, O. D., Berkers, C. R., Mason, S. M., Zheng, L., Blyth, K., Gottlieb, E., & Vousden, K. H. (2013). Serine starvation induces stress and p53-dependent metabolic remodelling in cancer cells. *Nature, 493*(7433), 542-546. doi:10.1038/nature11743

Maddocks, O. D. K., Athineos, D., Cheung, E. C., Lee, P., Zhang, T., van den Broek, N. J. F., . . . Vousden, K. H. (2017). Modulating the therapeutic response of tumours to dietary serine and glycine starvation. *Nature, 544*(7650), 372-376. doi:10.1038/nature22056

Maddocks, O. D. K., Labuschagne, C. F., Adams, P. D., & Vousden, K. H. (2016). Serine Metabolism Supports the Methionine Cycle and DNA/RNA Methylation through De Novo ATP Synthesis in Cancer Cells. *Mol Cell, 61*(2), 210-221. doi:10.1016/j.molcel.2015.12.014

Maio, N., Kim, K. S., Singh, A., & Rouault, T. A. (2017). A Single Adaptable Cochaperone-Scaffold Complex Delivers Nascent Iron-Sulfur Clusters to Mammalian Respiratory

Chain Complexes I-III. *Cell Metab, 25*(4), 945-953.e946. doi:10.1016/j.cmet.2017.03.010

Majumder, B., Baraneedharan, U., Thiyagarajan, S., Radhakrishnan, P., Narasimhan, H., Dhandapani, M., . . . Majumder, P. K. (2015). Predicting clinical response to anticancer drugs using an ex vivo platform that captures tumour heterogeneity. *Nat Commun, 6*, 6169. doi:10.1038/ncomms7169

Mali, P., Yang, L., Esvelt, K. M., Aach, J., Guell, M., DiCarlo, J. E., . . . Church, G. M. (2013). RNA-guided human genome engineering via Cas9. *Science (New York, N.Y.), 339*(6121), 823-826. doi:10.1126/science.1232033

Man, A. L., Bertelli, E., Rentini, S., Regoli, M., Briars, G., Marini, M., . . . Nicoletti, C. (2015). Age-associated modifications of intestinal permeability and innate immunity in human small intestine. *Clinical science (London, England : 1979), 129*(7), 515-527. doi:10.1042/cs20150046

Manchekar, M., Scissum-Gunn, K., Song, D., Khazi, F., McLean, S. L., & Nielsen, B. L. (2006). DNA recombination activity in soybean mitochondria. *J Mol Biol, 356*(2), 288-299. doi:10.1016/j.jmb.2005.11.070

Mancuso, M., Orsucci, D., Angelini, C., Bertini, E., Carelli, V., Comi, G. P., . . . Siciliano, G. (2015). Redefining phenotypes associated with mitochondrial DNA single deletion. *J Neurol, 262*(5), 1301-1309. doi:10.1007/s00415-015-7710-y

Marais, R., & Marshall, C. J. (1996). Control of the ERK MAP kinase cascade by Ras and Raf. *Cancer surveys, 27*, 101-125.

Maranzana, E., Barbero, G., Falasca, A. I., Lenaz, G., & Genova, M. L. (2013). Mitochondrial respiratory supercomplex association limits production of reactive oxygen species from complex I. *Antioxidants & redox signaling, 19*(13), 1469-1480. doi:10.1089/ars.2012.4845

Mariotti, C., Tiranti, V., Carrara, F., Dallapiccola, B., DiDonato, S., & Zeviani, M. (1994). Defective respiratory capacity and mitochondrial protein synthesis in transformant cybrids harboring the tRNA(Leu(UUR)) mutation associated with maternally inherited myopathy and cardiomyopathy. *J Clin Invest, 93*(3), 1102-1107. doi:10.1172/jci117061

Markowitz, S., Wang, J., Myeroff, L., Parsons, R., Sun, L., Lutterbaugh, J., . . . et al. (1995). Inactivation of the type II TGF-beta receptor in colon cancer cells with microsatellite instability. *Science, 268*(5215), 1336-1338. doi:10.1126/science.7761852

Marliot, F., Chen, X., Kirilovsky, A., Sbarrato, T., El Sissy, C., Batista, L., . . . Pagès, F. (2020). Analytical validation of the Immunoscore and its associated prognostic value in patients with colon cancer. *Journal for ImmunoTherapy of Cancer, 8*(1), e000272. doi:10.1136/jitc-2019-000272

Marsters, S. A., Sheridan, J. P., Pitti, R. M., Huang, A., Skubatch, M., Baldwin, D., . . . Ashkenazi, A. (1997). A novel receptor for Apo2L/TRAIL contains a truncated death domain. *Curr Biol, 7*(12), 1003-1006. doi:10.1016/s0960-9822(06)00422-2

Martens, P. A., & Clayton, D. A. (1979). Mechanism of mitochondrial DNA replication in mouse L-cells: localization and sequence of the light-strand origin of replication. *J Mol Biol, 135*(2), 327-351. doi:10.1016/0022-2836(79)90440-6

Martí, R., Dorado, B., & Hirano, M. (2012). Measurement of mitochondrial dNTP pools. *Methods Mol Biol, 837*, 135-148. doi:10.1007/978-1-61779-504-6_9

Martin, K., Kirkwood, T. B., & Potten, C. S. (1998). Age changes in stem cells of murine small intestinal crypts. *Exp Cell Res, 241*(2), 316-323. doi:10.1006/excr.1998.4001

Martin, M., Cho, J., Cesare, A. J., Griffith, J. D., & Attardi, G. (2005a). Termination factor-mediated DNA loop between termination and initiation sites drives mitochondrial rRNA synthesis. *Cell, 123*(7), 1227-1240. doi:10.1016/j.cell.2005.09.040

Martin, M. C., Allan, L. A., Lickrish, M., Sampson, C., Morrice, N., & Clarke, P. R. (2005b). Protein kinase A regulates caspase-9 activation by Apaf-1 downstream of cytochrome c. *J Biol Chem, 280*(15), 15449-15455. doi:10.1074/jbc.M414325200

Martin, W., & Müller, M. (1998). The hydrogen hypothesis for the first eukaryote. *Nature, 392*(6671), 37-41. doi:10.1038/32096

Martínez-Reyes, I., Cardona, L. R., Kong, H., Vasan, K., McElroy, G. S., Werner, M., . . . Chandel, N. S. (2020). Mitochondrial ubiquinol oxidation is necessary for tumour growth. *Nature, 585*(7824), 288-292. doi:10.1038/s41586-020-2475-6

Martinez-Torres, C., Cubeddu, L., Dillmann, E., Brengelmann, G. L., Leets, I., Layrisse, M., . . . Finch, C. (1984). Effect of exposure to low temperature on normal and iron-deficient subjects. *Am J Physiol, 246*(3 Pt 2), R380-383. doi:10.1152/ajpregu.1984.246.3.R380

Masclee, A., Geuskens, L., Driessen, W., Jansen, J., & Lamers, C. (1988). Effect of aging on plasma cholecystokinin secretion and gallbladder emptying. *Age, 11*(4), 136-140.

Mason, P. A., Matheson, E. C., Hall, A. G., & Lightowlers, R. N. (2003). Mismatch repair activity in mammalian mitochondria. *Nucleic Acids Res, 31*(3), 1052-1058. doi:10.1093/nar/gkg167

Massudi, H., Grant, R., Braidy, N., Guest, J., Farnsworth, B., & Guillemin, G. J. (2012). Age-associated changes in oxidative stress and NAD+ metabolism in human tissue. *PloS one, 7*(7), e42357. doi:10.1371/journal.pone.0042357

Matano, M., Date, S., Shimokawa, M., Takano, A., Fujii, M., Ohta, Y., . . . Sato, T. (2015). Modeling colorectal cancer using CRISPR-Cas9-mediated engineering of human intestinal organoids. *Nat Med, 21*(3), 256-262. doi:10.1038/nm.3802

Matoba, S., Kang, J. G., Patino, W. D., Wragg, A., Boehm, M., Gavrilova, O., . . . Hwang, P. M. (2006). p53 regulates mitochondrial respiration. *Science, 312*(5780), 1650-1653. doi:10.1126/science.1126863

McCall, I. C., Betanzos, A., Weber, D. A., Nava, P., Miller, G. W., & Parkos, C. A. (2009). Effects of phenol on barrier function of a human intestinal epithelial cell line correlate with altered tight junction protein localization. *Toxicol Appl Pharmacol, 241*(1), 61-70. doi:10.1016/j.taap.2009.08.002

McCance, K. L., & Huether, S. E. (2015). *Pathophysiology-E-Book: The Biologic Basis for Disease in Adults and Children*: Elsevier Health Sciences.

McCormack, J. G., Halestrap, A. P., & Denton, R. M. (1990). Role of calcium ions in regulation of mammalian intramitochondrial metabolism. *Physiol Rev, 70*(2), 391-425. doi:10.1152/physrev.1990.70.2.391

McDonald, S. A., Greaves, L. C., Gutierrez-Gonzalez, L., Rodriguez-Justo, M., Deheragoda, M., Leedham, S. J., . . . Wright, N. A. (2008). Mechanisms of field cancerization in the human stomach: the expansion and spread of mutated gastric stem cells. *Gastroenterology, 134*(2), 500-510. doi:10.1053/j.gastro.2007.11.035

McFarland, R., Kirby, D. M., Fowler, K. J., Ohtake, A., Ryan, M. T., Amor, D. J., . . . Thorburn, D. R. (2004). De novo mutations in the mitochondrial ND3 gene as a cause of infantile mitochondrial encephalopathy and complex I deficiency. *Ann Neurol, 55*(1), 58-64. doi:10.1002/ana.10787

Medawar, P. B. (1952). *An unsolved problem of biology*: College.

Medema, J. P., & Vermeulen, L. (2011). Microenvironmental regulation of stem cells in intestinal homeostasis and cancer. *Nature, 474*(7351), 318-326. doi:10.1038/nature10212

Meiser, J., Schuster, A., Pietzke, M., Vande Voorde, J., Athineos, D., Oizel, K., . . . Vazquez, A. (2018). Increased formate overflow is a hallmark of oxidative cancer. *Nature Communications, 9*(1), 1368-1368. doi:10.1038/s41467-018-03777-w

Mentch, Samantha J., Mehrmohamadi, M., Huang, L., Liu, X., Gupta, D., Mattocks, D., . . . Locasale, Jason W. (2015). Histone Methylation Dynamics and Gene Regulation Occur through the Sensing of One-Carbon Metabolism. *Cell Metab, 22*(5), 861-873. doi:https://doi.org/10.1016/j.cmet.2015.08.024

Metallo, C. M., Gameiro, P. A., Bell, E. L., Mattaini, K. R., Yang, J., Hiller, K., . . . Stephanopoulos, G. (2012). Reductive glutamine metabolism by IDH1 mediates lipogenesis under hypoxia. *Nature, 481*(7381), 380-384. doi:10.1038/nature10602

Michaloglou, C., Vredeveld, L. C., Soengas, M. S., Denoyelle, C., Kuilman, T., van der Horst, C. M., . . . Peeper, D. S. (2005). BRAFE600-associated senescence-like cell cycle arrest of human naevi. *Nature, 436*(7051), 720-724. doi:10.1038/nature03890

Michan, S., & Sinclair, D. (2007). Sirtuins in mammals: insights into their biological function. *Biochem J, 404*(1), 1-13. doi:10.1042/bj20070140

Minczuk, M., He, J., Duch, A. M., Ettema, T. J., Chlebowski, A., Dzionek, K., . . . Holt, I. J. (2011). TEFM (c17orf42) is necessary for transcription of human mtDNA. *Nucleic Acids Res, 39*(10), 4284-4299. doi:10.1093/nar/gkq1224

Miralles Fuste, J., Shi, Y., Wanrooij, S., Zhu, X., Jemt, E., Persson, O., . . . Falkenberg, M. (2014). In vivo occupancy of mitochondrial single-stranded DNA binding protein supports the strand displacement mode of DNA replication. *PLoS Genet, 10*(12), e1004832. doi:10.1371/journal.pgen.1004832

Mirvish, S. S. (1995). Role of N-nitroso compounds (NOC) and N-nitrosation in etiology of gastric, esophageal, nasopharyngeal and bladder cancer and contribution to cancer of known exposures to NOC. *Cancer Lett, 93*(1), 17-48. doi:10.1016/0304-3835(95)03786-v

Mitchell, P. (1961). Coupling of Phosphorylation to Electron and Hydrogen Transfer by a Chemi-Osmotic type of Mechanism. *Nature, 191*(4784), 144-148. doi:10.1038/191144a0

Mitchell, P. (1975a). The protonmotive Q cycle: a general formulation. *FEBS Lett, 59*(2), 137-139. doi:10.1016/0014-5793(75)80359-0

Mitchell, P. (1975b). Protonmotive redox mechanism of the cytochrome b-c1 complex in the respiratory chain: protonmotive ubiquinone cycle. *FEBS Lett, 56*(1), 1-6. doi:10.1016/0014-5793(75)80098-6

Mitchell, P. (1976). Possible molecular mechanisms of the protonmotive function of cytochrome systems. *J Theor Biol, 62*(2), 327-367. doi:10.1016/0022-5193(76)90124-7

Mitra, K., Wunder, C., Roysam, B., Lin, G., & Lippincott-Schwartz, J. (2009). A hyperfused mitochondrial state achieved at G1-S regulates cyclin E buildup and entry into S phase. *Proc Natl Acad Sci U S A, 106*(29), 11960-11965. doi:10.1073/pnas.0904875106

Mitsuoka, T. (1990). Bifidobacteria and their role in human health. *Journal of Industrial Microbiology, 6*(4), 263-267. doi:10.1007/BF01575871

Mohrin, M., Shin, J., Liu, Y., Brown, K., Luo, H., Xi, Y., . . . Chen, D. (2015). Stem cell aging. A mitochondrial UPR-mediated metabolic checkpoint regulates hematopoietic stem cell aging. *Science, 347*(6228), 1374-1377. doi:10.1126/science.aaa2361

Mok, B. Y., de Moraes, M. H., Zeng, J., Bosch, D. E., Kotrys, A. V., Raguram, A., . . . Liu, D. R. (2020). A bacterial cytidine deaminase toxin enables CRISPR-free mitochondrial base editing. *Nature, 583*(7817), 631-637. doi:10.1038/s41586-020-2477-4

Montoya, J., Christianson, T., Levens, D., Rabinowitz, M., & Attardi, G. (1982). Identification of initiation sites for heavy-strand and light-strand transcription in human mitochondrial DNA. *Proc Natl Acad Sci U S A, 79*(23), 7195-7199. doi:10.1073/pnas.79.23.7195

Montoya, J., Gaines, G. L., & Attardi, G. (1983). The pattern of transcription of the human mitochondrial rRNA genes reveals two overlapping transcription units. *Cell, 34*(1), 151-159. doi:10.1016/0092-8674(83)90145-9

Moodie, S. A., Willumsen, B. M., Weber, M. J., & Wolfman, A. (1993). Complexes of Ras.GTP with Raf-1 and mitogen-activated protein kinase kinase. *Science, 260*(5114), 1658. doi:10.1126/science.8503013

Moran, D. M., Trusk, P. B., Pry, K., Paz, K., Sidransky, D., & Bacus, S. S. (2014). KRAS mutation status is associated with enhanced dependency on folate metabolism pathways in non-small cell lung cancer cells. *Mol Cancer Ther, 13*(6), 1611-1624. doi:10.1158/1535-7163.Mct-13-0649

Morel, F., Renoux, M., Lachaume, P., & Alziari, S. (2008). Bleomycin-induced double-strand breaks in mitochondrial DNA of Drosophila cells are repaired. *Mutat Res, 637*(1-2), 111-117. doi:10.1016/j.mrfmmm.2007.07.007

Morgan, R. G., Mortensson, E., & Williams, A. C. (2018). Targeting LGR5 in Colorectal Cancer: therapeutic gold or too plastic? *British journal of cancer, 118*(11), 1410-1418. doi:10.1038/s41416-018-0118-6

Morita, H., Mazerbourg, S., Bouley, D. M., Luo, C.-W., Kawamura, K., Kuwabara, Y., . . . Hsueh, A. J. W. (2004). Neonatal lethality of LGR5 null mice is associated with ankyloglossia and gastrointestinal distension. *Molecular and cellular biology, 24*(22), 9736-9743. doi:10.1128/MCB.24.22.9736-9743.2004

Mörner, M. E., Edgren, G., Martling, A., Gunnarsson, U., & Egenvall, M. (2017). Preoperative anaemia and perioperative red blood cell transfusion as prognostic factors for recurrence and mortality in colorectal cancer-a Swedish cohort study. *International journal of colorectal disease, 32*(2), 223-232. doi:10.1007/s00384-016-2678-3

Moser, A. R., Pitot, H. C., & Dove, W. F. (1990). A dominant mutation that predisposes to multiple intestinal neoplasia in the mouse. *Science, 247*(4940), 322. doi:10.1126/science.2296722

Moskalev, A. A., Shaposhnikov, M. V., Plyusnina, E. N., Zhavoronkov, A., Budovsky, A., Yanai, H., & Fraifeld, V. E. (2013). The role of DNA damage and repair in aging through the prism of Koch-like criteria. *Ageing Research Reviews, 12*(2), 661-684. doi:https://doi.org/10.1016/j.arr.2012.02.001

Moskovitz, J., Yim, M. B., & Chock, P. B. (2002). Free Radicals and Disease. *Archives of Biochemistry and Biophysics, 397*(2), 354-359. doi:https://doi.org/10.1006/abbi.2001.2692

Moss, C., Dhillo, W. S., Frost, G., & Hickson, M. (2012). Gastrointestinal hormones: the regulation of appetite and the anorexia of ageing. *J Hum Nutr Diet, 25*(1), 3-15. doi:10.1111/j.1365-277X.2011.01211.x

Moullan, N., Mouchiroud, L., Wang, X., Ryu, D., Williams, E. G., Mottis, A., . . . Auwerx, J. (2015). Tetracyclines Disturb Mitochondrial Function across Eukaryotic Models: A Call for Caution in Biomedical Research. *Cell Rep, 10*(10), 1681-1691. doi:10.1016/j.celrep.2015.02.034

Moussaieff, A., Rouleau, M., Kitsberg, D., Cohen, M., Levy, G., Barasch, D., . . . Nahmias, Y. (2015). Glycolysis-mediated changes in acetyl-CoA and histone acetylation control the early differentiation of embryonic stem cells. *Cell Metab, 21*(3), 392-402. doi:10.1016/j.cmet.2015.02.002

Muise, E. S., Azzolina, B., Kuo, D. W., El-Sherbeini, M., Tan, Y., Yuan, X., . . . Wong, K. K. (2008). Adipose Fibroblast Growth Factor 21 Is Up-Regulated by Peroxisome Proliferator-Activated Receptor γ and Altered Metabolic States. *Molecular Pharmacology, 74*(2), 403-412. doi:10.1124/mol.108.044826

Mullen, A. R., Hu, Z., Shi, X., Jiang, L., Boroughs, L. K., Kovacs, Z., . . . DeBerardinis, R. J. (2014). Oxidation of alpha-ketoglutarate is required for reductive carboxylation in cancer cells with mitochondrial defects. *Cell Rep, 7*(5), 1679-1690. doi:10.1016/j.celrep.2014.04.037

Mullen, A. R., Wheaton, W. W., Jin, E. S., Chen, P.-H., Sullivan, L. B., Cheng, T., . . . DeBerardinis, R. J. (2011). Reductive carboxylation supports growth in tumour cells with defective mitochondria. *Nature, 481*(7381), 385-388. doi:10.1038/nature10642

Muller-Hocker, J. (1989). Cytochrome-c-oxidase deficient cardiomyocytes in the human heart--an age-related phenomenon. A histochemical ultracytochemical study. *Am J Pathol, 134*(5), 1167-1173.

Muller, F. L., Liu, Y., & Van Remmen, H. (2004). Complex III releases superoxide to both sides of the inner mitochondrial membrane. *J Biol Chem, 279*(47), 49064-49073. doi:10.1074/jbc.M407715200

Muller, H. J. (1964). THE RELATION OF RECOMBINATION TO MUTATIONAL ADVANCE. *Mutat Res, 106*, 2-9. doi:10.1016/0027-5107(64)90047-8

Muller, P. A. J., Caswell, P. T., Doyle, B., Iwanicki, M. P., Tan, E. H., Karim, S., . . . Vousden, K. H. (2009). Mutant p53 Drives Invasion by Promoting Integrin Recycling. *Cell, 139*(7), 1327-1341. doi:https://doi.org/10.1016/j.cell.2009.11.026

Munoz, J., Stange, D. E., Schepers, A. G., van de Wetering, M., Koo, B. K., Itzkovitz, S., . . . Clevers, H. (2012). The Lgr5 intestinal stem cell signature: robust expression of proposed quiescent '+4' cell markers. *Embo j, 31*(14), 3079-3091. doi:10.1038/emboj.2012.166

Munscher, C., Rieger, T., Muller-Hocker, J., & Kadenbach, B. (1993). The point mutation of mitochondrial DNA characteristic for MERRF disease is found also in healthy people of different ages. *FEBS Lett, 317*(1-2), 27-30. doi:10.1016/0014-5793(93)81484-h

Murata, K., Jadhav, U., Madha, S., van Es, J., Dean, J., Cavazza, A., . . . Shivdasani, R. A. (2020). Ascl2-Dependent Cell Dedifferentiation Drives Regeneration of Ablated Intestinal Stem Cells. *Cell Stem Cell, 26*(3), 377-390.e376. doi:10.1016/j.stem.2019.12.011

Murphy, M. P. (2009). How mitochondria produce reactive oxygen species. *Biochem J, 417*(1), 1-13. doi:10.1042/bj20081386

Muzio, M., Chinnaiyan, A. M., Kischkel, F. C., O'Rourke, K., Shevchenko, A., Ni, J., . . . Dixit, V. M. (1996). FLICE, a novel FADD-homologous ICE/CED-3-like protease, is recruited to the CD95 (Fas/APO-1) death--inducing signaling complex. *Cell, 85*(6), 817-827. doi:10.1016/s0092-8674(00)81266-0

Muzny, D. M., Bainbridge, M. N., Chang, K., Dinh, H. H., Drummond, J. A., Fowler, G., . . . disease working, g. (2012). Comprehensive molecular characterization of human colon and rectal cancer. *Nature, 487*(7407), 330-337. doi:10.1038/nature11252

Myers, K. A., Saffhill, R., & O'Connor, P. J. (1988). Repair of alkylated purines in the hepatic DNA of mitochondria and nuclei in the rat. *Carcinogenesis, 9*(2), 285-292. doi:10.1093/carcin/9.2.285

Nagaike, T., Suzuki, T., Katoh, T., & Ueda, T. (2005). Human mitochondrial mRNAs are stabilized with polyadenylation regulated by mitochondria-specific poly(A) polymerase and polynucleotide phosphorylase. *J Biol Chem, 280*(20), 19721-19727. doi:10.1074/jbc.M500804200

Nagaike, T., Suzuki, T., Tomari, Y., Takemoto-Hori, C., Negayama, F., Watanabe, K., & Ueda, T. (2001). Identification and characterization of mammalian mitochondrial tRNA nucleotidyltransferases. *J Biol Chem, 276*(43), 40041-40049. doi:10.1074/jbc.M106202200

Neiman, P. E., Thomas, S. J., & Loring, G. (1991). Induction of apoptosis during normal and neoplastic B-cell development in the bursa of Fabricius. *Proc Natl Acad Sci U S A, 88*(13), 5857-5861. doi:10.1073/pnas.88.13.5857

Netz, D. J., Stith, C. M., Stumpfig, M., Kopf, G., Vogel, D., Genau, H. M., . . . Pierik, A. J. (2011). Eukaryotic DNA polymerases require an iron-sulfur cluster for the formation of active complexes. *Nat Chem Biol, 8*(1), 125-132. doi:10.1038/nchembio.721

Neuhaus, F. C., & Byrne, W. L. (1960). Metabolism of Phosphoserine: III. MECHANISM OF O-PHOSPHOSERINE PHOSPHATASE. *Journal of Biological Chemistry, 235*(7), 2019-2024.

Neves, J., Sousa-Victor, P., & Jasper, H. (2017). Rejuvenating Strategies for Stem Cell-Based Therapies in Aging. *Cell Stem Cell, 20*(2), 161-175. doi:10.1016/j.stem.2017.01.008

Newman, A. C., & Maddocks, O. D. K. (2017). Serine and Functional Metabolites in Cancer. *Trends in Cell Biology, 27*(9), 645-657. doi:https://doi.org/10.1016/j.tcb.2017.05.001

Ngo, H. B., Kaiser, J. T., & Chan, D. C. (2011). The mitochondrial transcription and packaging factor Tfam imposes a U-turn on mitochondrial DNA. *Nature Structural & Molecular Biology, 18*(11), 1290-1296. doi:10.1038/nsmb.2159

Ni, Y., Hagras, M. A., Konstantopoulou, V., Mayr, J. A., Stuchebrukhov, A. A., & Meierhofer, D. (2019). Mutations in NDUFS1 Cause Metabolic Reprogramming and Disruption of the Electron Transfer. *Cells, 8*(10), 1149. doi:10.3390/cells8101149

Nicholls, T. J., Nadalutti, C. A., Motori, E., Sommerville, E. W., Gorman, G. S., Basu, S., . . . Gustafsson, C. M. (2018). Topoisomerase 3α Is Required for Decatenation and Segregation of Human mtDNA. *Mol Cell, 69*(1), 9-23.e26. doi:10.1016/j.molcel.2017.11.033

Nikkanen, J., Forsström, S., Euro, L., Paetau, I., Kohnz, Rebecca A., Wang, L., . . . Suomalainen, A. (2016). Mitochondrial DNA Replication Defects Disturb Cellular dNTP Pools and Remodel One-Carbon Metabolism. *Cell Metab, 23*(4), 635-648. doi:https://doi.org/10.1016/j.cmet.2016.01.019

Nilsson, R., Jain, M., Madhusudhan, N., Sheppard, N. G., Strittmatter, L., Kampf, C., . . . Mootha, V. K. (2014). Metabolic enzyme expression highlights a key role for MTHFD2 and the mitochondrial folate pathway in cancer. *Nature Communications, 5*(1), 3128. doi:10.1038/ncomms4128

Nishimura, T., Nakata, A., Chen, X., Nishi, K., Meguro-Horike, M., Sasaki, S., . . . Gotoh, N. (2019). Cancer stem-like properties and gefitinib resistance are dependent on purine synthetic metabolism mediated by the mitochondrial enzyme MTHFD2. *Oncogene, 38*(14), 2464-2481. doi:10.1038/s41388-018-0589-1

Nishimura, T., Nakatake, Y., Konishi, M., & Itoh, N. (2000). Identification of a novel FGF, FGF-21, preferentially expressed in the liver11The nucleotide sequence data reported in this paper will appear in the DDBJ, EMBL and GenBank nucleotide sequence databases with accession numbers AB021975 and AB025718. *Biochimica et Biophysica Acta (BBA) - Gene Structure and Expression, 1492*(1), 203-206. doi:https://doi.org/10.1016/S0167-4781(00)00067-1

Nissanka, N., Bacman, S. R., Plastini, M. J., & Moraes, C. T. (2018). The mitochondrial DNA polymerase gamma degrades linear DNA fragments precluding the formation of deletions. *Nature Communications, 9*(1), 2491. doi:10.1038/s41467-018-04895-1

Noji, H., Yasuda, R., Yoshida, M., & Kinosita, K. (1997). Direct observation of the rotation of F1-ATPase. *Nature, 386*(6622), 299-302. doi:10.1038/386299a0

Norddahl, Gudmundur L., Pronk, Cornelis J., Wahlestedt, M., Sten, G., Nygren, Jens M., Ugale, A., . . . Bryder, D. (2011). Accumulating Mitochondrial DNA Mutations Drive Premature Hematopoietic Aging Phenotypes Distinct from Physiological Stem Cell Aging. *Cell Stem Cell, 8*(5), 499-510. doi:https://doi.org/10.1016/j.stem.2011.03.009

Nusse, R., & Clevers, H. (2017). Wnt/β-Catenin Signaling, Disease, and Emerging Therapeutic Modalities. *Cell, 169*(6), 985-999. doi:10.1016/j.cell.2017.05.016

O'Brien, C. A., Pollett, A., Gallinger, S., & Dick, J. E. (2007). A human colon cancer cell capable of initiating tumour growth in immunodeficient mice. *Nature, 445*(7123), 106-110. doi:10.1038/nature05372

O'Brien, L. C., Keeney, P. M., & Bennett, J. P., Jr. (2015). Differentiation of Human Neural Stem Cells into Motor Neurons Stimulates Mitochondrial Biogenesis and Decreases Glycolytic Flux. *Stem Cells Dev, 24*(17), 1984-1994. doi:10.1089/scd.2015.0076

O'Brien, M. J., Yang, S., Mack, C., Xu, H., Huang, C. S., Mulcahy, E., . . . Farraye, F. A. (2006). Comparison of microsatellite instability, CpG island methylation phenotype, BRAF and KRAS status in serrated polyps and traditional adenomas indicates separate pathways to distinct colorectal carcinoma end points. *Am J Surg Pathol, 30*(12), 1491-1501. doi:10.1097/01.pas.0000213313.36306.85

O'Mahony, D., O'Leary, P., & Quigley, E. M. (2002). Aging and intestinal motility: a review of factors that affect intestinal motility in the aged. *Drugs Aging, 19*(7), 515-527. doi:10.2165/00002512-200219070-00005

Oellers, N., Dehio, M., & Knust, E. (1994). bHLH proteins encoded by the Enhancer of split complex of Drosophila negatively interfere with transcriptional activation mediated by proneural genes. *Mol Gen Genet, 244*(5), 465-473. doi:10.1007/bf00583897

Ojala, D., Montoya, J., & Attardi, G. (1981). tRNA punctuation model of RNA processing in human mitochondria. *Nature, 290*(5806), 470-474. doi:10.1038/290470a0

Oláhová, M., Ceccatelli Berti, C., Collier, J. J., Alston, C. L., Jameson, E., Jones, S. A., . . . Sayer, J. A. (2019). Molecular genetic investigations identify new clinical phenotypes associated with BCS1L-related mitochondrial disease. *Hum Mol Genet, 28*(22), 3766-3776. doi:10.1093/hmg/ddz202

Olive, K. P., Tuveson, D. A., Ruhe, Z. C., Yin, B., Willis, N. A., Bronson, R. T., . . . Jacks, T. (2004). Mutant p53 gain of function in two mouse models of Li-Fraumeni syndrome. *Cell, 119*(6), 847-860. doi:10.1016/j.cell.2004.11.004

Olovnikov, A. M. (1973). A theory of marginotomy: The incomplete copying of template margin in enzymic synthesis of polynucleotides and biological significance of the phenomenon. *Journal of Theoretical Biology, 41*(1), 181-190. doi:https://doi.org/10.1016/0022-5193(73)90198-7

Olsson, C., Johnsen, E., Nilsson, M., Wilander, E., Syvänen, A.-C., & Lagerström-Fermér, M. (2001). The level of the mitochondrial mutation A3243G decreases upon ageing in epithelial cells from individuals with diabetes and deafness. *European Journal of Human Genetics, 9*(12), 917-921. doi:10.1038/sj.ejhg.5200742

Ooft, S. N., Weeber, F., Dijkstra, K. K., McLean, C. M., Kaing, S., van Werkhoven, E., . . . Voest, E. E. (2019). Patient-derived organoids can predict response to chemotherapy in metastatic colorectal cancer patients. *Sci Transl Med, 11*(513). doi:10.1126/scitranslmed.aay2574

Osborn, M. J., Freeman, M., & Huennekens, F. M. (1958). Inhibition of dihydrofolic reductase by aminopterin and amethopterin. *Proc Soc Exp Biol Med, 97*(2), 429-431. doi:10.3181/00379727-97-23764

Osthus, R. C., Shim, H., Kim, S., Li, Q., Reddy, R., Mukherjee, M., . . . Dang, C. V. (2000). Deregulation of glucose transporter 1 and glycolytic gene expression by c-Myc. *J Biol Chem, 275*(29), 21797-21800. doi:10.1074/jbc.C000023200

Ouellette, A. J. (1997). Paneth cells and innate immunity in the crypt microenvironment. *Gastroenterology, 113*(5), 1779-1784. doi:10.1053/gast.1997.v113.pm9352884

Pacold, M. E., Brimacombe, K. R., Chan, S. H., Rohde, J. M., Lewis, C. A., Swier, L. J. Y. M., . . . Sabatini, D. M. (2016). A PHGDH inhibitor reveals coordination of serine synthesis and one-carbon unit fate. *Nat Chem Biol, 12*(6), 452-458. doi:10.1038/nchembio.2070

Pagès, F., Galon, J., Dieu-Nosjean, M. C., Tartour, E., Sautès-Fridman, C., & Fridman, W. H. (2010). Immune infiltration in human tumors: a prognostic factor that should not be ignored. *Oncogene, 29*(8), 1093-1102. doi:10.1038/onc.2009.416

Palade, G. E. (1952). The fine structure of mitochondria. *Anat Rec, 114*(3), 427-451. doi:10.1002/ar.1091140304

Palmer, C. S., Osellame, L. D., Laine, D., Koutsopoulos, O. S., Frazier, A. E., & Ryan, M. T. (2011). MiD49 and MiD51, new components of the mitochondrial fission machinery. *EMBO Rep, 12*(6), 565-573. doi:10.1038/embor.2011.54

Pan, G., Ni, J., Wei, Y. F., Yu, G., Gentz, R., & Dixit, V. M. (1997). An antagonist decoy receptor and a death domain-containing receptor for TRAIL. *Science, 277*(5327), 815-818. doi:10.1126/science.277.5327.815

Pandey, A., Golla, R., Yoon, H., Dancis, A., & Pain, D. (2012). Persulfide formation on mitochondrial cysteine desulfurase: enzyme activation by a eukaryote-specific interacting protein and Fe-S cluster synthesis. *Biochem J, 448*(2), 171-187. doi:10.1042/bj20120951

Pang, W., Su, J., Wang, Y., Feng, H., Dai, X., Yuan, Y., . . . Yao, W. (2015). Pancreatic cancer-secreted miR-155 implicates in the conversion from normal fibroblasts to cancer-associated fibroblasts. *Cancer Sci, 106*(10), 1362-1369. doi:10.1111/cas.12747

Papa, L., & Germain, D. (2014). SirT3 regulates the mitochondrial unfolded protein response. *Molecular and cellular biology, 34*(4), 699-710. doi:10.1128/MCB.01337-13

Papa, S., Francavilla, A., Paradies, G., & Meduri, B. (1971). The transport of pyruvate in rat liver mitochondria. *FEBS Lett, 12*(5), 285-288. doi:10.1016/0014-5793(71)80200-4

Papandreou, I., Cairns, R. A., Fontana, L., Lim, A. L., & Denko, N. C. (2006). HIF-1 mediates adaptation to hypoxia by actively downregulating mitochondrial oxygen consumption. *Cell Metab, 3*(3), 187-197. doi:10.1016/j.cmet.2006.01.012

Paradkar, P. N., Zumbrennen, K. B., Paw, B. H., Ward, D. M., & Kaplan, J. (2009). Regulation of mitochondrial iron import through differential turnover of mitoferrin 1 and mitoferrin 2. *Molecular and cellular biology, 29*(4), 1007-1016. doi:10.1128/mcb.01685-08

Parisi, M. A., & Clayton, D. A. (1991). Similarity of human mitochondrial transcription factor 1 to high mobility group proteins. *Science, 252*(5008), 965. doi:10.1126/science.2035027

Park, J. H., McMillan, D. C., Powell, A. G., Richards, C. H., Horgan, P. G., Edwards, J., & Roxburgh, C. S. D. (2015). Evaluation of a Tumor Microenvironment–Based Prognostic Score in Primary Operable Colorectal Cancer. *Clinical Cancer Research, 21*(4), 882. doi:10.1158/1078-0432.CCR-14-1686

Park, J. S., Sharma, L. K., Li, H., Xiang, R., Holstein, D., Wu, J., . . . Bai, Y. (2009). A heteroplasmic, not homoplasmic, mitochondrial DNA mutation promotes tumorigenesis via alteration in reactive oxygen species generation and apoptosis. *Hum Mol Genet, 18*(9), 1578-1589. doi:10.1093/hmg/ddp069

Park, S. M., Ou, J., Chamberlain, L., Simone, T. M., Yang, H., Virbasius, C.-M., . . . Green, M. R. (2016). U2AF35(S34F) Promotes Transformation by Directing Aberrant ATG7 Pre-mRNA 3' End Formation. *Mol Cell, 62*(4), 479-490. doi:10.1016/j.molcel.2016.04.011

Park, Y., Reyna-Neyra, A., Philippe, L., & Thoreen, C. C. (2017). mTORC1 Balances Cellular Amino Acid Supply with Demand for Protein Synthesis through Post-transcriptional Control of ATF4. *Cell Rep, 19*(6), 1083-1090. doi:10.1016/j.celrep.2017.04.042

Parsons, D. W., Wang, T.-L., Samuels, Y., Bardelli, A., Cummins, J. M., DeLong, L., . . . Velculescu, V. E. (2005). Mutations in a signalling pathway. *Nature, 436*(7052), 792-792. doi:10.1038/436792a

Passos, J. F., Saretzki, G., Ahmed, S., Nelson, G., Richter, T., Peters, H., . . . von Zglinicki, T. (2007). Mitochondrial dysfunction accounts for the stochastic heterogeneity in telomere-dependent senescence. *PLoS Biol, 5*(5), e110. doi:10.1371/journal.pbio.0050110

Pastò, A., Bellio, C., Pilotto, G., Ciminale, V., Silic-Benussi, M., Guzzo, G., . . . Amadori, A. (2014). Cancer stem cells from epithelial ovarian cancer patients privilege oxidative phosphorylation, and resist glucose deprivation. *Oncotarget, 5*(12), 4305-4319. doi:10.18632/oncotarget.2010

Pate, K. T., Stringari, C., Sprowl-Tanio, S., Wang, K., TeSlaa, T., Hoverter, N. P., . . . Waterman, M. L. (2014). Wnt signaling directs a metabolic program of glycolysis and angiogenesis in colon cancer. *Embo j, 33*(13), 1454-1473. doi:10.15252/embj.201488598

Patra, K. C., & Hay, N. (2014). The pentose phosphate pathway and cancer. *Trends in biochemical sciences, 39*(8), 347-354. doi:10.1016/j.tibs.2014.06.005

Pearce, S. F., Rorbach, J., Van Haute, L., D'Souza, A. R., Rebelo-Guiomar, P., Powell, C. A., . . . Minczuk, M. (2017). Maturation of selected human mitochondrial tRNAs requires deadenylation. *Elife, 6*, e27596. doi:10.7554/eLife.27596

Pebay-Peyroula, E., Dahout-Gonzalez, C., Kahn, R., Trezeguet, V., Lauquin, G. J., & Brandolin, G. (2003). Structure of mitochondrial ADP/ATP carrier in complex with carboxyatractyloside. *Nature, 426*(6962), 39-44. doi:10.1038/nature02056

Pedersen, G., Brynskov, J., & Saermark, T. (2002). Phenol toxicity and conjugation in human colonic epithelial cells. *Scand J Gastroenterol, 37*(1), 74-79. doi:10.1080/003655202753387392

Peeva, V., Blei, D., Trombly, G., Corsi, S., Szukszto, M. J., Rebelo-Guiomar, P., . . . Kunz, W. S. (2018). Linear mitochondrial DNA is rapidly degraded by components of the replication machinery. *Nat Commun, 9*(1), 1727. doi:10.1038/s41467-018-04131-w

Permuth-Wey, J., Chen, Y. A., Tsai, Y.-Y., Chen, Z., Qu, X., Lancaster, J. M., . . . Sellers, T. A. (2011). Inherited variants in mitochondrial biogenesis genes may influence epithelial ovarian cancer risk. *Cancer epidemiology, biomarkers & prevention : a publication of the American Association for Cancer Research, cosponsored by the American Society of Preventive Oncology, 20*(6), 1131-1145. doi:10.1158/1055-9965.EPI-10-1224

Persad, S., Troussard, A. A., McPhee, T. R., Mulholland, D. J., & Dedhar, S. (2001). Tumor suppressor PTEN inhibits nuclear accumulation of beta-catenin and T cell/lymphoid enhancer factor 1-mediated transcriptional activation. *The Journal of Cell Biology, 153*(6), 1161-1174. doi:10.1083/jcb.153.6.1161

Persson, Ö., Muthukumar, Y., Basu, S., Jenninger, L., Uhler, J. P., Berglund, A. K., . . . Falkenberg, M. (2019). Copy-choice recombination during mitochondrial L-strand synthesis causes DNA deletions. *Nat Commun, 10*(1), 759. doi:10.1038/s41467-019-08673-5

Petros, J. A., Baumann, A. K., Ruiz-Pesini, E., Amin, M. B., Sun, C. Q., Hall, J., . . . Wallace, D. C. (2005). mtDNA mutations increase tumorigenicity in prostate cancer. *Proc Natl Acad Sci U S A, 102*(3), 719-724. doi:10.1073/pnas.0408894102

Pflügler, S., Svinka, J., Scharf, I., Crncec, I., Filipits, M., Charoentong, P., . . . Eferl, R. (2020). IDO1(+) Paneth cells promote immune escape of colorectal cancer. *Communications biology, 3*(1), 252-252. doi:10.1038/s42003-020-0989-y

Pietrantonio, F., Petrelli, F., Coinu, A., Di Bartolomeo, M., Borgonovo, K., Maggi, C., . . . Barni, S. (2015). Predictive role of BRAF mutations in patients with advanced colorectal cancer receiving cetuximab and panitumumab: a meta-analysis. *Eur J Cancer, 51*(5), 587-594. doi:10.1016/j.ejca.2015.01.054

Pietromonaco, S. F., Denslow, N. D., & O'Brien, T. W. (1991). Proteins of mammalian mitochondrial ribosomes. *Biochimie, 73*(6), 827-835. doi:10.1016/0300-9084(91)90062-6

Piskounova, E., Agathocleous, M., Murphy, M. M., Hu, Z., Huddlestun, S. E., Zhao, Z., . . . Morrison, S. J. (2015). Oxidative stress inhibits distant metastasis by human melanoma cells. *Nature, 527*(7577), 186-191. doi:10.1038/nature15726

Pitti, R. M., Marsters, S. A., Lawrence, D. A., Roy, M., Kischkel, F. C., Dowd, P., . . . Ashkenazi, A. (1998). Genomic amplification of a decoy receptor for Fas ligand in lung and colon cancer. *Nature, 396*(6712), 699-703. doi:10.1038/25387

Polyak, K., Li, Y., Zhu, H., Lengauer, C., Willson, J. K., Markowitz, S. D., . . . Vogelstein, B. (1998). Somatic mutations of the mitochondrial genome in human colorectal tumours. *Nat Genet, 20*(3), 291-293. doi:10.1038/3108

Popat, S., & Houlston, R. S. (2005). A systematic review and meta-analysis of the relationship between chromosome 18q genotype, DCC status and colorectal cancer prognosis. *Eur J Cancer, 41*(14), 2060-2070. doi:10.1016/j.ejca.2005.04.039

Posse, V., & Gustafsson, C. M. (2017). Human Mitochondrial Transcription Factor B2 Is Required for Promoter Melting during Initiation of Transcription. *J Biol Chem, 292*(7), 2637-2645. doi:10.1074/jbc.M116.751008

Possemato, R., Marks, K. M., Shaul, Y. D., Pacold, M. E., Kim, D., Birsoy, K., . . . Sabatini, D. M. (2011). Functional genomics reveal that the serine synthesis pathway is essential in breast cancer. *Nature, 476*(7360), 346-350. doi:10.1038/nature10350

Potten, C. S., Kovacs, L., & Hamilton, E. (1974). Continuous labelling studies on mouse skin and intestine. *Cell Tissue Kinet, 7*(3), 271-283. doi:10.1111/j.1365-2184.1974.tb00907.x

Potten, C. S., & Loeffler, M. (1990). Stem cells: attributes, cycles, spirals, pitfalls and uncertainties. Lessons for and from the crypt. *Development, 110*(4), 1001-1020.

Powell, C. A., & Minczuk, M. (2020). TRMT2B is responsible for both tRNA and rRNA m(5)U-methylation in human mitochondria. *RNA biology, 17*(4), 451-462. doi:10.1080/15476286.2020.1712544

Pratilas, C. A., Taylor, B. S., Ye, Q., Viale, A., Sander, C., Solit, D. B., & Rosen, N. (2009). (V600E)BRAF is associated with disabled feedback inhibition of RAF-MEK signaling and elevated transcriptional output of the pathway. *Proc Natl Acad Sci U S A, 106*(11), 4519-4524. doi:10.1073/pnas.0900780106

Priebe, M. G., Vonk, R. J., Sun, X., He, T., Harmsen, H. J., & Welling, G. W. (2002). The physiology of colonic metabolism. Possibilities for interventions with pre- and probiotics. *Eur J Nutr, 41 Suppl 1*, I2-10. doi:10.1007/s00394-002-1101-8

Pyle, A., Hudson, G., Wilson, I. J., Coxhead, J., Smertenko, T., Herbert, M., . . . Chinnery, P. F. (2015). Extreme-Depth Re-sequencing of Mitochondrial DNA Finds No Evidence of

Paternal Transmission in Humans. *PLoS Genet, 11*(5), e1005040-e1005040. doi:10.1371/journal.pgen.1005040

Qi, J., Cui, C., Deng, Q., Wang, L., Chen, R., Zhai, D., . . . Yu, J. (2018). Downregulated SIRT6 and upregulated NMNAT2 are associated with the presence, depth and stage of colorectal cancer. *Oncology letters, 16*(5), 5829-5837. doi:10.3892/ol.2018.9400

Qi, Y., Yan, L., Yu, C., Guo, X., Zhou, X., Hu, X., . . . Hu, J. (2016). Structures of human mitofusin 1 provide insight into mitochondrial tethering. *The Journal of Cell Biology, 215*(5), 621-629. doi:10.1083/jcb.201609019

Qi, Z., Li, Y., Zhao, B., Xu, C., Liu, Y., Li, H., . . . Chen, Y.-G. (2017). BMP restricts stemness of intestinal Lgr5+ stem cells by directly suppressing their signature genes. *Nature Communications, 8*(1), 13824. doi:10.1038/ncomms13824

Rabelo, R., Schifman, A., Rubio, A., Sheng, X., & Silva, J. E. (1995). Delineation of thyroid hormone-responsive sequences within a critical enhancer in the rat uncoupling protein gene. *Endocrinology, 136*(3), 1003-1013. doi:10.1210/endo.136.3.7867554

Rad, R., Cadiñanos, J., Rad, L., Varela, I., Strong, A., Kriegl, L., . . . Bradley, A. (2013). A Genetic Progression Model of BrafV600E-Induced Intestinal Tumorigenesis Reveals Targets for Therapeutic Intervention. *Cancer Cell, 24*(1), 15-29. doi:https://doi.org/10.1016/j.ccr.2013.05.014

Ragan, C. I., & Hatefi, Y. (1986). Isolation of the iron-sulfur-containing polypeptides of NADH: oxidoreductase ubiquinone. *Methods Enzymol, 126*, 360-369. doi:10.1016/s0076-6879(86)26036-x

Rahman, S., Poulton, J., Marchington, D., & Suomalainen, A. (2001). Decrease of 3243 A-->G mtDNA mutation from blood in MELAS syndrome: a longitudinal study. *American journal of human genetics, 68*(1), 238-240. doi:10.1086/316930

Rajagopalan, H., Bardelli, A., Lengauer, C., Kinzler, K. W., Vogelstein, B., & Velculescu, V. E. (2002). RAF/RAS oncogenes and mismatch-repair status. *Nature, 418*(6901), 934-934. doi:10.1038/418934a

Rajala, N., Gerhold, J. M., Martinsson, P., Klymov, A., & Spelbrink, J. N. (2014). Replication factors transiently associate with mtDNA at the mitochondrial inner membrane to facilitate replication. *Nucleic Acids Res, 42*(2), 952-967. doi:10.1093/nar/gkt988

Rampino, N., Yamamoto, H., Ionov, Y., Li, Y., Sawai, H., Reed, J. C., & Perucho, M. (1997). Somatic frameshift mutations in the BAX gene in colon cancers of the microsatellite mutator phenotype. *Science, 275*(5302), 967-969. doi:10.1126/science.275.5302.967

Ramsey, M. J., Moore, D. H., 2nd, Briner, J. F., Lee, D. A., Olsen, L., Senft, J. R., & Tucker, J. D. (1995). The effects of age and lifestyle factors on the accumulation of cytogenetic damage as measured by chromosome painting. *Mutat Res, 338*(1-6), 95-106. doi:10.1016/0921-8734(95)00015-x

Ramzan, R., Rhiel, A., Weber, P., Kadenbach, B., & Vogt, S. (2019). Reversible dimerization of cytochrome c oxidase regulates mitochondrial respiration. *Mitochondrion, 49*, 149-155. doi:10.1016/j.mito.2019.08.002

Reaven, G. M. (1988). Banting lecture 1988. Role of insulin resistance in human disease. *Diabetes, 37*(12), 1595-1607. doi:10.2337/diab.37.12.1595

Rebelo-Guiomar, P., Powell, C. A., Van Haute, L., & Minczuk, M. (2019). The mammalian mitochondrial epitranscriptome. *Biochimica et biophysica acta. Gene regulatory mechanisms, 1862*(3), 429-446. doi:10.1016/j.bbagrm.2018.11.005

Red Brewer, M., Yun, C. H., Lai, D., Lemmon, M. A., Eck, M. J., & Pao, W. (2013). Mechanism for activation of mutated epidermal growth factor receptors in lung cancer. *Proc Natl Acad Sci U S A, 110*(38), E3595-3604. doi:10.1073/pnas.1220050110

Reid, M. A., Dai, Z., & Locasale, J. W. (2017). The impact of cellular metabolism on chromatin dynamics and epigenetics. *Nat Cell Biol, 19*(11), 1298-1306. doi:10.1038/ncb3629

Reina-Campos, M., Linares, J. F., Duran, A., Cordes, T., L'Hermitte, A., Badur, M. G., . . . Diaz-Meco, M. T. (2019). Increased Serine and One-Carbon Pathway Metabolism by PKCλ/ι Deficiency Promotes Neuroendocrine Prostate Cancer. *Cancer Cell, 35*(3), 385-400.e389. doi:https://doi.org/10.1016/j.ccell.2019.01.018

Reitmair, A. H., Schmits, R., Ewel, A., Bapat, B., Redston, M., Mitri, A., . . . Mak, T. W. (1995). MSH2 deficient mice are viable and susceptible to lymphoid tumours. *Nature Genetics, 11*(1), 64-70. doi:10.1038/ng0995-64

Reya, T., & Clevers, H. (2005). Wnt signalling in stem cells and cancer. *Nature, 434*(7035), 843-850. doi:10.1038/nature03319

Reya, T., Morrison, S. J., Clarke, M. F., & Weissman, I. L. (2001). Stem cells, cancer, and cancer stem cells. *Nature, 414*(6859), 105-111. doi:10.1038/35102167

Rheinwald, J. G., & Green, H. (1975). Serial cultivation of strains of human epidermal keratinocytes: the formation of keratinizing colonies from single cells. *Cell, 6*(3), 331-343. doi:10.1016/s0092-8674(75)80001-8

Ribeiro, M. O., Carvalho, S. D., Schultz, J. J., Chiellini, G., Scanlan, T. S., Bianco, A. C., & Brent, G. A. (2001). Thyroid hormone--sympathetic interaction and adaptive thermogenesis

are thyroid hormone receptor isoform--specific. *J Clin Invest, 108*(1), 97-105. doi:10.1172/jci12584

Ribic, C. M., Sargent, D. J., Moore, M. J., Thibodeau, S. N., French, A. J., Goldberg, R. M., . . . Gallinger, S. (2003). Tumor microsatellite-instability status as a predictor of benefit from fluorouracil-based adjuvant chemotherapy for colon cancer. *N Engl J Med, 349*(3), 247-257. doi:10.1056/NEJMoa022289

Ricci-Vitiani, L., Lombardi, D. G., Pilozzi, E., Biffoni, M., Todaro, M., Peschle, C., & De Maria, R. (2007). Identification and expansion of human colon-cancer-initiating cells. *Nature, 445*(7123), 111-115. doi:10.1038/nature05384

Ricquier, D., & Kader, J. C. (1976). Mitochondrial protein alteration in active brown fat: a soidum dodecyl sulfate-polyacrylamide gel electrophoretic study. *Biochem Biophys Res Commun, 73*(3), 577-583. doi:10.1016/0006-291x(76)90849-4

Ritsma, L., Ellenbroek, S. I. J., Zomer, A., Snippert, H. J., de Sauvage, F. J., Simons, B. D., . . . van Rheenen, J. (2014). Intestinal crypt homeostasis revealed at single-stem-cell level by in vivo live imaging. *Nature, 507*(7492), 362-365. doi:10.1038/nature12972

Robberson, D. L., Kasamatsu, H., & Vinograd, J. (1972). Replication of mitochondrial DNA. Circular replicative intermediates in mouse L cells. *Proc Natl Acad Sci U S A, 69*(3), 737-741. doi:10.1073/pnas.69.3.737

Rocha, M. C., Grady, J. P., Grünewald, A., Vincent, A., Dobson, P. F., Taylor, R. W., . . . Rygiel, K. A. (2015). A novel immunofluorescent assay to investigate oxidative phosphorylation deficiency in mitochondrial myopathy: understanding mechanisms and improving diagnosis. *Scientific Reports, 5*, 15037. doi:10.1038/srep15037

https://www.nature.com/articles/srep15037#supplementary-information

Rodríguez-Colman, M. J., Schewe, M., Meerlo, M., Stigter, E., Gerrits, J., Pras-Raves, M., . . . Burgering, B. M. (2017). Interplay between metabolic identities in the intestinal crypt supports stem cell function. *Nature, 543*(7645), 424-427. doi:10.1038/nature21673

Rodríguez-Viciana, P., Warne, P. H., Dhand, R., Vanhaesebroeck, B., Gout, I., Fry, M. J., . . . Downward, J. (1994). Phosphatidylinositol-3-OH kinase as a direct target of Ras. *Nature, 370*(6490), 527-532. doi:10.1038/370527a0

Roediger, W. E. (1982). Utilization of nutrients by isolated epithelial cells of the rat colon. *Gastroenterology, 83*(2), 424-429.

Rojansky, R., Cha, M.-Y., & Chan, D. C. (2016). Elimination of paternal mitochondria in mouse embryos occurs through autophagic degradation dependent on PARKIN and MUL1. *Elife, 5*, e17896. doi:10.7554/eLife.17896

Rorbach, J., Nicholls, T. J., & Minczuk, M. (2011). PDE12 removes mitochondrial RNA poly(A) tails and controls translation in human mitochondria. *Nucleic Acids Res, 39*(17), 7750-7763. doi:10.1093/nar/gkr470

Rorbach, J., Richter, R., Wessels, H. J., Wydro, M., Pekalski, M., Farhoud, M., . . . Chrzanowska-Lightowlers, Z. M. (2008). The human mitochondrial ribosome recycling factor is essential for cell viability. *Nucleic Acids Res, 36*(18), 5787-5799. doi:10.1093/nar/gkn576

Rosenberg, I. H. (1997). Sarcopenia: Origins and Clinical Relevance. *The Journal of Nutrition, 127*(5), 990S-991S. doi:10.1093/jn/127.5.990S

Rosenzweig, P. H., & Volpe, S. L. (1999). Iron, thermoregulation, and metabolic rate. *Crit Rev Food Sci Nutr, 39*(2), 131-148. doi:10.1080/10408399908500491

Roseweir, A. K., McMillan, D. C., Horgan, P. G., & Edwards, J. (2017). Colorectal cancer subtypes: Translation to routine clinical pathology. *Cancer Treat Rev, 57*, 1-7. doi:10.1016/j.ctrv.2017.04.006

Roseweir, A. K., Park, J. H., Hoorn, S. T., Powell, A. G., Aherne, S., Roxburgh, C. S., . . . Edwards, J. (2020). Histological phenotypic subtypes predict recurrence risk and response to adjuvant chemotherapy in patients with stage III colorectal cancer. *J Pathol Clin Res, 6*(4), 283-296. doi:10.1002/cjp2.171

Rothenberg, M. E., Nusse, Y., Kalisky, T., Lee, J. J., Dalerba, P., Scheeren, F., . . . Clarke, M. F. (2012). Identification of a cKit(+) colonic crypt base secretory cell that supports Lgr5(+) stem cells in mice. *Gastroenterology, 142*(5), 1195-1205.e1196. doi:10.1053/j.gastro.2012.02.006

Rothwell, N. J., & Stock, M. J. (1997). A role for brown adipose tissue in diet-induced thermogenesis. *Obes Res, 5*(6), 650-656. doi:10.1002/j.1550-8528.1997.tb00591.x

Rotig, A., Cormier, V., Blanche, S., Bonnefont, J. P., Ledeist, F., Romero, N., . . . et al. (1990). Pearson's marrow-pancreas syndrome. A multisystem mitochondrial disorder in infancy. *J Clin Invest, 86*(5), 1601-1608. doi:10.1172/jci114881

Rottenberg, H., Covian, R., & Trumpower, B. L. (2009). Membrane potential greatly enhances superoxide generation by the cytochrome bc1 complex reconstituted into

phospholipid vesicles. *J Biol Chem, 284*(29), 19203-19210. doi:10.1074/jbc.M109.017376

Rotter, V., Witte, O. N., Coffman, R., & Baltimore, D. (1980). Abelson murine leukemia virus-induced tumors elicit antibodies against a host cell protein, P50. *J Virol, 36*(2), 547-555. doi:10.1128/jvi.36.2.547-555.1980

Rouault, T. A. (2019). The indispensable role of mammalian iron sulfur proteins in function and regulation of multiple diverse metabolic pathways. *Biometals, 32*(3), 343-353. doi:10.1007/s10534-019-00191-7

Roubenoff, R. (1999). The Pathophysiology of Wasting in the Elderly. *The Journal of Nutrition, 129*(1), 256S-259S. doi:10.1093/jn/129.1.256S

Roy, N., Deveraux, Q. L., Takahashi, R., Salvesen, G. S., & Reed, J. C. (1997). The c-IAP-1 and c-IAP-2 proteins are direct inhibitors of specific caspases. *Embo j, 16*(23), 6914-6925. doi:10.1093/emboj/16.23.6914

Rubner, M. (1883). Ueber den einfluss der korpergrosse auf stoffund kaftwechsel. *Zeitschrift fur Biologie, 19*, 535-562.

Rubner, M. (1908). *Das Problem der Lebensdauer und seine Beziehungen zu wachstum und ernährung*: Oldenbourg.

Rutkowski, D. T., & Kaufman, R. J. (2003). All Roads Lead to ATF4. *Developmental Cell, 4*(4), 442-444. doi:https://doi.org/10.1016/S1534-5807(03)00100-X

Saffrey, M. J. (2013). Cellular changes in the enteric nervous system during ageing. *Developmental Biology, 382*(1), 344-355. doi:https://doi.org/10.1016/j.ydbio.2013.03.015

Sagan, L. (1967). On the origin of mitosing cells. *Journal of Theoretical Biology, 14*(3), 225-IN226. doi:https://doi.org/10.1016/0022-5193(67)90079-3

Samuels, Y., Wang, Z., Bardelli, A., Silliman, N., Ptak, J., Szabo, S., . . . Velculescu, V. E. (2004). High frequency of mutations of the PIK3CA gene in human cancers. *Science, 304*(5670), 554. doi:10.1126/science.1096502

Sancho, R., Cremona, C. A., & Behrens, A. (2015). Stem cell and progenitor fate in the mammalian intestine: Notch and lateral inhibition in homeostasis and disease. *EMBO Rep, 16*(5), 571-581. doi:10.15252/embr.201540188

Sangiorgi, E., & Capecchi, M. R. (2008). Bmi1 is expressed in vivo in intestinal stem cells. *Nat Genet, 40*(7), 915-920. doi:10.1038/ng.165

Sano, S., Inoue, S., Tanabe, Y., Sumiya, C., & Koike, S. (1959). Significance of mitochondria for porphyrin and heme biosynthesis. *Science (New York, N.Y.), 129*(3344), 275-276. doi:10.1126/science.129.3344.275

Sansom, O. J., Meniel, V., Wilkins, J. A., Cole, A. M., Oien, K. A., Marsh, V., . . . Clarke, A. R. (2006). Loss of Apc allows phenotypic manifestation of the transforming properties of an endogenous K-ras oncogene in vivo. *Proc Natl Acad Sci U S A, 103*(38), 14122-14127. doi:10.1073/pnas.0604130103

Sansom, O. J., Meniel, V. S., Muncan, V., Phesse, T. J., Wilkins, J. A., Reed, K. R., . . . Clarke, A. R. (2007). Myc deletion rescues Apc deficiency in the small intestine. *Nature, 446*(7136), 676-679. doi:10.1038/nature05674

Sansom, O. J., Reed, K. R., Hayes, A. J., Ireland, H., Brinkmann, H., Newton, I. P., . . . Winton, D. J. (2004). Loss of Apc in vivo immediately perturbs Wnt signaling, differentiation, and migration. *Genes & development, 18*(12), 1385-1390. doi:10.1101/gad.287404

Santidrian, A. F., Matsuno-Yagi, A., Ritland, M., Seo, B. B., LeBoeuf, S. E., Gay, L. J., . . . Felding-Habermann, B. (2013). Mitochondrial complex I activity and NAD+/NADH balance regulate breast cancer progression. *J Clin Invest, 123*(3), 1068-1081. doi:10.1172/jci64264

Saraste, A., & Pulkki, K. (2000). Morphologic and biochemical hallmarks of apoptosis. *Cardiovasc Res, 45*(3), 528-537. doi:10.1016/s0008-6363(99)00384-3

Sasaki, N., Sachs, N., Wiebrands, K., Ellenbroek, S. I., Fumagalli, A., Lyubimova, A., . . . Clevers, H. (2016). Reg4+ deep crypt secretory cells function as epithelial niche for Lgr5+ stem cells in colon. *Proc Natl Acad Sci U S A, 113*(37), E5399-5407. doi:10.1073/pnas.1607327113

Sato, T., Stange, D. E., Ferrante, M., Vries, R. G. J., van Es, J. H., van den Brink, S., . . . Clevers, H. (2011a). Long-term Expansion of Epithelial Organoids From Human Colon, Adenoma, Adenocarcinoma, and Barrett's Epithelium. *Gastroenterology, 141*(5), 1762-1772. doi:https://doi.org/10.1053/j.gastro.2011.07.050

Sato, T., van Es, J. H., Snippert, H. J., Stange, D. E., Vries, R. G., van den Born, M., . . . Clevers, H. (2011b). Paneth cells constitute the niche for Lgr5 stem cells in intestinal crypts. *Nature, 469*(7330), 415-418. doi:10.1038/nature09637

Sato, T., Vries, R. G., Snippert, H. J., van de Wetering, M., Barker, N., Stange, D. E., . . . Clevers, H. (2009). Single Lgr5 stem cells build crypt-villus structures in vitro without a mesenchymal niche. *Nature, 459*(7244), 262-265. doi:10.1038/nature07935

Satoh, M., & Kuroiwa, T. (1991). Organization of multiple nucleoids and DNA molecules in mitochondria of a human cell. *Exp Cell Res, 196*(1), 137-140. doi:10.1016/0014-4827(91)90467-9

Saxton, R. A., & Sabatini, D. M. (2017). mTOR Signaling in Growth, Metabolism, and Disease. *Cell, 168*(6), 960-976. doi:10.1016/j.cell.2017.02.004

Scarpulla, R. C. (2008). Nuclear control of respiratory chain expression by nuclear respiratory factors and PGC-1-related coactivator. *Annals of the New York Academy of Sciences, 1147*, 321-334. doi:10.1196/annals.1427.006

Schafer, Z. T., Grassian, A. R., Song, L., Jiang, Z., Gerhart-Hines, Z., Irie, H. Y., . . . Brugge, J. S. (2009). Antioxidant and oncogene rescue of metabolic defects caused by loss of matrix attachment. *Nature, 461*(7260), 109-113.

Schägger, H., de Coo, R., Bauer, M. F., Hofmann, S., Godinot, C., & Brandt, U. (2004). Significance of respirasomes for the assembly/stability of human respiratory chain complex I. *J Biol Chem, 279*(35), 36349-36353. doi:10.1074/jbc.M404033200

Schägger, H., & Pfeiffer, K. (2000). Supercomplexes in the respiratory chains of yeast and mammalian mitochondria. *Embo j, 19*(8), 1777-1783. doi:10.1093/emboj/19.8.1777

Schriner, S. E., Linford, N. J., Martin, G. M., Treuting, P., Ogburn, C. E., Emond, M., . . . Rabinovitch, P. S. (2005). Extension of Murine Life Span by Overexpression of Catalase Targeted to Mitochondria. *Science, 308*(5730), 1909. doi:10.1126/science.1106653

Schuijers, J., van der Flier, L. G., van Es, J., & Clevers, H. (2014). Robust cre-mediated recombination in small intestinal stem cells utilizing the olfm4 locus. *Stem Cell Reports, 3*(2), 234-241. doi:10.1016/j.stemcr.2014.05.018

Schwartz, M., & Vissing, J. (2002). Paternal inheritance of mitochondrial DNA. *N Engl J Med, 347*(8), 576-580. doi:10.1056/NEJMoa020350

Schwartzenberg-Bar-Yoseph, F., Armoni, M., & Karnieli, E. (2004). The tumor suppressor p53 down-regulates glucose transporters GLUT1 and GLUT4 gene expression. *Cancer Res, 64*(7), 2627-2633. doi:10.1158/0008-5472.can-03-0846

Schwitalla, S., Fingerle, A. A., Cammareri, P., Nebelsiek, T., Goktuna, S. I., Ziegler, P. K., . . . Greten, F. R. (2013). Intestinal tumorigenesis initiated by dedifferentiation and acquisition of stem-cell-like properties. *Cell, 152*(1-2), 25-38. doi:10.1016/j.cell.2012.12.012

Sciacovelli, M., Gonçalves, E., Johnson, T. I., Zecchini, V. R., da Costa, A. S. H., Gaude, E., . . . Frezza, C. (2016). Fumarate is an epigenetic modifier that elicits epithelial-to-mesenchymal transition. *Nature, 537*(7621), 544-547. doi:10.1038/nature19353

Scorrano, L., Ashiya, M., Buttle, K., Weiler, S., Oakes, S. A., Mannella, C. A., & Korsmeyer, S. J. (2002). A distinct pathway remodels mitochondrial cristae and mobilizes cytochrome c during apoptosis. *Dev Cell, 2*(1), 55-67. doi:10.1016/s1534-5807(01)00116-2

Sekine, S., Yamashita, S., Tanabe, T., Hashimoto, T., Yoshida, H., Taniguchi, H., . . . Ochiai, A. (2016). Frequent PTPRK-RSPO3 fusions and RNF43 mutations in colorectal traditional serrated adenoma. *J Pathol, 239*(2), 133-138. doi:10.1002/path.4709

Selak, M. A., Armour, S. M., MacKenzie, E. D., Boulahbel, H., Watson, D. G., Mansfield, K. D., . . . Gottlieb, E. (2005). Succinate links TCA cycle dysfunction to oncogenesis by inhibiting HIF-α prolyl hydroxylase. *Cancer Cell, 7*(1), 77-85. doi:https://doi.org/10.1016/j.ccr.2004.11.022

Semenza, G. L., Roth, P. H., Fang, H. M., & Wang, G. L. (1994). Transcriptional regulation of genes encoding glycolytic enzymes by hypoxia-inducible factor 1. *J Biol Chem, 269*(38), 23757-23763.

Sena, L. A., & Chandel, N. S. (2012). Physiological roles of mitochondrial reactive oxygen species. *Mol Cell, 48*(2), 158-167. doi:10.1016/j.molcel.2012.09.025

Serrano, M., Lin, A. W., McCurrach, M. E., Beach, D., & Lowe, S. W. (1997). Oncogenic ras provokes premature cell senescence associated with accumulation of p53 and p16INK4a. *Cell, 88*(5), 593-602. doi:10.1016/s0092-8674(00)81902-9

Seshagiri, S., Stawiski, E. W., Durinck, S., Modrusan, Z., Storm, E. E., Conboy, C. B., . . . de Sauvage, F. J. (2012). Recurrent R-spondin fusions in colon cancer. *Nature, 488*(7413), 660-664. doi:10.1038/nature11282

Seth Nanda, C., Venkateswaran, S. V., Patani, N., & Yuneva, M. (2020). Defining a metabolic landscape of tumours: genome meets metabolism. *British journal of cancer, 122*(2), 136-149. doi:10.1038/s41416-019-0663-7

Shabalina, I. G., Vyssokikh, M. Y., Gibanova, N., Csikasz, R. I., Edgar, D., Hallden-Waldemarson, A., . . . Nedergaard, J. (2017). Improved health-span and lifespan in mtDNA mutator mice treated with the mitochondrially targeted antioxidant SkQ1. *Aging (Albany NY), 9*(2), 315-339. doi:10.18632/aging.101174

Shang, J., & Clayton, D. A. (1994). Human mitochondrial transcription termination exhibits RNA polymerase independence and biased bipolarity in vitro. *Journal of Biological Chemistry, 269*(46), 29112-29120.

Shanske, S., Coku, J., Lu, J., Ganesh, J., Krishna, S., Tanji, K., . . . DiMauro, S. (2008). The G13513A mutation in the ND5 gene of mitochondrial DNA as a common cause of MELAS or Leigh syndrome: evidence from 12 cases. *Arch Neurol, 65*(3), 368-372. doi:10.1001/archneurol.2007.67

Sharma, L. K., Fang, H., Liu, J., Vartak, R., Deng, J., & Bai, Y. (2011). Mitochondrial respiratory complex I dysfunction promotes tumorigenesis through ROS alteration and AKT activation. *Hum Mol Genet, 20*(23), 4605-4616. doi:10.1093/hmg/ddr395

Shen, X., Kolluru, G. K., Yuan, S., & Kevil, C. G. (2015). Measurement of H2S in vivo and in vitro by the monobromobimane method. *Methods in enzymology, 554*, 31-45. doi:10.1016/bs.mie.2014.11.039

Sheridan, J. P., Marsters, S. A., Pitti, R. M., Gurney, A., Skubatch, M., Baldwin, D., . . . Ashkenazi, A. (1997). Control of TRAIL-induced apoptosis by a family of signaling and decoy receptors. *Science, 277*(5327), 818-821. doi:10.1126/science.277.5327.818

Shi, R., Proteau, A., Villarroya, M., Moukadiri, I., Zhang, L., Trempe, J. F., . . . Cygler, M. (2010). Structural basis for Fe-S cluster assembly and tRNA thiolation mediated by IscS protein-protein interactions. *PLoS Biol, 8*(4), e1000354. doi:10.1371/journal.pbio.1000354

Shi, Y., Ghosh, M. C., Tong, W.-H., & Rouault, T. A. (2009). Human ISD11 is essential for both iron-sulfur cluster assembly and maintenance of normal cellular iron homeostasis. *Human Molecular Genetics, 18*(16), 3014-3025. doi:10.1093/hmg/ddp239

Shidara, Y., Yamagata, K., Kanamori, T., Nakano, K., Kwong, J. Q., Manfredi, G., . . . Ohta, S. (2005). Positive contribution of pathogenic mutations in the mitochondrial genome to the promotion of cancer by prevention from apoptosis. *Cancer Res, 65*(5), 1655-1663. doi:10.1158/0008-5472.Can-04-2012

Shigenaga, M. K., Hagen, T. M., & Ames, B. N. (1994). Oxidative damage and mitochondrial decay in aging. *Proc Natl Acad Sci U S A, 91*(23), 10771-10778. doi:10.1073/pnas.91.23.10771

Shmelkov, S. V., Butler, J. M., Hooper, A. T., Hormigo, A., Kushner, J., Milde, T., . . . Rafii, S. (2008). CD133 expression is not restricted to stem cells, and both CD133+ and

CD133- metastatic colon cancer cells initiate tumors. *J Clin Invest, 118*(6), 2111-2120. doi:10.1172/jci34401

Shoemaker, A. R., Gould, K. A., Luongo, C., Moser, A. R., & Dove, W. F. (1997). Studies of neoplasia in the Min mouse. *Biochim Biophys Acta, 1332*(2), F25-48. doi:10.1016/s0304-419x(96)00041-8

Shoffner, J. M., Lott, M. T., Voljavec, A. S., Soueidan, S. A., Costigan, D. A., & Wallace, D. C. (1989). Spontaneous Kearns-Sayre/chronic external ophthalmoplegia plus syndrome associated with a mitochondrial DNA deletion: a slip-replication model and metabolic therapy. *Proc Natl Acad Sci U S A, 86*(20), 7952-7956. doi:10.1073/pnas.86.20.7952

Shtutman, M., Zhurinsky, J., Simcha, I., Albanese, C., D'Amico, M., Pestell, R., & Ben-Ze'ev, A. (1999). The cyclin D1 gene is a target of the beta-catenin/LEF-1 pathway. *Proc Natl Acad Sci U S A, 96*(10), 5522-5527. doi:10.1073/pnas.96.10.5522

Siegel, R. L., Miller, K. D., & Jemal, A. (2015). Cancer statistics, 2015. *CA Cancer J Clin, 65*(1), 5-29. doi:10.3322/caac.21254

Silva, J. P., Kohler, M., Graff, C., Oldfors, A., Magnuson, M. A., Berggren, P. O., & Larsson, N. G. (2000). Impaired insulin secretion and beta-cell loss in tissue-specific knockout mice with mitochondrial diabetes. *Nat Genet, 26*(3), 336-340. doi:10.1038/81649

Simsek, T., Kocabas, F., Zheng, J., Deberardinis, R. J., Mahmoud, A. I., Olson, E. N., . . . Sadek, H. A. (2010). The distinct metabolic profile of hematopoietic stem cells reflects their location in a hypoxic niche. *Cell Stem Cell, 7*(3), 380-390. doi:10.1016/j.stem.2010.07.011

Sinha, M., Jang, Y. C., Oh, J., Khong, D., Wu, E. Y., Manohar, R., . . . Pancoast, J. R. (2014). Restoring systemic GDF11 levels reverses age-related dysfunction in mouse skeletal muscle. *Science, 344*(6184), 649-652.

Sjölander, A., Yamamoto, K., Huber, B. E., & Lapetina, E. G. (1991). Association of p21ras with phosphatidylinositol 3-kinase. *Proc Natl Acad Sci U S A, 88*(18), 7908-7912. doi:10.1073/pnas.88.18.7908

Smith, A. L. M., Whitehall, J. C., Bradshaw, C., Gay, D., Robertson, F., Blain, A. P., . . . Greaves, L. C. (2020). Age-associated mitochondrial DNA mutations cause metabolic remodeling that contributes to accelerated intestinal tumorigenesis. *Nature Cancer*. doi:10.1038/s43018-020-00112-5

Smith, C. A., Farrah, T., & Goodwin, R. G. (1994). The TNF receptor superfamily of cellular and viral proteins: activation, costimulation, and death. *Cell, 76*(6), 959-962. doi:10.1016/0092-8674(94)90372-7

Smith, R. E., & Roberts, J. C. (1964). THERMOGENESIS OF BROWN ADIPOSE TISSUE IN COLD-ACCLIMATED RATS. *Am J Physiol, 206*, 143-148. doi:10.1152/ajplegacy.1964.206.1.143

Snell, K. (1984). Enzymes of serine metabolism in normal, developing and neoplastic rat tissues. *Advances in Enzyme Regulation, 22*, 325-400. doi:https://doi.org/10.1016/0065-2571(84)90021-9

Snell, K. (1985). Enzymes of serine metabolism in normal and neoplastic rat tissues. *Biochimica et Biophysica Acta (BBA) - General Subjects, 843*(3), 276-281. doi:https://doi.org/10.1016/0304-4165(85)90149-7

Soengas, M. S., Capodieci, P., Polsky, D., Mora, J., Esteller, M., Opitz-Araya, X., . . . Lowe, S. W. (2001). Inactivation of the apoptosis effector Apaf-1 in malignant melanoma. *Nature, 409*(6817), 207-211. doi:10.1038/35051606

Sohal, R. S., Svensson, I., Sohal, B. H., & Brunk, U. T. (1989). Superoxide anion radical production in different animal species. *Mech Ageing Dev, 49*(2), 129-135. doi:https://doi.org/10.1016/0047-6374(89)90096-1

Soleimanpour-Lichaei, H. R., Kühl, I., Gaisne, M., Passos, J. F., Wydro, M., Rorbach, J., . . . Chrzanowska-Lightowlers, Z. (2007). mtRF1a is a human mitochondrial translation release factor decoding the major termination codons UAA and UAG. *Mol Cell, 27*(5), 745-757. doi:10.1016/j.molcel.2007.06.031

Song, I. S., Jeong, Y. J., Jeong, S. H., Heo, H. J., Kim, H. K., Bae, K. B., . . . Han, J. (2015). FOXM1-Induced PRX3 Regulates Stemness and Survival of Colon Cancer Cells via Maintenance of Mitochondrial Function. *Gastroenterology, 149*(4), 1006-1016.e1009. doi:10.1053/j.gastro.2015.06.007

Sorge, S., Theelke, J., Yildirim, K., Hertenstein, H., McMullen, E., Müller, S., . . . Lohmann, I. (2020). ATF4-Induced Warburg Metabolism Drives Over-Proliferation in Drosophila. *Cell Rep, 31*(7), 107659. doi:https://doi.org/10.1016/j.celrep.2020.107659

Soucie, E. L., Annis, M. G., Sedivy, J., Filmus, J., Leber, B., Andrews, D. W., & Penn, L. Z. (2001). Myc potentiates apoptosis by stimulating Bax activity at the mitochondria. *Molecular and cellular biology, 21*(14), 4725-4736. doi:10.1128/mcb.21.14.4725-4736.2001

Sovran, B., Hugenholtz, F., Elderman, M., Van Beek, A. A., Graversen, K., Huijskes, M., . . . Wells, J. M. (2019). Age-associated Impairment of the Mucus Barrier Function is Associated with Profound Changes in Microbiota and Immunity. *Sci Rep, 9*(1), 1437. doi:10.1038/s41598-018-35228-3

Spelbrink, J. N., Li, F.-Y., Tiranti, V., Nikali, K., Yuan, Q.-P., Tariq, M., . . . Larsson, C. (2001). Human mitochondrial DNA deletions associated with mutations in the gene encoding Twinkle, a phage T7 gene 4-like protein localized in mitochondria. *Nature Genetics, 28*(3), 223-231. doi:10.1038/90058

Spring, F. A., Dalchau, R., Daniels, G. L., Mallinson, G., Judson, P. A., Parsons, S. F., . . . Anstee, D. J. (1988). The Ina and Inb blood group antigens are located on a glycoprotein of 80,000 MW (the CDw44 glycoprotein) whose expression is influenced by the In(Lu) gene. *Immunology, 64*(1), 37-43.

Srinivasan, S., Guha, M., Dong, D. W., Whelan, K. A., Ruthel, G., Uchikado, Y., . . . Avadhani, N. G. (2016). Disruption of cytochrome c oxidase function induces the Warburg effect and metabolic reprogramming. *Oncogene, 35*(12), 1585-1595. doi:10.1038/onc.2015.227

Srinivasula, S. M., Ahmad, M., Fernandes-Alnemri, T., & Alnemri, E. S. (1998). Autoactivation of Procaspase-9 by Apaf-1-Mediated Oligomerization. *Mol Cell, 1*(7), 949-957. doi:https://doi.org/10.1016/S1097-2765(00)80095-7

Srivastava, S., & Moraes, C. T. (2005). Double-strand breaks of mouse muscle mtDNA promote large deletions similar to multiple mtDNA deletions in humans. *Hum Mol Genet, 14*(7), 893-902. doi:10.1093/hmg/ddi082

St-Pierre, J., Buckingham, J. A., Roebuck, S. J., & Brand, M. D. (2002). Topology of superoxide production from different sites in the mitochondrial electron transport chain. *J Biol Chem, 277*(47), 44784-44790. doi:10.1074/jbc.M207217200

St John, J. C., & Schatten, G. (2004). Paternal mitochondrial DNA transmission during nonhuman primate nuclear transfer. *Genetics, 167*(2), 897-905. doi:10.1534/genetics.103.025049

St. Clair, D. K., Steven Wan, X., Oberley, T. D., Muse, K. E., & St. Clair, W. H. (1992). Suppression of radiation-induced neoplastic transformation by overexpression of mitochondrial superoxide dismutase. *Molecular carcinogenesis, 6*(4), 238-242.

Stamp, C., Zupanic, A., Sachdeva, A., Stoll, E. A., Shanley, D. P., Mathers, J. C., . . . Greaves, L. C. (2018). Predominant Asymmetrical Stem Cell Fate Outcome Limits the Rate of

Niche Succession in Human Colonic Crypts. *EBioMedicine, 31*, 166-173. doi:https://doi.org/10.1016/j.ebiom.2018.04.017

Stehling, O., Vashisht, A. A., Mascarenhas, J., Jonsson, Z. O., Sharma, T., Netz, D. J., . . . Lill, R. (2012). MMS19 assembles iron-sulfur proteins required for DNA metabolism and genomic integrity. *Science, 337*(6091), 195-199. doi:10.1126/science.1219723

Stennicke, H. R., Jürgensmeier, J. M., Shin, H., Deveraux, Q., Wolf, B. B., Yang, X., . . . Salvesen, G. S. (1998). Pro-caspase-3 Is a Major Physiologic Target of Caspase-8. *Journal of Biological Chemistry, 273*(42), 27084-27090. doi:10.1074/jbc.273.42.27084

Sternberg, N. (1979). Demonstration and analysis of P1 site-specific recombination using lambda-P1 hybrid phages constructed in vitro. *Cold Spring Harb Symp Quant Biol, 43 Pt 2*, 1143-1146.

Sternberg, N., & Hamilton, D. (1981). Bacteriophage P1 site-specific recombination. I. Recombination between loxP sites. *J Mol Biol, 150*(4), 467-486.

Stzepourginski, I., Nigro, G., Jacob, J. M., Dulauroy, S., Sansonetti, P. J., Eberl, G., & Peduto, L. (2017). CD34+ mesenchymal cells are a major component of the intestinal stem cells niche at homeostasis and after injury. *Proc Natl Acad Sci U S A, 114*(4), E506-e513. doi:10.1073/pnas.1620059114

Su, L. K., Kinzler, K. W., Vogelstein, B., Preisinger, A. C., Moser, A. R., Luongo, C., . . . Dove, W. F. (1992). Multiple intestinal neoplasia caused by a mutation in the murine homolog of the APC gene. *Science, 256*(5057), 668. doi:10.1126/science.1350108

Su, T., Grady, J. P., Afshar, S., McDonald, S. A., Taylor, R. W., Turnbull, D. M., & Greaves, L. C. (2018). Inherited pathogenic mitochondrial DNA mutations and gastrointestinal stem cell populations. *The Journal of pathology, 246*(4), 427-432. doi:10.1002/path.5156

Sullivan, Lucas B., Gui, Dan Y., Hosios, Aaron M., Bush, Lauren N., Freinkman, E., & Vander Heiden, Matthew G. (2015). Supporting Aspartate Biosynthesis Is an Essential Function of Respiration in Proliferating Cells. *Cell, 162*(3), 552-563. doi:https://doi.org/10.1016/j.cell.2015.07.017

Sun, D., Luo, M., Jeong, M., Rodriguez, B., Xia, Z., Hannah, R., . . . Goodell, M. A. (2014). Epigenomic profiling of young and aged HSCs reveals concerted changes during aging that reinforce self-renewal. *Cell Stem Cell, 14*(5), 673-688. doi:10.1016/j.stem.2014.03.002

Sun, L., Song, L., Wan, Q., Wu, G., Li, X., Wang, Y., . . . Zhang, H. (2015). cMyc-mediated activation of serine biosynthesis pathway is critical for cancer progression under nutrient deprivation conditions. *Cell Res, 25*(4), 429-444. doi:10.1038/cr.2015.33

Suomalainen, A., Elo, J. M., Pietiläinen, K. H., Hakonen, A. H., Sevastianova, K., Korpela, M., . . . Tyynismaa, H. (2011). FGF-21 as a biomarker for muscle-manifesting mitochondrial respiratory chain deficiencies: a diagnostic study. *The Lancet Neurology, 10*(9), 806-818. doi:https://doi.org/10.1016/S1474-4422(11)70155-7

Sutovsky, P., Moreno, R. D., Ramalho-Santos, J., Dominko, T., Simerly, C., & Schatten, G. (1999). Ubiquitin tag for sperm mitochondria. *Nature, 402*(6760), 371-372. doi:10.1038/46466

Sutovsky, P., Moreno, R. D., Ramalho-Santos, J., Dominko, T., Simerly, C., & Schatten, G. (2000). Ubiquitinated sperm mitochondria, selective proteolysis, and the regulation of mitochondrial inheritance in mammalian embryos. *Biol Reprod, 63*(2), 582-590. doi:10.1095/biolreprod63.2.582

Svoboda, L. K., Teh, S. S. K., Sud, S., Kerk, S., Zebolsky, A., Treichel, S., . . . Lawlor, E. R. (2018). Menin regulates the serine biosynthetic pathway in Ewing sarcoma. *J Pathol, 245*(3), 324-336. doi:10.1002/path.5085

Sykora, P., Croteau, D. L., Bohr, V. A., & Wilson, D. M., 3rd. (2011). Aprataxin localizes to mitochondria and preserves mitochondrial function. *Proc Natl Acad Sci U S A, 108*(18), 7437-7442. doi:10.1073/pnas.1100084108

Szatrowski, T. P., & Nathan, C. F. (1991). Production of large amounts of hydrogen peroxide by human tumor cells. *Cancer Res, 51*(3), 794-798.

Tabernero, J., Rojo, F., Calvo, E., Burris, H., Judson, I., Hazell, K., . . . Baselga, J. (2008). Dose- and schedule-dependent inhibition of the mammalian target of rapamycin pathway with everolimus: a phase I tumor pharmacodynamic study in patients with advanced solid tumors. *J Clin Oncol, 26*(10), 1603-1610. doi:10.1200/jco.2007.14.5482

Taguchi, N., Ishihara, N., Jofuku, A., Oka, T., & Mihara, K. (2007). Mitotic phosphorylation of dynamin-related GTPase Drp1 participates in mitochondrial fission. *J Biol Chem, 282*(15), 11521-11529. doi:10.1074/jbc.M607279200

Takaku, K., Oshima, M., Miyoshi, H., Matsui, M., Seldin, M. F., & Taketo, M. M. (1998). Intestinal tumorigenesis in compound mutant mice of both Dpc4 (Smad4) and Apc genes. *Cell, 92*(5), 645-656. doi:10.1016/s0092-8674(00)81132-0

Takeda, N., Jain, R., LeBoeuf, M. R., Wang, Q., Lu, M. M., & Epstein, J. A. (2011). Interconversion between intestinal stem cell populations in distinct niches. *Science, 334*(6061), 1420-1424. doi:10.1126/science.1213214

Takubo, K., Nagamatsu, G., Kobayashi, C. I., Nakamura-Ishizu, A., Kobayashi, H., Ikeda, E., . . . Suda, T. (2013). Regulation of glycolysis by Pdk functions as a metabolic checkpoint for cell cycle quiescence in hematopoietic stem cells. *Cell Stem Cell, 12*(1), 49-61. doi:10.1016/j.stem.2012.10.011

Tan, An S., Baty, James W., Dong, L.-F., Bezawork-Geleta, A., Endaya, B., Goodwin, J., . . . Berridge, Michael V. (2015). Mitochondrial Genome Acquisition Restores Respiratory Function and Tumorigenic Potential of Cancer Cells without Mitochondrial DNA. *Cell Metab, 21*(1), 81-94. doi:https://doi.org/10.1016/j.cmet.2014.12.003

Tan, B. H., & Fearon, K. C. (2008). Cachexia: prevalence and impact in medicine. *Curr Opin Clin Nutr Metab Care, 11*(4), 400-407. doi:10.1097/MCO.0b013e328300ecc1

Taylor, R. W., Barron, M. J., Borthwick, G. M., Gospel, A., Chinnery, P. F., Samuels, D. C., . . . Turnbull, D. M. (2003). Mitochondrial DNA mutations in human colonic crypt stem cells. *J Clin Invest, 112*(9), 1351-1360. doi:10.1172/jci19435

Temin, H. M., & Mizutani, S. (1970). RNA-dependent DNA polymerase in virions of Rous sarcoma virus. *Nature, 226*(5252), 1211-1213. doi:10.1038/2261211a0

Temperley, R., Richter, R., Dennerlein, S., Lightowlers, R. N., & Chrzanowska-Lightowlers, Z. M. (2010). Hungry codons promote frameshifting in human mitochondrial ribosomes. *Science, 327*(5963), 301. doi:10.1126/science.1180674

Terzioglu, M., Ruzzenente, B., Harmel, J., Mourier, A., Jemt, E., López, M. D., . . . Larsson, N. G. (2013). MTERF1 binds mtDNA to prevent transcriptional interference at the light-strand promoter but is dispensable for rRNA gene transcription regulation. *Cell Metab, 17*(4), 618-626. doi:10.1016/j.cmet.2013.03.006

Tetsu, O., & McCormick, F. (1999). Beta-catenin regulates expression of cyclin D1 in colon carcinoma cells. *Nature, 398*(6726), 422-426. doi:10.1038/18884

The Cancer Genome Atlas, N., Muzny, D. M., Bainbridge, M. N., Chang, K., Dinh, H. H., Drummond, J. A., . . . Thomson, E. (2012). Comprehensive molecular characterization of human colon and rectal cancer. *Nature, 487*, 330. doi:10.1038/nature11252

https://www.nature.com/articles/nature11252#supplementary-information

Thompson, K., Mai, N., Oláhová, M., Scialó, F., Formosa, L. E., Stroud, D. A., . . . Taylor, R. W. (2018). OXA1L mutations cause mitochondrial encephalopathy and a combined

oxidative phosphorylation defect. *EMBO molecular medicine, 10*(11). doi:10.15252/emmm.201809060

Thorslund, T., Sunesen, M., Bohr, V. A., & Stevnsner, T. (2002). Repair of 8-oxoG is slower in endogenous nuclear genes than in mitochondrial DNA and is without strand bias. *DNA repair, 1*(4), 261-273. doi:10.1016/s1568-7864(02)00003-4

Tian, H., Biehs, B., Warming, S., Leong, K. G., Rangell, L., Klein, O. D., & de Sauvage, F. J. (2011). A reserve stem cell population in small intestine renders Lgr5-positive cells dispensable. *Nature, 478*(7368), 255-259. doi:10.1038/nature10408

Tibbetts, A. S., & Appling, D. R. (2010). Compartmentalization of Mammalian Folate-Mediated One-Carbon Metabolism. *Annual Review of Nutrition, 30*(1), 57-81. doi:10.1146/annurev.nutr.012809.104810

Todaro, M., Alea, M. P., Di Stefano, A. B., Cammareri, P., Vermeulen, L., Iovino, F., . . . Stassi, G. (2007). Colon cancer stem cells dictate tumor growth and resist cell death by production of interleukin-4. *Cell Stem Cell, 1*(4), 389-402. doi:10.1016/j.stem.2007.08.001

Tomecki, R., Dmochowska, A., Gewartowski, K., Dziembowski, A., & Stepien, P. P. (2004). Identification of a novel human nuclear-encoded mitochondrial poly(A) polymerase. *Nucleic Acids Res, 32*(20), 6001-6014. doi:10.1093/nar/gkh923

Toyota, M., Ahuja, N., Ohe-Toyota, M., Herman, J. G., Baylin, S. B., & Issa, J.-P. J. (1999). CpG island methylator phenotype in colorectal cancer. *Proceedings of the National Academy of Sciences, 96*(15), 8681. doi:10.1073/pnas.96.15.8681

Trahey, M., & McCormick, F. (1987). A cytoplasmic protein stimulates normal N-ras p21 GTPase, but does not affect oncogenic mutants. *Science, 238*(4826), 542-545. doi:10.1126/science.2821624

Trifunovic, A., Hansson, A., Wredenberg, A., Rovio, A. T., Dufour, E., Khvorostov, I., . . . Larsson, N. G. (2005). Somatic mtDNA mutations cause aging phenotypes without affecting reactive oxygen species production. *Proc Natl Acad Sci U S A, 102*(50), 17993-17998. doi:10.1073/pnas.0508886102

Trifunovic, A., Wredenberg, A., Falkenberg, M., Spelbrink, J. N., Rovio, A. T., Bruder, C. E., . . . Larsson, N. G. (2004). Premature ageing in mice expressing defective mitochondrial DNA polymerase. *Nature, 429*(6990), 417-423. doi:10.1038/nature02517

Trobridge, P., Knoblaugh, S., Washington, M. K., Munoz, N. M., Tsuchiya, K. D., Rojas, A., . . . Grady, W. M. (2009). TGF-β Receptor Inactivation and Mutant Kras Induce Intestinal

Neoplasms in Mice via a β-Catenin-Independent Pathway. *Gastroenterology, 136*(5), 1680-1688.e1687. doi:https://doi.org/10.1053/j.gastro.2009.01.066

Tsai, J. H., & Yang, J. (2013). Epithelial-mesenchymal plasticity in carcinoma metastasis. *Genes Dev, 27*(20), 2192-2206. doi:10.1101/gad.225334.113

Tsuboi, M., Morita, H., Nozaki, Y., Akama, K., Ueda, T., Ito, K., . . . Takeuchi, N. (2009). EF-G2mt is an exclusive recycling factor in mammalian mitochondrial protein synthesis. *Mol Cell, 35*(4), 502-510. doi:10.1016/j.molcel.2009.06.028

Tucker, Elena J., Hershman, Steven G., Köhrer, C., Belcher-Timme, Casey A., Patel, J., Goldberger, Olga A., . . . Mootha, Vamsi K. (2011). Mutations in MTFMT Underlie a Human Disorder of Formylation Causing Impaired Mitochondrial Translation. *Cell Metab, 14*(3), 428-434. doi:https://doi.org/10.1016/j.cmet.2011.07.010

Tucker, J. D., Spruill, M. D., Ramsey, M. J., Director, A. D., & Nath, J. (1999). Frequency of spontaneous chromosome aberrations in mice: effects of age. *Mutation research, 425*(1), 135-141. doi:10.1016/s0027-5107(99)00036-6

Tuppen, H. A., Fehmi, J., Czermin, B., Goffrini, P., Meloni, F., Ferrero, I., . . . Taylor, R. W. (2010). Long-term survival of neonatal mitochondrial complex III deficiency associated with a novel BCS1L gene mutation. *Molecular genetics and metabolism, 100*(4), 345-348. doi:10.1016/j.ymgme.2010.04.010

Turrens, J. F., Alexandre, A., & Lehninger, A. L. (1985). Ubisemiquinone is the electron donor for superoxide formation by complex III of heart mitochondria. *Arch Biochem Biophys, 237*(2), 408-414. doi:10.1016/0003-9861(85)90293-0

Twig, G., Elorza, A., Molina, A. J., Mohamed, H., Wikstrom, J. D., Walzer, G., . . . Shirihai, O. S. (2008). Fission and selective fusion govern mitochondrial segregation and elimination by autophagy. *Embo j, 27*(2), 433-446. doi:10.1038/sj.emboj.7601963

Tyynismaa, H., Carroll, C. J., Raimundo, N., Ahola-Erkkilä, S., Wenz, T., Ruhanen, H., . . . Suomalainen, A. (2010). Mitochondrial myopathy induces a starvation-like response. *Human Molecular Genetics, 19*(20), 3948-3958. doi:10.1093/hmg/ddq310

Tyynismaa, H., Mjosund, K. P., Wanrooij, S., Lappalainen, I., Ylikallio, E., Jalanko, A., . . . Suomalainen, A. (2005). Mutant mitochondrial helicase Twinkle causes multiple mtDNA deletions and a late-onset mitochondrial disease in mice. *Proc Natl Acad Sci U S A, 102*(49), 17687-17692. doi:10.1073/pnas.0505551102

Ugalde, C., Hinttala, R., Timal, S., Smeets, R., Rodenburg, R. J. T., Uusimaa, J., . . . Smeitink, J. A. M. (2007). Mutated ND2 impairs mitochondrial complex I assembly and leads to

Leigh syndrome. *Molecular genetics and metabolism, 90*(1), 10-14. doi:10.1016/j.ymgme.2006.08.003

Ugalde, C., Triepels, R. H., Coenen, M. J. H., van den Heuvel, L. P., Smeets, R., Uusimaa, J., . . . Nijtmans, L. G. J. (2003). Impaired complex I assembly in a Leigh syndrome patient with a novel missense mutation in the ND6 gene. *Ann Neurol, 54*(5), 665-669. doi:10.1002/ana.10734

Uhrigshardt, H., Singh, A., Kovtunovych, G., Ghosh, M., & Rouault, T. A. (2010). Characterization of the human HSC20, an unusual DnaJ type III protein, involved in iron–sulfur cluster biogenesis. *Human Molecular Genetics, 19*(19), 3816-3834. doi:10.1093/hmg/ddq301

Umar, S. (2010). Intestinal stem cells. *Current gastroenterology reports, 12*(5), 340-348. doi:10.1007/s11894-010-0130-3

van den Ouweland, J. M., Lemkes, H. H., Ruitenbeek, W., Sandkuijl, L. A., de Vijlder, M. F., Struyvenberg, P. A., . . . Maassen, J. A. (1992). Mutation in mitochondrial tRNA(Leu)(UUR) gene in a large pedigree with maternally transmitted type II diabetes mellitus and deafness. *Nat Genet, 1*(5), 368-371. doi:10.1038/ng0892-368

van der Flier, L. G., & Clevers, H. (2009). Stem cells, self-renewal, and differentiation in the intestinal epithelium. *Annu Rev Physiol, 71*, 241-260. doi:10.1146/annurev.physiol.010908.163145

van der Flier, L. G., van Gijn, M. E., Hatzis, P., Kujala, P., Haegebarth, A., Stange, D. E., . . . Clevers, H. (2009). Transcription factor achaete scute-like 2 controls intestinal stem cell fate. *Cell, 136*(5), 903-912. doi:10.1016/j.cell.2009.01.031

van Es, J. H., Sato, T., van de Wetering, M., Lyubimova, A., Yee Nee, A. N., Gregorieff, A., . . . Clevers, H. (2012). Dll1+ secretory progenitor cells revert to stem cells upon crypt damage. *Nat Cell Biol, 14*(10), 1099-1104. doi:10.1038/ncb2581

Van Haute, L., Hendrick, A. G., D'Souza, A. R., Powell, C. A., Rebelo-Guiomar, P., Harbour, M. E., . . . Minczuk, M. (2019). METTL15 introduces N4-methylcytidine into human mitochondrial 12S rRNA and is required for mitoribosome biogenesis. *Nucleic Acids Res, 47*(19), 10267-10281. doi:10.1093/nar/gkz735

Van Vranken, J. G., Jeong, M. Y., Wei, P., Chen, Y. C., Gygi, S. P., Winge, D. R., & Rutter, J. (2016). The mitochondrial acyl carrier protein (ACP) coordinates mitochondrial fatty acid synthesis with iron sulfur cluster biogenesis. *Elife, 5*. doi:10.7554/eLife.17828

Vasconcelos-dos-Santos, A., Loponte, H. F. B. R., Mantuano, N. R., Oliveira, I. A., de Paula, I. F., Teixeira, L. K., . . . Todeschini, A. R. (2017). Hyperglycemia exacerbates colon cancer malignancy through hexosamine biosynthetic pathway. *Oncogenesis, 6*(3), e306-e306. doi:10.1038/oncsis.2017.2

Väyrynen, J. P., Tuomisto, A., Väyrynen, S. A., Klintrup, K., Karhu, T., Mäkelä, J., . . . Mäkinen, M. J. (2018). Preoperative anemia in colorectal cancer: relationships with tumor characteristics, systemic inflammation, and survival. *Scientific Reports, 8*(1), 1126-1126. doi:10.1038/s41598-018-19572-y

Venook, A. P., Niedzwiecki, D., Innocenti, F., Fruth, B., Greene, C., O'Neil, B. H., . . . Lenz, H.-J. (2016). Impact of primary (1º) tumor location on overall survival (OS) and progression-free survival (PFS) in patients (pts) with metastatic colorectal cancer (mCRC): Analysis of CALGB/SWOG 80405 (Alliance). *Journal of Clinical Oncology, 34*(15_suppl), 3504-3504. doi:10.1200/JCO.2016.34.15_suppl.3504

Venook, A. P., Niedzwiecki, D., Lenz, H. J., Innocenti, F., Fruth, B., Meyerhardt, J. A., . . . Blanke, C. (2017). Effect of First-Line Chemotherapy Combined With Cetuximab or Bevacizumab on Overall Survival in Patients With KRAS Wild-Type Advanced or Metastatic Colorectal Cancer: A Randomized Clinical Trial. *Jama, 317*(23), 2392-2401. doi:10.1001/jama.2017.7105

Vermeulen, L., De Sousa, E. M. F., van der Heijden, M., Cameron, K., de Jong, J. H., Borovski, T., . . . Medema, J. P. (2010). Wnt activity defines colon cancer stem cells and is regulated by the microenvironment. *Nat Cell Biol, 12*(5), 468-476. doi:10.1038/ncb2048

Vermeulen, L., Sprick, M. R., Kemper, K., Stassi, G., & Medema, J. P. (2008). Cancer stem cells--old concepts, new insights. *Cell Death Differ, 15*(6), 947-958. doi:10.1038/cdd.2008.20

Vermulst, M., Bielas, J. H., Kujoth, G. C., Ladiges, W. C., Rabinovitch, P. S., Prolla, T. A., & Loeb, L. A. (2007). Mitochondrial point mutations do not limit the natural lifespan of mice. *Nature Genetics, 39*(4), 540-543. doi:10.1038/ng1988

Vermulst, M., Wanagat, J., Kujoth, G. C., Bielas, J. H., Rabinovitch, P. S., Prolla, T. A., & Loeb, L. A. (2008). DNA deletions and clonal mutations drive premature aging in mitochondrial mutator mice. *Nat Genet, 40*(4), 392-394. doi:10.1038/ng.95

Viale, A., Pettazzoni, P., Lyssiotis, C. A., Ying, H., Sánchez, N., Marchesini, M., . . . Draetta, G. F. (2014). Oncogene ablation-resistant pancreatic cancer cells depend on mitochondrial function. *Nature, 514*(7524), 628-632. doi:10.1038/nature13611

Villeda, S. A., Luo, J., Mosher, K. I., Zou, B., Britschgi, M., Bieri, G., . . . Wyss-Coray, T. (2011). The ageing systemic milieu negatively regulates neurogenesis and cognitive function. *Nature, 477*(7362), 90-94. doi:10.1038/nature10357

Vincent, A. E., Rosa, H. S., Pabis, K., Lawless, C., Chen, C., Grünewald, A., . . . Picard, M. (2018). Subcellular origin of mitochondrial DNA deletions in human skeletal muscle. *Ann Neurol, 84*(2), 289-301. doi:10.1002/ana.25288

Virbasius, C. A., Virbasius, J. V., & Scarpulla, R. C. (1993a). NRF-1, an activator involved in nuclear-mitochondrial interactions, utilizes a new DNA-binding domain conserved in a family of developmental regulators. *Genes Dev, 7*(12a), 2431-2445. doi:10.1101/gad.7.12a.2431

Virbasius, J. V., Virbasius, C. A., & Scarpulla, R. C. (1993b). Identity of GABP with NRF-2, a multisubunit activator of cytochrome oxidase expression, reveals a cellular role for an ETS domain activator of viral promoters. *Genes Dev, 7*(3), 380-392. doi:10.1101/gad.7.3.380

Vogelstein, B., & Kinzler, K. W. (2002). *The genetic basis of human cancer*: McGraw-Hill.

von Zglinicki, T. (2002). Oxidative stress shortens telomeres. *Trends Biochem Sci, 27*(7), 339-344. doi:10.1016/s0968-0004(02)02110-2

Vozza, A., Parisi, G., De Leonardis, F., Lasorsa, F. M., Castegna, A., Amorese, D., . . . Fiermonte, G. (2014). UCP2 transports C4 metabolites out of mitochondria, regulating glucose and glutamine oxidation. *Proc Natl Acad Sci U S A, 111*(3), 960-965. doi:10.1073/pnas.1317400111

Vucic, D., Franklin, M. C., Wallweber, H. J., Das, K., Eckelman, B. P., Shin, H., . . . Fairbrother, W. J. (2005). Engineering ML-IAP to produce an extraordinarily potent caspase 9 inhibitor: implications for Smac-dependent anti-apoptotic activity of ML-IAP. *Biochem J, 385*(Pt 1), 11-20. doi:10.1042/bj20041108

Wagner, A. J., Kokontis, J. M., & Hay, N. (1994). Myc-mediated apoptosis requires wild-type p53 in a manner independent of cell cycle arrest and the ability of p53 to induce p21waf1/cip1. *Genes Dev, 8*(23), 2817-2830. doi:10.1101/gad.8.23.2817

Wall, C. E., Whyte, J., Suh, J. M., Fan, W., Collins, B., Liddle, C., . . . Evans, R. M. (2015). High-fat diet and FGF21 cooperatively promote aerobic thermogenesis in mtDNA mutator mice. *Proc Natl Acad Sci U S A, 112*(28), 8714-8719. doi:10.1073/pnas.1509930112

Wallace, D. C. (1989). Mitochondrial DNA mutations and neuromuscular disease. *Trends Genet, 5*(1), 9-13. doi:10.1016/0168-9525(89)90005-x

Wallace, D. C. (2010). Bioenergetics, the origins of complexity, and the ascent of man. *Proceedings of the National Academy of Sciences, 107*(Supplement 2), 8947. doi:10.1073/pnas.0914635107

Wallace, D. C., Zheng, X. X., Lott, M. T., Shoffner, J. M., Hodge, J. A., Kelley, R. I., . . . Hopkins, L. C. (1988). Familial mitochondrial encephalomyopathy (MERRF): genetic, pathophysiological, and biochemical characterization of a mitochondrial DNA disease. *Cell, 55*(4), 601-610. doi:10.1016/0092-8674(88)90218-8

Wang, C., Guo, K., Gao, D., Kang, X., Jiang, K., Li, Y., . . . Liu, Y. (2011). Identification of transaldolase as a novel serum biomarker for hepatocellular carcinoma metastasis using xenografted mouse model and clinic samples. *Cancer Lett, 313*(2), 154-166. doi:10.1016/j.canlet.2011.08.031

Wang, C., & Youle, R. J. (2009). The Role of Mitochondria in Apoptosis. *Annual Review of Genetics, 43*(1), 95-118. doi:10.1146/annurev-genet-102108-134850

Wang, J., Silva, J. P., Gustafsson, C. M., Rustin, P., & Larsson, N. G. (2001). Increased in vivo apoptosis in cells lacking mitochondrial DNA gene expression. *Proc Natl Acad Sci U S A, 98*(7), 4038-4043. doi:10.1073/pnas.061038798

Wang, J., Wilhelmsson, H., Graff, C., Li, H., Oldfors, A., Rustin, P., . . . Larsson, N. G. (1999). Dilated cardiomyopathy and atrioventricular conduction blocks induced by heart-specific inactivation of mitochondrial DNA gene expression. *Nat Genet, 21*(1), 133-137. doi:10.1038/5089

Wang, Q., Liberti, M. V., Liu, P., Deng, X., Liu, Y., Locasale, J. W., & Lai, L. (2017). Rational Design of Selective Allosteric Inhibitors of PHGDH and Serine Synthesis with Anti-tumor Activity. *Cell chemical biology, 24*(1), 55-65. doi:10.1016/j.chembiol.2016.11.013

Wang, Y., & Bogenhagen, D. F. (2006). Human mitochondrial DNA nucleoids are linked to protein folding machinery and metabolic enzymes at the mitochondrial inner membrane. *J Biol Chem, 281*(35), 25791-25802. doi:10.1074/jbc.M604501200

Warburg, O. (1927). Über den heutigen Stand des Carcinomproblems. *Naturwissenschaften, 15*(1), 1-4. doi:10.1007/BF01504870

Warburg, O. (1956). On the origin of cancer cells. *Science, 123*(3191), 309-314. doi:10.1126/science.123.3191.309

Ward, P. S., Patel, J., Wise, D. R., Abdel-Wahab, O., Bennett, B. D., Coller, H. A., . . . Thompson, C. B. (2010). The common feature of leukemia-associated IDH1 and IDH2 mutations is a neomorphic enzyme activity converting alpha-ketoglutarate to 2-hydroxyglutarate. *Cancer Cell, 17*(3), 225-234. doi:10.1016/j.ccr.2010.01.020

Warne, P. H., Vician, P. R., & Downward, J. (1993). Direct interaction of Ras and the amino-terminal region of Raf-1 in vitro. *Nature, 364*(6435), 352-355. doi:10.1038/364352a0

Warren, C., McDonald, D., Capaldi, R., Deehan, D., Taylor, R. W., Filby, A., . . . Vincent, A. E. (2020). Decoding mitochondrial heterogeneity in single muscle fibres by imaging mass cytometry. *Scientific Reports, 10*(1), 15336. doi:10.1038/s41598-020-70885-3

Warthin, A. S. (1913). HEREDITY WITH REFERENCE TO CARCINOMA: AS SHOWN BY THE STUDY OF THE CASES EXAMINED IN THE PATHOLOGICAL LABORATORY OF THE UNIVERSITY OF MICHIGAN, 1895-1913. *Archives of Internal Medicine, XII*(5), 546-555. doi:10.1001/archinte.1913.00070050063006

Watanabe, K., Ueno, M., Kamiya, D., Nishiyama, A., Matsumura, M., Wataya, T., . . . Sasai, Y. (2007). A ROCK inhibitor permits survival of dissociated human embryonic stem cells. *Nature Biotechnology, 25*(6), 681-686. doi:10.1038/nbt1310

Watson, J. D. (1972). Origin of Concatemeric T7DNA. *Nature New Biology, 239*(94), 197-201. doi:10.1038/newbio239197a0

Wei, W., Pagnamenta, A. T., Gleadall, N., Sanchis-Juan, A., Stephens, J., Broxholme, J., . . . Chinnery, P. F. (2020). Nuclear-mitochondrial DNA segments resemble paternally inherited mitochondrial DNA in humans. *Nature Communications, 11*(1), 1740-1740. doi:10.1038/s41467-020-15336-3

Weinberg, F., Hamanaka, R., Wheaton, W. W., Weinberg, S., Joseph, J., Lopez, M., . . . Chandel, N. S. (2010). Mitochondrial metabolism and ROS generation are essential for Kras-mediated tumorigenicity. *Proc Natl Acad Sci U S A, 107*(19), 8788-8793. doi:10.1073/pnas.1003428107

Weisenberger, D. J., Siegmund, K. D., Campan, M., Young, J., Long, T. I., Faasse, M. A., . . . Laird, P. W. (2006). CpG island methylator phenotype underlies sporadic

microsatellite instability and is tightly associated with BRAF mutation in colorectal cancer. *Nat Genet, 38*(7), 787-793. doi:10.1038/ng1834

Weisiger, R. A., & Fridovich, I. (1973). Superoxide dismutase. Organelle specificity. *J Biol Chem, 248*(10), 3582-3592.

Weismann, A., Poulton, E. B., Schönland, S., & Shipley, A. E. (1891). *Essays Upon Heredity and Kindred Biological Problems*: Clarendon Press.

Weissbach, A., Baltimore, D., Bollum, F., Gallo, R., & Korn, D. (1975). Nomenclature of eukaryotic DNA polymerases. *Science, 190*(4212), 401-402. doi:10.1126/science.1179222

Welter, C., Kovacs, G., Seitz, G., & Blin, N. (1989). Alteration of mitochondrial DNA in human oncocytomas. *Genes Chromosomes Cancer, 1*(1), 79-82. doi:10.1002/gcc.2870010112

Wiedemann, N., Kozjak, V., Chacinska, A., Schonfisch, B., Rospert, S., Ryan, M. T., . . . Meisinger, C. (2003). Machinery for protein sorting and assembly in the mitochondrial outer membrane. *Nature, 424*(6948), 565-571. doi:10.1038/nature01753

Wikström, M. (1977). Proton pump coupled to cytochrome c oxidase in mitochondria. *Nature, 266*(5599), 271-273. doi:10.1038/266271a0

Wikström, M. (1984). Two protons are pumped from the mitochondrial matrix per electron transferred between NADH and ubiquinone. *FEBS Lett, 169*(2), 300-304. doi:10.1016/0014-5793(84)80338-5

Wiley, S. R., Schooley, K., Smolak, P. J., Din, W. S., Huang, C. P., Nicholl, J. K., . . . et al. (1995). Identification and characterization of a new member of the TNF family that induces apoptosis. *Immunity, 3*(6), 673-682. doi:10.1016/1074-7613(95)90057-8

Williams, G. C. (1957). Pleiotropy, Natural Selection, and the Evolution of Senescence. *Evolution, 11*(4), 398-411. doi:10.2307/2406060

Williams, G. M., Iatropoulos, M. J., Djordjevic, M. V., & Kaltenberg, O. P. (1993). The triphenylethylene drug tamoxifen is a strong liver carcinogen in the rat. *Carcinogenesis, 14*(2), 315-317. doi:10.1093/carcin/14.2.315

Wilms, E., Troost, F. J., Elizalde, M., Winkens, B., de Vos, P., Mujagic, Z., . . . Masclee, A. A. M. (2020). Intestinal barrier function is maintained with aging – a comprehensive study in healthy subjects and irritable bowel syndrome patients. *Scientific Reports, 10*(1), 475. doi:10.1038/s41598-019-57106-2

Wilson, K. J., Mill, C., Lambert, S., Buchman, J., Wilson, T. R., Hernandez-Gordillo, V., . . . Riese, D. J., 2nd. (2012). EGFR ligands exhibit functional differences in models of paracrine and autocrine signaling. *Growth Factors, 30*(2), 107-116. doi:10.3109/08977194.2011.649918

Wilson, M. J., Dekker, J. W. T., Harlaar, J. J., Jeekel, J., Schipperus, M., & Zwaginga, J. J. (2017). The role of preoperative iron deficiency in colorectal cancer patients: prevalence and treatment. *International journal of colorectal disease, 32*(11), 1617-1624. doi:10.1007/s00384-017-2898-1

Winton, D. J., Blount, M. A., & Ponder, B. A. J. (1988). A clonal marker induced by mutation in mouse intestinal epithelium. *Nature, 333*(6172), 463-466. doi:10.1038/333463a0

Wittig, I., Velours, J., Stuart, R., & Schägger, H. (2008). Characterization of Domain Interfaces in Monomeric and Dimeric ATP Synthase. *Molecular & Cellular Proteomics, 7*(5), 995. doi:10.1074/mcp.M700465-MCP200

Wolin, K. Y., Yan, Y., Colditz, G. A., & Lee, I. M. (2009). Physical activity and colon cancer prevention: a meta-analysis. *British journal of cancer, 100*(4), 611-616. doi:10.1038/sj.bjc.6604917

Wollert, K. C., Kempf, T., & Wallentin, L. (2017). Growth Differentiation Factor 15 as a Biomarker in Cardiovascular Disease. *Clinical Chemistry, 63*(1), 140-151. doi:10.1373/clinchem.2016.255174

Woo, D. K., Green, P. D., Santos, J. H., D'Souza, A. D., Walther, Z., Martin, W. D., . . . Shadel, G. S. (2012). Mitochondrial genome instability and ROS enhance intestinal tumorigenesis in APC(Min/+) mice. *Am J Pathol, 180*(1), 24-31. doi:10.1016/j.ajpath.2011.10.003

Wright, D. C., Geiger, P. C., Han, D. H., Jones, T. E., & Holloszy, J. O. (2007). Calcium induces increases in peroxisome proliferator-activated receptor gamma coactivator-1alpha and mitochondrial biogenesis by a pathway leading to p38 mitogen-activated protein kinase activation. *J Biol Chem, 282*(26), 18793-18799. doi:10.1074/jbc.M611252200

Wu, H., Rao, G. N., Dai, B., & Singh, P. (2000). Autocrine gastrins in colon cancer cells Up-regulate cytochrome c oxidase Vb and down-regulate efflux of cytochrome c and activation of caspase-3. *J Biol Chem, 275*(42), 32491-32498. doi:10.1074/jbc.M002458200

Wu, S. P., Theodorescu, D., Kerbel, R. S., Willson, J. K., Mulder, K. M., Humphrey, L. E., & Brattain, M. G. (1992). TGF-beta 1 is an autocrine-negative growth regulator of

human colon carcinoma FET cells in vivo as revealed by transfection of an antisense expression vector. *The Journal of Cell Biology, 116*(1), 187. doi:10.1083/jcb.116.1.187

Wüst, S., Dröse, S., Heidler, J., Wittig, I., Klockner, I., Franko, A., . . . Braun, T. (2018). Metabolic Maturation during Muscle Stem Cell Differentiation Is Achieved by miR-1/133a-Mediated Inhibition of the Dlk1-Dio3 Mega Gene Cluster. *Cell Metab, 27*(5), 1026-1039.e1026. doi:10.1016/j.cmet.2018.02.022

Wyllie, A. H., Rose, K. A., Morris, R. G., Steel, C. M., Foster, E., & Spandidos, D. A. (1987). Rodent fibroblast tumours expressing human myc and ras genes: growth, metastasis and endogenous oncogene expression. *British journal of cancer, 56*(3), 251-259. doi:10.1038/bjc.1987.186

Xiao, M., Yang, H., Xu, W., Ma, S., Lin, H., Zhu, H., . . . Guan, K.-L. (2012). Inhibition of α-KG-dependent histone and DNA demethylases by fumarate and succinate that are accumulated in mutations of FH and SDH tumor suppressors. *Genes & development, 26*(12), 1326-1338. doi:10.1101/gad.191056.112

Xu, X., Zur Hausen, A., Coy, J. F., & Löchelt, M. (2009). Transketolase-like protein 1 (TKTL1) is required for rapid cell growth and full viability of human tumor cells. *Int J Cancer, 124*(6), 1330-1337. doi:10.1002/ijc.24078

Yadav, N., Kumar, S., Marlowe, T., Chaudhary, A. K., Kumar, R., Wang, J., . . . Chandra, D. (2015). Oxidative phosphorylation-dependent regulation of cancer cell apoptosis in response to anticancer agents. *Cell Death & Disease, 6*(11), e1969-e1969. doi:10.1038/cddis.2015.305

Yakes, F. M., & Van Houten, B. (1997). Mitochondrial DNA damage is more extensive and persists longer than nuclear DNA damage in human cells following oxidative stress. *Proc Natl Acad Sci U S A, 94*(2), 514-519.

Yakubovskaya, E., Chen, Z., Carrodeguas, J. A., Kisker, C., & Bogenhagen, D. F. (2006). Functional human mitochondrial DNA polymerase gamma forms a heterotrimer. *J Biol Chem, 281*(1), 374-382. doi:10.1074/jbc.M509730200

Yakubovskaya, E., Mejia, E., Byrnes, J., Hambardjieva, E., & Garcia-Diaz, M. (2010). Helix unwinding and base flipping enable human MTERF1 to terminate mitochondrial transcription. *Cell, 141*(6), 982-993. doi:10.1016/j.cell.2010.05.018

Yan, K. S., Chia, L. A., Li, X., Ootani, A., Su, J., Lee, J. Y., . . . Kuo, C. J. (2012). The intestinal stem cell markers Bmi1 and Lgr5 identify two functionally distinct populations. *Proc Natl Acad Sci U S A, 109*(2), 466-471. doi:10.1073/pnas.1118857109

Yang, J., Liu, X., Bhalla, K., Kim, C. N., Ibrado, A. M., Cai, J., . . . Wang, X. (1997). Prevention of apoptosis by Bcl-2: release of cytochrome c from mitochondria blocked. *Science, 275*(5303), 1129-1132. doi:10.1126/science.275.5303.1129

Yang, L., Garcia Canaveras, J. C., Chen, Z., Wang, L., Liang, L., Jang, C., . . . Rabinowitz, J. D. (2020). Serine Catabolism Feeds NADH when Respiration Is Impaired. *Cell Metab, 31*(4), 809-821.e806. doi:https://doi.org/10.1016/j.cmet.2020.02.017

Yang, Q., Bermingham, N. A., Finegold, M. J., & Zoghbi, H. Y. (2001). Requirement of Math1 for secretory cell lineage commitment in the mouse intestine. *Science, 294*(5549), 2155-2158. doi:10.1126/science.1065718

Yasukawa, T., Reyes, A., Cluett, T. J., Yang, M.-Y., Bowmaker, M., Jacobs, H. T., & Holt, I. J. (2006). Replication of vertebrate mitochondrial DNA entails transient ribonucleotide incorporation throughout the lagging strand. *Embo j, 25*(22), 5358-5371. doi:10.1038/sj.emboj.7601392

Yatsuga, S., Fujita, Y., Ishii, A., Fukumoto, Y., Arahata, H., Kakuma, T., . . . Koga, Y. (2015). Growth differentiation factor 15 as a useful biomarker for mitochondrial disorders. *Ann Neurol, 78*(5), 814-823. doi:10.1002/ana.24506

Ye, J., Mancuso, A., Tong, X., Ward, P. S., Fan, J., Rabinowitz, J. D., & Thompson, C. B. (2012). Pyruvate kinase M2 promotes de novo serine synthesis to sustain mTORC1 activity and cell proliferation. *Proc Natl Acad Sci U S A, 109*(18), 6904-6909. doi:10.1073/pnas.1204176109

Ye, X. Q., Li, Q., Wang, G. H., Sun, F. F., Huang, G. J., Bian, X. W., . . . Qian, G. S. (2011). Mitochondrial and energy metabolism-related properties as novel indicators of lung cancer stem cells. *Int J Cancer, 129*(4), 820-831. doi:10.1002/ijc.25944

Yin, A. H., Miraglia, S., Zanjani, E. D., Almeida-Porada, G., Ogawa, M., Leary, A. G., . . . Buck, D. W. (1997). AC133, a novel marker for human hematopoietic stem and progenitor cells. *Blood, 90*(12), 5002-5012.

Yoshida, M., Muneyuki, E., & Hisabori, T. (2001). ATP synthase--a marvellous rotary engine of the cell. *Nat Rev Mol Cell Biol, 2*(9), 669-677. doi:10.1038/35089509

Yoshida, T., & Kikuchi, G. (1970). Major pathways of glycine and serine catabolism in rat liver. *Archives of Biochemistry and Biophysics, 139*(2), 380-392. doi:https://doi.org/10.1016/0003-9861(70)90490-X

Yu, M., Trobridge, P., Wang, Y., Kanngurn, S., Morris, S. M., Knoblaugh, S., & Grady, W. M. (2014). Inactivation of TGF-β signaling and loss of PTEN cooperate to induce colon cancer in vivo. *Oncogene, 33*(12), 1538-1547. doi:10.1038/onc.2013.102

Yuan, Y., Ju, Y. S., Kim, Y., Li, J., Wang, Y., Yoon, C. J., . . . Consortium, P. (2020). Comprehensive molecular characterization of mitochondrial genomes in human cancers. *Nature Genetics, 52*(3), 342-352. doi:10.1038/s41588-019-0557-x

Yuan, Y., Wang, W., Li, H., Yu, Y., Tao, J., Huang, S., & Zeng, Z. (2015). Nonsense and missense mutation of mitochondrial ND6 gene promotes cell migration and invasion in human lung adenocarcinoma. *BMC cancer, 15*, 346-346. doi:10.1186/s12885-015-1349-z

Yue, L., Pei, Y., Zhong, L., Yang, H., Wang, Y., Zhang, W., . . . Han, J. (2020). Mthfd2 Modulates Mitochondrial Function and DNA Repair to Maintain the Pluripotency of Mouse Stem Cells. *Stem Cell Reports, 15*(2), 529-545. doi:10.1016/j.stemcr.2020.06.018

Yukawa, K., Tanaka, T., Tsuji, S., & Akira, S. (1999). Regulation of transcription factor C/ATF by the cAMP signal activation in hippocampal neurons, and molecular interaction of C/ATF with signal integrator CBP/p300. *Molecular Brain Research, 69*(1), 124-134. doi:https://doi.org/10.1016/S0169-328X(99)00086-8

Zacharakis, M., Xynos, I. D., Lazaris, A., Smaro, T., Kosmas, C., Dokou, A., . . . Tsavaris, N. (2010). Predictors of survival in stage IV metastatic colorectal cancer. *Anticancer Res, 30*(2), 653-660.

Zakikhani, M., Dowling, R., Fantus, I. G., Sonenberg, N., & Pollak, M. (2006). Metformin Is an AMP Kinase–Dependent Growth Inhibitor for Breast Cancer Cells. *Cancer Res, 66*(21), 10269. doi:10.1158/0008-5472.CAN-06-1500

Zha, H., Aimé-Sempé, C., Sato, T., & Reed, J. C. (1996). Proapoptotic protein Bax heterodimerizes with Bcl-2 and homodimerizes with Bax via a novel domain (BH3) distinct from BH1 and BH2. *J Biol Chem, 271*(13), 7440-7444. doi:10.1074/jbc.271.13.7440

Zhang, C., Skamagki, M., Liu, Z., Ananthanarayanan, A., Zhao, R., Li, H., & Kim, K. (2017). Biological Significance of the Suppression of Oxidative Phosphorylation in Induced Pluripotent Stem Cells. *Cell Rep, 21*(8), 2058-2065. doi:10.1016/j.celrep.2017.10.098

Zhang, C. F., Linnane, A. W., & Nagley, P. (1993). Occurrence of a Particular Base Substitution (3243 A to G) in Mitochondrial DNA of Tissues of Ageing Humans. *Biochemical and Biophysical Research Communications, 195*(2), 1104-1110. doi:https://doi.org/10.1006/bbrc.1993.2158

Zhang, L., Zhu, H., Teraishi, F., Davis, J. J., Guo, W., Fan, Z., & Fang, B. (2005). Accelerated degradation of caspase-8 protein correlates with TRAIL resistance in a DLD1 human colon cancer cell line. *Neoplasia (New York, N.Y.), 7*(6), 594-602. doi:10.1593/neo.04688

Zhang, X.-Y., Pfeiffer, H. K., Mellert, H. S., Stanek, T. J., Sussman, R. T., Kumari, A., . . . McMahon, S. B. (2011). Inhibition of the single downstream target BAG1 activates the latent apoptotic potential of MYC. *Molecular and cellular biology, 31*(24), 5037-5045. doi:10.1128/mcb.06297-11

Zhang, Y., Ikeno, Y., Qi, W., Chaudhuri, A., Li, Y., Bokov, A., . . . Van Remmen, H. (2009). Mice deficient in both Mn superoxide dismutase and glutathione peroxidase-1 have increased oxidative damage and a greater incidence of pathology but no reduction in longevity. *The journals of gerontology. Series A, Biological sciences and medical sciences, 64*(12), 1212-1220. doi:10.1093/gerona/glp132

Zhang, Y., Riesterer, C., Ayrall, A. M., Sablitzky, F., Littlewood, T. D., & Reth, M. (1996). Inducible site-directed recombination in mouse embryonic stem cells. *Nucleic Acids Res, 24*(4), 543-548. doi:10.1093/nar/24.4.543

Zhao, H., French, J. B., Fang, Y., & Benkovic, S. J. (2013a). The purinosome, a multi-protein complex involved in the de novo biosynthesis of purines in humans. *Chem Commun (Camb), 49*(40), 4444-4452. doi:10.1039/c3cc41437j

Zhao, J., Zhang, J., Yu, M., Xie, Y., Huang, Y., Wolff, D. W., . . . Tu, Y. (2013b). Mitochondrial dynamics regulates migration and invasion of breast cancer cells. *Oncogene, 32*(40), 4814-4824. doi:10.1038/onc.2012.494

Zhao, Q., Wang, J., Levichkin, I. V., Stasinopoulos, S., Ryan, M. T., & Hoogenraad, N. J. (2002). A mitochondrial specific stress response in mammalian cells. *Embo j, 21*(17), 4411-4419. doi:10.1093/emboj/cdf445

Zhen, L., Zhe, S., Zhenning, W., Zhifeng, M., Zhidong, L., Xiaoxia, L., . . . Huimian, X. (2012). Iron-deficiency anemia: A predictor of diminished disease-free survival of T3N0M0 stage colon cancer. *Journal of Surgical Oncology, 105*(4), 371-375. doi:10.1002/jso.22032

Zheng, W., Khrapko, K., Coller, H. A., Thilly, W. G., & Copeland, W. C. (2006). Origins of human mitochondrial point mutations as DNA polymerase γ-mediated errors. *Mutation Research/Fundamental and Molecular Mechanisms of Mutagenesis, 599*(1), 11-20. doi:https://doi.org/10.1016/j.mrfmmm.2005.12.012

Zheng, X., Boyer, L., Jin, M., Mertens, J., Kim, Y., Ma, L., . . . Hunter, T. (2016). Metabolic reprogramming during neuronal differentiation from aerobic glycolysis to neuronal oxidative phosphorylation. *Elife, 5*. doi:10.7554/eLife.13374

Zhou, G., Myers, R., Li, Y., Chen, Y., Shen, X., Fenyk-Melody, J., . . . Moller, D. E. (2001). Role of AMP-activated protein kinase in mechanism of metformin action. *J Clin Invest, 108*(8), 1167-1174. doi:10.1172/JCI13505

Zong, S., Wu, M., Gu, J., Liu, T., Guo, R., & Yang, M. (2018). Structure of the intact 14-subunit human cytochrome c oxidase. *Cell Research, 28*(10), 1026-1034. doi:10.1038/s41422-018-0071-1

Zuchner, S., Mersiyanova, I. V., Muglia, M., Bissar-Tadmouri, N., Rochelle, J., Dadali, E. L., . . . Vance, J. M. (2004). Mutations in the mitochondrial GTPase mitofusin 2 cause Charcot-Marie-Tooth neuropathy type 2A. *Nat Genet, 36*(5), 449-451. doi:10.1038/ng1341